REINFORCEMENT OF CEMENT-BASED MATRICES WITH GRAPHITE NANOMATERIALS

By

Muhammad Maqbool Sadiq

A DISSERTATION

Submitted to
Michigan State University
in partial fulfillment of the requirements
for the degree of

Civil Engineering – Doctor of Philosophy

ABSTRACT

REINFORCEMENT OF CEMENT-BASED MATRICES WITH GRAPHITE NANOMATERIALS

By

Muhammad Maqbool Sadiq

Cement-based materials offer a desirable balance of compressive strength, moisture resistance, durability, economy and energy-efficiency; their tensile strength, fracture energy and durability in aggressive environments, however, could benefit from further improvements. An option for realizing some of these improvements involves introduction of discrete fibers into concrete. When compared with today's micro-scale (steel, polypropylene, glass, etc.) fibers, graphite nanomaterials (carbon nanotube, nanofiber and graphite nanoplatelet) offer superior geometric, mechanical and physical characteristics. Graphite nanomaterials would realize their reinforcement potential as far as they are thoroughly dispersed within cement-based matrices, and effectively bond to cement hydrates.

The research reported herein developed non-covalent and covalent surface modification techniques to improve the dispersion and interfacial interactions of graphite nanomaterials in cement-based matrices with a dense and well graded micro-structure. The most successful approach involved polymer wrapping of nanomaterials for increasing the density of hydrophilic groups on the nanomaterial surface without causing any damage to the their structure.

The nanomaterials were characterized using various spectrometry techniques, and SEM (Scanning Electron Microscopy). The graphite nanomaterials were dispersed via selected sonication procedures in the mixing water of the cement-based matrix; conventional mixing and sample preparation techniques were then employed to prepare the cement-based nanocomposite

samples, which were subjected to steam curing. Comprehensive engineering and durability characteristics of cement-based nanocomposites were determined and their chemical composition, microstructure and failure mechanisms were also assessed through various spectrometry, thermogravimetry, electron microscopy and elemental analyses.

Both functionalized and non-functionalized nanomaterials as well as different micro-scale fibers were used for comparison purposes at different volume fractions. Replicated mixes and tests were considered to provide the basis for statistically reliable inferences.

Theoretical studies were conducted in order to develop insight into the reinforcement mechanisms of properly functionalized graphite nanomaterials. The results suggested that modified graphite nanomaterials improve the mechanical performance of cement-based matrices primarily through control of microcrack size and propagation, relying on their close spacing within matrix and dissipation of substantial energy by debonding and frictional pullout over their enormous surface areas. The gains in barrier qualities of cement-based materials with introduction of modified graphite nanomaterials could be attributed to the increased tortuosity of diffusion paths in the presence of closely spaced nanomaterials.

Experimental investigations were designed and implemented towards identification of the optimum (nano- and micro-scale) reinforcement systems for high-performance concrete through RSA (Response Surface Analysis). A comprehensive experimental data base was developed on the mechanical, physical and durability characteristics as well as the structure and composition of high-performance cementitious nanocomposites reinforced with modified graphite nanomaterials and/ or different micro-fibers.

DEDICATION

To my *Ammi*, *Abbu* and *Brothers* for their endless love, support and encouragement...

Also, to *My Wife* and the *Four Fairies* in my life who have made my life so beautiful and are a constant source of love, motivation and inspiration...

ACKNOWLEDGMENTS

All Praises to Allah Almighty for giving me the ability and serenity to conduct this research, strength to persevere through hard times and for showering His countless blessings on me. I would also like to express my humble gratitude to my great country Pakistan for providing me with all the wonderful opportunities in my life, especially to Pakistan Army for giving me this chance to pursue this advance degree.

It is with immense gratitude that I acknowledge my Academic Advisor and my Committee Chair, Professor Parviz Soroushian for his tugs and pushes as well as support and guidance during the course of my research. I would also like to thank Professor Rigoberto Burgueño, Professor Lawrence T. Drzal and Professor Venkatesh Kodur for joining my PhD committee, and for their valuable advice throughout my education at MSU. Many thanks and appreciation for Dr. Anagi Balachandra for all her help during the initial chemistry part of this research work.

I would especially like to thank Professor and Chairperson Neeraj Buch, Professor and Associate Dean of Graduate Studies and Faculty Development M. Koochesfahani and Director Office of International Students and Scholars Peter Briggs for supporting me through some very hard times. And, I would also like to extend my thanks to Laura Taylor, Mary Mroz, and Margaret Conner for all the help they provided.

I would also like to thank my fellow graduate students for their advice and support through out the duration of my graduate studies. Last but not the least I would like to thank Michigan State University as a whole for providing such a wonderful atmosphere of learning and development. Hats off to you my *Alma Mater* – Go Green, Go White.

TABLE OF CONTENTS

LIST OF TABLESx	iii
LIST OF FIGURES.	XX
Chapter 1	1
1 Introduction	
1.1 General	
1.2 Graphite Nanomaterials	
1.2.1 Carbon Nanotubes	
1.2.2 Carbon Nanofibers	
1.2.3 Graphite Nanoplatelets	
1.3 Merits of Graphite Nanomaterials	
1.4 The Need and Routes for Functionalization of Graphite Nanomaterials	
1.5 Fresh Cement Past and Hydrates: Morphological Relationships with Graph	
Nanomaterials	
1.6 Research Hypothesis	
1.7 Research Objectives	
1.8 Scope	
Chapter 2	38
2 Literature Review, Materials and Methods	
2.1 General	
2.2 Experimental Studies	
2.2.1 Carbon Nanotubes	
2.3 Knowledge Gaps	
2.4 Graphite Nanomaterials and Microfibers.	
2.5 Cementitious Matrix and Processing Techniques	
2.5.1 Cementitious Matrix	
2.5.2 Dispersion and Mixing Procedure	
2.6 Experimental Methods	
2.0 Experimental Methods	00
Chapter 3	
Reinforcement of High-Performance Cementitious Matrices with Relatively L	
Volume Fractions of Graphite Nanomaterials	
3.1 General	
3.2 Introduction	
3.3 Materials and Methods	
3.3.1 Graphite Nanomaterials and Microfibers	
3.3.2 Cementitious Matrices, Mixing and Curing Procedure	
3.3.3 Experimental Methods	
3.4 Characterization of Non-Functionalized and Functionalized Graph	
	98
3.4.1 FTIR Spectrometry	
3.4.2 Scanning Electron Microscopy	99

3.4.3 Raman Spectrometry	99
3.4.4 X-Ray Photoelectron Spectroscopy (XPS)	
3.5 Engineering Properties, Structure and Failure Modes of Cer	
Nanocomposites	101
3.5.1 Engineering Properties	101
3.5.2 Transmission and Scanning Electron Microscopic Investigations	
3.5.3 X-Ray Diffraction (XRD) Analysis	104
3.5.4 Thermogravimetric Analysis (TGA)	105
3.5.5 Energy-Dispersive Spectroscopy (EDS)	107
3.6 Summary	108
Chapter 4	137
4 Effect of Refined Functionalization of Nanotubes on their Reinforcement Effe	eciency at
Different Volume Fraction in Cementitious Matrices	137
4.1 General	137
4.2 Materials and Methods	
4.2.1 Materials	
4.2.2 Cementitious Matrices, Mixing and Curing Procedure	
4.2.3 Experimental Methods	
4.3 Further Functionalization and Characterization of Carbon Nanotubes	139
4.3.1 Polymer Physisorption	
4.3.2 Covalent Tethering of Polymers onto Nanotube Walls	
4.3.3 Further Functionalization of Carboxylated Nanotubes Starting from	
Groups	
4.3.4 Microwave Irradiation	
4.4 Experimental Results	
4.4.1 Reinforcement Efficiency of Carbon Nanotubes with Different Function	
Conditions	
4.4.2 Scanning Electron Microscope Investigations	
4.4.3 X-Ray Diffraction Analysis (XRD)	
4.4.4 Thermogravimetric Analysis (TGA)	
4.5 Summary	149
Chapter 5	170
5 Reinforcing Effects of Multiwalled Carbon Nanotubes and Fibers in High-Per	formance
Cementitious Materials	170
5.1 General	170
5.2 Materials and Methods	170
5.2.1 Graphite Nanomaterials and Microfibers	171
5.2.2 Cementitious Matrices, Mixing and Curing Procedure	
5.2.3 Experimental Methods	171
5.3 Experimental Results and Discussion	
5.3.1 Multiwalled Carbon Nanotube Aspect Ratio and Volume Fraction	
5.3.2 Effects of Hybrid (nano- and micro-scale) Reinforcement Systems	177
5.4 Summary	180

Chapter 6
6 Reinforcing Effects of Multiwalled Carbon Nanotubes at Different Volume Fractions
in Cementitious Pastes
6.1 General 193
6.2 Materials and Methods
6.2.1 Graphite Nanomaterials
6.2.2 Cementitious Matrices, Mixing and Curing Procedure
6.2.3 Experimental Methods 194
6.3 Experimental Results and Discussion 195
6.3.1 Effects of MWNT D Volume Fraction and Superplasticizer Type
6.3.2 Effect of Dispersing Multiwalled Carbon Nanotubes in Different Fractions of
Mixing Water
6.4 Summary
Chapter 7
7 Nano- and/or Micro-Scale Reinforcements of High-Performance Cementitious
Mortar
7.1 General
7.2 Materials and Methods
7.2.1 Materials, Graphite Nanomaterials and Microfibers
7.2.2 Cementitious Matrices, Mixing and Curing Procedure
7.2.3 Experimental Methods 207
7.3 Experimental Results and Discussion 207
7.3.1 Carbon Nanotubes and/ or Carbon Microfibers at Different Volume Fractions and
with Different Superplasticizers 208
7.3.2 Enhanced Hybrid Reinforcement of High-Performance Cementitious Mortar 212
7.4 Summary
Chapter 8
•
8 Damage-Sensitive Electrical Conductivity of High-Performacne Mortars Reinforced with Multiwalled Carbon Nanotubes
8.1 General 229
8.2 Materials and Methods
8.2.1 Materials and Graphite Nanomaterials 230
8.2.2 Cementitious Matrices, Mixing and Curing Procedure
8.2.3 Experimental Methods 231
8.3 Experimental Results and Discussion 232
8.3.1 Effects of Modified Multiwalled Carbon Nanotubes on the Electrical
Conductivity of High-Performance Cementitious Mortars
8.3.2 Damage-Sensitivity of the Electrical Conductivity of High-Performance
Cementitious Mortars Incorporating Modified Carbon Nanotubes
8.3.3 Scanning Electron Microscope Observations 233
8.4 Summary 234

Chapter 9.	.240
9 Evaluation of Hybrid (Nano- and Micro-scale) Reinforcemet Effects on	the
Engineering of High-Performance Concrete	
9.1 General	
9.2 Materials and Methods	
9.2.1 Graphite Nanomaterials and Microfibers	. 242
9.2.2 Cementitious Matrices, Mixing and Curing Procedure	. 242
9.2.3 Experimental Methods	. 243
9.3 Experimental Results and Discussion	
9.3.1 Carbon Nanotubes and/ or Carbon Microfibers at Different Volume Fractions	and
with Different Superplasticizers	
9.4 Summary	. 249
Chapter 10	.260
Chapter 10	
Properties of High Strength Concrete and Comparison with High-Performance Concrete	_
10.1 General	
10.1 General	
10.2.1 Graphite Nanomaterials and Microfibers	
10.2.2 Cementitious Matrices, Mixing and Curing Procedure	
1	
10.3 Experimental Results and Discussion	
10.3.1 Flexural Performance	
10.3.2 Compressive Strength	
10.3.3 Impact Resistance	
10.3.4 Abrasion Resistance	
10.4 Summary	. 200
Chapter 11	.269
Evaluation of Reinforcement Efficiency of Carbon Nano- and Micro-fibers in H	Iigh-
Performance Cementitious Paste	
11.1 General	. 269
11.2 Materials and Methods	271
11.2.1 Graphite Nanomaterials and Microfibers.	
11.2.2 Cementitious Matrices, Mixing and Curing Procedure	
11.2.3 Experimental Methods	
11.3 Experimental Results and Discussion	
11.3.1 Effects of Carbon Nanofiber Surface Functionalization on Engineer	
Properties.	_
11.3.2 Effects of Hybrid (Nano- and Micro-scale) Reinforcement Systems	
11.4 Summary	
Chapter 12	.290
12 Evaluation of Reinforcement Efficiency of Carbon Nano- and Micro-fibers in H	ligh-
Performance Cementitious Mortar	
12.1 General	290

12.2 Materials and Methods	292
12.2.1 Graphite Nanomaterials and Microfibers.	
12.2.2 Cementitious Matrices, Mixing and Curing Procedure	
12.2.3 Experimental Methods	
12.3 Experimental Results and Discussion	
12.3.1 Effects of Carbon Nano- and/or Micro-fibers Used at Different Volume	
and with Different Superplasticizers	293
12.3.2 Energy-Dispersive Spectroscopy (EDS)	297
12.3.3 Response Surface Analysis of High-Performance Cementitious Mortar	297
12.4 Summary	298
Chapter 13	306
Evaluation of Reinforcement Efficiency of Carbon Nano- and Micro-fibers	
Performance Cementitious Concrete	_
13.1 General	306
13.2 Materials and Methods	308
13.2.1 Graphite Nanomaterials and Microfibers	308
13.2.2 Cementitious Matrices, Mixing and Curing Procedure	
13.2.3 Experimental Methods	
13.3 Experimental Results and Discussion	309
13.3.1 Flexural Performance	309
13.3.2 Compressive Strength	312
13.3.3 Impact Resistance	312
13.3.4 Abrasion Resistance	313
13.3.5 Response Surface Analysis	313
13.3.6 Scanning Electron Microscope Observations	315
13.4 Summary	316
Chapter 14.	324
Graphite Nanoplatelets in High-Performance Matrices	
14.1 General	
14.2 Materials and Methods	326
14.2.1 Graphite Nanomaterials and Microfibers	326
14.2.2 Cementitious Matrices, Mixing and Curing Procedure	
14.2.3 Experimental Methods	
14.3 Experimental Results and Discussion	327
14.3.1 Effects of Graphite Platelets and Carbon Microfibers on Engineering Prop	erties of
DSP Paste	327
14.3.2 Effects of Graphite Platelets and Carbon Microfibers on Engineering Prop	
DSP Mortar	
14.3.3 Effects of Graphite Platelets and Different Microfibers on Engineering P	-
of DSP Concrete	
14.4 Summary	336

Chapter 15	343
Durability Characteristics of High-Performance Cementitious Matric Reinfor	ced with
Nano and/or Micro Reinforcements	343
15.1 General	343
15.2 Materials and Methods	344
15.2.1 Graphite Nanomaterials and Microfibers	344
15.2.2 Cementitious Matrices, Mixing and Curing Procedure	
15.2.3 Experimental Methods	
15.3 Test Results and Discussion of DSP Mortar Matrix	345
15.3.1 DSP Mortar with Different Nano and/ or Micro Reinforcements	
15.3.2 DSP Mortar with Refined Nano and/ or Micro Reinforcements	349
15.4 Test Results and Discussion of DSP Concrete Matrix	352
15.4.1 Exposure to Elevated Temperature	352
15.4.2 Freeze-Thaw Cycles	353
15.4.3 Wet-Dry Cycles	354
15.4.4 Hot Water Immersion	355
15.5 Summary	356
Chapter 16	374
16 Effects of Modified Graphite Nanomaterials on the Moisture Sorption Chara	
of High-Performance Cementitious Materials	
16.1 General	
16.2 Materials and Methods	
16.2.1 Graphite Nanomaterials and Microfibers.	
16.2.2 Cementitious Matrices, Mixing and Curing Procedure	
16.2.3 Experimental Methods	
16.3 Experimental Results and Discussion	
16.3.1 Rate of Moisture Absorption of DSP Paste Matrix	
16.3.2 Rate of Moisture Absorption of DSP Mortar Matrix	
16.3.3 Rate of Moisture Absorption of DSP Concrete Matrix	
16.4 Comparison of Graphite Nanomaterials with other Methods of I	
Permeability of Concrete	_
16.5 Summary	384
Chapter 17.	
17 Plant Production and Placement of Nanocomposites – Challenges and Results.	
17.1 General	
17.2 Materials and Methods	
17.2.1 Graphite Nanomaterials and Microfibers	
17.2.2 Cementitious Matrices, Dispersion, Mixing and Curing Procedure	
17.2.3 Challenges Associated with Plant Production	
17.2.4 Experimental Methods	402
17.3 Experimental Results and Discussion	
17.3.1 Flexural Performance	
17.3.2 Compressive Strength	
17.3.3 Impact Resistance	405

17.3	3.4 Abrasion Resistance	406
17.3	3.5 Rate of Moisture Absorption by Capillary Rise	407
	3.6 General Observations	
17.4	Summary	409
Chapter 18.		420
18 T	heoratical Studies and Performance to Cost Analysis of DSP Matrices I	Reinforced
	ite Nanomaterials	
18.1	General	420
18.2	Merits of Graphite Nanomaterials	422
18.2	2.1 Average Spacing and Specific Surface Area of Nanomaterials in Ce	mentitious
	rices	
18.3	Reinforcement Efficiency of Multiwalled Carbon Nanotubes	424
18.3	3.1 Optimum Volume Fraction of MWNTs	
18.4	Analysis of the Debonding Process of Functionalized Carbon Nanotubes,	and Their
Contri	bution to Tensile Strength	426
18.4	1.1 DSP Paste	
18.5	<i>y</i>	
Fractu	re Energy	429
18.6	Elastic Modulus and Tensile Strength Based on the Composite	
	ach	
18.7	r i i i i i i i i i i i i i i i i i i i	
	ntitious Paste, Mortar and Concrete	
	7.1 High-Performance Paste	
	7.2 High Performance Mortar and Concrete	
18.8	Synergistic Role of Nano- and Micro-scale Reinforcement	
18.9	Diffusion Resistance of Cement-Based Nanocomposites	
18.10	Electric Conductivity and Its Damage Sensitivity	
18.11	1	
18.12	Targeted Applications	
18.13	Summary	447
Chapter 19.		469
-	Conclusions	
19.1	General	469
19.2	Key Findings	472
19.3	Recommendations for Future Research	493
19.4	Impact of the Research Effort	495
REFEREN	CES	496

LIST OF TABLES

Table 1.1- Applications, performance requirements, and competing fibers
Table 1.2- Typical properties of graphite nanomaterials and carbon fiber
Table 1.3- Key properties governing the reinforcement efficiency of multi-walled carbon nanotubes versus conventional steel, polypropylene and glass fibers
Table 2.1- Summary review of experimental studies reported on the use of nanomaterials in cement-based matrices
Table 2.2- Strength test results after 28 days of curing (Li, Wang et al. 2005)
Table 2.3- Physical attributes of all graphite nano and micro-scale reinforcement systems 81
Table 2.4- The cementitious matrices selected for evaluation of the reinforcement efficiency of graphite nanomaterials
Table 2.5- Chemical composition of Type I Portland cement. 82
Table 3.1- Elemental analysis of fluorinated MWNTs and ethyl carboxylated MWNTs 109
Table 3.2- Mix designations of DSP pastes reinforced with non-functionalized and functionalized graphite nano and micro reinforcements at 0.08 vol.%
Table 3.3- Mix designation of high-performance DSP mortar with functionalized graphite nanomaterials at 0.03 vol.%
Table 5.1- Mean values of flexural strength, maximum deflection and energy absorption capacity of DPS paste matrix reinforced with 0%, 0.24% and 0.48% volume fractions of non-functionalized and acid-functionalized MWNT D & E
Table 5.2- Mean values of compressive strength test results for DSP paste matrix reinforced with 0%, 0.24% and 0.48% volume fractions of non-functionalized and acid-functionalized carbon nanotubes.
Table 5.3- Mean values of impact resistance test results for DSP paste reinforced with 0%, 0.24% and 0.48% volume fractions of non-functionalized and acid-functionalized carbon nanotubes MWNT D & E
Table 5.4- Mean weight loss test results after abrasion for DSP paste reinforced with 0%, 0.24% and 0.48% volume fractions of non-functionalized and acid-functionalized carbon nanotubes MWNT D & E

Table 5.5- Mean values of flexural strength, maximum deflection and energy absorption capacity of DSP paste reinforced different vol. fractions of micro- and/or nano-scale reinforcement 183
Table 5.6- Compressive strength test results for the DSP paste matrix reinforced with different volume fractions of nano and micro-scale reinforcements
Table 5.7- Impact resistance test results of DSP pastes with nano- and/or micro-scale reinforcement
Table 5.8- Abrasion weight losses of DSP pastes with nano- and/or micro-scale reinforcement.
Table 6.1- Mean values of the flexural properties of DSP pastes with functionalized and non-functionalized MWNT D at 0.24 vol.% and 0.48vol.%, prepared using different carboxylic-based superplasticizers
Table 6.2- Mean values and standard errors of the compressive strength test results for DSP pastes with functionalized and non-functionalized MWNT D at 0.24 vol.% and 0.48 vol.%, prepared using different poly carboxylate-based superplasticizers
Table 6.3- Mean values of flexural strength, maximum deflection and energy absorption capacity of DSP paste with and without 0.24 vol.% of polymer-wrapped and non-functionalized MWNT D dispersed in different fractions of mixing water.
Table 6.4- Mean values and standard errors of the compressive strength test results for DSP paste with and without 0.24 vol.% polymer-wrapped and non-functionalized MWNT D dispersed in different fractions of the mixing water
Table 7.1- Mean values of the flexural attributes high-performance cementitious mortars with nano- and/or micro-scale reinforcement systems
Table 7.2- Mean values and standard errors of the compressive strength of the high-performance cementitious mortar matrices with nano- and/or micro-scale reinforcement systems
Table 7.3- Mean values of the impact resistance test results for high-performance cementitious mortars reinforced with nano- and/or micro-scale reinforcement systems
Table 7.4- Mean values of the abrasion resistance test results for high-performance cementitious mortars reinforced with nano- and/or micro-scale reinforcement systems
Table 7.5- Mean values of flexural strength, maximum deflection and energy absorption capacity of high-performance cementitious mortars with nano- and/or micro-scale reinforcement systems
Table 7.6- Mean values and standard errors of the compressive strength test results for high – performance cementitious mortars with nano- and/or micro-scale reinforcement systems 220

Table 7.7- Mean values of the impact resistance test results for high-performance cementitious mortars with nano- and/or micro-scale reinforcement. 221
Table 8.1- Mean values of the electrical conductivity test results for high-performance cementitious mortars with different volume fractions of modified multiwalled carbon nanotubes prepared using two different superplasticizers.
Table 8.2- Mean values of the electrical conductivity of high-performance cementitious mortar specimens with different volume fractions of functionalized multiwalled carbon nanotubes after application of different compressive stress levels.
Table 9.1- Mean values of flexural attributes of high-performance concrete with and without different nano- and/ or micro-scale reinforcement systems
Table 9.2- Mean values and standard errors of the compressive strength test results for high-performance concrete with and without nano- and/ or micro-scale reinforcement systems 250
Table 9.3- Impact resistance test results for high-performance concrete with and without nano-and/or micro-scale reinforcement
Table 9.4- Mean abrasion weight losses of high-performance concretes with and without nano- and/ or micro-scale reinforcement systems
Table 9.5- Outcomes of Ridge analysis of the flexural attributes and impact resistance test data for high performance concrete with nano- and/or micro-scale reinforcement
Table 10.1- Starting material selections and mix proportions (weight ratios) of high-performance and high-strength concrete matrix
Table 10.2- Mean values of flexural attributes of high-strength concrete with and without nano-and/ or micro-scale reinforcement systems and comparison with high-performance concrete 267
Table 10.3- Compressive strength values of high-strength concrete with and without nano- and/or micro-scale reinforcement systems and comparison with high-performance concrete 267
Table 10.4- Impact resistance test results for high-strength concretes with and without nano- and/ or micro-scale reinforcement systems and comparison with high-performance concrete 268
Table 10.5- Mean abrasion weight losses of high-strength concretes with and without nano- and/ or micro-scale reinforcement systems and comparison with high-performance concrete 268
Table 11.1- Mean values of the flexural strength, maximum deflection and energy absorption capacity test results for high-performance cementitious pastes with 0% and 0.24% (by volume of cement plus silica fume) of non-functionalized and acid-functionalized CNFs

Table 11.2- Mean values of the flexural strength, maximum deflection and energy absorption capacity test results for high-performance cementitious paste with carbon nanofiber and/or microfiber reinforcement systems
Table 11.3- Mean values and standard errors of the compressive strength test results for high-performance cementitious paste reinforced with CNFs and/or microfibers
Table 11.4- Mean values of the impact resistance test results for high-performance cementitious pastes with carbon nanofiber and/or microfiber reinforcement systems
Table 12.1- Mean values of the flexural attributes of high-performance (DSP) cementitious mortar with nano- and/or micro-scale reinforcement systems
Table 12.2- Mean values and standard errors of the compressive strength test results for DSP mortar with nano- and/or micro-scale reinforcement systems
Table 12.3- Impact resistance test results for high-performance (DSP) cementitious mortar with nano- and/or micro-scale reinforcement systems
Table 12.4 - Mean abrasion weight losses of high-performance DSP cementitious mortars with nano- and/or micro-scale reinforcement
Table 13.1- Mean values of flexural attributes of plain high-performance concrete and those reinforced with different nano- and/ or micro-scale reinforcement systems
Table 13.2- Mean values and standard errors of the compressive strength test results for plain DSP concrete and those reinforced with nano- and/ or micro-scale reinforcement systems 317
Table 13.3- Impact resistance test results for high-performance concrete with and without nano-and/or micro-scale reinforcement
Table 13.4- Mean abrasion weight losses of DSP concretes with and without nano- and/ or micro-scale reinforcement systems
Table 13.5- Outcomes of Ridge analysis of the flexural attributes and impact resistance test data for high performance concrete with nano- and/or micro-scale reinforcement
Table 14.1- Mean values of the flexural properties of DSP pastes with graphite nanoplatelet and/or carbon microfiber reinforcement
Table 14.2- Mean values and standard errors of the compressive strength test results for DSP pastes with graphite nanoplatelet and/or carbon microfiber reinforcement

Table 14.3- Mean values and standard errors of the impact resistance test results for DSP paster with graphite nanoplatelet and/or carbon microfiber reinforcement
Table 14.4- Mean values and standard errors of the abrasion weight loss test results for DSI pastes with graphite nanoplatelet and/or carbon microfiber reinforcement
Table 14.5- Mean values of flexural strength, maximum deflection and energy absorption capacity of DSP mortar with nano- and/or micro-scale reinforcement systems
Table 14.6- Mean values and standard errors of compressive strength test results for DSP morta with nano- and/or micro-scale reinforcement systems
Table 14.7- Mean values of impact resistance test results for DSP mortar reinforced with nanoand/or micro-scale reinforcement systems
Table 14.8- Mean values of abrasion resistance test results for DSP mortar reinforced with nanoand/or micro-scale reinforcement systems
Table 14.9- Mean values of flexural attributes of plain DSP concrete and those reinforced with different nano- and/ or micro-scale reinforcement systems
Table 14.10- Mean values and standard errors of the compressive strength test results for plain DSP concrete and those reinforced with nano- and/ or micro-scale reinforcement systems 340
Table 14.11- Impact resistance test results for DSP concrete with and without nano- and/o micro-scale reinforcement
Table 14.12- Mean abrasion weight losses of DSP concretes with and without nano- and/ o micro-scale reinforcement systems
Table 15.1- Mean values of flexural attributes of DSP mortar reinforced with micro- and/o nano-scale reinforcement prior to and after exposure to elevated temperature (ET)
Table 15.2 - Mean values of the flexural attributes of DSP mortar samples with micro- and/o nano-scale reinforcement before and after exposure to 300 cycles of freeze-thaw (FT) 357
Table 15.3- Mean values of the flexural attributes of DSP mortars with micro- and/or nano-scale reinforcement prior to and after exposure to 300 wet-dry (WD) cycles
Table 15.4- Mean values of the flexural attributes of DSP mortars with micro- and/or nano-scale reinforcement prior to and after 56 days of hot water (HW) immersion
Table 15.5- Mean values of flexural attributes of DSP mortar reinforced with preferred hybric reinforcement systems prior to and after exposure to elevated temperature (ET)

Table 15.6- Mean values of the flexural attributes of DSP mortar specimens with preferred hybrid reinforcement systems prior to and after 56 days of immersion in hot water (HW) 359
Table 15.7- Mean values of flexural attributes of DSP concrete reinforced with micro- and/or nano-scale reinforcement prior to and after exposure to elevated temperature (ET)
Table 15.8- Mean values of the flexural properties of DSP concrete samples with micro- and/or nano-scale reinforcement before and after exposure to 300 cycles of freeze-thaw (FT)
Table 15.9- Mean values of the flexural properties of DSP concrete samples with micro- and/or nano-scale reinforcement before and after exposure to 300 wet-dry cycles (WD)
Table 15.10- Mean values of the flexural properties of DSP concrete samples with micro- and/or nano-scale reinforcement before and after exposure to 56 days in hot water (HW)
Table 17.1- Starting material selections and mix proportions of high-strength concrete matrix for plant production
Table 17.2- Mean values of flexural attributes of plain high-performance concrete and those reinforced with different nano- and/ or micro-scale reinforcement systems
Table 17.3- Mean values and standard errors of the compressive strength test results for plain DSP concrete and those reinforced with nano- and/ or micro-scale reinforcement systems 412
Table 17.4- Impact resistance test results for high-performance concrete with and without nano-and/or micro-scale reinforcement
Table 17.5- Mean abrasion weight losses of DSP concretes with and without nano- and/ or micro-scale reinforcement systems
Table 18.1- Typical improvements in properties of high-performance cement-based materials (concrete/mortar/paste) with 0.16 vol.% graphite nanomaterials, 0.24 vol.% carbon microfibers, or hybrid reinforcement comprising 0.16 vol.% functionalized carbon nanotube and 0.24 vol.% carbon microfibers.
Table 18.2- Mean values of the electrical conductivity test results for high-performance cementitious mortars with different volume fractions of modified multiwalled carbon nanotubes prepared using two different superplasticizers. 448
Table 18.3- Mean values of the electrical conductivity of high-performance cementitious mortar specimens with different volume fractions of functionalized multiwalled carbon nanotubes after application of different compressive stress levels
Table 18.4- Performance gains of high-performance concrete per vol.% of reinforcement, normalized with respect to the reinforcement cost.

Table	18.5-	Typical	performance	gains	of	cement-based	materials	with	introduction	of the
specifi	ed vol	lume frac	tions of functi	ionaliz	ed o	carbon nanotub	e, and stee	l, poly	ypropylene an	d glass
fibers.										450

LIST OF FIGURES

Figure 1.1- Arrangement of graphene sheets in carbon nanotube and nanofiber, graphit nanoplatelet, and carbon micro-fiber	
Figure 1.2- Carbon nanotube	5
Figure 1.3- Multi-walled carbon nanotubes.	6
Figure 1.4- Roll-up of a graphene sheet to form different nanotube types.	6
Figure 1.5- Schematic depiction and electron microscope images of carbon nanofiber	7
Figure 1.6- SEM and TEM images of exfoliated graphite nanoplatelets (Li, Sham et al. 2007). 2	8
Figure 1.7- Reinforcement mechanisms of discrete reinforcement systems in composites 2	8
Figure 1.8- Loss of mechanical properties of carbon nanotubes due to agglomeration (Ajayan et al, 2003).	
Figure 1.9- Schematics of the interactions of pristine and functionalized nanotubes with cemer hydration products.	
Figure 2.1- Modulus-of-rupture (a) and compression resistance (b) test results for cement mortar with and without MWNTs (Musso, Tulliani et al. 2009).	
Figure 2.2- Schematic representation of the experimental setup based on continuous feeding of cement particles using a screw feeder (Nasibulin, Shandakov et al. 2009)	
Figure 2.3- TEM and SEM micrographs of different nano- and micro-scale reinforcement systems.	
Figure 2.4- DSP cementitious paste, mortar and concrete.(Guerrini 2000)	9
Figure 2.5- Steric and electrostatic repulsion of separated nanotubes.	0
Figure 2.6- Dispersion and stability conditions of carbon nanotubes in aqueous media90	0
Figure 2.7- Dispersion equipment: (a) Magnetic stirrer (b) Sonic horn	1
Figure 2.8- Experimental setups. 9	1
Figure 2.9- Durability test systems.	2
Figure 3.1 - FTIR spectra of pristine and acid-functionalized carbon nanotubes and nanofibers	

Figure 3.2- FTIR spectra for MWNTs A prior to and after fluorination, and after ethyl carboxylation upon fluorination
Figure 3.3 - SEM images of MWNTs B prior to and after fluorination
Figure 3.4- Raman spectra for MWNT A and B prior to and after fluorination
Figure 3.5- XPS spectrum.
Figure 3.6-Typical flexural load-deflection behavior of DSP paste with 0% and 0.08% volume fractions of various non-functionalized and acid-functionalized graphite nanomaterials 119
Figure 3.7- Mean and standard error of various engineering properties of DSP paste reinforced with non-functionalized and functionalized graphite nano and micro reinforcements at 0.08 vol.%
Figure 3.8- Effects of functionalized graphite nanomaterials at 0.03% on the engineering properties of high-performance DSP mortar (means & standard errors)
Figure 3.9- Visual appearances of failed specimens after different tests
Figure 3.10- TEM image of functionalized MWNT B, and SEM images of the fractured surface of a cementitious matrix with 0.04 vol.% of functionalized MWNT C
Figure 3.11- Bridging of micro-cracks by acid-functionalized graphite nanomaterials introduced into cementitious matrices at 0.08% volume fraction
Figure 3.12- Arrest and deflection of a micro-crack by a bundle of CNFs within the cementitious matrix.
Figure 3.13- SEM images of DSP paste with 0.08 vol.% of carbon micro-fiber exhibiting showing pulled-out micro-fibers on a crack surface
Figure 3.14- XRD graphs of the high-performance cementitious paste matrix with 0% and 0.04 vol.% of acid-functionalized MWNT A
Figure 3.15- Results of TGA for conventional mortar and for the DSP paste with 0% and 0.08 vol.% acid-functionalized MWNT A, MWNT B, carbon nano-fiber, fluorinated MWNT A 136
Figure 4.1- Schematic depiction of the random and disordered adsorption of polymers upon carbon nanotube walls
Figure 4.2- FTIR spectra for acid-functionalized carbon nanotubes (CNT-COOH), Gum Arabic (GA), and acid-functionalized nanotubes modified with Gum Arabic (GA-CNTCOOH) 151

Figure 4.3- FTIR spectra of acid-functionalized carbon nanotubes (CNT-COOH), PAA, and acid-functionalized nanotubes modified with PAA (PAA-CNTCOOH)
Figure 4.4- FTIR spectra of acid-functionalize carbon nanotubes (CNT-COOH), Glenium®, and acid-functionalized nanotubes modified with Glenium® (Glenium-CNTCOOH)
Figure 4.5- Schematic depiction of the tethering (covalent attachment) of polymer chains via functional groups onto nanotube walls
Figure 4.6- Covalent tethering of PAA onto carboxylated carbon nanotube
Figure 4.7- Tethering of Glenium® onto carboxylated nanotube
Figure 4.8- FTIR spectra of carboxylated nanotubes (CNT-COOH), PAA and PAA-tethered carboxylated nanotubes (PAA-CNTCOOH).
Figure 4.9- FTIR spectra of carboxylated nanotubes (CNT-COOH), Glenium® and Glenium®-tethered carboxylated nanotubes (Glenium-CNTCOOH).
Figure 4.10- Schematic depiction of covalent tethering of PEI to carboxylated nanotubes 155
Figure 4.11- FTIR spectra of carboxylated nanotubes (CNT-COOH), PEI, and PEI-tethered carboxylated nanotubes (PEI-CNTCOOH).
Figure 4.12- Mean values and standard errors of the flexural attributes and compressive strength of DSP paste reinforced with 0%, 0.16% and 0.24% volume fractions of acid-functionalized and non-functionalized MWNT D with different further treatments
Figure 4.13- Mean values and standard errors of the flexural attributes and compressive strength of cementitious (DSP) pastes reinforced with 0%, 0.16% and 0.24% volume fractions of acid-functionalized and non-functionalized MWNT E with different further treatments
Figure 4.14- Mean values and standard deviations of the flexural strength and energy absorption capacity test results for cementitious (DSP) pastes reinforced with 0% and 0.16% volume fractions of non-functionalized MWNT F with different polymer treatments
Figure 4.15- Flexural strength and energy absorption capacity of DSP cement pastes reinforced with 0% and 0.16% volume fractions of microwave treated MWNTs F and G
Figure 4.16- Scanning electron microscope images of the cementitious DSP paste with different volume fractions of surface-modified carbon nanotubes
Figure 4.17- XRD spectrographs of DSP pastes with 0% and 0.16% volume fractions of acid-functionalized MWNT D and MWNT E, that are further modified with Gum Arabic 168
Figure 4.18- Results of thermogravimetric analysis showing weight loss versus temperature 169

Figure 5.1- Flexural strength and energy absorption capacity of DSP cement pastes with 0.24 and 0.48 vol.% non-functionalized and acid-functionalized MWNT D & E
Figure 5.2- Excessive clumping of carbon nanotubes in DSP paste at 0.48% volume fraction. 187
Figure 5.3- Typical SEM images of DSP paste. 187
Figure 5.4- The results of thermogravimetric analysis of DSP cement paste with 0% and 0.24% volume fractions of functionalized multi-walled carbon nanotubes MWNT D & E
Figure 5.5- Typical SEM mages of DSP paste reinforced with 0.16 vol.% of MWNT D-PAA and 0.24 vol.% of CMF: (a) dispersed MWNTs; and (b) failure mechanism of micro-scale fibers. 191
Figure 5.6- Results of thermogravimetric analysis (weight loss vs. temperature) for the high-performance cementitious matrix (DSP paste) with different volume fractions of micro and nano reinforcements.
Figure 6.1- SEM mages of DSP paste reinforced with 0.24 vol.% of MWNT D casted with ADVA® Cast 575 superplasticizer
Figure 7.1- SEM image of a cement-based material incorporating well dispersed PAA-physisorbed multiwalled carbon nanotubes (CNT D-PAA)
Figure 7.2- Transmission electron microscope image of PAA physisorbed multiwalled carbon nanotube Type D
Figure 7.3- Complementary roles of nano- and micro-scale reinforcement in damage control by suppression of micro-crack inception and control of microcrack growth
Figure 7.4- Typical SEM images of the fractured surfaces of high-performance cementitious mortars with nano- and micro-scale reinforcement systems
Figure 8.1- Percolated network
Figure 8.2- Electrical conductivity test setup and specimens. 236
Figure 8.3- Typical SEM mages of high-performance cementitious mortar reinforced with modified multiwalled carbon nanotube.
Figure 9.1- SEM images of fractured surfaces of high performance concrete
Figure 11.1- Representative flexural load-deflection curves of high-performance cementitious pastes with 0 and 0.24 vol.% of non-functionalized and oxidized nanofibers
Figure 11.2- Flexural attributes of high-performance cementitious pastes

Figure 11.3- Clumping of non-functionalized CNFs in the high-performance cementitious paste at 0.24% by volume of cement plus silica fume.
Figure 11.4- Mean values and standard errors of the compressive strength test results for high-performance cementitious paste reinforced with 0 and 0.24 vol.% of non-functionalized and acid-functionalized CNFs
Figure 11.5- Failed impact test specimens.
Figure 11.6- Mean values and standard errors of the impact resistance test results for high-performance cementitious paste reinforced with 0 and 0.24 vol.% of non-functionalized and acid-functionalized CNFs. 284
Figure 11.7- Abrasion test specimens after test. 284
Figure 11.8- Mean values of abrasion weight loss for high-performance cementitious pastes reinforced with 0% and 0.24% of non-functionalized and acid-functionalized CNFs
Figure 11.9- Typical SEM images of high-performance pastes reinforced with 0.24 vol.% of CNFs
Figure 11.10- Typical SEM mages of DSP cementitious paste reinforced with carbon microfibers and/or oxidized CNFs
Figure 12.1- Typical SEM images of high-performance cementitious mortar reinforced with different contents of polymer-wrapped or acid- functionalized CNFs
Figure 12.2- Typical SEM images of DSP cementitious materials reinforced with CNFs and/or CMFs
Figure 13.1- SEM images of fractured surfaces of high performance concrete
Figure 14.1- SEM images of failed specimens of DSP paste reinforced with GP, providing indications of the graphite nanoplatelet delamination and their interactions with microcracks. 342
Figure 15.1- Tortuous diffusion paths forced by nano-scale reinforcement
Figure 15.2- DSP mortar specimens with different reinforcement conditions after exposure to elevated temperature
Figure 15.3- Effects of exposure to freeze-thaw on the dynamic modulus of DSP mortars with micro- and/or nano-scale reinforcement after 300 cycles
Figure 15.4- Effects of exposure to wet-dry cycles on the dynamic modulus of DSP mortars with micro- and/or pano-scale reinforcement

Figure 15.5- Effects of immersion in hot water on the dynamic modulus of DSP mortars with micro- and/or nano-scale reinforcement
Figure 15.6- High-performance (DSP) mortar specimens with different reinforcement conditions after exposure to elevated temperature
Figure 15.7- Effects of immersion in hot water on the dynamic modulus of DSP mortars with preferred hybrid reinforcement systems after 56 days
Figure 15.8- DSP concrete specimens with different reinforcement conditions after exposure to elevated temperature
Figure 15.9- Effects of exposure to freeze-thaw on the dynamic modulus of DSP concrete with micro- and/or nano-scale reinforcement after 300 cycles
Figure 15.10- Effects of exposure to wet-dry on the dynamic modulus of DSP concrete with micro- and/or nano-scale reinforcement
Figure 15.11- Effects of immersion in hot water on the dynamic modulus of DSP concrete with micro- and/or nano-scale reinforcement
Figure 17.1- Mean ROMS in HSC matrix reinforced with and without different volume fraction of graphite nanomaterials and microfibers produced in laboratory and concrete mixing plant. 414
Figure 17.2- Average TWA in HSC matrix reinforced with and without different volume fraction of graphite nanomaterials and microfibers produced in laboratory and concrete mixing plant. 415
Figure 17.3- Photos of Plant Production and laying of slab overlay
Figure 18.1- Evolution of DSP paste into DSP mortar and RPC cementitious products (Guerrini 2000)
Figure 18.2- Average nanotube spacing versus nanotube diameter at different nanotube volume fractions ranging from 0.1% to 1% (K=1.38 for 3-D random orientation of nanotubes) 452
Figure 18.3- The specific surface area of nanotubes versus nanotube diameter for different nanotube volume fractions
Figure 18.4- The crack suppression effect of closely spaced nanotubes. 454
Figure 18.5- Schematic depiction of the relationship between first-crack stress and nanotube spacing
Figure 18.6- The trends in measured values of flexural strength at different volume fractions of MWNTs. 455

Figure 18.7- Typical SEM mages of the fractured surfaces of DSP paste reinforced with 0.48% volume fraction of acid-functionalized and non- functionalized MWNT E
Figure 18.8- The debonding model
Figure 18.9- Interfacial shear stress distribution for critical length (l _c) calculation
Figure 18.10- Pullout load versus displacement for various ratios of adhesion shear to interfacial friction resistance
Figure 18.11- Gains in engineering properties of high-performance concrete brought about by 0.16 vol.% functionalized carbon nanotube and/or 0.24 vol.% carbon (micro)fiber
Figure 18.12- Three-dimensional assembly of carbon nanotubes within a cement-based matrix.
Figure 18.13- Tortuous diffusion paths forced by nano-scale reinforcement
Figure 18.14- Diffusivity factor versus the reinforcement diameter at 0.24% volume fraction for a diameter range covering multi-walled carbon nanotubes and conventional micro-scale fibers.
Figure 18.15- Relative decrease in rate of moisture sorption for different high-performance matrices incorporating 0.24 vol.% of different nano and micro-scale reinforcements
Figure 18.16- Percolated network. 466
Figure 18.17- Percolation of conductive inclusions within a matrix
Figure 18.18- Electrical conductivity values plotted for different volume fractions of PAA-physisorbed MWNT D using different β values
Figure 18.19- Typical SEM image of high-performance cementitious mortar reinforced with modified MWNTs showing uniform dispersion and percolation of nanotubes within the matrix.
Figure 18.20- Self-sensing smart concrete (Baoguo, Xun et al. 2009)

CHAPTER 1

1 INTRODUCTION

1.1 General

This research focuses on enhancement of the cement- and concrete-based civilian and military infrastructure with functionalized graphite nanomaterials (carbon nanotube and nanofiber, and graphite nanoplatelet). Concrete-based materials offer suitable engineering properties (compressive strength, moisture resistance and durability) at low cost, combined with energy-saving and ecological benefits. They constitute the most widely used class of manufactured materials worldwide. The energy consumption for production of concrete is only 3% that of steel (per unit weight), and cement-based materials are far superior to competing construction materials in terms of ecological impact (pollution, deforestation, use of exhaustible raw materials, etc.) (Mehta 1993). Cement-based materials, however, lack adequate toughness, impact resistance and durability in aggressive environments. These are properties targeted to be improved through reinforcement with discrete reinforcement systems, including micro-scale fibers and functionalized graphite nanomaterials.

Introduction of functionalized graphite nanomaterials promises major gains in the structural performance, durability (weathering resistance and fatigue life), and safety (under fire, explosion and earthquake) of cement- and concrete-based infrastructure systems. Enhancement of cement-based materials with functionalized graphite nanomaterials promises qualitative improvements over the successful and growing practice of reinforcing cement-based materials with micro-scale

steel, polypropylene, glass, cellulose, carbon and other fibers (Li 2002). The worldwide consumption rate of these fibers in cement- and concrete-based infrastructure exceeds 1.5 million tons/yr, representing close to 1 billion tons/year global consumption of fiber cement and fiber concrete products. Existing fiber cement and fiber concrete applications, especially those with greater demands for structural performance, durability and safety, represent viable entry points for market introduction of functionalized graphite nanomaterials. These applications are introduced in Table 1.1 together with the relevant performance considerations and the competing fibers.

The targeted applications are of value to both the military and civilian infrastructure systems. Applications of graphite nanomaterials towards development of explosion-resistant infrastructure represent a priority topic actively pursued by the U.S. Army (Survivability Branch).

Graphite nanomaterials (e.g., carbon nanotubes), when compared with today's (micro-scale) fibers, offer distinctly high mechanical and physical attributes as well as enormous surface areas and very close spacing within matrix even at low volume fractions (below 0.1%). The high reinforcement efficiency of graphite nanomaterials in cement-based matrices could be realized only if steps are taken to ensure thorough dispersion of nanomaterials within the matrix and effective interfacial interactions between nanomaterials and cement hydrates. The high surface area of nanomaterials generates strong tendencies towards agglomeration (via van der Waals adhesion forces). The largely inert surfaces of graphite nanomaterials also offer limited potentials for chemical bonding to cement hydrates.

1.2 Graphite Nanomaterials

The graphite nanomaterials considered in this investigation (Fig. 1.1a) include carbon nanotube, carbon nanofiber, and graphite nanoplatelet. When compared with the near-perfect structure of, say, carbon nanotube, the imperfect arrangement of graphene sheets in conventional (microscale) carbon fibers (Fig. 1.1b) generates substantial defects which greatly compromise engineering properties.

1.2.1 Carbon Nanotubes

CNTs (Carbon nanotubes) are cylinder-shaped macromolecules with nano-scale diameter and micro-scale (or larger) length. The walls of nanotubes are made up of a hexagonal lattice of carbon atoms analogous to the atomic planes of graphite. They are capped at their ends by one half of a fullerene-like (semi-spherical) molecule (Fig. 1.2). In the most general case, a CNT is composed of a concentric arrangement of many cylinders (Fig. 1.3) bound together by weak van der Waals interactions (Breuer and Sundararaj 2004). Such MWNTs (Multi-walled Carbon Nanotubes) have diameters ranging from few up to 100 nm (nanometer), with lengths ranging from few micrometers to several centimeters. SWNTs (Single-walled Carbon Nanotubes) possess the simplest geometry, and have been observed with diameters ranging from 0.4 to 3 nm. The formation of a SWCNT can be visualized through the rolling of a graphene sheet. Based on the orientation of the tube axis with respect to the hexagonal lattice, the structure of a nanotube can be completely specified through its chiral vector (Fig. 1.4), which is denoted by the chiral indices (n, m). The diameter and chirality of carbon nanotubes influence their properties. Historically the multi-walled nanotubes were the first to be discovered (1991), followed by their single-walled counterparts (1993). Different methods are now well established for the production

of SWNTs, including catalytic decomposition of a gaseous carbon feedstock, laser ablation, and electric arc-discharge (Balasubramanian and Burghard 2005).

Although carbon nanotubes (CNTs) are similar in composition to graphite, CNTs are highly isotropic; it is this topology that distinguishes nanotube from other carbon structures, and gives them their unique properties. Since carbon-carbon covalent bonds are among the strongest bonds in nature, a structure based on perfect arrangement of these bonds oriented along the axis of the nanotubes produces a very strong material with an extremely high strength-to-weight ratio. The mechanical properties of various nanotube types have been extensively investigated. Their tensile strength (~100-600 GPa (Giga Pascal) is about two orders of magnitude higher than that of current high-strength carbon fibers, and their density is around 1.3 g/cm³ (Grams per Centimeter Cube), lower than the density of commercial carbon fibers (1.8-1.9 g/cm³). The compressive strength of carbon nanotubes is approximately two orders of magnitude higher than the compressive strength of any known fiber. Carbon nanotubes are also one of the stiffest structures ever made; compared to carbon fibers, which typically have Young's moduli of about 380 GPa, moduli of nanotubes range between 1 and 5 TPa (Tera Pascal). The most striking effect, however, is the combination of high ductility with high stiffness and strength, a property that is absent in carbon fibers. Carbon nanotubes can accommodate large deformations without rupture: the ultimate tensile strain of carbon nanotubes ranges from 10% to 30%, compared to 0.1% to 2% for carbon fibers. They can be flattened, twister and buckled as they deform reversibly. The high aspect ratio of carbon nanotubes (as high as 10,000) favors their use in composites to impart conductivity and reinforcement effects (Breuer and Sundararaj 2004). The strength and modulus data for carbon nanotubes are occasionally calculated using the crosssectional area of wall(s) and not that of the nanotube (with an individual wall thickness of 0.34

nm). When multi-walled carbon nanotubes are evaluated in the context of composites, an important consideration is that direct stress transfer occurs between the matrix and the outer wall of the nanotube. The weak van der Waals interactions between nanotube walls limit the contributions of inner walls. This would reduce the effective strength and modulus of multi-walled carbon nanotubes which can be mobilized to render reinforcing effects within composites. A conservative approach is to neglect the contributions of inner tubes to the strength and modulus of multi-walled carbon nanotubes when they are used in composites.

Carbon nanotubes have a unique electronic character which depends upon their chirality, and ranges from high-conductivity metallic behavior to semiconducting with a large band gap. Metallic carbon nanotubes exhibit ballistic transport with zero resistance along the tube, and they can have conductivities several times that of copper. Because of their very low energy dissipation, nanotubes carry tremendous current densities, higher than 100 MA/cm² (Milli-Amperes per Centimeter Square) for multi-walled carbon nanotubes, compared to tens of kA/cm² for superconducting wires. The thermal conductivity of carbon nanotubes is highly anisotropic; it is diamond-like over the length of the tube, and insulting in the transverse direction. The room-temperature thermal conductivity (along the length) of carbon nanotubes is measured at 200 W/(m.K) (Watts per Meter Kelvin), compared to the theoretical prediction of 6,000 W/(m.K) (Breuer and Sundararaj 2004).

Carbon nanotubes have important surface characteristics, which affect their dispersion within a matrix. The strong van der Waals interactions between the large SSA (Specific Surface Area) of nanotubes encourage their agglomeration. These agglomerates may break by shearing along their axes, causing failure between nanotubes at stresses much below the intrinsic capabilities of

individual nanotubes. The nanotube surface characteristics can be tailored through functionalization.

1.2.2 Carbon Nanofibers

CNFs (Carbon Nanofibers) consist of stacked conical graphite planes with a hollow core (Fig. 1.5a); the graphite basal planes are oriented at about 25° with respect to the nanofiber longitudinal axis (Tibbetts, Lake et al. 2007). TEM (Transmission Electron Microscope) and SEM (Scanning Electron Microscope) images of CNFs are shown in Figs. 1.5b and 1.5c, respectively.

CNFs generally have larger diameters (50-100 nm) when compared with multi-walled carbon nanotubes. Their inner diameter ranges from 30 to 90 nanometer, and their length from 50 to 100 µm (micrometer) (with aspect ratios ranging from 100 to 500). The tensile strength and elastic modulus of CNFs are about 3 GPa and 240 GPa, respectively, and their thermal conductivity is quite high with a value of 1,950 W/(m.K). CNFs, when compared with carbon nanotubes, have a higher defect concentration, which lowers their mechanical properties below those of carbon nanotubes. On the other hand, CNFs are now produced at relatively large quantities, and their current cost is much lower than that of carbon nanotubes (Breuer and Sundararaj 2004). One of the most outstanding features of CNFs is the presence of a large number of edges on their surfaces, which present sites readily available for functionalization. CNFs are generally vapor-grown; this process tends to deposit a layer of (less graphitic) carbon upon nanofibers which could cement the nanofibers together (Tibbetts, Lake et al. 2007).

1.2.3 Graphite Nanoplatelets

GP (Graphite Nanoplatelets) (Fig. 1.6) are obtained by exfoliation of natural graphite; their thickness can be controlled in a range from 1 to 25 nm (with about 0.5 nm thickness of each grapheme layer), and their diameter from the sub-micron level to tens of microns. Graphite, in its basal plane, offers elastic modulus of 1,060 GPa, thermal conductivity of 250 W/m.K, and electrical resistivity of $4 \times 10^{-5} \Omega$.cm (Ohm Centimeter) (Kalaitzidou, Fukushima et al. 2007; Kalaitzidou, Fukushima et al. 2007; Li, Sham et al. 2007). Stress concentrations at the rough edges of graphite nanoplatelets lower their tensile strength below that of carbon nanotubes.

1.3 Merits of Graphite Nanomaterials

Typical properties of three graphite nanomaterials (multi-walled carbon nanotube, carbon nanofiber and graphite nanoplatelet) are presented in Table 1.2, and compared with typical properties of carbon fibers. Multi-walled carbon nanotubes are observed to be distinguished from carbon fibers by their high aspect ratio, specific surface area, elastic modulus, tensile strength, thermal conductivity, electrical conductivity and strain capacity. The advantages of graphite nanomaterials over carbon fibers include high aspect ratio, specific surface area, and thermal and electrical conductivity. The high surface area and elastic modulus of graphite nanoplatelets as well as their distinct geometry distinguish them from carbon fibers. The costs of graphite nanomaterials have experienced tremendous drops in recent years; their performance-to-cost ratios are starting to match and surpass those of carbon fibers.

The geometric features of graphite nanomaterials provide them with distinct capabilities for: (i) control of defect size and propagation within composites; (ii) energy dissipation via frictional pullout; and (iii) adding to the tortuosity of crack propagation and diffusion paths. These unique

features of graphite nanomaterials are compared in the following with those of conventional (micro-scale) carbon fibers.

Close spacing of discrete reinforcement systems in composites offer important advantages. With proper selection of materials and processing conditions, the defect size in composites would be limited to the spacing between the discrete reinforcement systems. For uniformly dispersed discrete reinforcement (with different orientation conditions) within a matrix, the average spacing (S) of the reinforcement can be expressed in terms of the reinforcement diameter (d) and volume fraction (V_f) as $S=K.d/V_f^{0.5}$. The coefficient K in this equation is a constant which ranges from 0.8 to 1.38 depending on the reinforcement orientation condition (1-, 2- or 3-D) and the assumptions made in the calculation. At 0.1% volume fraction, for the typical diameters introduced in Table 1, the average reinforcement spacing within composites, calculated using the above equation (with K=1), are 632, 3160 and 221,200 nm. For multi-walled carbon nanotube, carbon nanofiber and carbon fiber, respectively. The average spacing of carbon fiber is thus about 350 times that of multi-walled carbon nanotube at similar volume fraction. This provides nanotubes with superior capabilities for control of defect size and propagation within composites.

A primary purpose of using discrete reinforcement systems in brittle matrices (including cementitious materials) is to enhance their toughness characteristics. One key mechanism contributing to fracture toughness is energy dissipation through frictional pullout (Fig. 1.7a) of the discrete reinforcement, which is proportional to N_1 .(L/4).(π .d) where N_1 is the number of reinforcement crossing a unit area of the crack (N_1 =0.53 V_f /d²), and L and d are the length and diameter of the reinforcement. At a reinforcement volume fraction of 0.1%, with the typical

geometric attributes of Table 1.1, the frictional pullout energy dissipation (per unit crack area) of carbon nanotube, carbon nanofiber and carbon fiber would be proportional to 0.42, 0.21 and 0.059, respectively. Hence, the (geometric) potential of multi-walled carbon nanotubes for toughening of composites via frictional pullout is about an order of magnitude greater than that of conventional (micro-scale) carbon fibers.

Another measure of the reinforcement efficiency of discrete reinforcement systems in composites is the tortousity of a (crack or diffusion) path within the matrix and interfaces (avoiding the reinforcement), as shown in Fig. 1.7b. This tortuosity can enhance the fracture toughness and diffusion resistance of composites in the presence of discrete reinforcement systems. The tortuosity factor (t) is defined as the ratio of the actual distance that a crack or penetrant must travel (for avoiding the reinforcement) to the shortest distance that it would have traveled in the absence of the reinforcement, and can be expressed (for reinforcement with platelet geometry, length L and thickness T) as $t=1+V_fL/(2T)$. This equation can be strictly applied only to carbon nanoplatelets; we assume that it would also be applicable to carbon nanotube, nanofiber and microfiber. The tortuosity factor for carbon nanotube, carbon nanofiber, graphite nanoplatelet and carbon microfiber at 0.1% volume fraction would thus be (for the typical geometric attributes of Table 1.2) 1.5, 1.25, 1.15 and 1.07, respectively. While this approximate approach could underestimate the tortuosity factor of graphite nanoplatelet, it still shows that graphite nanomaterials, when compared with carbon fiber, are more effective in enhancing the diffusion resistance and fracture toughness of composites.

Existing markets for fiber reinforced cement composites are dominated by steel, polypropylene and glass fibers. Table 1.3 compares the key properties (governing reinforcement efficiency) of multi-walled carbon nanotube with those of steel, polypropylene and glass fibers. This

comparison further highlights the distinctly high reinforcement efficiency of graphite nanomaterials in cement-based materials.

1.4 The Need and Routes for Functionalization of Graphite Nanomaterials

Successful use of graphite nanomaterials in cement-based matrices requires: (i) thorough dispersion of individual nanomaterials within the aqueous fresh mix; and (ii) adequate bonding of cement hydration products to the nanomaterial surfaces for effective stress transfer across interfaces. The surfaces of graphite nanomaterials are, disregarding the presence of minor defects, hydrophobic and atomically smooth (i.e., without sites for primary bond development). The hydrophobic surfaces of graphite nanomaterials would, in an aqueous solution (e.g., fresh cement mix), have the energetic preference for bonding to each other (i.e., agglomerating) versus exposing their surfaces to the aqueous environment. Agglomeration of nanotubes undermines all key features governing their reinforcement efficiency in composites. For example, the mechanical properties of nanotube agglomerates are dominated by the secondary (weak) intertube interactions and not the mechanical properties of individual nanotubes. Fig. 1.8 shows the sharp drop in elastic modulus of nanotube agglomerates with increasing diameter (number) of agglomerated nanotubes. Agglomeration also compromises the unique geometric advantages of nanotubes (high surface area and aspect ratio, close spacing, and large tortuosity factor). The hydrophobic surfaces of carbon nanotubes can be made hydrophilic through introduction of selected functional groups to facilitate their thorough dispersion in aqueous media.

Besides thorough dispersion in aqueous media, effective bonding to cement hydration products is another criterion governing the reinforcement efficiency of graphite nanomaterials in cement-based materials. The atomically smooth surfaces of graphite nanomaterials do not offer any sites for development of strong (primary) bonds to cement hydration products (Fig. 1.9a). The absence

of such bonds prevents effective mechanical and physical interactions (e.g., for stress and heat transfer) between nanotubes and the cement-based matrix. Therefore, the distinctly high mechanical and physical attributes of nanotubes cannot be mobilized toward enhancement of the cementitious matrix. In order to develop primary bonds between cement hydration products and graphite nanomaterials, one can introduce functional groups via primary bonds (to carbon atoms) upon nanotubes, which can also develop primary bonds with cement hydration products (Fig. 1.9b). Functional groups, when present at adequate concentrations on nanotube surfaces, would provide enhanced interfacial stiffness, strength, thermal conductivity, etc. for effective mechanical and physical interactions between carbon nanotubes and cement hydration products. These interfacial interactions enable mobilization of the distinct mechanical and physical attributes of graphite nanomaterials towards enhancement of the performance characteristics of cement-based materials.

Hydrated cement comprises primarily of calcium silicate hydrate and calcium hydroxide. An effective way of interacting with these products of cement hydration is through introduction of COOH functional groups upon graphite nanomaterials. These functional groups promote formation of strong covalent bonds between carbon nanotubes and cement hydration products, and therefore increase the load transfer efficiency at the interface (and lower the interfacial electrical and thermal resistance). Introduction of COOH functional groups also makes the nanotube surfaces more hydrophilic, and thus benefits their dispersion in aqueous media.

Refluxing of carbon nanotubes in a H_2SO_4/HNO_3 mixture yields functionalized nanotubes with main functionalities comprising -COOH, -C=O, and -OH groups (Fig. 1.10) approximately in 4:2:1 proportions. The concentration of these groups in nanotubes treated by different oxidants varies in the range of 2 x 10^{20} to 10×10^{20} sites/gram. On a molar basis, the concentration of

functional groups is about 4% to 6%. The carboxyl and other functional groups introduced upon carbon nanotubes represent useful sites for covalent bonding to cement hydration products (and also to other molecules for introduction of a wide range of functional moieties for diverse fields of application) (Balasubramanian and Burghard 2005).

The acid-functionalization process introduces the functional groups at defects which are either pre-existing or are generated in the course of acid-functionalization. Typically around 1-3% of the carbon atoms in a nanotube are located at defect sites formed during its synthesis. Acid-functionalization also introduces defects (holes) the concentration of which depends upon the severity of the acid exposure conditions. Carboxyl and other oxygen-containing functional groups bond to nanotubes at such defect sites. The defects associated with the functional groups introduced via functionalization tend to compromise the mechanical and physical characteristics of nanotubes; such negative effects, however, can be minimized with less vigorous conditions such as refluxing with nitric acid (Balasubramanian and Burghard 2005).

Dispersion of graphite nanomaterials in the aqueous fresh cement mix environment benefits from the hydrophilic nature of functionalized nanomaterials and also from the reduction in of van der Waals interactions in the presence of carboxyl groups, which strongly facilitates the separation of nanotube agglomerates into individual nanotubes (Balasubramanian and Burghard 2005).

The association of acid-functionalization (oxidation) with defects implies some damage to the mechanical and physical properties of acid-functionalized graphite nanomaterials. "Addition functionalization" offers the potential for less association of functional groups with defects. Addition reactions involve direct coupling of functional groups onto the conjugated carbon framework of nanotubes. The required reactive species are in general made available through thermally activated reactions. A variety of addition reactions are possible, and the most

important one are schematically shown in Fig. 1.11a. In principle, addition reactions can be initiated exclusively on the intact sidewall (in the absence of defects), or in parallel at defect sites from where the reaction could proceed further. An exception is fluorination, for which direct addition to defect-free sidewalls is viable (Balasubramanian and Burghard 2005). Slightly elevated temperatures are needed to overcome the activation barrier to fluorination. The fluorine atoms in fluorinated graphite nanomaterials can be replaced through nucleophilic substitution reactions with relative ease, thus opening a flexible approach for providing the sidewall with various types of functional groups, as illustrated in Fig. 1.11b.

Analogous with functionalization with carboxyl groups, the direct covalent attachment of functional moieties followed by substitution reactions can be used to significantly facilitate dispersion of graphite nanomaterials in aqueous media (Balasubramanian and Burghard 2005).

The enormous specific surface area of nanotubes together with their high aspect ratio and relative flexibility generates strong tendencies toward agglomeration and entanglement. Aggressive covalent treatment (e.g., acid-functionalization) of carbon nanotubes could compromise their desirable performance attributes. Non-covalent treatment could be used to further facilitate the dispersion of nanotubes at increased concentrations in aqueous media without damaging the nanotubes (except for altering their electrical properties). Non-covalent surface treatment by surfactants is a versatile route to enhance the dispersion of nanotubes in aqueous media. Surfactants (surface acting agents) are amphilic compounds, containing both hydrophobic groups (tails) and hydrophilic groups (heads). The association of hydrophobic tails with nanotubes and the hydrophilic heads with water (schematically depicted in Fig. 1.12) is the fundamental mechanism facilitating dispersion of nanotubes in aqueous media with surfactants.

In a typical approach to dispersion of nanotubes with surfactants, the nanotubes are mechanically exfoliation, and the surfactant is adsorbed on their surfaces; further ultrasonication then helps the surfactant to debundle nanomaterials by steric or electrostatic repulsions. Ultrasonic treatment of carbon nanotube agglomerate (Fig. 1.13i) generates high local shear, particularly at the nanotube bundle end (Fig. 1.13ii). Once spaces or gaps at the bundle ends are formed, they are propagated by surfactant adsorption (Fig. 1.13iii), ultimately separating the individual nanotubes from the bundle (Fig. 1.13iv). Generally, ionic surfactants are preferred for dispersion of carbon nanotubes in aqueous media.

Carbon nanotubes can be dispersed in water when coated by adsorbed surfactants, preferentially with those that have relatively high HLB (Hydrophile-Lydrophyle Balance). The nature of surfactant, its concentration, and type of interaction play crucial roles in the dispersion process. Knowing the surface charge of carbon nanotubes in different media is essential for understanding the interaction (adsorption) mechanism with ionic surfactants, and to predict colloidal stability of nanotube dispersions. The adsorption mechanism of ionic surfactants, which is promoted by electrostatic interactions with the nanotube surface, is heavily controlled by the purification process and functionalization of nanotubes, which in turn determine their surface charge. Fig. 1.14 shows examples of the structure of adsorbed surfactants on carbon nanotubes.

Experience with the use of functionalized carbon nanotubes in biominerals and ceramics indicate that introduction of a coating of matrix on nanotubes (by precipitation of biominerals or adsorption of nanoparticles) yields important gains in performance characteristics of inorganic matrix nanocomposites (Wang, Ye et al. 2007). An example involved reinforcement of calcium phosphate cement with carboxyl-functionalized carbon nanotube (for development of a new bone repair material). When calcium phosphate cement was exposed to simulated body fluid prior to

introduction into calcium phosphate cement, a uniform layer of ydroxyapatite precipitated on the functionalized nanotubes (Fig. 1.15). The resulting (biomineralized) carbon nanotubes proved to be a more effective reinforcement in calcium phosphate cement when compared with functionalized (but not biomineralized) nanotubes (Wang, Ye et al. 2007). Similar improvements in the reinforcement efficiency of carbon nanotubes in ceramic matrices have been detected when the acid-functionalized nanotubes are coated with ceramic nano-particles (Fig. 1.16) prior to their use for processing ceramic matrix nanocomposites (Gao, Jiang et al. 2006).

1.5 Fresh Cement Past and Hydrates: Morphological Relationships with Graphite Nanomaterials

Carbon nanotubes (and other graphite nanomaterials) offer exceptional mechanical, physical and functional attributes. Development of cement-based nanocomposites which make effective use of the exceptional mechanical, physical and geometric attributes of graphite nanomaterials requires thorough dispersion and intimate interfacial interactions of the nanomaterials within matrix. Efforts to meet these requirements encounter particular challenges relating to the morphological attributes of cement-based matrices. The fresh cementitious paste is a dispersion of micro-scale particles in an aqueous solution, which complicates the dispersion process of graphite nanomaterials. After curing, conventional cement-based matrices incorporate large quantities of micro- to nano-scale pores which mitigate intimate interfacial contacts over the surface area of graphite nanomaterials.

Fig. 1.17a depicts the relative dimensions of carbon nanotubes, cement particles, and carbon fibers. The micro-scale dimensions of carbon fibers facilitate their dispersion within a suspension of micro-scale cement particles (Fig. 1.17b). Graphite nanomaterials with at least one dimension

that is three orders of magnitude smaller than cement particles, on the other hand, would be squeezed into the space between the micro-scale particles in fresh cement paste (Fig. 1.17c). This phenomenon increases the chances for agglomeration of the nanomaterials.

The potential for thorough dispersion of carbon nanotubes and other graphite nanomaterials within a cementitious matrix can be improved through partial replacement of micro-scale cement particles with nano-scale silica fume particles in order to improve generate a smooth particle size distribution which facilitates uniform dispersion of nanomaterials. Fig. 1.18a depicts the relative dimensions of carbon nanotubes, silica fume particles and cement particles. Cementitious pastes with relatively high replacement levels of cement with silica fume are referred to as DSP (Densified with Cement Particles). The fresh DSP cementitious paste offers a particle size distribution (in aqueous solution) which favors dispersion of carbon nanotubes, Fig. 1.18b.

During hydration, the cement particles (dispersed in water) react with water and form hydration products which partially fill the space between them, Fig. 1.19a; the unfilled fraction of space forms micro-scale capillary pores. The structure of hydrated cement, Fig. 1.19b, comprises nanoscale C-S-H (Calcium Silicate Hydrate) particles (their van der Waals interaction is the primary binding force within hydrated cement paste), micro-scale C-H (Calcium Hydroxide) crystals, capillary pores, gel pores within calcium silicate hydrate, and other hydration products. Capillary pores constitute several percent (depending on the water/cement ratio) of hydrated cement. The micro-scale calcium hydroxide crystals have a relatively low specific surface area and thus limited binding capability. The prevalence of micro-scale pores and crystals limit the potential for effective interactions between hydrated cement and graphite nanomaterials, Fig. 1.19c. Improving the gradation of particles in fresh cement paste by introduction of (nano-scale) silica fume particles, Fig. 1.18b, together with the use of superplasticizers (surfactants) to lower the

required water content (for fresh mix workability) yield dense hydrated cements, Fig. 1.19d, where micro-scale calcium hydroxide crystals and (through pozzolanic reactions) converted to calcium silicate hydrate (comprising nano-scale particles with desirable binding qualities). The improved physical compatibility of the refined cement hydrates with graphite nanomaterials, compare Figs. 1.19c & 1.19d, are expected to enhance the reinforcement efficiency of nanomaterials in modified cement-based matrices. Further gains would be realized by functionalization of graphite nanomaterials to improve their chemical compatibility with cement hydrates.

1.6 Research Hypothesis

This research was conducted primarily with two hypotheses in mind:

- Properly functionalized graphite nanomaterials when used in an appropriately graded matrix can bring about substantial increase in all engineering and durability characteristics of high-performance cement based matrices.
- Complementary use of nano- and micro-scale reinforcement can provide cementitious materials with desired balances of engineering properties.

1.7 Research Objectives

In order to verify the above hypothesis, the main thrust of this research is to develop and thoroughly characterize high-performance cement-based materials (paste, mortar and concrete) reinforced with functionalized graphite nanomaterials and suitable micro-scale fibers. A theoretical framework will also be developed to rationalize the experimental results and to guide further development of the technology. The objectives to be accomplished in the project are presented below together with the approach followed for meeting each objective.

Objective 1. Select cementitious materials, mix designs and production conditions for enhancing the reinforcement efficiency of graphite nanomaterials.

Cementitious materials were selected to effectively interact with nanomaterials of distinctly high specific surface area, close spacing and fine geometry in order to enhance the benefits of functionalized nanomaterials to mechanical, barrier and durability characteristics. Fundamental studies using cementitious paste provided the basis to design and evaluate cementitious nanocomposites incorporating fine and eventually coarse aggregates for introduction into mainstream concrete construction practices.

Objective 2. Identify surface functionalization conditions which benefit the dispersion and reinforcing action of graphite nanomaterials in cement-based matrices.

Covalent functionalization techniques as well as non-covalent (physisorption) methods were evaluated for enhancing the dispersion of graphite nanomaterials in aqueous media, and their interfacial bonding to cement hydrates. Due consideration was given to achieving desired compatibility with aqueous media and cement hydrates without excessively damaging the nanomaterials.

Objective 3. Make complementary use of graphite nanomaterials and micro-scale discrete reinforcement towards achieving balanced gains in engineering properties.

The potential for positive interactions between nano- and micro-scale reinforcement in cementitious matrices were evaluated. Optimization experimental programs were implemented in order to identify hybrid reinforcement systems which bring about balanced gains in key engineering properties of cementitious materials. The experimental results were used to verify and refine the theoretical models.

Objective 4. Thoroughly characterize selected cement-based materials with nano-scale and hybrid reinforcement systems.

Selected cementitious (mortar and concrete) materials with optimum nano-scale and hybrid reinforcement systems were thoroughly characterized through evaluation of their mechanical, barrier, durability and physical characteristics as well as their structure and failure mechanisms. Control tests were conducted on cementitious matrices. Statistical analyses were undertaken to verify the performance gains realized by cementitious mortar and concrete materials through nano-scale and hybrid reinforcement.

Objective 5. Develop a theoretical framework for the reinforcing action of graphite nanomaterials in cement-based matrices. Assess competitive performance and cost of cement-based nanocomposites, and identify priority applications.

The interfacial interactions, geometric characteristics, spacing and percolation conditions of functionalized (and non-functionalized) graphite nanomaterials in cementitious matrices were used towards development of theoretical models for prediction of the mechanical performance, moisture transport characteristics and electrical conductivity of cementitious materials with nano-scale and hybrid (nano- and micro-scale) reinforcement systems as evident from the experimental results. The performance characteristics and economics of cementitious mortar and concrete materials with nano-scale and hybrid reinforcement systems were evaluated against those of high-performance concrete materials (without and with micro-scale discrete reinforcement) in order to identify priority applications for cementitious nanocomposites.

1.8 Scope

The research undertaken to address the above objectives is organized in a number of chapters, as described below:

- Chapter 1 provides introduction to different nanomaterials, a general background and considerations for use of nanomaterials in cement-based matrices, and the objectives of this study.
- Chapter 2 covers a review the literature on the use of graphite nanomaterials in cement-based matrices, identifying key knowledge gaps in the field.
- Chapter 3 deals with the preliminary results generated on the use of graphite nanomaterials (both pristine and functionalized) and carbon microfibers at relatively low volume fractions in high-performance cementitious paste and mortar matrices.
- Chapter 4 presents an evaluation of different covalent and non-covalent surface modification techniques for enhancing the concentration, dispersion and interaction of carbon nanotubes in high-strength cementitious matrix.
- Chapter 5, 6 and 7 present the results of addition of various multiwalled carbon nanotubes, non-functionalized as well as functionalized, at different volume fraction in high-performance (densified with small particles DSP) paste and mortar matrices along with the use of hybrid reinforcement with different microfibers, and outcomes of statistical analyses and optimization efforts.
- Chapter 8 evaluates the effects of nanotubes on the electrical conductivity of the cementitious mortar and the damage-sensitivity of electrical conductivity under compressive loads.

- Chapter 9 presents the experimental results of addition of non-functionalized and PAA-physisorbed multiwalled carbon nanotubes and their hybrid combination with different microfibers at different volume fraction on the engineering properties and microstructure of DSP concrete. Whereas, Chapter 10 compares the results of reinforcement of high strength concrete with PAA-physisorbed multiwalled carbon nanotubes and its hybrid combination with carbon microfibers.
- Chapter 11, 12 and 13 presents effects on the engineering properties of high-performance DSP paste, mortar and concrete matrices with the addition of functionalized and non-functionalized nanofibers at different volume fraction along with the use of hybrid reinforcement with different microfibers, and outcomes of statistical analyses and optimization efforts.
- Chapter 14 deals with the effects on the engineering properties of high-performance DSP paste, mortar and concrete matrices with the addition of functionalized and graphite nanoplatelets at different volume fraction along with the use of hybrid reinforcement with different microfibers, and outcomes of statistical analyses and optimization efforts.
- Chapter 15 and 16 present the experimental results on the effects of modified nanomaterials and their hybrid combinations on the durability characteristics of high-performance cementitious materials.
- Chapter 17 presents the results of plant production and field project highlighting the challenges and results of first ever scale up plant production of high-strength concrete nanocomposites.

- Chapter 18 develops a theoretical framework for contributions of graphite nanomaterials (emphasizing carbon nanotubes) to diverse aspects of concrete engineering properties and competitive performance and cost analyses of cementitious nanocomposites.
- Chapter 19 reviews the main findings and conclusions of the research.

Table 1.1- Applications, performance requirements, and competing fibers.

Application	Primary Performance Considerations	Competing Fibers
Explosion-resistant infrastructure systems (e.g., military shelters and mission-critical structures), armor, antiblast doors, security products	Impact resistance, energy absorption capacity, ductility, fire resistance, weight (thickness) reduction	Steel, Glass
Tunnel linings, water and sewage network linings, hydraulic structures wear linings	Flexural strength, toughness, ductility, abrasion resistance, moisture diffusion resistance, durability, fatigue life, shrinkage crack control, adhesion capacity, fire resistance	Steel, Glass
Repair and retrofit of civilian and military infrastructure systems (bridges, building structures, shelters, pavements, etc.)	Ductility, tensile and flexural strength, adhesion capacity, shrinkage crack control, toughness and energy absorption capacity, impact resistance, fatigue life, abrasion resistance, durability	Steel, Polypropylene, Glass
Water, wastewater and nuclear waste containment infrastructure systems (pipes, canals, tanks, containers)	Flexural strength, ductility, moisture diffusion resistance, durability, fatigue life, shrinkage crack control, fire resistance, impact resistance	Steel, Polypropylene, Glass
Thin-sheet products (roofing, siding)	Flexural and tensile strength, toughness, ductility, impact resistance, moisture diffusion resistance, durability, fire resistance, shrinkage crack control	Cellulose, PVA, polypropylene, Glass, Carbon
Highway and airfield pavement, bridge decks, parking garage and industrial floors	Fatigue life, durability, flexural strength, ductility, abrasion resistance, impact resistance, shrinkage crack control	Steel, Polypropylene, Glass
Structural components (beams, columns, walls, joints)	Flexural and tensile strength, ductility, toughness, energy absorption capacity, impact resistance, bond strength to conventional reinforcement	Steel, Glass

Table 1.2- Typical properties of graphite nanomaterials and carbon fiber.

Graphite Nanomat.	Length, μm	Dia., nm	Aspect Ratio	Surface Area, m ² /g	Elastic Modulus, GPa	Tensile Strength, GPa	Thermal Conductivity, W/m.K *	Cost, \$/kg
MWNT	20	20	1,000	500	1,200 ***	350 ***	2,800 ***	45**
Nanofiber	50	100	500	500	240	3	1,950	10
Nanoplatelet	3	10	300	100	1,000	~(10-20)	250	10
CarbonFiber	1,000	7,000	140	16	350	3	600	12

^{*} Property measured in basal plane or along length

Measurements are 'true' values based on wall cross-sectional area

**** Mid-term price target- Pyrograf Product Inc; a subsidiary of ASZ

Mid-term price target- XG Sciences

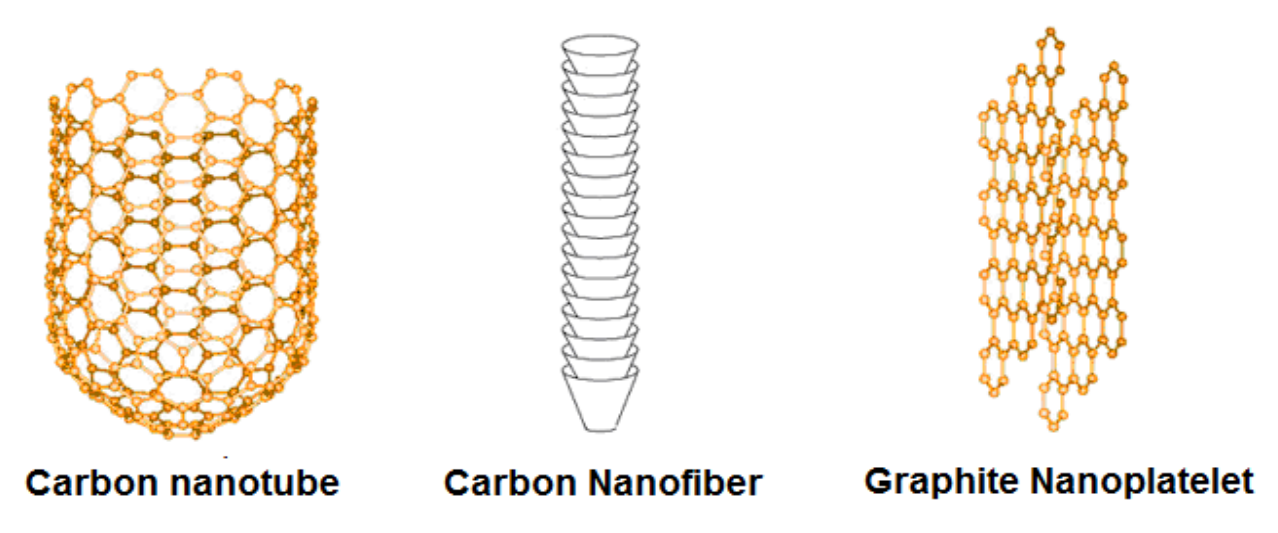
Table 1.3- Key properties governing the reinforcement efficiency of multi-walled carbon nanotubes versus conventional steel, polypropylene and glass fibers.

Reinforcement	Dia µm	Aspect Ratio	Density, g/cm ³	Surface Area, m ² /g	Elastic Modulus, GPa	Tensile Strength, GPa	Strain Capacity, %	Spacing @ 1 Vol.%, µm	Tortuosity Factor @ 1 Vol.%
Nanotube	0.02	1,000	2.1*	500	1,200*	350*	20	0.2	6
Steel	540	65	7.8	0.00095	200	1.2	20	5,400	1.3
Polypropylene	50	450	0.9	0.089	4	0.35	15	500	3.2
AR Glass	14	700	2.7	0.11	72	1.7	2.4	140	4.5

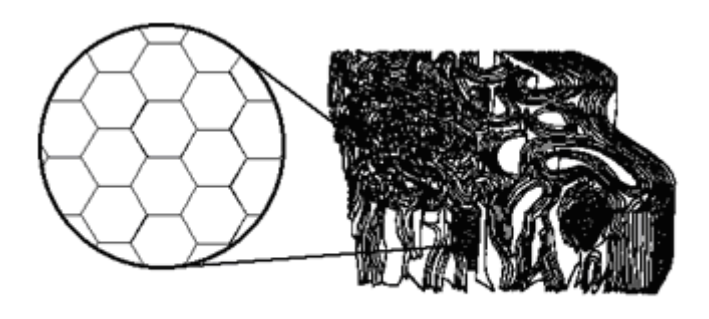
Measurements are 'true' values based on wall cross-sectional area ('apparent' values based on total cross-sectional area would by 75% of 'true' values, assuming a typical inner-to-outer diameter ratio of 0.5 for MWNT)

Mid-term price target

For the interpretation of the references to colors in this and all other figures, the reader is referred to the electronic version of this dissertation



(a) Graphite nanomaterials



Carbon Micro-Fiber

(b) Micro-scale carbon fiber

Figure 1.1- Arrangement of graphene sheets in carbon nanotube and nanofiber, graphite nanoplatelet, and carbon micro-fiber.

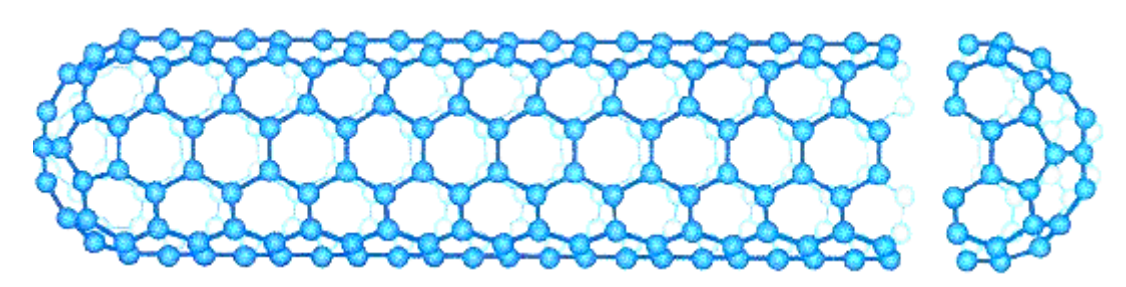


Figure 1.2- Carbon nanotube

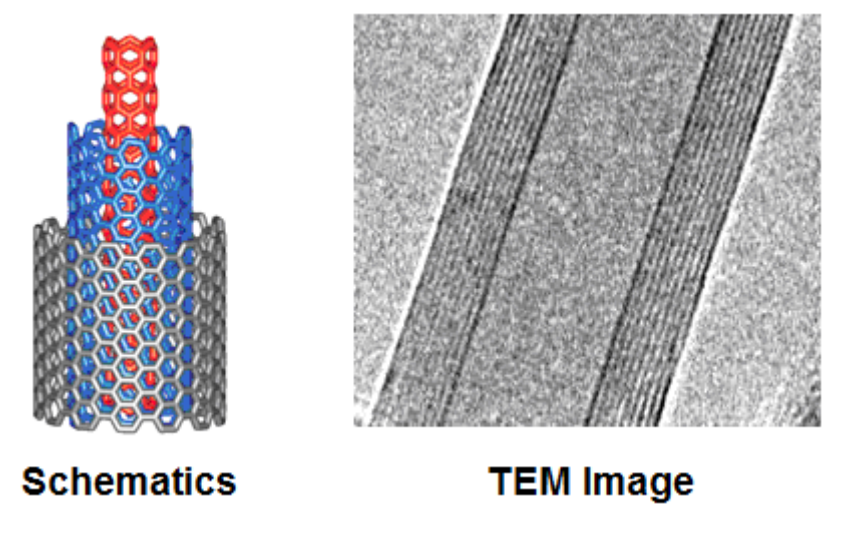


Figure 1.3- Multi-walled carbon nanotubes.

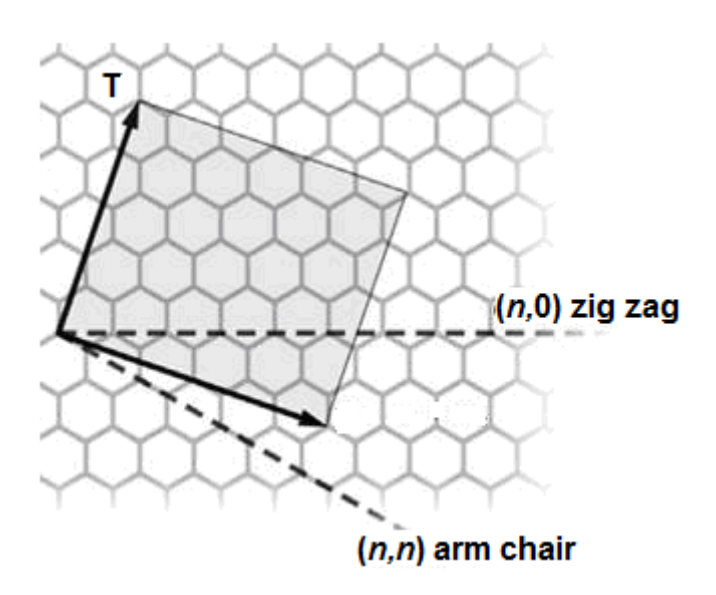
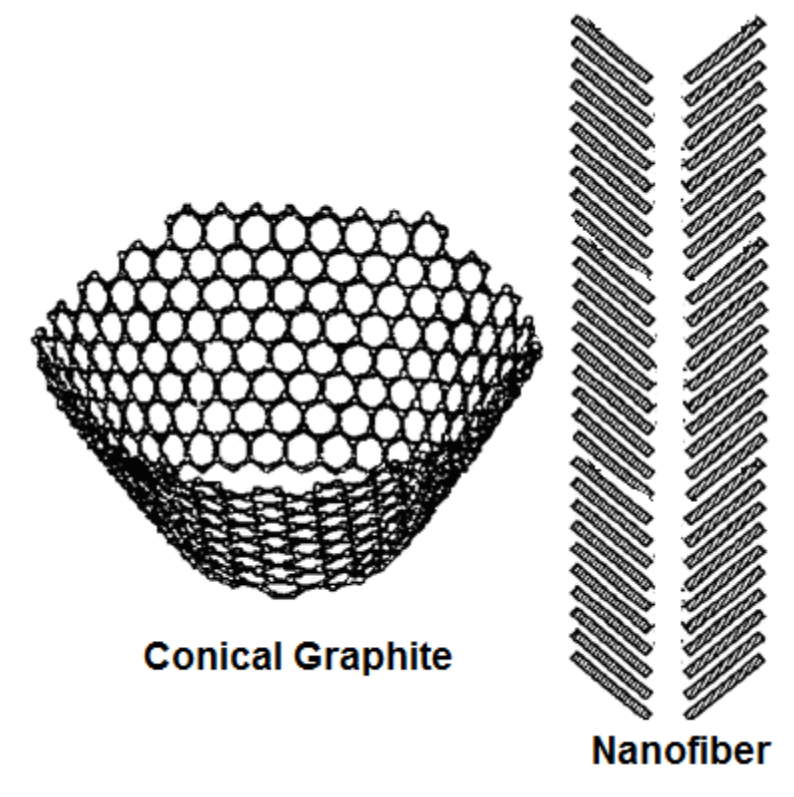
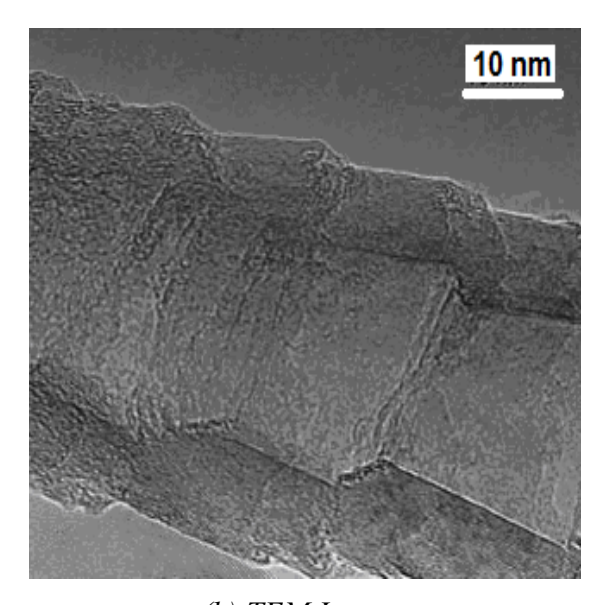


Figure 1.4- Roll-up of a graphene sheet to form different nanotube types.



(a) Schematics



(b) TEM Images

Figure 1.5- Schematic depiction and electron microscope images of carbon nanofiber.

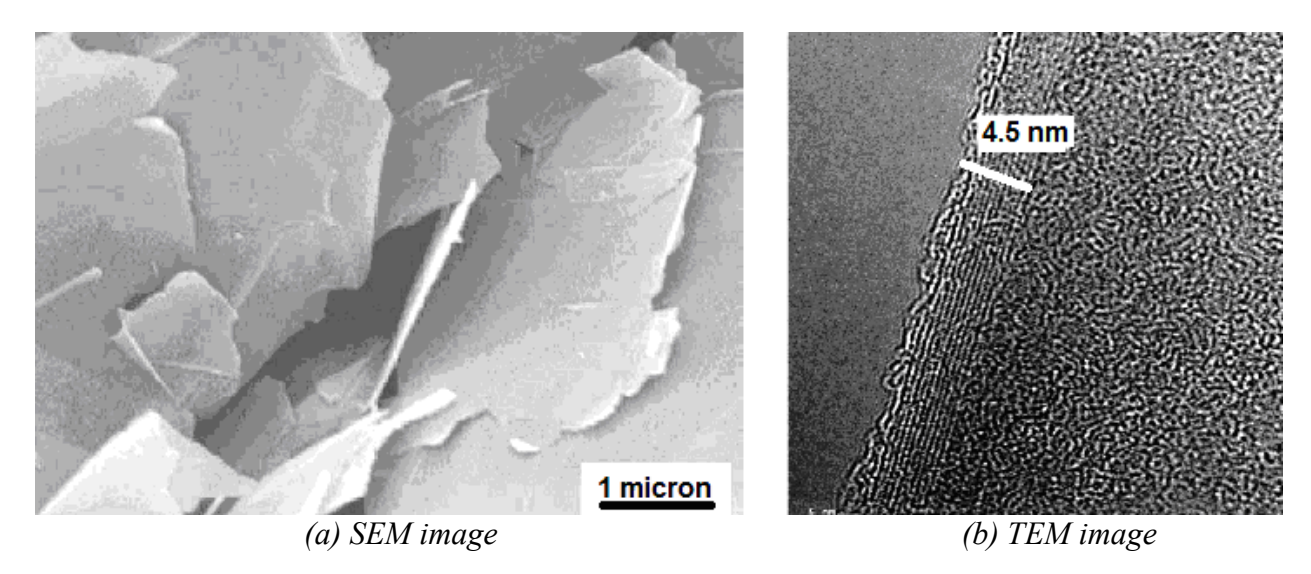


Figure 1.6- SEM and TEM images of exfoliated graphite nanoplatelets (Li, Sham et al. 2007).

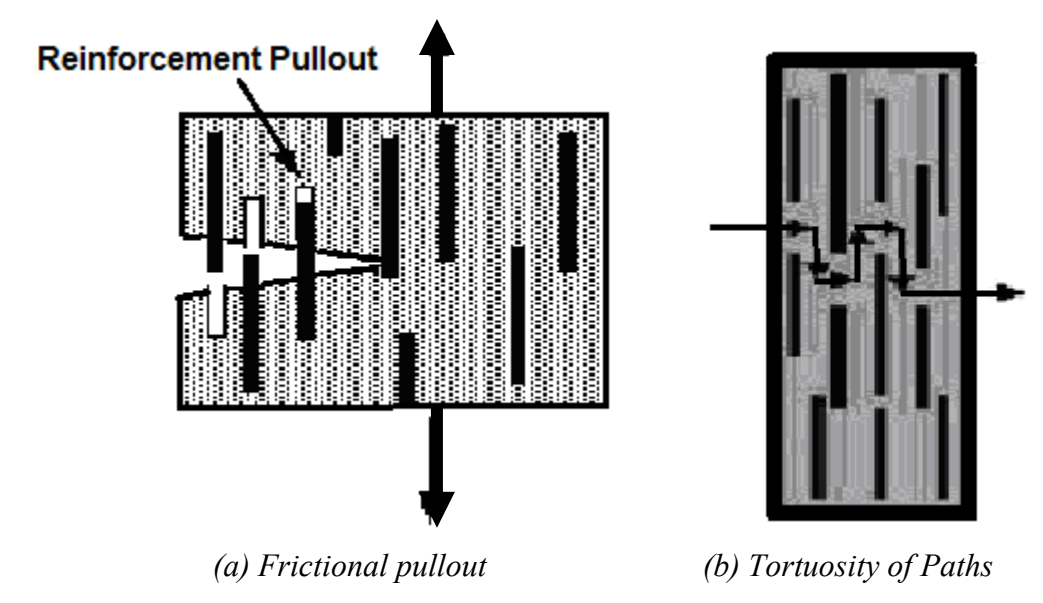


Figure 1.7- Reinforcement mechanisms of discrete reinforcement systems in composites.

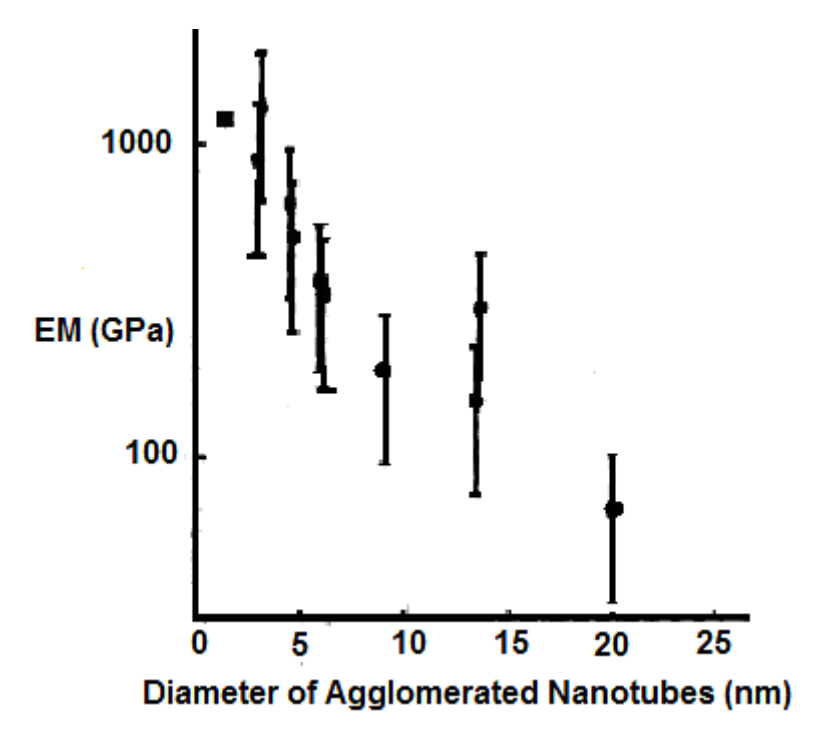
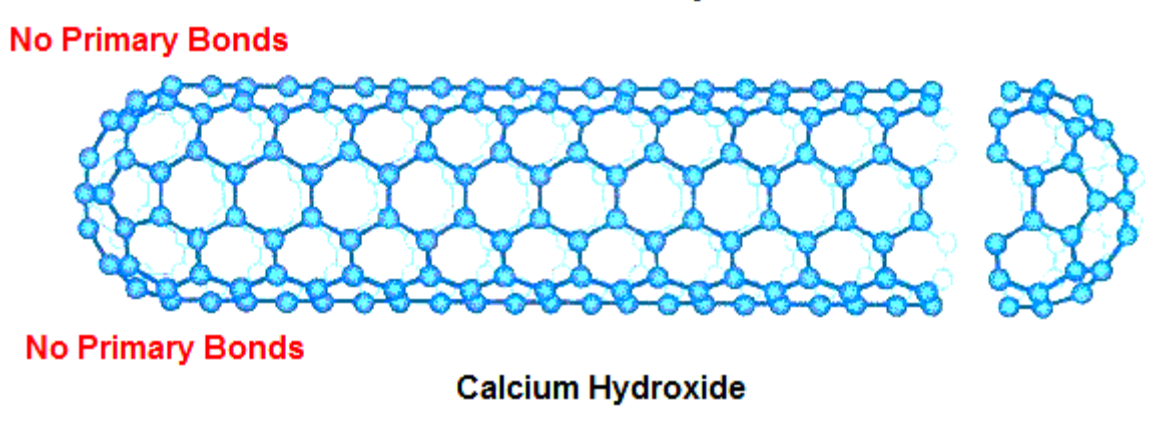
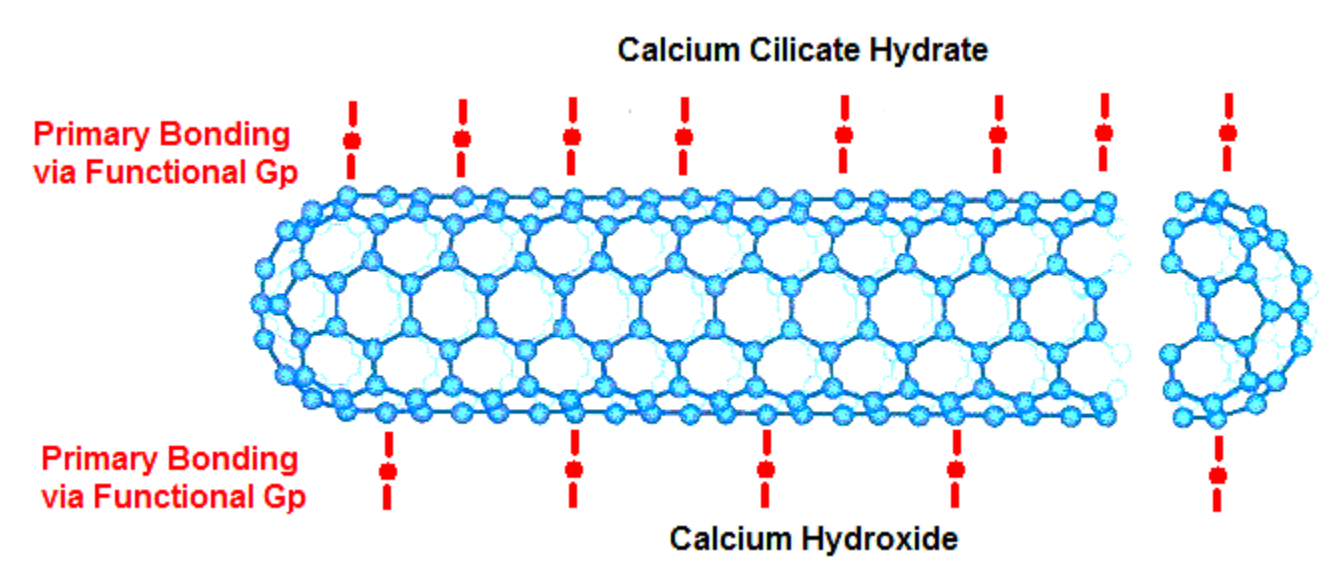


Figure 1.8- Loss of mechanical properties of carbon nanotubes due to agglomeration (Ajayan et al, 2003).

Calcium Cilicate Hydrate



(a) Lack of primary bonding with pristine nanotube



(b) Primary bonding with functionalized nanotube

Figure 1.9- Schematics of the interactions of pristine and functionalized nanotubes with cement hydration products.

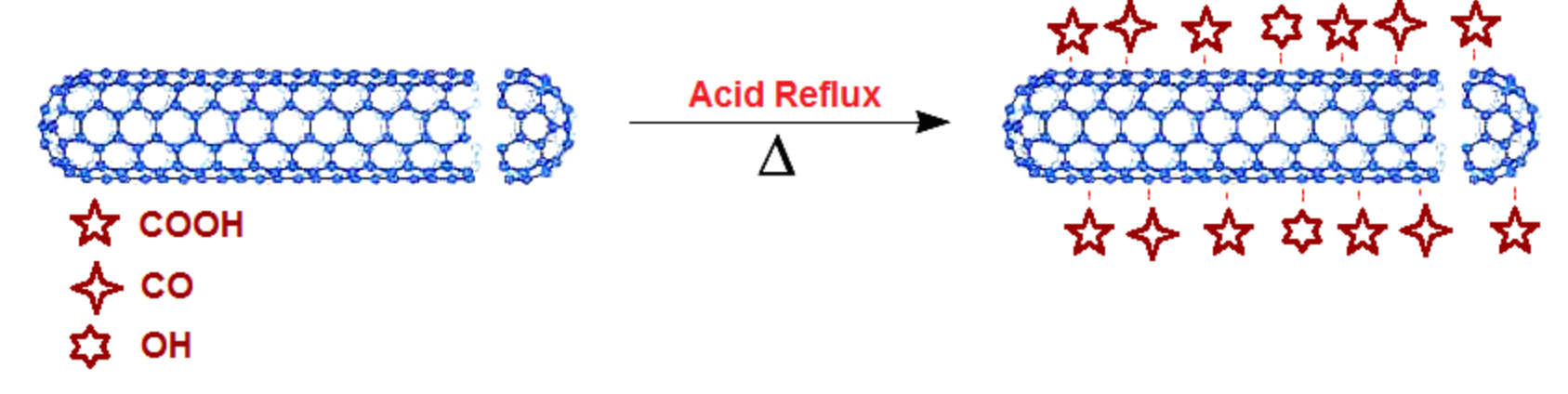


Figure 1.10- Schematic depiction of acid-functionalization of carbon nanotube.

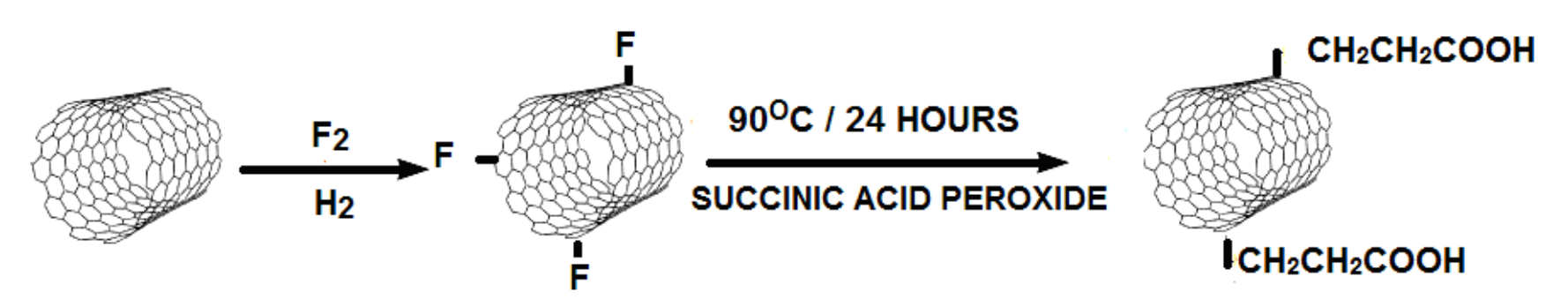


Figure 1.11- Fluorination followed by ethylcarboxylation of carbon nanotube.

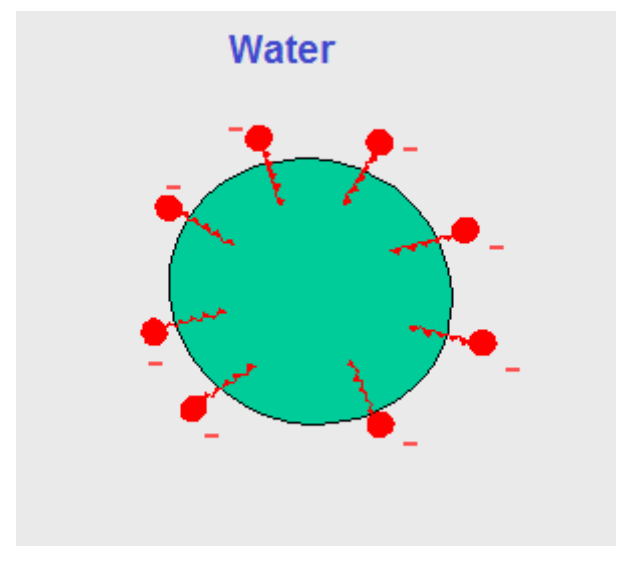


Figure 1.12- Schematic depiction of the dispersion mechanism of surfactants.

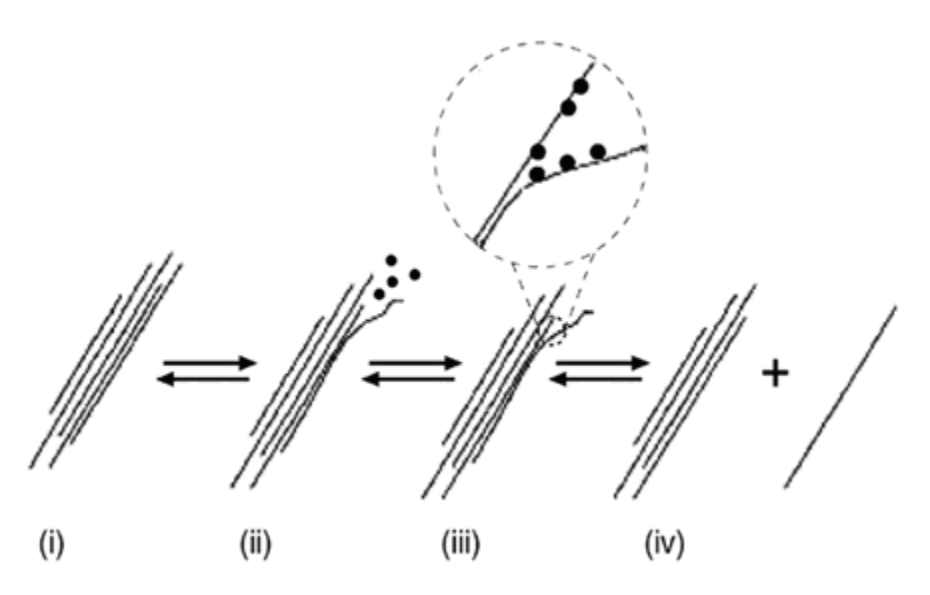


Figure 1.13- Mechanisms of nanotube separation from bundle by ultrasonicaiton and surfactant stabilization (Vaisman, Wagner et al. 2006).



(a) Encapsulation in a cylindrical surfactant micelle

(b) Hemimicellar adsorption of surfactant molecules

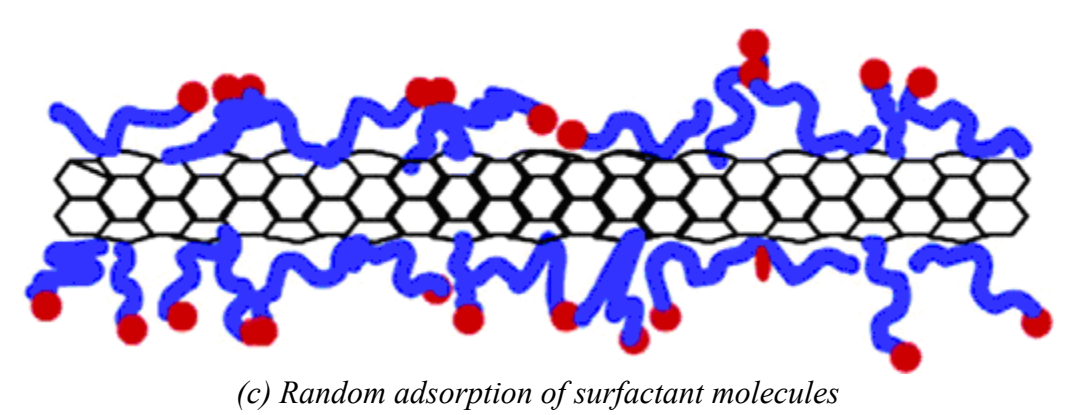


Figure 1.14- Schematic presentation of the surfactant assembly structures on carbon nanotubes (Vaisman, Wagner et al. 2006).

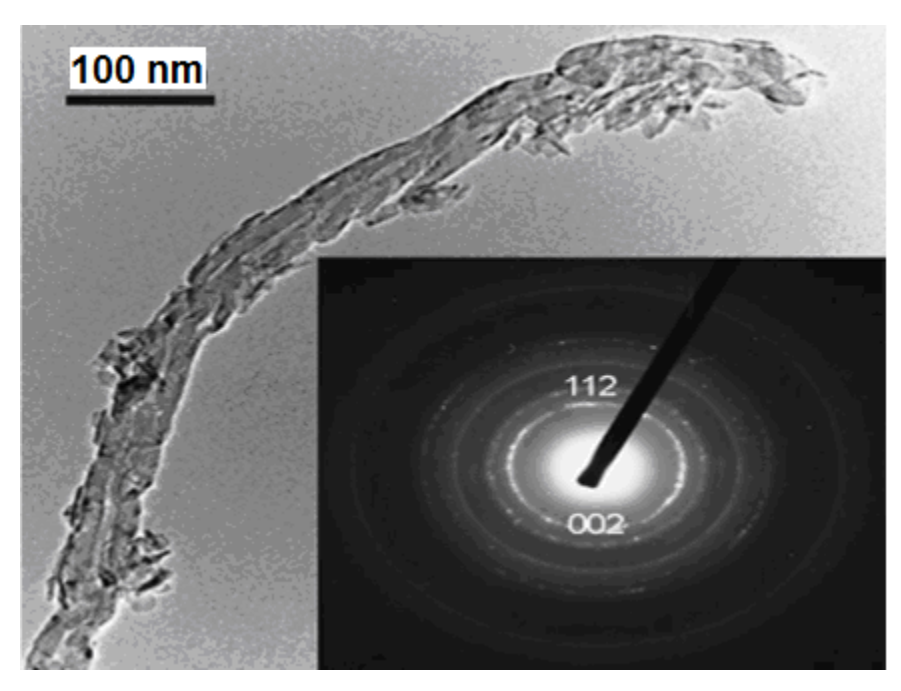


Figure 1.15- TEM image and selected area diffraction pattern of biomineralized nanotube in simulated body fluid (SBF) for use in calcium phosphate cement (Wang, Ye et al. 2007).

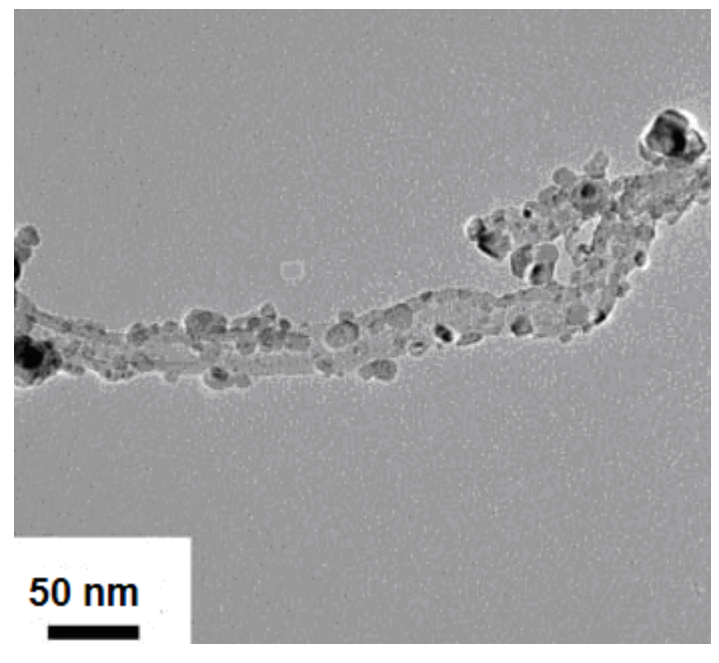
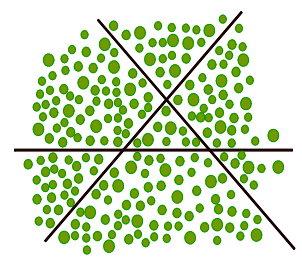
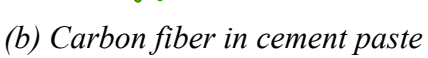
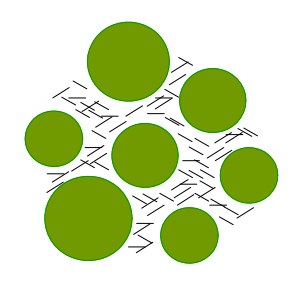


Figure 1.16- TEM image of carbon nanotube coated with ceramic nanoparticles (Gao, Jiang et al. 2006).

(a) Relative dimensions





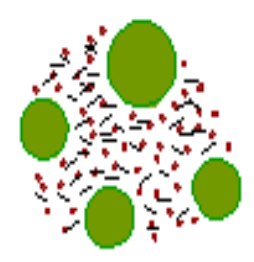


(c) Carbon nanotube in cement paste

Figure 1.17- Relative dimensions and dispersion conditions of carbon nanotubes and fibers.



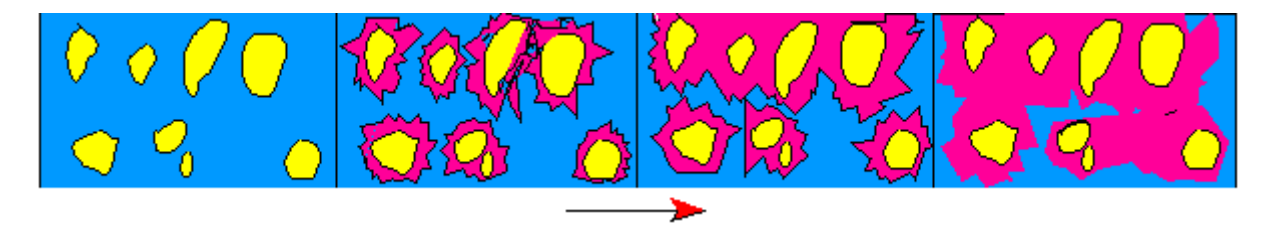




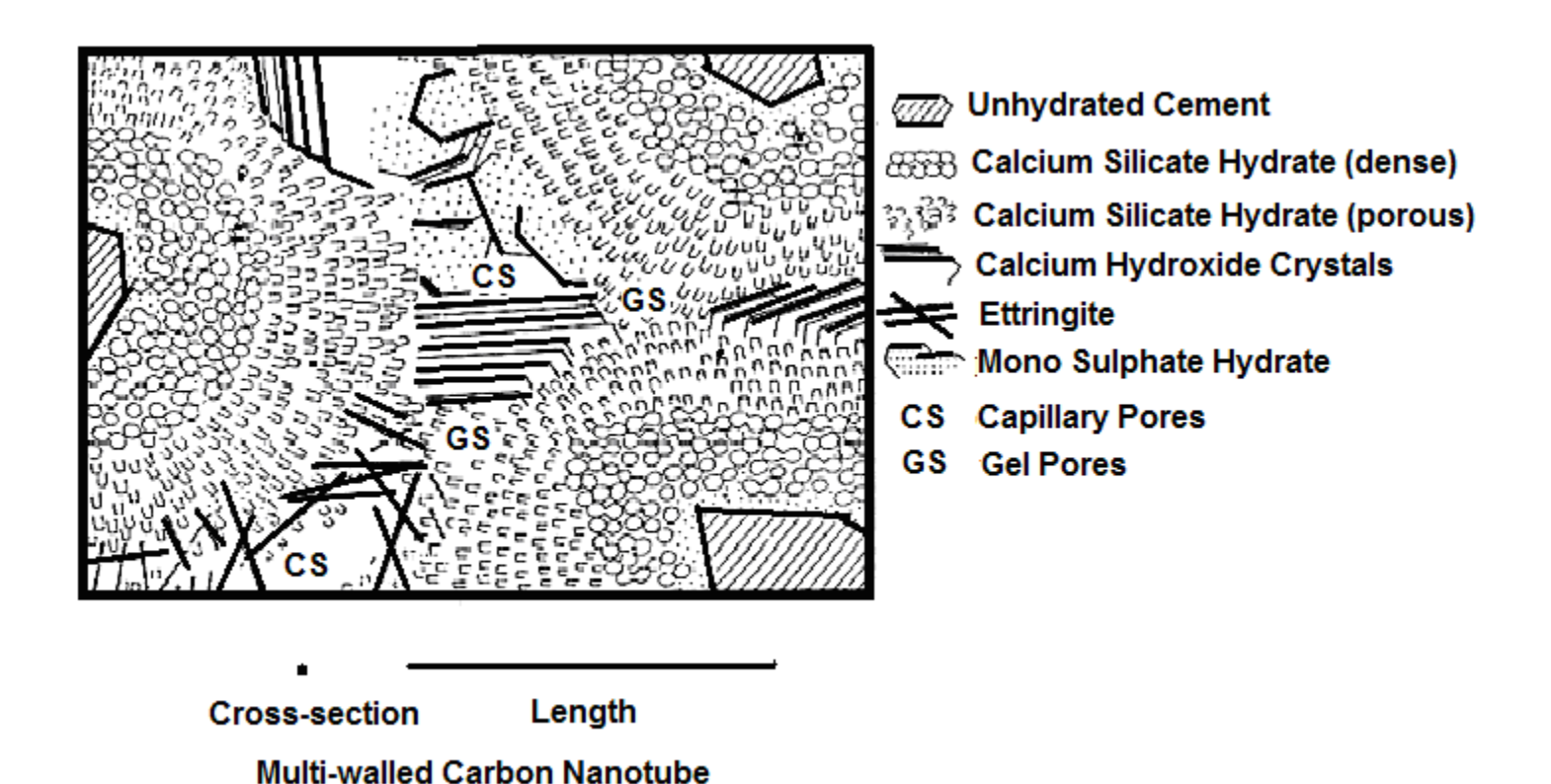
(a) Relative dimensions

(b) CNT in cement (left) & cement/silica fume (right)

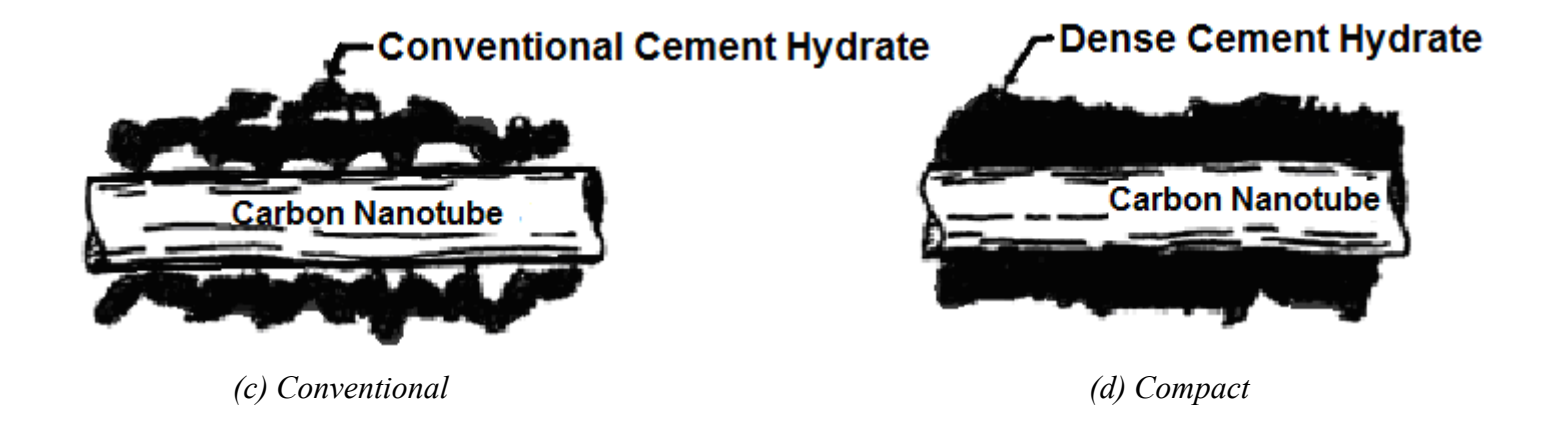
Figure 1.18- Improved dispersion of carbon nanotubes in DSP (cement/silica fume) cement paste.



(a) Hydration of cement particles partially filling the space between them Figure 1.19- The interactions of cement hydrates with graphite nanomaterials



(b) Structure of hydrated cement depicted with carbon nanotube length scale



CHAPTER 2

2 LITERATURE REVIEW, MATERIALS AND METHODS

2.1 General

Advances in concrete admixtures have played enabling roles in development of high-performance concrete materials with increasing strength levels. These high-performance concrete materials, however, tend to be brittle with low tensile strength and sensitivity to early-age microcracking under restrained (drying/autogeneous) shrinkage and thermal stresses. These drawbacks in development of high-performance and ultra-high-performance concrete materials can be addressed through discrete (millimeter- and micrometer-scale) fiber reinforcement Cementitious materials, however, incorporate flaws at different scales; finer flaws with nanoscale size and spacing challenge the effectiveness of conventional reinforcing fibers; these finer flaws can form and grow within the cementitious matrix in between conventional (coarser) fibers without encountering the fibers. The use of nano-scale fibers (with nano-scale spacing) in high-performance cementitious materials can overcome this drawback of conventional reinforcing fibers.

Graphite Nanomaterials, including carbon nanotubes (CNTs), present several distinct advantages over conventional (micro-scale) fibers as reinforcement in high-performance cementitious materials. Graphite nanomaterials generally provide significantly higher strength and modulus than conventional fibers. These nanomaterials also provide distinctly high specific surface areas and aspect ratios, which benefit their interactions with the cementitious matrix and effectiveness

in crack arrest. Provided that the nanomaterials are uniformly dispersed within the cementitious matrix, due to their nano-scale cross-sectional dimensions, the spacing between nanomaterials tends to be very small. The inception and propagation of microcracks in the space between nanoscale reinforcement would thus be effectively hindered.

Few attempts have been made to introduce graphite nanomaterials as reinforcement in cementitious matrices. A comprehensive review of the literature in this field is presented in the following. This review covers material selections, the approach to dispersion of nanomaterials, and their mixing into the cementitious matrix; benefits of nanomaterials to performance characteristics of cementitious materials are also discussed.

2.2 Experimental Studies

The addition of carbon nanotubes (CNTs), carbon nanofibers (CNFs) and exfoliated graphite nanoplatelets (GPs) to polymer-based matrices is among the highly developed areas of research. The results indicate that CNTs and CNFs can tremendously benefit the strength and energy-absorbing capacity of polymers, and also improve their electrical and thermal conductivity. Graphite nanoplatelets are incorporated into polymer matrices as low-cost alternatives to CNTs for realizing such benefits as vibration damping, and electric and heat conduction.

Applications of graphite nanomaterials in cementitious matrices are at early stages of development. A summary of notable research on nanocomposites involving CNTs is presented in Table 2.1. For each investigation, the objectives, the test parameters, the test methods/features, and major conclusions have been summarized in this table. In addition, the strengths and drawbacks, if any, of each investigation are also presented. Additional details, including significant findings of these studies are discussed in the following.

2.2.1 Carbon Nanotubes

In one of the earliest uses of carbon nanotubes in cement-based materials, reported by Fu et al.(Fu and Chung 1998), it was found that surface treatment of carbon by ozone gas (0.3 vol% in air, 160° C, 10 minutes) can benefit the tensile and compressive strengths or cementitious nanocomposites.

Campillo et al. tested carbon nanotube/cement nanocomposite under compression, and found that single- and multi-walled carbon nanotubes increased the strength of plain cement paste by 6% and 30%, respectively.

Kowald (Kowald 2004) found that 0.5% (by weight of cement) multiwalled carbon nanotubes (MWNTs) produced 12% gain in the compressive strength or the cementitious matrix; the consistency of the paste (i.e. the ability of freshly mixed cement paste to flow) was, however, reduced substantially, and pressures up to 125 MPa had to be applied for more than 45 min to adequately compact the fresh cementitious nanocomposite.

Makar et al.(Makar and Beaudoin 2004; Makar, Margeson et al. 2005) investigated the reinforcing effect of 2.0 wt.% CNTs in cement using Vickers hardness measurements and scanning electron microscope observations. The results indicated that carbon nanotubes may affect the early progress of hydration, producing higher hydration rates.

Li et al.(Li, Wang et al. 2005) used multiwalled carbon nanotubes, treated by sulfuric and nitric acid, at 0.5% by weight of cement, in a cement mortar (0.45:1:1.5). Experimental results indicated that the compressive and flexural strength of mortar could be increased by 19% and 25% with the addition of nanotubes. Moreover, the addition of carbon nanotubes reduced the porosity and produced a finer pore size distribution in the cementitious mortar. It is worth

mentioning that carbon fibers at similar volume fractions could increase the flexural of the cementitious mortar by 22%, but produced loss of compressive strength (Table 2.2).

Ibarra et al.(Saez De Ibarra, Gaitero et al. 2006) used both single walled carbon nanotubes (SWNTs) and multiwalled carbon nanotubes (MWNTs) in cement paste matrix at 0.05 to 0.20 percent by weight of cement. Dispersion of nanotubes was found to be a key to their successful use in cement paste. When gum Arabic was used to disperse nanotubes in the aqueous environment, the addition of nanotubes benefited the Young's modulus and hardness of cement paste; this was particularly true in the case of single walled carbon nanotubes. Without gum Arabic, however, the addition of nanotubes damaged the mechanical performance of cement paste.

Cwirzen et al.(Cwirzen, Habermehl-Cwirzen et al. 2008) investigated the effects of surface treatment on the wetability of multi-walled carbon nanotubes (MWNTs) and the mechanical properties of cement pastes incorporating dispersions of both pristine and acid functionalized MWNTs. Experimental results indicated that stable and homogenous dispersions of MWNTs in water can be produced through surface functionalization of nanotubes followed by decoration with polyacrylic acid polymers. Cement pastes incorporating dispersions of these nanotubes provided good workability and an increase in the compressive strength of nearly 50% even with only a small addition of the MWNTs, namely 0.045–0.15% by weight of cement. These positive results may have resulted from the existence of chemical bonds between the OH groups of the functionalized MWNTs and the C–S–H phase of the cement matrix, which benefits interfacial stress transfer. The effects of decoration of MWNTs with polyacrylic acid polymers and gum Arabic were also investigated. These dispersions appeared to be homogeneous only for approximately 2 hours, after which a progressive sedimentation occurred. Good workability was

found for the cement pastes produced with all of nanotube dispersions; the only significant difference was the slower hydration of the cement paste incorporating gum Arabic. When the amount of gum Arabic was as high as 0.8%, hydration of the cement was hindered for over 3 days.

Musso et al.(Musso, Tulliani et al. 2009) compared the flexural and compressive of unreinforced cement mortar (0.4:1:1.5) versus three different cement-based composites containing as-grown, annealed and functionalized multiwalled carbon nanotubes at 0.5% by weight of cement. The phase composition of composites was also evaluated by thermogravimetric analysis (TGA) coupled with mass spectroscopy (MS), and the mineralogy and microstructure were analyzed using X-ray diffractometer (XRD) and scanning electron microscope (SEM) techniques. Flexure test results indicated that the addition of carboxyl functionalized MWNTs lowered the strength of cement-based materials by a factor of 2.5; addition of pristine MWNTs, on the other hand, produced close to 34% rise in flexural strength. Annealed MWNTs produced a slight gain of about 9% in the flexural strength of cement-based materials. Comparable trends were observed in compressive strength test results. While carboxyl-functionalized nanotubes produced a sharp drop in compressive strength, addition of pristine nanotubes led to 10-20% rise in compressive strength, Figure 2.1.

Konsta-Gdoutos et al. (Metaxa, Konsta-Gdoutos et al. 2010) found that small amounts of effectively dispersed MWNTs (0.025–0.08 wt.% of cement) can significantly increase the strength and stiffness of the cementitious matrix. In particular, lower dosages (0.025–0.048 wt.%) of relatively long MWNTs produced desired reinforcement effects; higher dosages (close to 0.08 wt.%) of short MWNTs were required to render similar reinforcement effects. Nanoindentation test results indicated that MWNTs can strongly modify and reinforce the

nanostructure of the cementitious matrix. Compared to plain cement matrix, nanocomposites appeared to have a larger amount of high-stiffness C–S–H accompanied with reduced nanoporosity. Due to their small diameters (20–40 nm), MWNTs appear to specifically reduce the amount of fine pores. This phenomenon leads to a reduction of capillary stresses, resulting in a beneficial effect on the early strain capacity of nanocomposites.

Nasibulin et al. (Nasibulin, Shandakov et al. 2009) synthesized "Cement Hybrid Material" (CHM) in a simple, one-step process by the chemical vapor deposition (CVD), Figure 2.2, where cement particles were used both as catalyst and as support material. This approach allowed synthesis of novel hybrid nano-structured materials, wherein carbon nanotubes and nanofibers were attached to cement particles, facilitating dispersion of carbon nanomaterials in the cement matrix. Investigations of the physical properties of the paste made of the CHM revealed as high as 2 times increase in compressive strength and 40 times rise in the electrical conductivity after 28 days of curing in water.

Makar and Chan (Makar and Chan 2009) examined the effect of 1% SWNT on the early stages of hydration of ordinary Portland cement using isothermal conduction calorimetry, high-resolution SEM and TGA (Thermogravimetric Analysis). Introduction of non-functionalized SWCNT bundles distributed by sonication in isopropanol on cement grains accelerated the hydration of cement as compared both with control cement-based materials sonicated alone and with as-delivered cement. SEM images showed the formation of C-S-H on the surface of nanotube bundles. The images also showed evidence of classical reinforcing behavior including bridging and pullout at microcracks.

Manzur and Yazdani (Manzur and Yazdani 2010) explored the effects of treated and untreated CNTs at different dosages on the mechanical properties of cement mortars with different w/c

ratios. An increase in mean strength was observed up to 0.5% MWNT addition with both types of MWNT; addition of 0.3% MWNTs produced the highest mean compressive strengths. The maximum gains in mean compressive strength were about 29% and 25% at 7 and 28 days, respectively, relative to the control samples. A smaller-sized MWNT produced higher mortar compressive strength. Smaller MWNTs were distributed at a much finer scale, and therefore filled the nano-pore space within the cement matrix more efficiently.

Wille and Loh (Wille and Loh 2010) designed a hybrid fiber-reinforced ultra-high-performance concrete (UHPC) that incorporated different sizes of fibers ranging from nanometer to millimeter length scales. MWNTs in the amount of 0.022% (relative to cement weight) were included in the mix design. The bond behavior of steel fibers pulled out of UHPC significantly increased with the addition of low concentrations of MWNTs to the concrete mix. MWNTs showed no significant influence on mechanical properties such as compressive and flexural strength.

Collins et al. (Collins, Lambert et al. 2012) reported results of preliminary investigations into the dispersion and rheology of cement pastes reinforced with carbon nanotubes, with and without dispersants/surfactants. Most paste mixtures were composed with water/cement ratio of 0.5. Mini-slump consistency increased with increasing w/c ratio (as expected). Addition of carbon nanotubes (at 0.5%, 1%, and 2% by weight of cement), significantly reduced the consistency of cement paste. Despite ultrasonication, the compressive strength of cement pastes decreased with increasing nanotube content. The paste with w/c of 0.4 demonstrated the most significant drop in compressive strength with the addition of nanotubes; at 2% CNT, compressive strength was only 24% of the compressive strength of the control paste made without nanotubes. The consistence of cement paste reinforced with carbon nanotube greatly improved with the addition of polycarboxylate-based superplasticizer, with a highly flowable mixtures achieved with w/c ratios

as low as 0.35. This cement paste provided a compressive strength that was 25% higher than that of the control cement paste made without nanotubes.

Chan and Andrawes (Chan and Andrawes 2010) utilized finite element (FE) models to study the improvements in tensile strength and ductility of cement brought about by the use of carbon nanotubes (CNTs) as reinforcement. Nano-scale and macro-scale models were used to investigate the interfacial bond behavior of an individual CNT embedded in cement matrix, and the flexural response of a CNT/cement composite beam. Experimental results on CNT/cement composite beams were used to calibrate the numerical models. It was found that CNTs increased the load-carrying capacity by about 47%. Moreover, toughness of the composite beams was greater by 25% on average when compared with the plain cement beams. However, the mechanical test results did not show any enhancement in the ductility of the composite beams.

A comparison between the experimental and numerical behavior of the composite beams suggested an effective average (nanotube/cement) interfacial shear strength value of 6.5 MPa. It was verified that the numerical models could successfully predict the behavior of CNT/cement composites. FE analysis also predicted that increasing the shear strength from 6.5 MPa to 20.0 MPa, would increase the composite's flexural strength, ductility, and toughness by 141%, 259%, and 1976%, respectively. These results were significant considering that the enhancement was provided by CNTs alone, and pointed at the great potential of surface-treating CNTs for enhancing their interfacial bond strength and thus reinforcement efficiency in cement-based matrices

2.3 Knowledge Gaps

The above literature review indicates that most developments conducted thus far in the area of cement-based nanocomposites have been directed towards processing of carbon nanotubes into cementitious materials, and understanding the mechanisms of action of nanotubes in cementitious matrices. Lower-cost graphite nanomaterials (carbon nanofiber and particularly graphite nanoplatelet) have so far received less attention as reinforcement/additive in cement-based materials. The investigations reviewed above and summarized in Table 2.1 represent exploratory studies which provide limited insight into the mechanisms of action and potential value of graphite nanomaterials in cement-based matrices. Some key issues pertaining to enhancement of the contributions of graphite nanomaterials in cementitious matrices are presented in the following.

- The high reinforcement efficiency of graphite nanomaterials in cement-based matrices could be realized only if steps are taken to ensure thorough dispersion of nanomaterials within the matrix and effective interfacial interactions between nanomaterials and cement hydrates. The hydrophobic surfaces of carbon nanotubes can be made hydrophilic through introduction of selected functional groups, surfactants and/or polyelectrolytes which facilitate their thorough dispersion in aqueous media. Non-covalent interactions of surfactants and polyelectrolytes with graphite nanomaterials can beneficially modify the nanomaterial surfaces without damaging their structure and properties. Scalability of the nanomaterial dispersion process would benefit from increasing the concentration of (modified) nanomaterials dispersed in aqueous media.
- Besides thorough dispersion in aqueous media, effective bonding to cement hydrates is a
 key criterion governing the reinforcement efficiency of graphite nanomaterials in cement-

based materials. In order to develop primary bonds between cement hydration products and graphite nanomaterials, one can introduce functional groups via primary bonds (to carbon atoms) upon nanotubes, which can also develop primary bonds with cement hydration products. Functional groups, when present at adequate concentrations on nanotube surfaces, would provide enhanced interfacial stiffness, strength, thermal conductivity, etc. for effective mechanical and physical interactions between carbon nanotubes and cement hydration products. Non-covalent treatments (involving surfactants and polyelectrolytes) could further benefit interfacial interactions with cement hydrates without damaging the graphite nanomaterials.

- The fresh cementitious paste is a dispersion of micro-scale particles in an aqueous solution, which complicates the dispersion of nanomaterials which would only have the residual space between cement particles for dispersion. After curing, conventional cement-based matrices incorporate large quantities of micro- to nano-scale pores which mitigate intimate interfacial contacts over the surface area of graphite nanomaterials. The potential for thorough dispersion of carbon nanotubes and other graphite nanomaterials within a cementitious matrix can be improved through partial replacement of micro-scale cement particles with nano-scale silica fume particles in order to generate a smooth particle size distribution which benefits the dispersion of nanomaterials and limit the porosity and the maximum pore size in cement hydrates. Therefore, proper selection of cementitious matrix with proper particle size gradation/packing would benefit the reinforcement efficiency of graphite nanomaterials.
- Nanomaterials should first be dispersed in water, and then introduced into the mixing process of cement-based materials. Some nanomaterial modification schemes (e.g.,

physisorption of surfactants and polyelectrolytes) can be implemented as they are being dispersed in water. The efforts needed for dispersion of nanomaterials in water have implications in terms of added cost and reduced throughput. Any modification of the conventional mixing process of cement for ensuring thorough dispersion of nanomaterials within the fresh cement-based matrix would also have implications in terms of cost and productivity. For a particular type and dosage of nanomaterials, the modification conditions of nanomaterials and the (tailored) mix proportions should be selected to minimize the dispersion efforts at different stages of production.

- Given the porous structure of cement-based materials and the presence of micro-scale crystalline constituents among cement hydrates, judicious selection of mix design and curing conditions is important for reducing the porosity and pore size, and hindering the formation of larger crystalline constituents during hydration of cement.
- Given a particular combination of nanomaterial type, functionalization/modification condition, dispersion method, and cementitious matrix mix design, mixing method and curing condition, there is an optimum nanomaterial dosage for achieving balanced improvements in the structure and engineering properties of the cement-based matrix.
- The reliability of cementitious nanocomposite production, in light of the variations in the qualities, dispersion and interfacial interactions of nanomaterials, need to be thoroughly assessed. Comprehensive experimental data are also needed on diverse engineering properties of cementitious nanocomposites.
- Theoretical explanations are needed for the effects of nanomaterials on the engineering properties of cementitious materials to support further development and improvement of this new class of cementitious materials.

2.4 Graphite Nanomaterials and Microfibers

Seven types of multi-walled carbon nanotubes (MWNT A, B, C, D, E, F & G), in both acid-functionalize and non-functionalized conditions, two types of carbon nanofiber in plain (CNF1 and CNF) and oxidized (CNF-OX) conditions, Two type of graphite nanoplatelets (GP and GP1), two types of carbon microfiber (TT 143 and TT 150), and polypropylene microfiber (PP) were used in the project. All graphite nano- and micro-scale reinforcement systems used during this research are introduced in Table 2.3. TEM and SEM images of these different fiber reinforcements are presented in Figure 2.3.

2.5 Cementitious Matrix and Processing Techniques

2.5.1 Cementitious Matrix

In high-performance cementitious matrices two lines of research have been followed. The first concerns compact granular matrix concretes (DSP), with high superplasticizer and silica fume content, also incorporating ultra-hard aggregate (calcinated bauxite or granite). The other line of research relates to MDF (Macro Defect Free) polymer pastes. These pastes have very high tensile strength (150 MPa or more), in particular when mixed with aluminous cements. In spite of these favorable properties, it is necessary to underline the problems concerning MDF's sensitivity to water that, in many application, could be a weak point.

Dense cement-based matrices with a smooth particle size gradation down to nano-scale range, capable of dispersing nanomaterials and effective interactions with their interfaces for effective mobilization of their tremendous mechanical qualities, were used in this research. The primary category of cement-based materials used here is referred to as densified with small particles (DSP). These cementitious materials comprise micro-scale cement and nano-scale silica fume

particles, dispersed and densified with the help of superplasticizer (Figure 2.4). The silica fume/binder ratio generally ranges from 0.15 to 0.25, and the water/binder ratio from 0.15 to 0.20 (Guerrini 2000). Using this basic concept, and introducing other ingredients (e.g., high-quality aggregates and reinforcing fibers), it is possible to produce high-performance cementitious materials with balanced qualities suiting different fields of application (Guerrini 2000). RPC (Reactive Powder Concrete) is a variation of DSP where the microstructure, particle packing density and thus mechanical properties are improved by steam or high-pressure steam curing (optionally accompanied with pressure compaction) in the presence of reactive microscale aggregates. The main thrust of this research is to evaluate the efficiency of different graphite nanomaterials in progressively coarser high-performance densified with small particles (DSP) matrices. Therefore, it is appropriate to delve in to details of the criterion to select such matrices and the influence of different constituent materials.

2.5.1.1 Homogeneity Enhancement

Conventional concrete is a heterogeneous material, in which the aggregates (sand and gravel) form a skeleton of contiguous granular elements in the cementitious paste (cement, additives and water). The hardness of the aggregates is greater than that of the paste. For example, the Young's modulus for silica is 50-70 GPa, compared with between 18 and 22 MPa for the paste. Heterogeneity-related problems are substantially reduced with DSP matrices for the following reasons (i) Elimination of classical coarse aggregates, replaced by fine sand, (600 µm maximum) and granite gravel (less than 9 mm), if required; (ii) Improved mechanical properties of the paste; and (iii) Reduction in the aggregate/matrix ratio.

<u>Effect of Aggregate Size</u>. Conventional concrete aggregates form a set of rigid inclusions.
 On application of a compression force shear and tensile stresses appearing at the

paste/aggregate interface generate cracks in the paste. The sizes of these cracks is related to the extent of the zone under tensile or shear stress. In the case of a spherical inclusion, the size of the equatorial crack is directly proportional, to the diameter of the inclusion. For DSP mortar matrix, with a reduction in the size of the coarsest aggregate by a factor of about 50 (e.g, 400 µm instead of 20 mm), a major reduction is obtained in the size of mechanical (external loads); chemical (autogenous shrinkage); and thermo-mechanical (differential expansion between paste and aggregate under the effects of heat-treatment) microcracks.

- Effect of Enhanced Mechanical Properties of Paste. In all cases, the increase in the Young's modulus for the DSP paste, by comparison with that of conventional cementitious pastes, tends to attenuate the effects associated with disturbance of the mechanical stress field.
- Effect of Sand Content. The effects mentioned above are linked to aggregate size, and can be described as "mesoeffects". Reduction of sand content represents a more global "macro-effect". In a conventional concrete, the aggregates (sand and gravel) are the majority components in terms of volume, and form a rigid skeleton of contiguous granular elements. This means that a major proportion of paste shrinkage is blocked by the granular skeleton, with results in increased porosity. In the case of a DSP, the volume of the paste is at least 20% greater than the voids index of non-compacted sand. Thus the aggregates used in DSP do not form a rigid skeleton, but a set of inclusions trapped in a continuous matrix. Paste shrinkage is blocked locally round each aggregate particle (with diminished consequences as a result of the size limitation effect mentioned above), whereas global shrinkage is not blocked by the rigid skeleton. Each grain can be

transported by the paste, and can migrate with respect to its neighbors. This advantage only concerns structures where global shrinkage is unrestricted by any external source (eg, form work).

2.5.1.2 Optimization of Granular Mixture

Optimization of the granular mixture can be achieved by the use of packing models. DSP mix design is based on the following principles:

- A mixture comprising a number of granular classes is obtained, with a tight granular range inside each class;
- Classes are separated, selecting a high ratio (exceeding 13) between mean diameter d, for two consecutive granular classes;
- Cement/superplasticizer compatibility is studied, and optimum ratios are determined by rheological analysis;
- Only the least agglomerated fine sand is selected.

2.5.1.3 Selection of Granular Components

• <u>Sand</u>. Sand selection parameters to be defined consist, (i) mineral composition; (ii) mean particle size; (iii) granular range; (iv) particle shape; and (v) mixture ratio by weight.

Insofar as mineral composition is concerned, silica offers the advantages of being a very hard material, excellent paste/aggregate interfaces and readily available and low cost. Mean particle size is defined in line with the homogeneity criterion, and the separation of granular classes criterion that have both already been described. The next lowest granular class is the cement, for which mean diameter d, can vary between 11 and 15µm. Sand

with a mean particle diameter of about 250 μ m is therefore selected. The particle size range is defined indirectly by the desirable maximum and minimum particle sizes. Maximum particle size is limited to less than 600 μ m, Fine sand is obtained by screening crushed silica sand, where the grains are highly angular, or natural quarry sand, where the grains are more spherical. Both types of sand can be used for DSP matrices. However water demand is slightly less for natural sand.

- Cement. The selection of cement cannot be dissociated from that of the superplasticizer. From the point of view of chemical composition, cements with low C₃A content give better results. As for particle size, over-ground cements with a high Blaine fineness are not satisfactory, due to their high water demand. The best cement in terms of rheological characteristics and mechanical performance is high-silica-modulus cement. However this type of cement has the disadvantage of a very slow setting rate, preventing its use for certain applications. Conventional quick-setting high performance cement offers very similar mechanical performance, despite a higher water demand. The most efficient superplasticizers are polycarboxylate-based dispersing agents, but which also exhibit a retarding characteristic which can present a problem for practical applications. The conventional superplasticizers (nepthalene-based) selected for their compatibility with the cement give slightly poorer results. For the low w/c ratios used for DSP concretes, the optimum superplasticizer ratio is high (solid content of approx. 1.6% of cement content).
- <u>Silica Fume</u>. The silica fume used in DSP matrices has three main functions, (i) filling the voids between the next larger class particles (cement); (ii) enhancement of rheological characteristics by the lubrication effect resulting from the perfect sphericity of the basic

particles; and (iii) production of secondary hydrates by pozzolanic reaction with the lime resulting from primary hydration.

Therefore, the following parameters are used for silica fume characterization: (i) degree of particle aggregation; (ii) nature and quantity of impurities; and (iii) basic particle size. The main quality of a silica fume is the absence of aggregates. This leads to the use of non-compacted silica fumes. Slurry cannot be used, as the quantity of water contained in the slurry exceeds the total quantity of water required for the mixture. Particle size is a secondary factor. Indeed the best results are obtained with silica fume procured from the zirconia industry, being free from impurities and totally disaggregated. However Blaine fineness is lower than that for conventional fumes (14m²/g compared with18m²/g). On the other hand, an impurity-free fume with a high Blaine fineness value (22m²/g) produced mediocre results, due to the aggregation of the finest particles. Typically the fume/cement ratio used for DSP is less than 0.25. This ratio corresponds to optimum filling performance (Collepardi, Corinaldesi et al. 2002) and it is close to the dosage required for complete consumption of the lime resulting from total hydration of the cement. However, cement hydration is incomplete in DSP matrices, and the available quantity of silica fume is more than required by the pozzolanic reaction.

• Crushed Silica Sand. Crushed crystalline silica powder is an essential ingredient for DSP mortar and concretes. Maximum reactivity during heat-treating is obtained for a mean particle size of between 5 and 39 μm (11). The mean particle size of the crushed silica used for DSP is 10μm, and is therefore in the same granular class as the cement. The ratio by weight adopted corresponds to the stoechiometric optimum for conversion of

amorphous hydrates into tobermorite characterized by a C/S molar ratio of 516 = 0.83. This is achieved with a silica/cement ratio of 0.56. This ratio is obtained by adding silica fume and crushed silica sand as a complement (see Table 2.4).

2.5.1.4 Microstructure Enhancement by Heat Treatment

Heat-treating is performed after the matrix has set, by simply heating at ambient pressure. Heat-treating at 70° - 90°C substantially accelerates the pozzolanic reaction, while modifying the microstructure of the hydrates which have formed. However, for our experimental regimen 70°C was selected to conserve on the energy requirement for production of high-performance DSP matrices.

2.5.1.5 Ductility Enhancement by Incorporation of Fibers

The behavior of DSP matrices is purely linear and elastic, corresponding to a fracture energy not exceeding 30 Jm⁻² Micro-fibers must be added to enhance DSP for ductility. The fibers are introduced into the mix at a ratio of between 1.5 and 3% by volume. The economic optimum corresponds to a ratio of 2%, or about 155kg/m³. However, most of the micro-fibers increase the toughness but tend to decrease the flexural strength of the matrix, especially at lower volume fractions. Besides, other draw-backs related to durability and long-term performance.

Keeping all the factors mentioned earlier in mind a comprehensive literature review was conducted on DSP (and RPC) cement-based materials (Tjiptobroto and Hansen 1991; Sun and Young 1993; Sun and Young 1993; Tjiptobroto and Hansen 1993; Tjiptobroto and Hansen 1993; Beaudoin, Feldman et al. 1994; Cheyrezy, Maret et al. 1995; Richard and Cheyrezy 1995; Shannag, Hansen et al. 1995; Feylessoufi, Villieras et al. 1996; Roux, Andrade et al. 1996;

Shannag, Brincker et al. 1996; Young 1996; Zanni, Cheyrezy et al. 1996; Shannag, Brincker et al. 1997; Hu, Fang et al. 1999; Matte and Moranville 1999; Shannag, Hansen et al. 1999; Zivica 1999; Guerrini 2000; Shannag and Hansen 2000; Moranville-Regourd 2001; Singh, Kumar et al. 2001; Collepardi, Corinaldesi et al. 2002; Morin, Cohen-Tenoudji et al. 2002; Badanoiu, Georgescu et al. 2003; Bayard and Ple 2003; Chan and Chu 2004; Washer, Fuchs et al. 2004; Camilleri, Montesin et al. 2006; Childs, Wong et al. 2007; Lee, Wang et al. 2007; Wong, Childs et al. 2007). Based on this literature review, the cementitious matrices introduced in Table 2.4 were selected for evaluation of the reinforcement effects of graphite nanomaterials in cement-based matrices. The polycarboxylate-based superplasticizers used for dispersion of graphite nanomaterials were also used in these cement-based matrices. The materials selected for use in the cement-based matrices (Table 2.4) are introduced in the following.

- <u>Portland Cement:</u> Type I Portland cement was acquired from Lafarge North America.
 The chemical composition of this cement is given in Table 2.5.
- <u>Silica Fume:</u> Undensified silica fume was acquired from Norchem, Inc. It comprises nano-scale (200 nm average particle size) amorphous silica particles, with a minimum silicon dioxide content of 85% and a specific gravity of 2.25. The specific surface area of this silica fume is 15 m²/g, and its minimum 7-day pozzolanic activity index is 105%.
- <u>Silica Sand:</u> Sand comprising more than 99.5% silicon dioxide was acquired from Fairmount Minerals, Chardon, Ohio. It was ball milled in our laboratory to average particle sizes of about 39 μm and 350 μm. Sand particles were used in high-performance mortar and concrete matrices.

- <u>Granite Gravel:</u> Granite gravel ranging in size from 1 mm to less than 9 mm, with average particle size of 3.55 mm was acquired from Fairmount Minerals, Chardon, Ohio. It was used in high-performance matrices.
- <u>Superplasticizer:</u> Glenium® 7700 and ADVA® Cast 575 polycarboxylate-based superplasticizers (high-range water reducers) were acquired from BASF and W.R. Grace, respectively. They offer excellent slump retention without compromising early-age compressive strength development and set time. These admixtures meet the ASTM C 494 requirements for Type F (high-range water-reducing) admixtures.

2.5.2 Dispersion and Mixing Procedure

Thorough dispersion of nanomaterials is a key step toward their effective use as reinforcement in various matrix systems. The strong tendencies toward physical interactions over the large surface area of nanomaterials seriously challenge development of (aqueous) dispersions with adequate nanomaterial concentrations. As-produced carbon nanotubes align parallel to each other and pack into crystalline ropes, which is due to the strong van der Waals attractions between nanotubes. The ropes further aggregate into tangled networks. The aggregation of nanotubes is an obstacle in most applications, diminishing the special mechanical, geometric and physical properties of individual nanotubes. Hence, effective use of carbon nanotubes in cementitious nanocomposites requires deagglomeration and dispersing of the nanotubes within the matrix. The surface of carbon nanotubes is atomically sharp, hydrophobic and inert. Functionalization of the nanotube surfaces to make them compatible with cementitious matrices would be another key step toward successful use of graphite nanomaterials as reinforcement in cementitious matrices.

Before mixing with the cementitious paste, graphite nanomaterials need to be well dispersed in aqueous media. The mechanical action needed for dispersion of CNT/graphite nanomaterials

will be applied through high-shear mixing using magnetic stirrers followed by ultrasonication (involving high-power sonication using a tip or horn). During ultasonication, high-frequency sound waves are applied to carbon nanotubes, which can agitate the molecules and breaks intermolecular bonds. The separated nanotubes can re-aggregate if the dispersion is not stabilized using steric and/or electrostatic effects (Fig. 2.5). The objective is to achieve a uniform and stable dispersion of individual graphite nanomaterials (Fig. 2.6).

Introduction of COOH groups (carboxyl groups) makes the surfaces of graphite nanomaterials hydrophilic, and thus facilitates their dispersion in the aqueous medium of fresh cementitious paste. In addition, stabilization of the dispersion is achieved through electrostatic effects, which is because the COOH groups will be negatively charged in aqueous media, and will thus repel each other. The COOH-functionalized nanotubes, however, yield stable dispersions as far as the nanotube concentration in the aqueous medium does not exceed a relatively low limit (about 3 gram/liter).

Introduction of surfactants also facilitates dispersion of graphite nanomaterials; this technique is commonly used with graphite nano-sheets. Polymer wrapping is yet another approach to uniform dispersion of carbon nanotubes. This research work is employing all these techniques for achieving uniform and stable dispersions of individual graphite nanomaterials with increased concentrations of nanomaterials.

The dispersion and mixing process was constantly modified throughout the project in order to achieve improved dispersion at increased volume fraction of graphite nanomaterials. The nanomaterial dispersion procedure that evolved in the course of implementing the project comprised the following steps:

- Add the required amount of graphite nanomaterial, superplasticizer, and polyelectrolyte (if used as modifier of nanomaterials) to the mixing water of cementitious material;
- Stir the mixture overnight (12 to 15 hours), Fig 2.7a;
- Sonicate, Fig 2.7b, the mixture using a probe as follows: (i) Sonicate for ten minutes at different amplitudes (30%, 45%, 65% and 75%) with 1-minute breaks between different amplitudes; (ii) Pulse (1 minute on & 30 seconds off) for 10 minutes at 85% amplitude; (iii) Turn off the sonic probe for 2 minutes, and repeat the pulsing cycle two more times; and (iv) Repeat the whole sonic probing cycle one more time.
- In cases with microfiber (or hybrid reinforcement systems), microfibers were added to the mixing water half an hour before mixing with cementitious materials, without using the above dispersion procedure (for hybrid reinforcement, the nanomaterials were first dispersed following the above procedure, and then microfibers were added half an hour before mixing).

Cementitious materials (with and without graphite nanomaterials dispersed in the mixing water) were prepared following ASTM C 192 and C 305 procedures. The high-performance (DSP) paste specimens, for example, were prepared as follows: (i) mix cement and silica fume for 3 minutes at speed 1 in a mortar mixer (HOBART, Model A200F – Fig. 2.8a); (ii) add water (with dispersed graphite nanomaterial, if any, at the concentration required to yield the targeted volume fraction) plus superplasticizer and micro-fibers (if any), and mix for approximately 2 minutes at each of the speeds 1, 2 and 3; (iii) cast specimens following ASTM C 192 procedures, using a vibrating table (FMC Syntron Power Plus) at vibration intensity of 10.

The specimens were moist-cured inside molds after casting (ASTM C 192) over a 24-hour period. They were subsequently demolded and subjected to 48 hours of steam curing at 70°C. The specimens were then conditioned at 50% relative humidity and room temperature for seven days prior to testing.

2.6 Experimental Methods

The test procedures employed to determine the engineering properties of cement-based materials are described in the following.

Compression tests (ASTM (American Society for Testing and Materials) C 109) were performed (Fig. 2.8b) on 50 mm cube specimens. Flexure tests (ASTM C 1185) were performed (Fig. 2.8c) on 12.5x50x150 mm specimens by center-point loading on a span of 125 mm using a deflection controlled Instron test system, with load and deflection data collected using a data acquisition system. Impact tests (ASTM D 7136) were performed (Fig. 2.8d) on 12x150x150 mm specimens. Abrasion tests (ASTM C 944) were conducted (Fig. 2.8e) on the surface of cylindrical specimens with 100 mm diameter (and 50 mm height). Moisture absorption rate tests (ASTM C 1585) were performed (Fig. 2.8f) on cylindrical specimens with 100 mm diameter and 100 mm height. The sides and top surfaces of specimens were covered with impermeable adhesive sheets, and the bottom surface was immersed (1-3 mm depth) in water. The mass gain of the specimen (due to capillary sorption of water) was measured at frequent time intervals (with the wet surfaces patted dry prior to weight measurement).

In order to evaluate the durability and stability of the high-performance (DSP) cementitious materials with different nano- and/or micro-scale reinforcement, accelerated aging tests were conducted. *Freeze-Thaw* tests were carried out following ASTM C666 – 03, Standard Test

Method for Resistance to Rapid Freezing and Thawing (with both freezing and thawing in water) and ASTM C1185 and 1186. The automated freeze-thaw machine used for testing the specimens is made by Humboldt Manufacturing Corporation, Model H 3185 (Fig. 2.9a). *Wet-dry* tests were carried out following ASTM C1185 – 03, Standard Test Method for Sampling and Testing Non-Asbestos Fiber-Cement Flat Sheets. An automated wet-dry machine (with CN 76000 Omega® controller) was used for exposing the specimens to wet-dry cycles (Fig. 2.9b). *Hot Water Immersion* tests were carried out according to ASTM C1185 – 03, Standard Test Method for Sampling and Testing Non-Asbestos Fiber-Cement Flat Sheets. A hot water bath (Precision Scientific Model 186) was used for hot water immersion of specimens (Fig. 2.9c). The *Elevated Temperature* tests were carried out in an electric furnace (Applied Test System, Inc.) shown in Fig. 2.9d, with temperature change controlled using a CN76000 Omega® controller. Temperature was ramped up at a rate of 2°C/minute to 300°C, where it was maintained for 3 hours before ramping down to room temperature.

During long-term exposures to different severe environments, the specimen degradation over the course of exposure was monitored by nondestructive evaluation of the dynamic elastic modulus using a sonometer (Geotest Instrument Corporation model C2010) shown in Fig.2.9e, in accordance with ASTM C215, Test Method for Fundamental Transverse, Longitudinal, and Torsional Frequencies of Concrete Specimens and ASTM C1198, Standard Test Method for Dynamic Young's Modulus, Shear Modulus, and Poisson's Ratio for Advanced Ceramics by Sonic Resonance.

In addition to above tests on the engineering properties of cement-based nanocomposites, the following experimental techniques were employed to provide further insight into the chemistry, crystallinity, microstructure and failure mechanisms of cement nanocomposites reinforced with

functionalized graphite nanomaterials: (i) SEM; (ii) XRD (X-Ray Diffraction); (iii) DT/TGA (Differential Thermal and Thermogravimetry Analyses); and (iv) FTIR (Fourier Transform Infrared Spectrometry).

Table 2.1- Summary review of experimental studies reported on the use of nanomaterials in cement-based matrices.

Author	Study Objectives / Detail	Features and Methodology	Observations / Conclusions	Strengths/ Drawbacks
Carbon N	lanotubes			
Li et al. [2004]	results of addition of acid treated MWNTs and carbon fibers in cement mortar Objectives: • Acidic treated carbon nanotubes were added to cement, and both the mechanical behavior and microstructure of the resulting nanocomposites were studied. • Phase composition was characterized by FTIR spectroscopy • Mineralogy and microstructure were studied using SEM. • Porosity and pore size	were prepared with water: cement: sand ratio of 0.45:1:1.5. Plain mortars and those with with 0.5% by weight of cement MWNT and 0.5% by weight of cement CMF were studied. • MWNTs had an outer dia of 10-30 nm and lengths ranging from 0.5-500 μm. • CMF had diameter of 10-14 μm and length of 6 mm. • 40x40x160 mm samples were casted using a flat beat mixer, and compacted by vibration. • Demolded after 1 day, cured in water at 30°C for 26 days. The samples were dried in oven at 50°C for 24 hours	 It was found that the addition of carbon nanotubes to cement can greatly enhance its flexural and compressive strengths, as well as failure strain. This enhancement is due to the improvement of material microstructure. Interfacial interactions between surface-modified nanotubes and cement hydrates (such as C-S-H and calcium hydroxide) produce high bond strength, and increase the load-transfer efficiency from cement matrix to the reinforcement. Moreover, the addition of carbon 	study showing the potential of CNTs in cement-based materials. • Preliminary results not covering all aspects of nanocomposite performance. • Dispersion of nanotubes in cementitious matrix is not emphasized.

Author	Study Objectives / Detail	Features and Methodology	Observations / Conclusions	Strengths/Drawbacks
al. [2006]	This paper presents preliminary results on the mechanical properties of cement pastes reinforced with carbon nanotubes. Objectives: Assess contributions of SWNTs and MWNTs to compressive and flexural strengths. Elastic modulus was obtained by nanoindentation and AFM observation.	 matrix using type I cement at 0.34 w/c ratio. Both SWNTs and MWNTs were used at 0.05 to 0.20 wt.%. These nanotubes were dispersed both in plain water and water containing Gum Arabic. SWNTs had an outer dia. of 2 nm and lengths of about 20 μm. MWNTs had an outer dia. of 10-20 nm and lengths of 1-50 μm. 	nanotubes without gum arabic provided lower mechanical properties than the plain cement paste due to the intrinsic hydrophobicity of the nanotubes and their effects on the hydration	on the use of CNTs in cement-base matrix.

Author	Study Objectives / Detail	Features and Methodology	Observations / Conclusions	Strengths/Drawbacks
(2008)	investigated the effects of surface decoration on the wettability of multiwalled carbon nanotubes (MWNTs), and the mechanical properties of the cement paste incorporating decorated nanotube dispersions. Objectives: Determine the effects of surfactants and surface functionalization	 matrix, using sulphateresistant CEM I 42.5 N cement with w/c ratio of 0.25 - 0.40. Two types of MWNTs were used: pure MWNT and MWNT functionalized with COOH groups. Pure MWNTs had an outer dia. of 10 nm and length of about 10 μm. Functionalized MWNTs had an outer dia. ranging from few to few hundred μm, with unspecified length. 	surface functionalization combined with decoration using polyacrylic acid. The cement paste specimens incorporating these dispersions offerred good workability and an increase in the compressive strength of nearly 50% with 0.045% by weight of cement addition of the PAA-treated MWNTs At 0.15 wt.%, functionalized	effects of both pristine and oxidized MWNTs on compressive strength of cement paste. Either GA or PAA was used for further treatment of MWNTs.

Table 2.1 (cont'd)

Author	Study Objectives / Detail	Features and Methodology	Observations / Conclusions	Strengths/Drawbacks
	influence of the type of surface decoration on the mechanical properties of the	 10x10x60 mm samples were casted using vacuum mixer in Teflon molds, and were not compacted using vibration. Demolded after 1 day, cured in water at 21°C for 27 days. Specimens were taken form samples after mechanical tests for nanoindentation tests and AFM observations. 	polyacrylic acid polymers and gum Arabic yielded dispersions which appeared to be homogeneous only for approximately 2 hr., after which a progressive sedimentation	

Author	Study Objectives / Detail	Features and Methodology	Observations / Conclusions	Strengths/Drawbacks
al. [2009].	Presents flexure and compression test results on cement mortar reinforced with as-grown, annealed and functionalized MWNTs.	 MWNTs. As-grown, annealed and carboxyl functionalized MWNTs were used. Pristine MWNTs had an outer dia. of 40-80 nm and lengths of 400-1000 μm. Annealed MWNTs had an outer dia of 40-80 nm and lengths of 200-400 μm. Carboxyl functionalized MWNTs 	made: • Both pristine and annealed MWNTs induced an improvement in the mechanical properties of cement-based matrix.	MWNTs were evaluated in mortar matrix. Carboxyl functionalized MWNTs produced a drop in mechanical properties, which is contrary to other reported results.

Table 2.1 (cont'd)

Author	Study Objectives / Detail	Features and Methodology	Observations / Conclusions	Strengths/Drawbacks
		atmosphere, and then demolded and cured for 27 days in 20 °C water.	 This hypothesis was supported by the low amounts of tobermorite gel produced during hydration per outcomes of TGA. A suitable hydration of cement was realized by only increasing the water/cement ratio from 0.4 to 0.56. Even if a significant number of defects in the CNT atomic network can produce curved CNTs with deteriorated mechanical properties, the ultimate strength of the nanocomposite can still be enhanced 	

Author	Study Objectives / Detail	Features and Methodology	Observations / Conclusions	Strengths/Drawbacks
Konsta-Gdoutos [2009]	 Development of high-performance cement pastes reinforced with multiwalled carbon nanotubes was investigated. Effective dispersion of MWNTs in the mixing water was 	• Mix proportions of sonicated suspensions with short MWNTs at 0.048, 0.08 and 0.10 wt.% of cement, and long MWNTs at 0.025,	of thoroughly dispersed MWNTs (0.025–0.08 wt.% of cement) can significantly increase the strength and modulus of the cementitious matrix. In particular, lower amounts of long MWNTs (0.025–0.048 wt.%) offered high reinforcement efficiency. Higher concentrations (close to 0.08 wt.%) of short MWNTs were required to produce the same reinforcing effects as long nanotubes. Nano-indentation test results suggesedt that MWNTs can strongly modify and reinforce the nanostructure of the cementitious matrix.	were evaluated in cement paste. • Functionalization of nanotubes was not given due consideration.

Table 2.1 (cont'd)

Author St	udy Objectives /	Features and Methodology	Observations / Conclusions	Strengths/Drawbacks
	Detail			
tes to eff rati con MV fra cha cer nar • De me pro pon con car nai • Au shr exp con eff ear	acture mechanics ts were performed investigate the fects of the aspect io and incentration of WNTs on the cture aracteristics of	A 6 mm notch was placed in specimens using a water-cooled diamond saw. The specimens were then subjected to three-point flexure tests at 3, 7 and 28 days of	• Due to their small dia. (20–40 nm) MWNTs appear to specifically reduce the amount of fine pores. This phenomenon leads to reduction of capillary stresses, resulting in a beneficial effect on the early strain capacity of nanocomposites.	

Author	Study Objectives / Detail	Features and Methodology	Observations / Conclusions	Strengths/Drawbacks
Nasibuli- n etal. [2009]	novel cement hybrid material (CHM), wherein CNTs and CNFs are adhered to cement particles, providing for thorough dispersion of carbon nanomaterials in the matrix.	 Two types of Portland cement with different concentrations of iron oxide (Fe₂O₃): sulphate-resistant (SR) (4 wt%) white (0.33 wt%) Portland cements. For synthesis of graphite nanomaterials, acetylene was chosen as the main carbon source due to its low decomposition temperature and cost-effectiveness. Carbon monoxide and carbon dioxide were used as promoting additives. The synthesis of CHM was carried out in a CVD reactor, which consists of a quartz tube (with an internal diameter of 34mm and a length of 100 cm) inserted in a resistively heated furnace (with a heated length of 60 cm), a powder feeder with an adjustable powder feeding rate, a copper screw feeder, a powder collector and a water cooling system to keep the ends of the tube at room temperature. 	 Cement particles were utilized both as catalyst and as support material, which enabled synthesis of novel hybrid nanostructured materials, wherein CNTs and CNFs attached to cement particles, and provided for desired dispersion of carbon nanomaterials in cement matrix. This hybrid material was synthesized by a simple onestep CVD method, which can be easily integrated into industrial cement production without a significant increase in cement cost. TEM, SEM, XRD, TGA and Raman investigations showed high efficiency of the method for low-temperature and high-yield synthesis of CNTs and CNFs. 	was introduced for production of cement with as-grown CNTs and CNFs. Only cement paste matrix was evaluated.

Author	Study Objectives / Detail	Features and Methodology	Observations / Conclusions	Strengths/Drawbacks
		 For the performance of mechanical tests, beams with dimensions of 60×10×10 mm³ were prepared using Teflon moulds and cured in water at 20°C for 7, 14 and 28 days. The structure of nanocomposites was evaluated by observation under SEM and TEM, and also by XRD, TGA and Raman. 	• Investigations of the physical properties of cement paste made with CHM revealed as high as 2 times increase in compressive strength and 40 times increase in electrical conductivity after 28 days of curing in water.	
Makar and Chan [2009]	• Examination of the effect of 1% SWCNT content on the early stages	 Type I cement paste was used with 0.5 w/c ratio. SWNTs were purified by a solvent-based method which does not functionalize. Samples of OPC were sonicated for 2 h in isopropanol both with and without 1 wt.% SWNT. Isopropanol was then removed in each case by dessication in a vacuum system, and the processed samples were stored under vacuum until needed. 	 Unfunctionalized SWCNT bundles distributed by sonication in isopropanol on OPC grains accelerated the hydration of OPC as compared with both OPC control samples sonicated alone and as-delivered OPC. The morphology and location of the C₃A hydration products were altered by the presence of SWCNT, but no evidence was observed for nucleation of C₃A hydration products on SWCNT bundles. 	• A fundamental study focusing on the early stages of hydration, providing valuable information on the development of cement hydrate structure in the presence of nanotubes, but limited information on the engineering properties of cementitious nanocomposites.

Table 2.1 (cont'd)

Author	Study Objectives / Detail	Features and Methodology	Observations / Conclusions	Strengths/Drawbacks
	Detail	 Calorimetry measurements were then made, and specific hydration durations were chosen for subsequent SEM examination. Times of 0, 60, 120, 135, 180, and 240 min were chosen for the samples sonicated with SWCNT, and times of 0, 60, 135, 150, 180, and 240 min were chosen for the samples sonicated without SWCNT. Image analysis was performed to determine the average surface area covered by the C₃A hydration products formed during the first 60 min of hydration. 	instead responsible for the observed change in hydration	

Author	Study Objectives / Detail	Features and Methodology	Observations / Conclusions	Strengths/Drawbacks
Manzur and Yazdani [2010]	 Evaluation of the effects of treated and untreated CNTs on the mechanical properties of cement mortar. Assessment of the effect of CNT dosage on the mechanical properties of cement mortar. Investigations of the effect of water/cement ratio 	form 0.485 to 0.65. • Type II cement was used with specially graded sand per ASTM C109. Two types of MWNTs were used: (i) MWNT1 had an outer dia. >50 nm and lengths ranging from 10 to 20 μm; (ii) MWNT2 had an outer dia. of 20-30 nm and lengths ranging from 10 to 30 μm. • All MWNTs were dispersed using a	typical mortar mix increased by addition of the two types of MWNT. • Mixing technique is important in enhancing the compressive strength of mortar nanocomposites. Proper mixing is necessary to distribute the MWNTs uniformly within the cement-based matrix, which results in higher-strength nanocomposites. This increase in strength indicated that nanotubes were properly anchored within the cement matrix.	the use of two different MWNTs in mortar matrix. No consideration given to functionalization of nanotubes. Modest increase in compressive strength reported with smaller-dia. MWNTs.

Table 2.1 (cont'd)

Author	Study Objectives / Features and Methodology Detail		Observations / Conclusions	Strengths/Drawbacks
	compressive and	 Compressive and flexural Strengths were evaluated. Structure was assessed by FE-SEM, TEM. Evaluation of lattice defects was performed by Raman. FT-IR and EDX (Energy Dispersive X-ray) analysis were used to assess the presence of reactive groups on CNT surfaces. Thermal oxidation of CNTs was by (TGA) analysis. 	in CNT-reinforced composites, and water–cement ratio plays a vital role. More water is required to reach proper workability in nanotube-reinforced cement composites. The control sample with higher	

Author	Study Objectives / Detail	Features and Methodology	Observations / Conclusions	Strengths/Drawbacks
	Objectives: Dispersion of low concentrations of MWNTs in cement paste, promoting nanotube—cement matrix interactions. Design of a hybrid fiber-reinforced UHPC that incorporates different sizes of fibers covering nanometer to	wt.% of cement. • MWNTs were mixed in diluted polyelectrolyte or diluted SPL solutions. The MWNT– polyelectrolyte solutions were subjected to 180 min. of ultrasonic bath treatment (135 W, 42 kHz) followed by 30 min. of high-powered probe sonication (3.175– mm tip, 150 W, 22.0 kHz). • Two different types of high-strength steel fibers were used: (i) straight fiber with dia. of 0.20 mm and length of 13 mm; and (ii) twisted fiber with dia. of 0.3 mm and length of 30 mm.	 By optimizing the dispersion of MWNTs in poly(carboxylate ether)- based SPLs, three initial goals were accomplished: (i) long-term stable MWNT suspensions; (ii) incorporation of MWNTs into the mix design without adversely influencing its workability; and (iii) enhancement of the interface properties between embedded steel fibers and the concrete matrix. Bond strength of steel fibers to UHPP and UHPC increased significantly with the addition of low concentrations of MWNTs (1 mg/mL in dispersion, or 0.022% of cement weight). MWNTs did not significantly influence the compressive and flexural strengths of highperformance concrete materials. 	reinforcement systems comprising MWNT and microfibers in a high-performance mortar. • The improvements in bond strength of microfibers with addition of MWNT were minor. • No gains in mechanical properties were obtained with the

Author	Study Objectives / Detail	Features and Methodology	Observations / Conclusions	Strengths/Drawbacks
		• Specimens for single fiber pullout, compression and flexure tests were cast and slightly compacted on a vibration table (30 s). After casting, the specimens were covered with plastic sheets and stored at room temperature for 24 h; they were then removed from molds, and stored in a water tank at 20°C for 25 days.		
	 Evaluation of the dispersion and rheology of CNT—OPC paste mixtures, with and without dispersants/ surfactants. Initial screening of aqueous solutions containing CNTs 	 Type I cement paste was used as the matrix, with 0.3 w/c ratio. Three types of commercially available purified multiwalled carbon nanotubes (MWNTs) were used. MWNT1020 had an outer dia. of 10-20 nm and lengths of 5-15 or 1-2 µm. MWNT1030 had an outer dia. of 10-30 nm and lengths of 5-15 or 1-2 µm. MWNT60100 had an outer dia. of 60-100 nm and lengths of 5-15 or 1- 	the following conclusions: In the case of CNTs airentrained aqueous solutions, however, sedimentation occurred within days following mixing. Mechanical agitation by ultrasonication greatly reduced sedimentation when observed 9 days following mixing. Ultrasonication of polycarboxylate and	to evaluate three different types of CNTs. Not dispersed properly.

Table 2.1 (cont'd)

Author S	Study Objectives / Features and Methodology Detail		Observations / Conclusions	Strengths/Drawbacks
	SEM observation of fractured surfaces of selected mixtures for evaluating the distribution of CNTs in cement-based matrix.	 Different types of dispersants/surfactants were chosen because of their compatibility when utilized in cement paste. Sedimentation in aqueous solution, mini slump and compressive strength tests as well as SEM investigations was undertaken. Mixing was performed in a planetary mixer. Paste cylinders, measuring 50 mm diameter by 100 mm height, were tested in compression at 28 days. Following mixing of paste, the molds were filled and compacted on a vibrating table for 30 s. Specimens were then covered with polyethylene film to ensure minimal air circulation over the sample. Following elapse of 24 h, the samples were removed from molds, and machine-finished at both ends to ensure smoothness. 	 in OPC paste mixtures, resulted in reduced consistency and strength. CNT-OPC paste consistency was greatly improved in the case of polycarboxylate 	

Author	Study Objectives / Detail	Features and Methodology	Observations / Conclusions	Strengths/Drawbacks
	 Finite element (FE) analysis of improvements in tensile strength and ductility of cement-based materials with carbon nanotube reinforcement. Use of nano-scale and macro-scale models to investigate the interfacial bond behavior of an individual CNT 	 Three-point flexure tests were performed on 13 mm x 26 mm x 165 mm beams. The CNTs used in this work were 	increased flexural strength by about 47%. Moreover, toughness increased by 25% with CNTs. • Deformation capacity, however, did not benefit significantly with introduction of CNTs. • A comparison between the experimental and numerical behavior of the composite beams suggested an effective average shear strength value of 6.5 MPa at the CNT/cementitious matrix	 Reported increase in both strength and toughness. Suggests that tremendous reinforcing effects can be realized

Table 2.1 (cont'd)

Author	Study Objectives / Features and Methodology		Observations / Conclusions	Strengths/Drawbacks
	Detail			
	• Use of experimental results on CNT/ cement composite beams to calibrate models.	\mathcal{E}	increasing the interfacial shear strength from 6.5 MPa to 20.0 MPa, would increase the composite's flexural strength, ductility, and toughness by 141%, 259% and 1976%, respectively. These findings pointed at the great potential of	

Table 2.2- Strength test results after 28 days of curing (Li, Wang et al. 2005).

Mix	Compressive Strength (MPa)	Flexural Strength (MPa)
PCC	52.27 (+/-) 1.4%	6.69 (+/-) 1.5%
PCCF	47.51 (+/-) 3.1%	8.14 (+/-) 2.6%
PCNT	62.13 (+/-) 2.3%	8.37 (+/-) 2.1%

Table 2.3- Physical attributes of all graphite nano and micro-scale reinforcement systems.

Reinforcement	Diameter	Length	Manufacturer	
MWNT A	20-40 nm	5-15 μm	NanoAmor, Inc.	
MWNT B	60-100 nm	5-15 μm	NanoAmor, Inc.	
MWNT C	5-15 nm	5-20 μm	NanoLab, Inc.	
MWNT D	8-15 nm	10-50 μm-oxidized 100 μm- pristine	Cheap Tubes, Inc.	
MWNT E	20-30 nm	10-30 μm-oxidized 50 μm- pristine	Cheap Tubes, Inc.	
MWNT F	8-15 nm	Up to 200 μm	Cheap Tubes, Inc.	
MWNT G	20-40 nm	Up to 200 μm	Cheap Tubes, Inc.	
CNF1	200-500 nm	10-40 μm	Pyrograf Products, Inc.	
CNF-OX	60-150 nm	30-100 μm	Pyrograf Products, Inc.	
CNF	60-150 nm	30-50 μm	Pyrograf Products, Inc.	
GP1	5-10 nm	15 μm	XG Sciences, Inc.	
GP	3-90 nm	500 μm (100-150 μm after sonication	XG Sciences, Inc.	
CMF (TT143)	6-7 μm	6 mm	Toho Tenax America, Inc.	
CMF1 (TT 150)	6-7 μm	3 mm	Toho Tenax America, Inc.	
PP Microfiber	50 μm	19 mm	New Nycon, Inc.	

All MWNTs have ~2.1 g/cm³ true density, and >95% purity.

All CNFs have \sim 1.95 g/cm³ true density, and >95% purity.

Table 2.4- The cementitious matrices selected for evaluation of the reinforcement efficiency of graphite nanomaterials.

Mix Proportions	DSP Paste	DSP Mortar	DSP Concrete
Silica Fume/Binder	0.20	0.20	0.20
Water/Binder	0.185 (0.24)*	0.185 (0.24)*	0.185 (0.26)*
Superplasticizer/Binder	Adjusted for diff reinforcements	Adjusted for diff reinforcements	Adjusted for diff reinforcements
Silica Sand (0 – 0.18 mm) / Binder	-	0.36	0.36
Silica Sand (0.18 -0.5 mm) / Binder	-	0.86	0.86
Granite Gravel/ Binder	-	-	0.50

^{*} including the water content of superplasticizer

Table 2.5- Chemical composition of Type I Portland cement.

Compound	Content (%)
C ₃ S	55
C ₂ S	19
C ₃ A	10
C ₄ AF	7
MgO	2.8
SO ₃	2.9
Ignition Loss	1.0
Free CaO	1.0

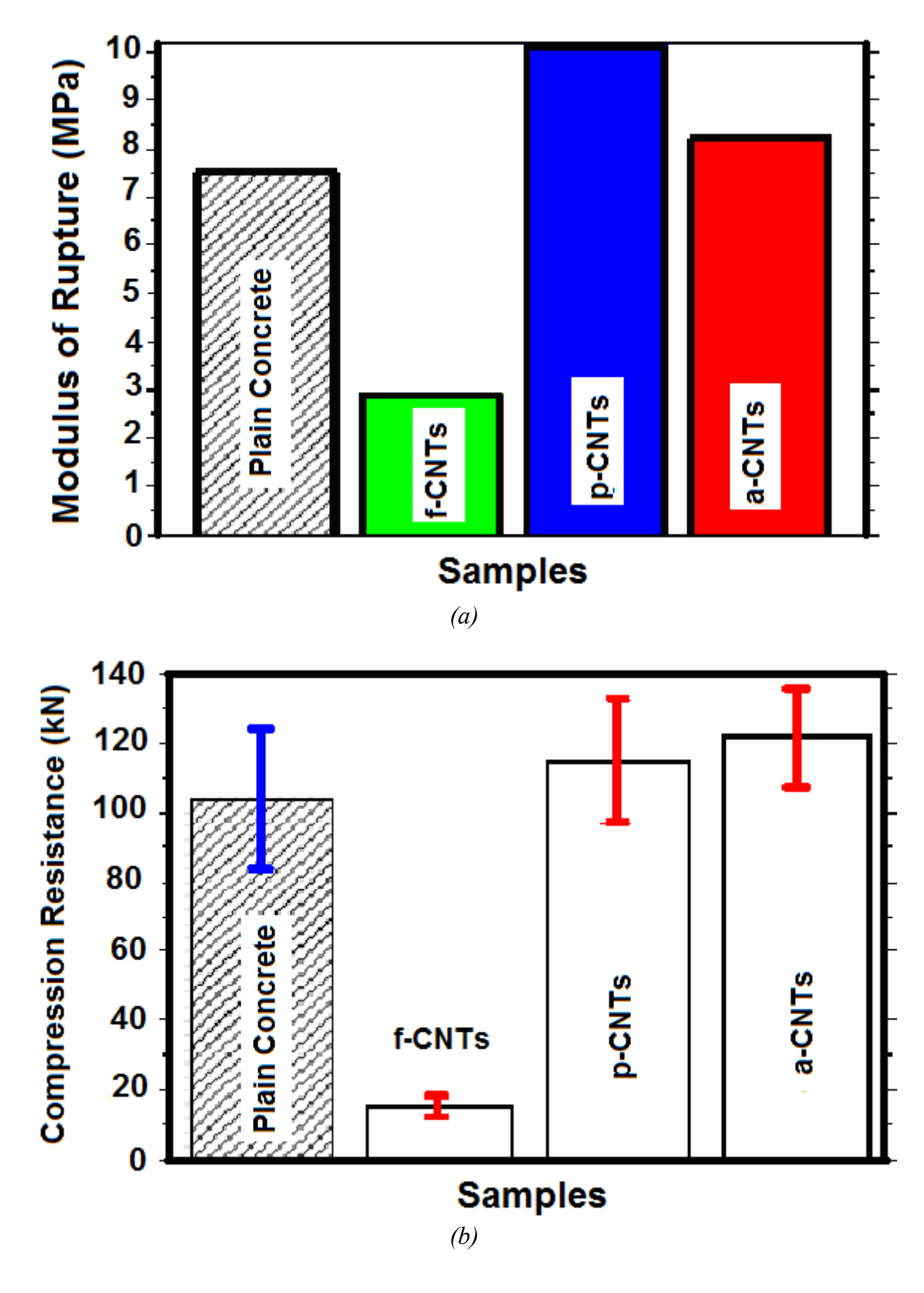


Figure 2.1- Modulus-of-rupture (a) and compression resistance (b) test results for cement mortars with and without MWNTs (Musso, Tulliani et al. 2009).

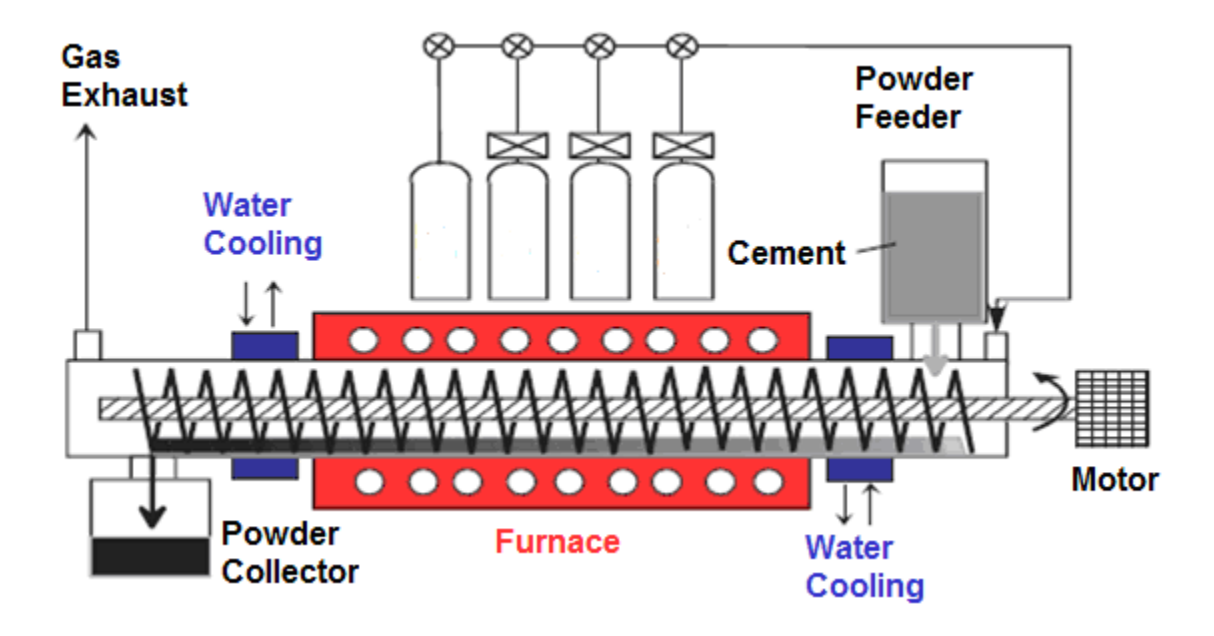


Figure 2.2- Schematic representation of the experimental setup based on continuous feeding of cement particles using a screw feeder (Nasibulin, Shandakov et al. 2009).

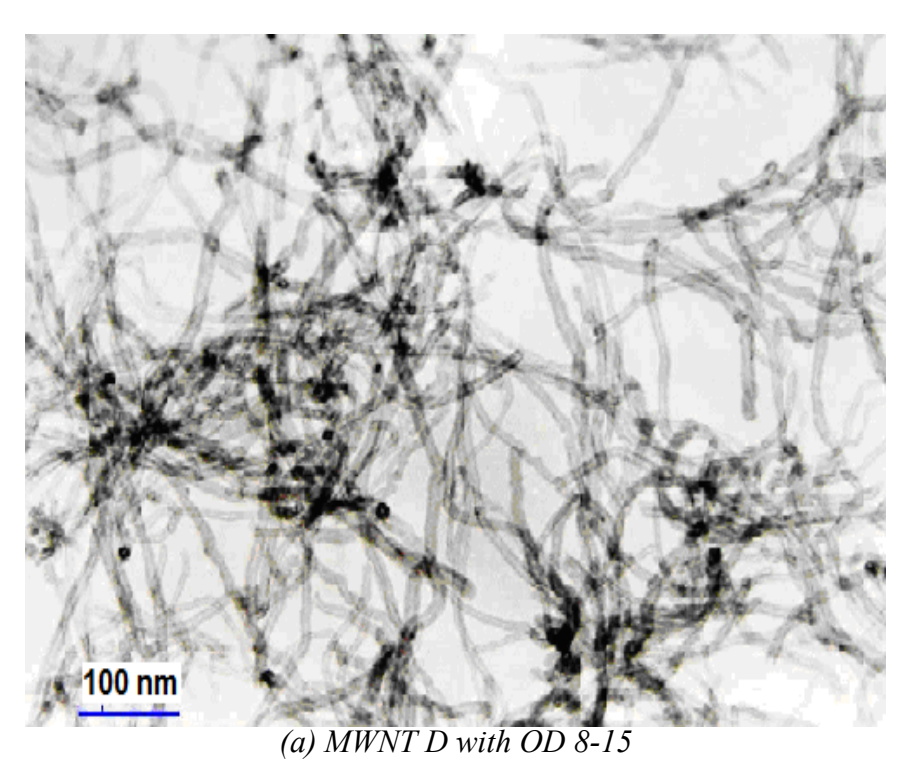
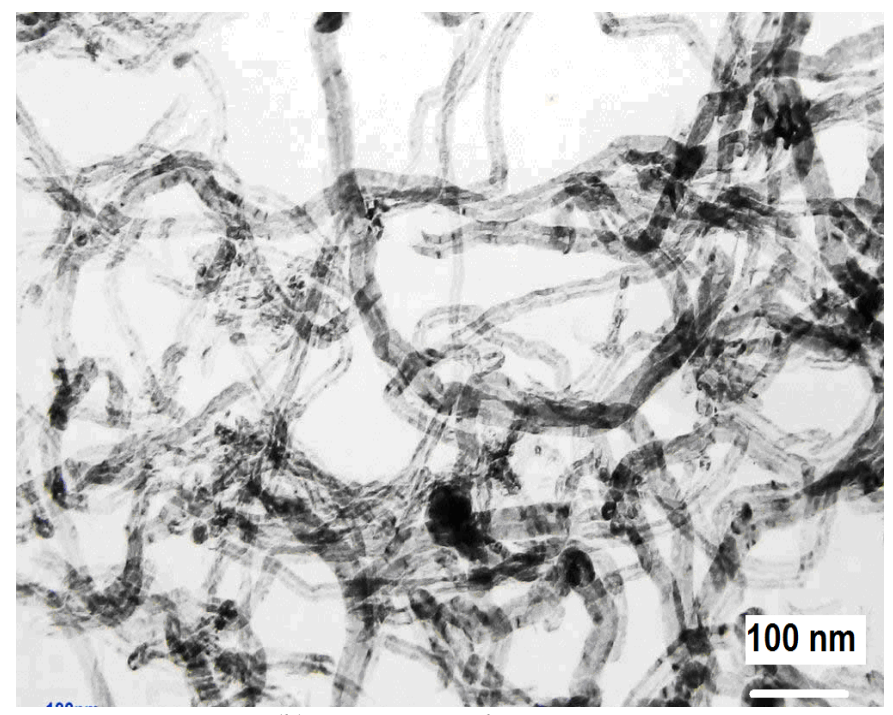
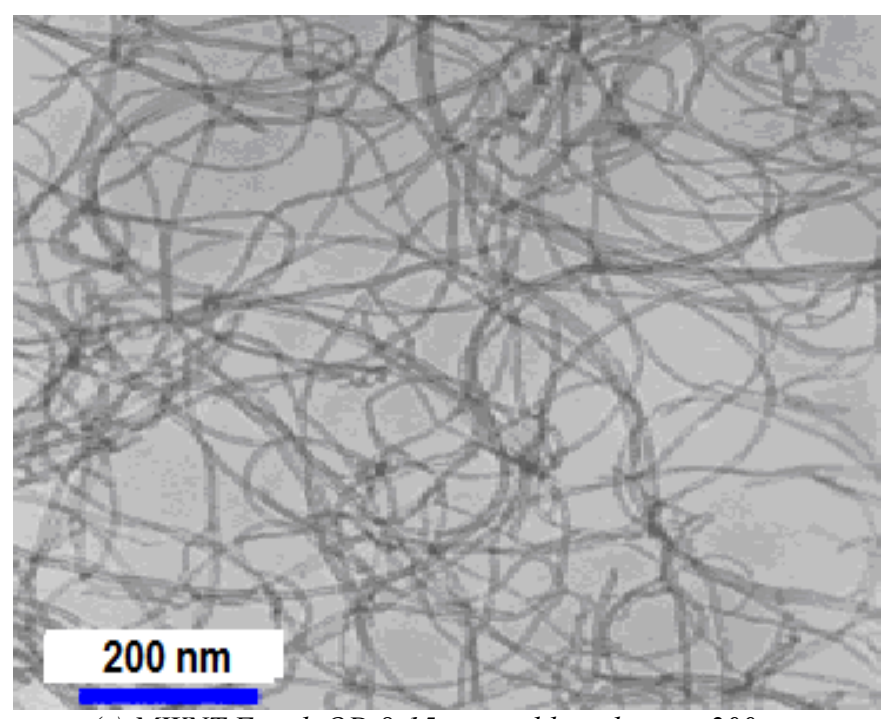


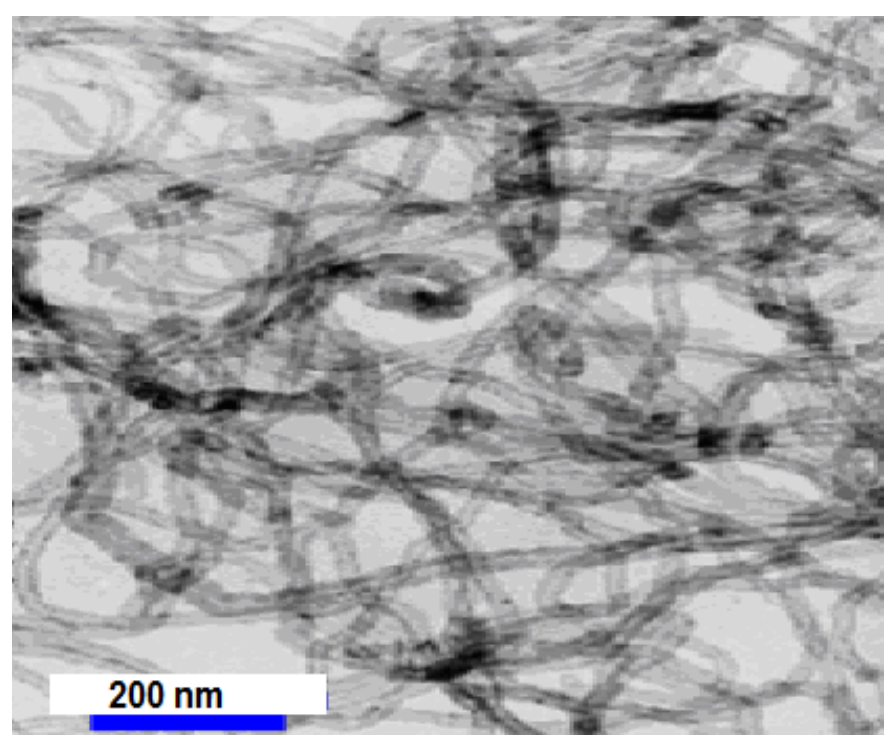
Figure 2.3- TEM and SEM micrographs of different nano- and micro-scale reinforcement systems.



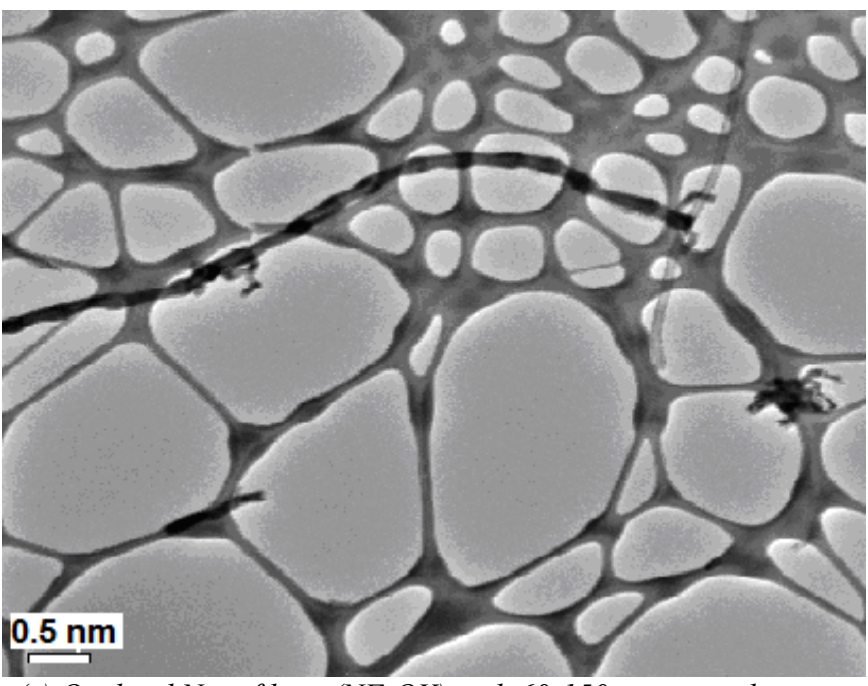
(b) MWNT E with OD 20-40 nm



(c) MWNT F with OD 8-15 nm and length up to 200 μ m

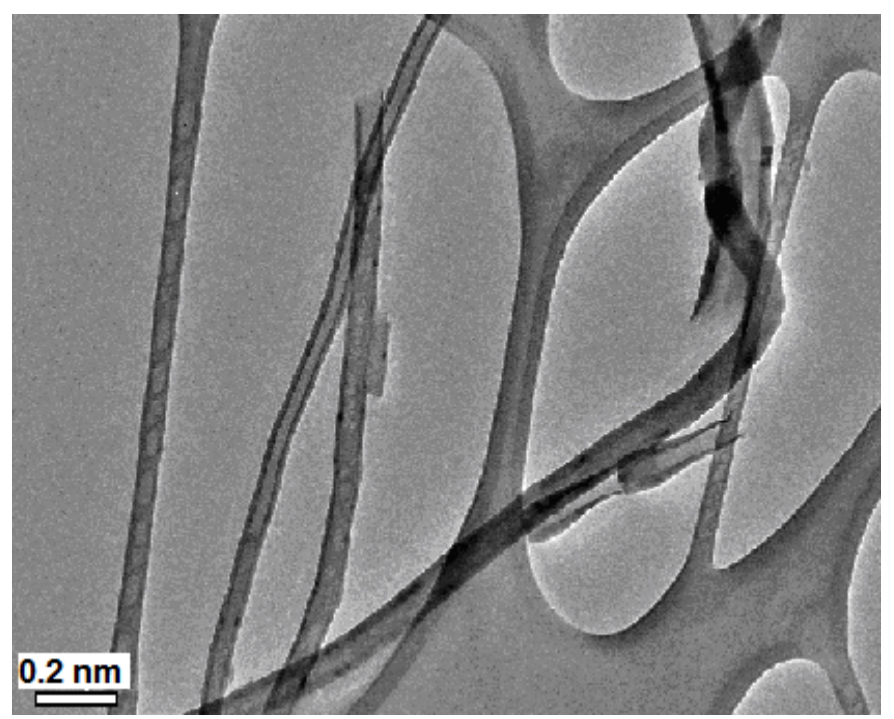


(d) MWNT G with OD 20-40 nm and length up to 200 μm

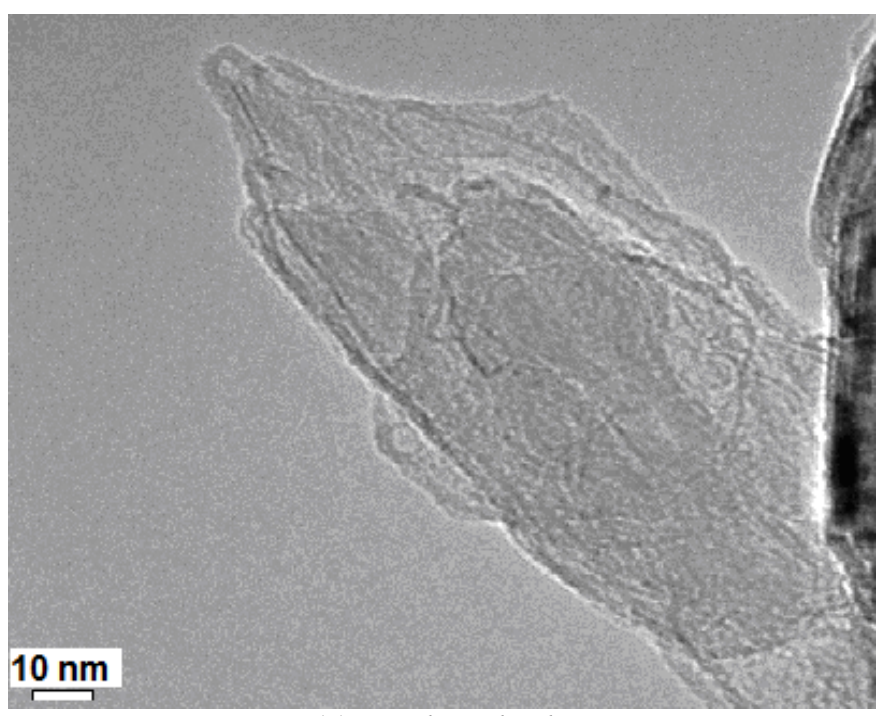


(e) Oxidized Nanofibers (NF-OX) with 60-150 nm outer diameter

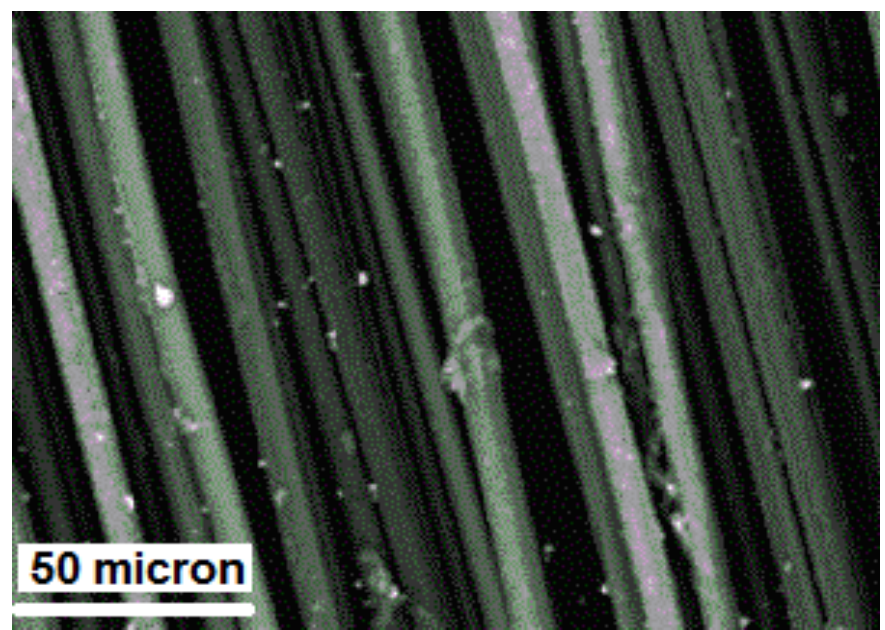
Figure 2.3 (cont'd)



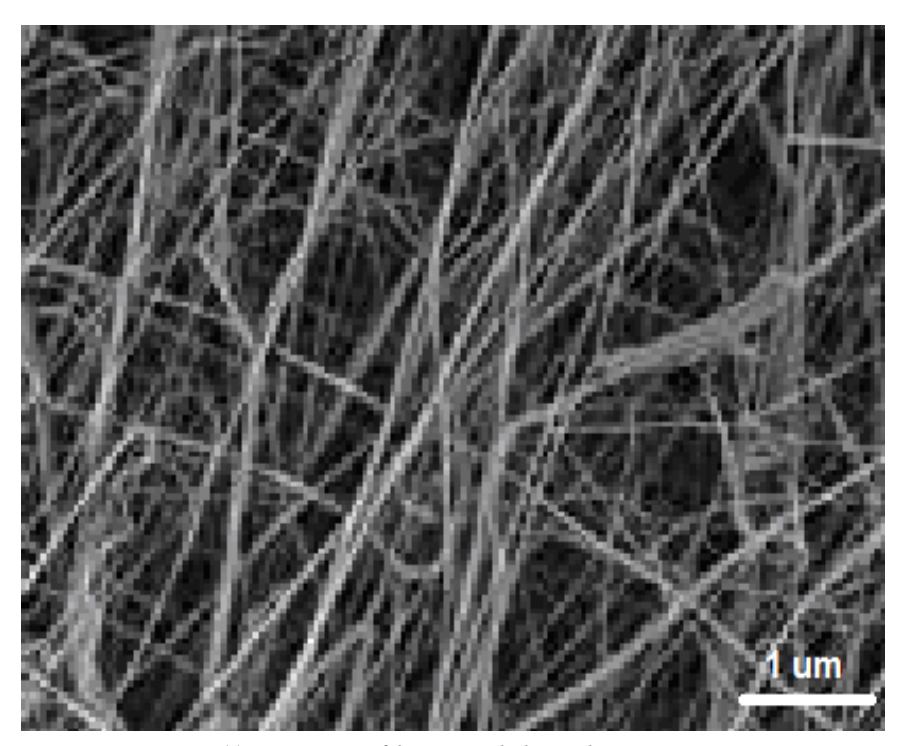
(f) Plain Nanofibers (NF) with 60-150 nm outer diameter



(g) Graphite platelet



(h) TT 143 microfibers with length of 6 mm



(i) PP microfibers with length 19 mm

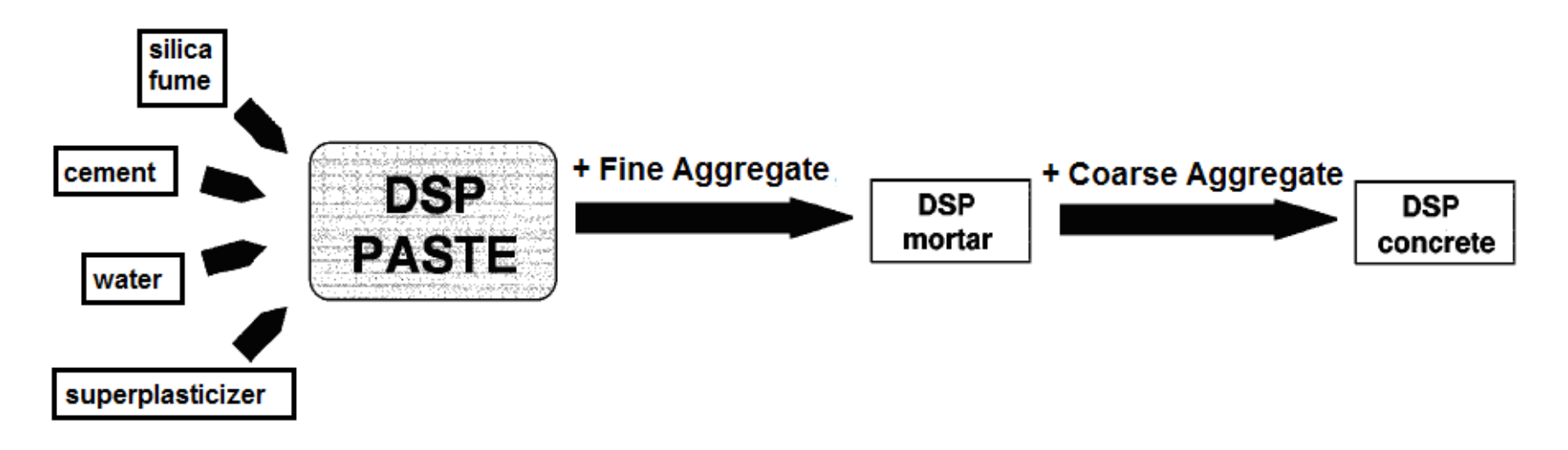


Figure 2.4- DSP cementitious paste, mortar and concrete.(Guerrini 2000)

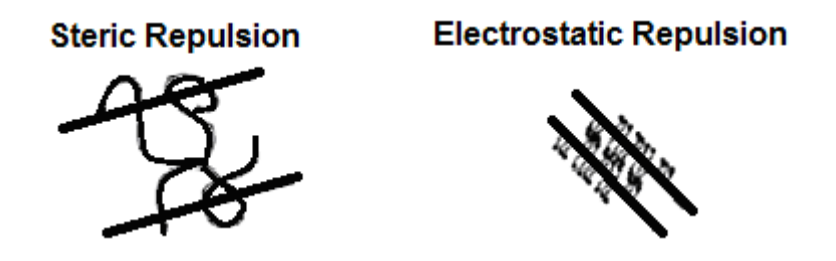


Figure 2.5- Steric and electrostatic repulsion of separated nanotubes.

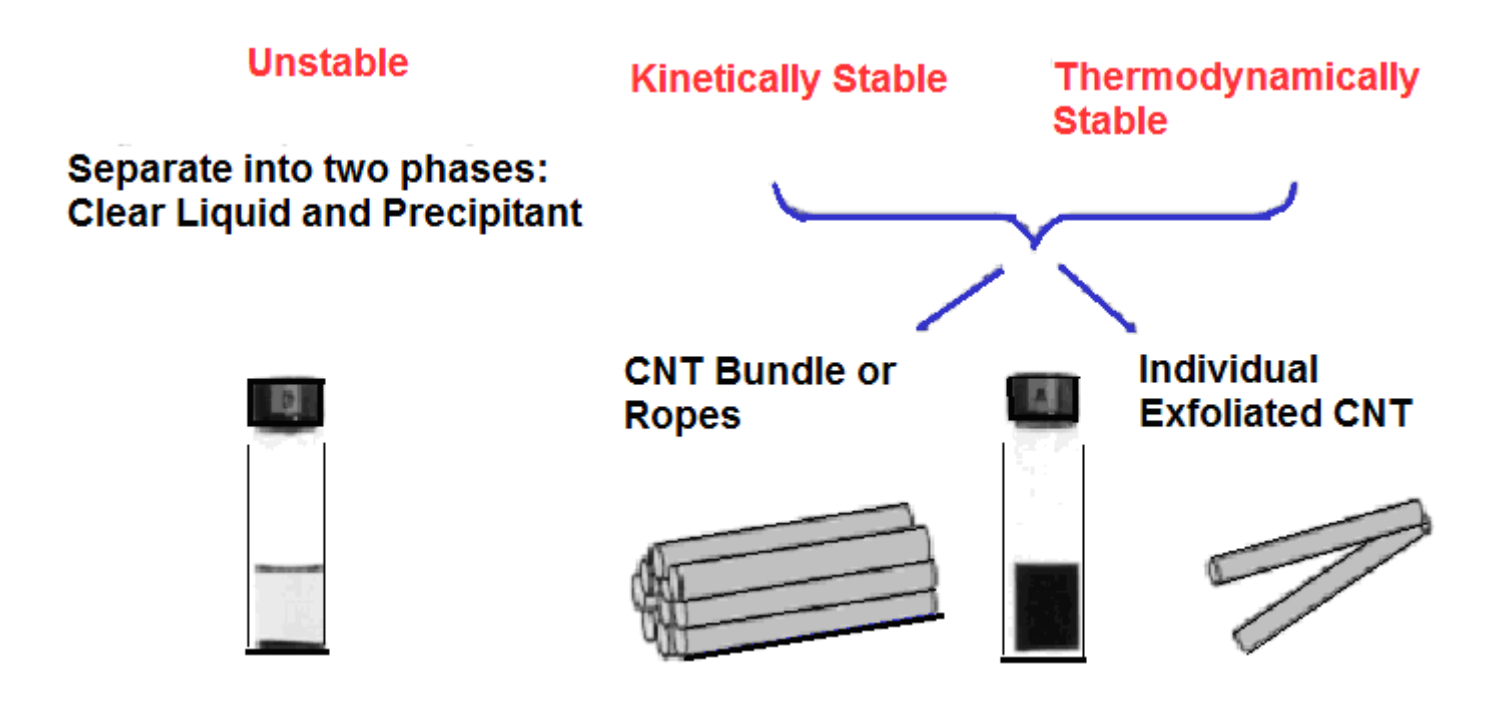


Figure 2.6- Dispersion and stability conditions of carbon nanotubes in aqueous media.

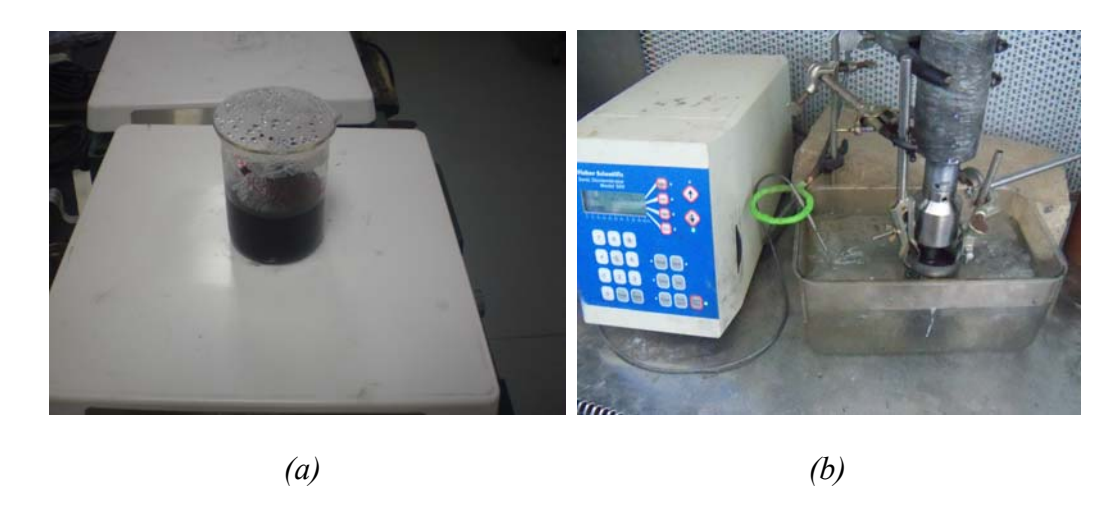


Figure 2.7- Dispersion equipment: (a) Magnetic stirrer (b) Sonic horn.



Figure 2.8- Experimental setups.

(e) Abrasion

(d) Impact

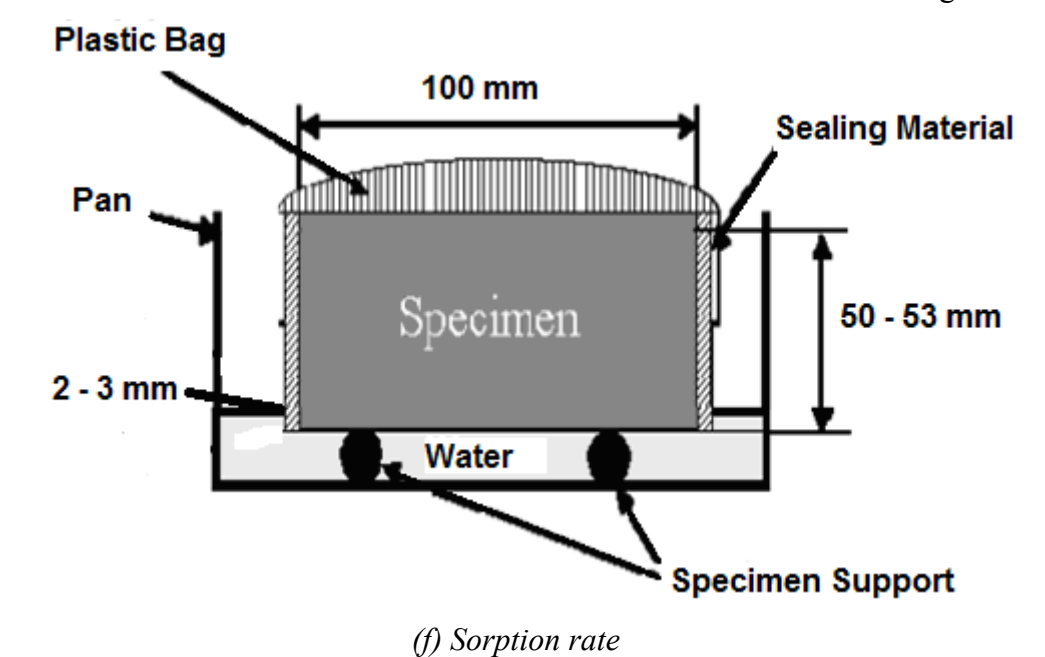




Figure 2.9- Durability test systems.

(d) Elevated Temperature

(c) Hot Water Immersion

Figure 2.9 (cont'd)



(e) Sonometer

3 REINFORCEMENT OF HIGH-PERFORMANCE CEMENTITIOUS MATRICES WITH RELATIVELY LOW VOLUME FRACTIONS OF GRAPHITE NANOMATERIALS

3.1 General

Graphite nanomaterials would realize their reinforcement potential as far as they are thoroughly dispersed within cement-based matrices, and also develop primary bonds with cement hydrates. Thorough dispersion of graphite nanomaterials in the aqueous medium of fresh cementitious matrix encounters challenges associated with the hydrophobic nature of nanomaterial surfaces as well as the strong tendency towards agglomeration due to the attractive van der Waals forces over the enormous surface area of graphite nanomaterials. Effective interfacial interactions with cement hydrates are further challenged by the largely inert nature of nanomaterial surfaces. The research reported herein developed surface functionalization techniques to improve the dispersion and interfacial interactions of graphite nanomaterials in cement-based matrices without compromising their highly desired structure and engineering properties. The covalent functionalization techniques considered here included acid-oxidation under mild conditions, and fluorination/carboxylation. The reinforcement efficiencies of different graphite nanomaterials were evaluated at relatively low volume fractions in a high performance cementitious matrix.

3.2 Introduction

Cement- and concrete-based materials offer suitable engineering properties (compressive strength, moisture resistance and durability) at low cost, combined with energy-saving and

ecological benefits. They are the most widely used class of manufactured materials worldwide. Cement-based materials offer important advantages over competing construction materials in terms of ecological impact (pollution, deforestation, use of exhaustible raw materials, etc.) (Mehta 1993). Cement-based materials, however, lack adequate toughness and impact resistance; further improvement of their durability in aggressive environments would also yield major benefits in terms of the life-cycle cost of infrastructure systems. The main thrust of this research is to make effective use of the unique geometric and mechanical attributes of graphite nanomaterials towards achieving these needed improvements in concrete properties.

Enhancement of cement-based materials with graphite nanomaterials draws upon the experience gained with reinforcement of cement-based materials with micro-scale fibers. Graphite nanomaterials offer unique reinforcement qualities in cementitious materials, which can benefit applications requiring high levels of structural performance, durability and safety.

Graphite nanomaterials, when compared with today's (micro-scale) fibers, offer distinctly high mechanical and physical attributes, tremendous specific surface areas, and close spacing within matrix even at relatively low volume fractions of about 0.1%. These advantages of graphite nanomaterials can be realized as far as they are thoroughly dispersed within the cementitious matrix, and effectively interact with cement hydrates. The high surface area of nanomaterials generates strong tendencies towards agglomeration via van der Waals interactions. The largely inert surfaces of graphite nanomaterials also offer limited potentials for strong bonding to cement hydrates. This paper presents an investigation into modifications of nanomaterials for enhancing their dispersion and interfacial interactions, and thus reinforcing effects in cementitious material.

3.3 Materials and Methods

3.3.1 Graphite Nanomaterials and Microfibers

Different types of acid-functionalized and non-functionalized multiwalled carbon nanotubes as well as carbon nanofibers, graphite nanoplatelets and chopped (micro-scale) carbon fibers were evaluated for use in cement-based nanocomposites. These graphite nanomaterials and carbon microfibers have been introduced in detail in Chapter 2, Section 2.4and Table 2.3. Multiwalled carbon nanotubes (MWNT A, MWNT B and MWNT C), carbon nanofibers (CNF1, CNF, CNF-OX), graphite nanoplatelets (GP1, GP) and carbon microfibers (CMF) were used in high-performance cement-based paste and mortar matrices, Fig 2.3.

Acid Oxidation (Fig. 1.11) involves refluxing graphite nanomaterials in sulfuric/nitric acid (3/1 volume ratio). The process can introduce a relatively high concentration of carboxyl (-COOH) groups on the surface of graphite nanomaterials; it also generates other (e.g. –OH) groups. After functionalization, carboxylated nanotubes would typically have 2-7 wt.% COOH (measured by titration).

Direct fluorination of carbon nanotubes adds fluorine to the sidewalls of nanotubes to dramatically enhance their chemical reactivity (accompanied by some changes in physical properties). Direct fluorination is carried out by heating carbon nanotubes in the presence of hydrogen and fluorine (Fig. 1.13). The reaction causes *in-situ* generation of HF which, in turn, acts as catalyst for fluorination. After fluorination, π -bonds get more activated, and other electron-rich molecules can be covalently added to fluorinated surfaces. For effective interactions with cement hydrates, fluorinated graphite nanomaterials were reacted with succinic acid peroxide (1:10 weight ratio of fluorinated nanomaterial to succinic acid peroxide) at 90° C

over 24 hours. The intermolecular elimination of HF in the reaction results in the formation of ethylcarboxylate-functionalized graphite nanomaterials.

3.3.2 Cementitious Matrices, Mixing and Curing Procedure

Dense cement-based matrices with a smooth particle size gradation covering nano- to microscale range promise to effectively mobilize the tremendous mechanical qualities of graphite nanomaterials within cementitious nanocomposites. The cementitious matrices selected have been introduced in detail in Chapter 2, Section 2.5. Both DSP (Densified with Small Particles) paste and mortar matrices were use to evaluate the reinforcement efficiency of both graphite nanomaterials and carbon microfibers at relatively low volume fractions.

Cementitious materials with and without functionalized and non-functionalized graphite nanomaterials dispersed in the mixing water via sonication, described in detail in Chapter 2, Section 2.5.2) and/or microfibers, were prepared following ASTM C 192 and C 305 procedures as described in the same section.

3.3.3 Experimental Methods

The test procedures employed to determine the engineering properties of cement-based nanocomposites are described in this section and have been discussed in detail in Chapter 2, Section 2.6. *Compressive Strength* tests (ASTM C 109), *flexure* tests (ASTM C 1185), *Impact* tests (ASTM D 7136), *abrasion* tests (ASTM C 944) and *moisture absorption rate* tests (ASTM C 1585) were performed to estimate the engineering and durability properties of high-performance cement-based nanocomposites.

The following experimental methods were also employed to gain further insight into the chemistry, crystallinity, microstructure and failure mechanisms of cement-based

nanocomposites: (i) SEM; (ii) XRD; (iii) DT/TGA; (iv) XPS; (v) Raman Spectrometry; and (vi) FTIR. Graphite nanomaterials were also evaluated prior to and after functionalization.

3.4 Characterization of Non-Functionalized and Functionalized Graphite Nanomaterials

3.4.1 FTIR Spectrometry

ATR FTIR spectra for three types of multiwalled carbon nanotubes and the carbon nanofiber considered in this experimental program were obtained after acid oxidation (Fig. 3.1a). Since surfaces of carbon nanotubes and nanofibers were oxidized with nitric acid, the peak at 1648 cm⁻¹ is associated with C=O stretching of carboxylic acids. This indicates that treatment with the strong oxidizing acid led to attachment of oxygen-containing groups (such as carboxylic and hydroxyl) to the carbon nanotube and nanofiber surfaces. The peak near 3400 cm⁻¹ is associated with the -OH stretching mode of the -COOH group.

Since ATR FTIR offers relatively low detection limit and sensitivity, a transmission FTIR device equipped with more sensitive MCT (Mercury Cadmium Telluride) detector was used to further investigate the relatively low concentration of functional groups introduced after acid oxidation upon carbon nanotubes and nanofibers. Fig. 3.1b and c present the transmission FTIR spectra of a multiwalled carbon nanotube prior to and after acid oxidation. Like graphite, pristine nanotubes have featureless FTIR spectra with extremely low infrared absorption intensities. After acid-oxidation, two new bands appear at 1715 and 1160 cm⁻¹, which are attributed to the C=O and C-O stretching vibrations, respectively, of the carboxylic group (-COOH). Peaks at 1635 and 1560 cm⁻¹ are due to C=C stretching. The intense, broad line centered at 3422 cm⁻¹ is associated with

the –OH stretching mode of the –COOH group. The increase in relative intensities of bands at 1068 and 3420 cm⁻¹ suggests a rise in –OH groups on nanotube surfaces after acid-oxidation. Similar trends are observed in the case of acid-functionalized carbon nanofiber (Fig. 3.1d).

The FTIR spectra for a multiwalled carbon nanotube prior to and after fluorination and ethyl carboxylation are presented in Fig. 3.2. After fluorination, the appearance of C=C and C-F bonds confirms the success of fluorination. No peaks at these wave numbers were observed in pristine multiwalled carbon nanotubes. After ethyl carboxylation, a new peak was observed at ~1700 cm⁻¹ confirming carboxylation.

3.4.2 Scanning Electron Microscopy

Comparison of the SEM images of multiwalled carbon nanotubes prior to and after fluorination (Fig. 3.3) did not reveal appearance of additional defects on nanotube surfaces after fluorination. The surfaces appear even smoother after fluorination (pointing at "Teflonization").

3.4.3 Raman Spectrometry

The Raman spectra of two types of multiwalled carbon nanotubes (MWNT A & B) prior to and after fluorination were used for diagnosis of the nanotube type. The D mode (the disorder band located between1330-1360 cm⁻¹, when excited with a visible laser) is associated with multiwalled nanotubes. However, when observed with single-walled nanotubes, one assumes that it is due to the presence of defects. The G mode or (TM- Tangential Mode), located around 1580 cm⁻¹, corresponds to the stretching mode in the graphite plane. The results presented in Fig. 3.4 suggest that, after fluorination, MWNT A shows downshifts in the positions of both D (~ 1300 cm⁻¹) and G (near 1600 cm⁻¹) peaks due to the fluorine groups attached to the nanotube

sidewalls. However, MWNT B shows a 4 cm⁻¹ downshift of only the G peak due to a smaller bulk amount of fluorine as compared to the smaller-diameter MWNT A.

3.4.4 X-Ray Photoelectron Spectroscopy (XPS)

Table 3.1 presents the elemental analyses obtained for MWNT A (20-40 nm diameter) and MWNT B (60-100 nm diameter) in pristine condition and after fluorination (at different temperatures) and subsequent ethyl carboxylation, confirming the introduction of fluorine and oxygen atoms upon fluorination and subsequent carboxylation, respectively.

Introduction of fluorine and oxygen atoms with electron negativity onto the MWNT surfaces can significantly change the chemical environment of carbon atoms. Figs 3.5a and 3.5b show the C_{1s} high resolution spectra (red curves) obtained for fluorinated (at two different temperatures) and subsequently carboxylated MWNTs (with two different diameters). Unlike pristine nanotubes, an asymmetric peak is observed for the C_{1s} high resolution XPS spectrum. This indicates that carbon atoms are in different environments, which is an indication of successful functionalization. The main peak centered at 284.12 eV (Electron Volts) was assigned to carbon atoms bound to hydrogen atoms. The peak at 284.32 eV originated from the sp3–hybridized carbon atoms. Peaks at 285.57, 288.65 and 290.95 eV are assigned to carbon atoms bound to oxygen atoms and fluorine atoms, respectively. Carbon atoms bound to oxygen and fluorine could lead to higher binding energies because of their high electron negativity.

3.5 Engineering Properties, Structure and Failure Modes of Cementitious Nanocomposites

3.5.1 Engineering Properties

Typical flexural load-deflection behavior of the high-performance cementitious (DSP) paste without any reinforcement and with 0.08 vol.% (volume fractions of dry cementitious materials) of different acid-functionalized graphite nanomaterials (and micro-scale carbon fibers) are presented in Fig. 3.6. With proper functionalization, graphite nanomaterials are observed to yield (at only 0.08 vol.%) important gains in the flexural strength and energy absorption capacity (area underneath the load-deflection curve) of cement-based matrix.

Fig. 3.7 with mix designation given in Table 3.2, summarizes the effects of different graphite nanomaterial types and functionalization conditions, at 0.08 vol.%, on the flexural performance, abrasion resistance, moisture sorption rate and compressive strength of the high-performance cementitious (DSP) paste. Analysis of variance of test results confirmed that functionalized graphite nanomaterials at 0.08 vol.% yield statistically significant gains (at 0.05 significance level) in the flexural strength and energy absorption capacity, abrasion resistance and moisture sorption resistance of the high-performance cementitious paste. The corresponding effects of graphite nanomaterials on compressive strength were not statistically significant. Functionalization of graphite nanomaterials via acid-oxidation and, to a generally smaller extent, fluorination/carboxylation, led to improved reinforcement efficiency of graphite nanomaterials in cementitious paste. Analysis of variance, followed by pair-wise comparisons, of test results indicated that the acid-oxidation effects on the reinforcement efficiency of graphite nanomaterials at 0.08 vol.% were statistically significant at 0.05 significance level as far as

flexural strength and energy absorption capacity, maximum deflection and abrasion resistance are concerned. In the case of resistance to moisture sorption, the acid-oxidation effect was statistically significant at 0.02 significance level. The maximum improvement in all engineering properties was achieved with oxidized MWNT B.

Analysis of variance of test results followed by pair-wise comparisons indicated that the microscale carbon fiber is inferior to all nano-scale reinforcement systems considered here (at 0.05 significance level) as far as the flexural strength and energy absorption capacity, and moisture sorption resistance of the cementitious paste are concerned. The large variations in abrasion test results lowered the statistical confidence in superiority of graphite nanomaterials over the microscale carbon fiber in improving the abrasion resistance of cementitious paste.

Graphite nanoplatelets were introduced in non-functionalized form into the high-performance (DSP) cementitious paste at 0.08 vol.% with the primary objective of lowering the moisture sorption rate by forcing a tortuous diffusion paths. The mean moisture sorption rate was lowered by more than 50% with 0.08 vol.% of non-functionalized graphite nanoplatelets. This effect was statistically significant at 0.05 level of significance.

Fig. 3.8 with mix designations in Table 3.3, summarizes the effects of introducing a very low volume fraction (0.03 vol.%) of acid-functionalized multi-walled carbon nanotube and oxidized carbon nanofiber on the flexural performance, abrasion resistance, moisture sorption rate and compressive strength of the high-performance (DSP) mortar. The gains in flexural energy absorption capacity, maximum deflection and abrasion resistance were statistically significant at 0.05 level of significance for both MWNT A and B. The gains in flexural strength and compressive strength were not statistically significant for this very low nanomaterial volume fraction.

The introduction of acid-functionalized multiwalled carbon nanotube MWNT B led to a more complex failure mode (involving more extensive cracking) of the high-performance cementitious (DSP) paste under impact loading (Fig. 3.9a). The failure modes in flexure (Fig. 3.9b) and abrasion (Fig. 3.9c) did not undergo obvious changes with introduction of ≤0.08 vol.% of graphite nanomaterials.

3.5.2 Transmission and Scanning Electron Microscopic Investigations

The failed surfaces of flexure and compression test specimens were evaluated under a high-precision scanning electron microscope (JOEL JM-6300F). All samples were coated with Osmium (Using Osmium Coater Neoc-AN, Meiwa Shoji) prior to SEM observations.

A transmission electron microscope (TEM) image of the multiwalled carbon nanotube MWNT B after acid-oxidation followed by nucleation of cement hydrates on their surfaces is shown in Fig. 3.10a. One can distinguish the nucleated cement hydrates formed upon the functionalized nanotube surfaces. SEM images of the cementitious matrix with 0.04% volume fraction of multiwalled carbon nanotubes subjected to acid-oxidation followed by nucleation of cement hydrates (Fig. 3.10b) suggest that the carbon nanotubes exposed at the failed surface of flexure test specimens are thoroughly coated with cement hydration products. Debonding seems to have taken place away from the actual interface within the matrix, which points at the adequately strong bond developed between the functionalized nanotubes and the cementitious matrix. The SEM images of Fig. 3.10b provide indications for the uniform dispersion of individual acid-functionalized carbon nanotubes within the cementitious matrix.

SEM images of cementitious pastes reinforced with 0.08% volume fraction of acidfunctionalized graphite nanomaterials provided strong evidence for the bridging and pull-out actions of carbon nanotubes and nanofibers at microcracks (Fig. 3.11), which are key to their contributions to the flexural strength and energy absorption capacity of cementitious matrices.

While the functionalized multiwalled carbon nanotubes and nanofibers were largely dispersed within the cementitious paste, some bundling of nanomaterials occurred at the higher volume fraction of 0.08 vol.%. Even the bundled graphite nanomaterials exhibited positive effects through arrest and deflection of microcracks (Fig. 3.12).

The cementitious paste matrix with 0.08 vol.% of acid-functionalized microfibers exhibited thorough dispersion of fibers, with relatively large fiber spacing. The prevalent failure mode involved pullout of microfibers (Fig. 3.13).

3.5.3 X-Ray Diffraction (XRD) Analysis

XRD Analysis was carried out on two cementitious pastes with 0% and 0.04 vol.% of acid-functionalized MWNT A using Rotaflex Rigaku 200B Analyzer. The spectrum was analyzed using JADE to identify various elements according to their crystalline structure.

The XRD graphs of the two cementitious materials (Fig. 3.14) exhibit no significant differences, indicating that there were no major changes in the crystalline structure of the matrix with introduction of a low volume fraction (0.04 vol.%) of acid-functionalized multi-walled carbon nanotube. The two major compounds identified in these two cementitious materials were calcium silicate (Ca₃SiO₅) and calcium silicate oxide (Ca₃(SiO₄)O). As compared to the XRD graph of a conventional cement mortar, the typical calcium hydroxide peaks were not observed; this points at substantial conversion of calcium hydroxide to calcium silicate hydrate via pozzolanic reactions involving silica fume.

3.5.4 Thermogravimetric Analysis (TGA)

Thermogravimetric analyses of the high-performance cementitious paste matrix, plain or with acid-functionalized graphite nanomaterials were performed using the TA Instrument Hi-Res TGA 2950 Thermogravimetric Analyzer. A sample of conventional mortar having 1: 1.22: 0.45, cement: sand: water ratio was also tested in order to identify their differences. A finely ground powder (passing 100 mesh) of the material was used in thermogravimetric analysis. The samples were heated at a constant rate of 10°C per minute up to 1000°C, with weight loss recorded as a function of temperature. Tests were conducted 21 days after casting of the cementitious samples. The results of thermogravimetric analysis are summarized in Fig. 3.15; some interpretations of these results are presented below.

- The peak in weight loss between 450°C and 500°C is assumed to be due to C-H dehydration. This peak is quite strong for conventional mortar, and weak for all high-performance (DSP) matrices, which indicates the presence of more calcium hydroxide in conventional mortar than in DSP matrices. This has been confirmed by scanning electron microscopic analyses where C-H crystals are found only rarely in DSP matrices. This finding could be anticipated because the relatively high dosage of silica fume used in DSP matrices converts C-H to C-S-H through pozzolanic reactions.
- The initial loss of mass from 100°C to 122°C is assumed to be due to the loss of physically held water, and from 600°C to around 797°C due to high-temperature decomposition of CaCO₃ (Calcium Carbonate). The physically held water content of DSP paste is greater than that of conventional mortar, which could be attributed to the higher

surface area of the hydration products present in DSP paste. The young age of the cementitious materials tested implies that the CaCO₃ content is relatively small. Over time, the higher C-H content of the conventional mortar (which is prone to carbonation) could increase its CaCO₃ content when compared with DSP paste.

- The mass loss from 819°C to 899°C, observed only for DSP samples which contain silica fume, is characteristic of the calcium silicate hydrate (C-S-H(I)) with CaO/SiO₂<1.5, which forms primarily through pozzolanic reaction. This effect is caused by the reorganization of the lattice network of anhydrous calcium silicate.
- For the purpose of evaluating the chemically bound water in C-S-H, with a certain degree of approximation, only the mass loss between 100°C to 400°C was considered. This approximation helps avoid the errors caused by the possible presence of CaCO₃ and the mass loss associated with its decomposition at higher temperatures (around 800°C), and by the presence of free water below 100°C. The maximum weight loss of 9.49% occurs for DSP Paste containing 0.08 vol.% of carbon nanofiber, followed by 7.88% for the case with acid-functionalized MWNT B. The acid-functionalized and fluorinated MWNT A had weight losses of 6.57% and 6.29%, respectively, as compared to 6.87% for plain DSP paste. In conventional mortar, the total weight loss was 3.93%. These results indicate that more water is chemically bound with C-S-H in the high-performance cementitious material (DSP paste) when compared with conventional mortar. The effect of a low

volume fraction (0.08%) of functionalized nanotubes on the C-S-H content of DSP paste is observed to be relatively small.

• Total weight loss is greater for the high-performance cementitious material (DSP paste), at 18.0% for plain DSP paste, and 17.5% with fluorinated MWNT A, 17.4% with carbon nanofiber, 17.3% with MWNT B and 16% with acid-functionalized MWNT A as compared to 10.2% for the conventional mortar. This could result from a greater content of hydration products in DSP paste when compared with the conventional mortar (which partly results from the presence of sand in conventional mortar).

The findings of thermogravimetric analysis confirm the outcomes of XRD analysis, which suggests that the introduction of acid-functionalized graphite nanomaterials does not alter the chemistry and crystalline structure of cement hydration products.

3.5.5 Energy-Dispersive Spectroscopy (EDS)

Elemental analyses were performed on 2.5x12x12 mm samples of cementitious materials with and without acid-functionalized graphite nanomaterials. The specimens were coated with carbon (using Carbon String Evaporator, Ernest F. Fullam) to make them more conductive for the purpose of EDS analysis. Elemental (EDS) analyses of cementitious matrices with 0 and 0.08 vol.% of acid - functionalized carbon nanotube or nanofiber indicated that cementitious matrices with graphite nanomaterials exhibit elemental compositions similar to those of the plain cementitious matrix, except for the higher carbon content in systems incorporating graphite nanomaterials. This is in line with the findings of x-ray diffraction and thermogravimetry analyses, indicating that introduction of functionalized graphite nanomaterials did not alter the chemistry of cement hydration products.

3.6 Summary

Graphite nanomaterials (multi-walled carbon nanotube, carbon nanofiber and graphite nanoplatelet) were evaluated as reinforcement systems in cement-based materials. While the excellent mechanical and physical characteristics as well as the distinct geometric attributes of graphite nanomaterials promise superior reinforcement efficiency in cement-based matrices, there are challenges associated with their dispersion and interfacial interactions within cementbased materials. Uniform dispersion of graphite nanomaterials in an aqueous medium is complicated by the predominantly hydrophobic nature of nanomaterial surfaces and the strong tendency towards agglomeration driven by van der Waals attractions between the enormous surface areas of graphite nanomaterials. The largely inert surfaces of nanomaterials cannot effectively bond to cement hydrates, which lower the interfacial stress transfer needed to mobilize the enormous mechanical qualities of graphite nanomaterials. Complementary covalent functionalization techniques were developed to address these challenges and improve the reinforcement efficiency of graphite nanomaterials in cement-based matrices. The methods developed for covalent functionalization included acid-oxidation under mild conditions, and fluorination/ethyl carboxylation, both of which introduced carboxyl groups via primary bonds upon graphite nanomaterials. Preparation of cement nanocomposites involved careful dispersion of functionalized graphite nanomaterials via sonication in the mixing water, followed by conventional mixing, molding and steam curing of the nanocomposites. The nanomaterial volume fractions considered included 0.04% and 0.08 vol.% (in cementitious pastes) and 0.03 vol.% in mortar. Replicated mixes and tests were considered to provide the basis for statistically reliable inferences.

Table 3.1- Elemental analysis of fluorinated MWNTs and ethyl carboxylated MWNTs.

Sample	C _{1s}	F _{1s}	O _{1s}	
MWNT A	97.4	1.0	1.6	
150°C F-MWNT A	70.4	25.8	3.7	
150°C F-MWNT A-(CH ₂) ₂ -COOH	74.2	19.7	6.1 (notable ethyl carboxylation)	
250°C F-MWNT A	69.8	29.1	1.1	
250°C F-MWNT A-(CH ₂) ₂ -COOH	72.7	24.8	2.6 (notable ethyl carboxylation)	
150°C F-MWNT B	70.2	25.9	3.9	
150°C F-MWNT B-(CH ₂) ₂ -COOH	74.7	20.8	4.4 (notable ethyl carboxylation)	
250°C F-MWNT B	63.5	33.7	2.8	
250°C F-MWNT B-(CH ₂) ₂ - COOH	65.4	31.2	3.4 (minor ethyl carboxylation)	

Table 3.2- Mix designations of DSP pastes reinforced with non-functionalized and functionalized graphite nano and micro reinforcements at 0.08 vol.%.

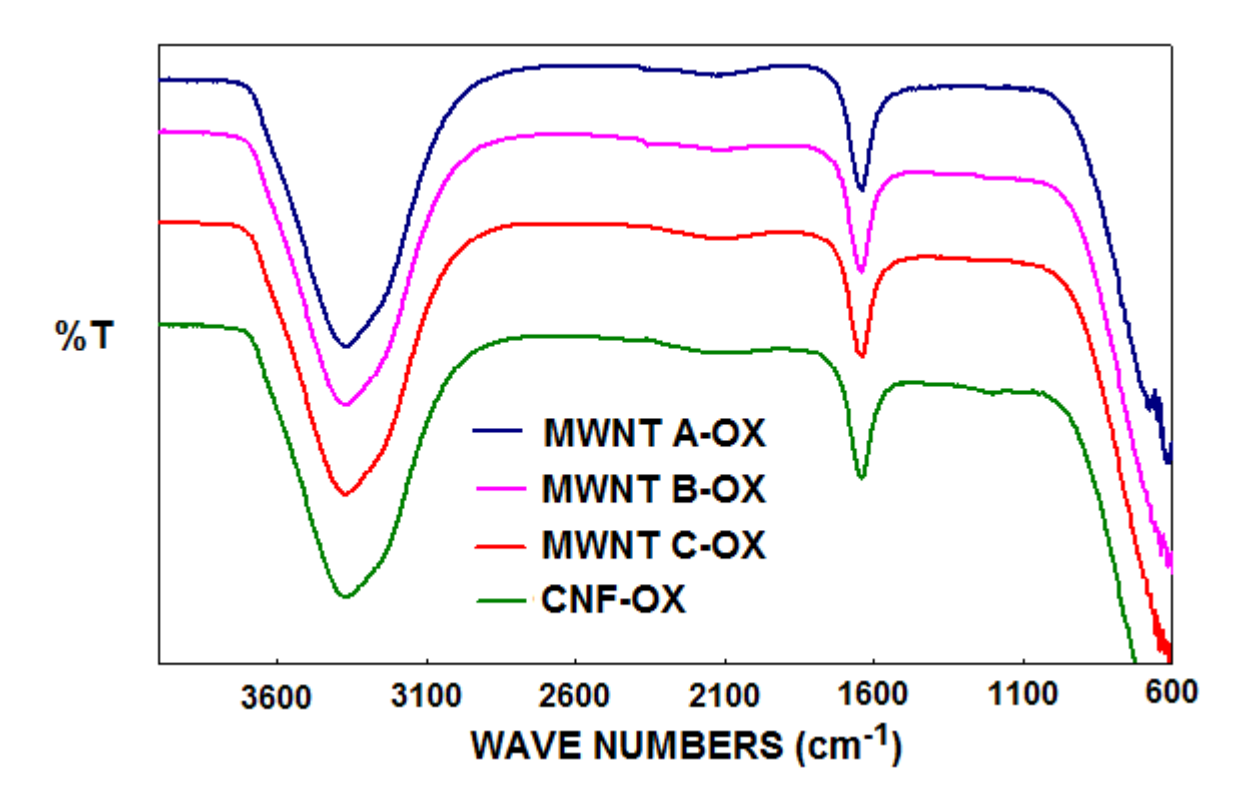
Reinforcement Condition	Mix Designation
Plain	1
Non-functionalized MWNT A, 0.08 vol.%	2
Acid-functionalized MWNT A, 0.08 vol.%	3
Fluorinated MWNT A, 0.08 vol.%	4
Non-functionalized MWNT B, 0.08 vol.%	5
Acid-functionalized MWNT B, 0.08 vol.%	6
Fluorinated MWNT B, 0.08 vol.%	7
Acid-functionalized CNF1, 0.08 vol.%	8
GP1, 0.08 vol.%	9
Acid-functionalized CMF, 0.08 vol.%	10

vol.% - volume percent with respect to dry cementitious materials

Table 3.3- Mix designation of high-performance DSP mortar with functionalized graphite nanomaterials at 0.03 vol.%.

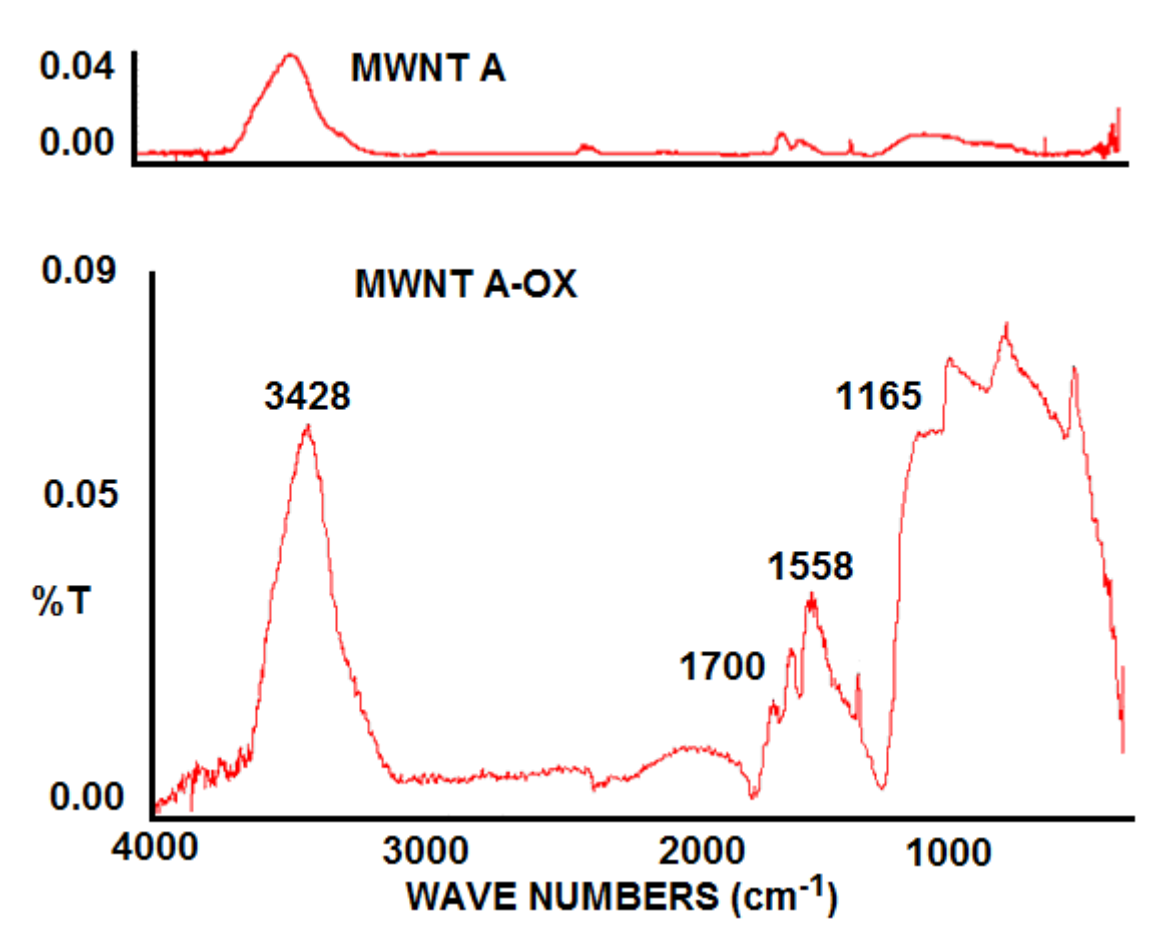
Reinforcement Condition	Mix
	Designation
Plain	1
Acid-functionalized MWNT A, 0.03 vol.%	2
Acid-functionalized MWNT B, 0.03 vol.%	3
Acid-functionalized Carbon Nanofiber, 0.03 vol.%	4

vol.% - volume percent with respect to dry cementitious materials



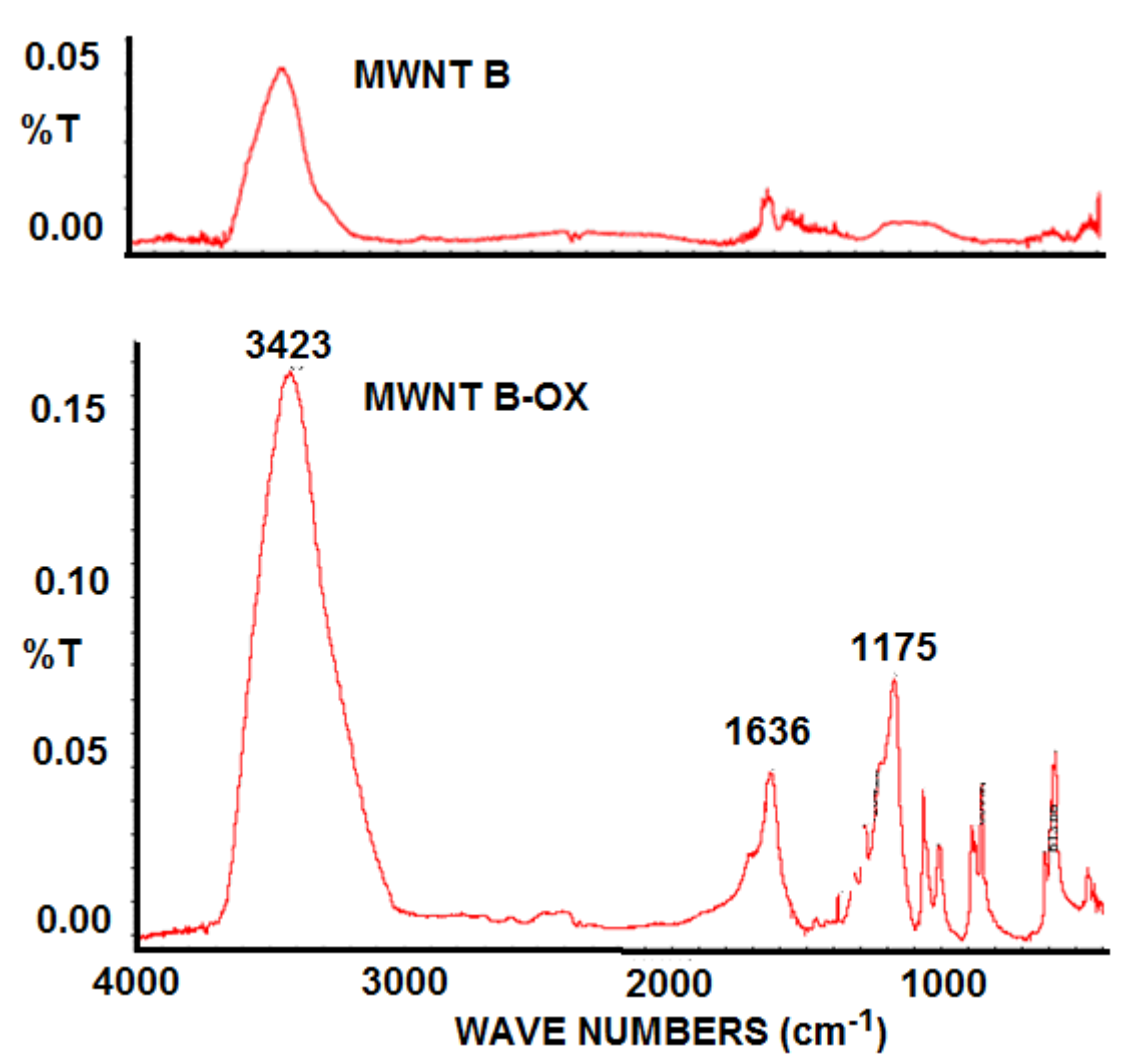
(a) FTIR spectra for three types of carbon nanotubes and one type of carbon nanofiber after acid oxidation

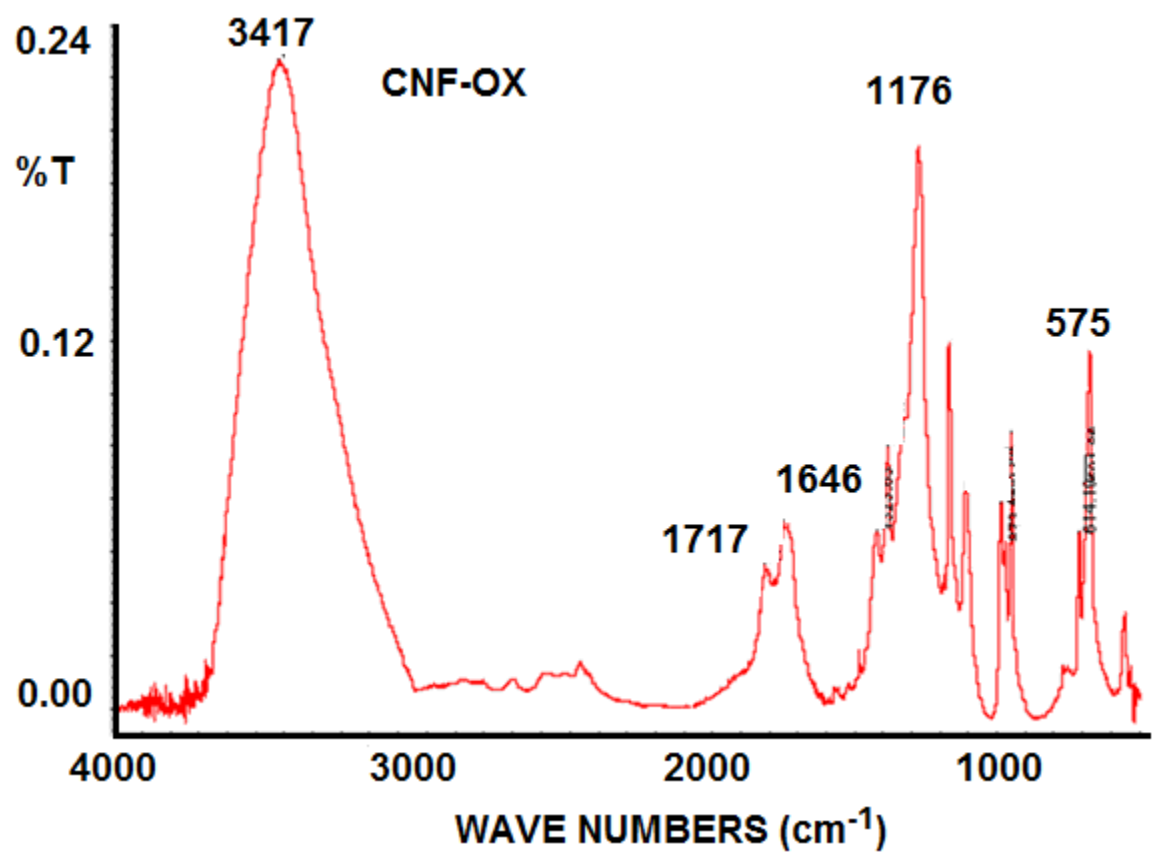
Figure 3.1 - FTIR spectra of pristine and acid-functionalized carbon nanotubes and nanofibers.



(b) MWNT A prior to and after acid-oxidation

Figure 3.1 (cont'd)





(d) Acid-oxidized carbon nanofiber

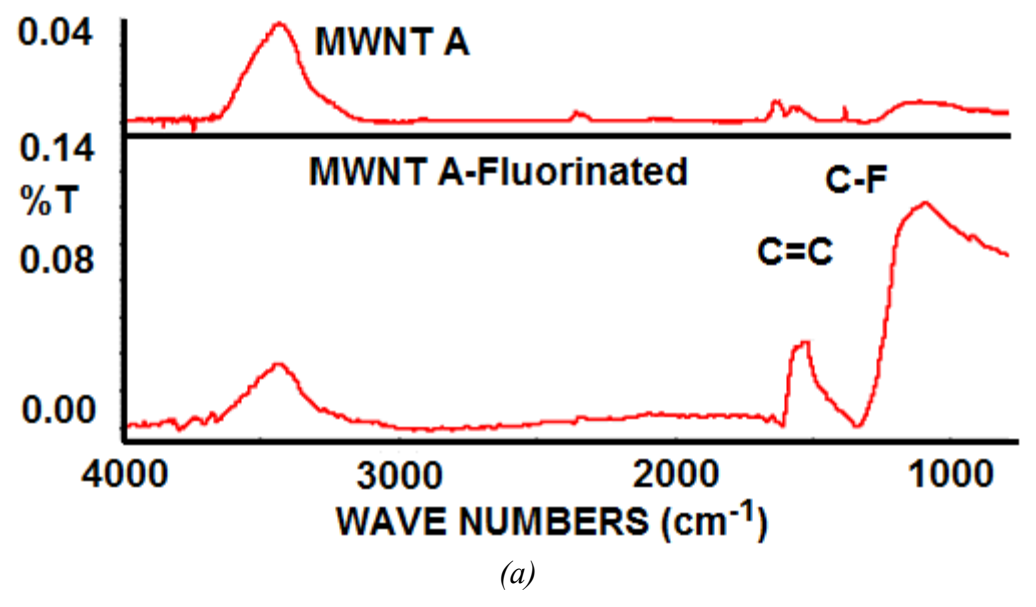
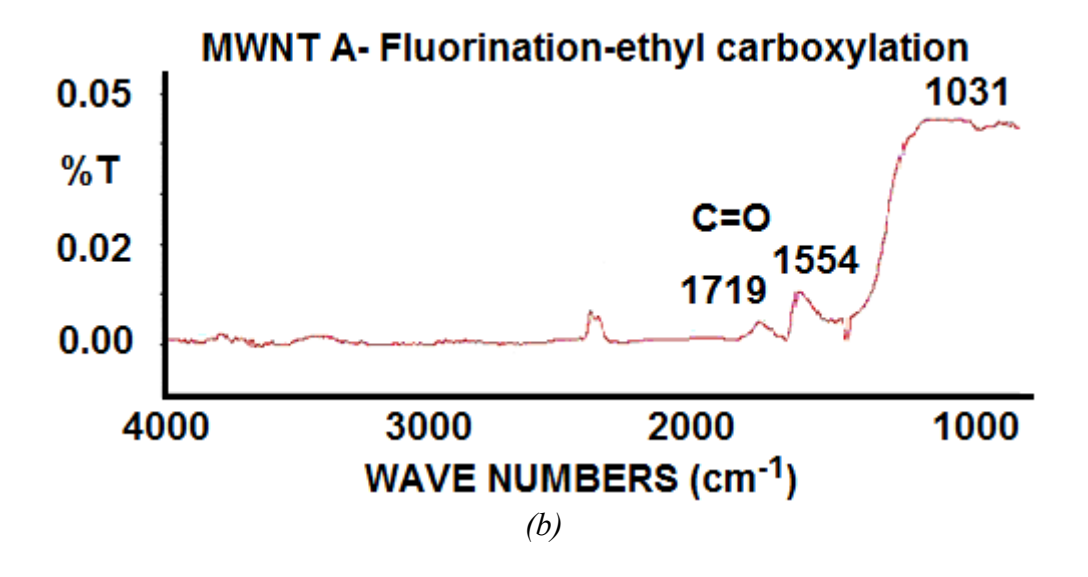


Figure 3.2- FTIR spectra for MWNTs A prior to and after fluorination, and after ethyl carboxylation upon fluorination.



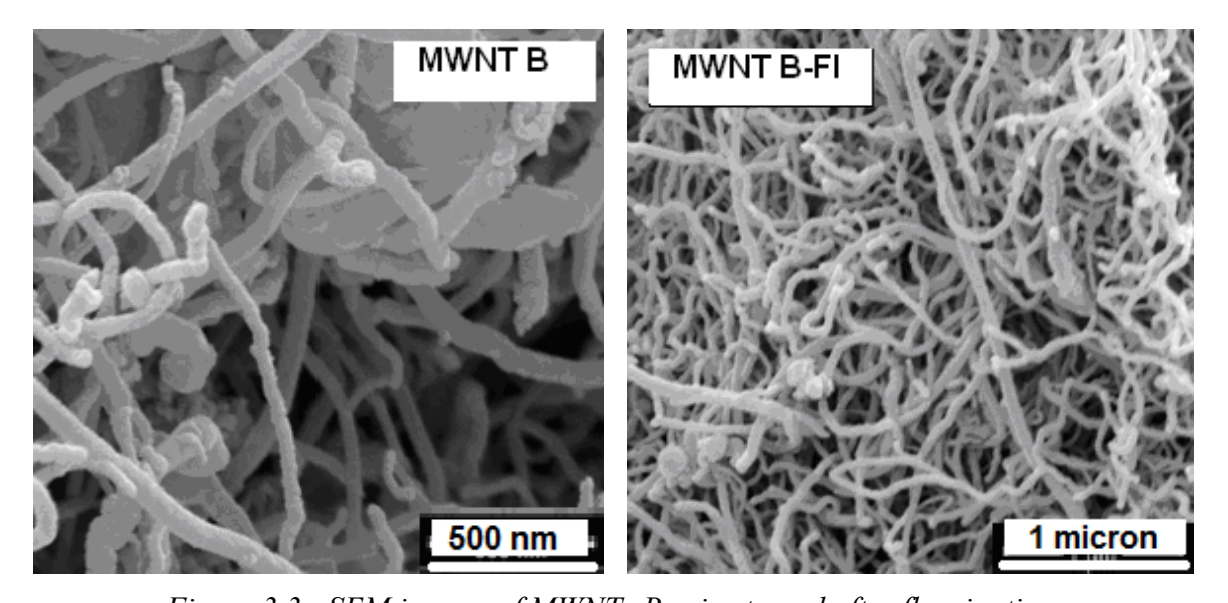


Figure 3.3 - SEM images of MWNTs B prior to and after fluorination.

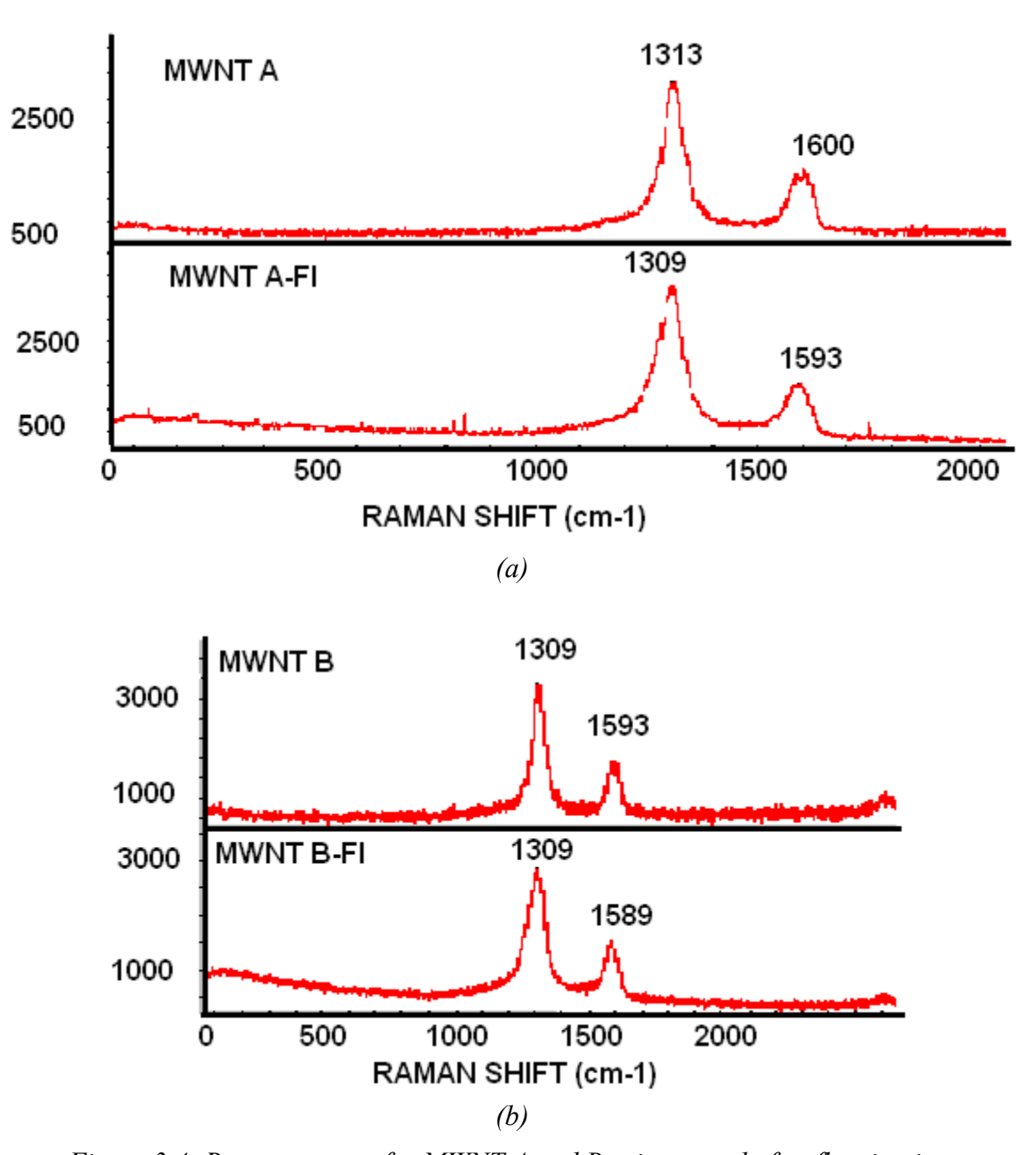


Figure 3.4- Raman spectra for MWNT A and B prior to and after fluorination.

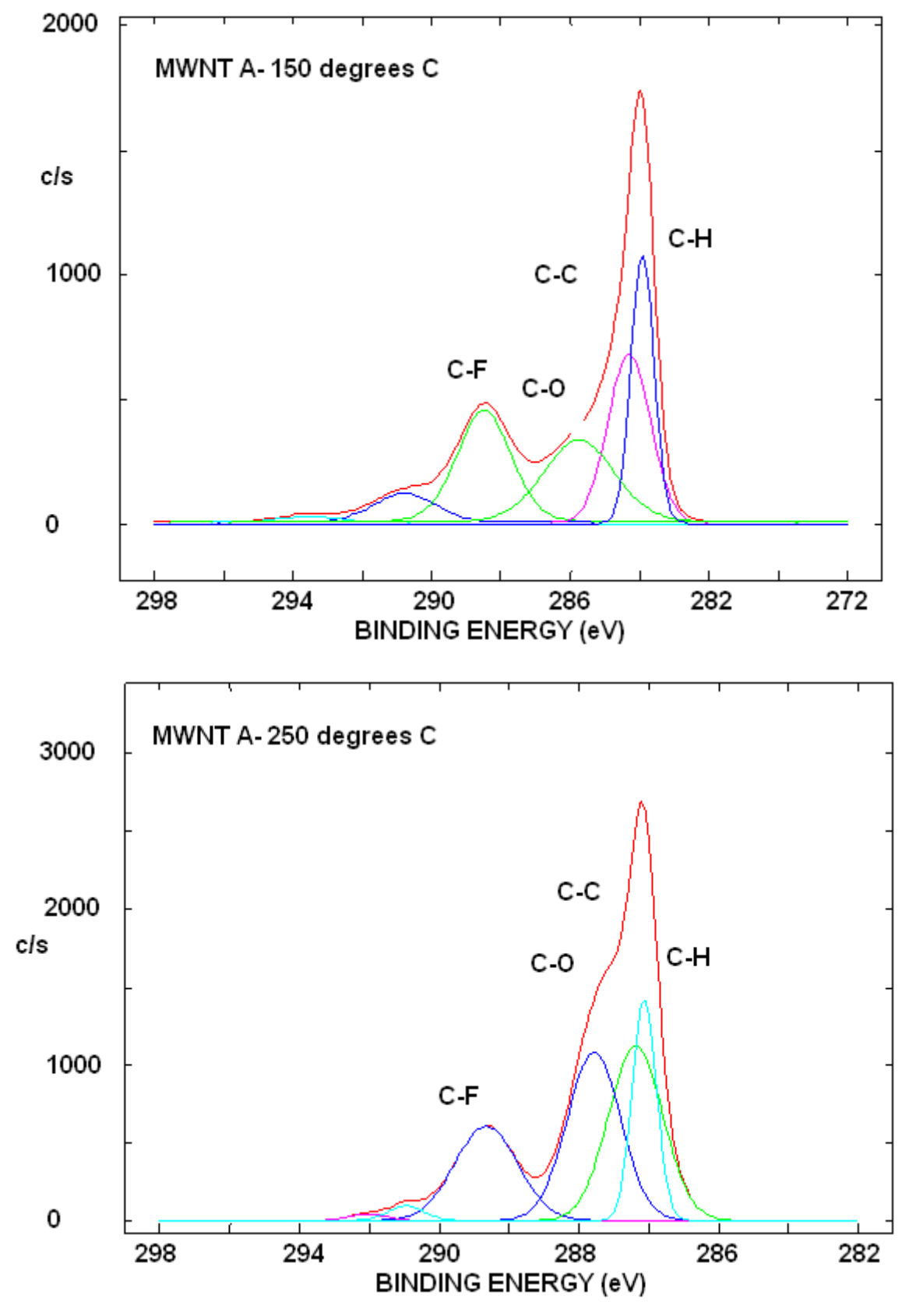
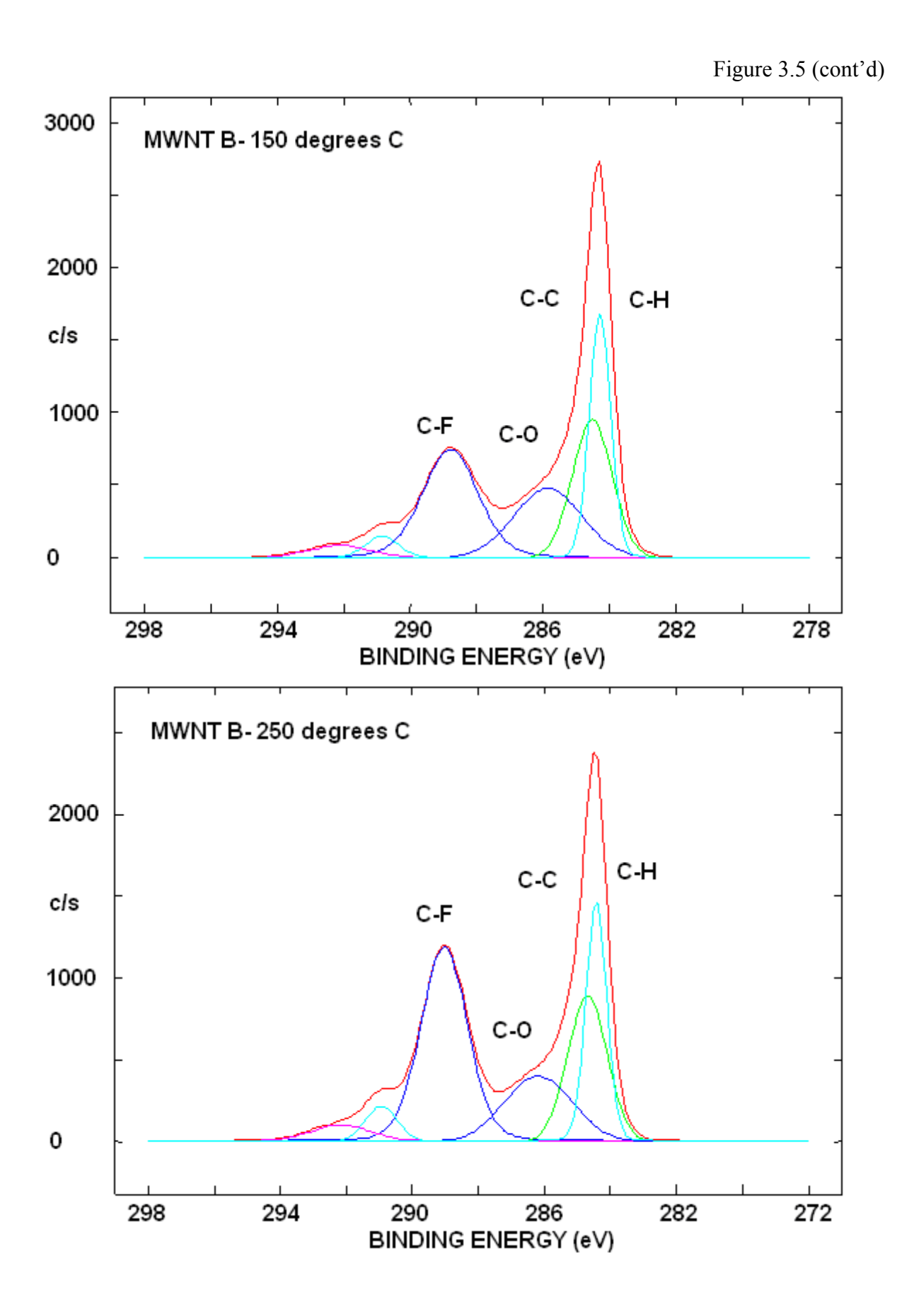


Figure 3.5- XPS spectrum.



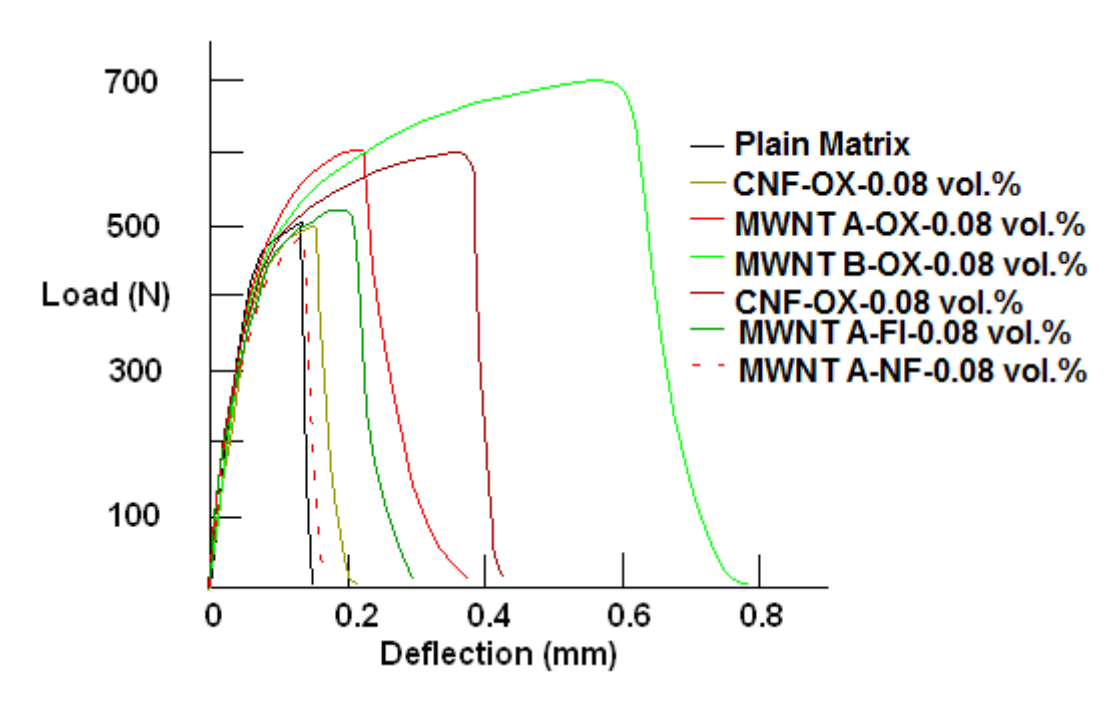
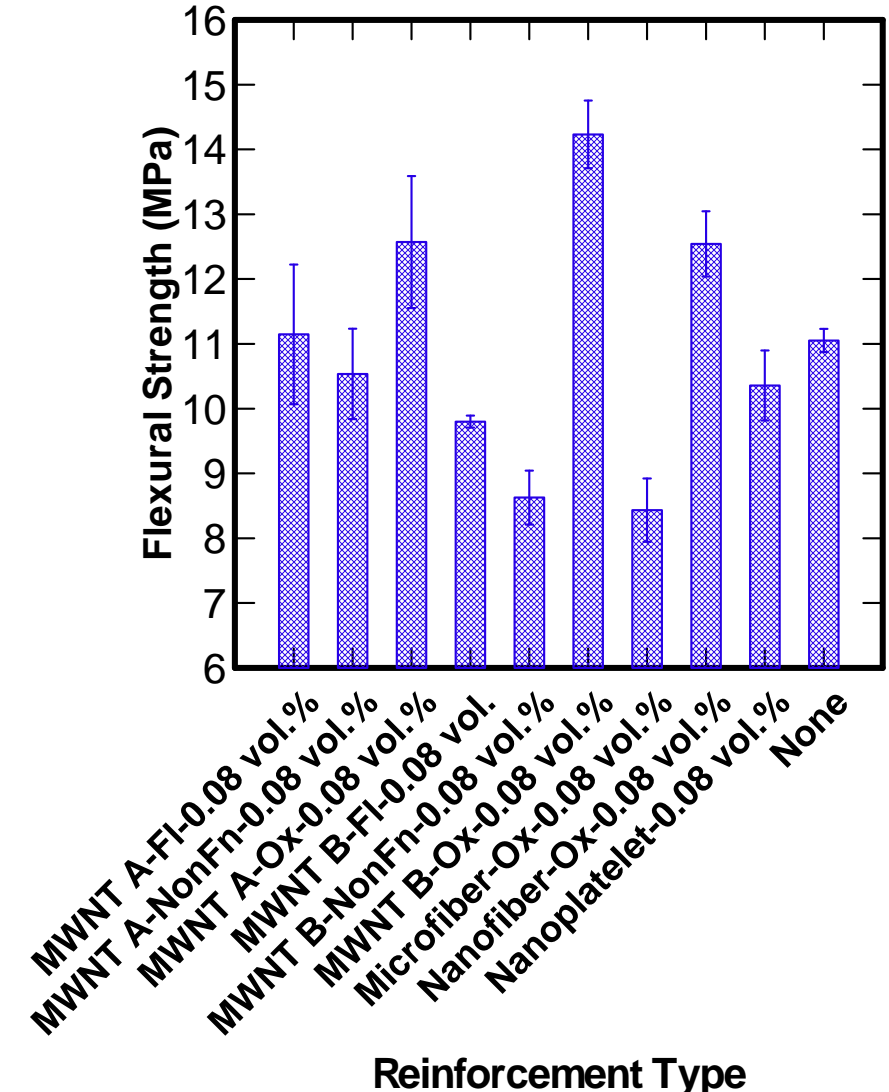
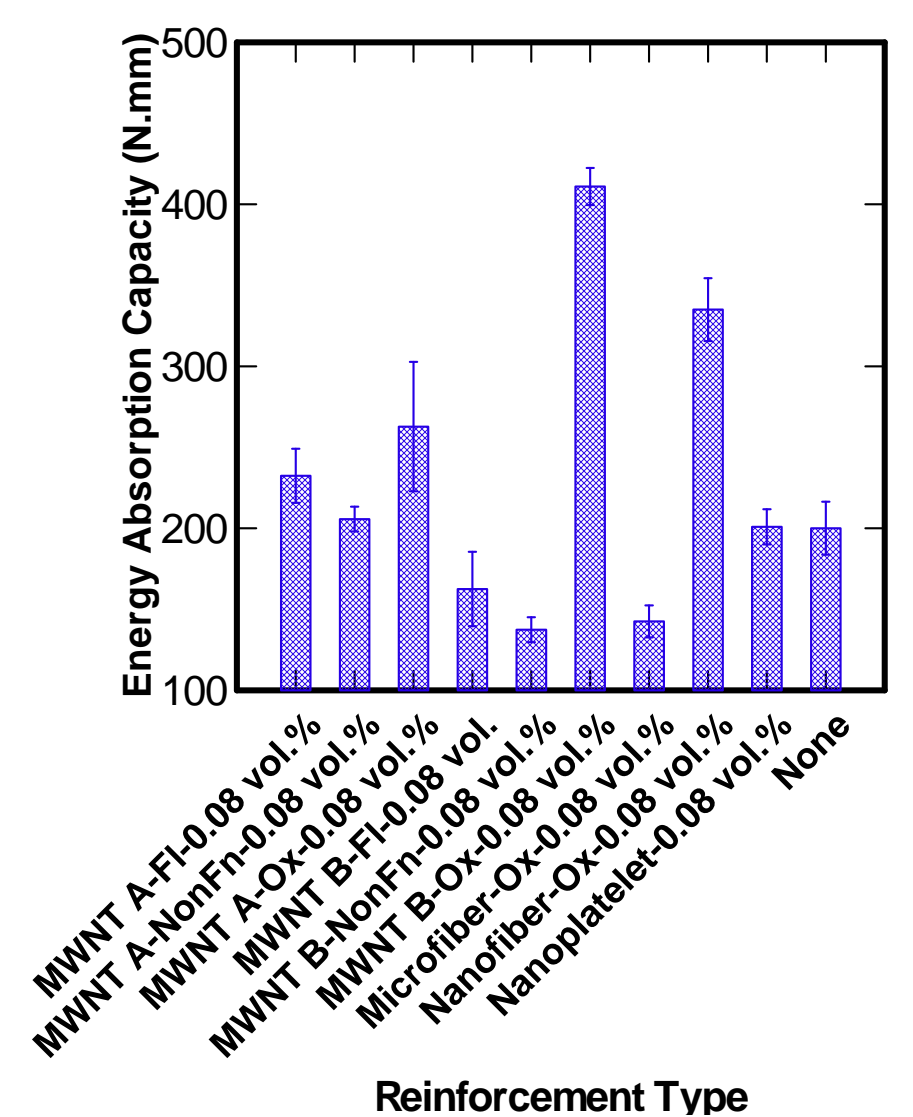


Figure 3.6-Typical flexural load-deflection behavior of DSP paste with 0% and 0.08% volume fractions of various non-functionalized and acid-functionalized graphite nanomaterials.



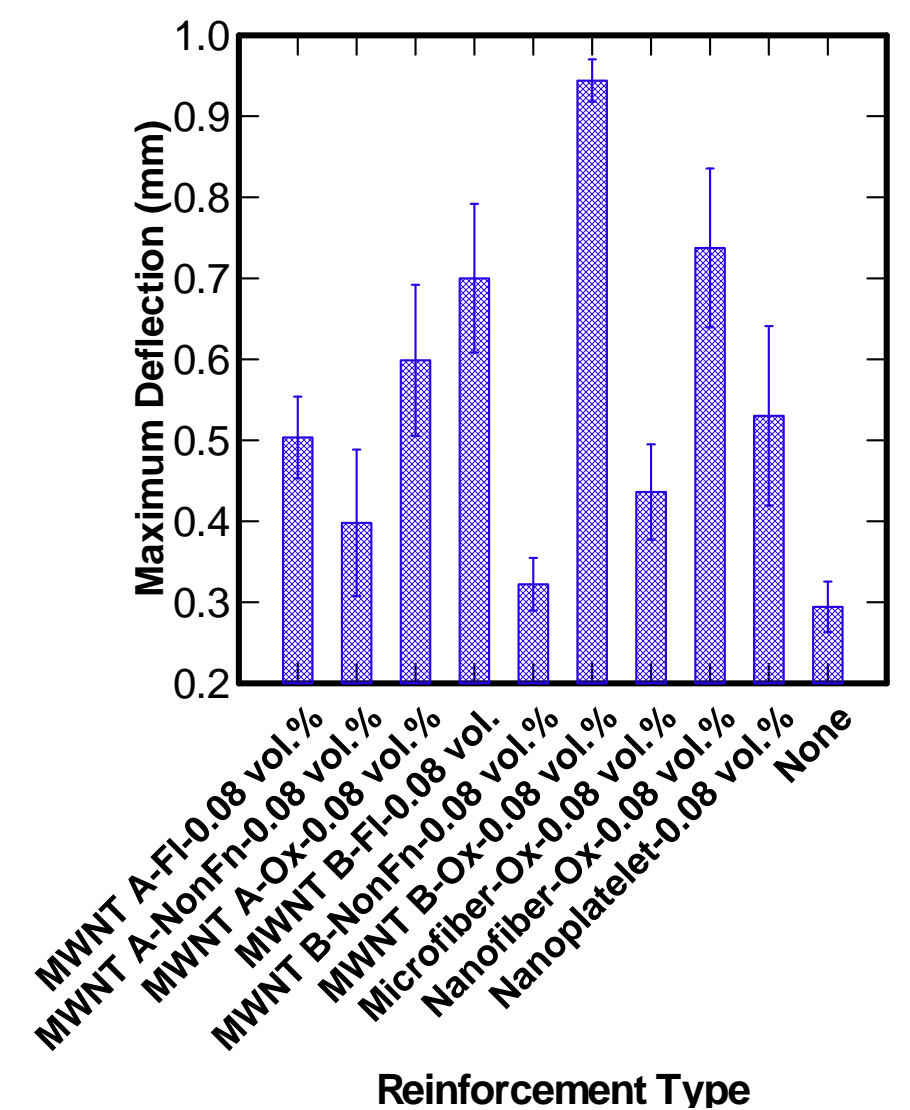
(a)

Figure 3.7- Mean and standard error of various engineering properties of DSP paste reinforced with non-functionalized and functionalized graphite nano and micro reinforcements at 0.08 vol.%.

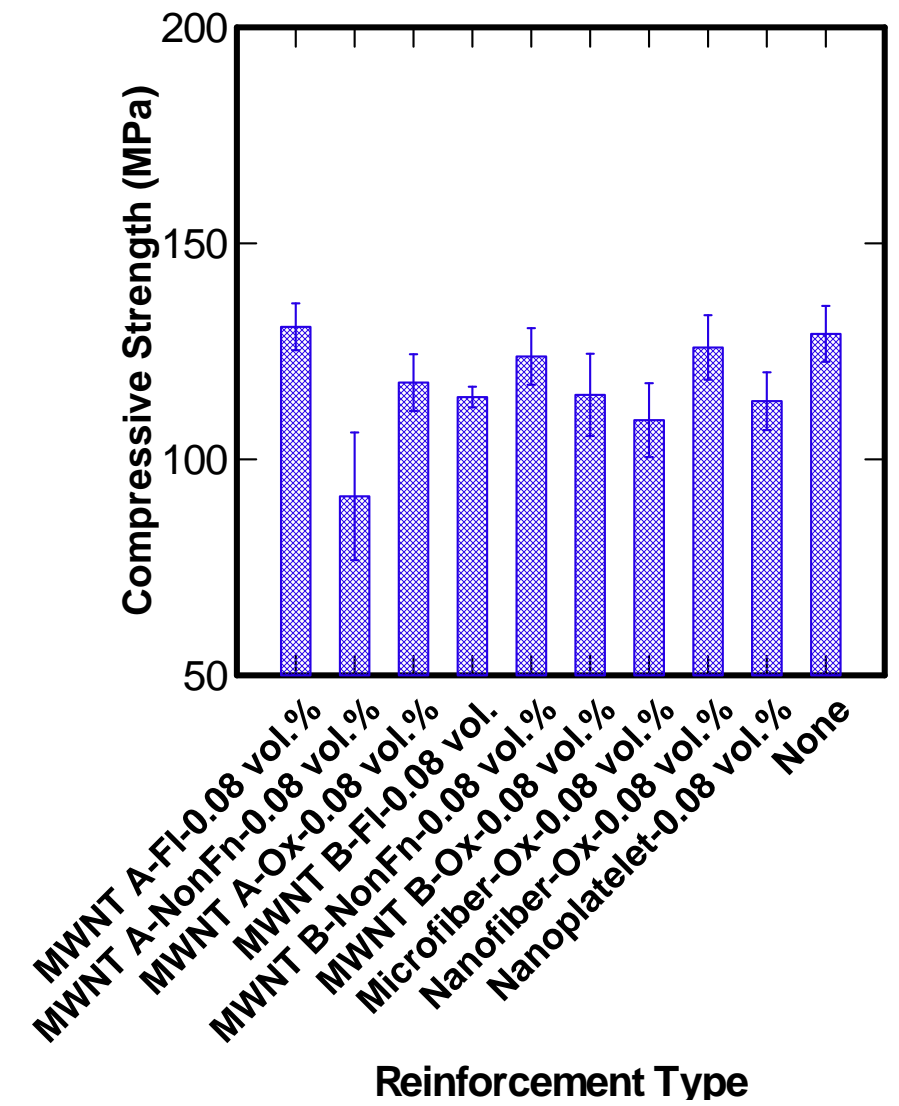


Reinforcement Type

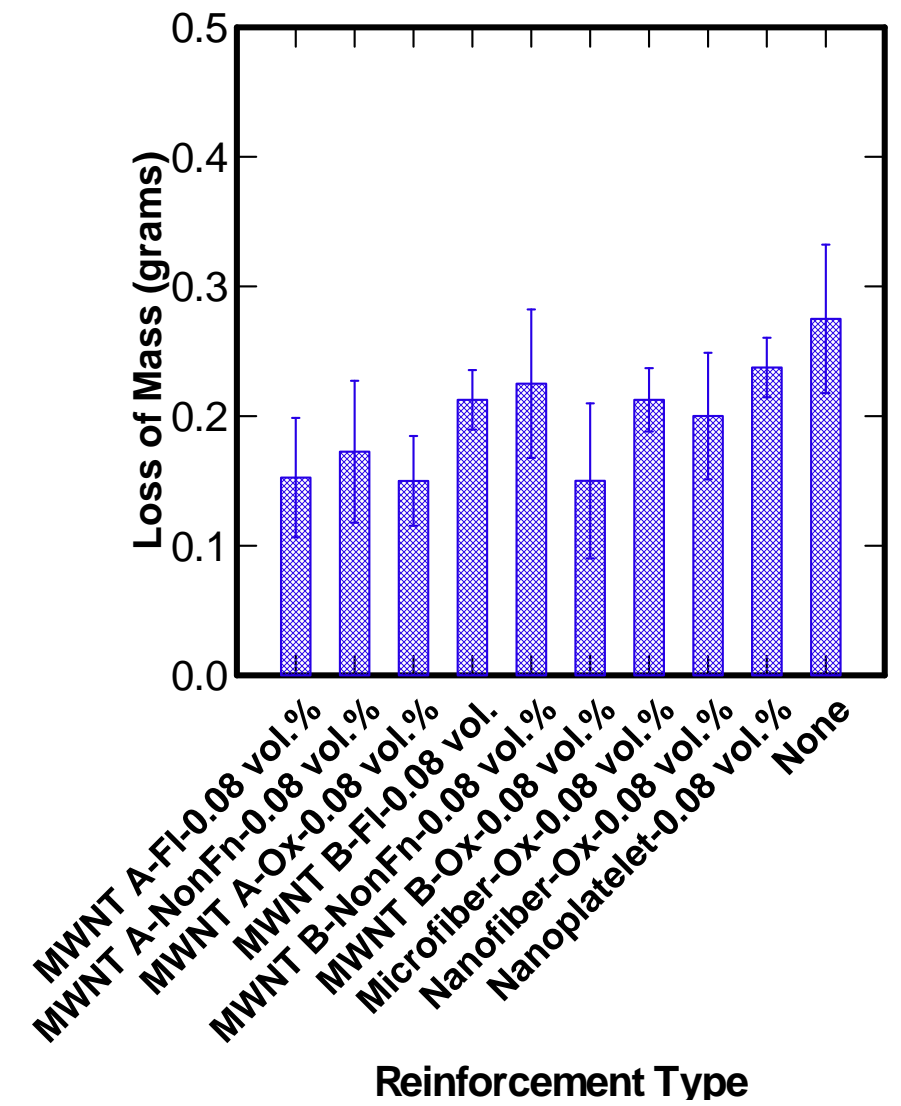
(b)



(c)

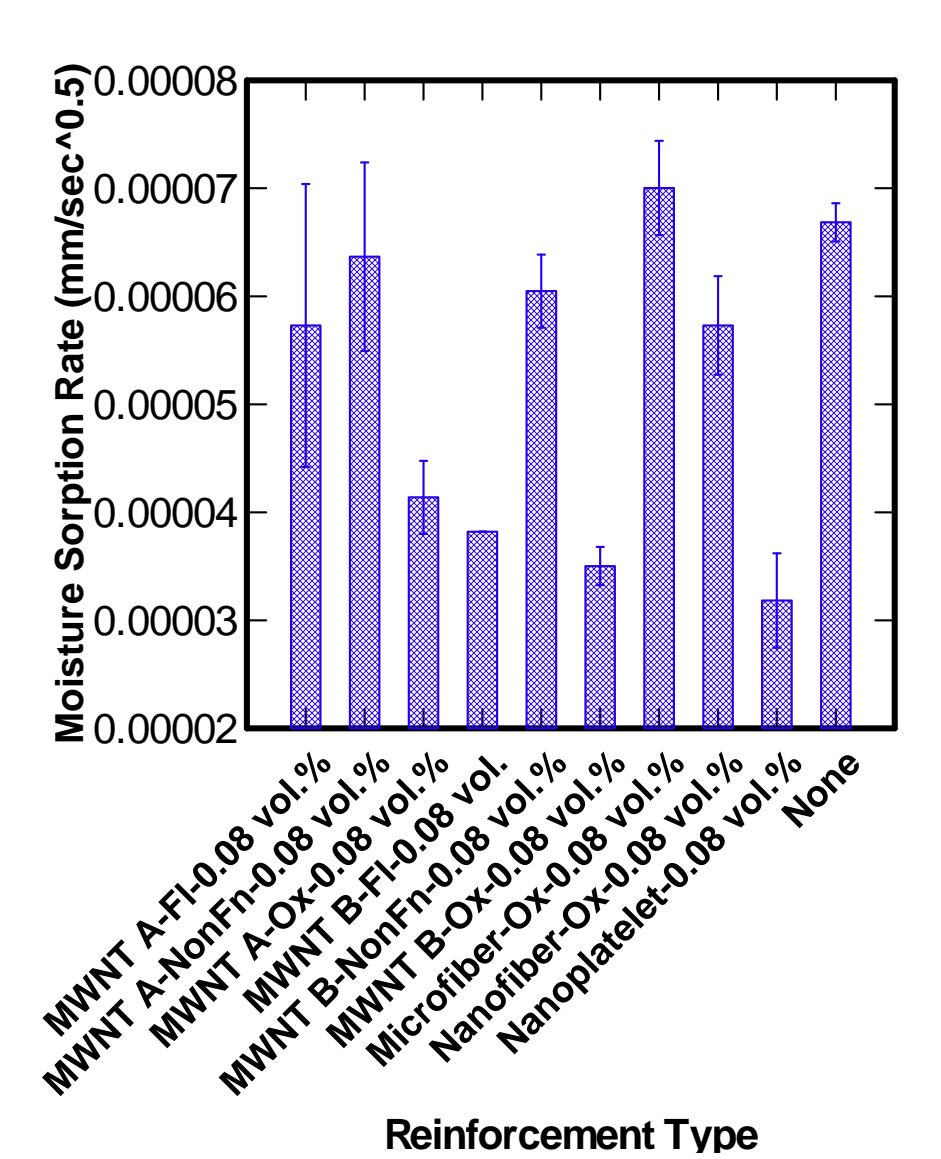


(d)



Reinforcement Type

(e)



(f)

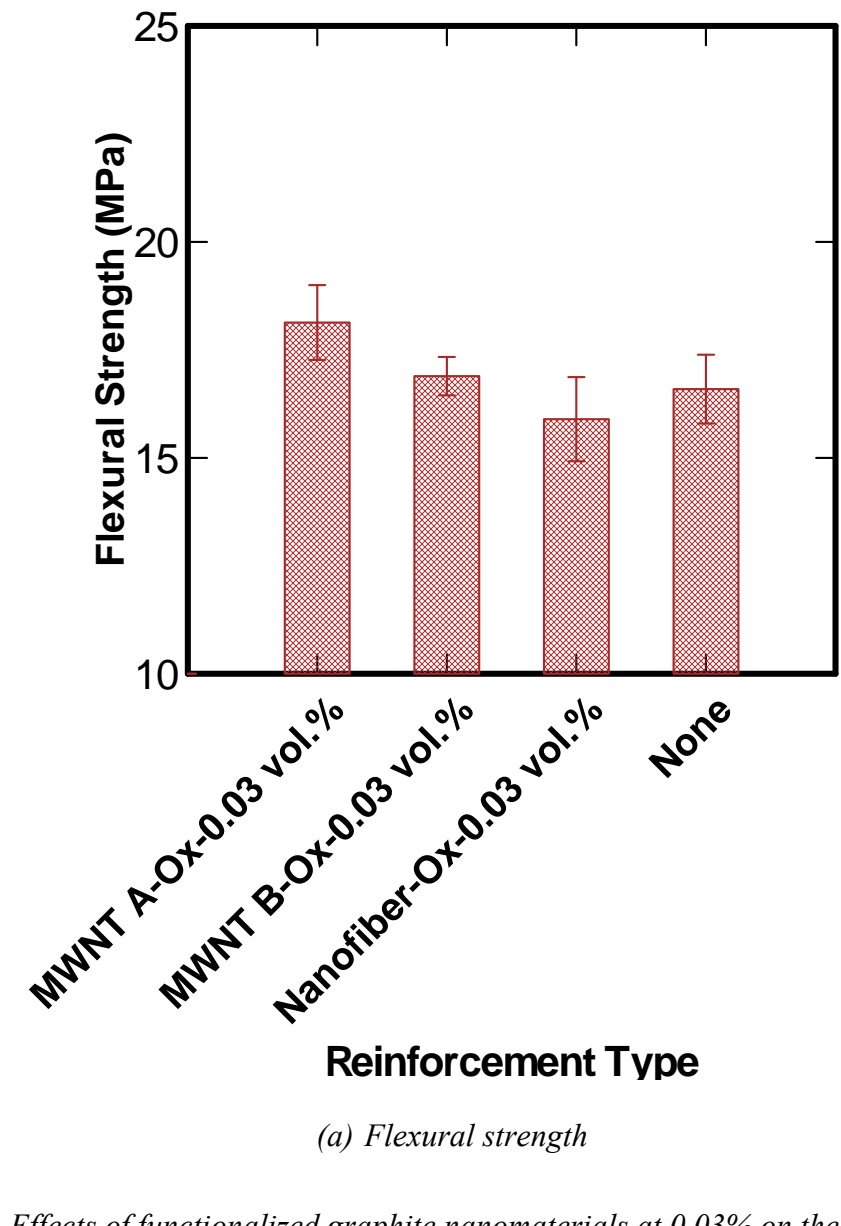
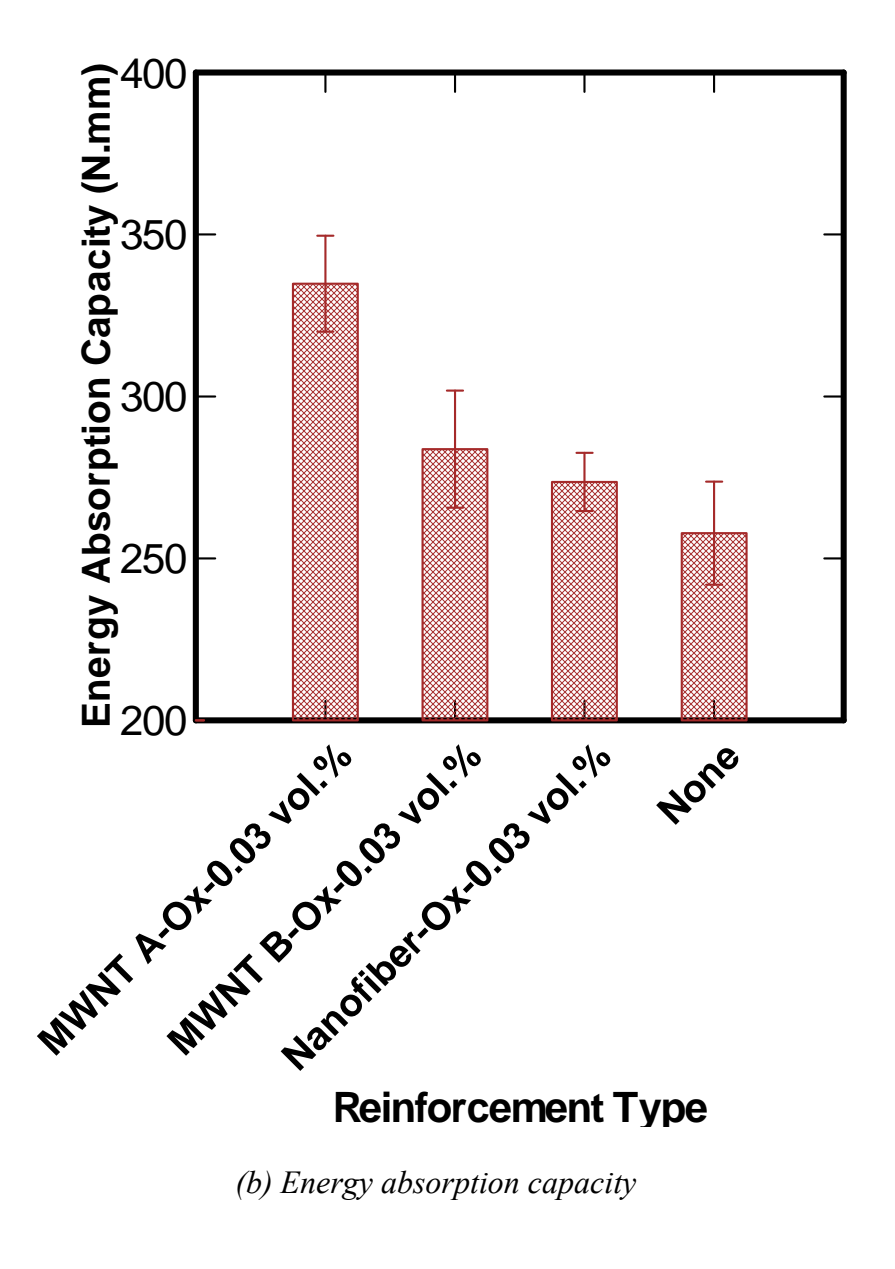
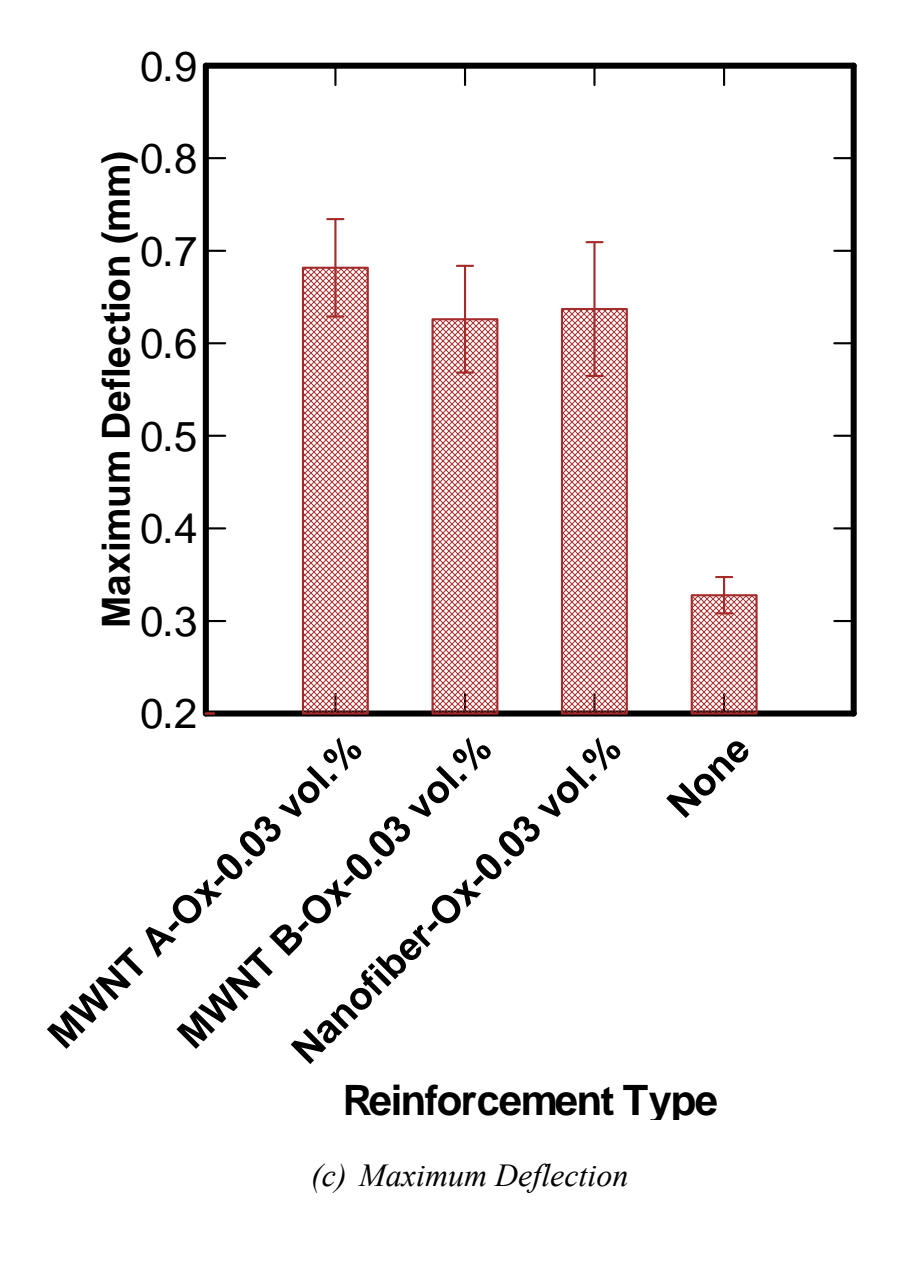
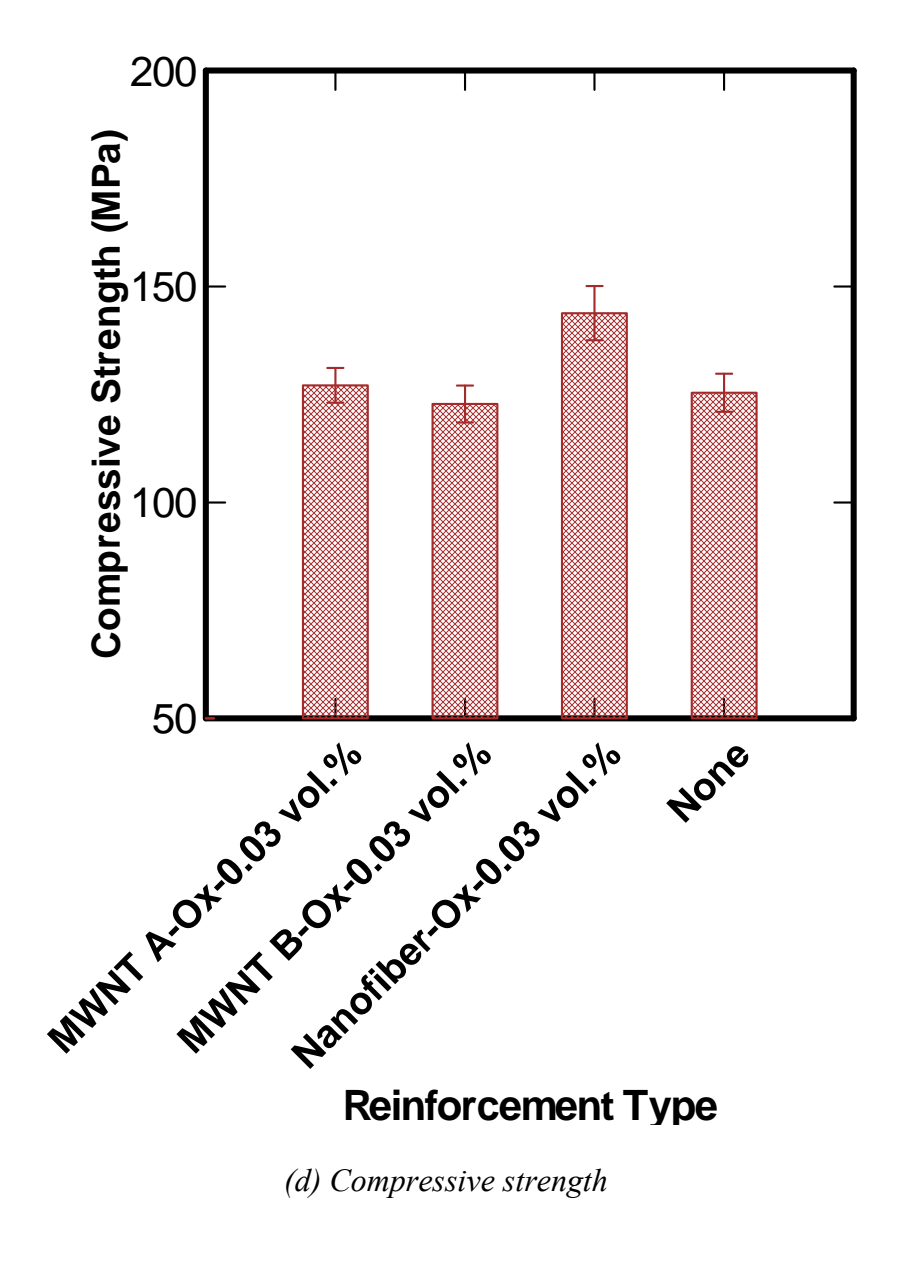
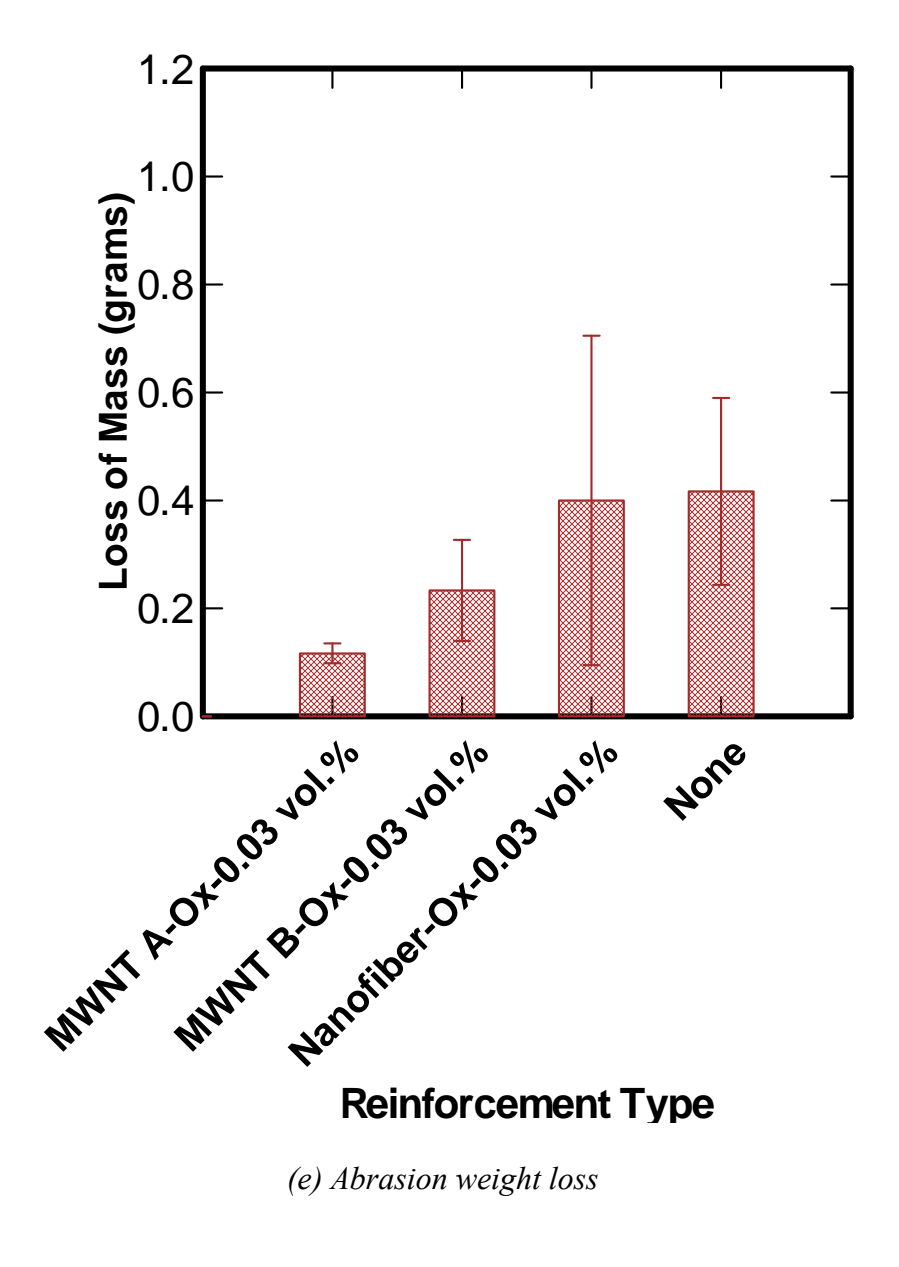


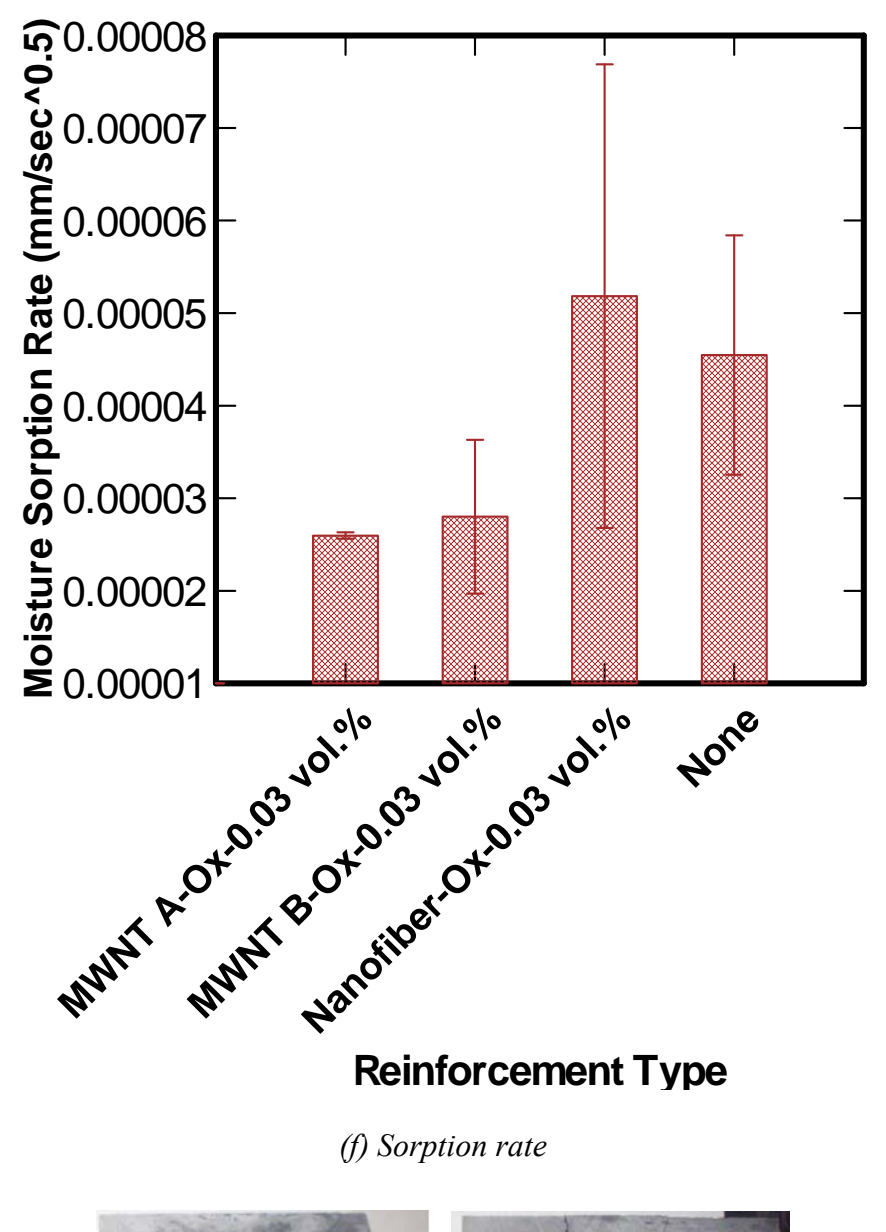
Figure 3.8- Effects of functionalized graphite nanomaterials at 0.03% on the engineering properties of high-performance DSP mortar (means & standard errors).











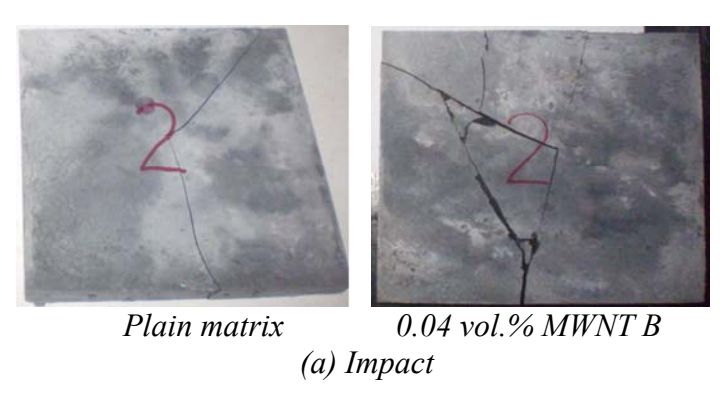


Figure 3.9- Visual appearances of failed specimens after different tests.

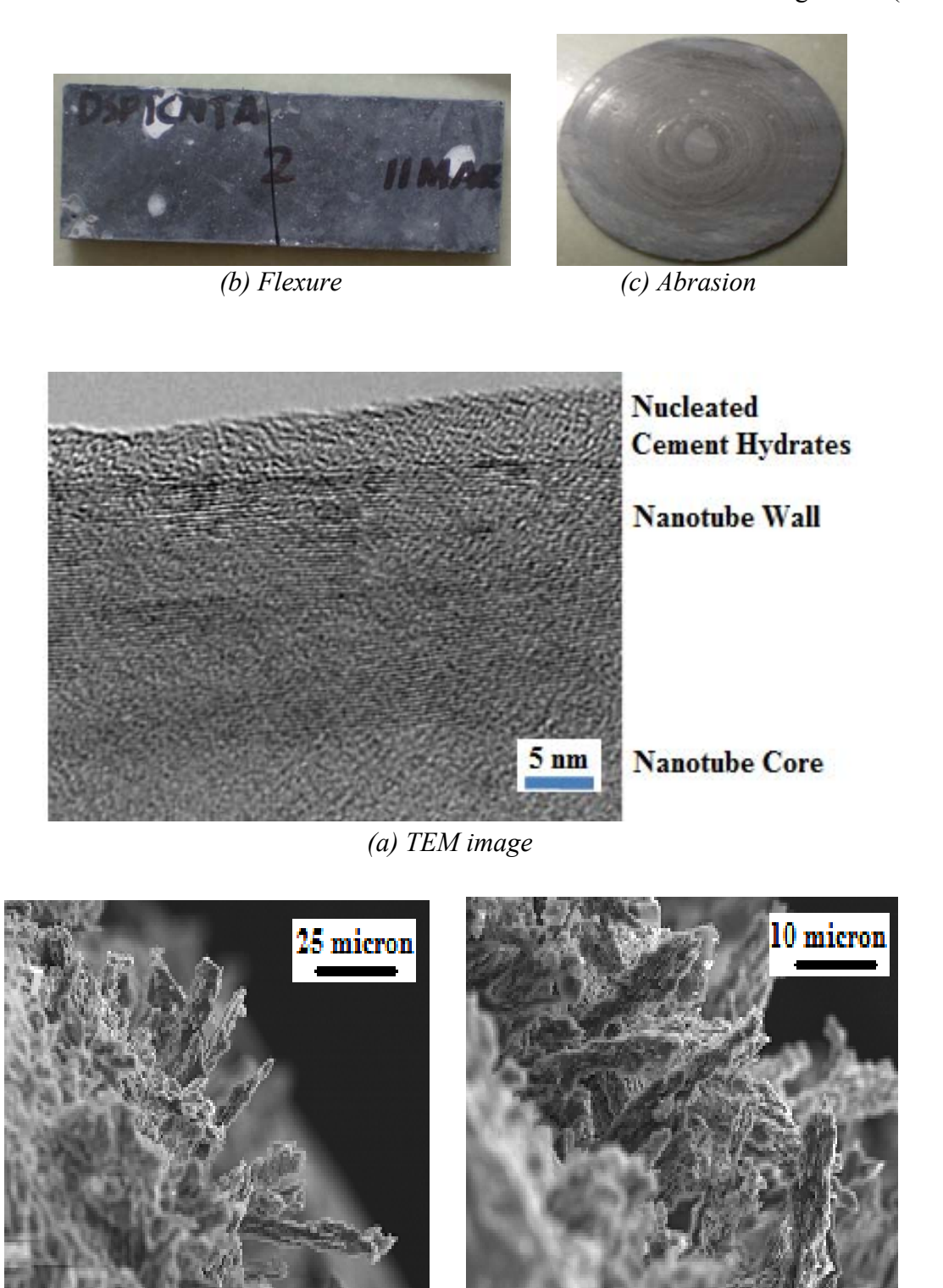
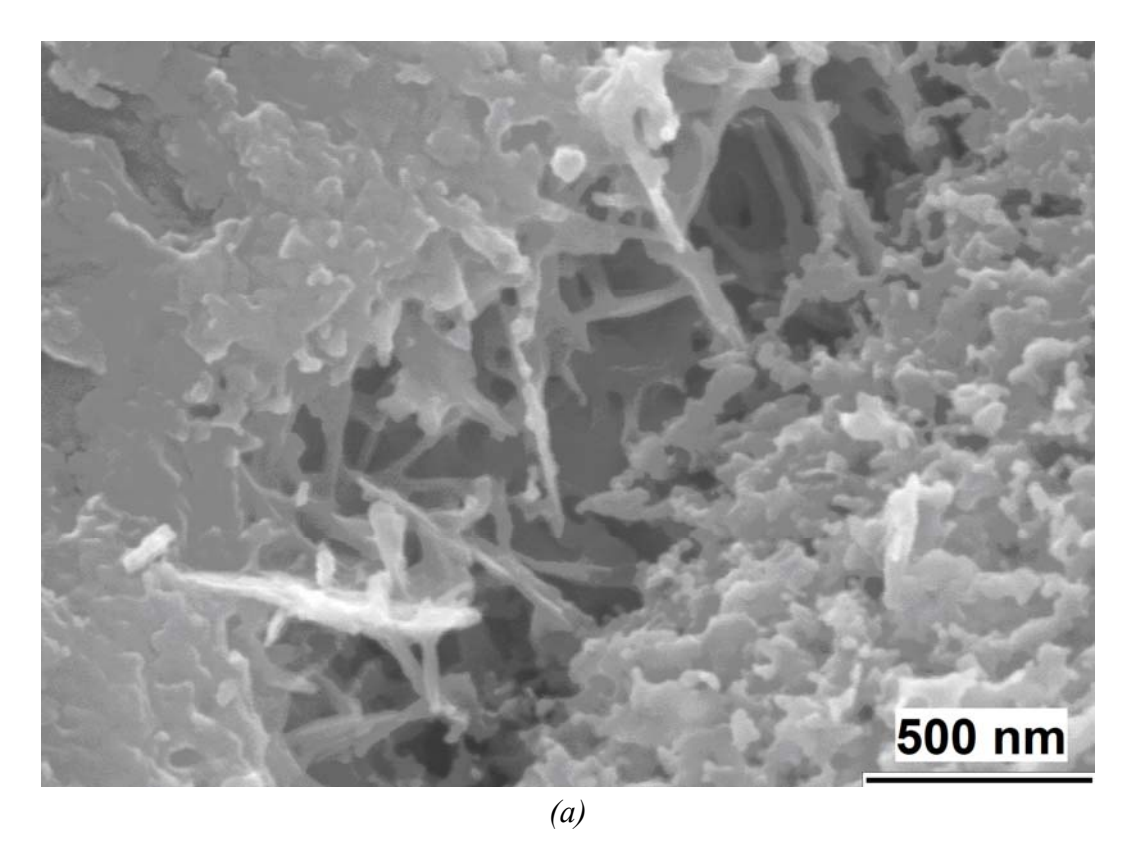


Figure 3.10- TEM image of functionalized MWNT B, and SEM images of the fractured surface of a cementitious matrix with 0.04 vol.% of functionalized MWNT C.

(b) SEM images



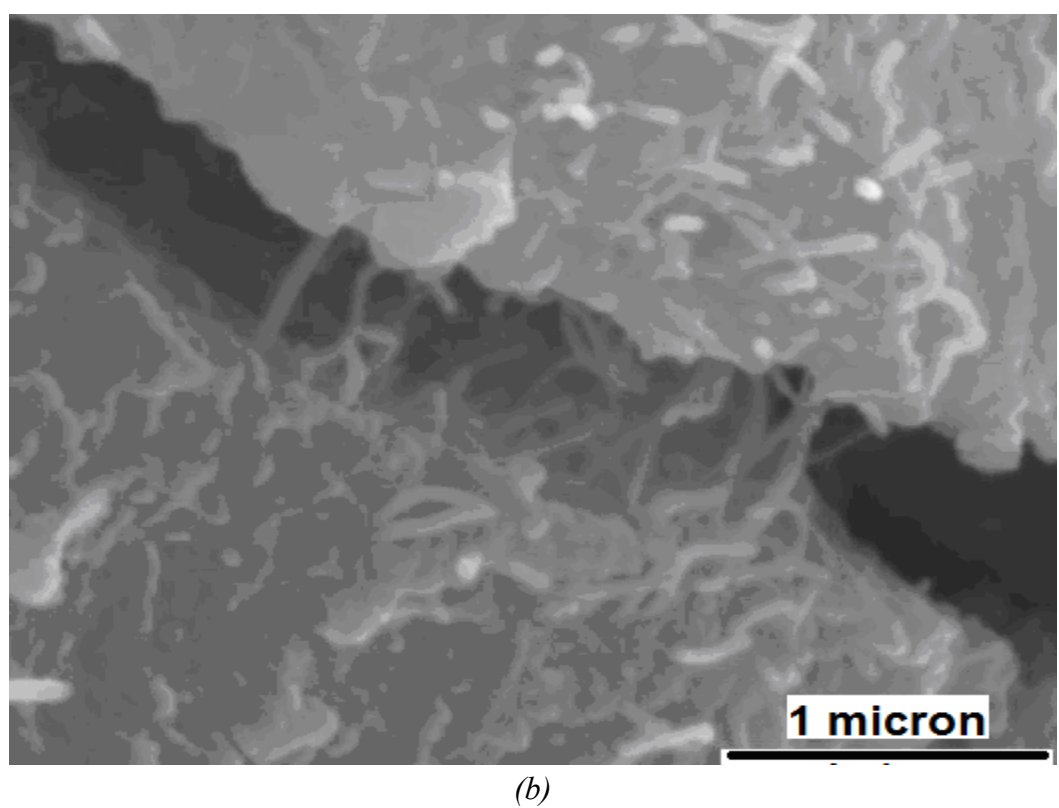


Figure 3.11- Bridging of micro-cracks by acid-functionalized graphite nanomaterials introduced into cementitious matrices at 0.08% volume fraction.

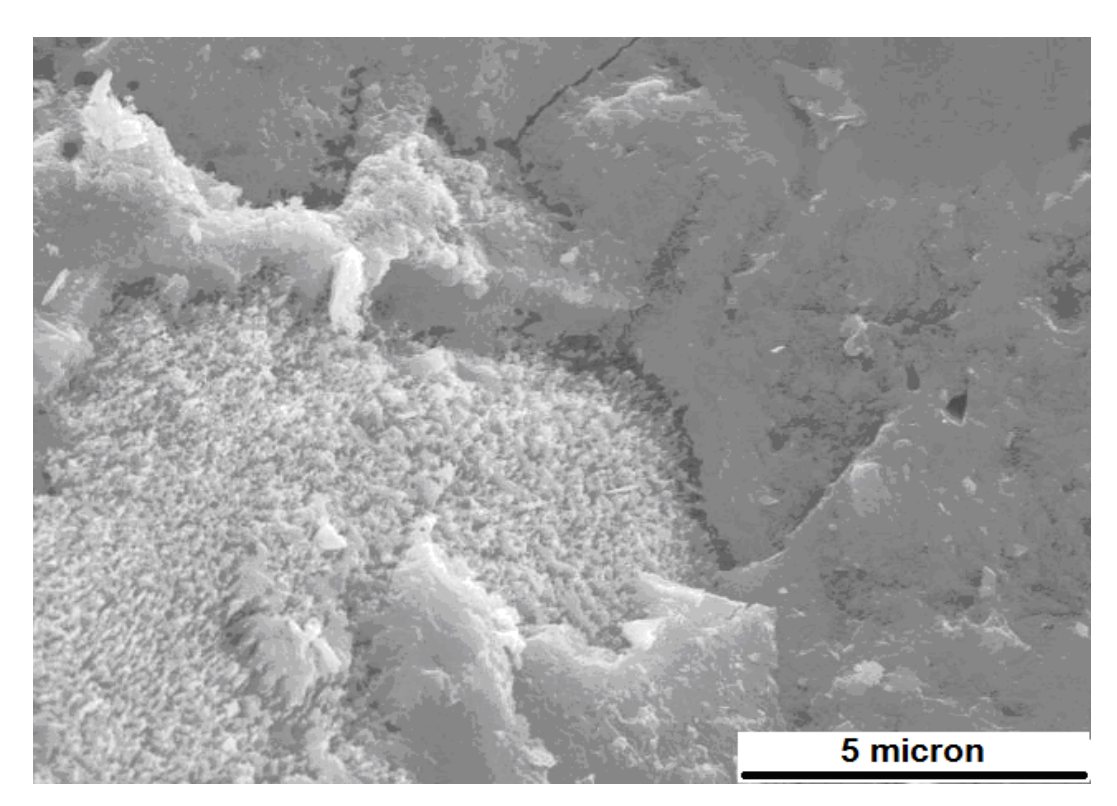


Figure 3.12- Arrest and deflection of a micro-crack by a bundle of CNFs within the cementitious matrix.

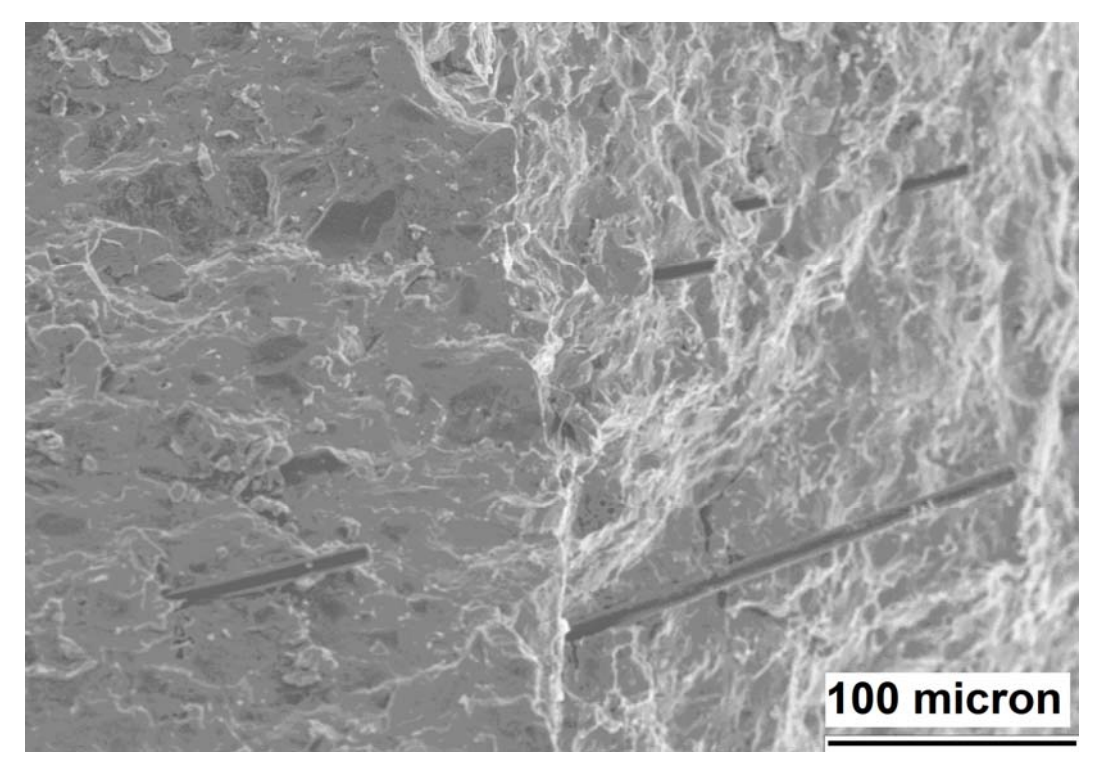


Figure 3.13- SEM images of DSP paste with 0.08 vol.% of carbon micro-fiber exhibiting showing pulled-out micro-fibers on a crack surface.

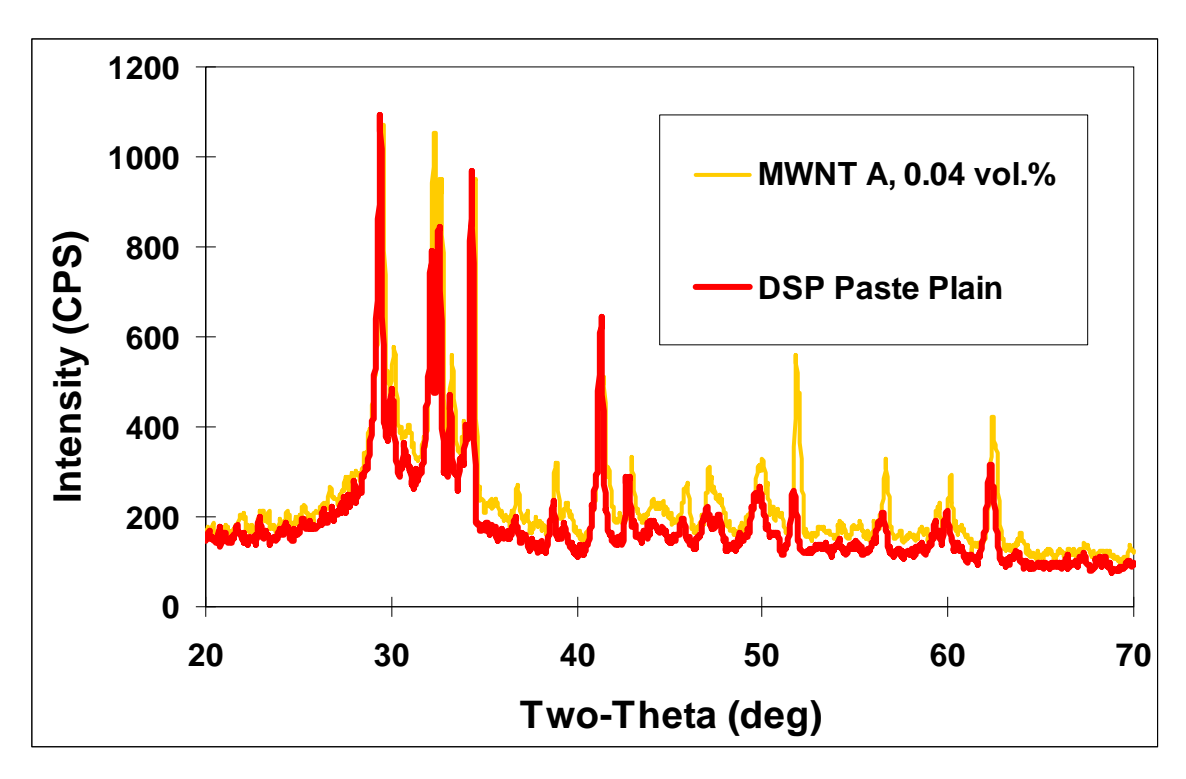


Figure 3.14- XRD graphs of the high-performance cementitious paste matrix with 0% and 0.04 vol.% of acid-functionalized MWNT A.

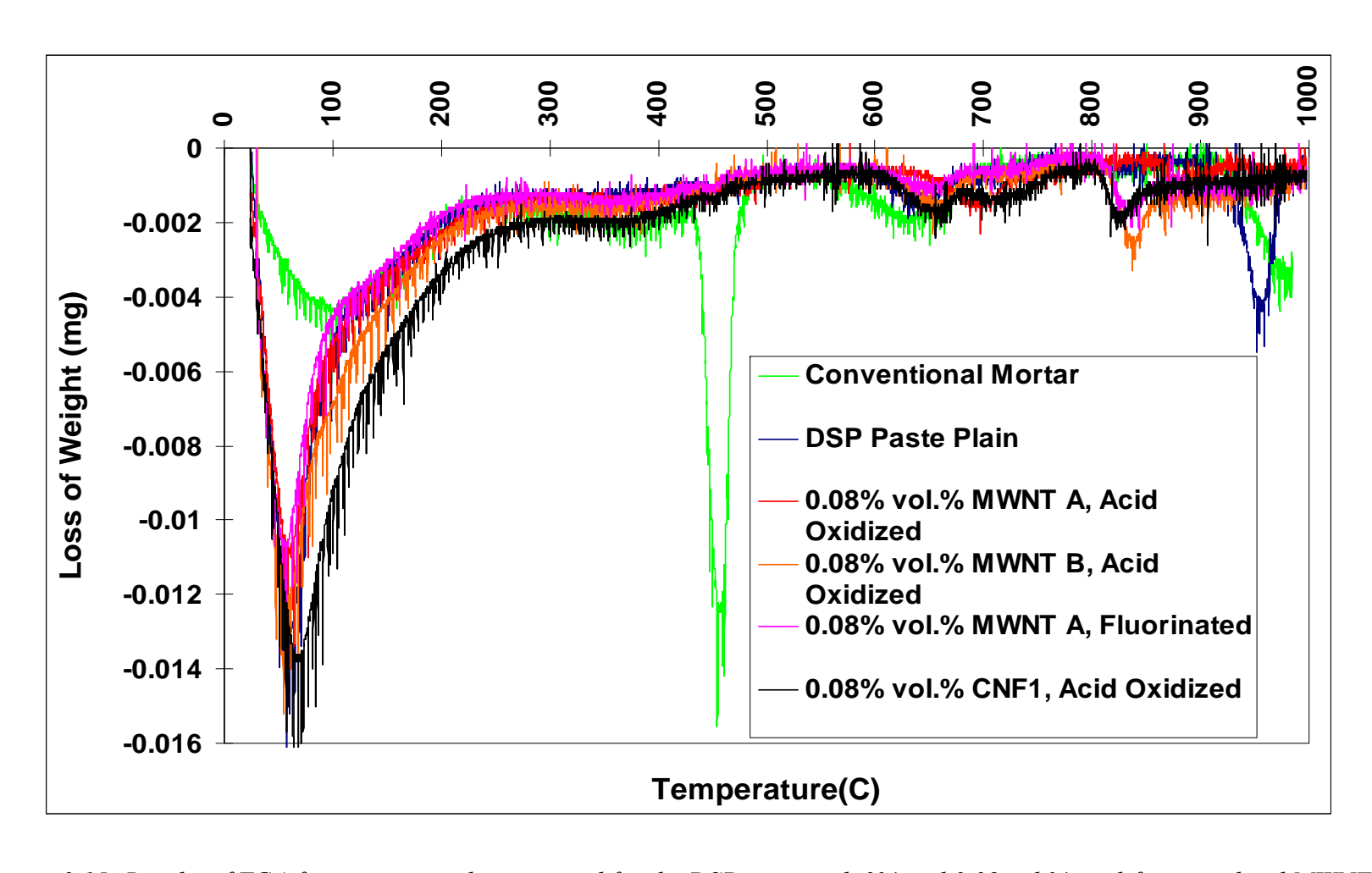


Figure 3.15- Results of TGA for conventional mortar and for the DSP paste with 0% and 0.08 vol.% acid-functionalized MWNT A, MWNT B, carbon nano-fiber, fluorinated MWNT A.

CHAPTER 4

4 EFFECT OF REFINED FUNCTIONALIZATION OF NANOTUBES ON THEIR REINFORCEMENT EFFECIENCY AT DIFFERENT VOLUME FRACTIONS IN CEMENTITIOUS MATRICES

4.1 General

Carbon nanotubes offer distinct engineering and geometric attributes for use as reinforcement in cementitious materials. The tendency of nanotubes towards clustering, via van der Waals interactions over their large specific surface area, and the hydrophobic nature of their surfaces challenge efforts to make effective use of the distinct qualities of nanotubes in cementitious materials. Functionalization/modification of the nanotube surfaces can enhance their wetting attributes for improved dispersion in aqueous media, and their potential for bonding with cement hydrates. Such surface functionalization/modification of nanotubes should not damage their structure and properties. The objective of modifying nanotube surfaces for increasing the density of hydrophilic groups on carbon nanotubes without damaging their structure can be achieved by wrapping nanotubes using selected polymer chains, which does not require introduction of defects or shortening of nanotube (unlike commonly used nanotube functionalization techniques, including acid-oxidation). Polymer-wrapping of nanotubes can be realized through: (i) physisorption of (water-soluble) polymer molecules upon COOH-functionalized nanotubes (O'Connell 2001; Banerjee, Kahn et al. 2003); or (ii) covalent tethering of polymers to nanotube walls (Xie, Xu et al. 2007). Other functionalization strategies have also been explored (Hawley 2002; Bensebaa, Zavaliche et al. 2004; Kubota, Sano et al. 2005).

4.2 Materials and Methods

4.2.1 Materials

Gum Arabic from acacia tree (GA, Reagent grade) and poly(acrylic acid) (PAA, average M_W ~100,000, 35 wt.% in H₂O), N,N'-dicyclohexyl carbodiimide (DCC, 99% purity), N,N-dimethylformamide (DMF, ACS reagent, \geq 99.8%), ethanol (ACS reagent, \geq 99.5%), N-(3-dimethylaminopropyl)-N'-ethylcarbodiimide (EDC, \geq 97.0% purity) and N-hydroxysuccinimide (NHS, 98% purity, 1-Hydroxy-2,5-pyrrolidinedione) were purchased from Sigma-Aldrich. Glenium® 7700 (40 wt.% solution in water) was purchased from BASF (Master Builders). Polyethyleneimine (PEI, branched, M_W ~70,000, 30% w/v aqueous solution) was purchased from Alfar Aesar, Ward Hill, MA. Two types of both carboxylic acid-functionalized and non-functionalized multiwalled carbon nanotubes (MWNT D and E) were used, introduced in detail in Chapter 2, Section 2.4, Fig. 2.3 and Table 2.3. Two longer non-functionalized multiwalled carbon nanotubes (MWNT F and G) were also used. All multiwalled carbon nanotubes had a purity of >95%. Deionized (DI) water was used for all solution preparations.

4.2.2 Cementitious Matrices, Mixing and Curing Procedure

Dense cement-based matrix selected has been introduced in detail in Chapter 2, Section 2.5.1 and Table 2.4. DSP (Densified with Small Particles) paste was use to evaluate the reinforcement efficiency of different multiwalled carbon nanotubes with different surface treatments.

Cementitious materials (with and without functionalized graphite nanomaterials dispersed in the mixing water via sonication, described in detail in Chapter 2, Section 2.5.2) were prepared and cured following ASTM procedures described in the same section.

4.2.3 Experimental Methods

The test procedures employed for determining the engineering properties of cement-based materials were *Compressive Strength* test (ASTM C 109) and *Flexural Strength* test (ASTM C 1185). The following experimental methods were also employed to gain further insight into the chemistry, crystallinity, microstructure and failure mechanisms of cement-based nanocomposites: (i) SEM; (ii) XRD; (iii) DT/TGA; and (vi) FTIR. The details of these experimental tests and methods have been covered in Chapter 2, Section 2.6.

4.3 Further Functionalization and Characterization of Carbon Nanotubes

4.3.1 Polymer Physisorption

Fig. 4.1 schematically depicts the adsorption of polymer/surfactants upon the nanotube sidewalls. The following three polymers were chosen to evaluate the potential of polymer physisorption in enhancing the dispersion and reinforcing effects of nanotubes in cement-based matrices: (i) Gum Arabic (GA); (ii) poly(acrylic acid) (PAA); and (iii) Glenium® (which is also used as a superplasticizer in the project).

The above mentioned polymers were introduced into DI water (1 wt.%), and the mixture was stirred to dissolve the polymers. Subsequently, a dispersion of either non-functionalized or acid-functionalized nanotubes was introduced (1 wt.%, with the dispersion mixed thoroughly overnight). The volume of the mix was adjusted to the targeted level (for use as the mixing water of the cementitious material) by addition of water. The dispersion was then sonicated, first at different amplitudes (30%, 45%, 65% and 75%) for 10 minutes each (with one-minute break intervals in between), and then subjected to three ten-minute intervals of pulsing (1 minute on 30 seconds off) at 85% amplitude with two-minute breaks in between. Finally, the whole sonication

process was repeated one more time. The resulting nanotube dispersion was immediately mixed with the cementitious paste; it was also characterized through Fourier Transform Infrared Spectrometry (FTIR).

Fig. 4.2 shows the FTIR spectra of acid-functionalized nanotubes, Gum Arabic, and the acid-functionalized nanotubes modified with Gum Arabic. The appearance of new peaks at 1600 cm⁻¹, 1720 cm⁻¹ and 3300 cm⁻¹ indicate that GA is physisorbed upon nanotubes. Further appearance of a new broad peak around 2900 cm⁻¹ due to alkane stretching confirms the presence of a polymer chain.

The FTIR spectra for acid-functionalized nanotubes, PAA and PAA-modified functionalized nanotubes are shown in Fig. 4.3. The appearance of new peaks for PAA-modified nanotubes at 1720 cm⁻¹ indicates that PAA is physisorbed upon acid-functionalized nanotubes. Further appearance of a new broad peak around 3000 cm⁻¹ indicates the presence of free OH groups. Hence, FTIR spectra confirm the presence of polymer chains associated with nanotubes.

Fig. 4.4 shows the FTIR spectra of acid-functionalized nanotubes, Glenium®, and Glenium®-modified functionalized nanotubes. The appearance of new peaks for Glenium®-modified nanotubes at 1545 cm⁻¹, 1720 cm⁻¹ and 3200 cm⁻¹ point at the association of Glenium® with acid-functionalized nanotubes. The peak at 1720 cm⁻¹ corresponds to the carbonyl group of Glenium®, and the one at 3200 cm⁻¹ corresponds to the OH stretching of the carboxylic acid groups in Glenium®. Further appearance of a new set of peaks around 2900 cm⁻¹ is due to alkane stretching, which confirms the presence of a polymer chain. The appearance of all these

peaks confirms that Glenium® is incorporated upon nanotube walls, probably through non-covalent interactions.

4.3.2 Covalent Tethering of Polymers onto Nanotube Walls

While nanotube dispersions can be prepared using surfactants and physisorbed polymers, the interactions between nanotubes and polymers or surfactants are non-covalent in these cases. Such interactions tend to weaken upon changes in pH, ionic strength and other attributes of the medium. In addition, polymer wrapping decreases the effective aspect ratio of the reinforcement. Covalent attachment of functional groups or polymers onto the nanotube wall can improve the load transfer efficiency. Oxidation is one of the most commonly used covalent functionalization methods, in which a mixture of sulfuric acid and nitric acid is commonly used to form carboxylic acid groups on nanotube surfaces. This approach involves tethering of water-soluble polymers upon carbon nanotubes (Fig. 4.5) via covalent bonding to the COOH groups introduced at nanotube surfaces by acid-oxidation. Two water-soluble polymers were chosen to be tethered to carboxylated nanotubes: (i) poly(acrylic acid) (PAA); and (ii) Glenium®. Both these polymers have high densities of COOH groups, and have been shown to improve the dispersability of nanotubes and their bonding to cementitious matrices.

PAA and Glenium® were chosen here as the anchoring polymers because of their water-solubility and high density of COOH groups. The process of tethering these polymers onto nanotube walls starts with acid-oxidation of nanotubes, resulting in covalent attachment of the carboxylic acid (COOH) groups onto the surface of nanotubes. This is followed by a coupling reaction of the COOH groups on nanotube surfaces with the COOH groups of PAA or Glenium® in the presence of coupling reagents (e.g, dicyclohexylcarbodiimide - DCC), as schematically depicted in Figs. 4.6 and 4.7. This procedure will covalently tether the polymer

chains onto the nanotube surfaces. Thorough dispersion of the resulting modified nanotubes in water was accomplished through sonication with a sonic probe as described earlier.

The FTIR spectra of carboxylated nanotubes, PAA and PAA-tethered carboxylated nanotubes are shown in Fig. 4.8. The appearance of new peaks for PAA-CNTCOOH (versus CNT-COOH) at ~3300 cm⁻¹, 2900 cm⁻¹, 2800 cm⁻¹, 1625 cm⁻¹, 1573 cm⁻¹, 1400 cm⁻¹, 1300 cm⁻¹ and 1200 cm⁻¹ points at tethering of PAA via COOH onto CNT. The appearance of a new set of peaks around 2900 cm⁻¹ and 2800 cm⁻¹, due to alkane (CH₂, CH₃ and CH) stretching, confirms the presence of a polymer chain. The peak at ~3300 cm⁻¹ is due to OH stretching in COOH groups; this is usually a broad peak, but it is sharp here indicating that the OH groups are not H-bonded. Peaks at 1625 cm⁻¹ and 1573 cm⁻¹, due to carbonyl stretching, occur lower than the corresponding neat PAA carbonyl peaks, indicating that the COOH groups of PAA are being reacted. The medium peak at 1400 cm⁻¹ is due to C-OH bending. Peaks at 1300 cm⁻¹ and 1200 cm⁻¹ are due to C-O stretching. In short, the FTIR spectra shown in Fig. 4.8 confirm that PAA is covalently bonded to carboxylated nanotubes.

Fig. 4.9 shows the FTIR spectra of carboxylated nanotubes, Glenium®, and Glenium®-tethered carboxylated nanotubes. Appearance of new peaks in Glenium®-CNTCOOH (versus CNT-COOH) at 1545 cm⁻¹, 1720 cm⁻¹ and 3200 cm⁻¹ indicates that Glenium® is tethered via COOH groups onto nanotubes. Further appearance of a new set of peaks around 2900 cm⁻¹, attributed to alkane stretching, confirms the presence of polymer chains in association with nanotubes.

4.3.3 Further Functionalization of Carboxylated Nanotubes Starting from Carboxyl Groups

Amino groups can be attached to carboxylated nanotubes in a way similar to those described above for attachment of carboxylic acid polymers. In an effort to employ amino groups towards further modification of carboxylated nanotubes, the water-soluble polymer polyethyleneimine (PEI), which carries amino groups, was chosen to interact with the carboxyl groups of nanotubes, as schematically depicted in Fig. 4.10, and also with cement hydrates (through mechanisms similar to COOH groups). Further functionalization of carboxylated nanotubes with PEI was accomplished in the presence of *N*-hydroxysuccinimide (NHS); the COOH groups on carboxylated nanotubes were activated to form NHS esters. Upon introduction of *N*,*N*-dicyclohexyl carbodiimide (EDC), PEI can react with the activated ester groups to form amide bonds between PEI and nanotubes.

As a first step, EDC (1 M) was mixed together with NHS (1 M) in the required amount of DI water, and stirred to achieve thorough dissolution. Carboxylated nanotubes were then added to the mixture (at 0.5 wt.%), followed by further stirring for 30 minutes. Conversion of the carboxylic acid groups of CNT-COOH into active esters (CNT-NHS) would occur upon exposure to the solution of EDC (1 M) and NHS (1 M) in water. Subsequently, PEI (0.5 wt.%) was added to the mix, and it was left for 24 hours at room temperature. During this period, the amino groups of PEI would covalently bind to CNT-NHS. After 24 hours of stirring, the residue (amine-anchored nanotube) was filtered, rinsed well with ethanol and DI water, and dried. It was then mixed with water (10 g/L), and stirred overnight for thorough mixing. Thorough dispersion of the modified nanotubes in water was accomplished through sonication with a sonic probe.

Fig. 4.11 shows the FTIR spectra of carboxylated nanotubes, PEI, and PEI-tethered carboxylated nanotubes. Peaks at ~3300 cm⁻¹, 2900 cm⁻¹, 2800 cm⁻¹, 1640 cm⁻¹, 1550 cm⁻¹, 1460 cm⁻¹, 1370 cm⁻¹, 1260 cm⁻¹ and 1060 cm⁻¹ point at the tethering of PEI upon nanotubes. The appearance of a new set of peaks upon tethering of PEI around 2900 cm⁻¹ and 2800 cm⁻¹, attributed to alkane (CH₂, CH₃ and CH) stretching, confirms the presence of polymer chains in association with nanotubes. Peaks at ~3300 cm⁻¹ (NH stretching), 1550 cm⁻¹ (NH₂ scissoring) and 1060 cm⁻¹ (C-N stretching) are attributed to the amine groups of PEI. The peak at ~1640 cm⁻¹ is attributed to carbonyl stretching of the newly formed amide bond between the amine groups of PEI and the COOH groups of carboxylated nanotubes. This bonding mechanism is further confirmed by the medium peak at 1460 cm⁻¹, which is attributed to amide N-H bending. In short, the FTIR spectra indicate that PEI is covalently bonded to carboxylated nanotubes.

4.3.4 Microwave Irradiation

Carbon nanotubes (0.75 g) were added to 350 ml (milli-liter) of a 1:1 mixture of 70% solution of nitric acid and 97% solution of sulphuric acid. The microwave power was set at 40% of a total of 1100 W, and microwave irradiation was performed at atmospheric pressure. The reaction vessel was subjected to 5 minutes of irradiation followed by a 1-minute break and another 5 minutes of microwave irradiation. For safety reasons, the microwave oven was placed in a fume hood. The mixture was then diluted with DI water and filtered through 5 µm hydrophilic poly (tetrafluoroethylene) (PTFE) filter paper under vacuum. Filtered MWNTs were washed until the washings were found to be neutral (using pH paper). The functionalized MWNTs were

allowed to dry in the filter paper. Further drying was achieved under vacuum. The extent of functionalization was evaluated using FTIR spectroscopy.

4.4 Experimental Results

4.4.1 Reinforcement Efficiency of Carbon Nanotubes with Different Functionalization Conditions

The functionalization conditions of carbon nanotubes were established in a systematic manner. First, the preferred dosages of different polymers introduced upon carbon nanotubes were identified and characterized. For many polymers, a 1:1 weight ratio of physisorbed polymer to carbon nanotube produced desired results. Cementitious nanocomposites were prepared and characterized with 0.16 vol.% (volume fraction of dry cementitious materials) or 0.24 vol.% functionalized carbon nanotubes. Flexure and Compression tests were carried out on samples in order to evaluate the effects of different functionalization conditions. The main findings of this experimental investigation are summarized below.

The refined functionalization process of carbon nanotubes is sensitive to both the functionalization condition as well as the diameter of nanotubes. For example, PEI introduction made positive contributions in the case of functionalized MWNT D (8-15 nm diameter) at 0.24 vol.%, but had negative effects on the flexural strength and energy absorption capacity when applied to acid-functionalized MWNT E (20-40 nm diameter) (Figs. 4.12 & 4.13). Similar trends were observed upon treatment of functionalized nanotubes with GA. Another observation is that a rise in the dosage of the treatment agent proportional with increasing nanotube concentration may not be optimal in the case of GA and PEI treatments.

Test results indicate that PAA is the preferred polymer for further functionalization of nanotubes via polymer physisorption/tethering. PAA has produced consistent results with both functionalized and non-functionalized MWNT D. Although some mixes with GA (0.16 vol.% of acid-functionalized MWNT D) and PEI (0.16 vol.% of non-functionalized MWNT D) gave the best results, these polymers produced inconsistent overall effects at different nanotube volume fractions and for different pre-functionalization conditions.

PAA produced positive effects on both the flexural strength and energy absorption capacity of cementitious nanocomposites at different volume fractions of MWNT D, and with different prefunctionalization conditions. As noted earlier, the exploratory word conducted in the course of this investigation indicated that further improvements in PAA-functionalized nanotubes can be realized by not increasing the PAA content in proportions with the nanotube volume fraction.

As was the case with MWNT D, with MWNT E also PAA emerged as the only polymer used for further functionalization via physisorption/tethering which consistently benefited the reinforcement efficiency of nanotubes. The increase in flexural strength was evident with increasing volume fraction of MWNT E. However, the maximum deflection and energy absorption capacity of cementitious nanocomposites with 0.24 vol.% of non-functionalized MWNT E were reduced, and the flexural strength was unaffected. This could indicate that these mixes can be further improved by not increasing the (functionalizing) polymer in proportion with the nanotube volume fraction.

Cementitious nanocomposites with desired flexural attributes did not exhibit any significant loss of compressive strength, while those with unfavorable flexural performance exhibited measurable losses of compressive strength, Fig.s 4.12c and 4.13c.

A comparison of the GA, PAA and PEI treatment effects on the MWNT F contributions to flexural performance at 0.16 vol.% (Fig. 4.14) indicated that only PAA treatment produced promising results; both GA and PEI treatments caused a marked reduction of flexural strength and energy absorption capacity of cementitious nanocomposites. A significant drop upon GA treatment of MWNT F can be attributed to its longer length which could complicate its dispersion under sonication.

Both MWNT F and G (functionalized through microwave irradiation) at 0.16 vol.% produced an increase in flexural strength, maximum deflection and energy absorption capacity (Fig. 4.15). This shows that both MWNT F and G act as effective reinforcement at this volume fraction, which is partly due to their longer lengths (200 µm). MWNT F, due to its smaller diameter (8-15 nm), showed more promise as reinforcement in DSP cementitious paste. The gains in flexural strength, maximum deflection and energy absorption capacity with 0.16 vol.% of MWNT F were 24%, 65% and 145%, respectively.

4.4.2 Scanning Electron Microscope Investigations

Observations of failed surfaces of flexure and compression test specimens using a high-precision scanning electron microscope (JOEL JM-6300F) provided further insight into the mechanisms of actions of nanotubes with different functionalization conditions in cementitious matrices. All specimens which provided high flexural strength and energy absorption capacity showed nanomaterials bridging across (and pulling out at) micro-cracks (Figs. 4.16a & b). Specimens that provided lower flexural and compressive strengths, on the other hand, exhibited compromised microstructures with reduced matrix density (Figs. 4.16c & d), which could be attributed to the presence of excess amounts of functionalizing polymer.

4.4.3 X-Ray Diffraction Analysis (XRD)

XRD Analysis of selected specimens was carried out using Rotaflex Rigaku 200B Analyzer. The spectrum was analyzed using JADE to identify various elements according to their crystalline structure. Typical XRD spectrographs for DSP Pastes with 0% and 0.16 vol.% of MWNT D and MWNT E (both acid-functionalized and carrying adsorbed GA) are presented in Fig. 4.17, noting that higher compressive and flexural strength levels were obtained with MWNT D. The spectrum for MWNT D shows no significant difference when compared with that for plain matrix. The two major compounds identified in these two samples were calcium silicate (Ca₃SiO₅) and calcium silicate oxide (Ca₃(SiO₄)O). However, the mix containing MWNT E shows peaks corresponding to calcium hydroxide which does not provide the high surface area and binding qualities of calcium silicate hydrate. This adverse effect of functionalized MWNT E on the matrix structure could be used to explain the relatively low flexural and compressive strengths provided by these nanocomposites (see Figs. 4.12 and 4.13). In other words, depending on the nanotube type and functionalization conditions, introduction of nano-scale reinforcement with high specific surface area could interfere with the hydration/pozzolanic reactions of cementitious matrix.

4.4.4 Thermogravimetric Analysis (TGA)

Thermogravimetric analyses of the cementitious matrix (DSP Paste) were performed using the TA Instrument Hi-Res TGA 2950 Thermogravimetric Analyzer. A finely ground powder (passing No. 100 mesh) of the material was used in thermogravimetric analysis. The samples were heated at a constant rate of 10°C per minute up to 1000°C, with the weight loss recorded as

a function of temperature. Tests on selected mixes were conducted 15 days after casting of cementitious specimens.

The TGA test results for the materials introduced in previous section (on XED) are shown in Fig. 4.18. The lower-strength cementitious nanocomposites with 0.16 vol% MWNT E (acid-functionalized, with physisorbed Gum Arabic) showed excess weight loss with increasing temperature. The loss of water is evident, which points at the presence of excess water that was not chemically bound with cement. In the case of the higher-strength cementitious nanocomposite reinforced with MWNT D (acid-functionalized, with physisorbed Gum Arabic), the mass loss trends were similar to those of the plain cementitious matrix.

4.5 Summary

Experimental studies were conducted on the reinforcement efficiency of multiwalled carbon nanotubes with different aspect ratios and surface modification conditions in high-performance cementitious materials. The surface modification conditions considered involved (acid) functionalization of carbon nanotubes and/or anchoring different polymers via chemical bonding or physical adsorption. Experimental results indicated that a combination of the surface modification specifics and the nanotube aspect ratio determines their reinforcement efficiency in high-performance cementitious matrices. The most consistent favorable effects were produced when poly(acrylic acid) (PAA) was physisorbed on nanotubes. Increased nanotube length and aspect ratio also benefited their reinforcement efficiency in high-performance cementitious matrices; excess nanotube lengths, however, complicate their dispersion in the mixing water of cementitious matrix at required concentrations. The best balance of mechanical properties was realized when longer multiwalled carbon nanotubes were used with physisorbed PAA, which were not acid-functionalized prior to introduction of PAA. It seems that the benefits of acid-

functionalization are more than compensated for by their damaging effects involving shortening of carbon nanotubes. The benefits realized by proper surface modification of nanotubes can be explained by their contributions towards uniform dispersion in aqueous media, and improved interfacial interactions with cement hydrates. The extent of surface modification as well as the concentration of nanotubes in cementitious matrix should be optimized, depending on the composition and processing conditions of cementitious nanocomposites, in order to avoid agglomeration of nanotubes and their potential interferences with the hydration process of cement.

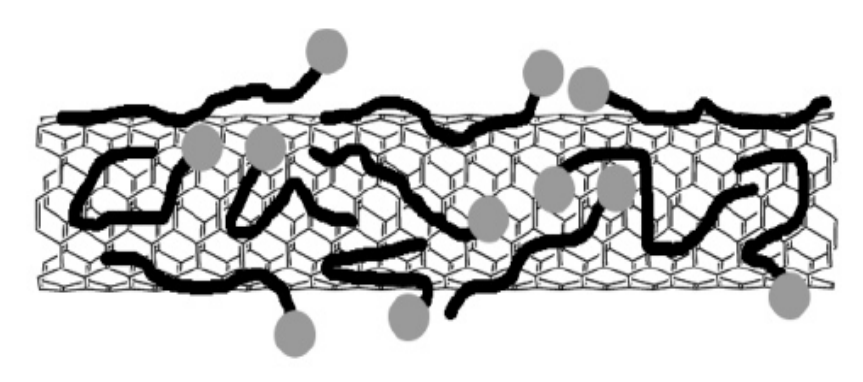


Figure 4.1- Schematic depiction of the random and disordered adsorption of polymers upon carbon nanotube walls.

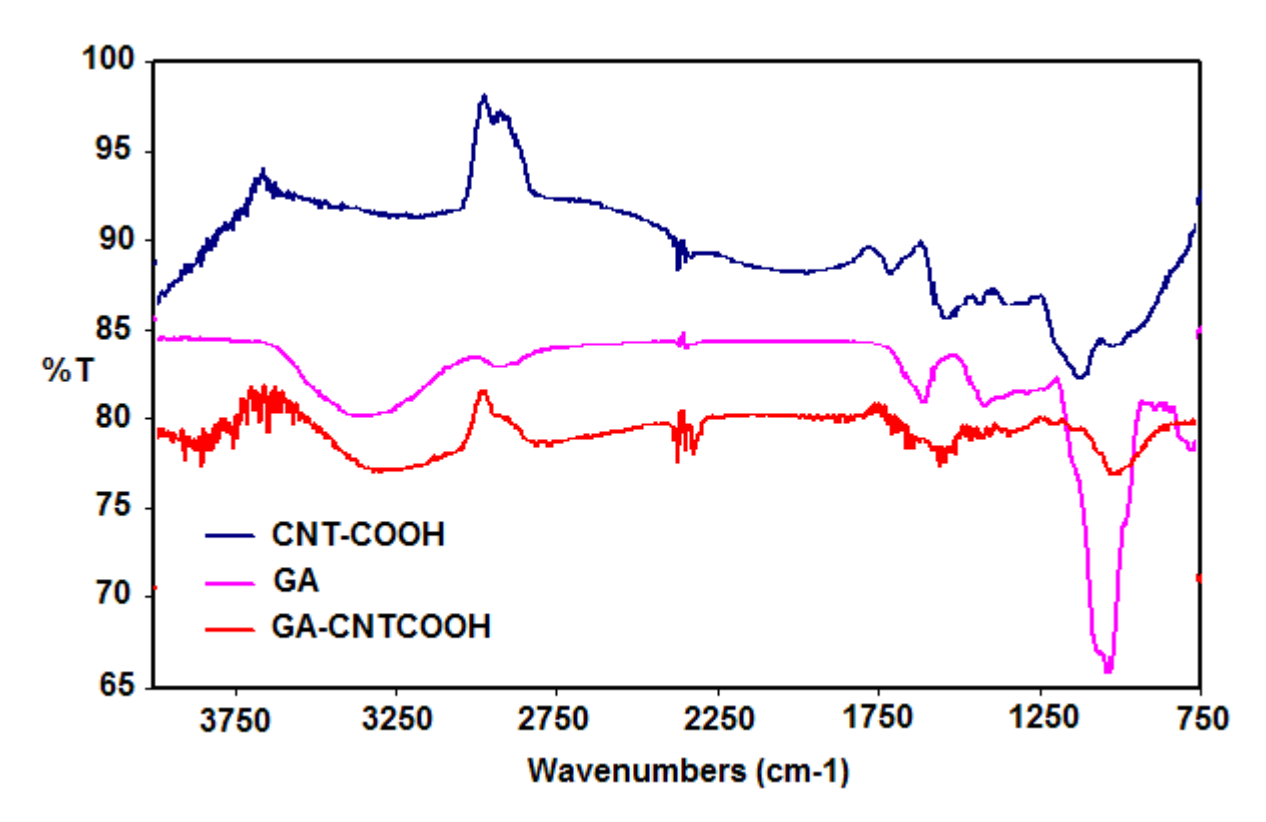


Figure 4.2- FTIR spectra for acid-functionalized carbon nanotubes (CNT-COOH), Gum Arabic (GA), and acid-functionalized nanotubes modified with Gum Arabic (GA-CNTCOOH).

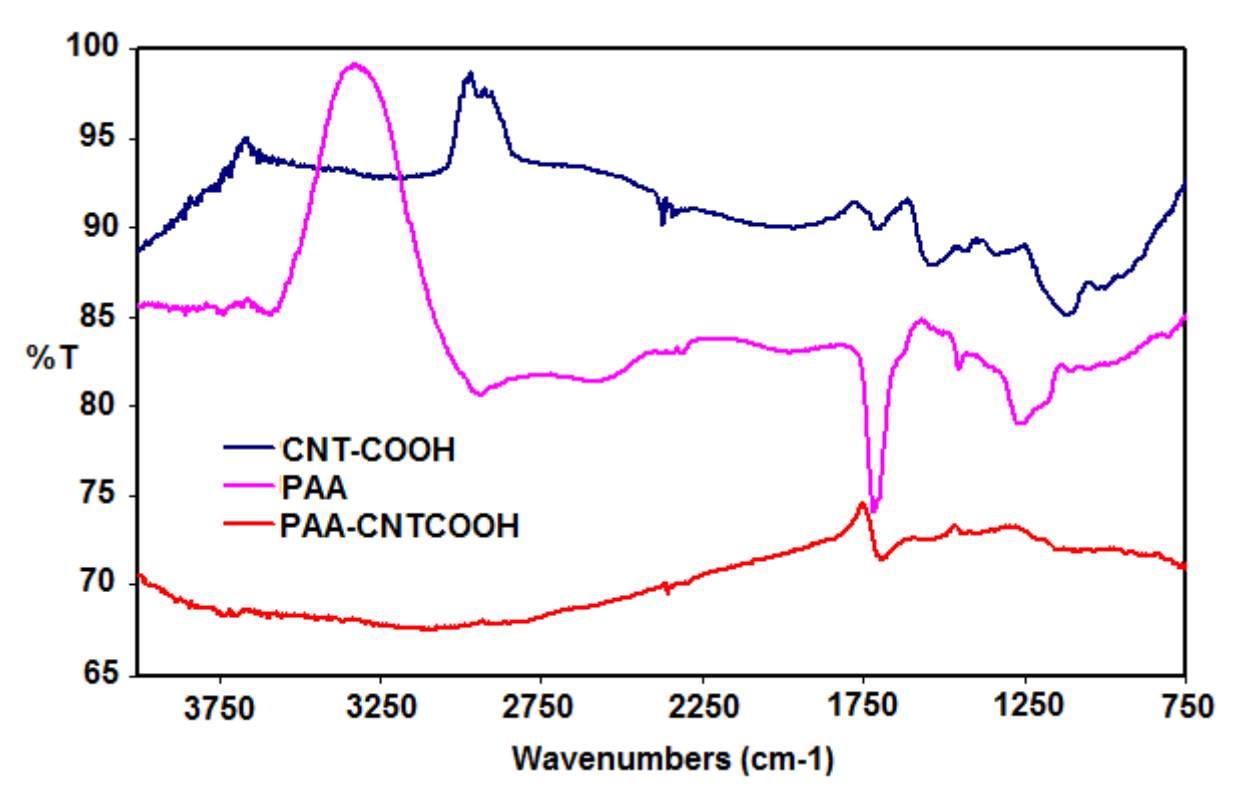


Figure 4.3- FTIR spectra of acid-functionalized carbon nanotubes (CNT-COOH), PAA, and acid-functionalized nanotubes modified with PAA (PAA-CNTCOOH).

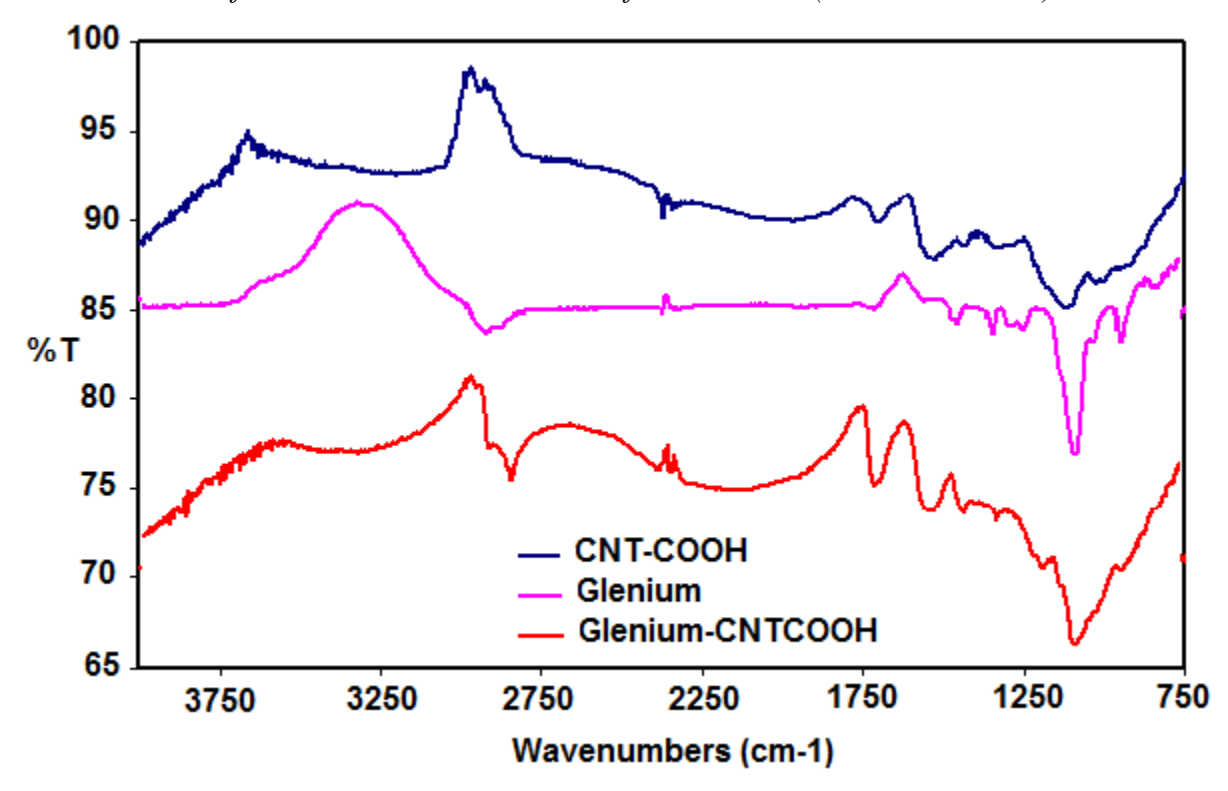


Figure 4.4- FTIR spectra of acid-functionalize carbon nanotubes (CNT-COOH), Glenium®, and acid-functionalized nanotubes modified with Glenium® (Glenium-CNTCOOH).

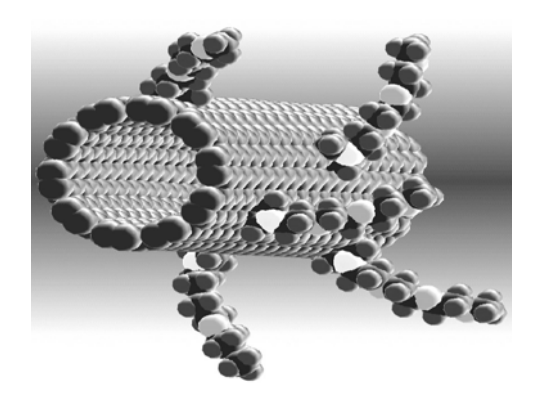


Figure 4.5- Schematic depiction of the tethering (covalent attachment) of polymer chains via functional groups onto nanotube walls.

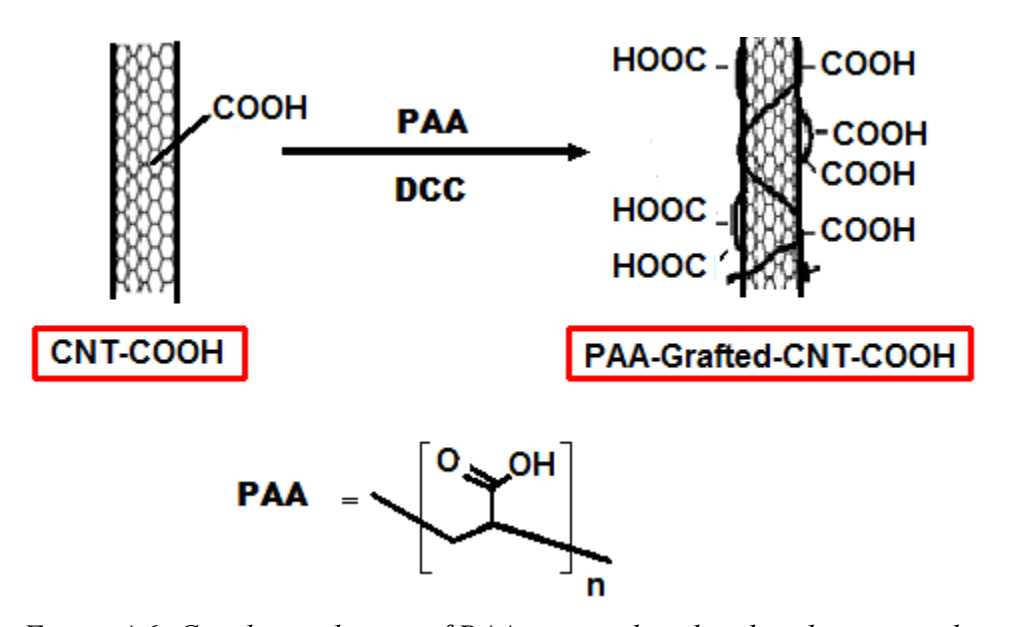


Figure 4.6- Covalent tethering of PAA onto carboxylated carbon nanotube.

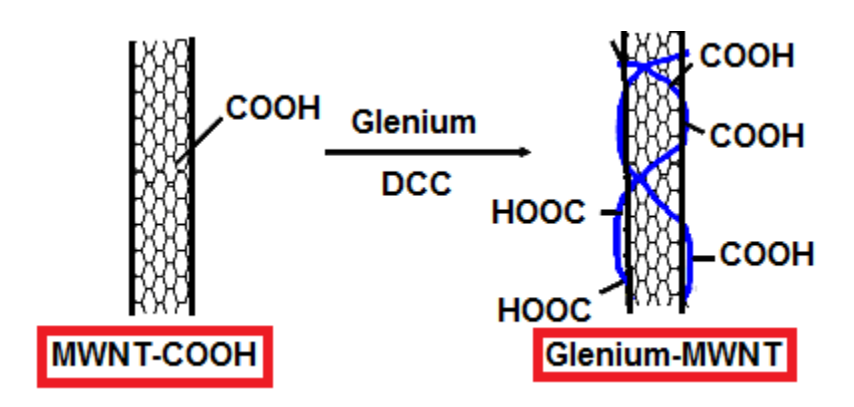


Figure 4.7- Tethering of Glenium® onto carboxylated nanotube.

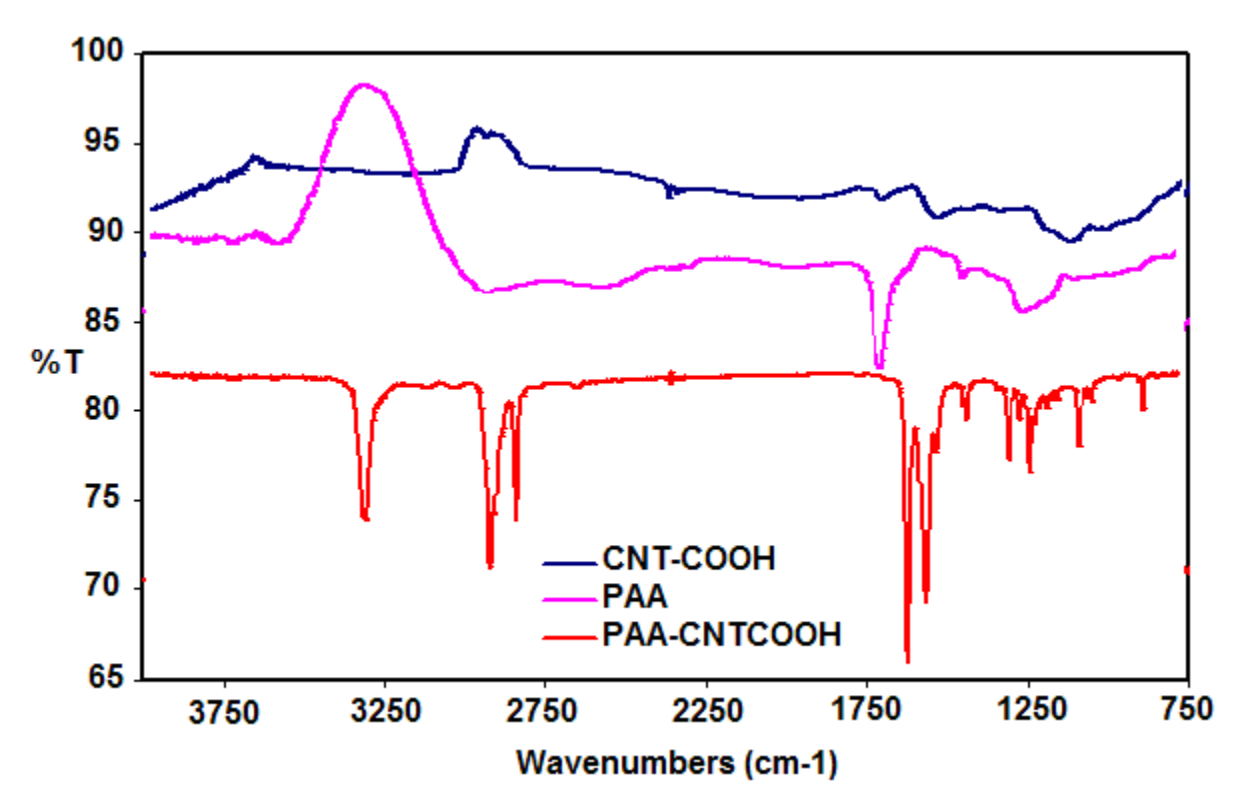


Figure 4.8- FTIR spectra of carboxylated nanotubes (CNT-COOH), PAA and PAA-tethered carboxylated nanotubes (PAA-CNTCOOH).

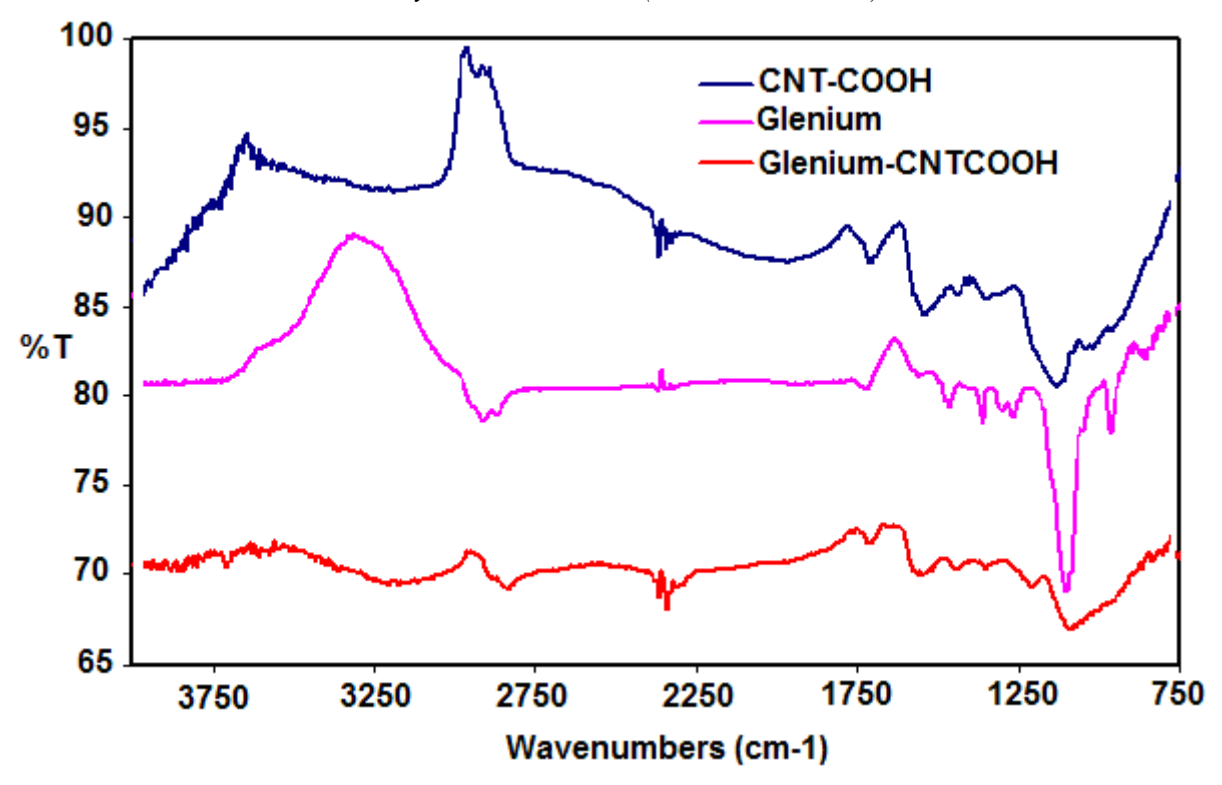


Figure 4.9- FTIR spectra of carboxylated nanotubes (CNT-COOH), Glenium® and Glenium®-tethered carboxylated nanotubes (Glenium-CNTCOOH).

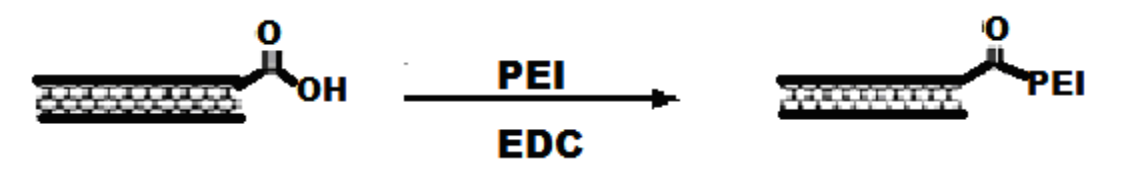


Figure 4.10- Schematic depiction of covalent tethering of PEI to carboxylated nanotubes.

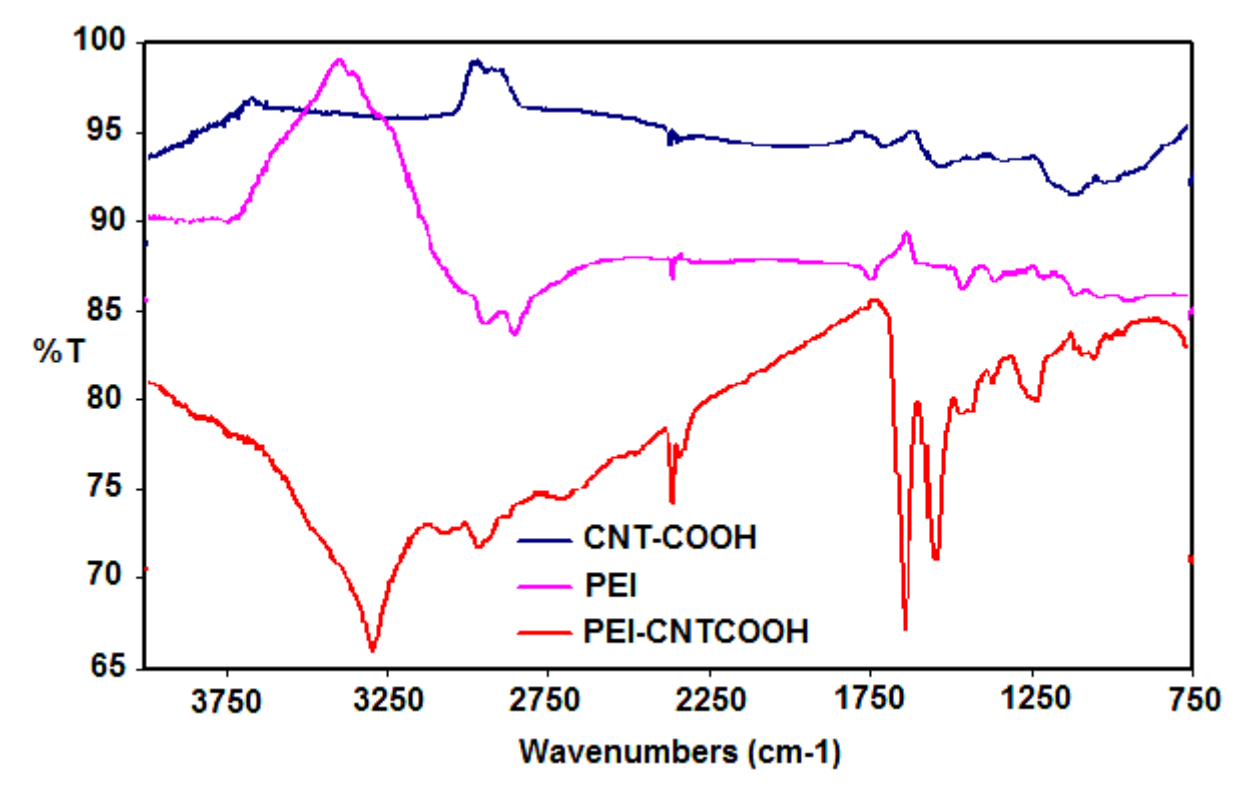


Figure 4.11- FTIR spectra of carboxylated nanotubes (CNT-COOH), PEI, and PEI-tethered carboxylated nanotubes (PEI-CNTCOOH).

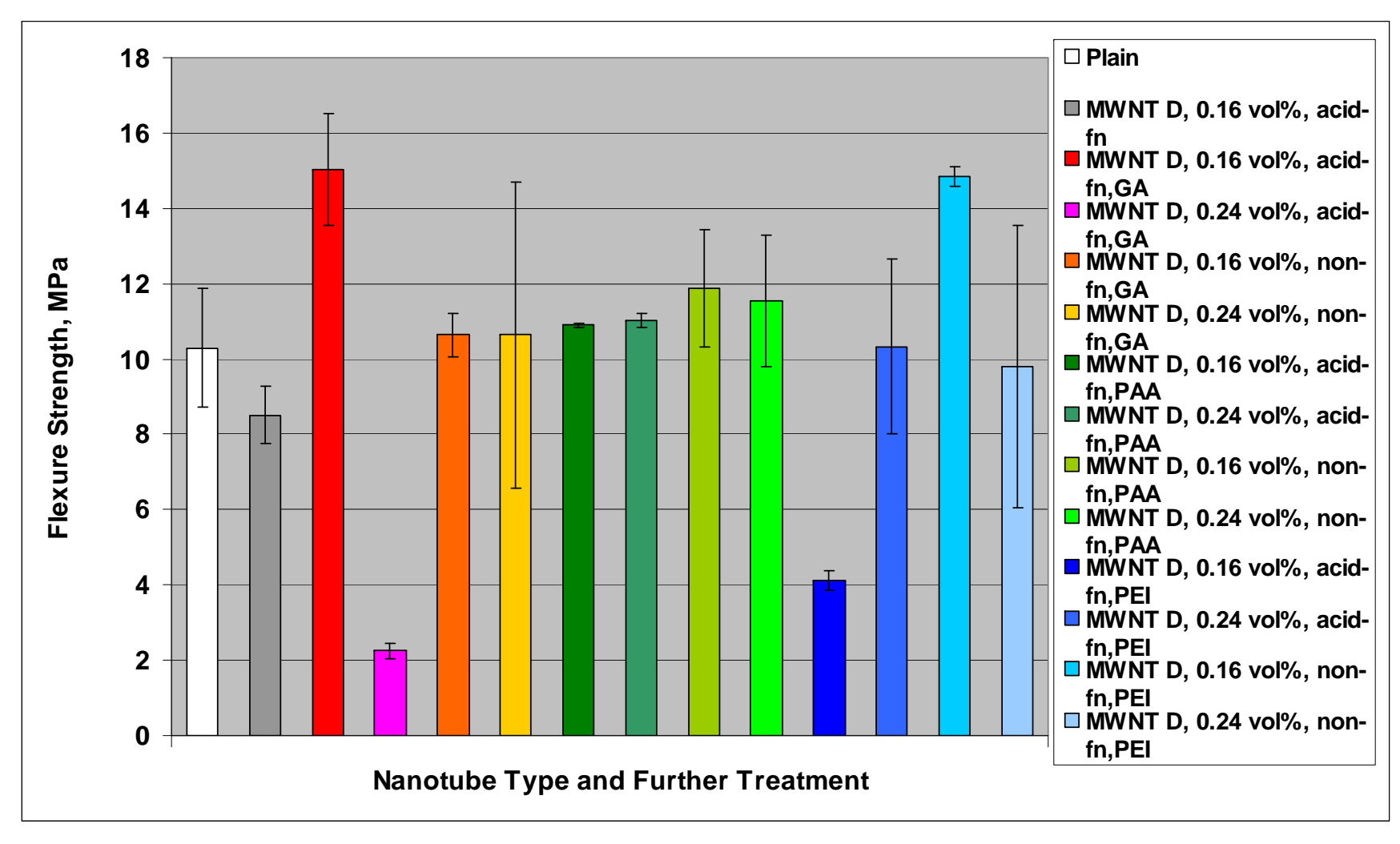
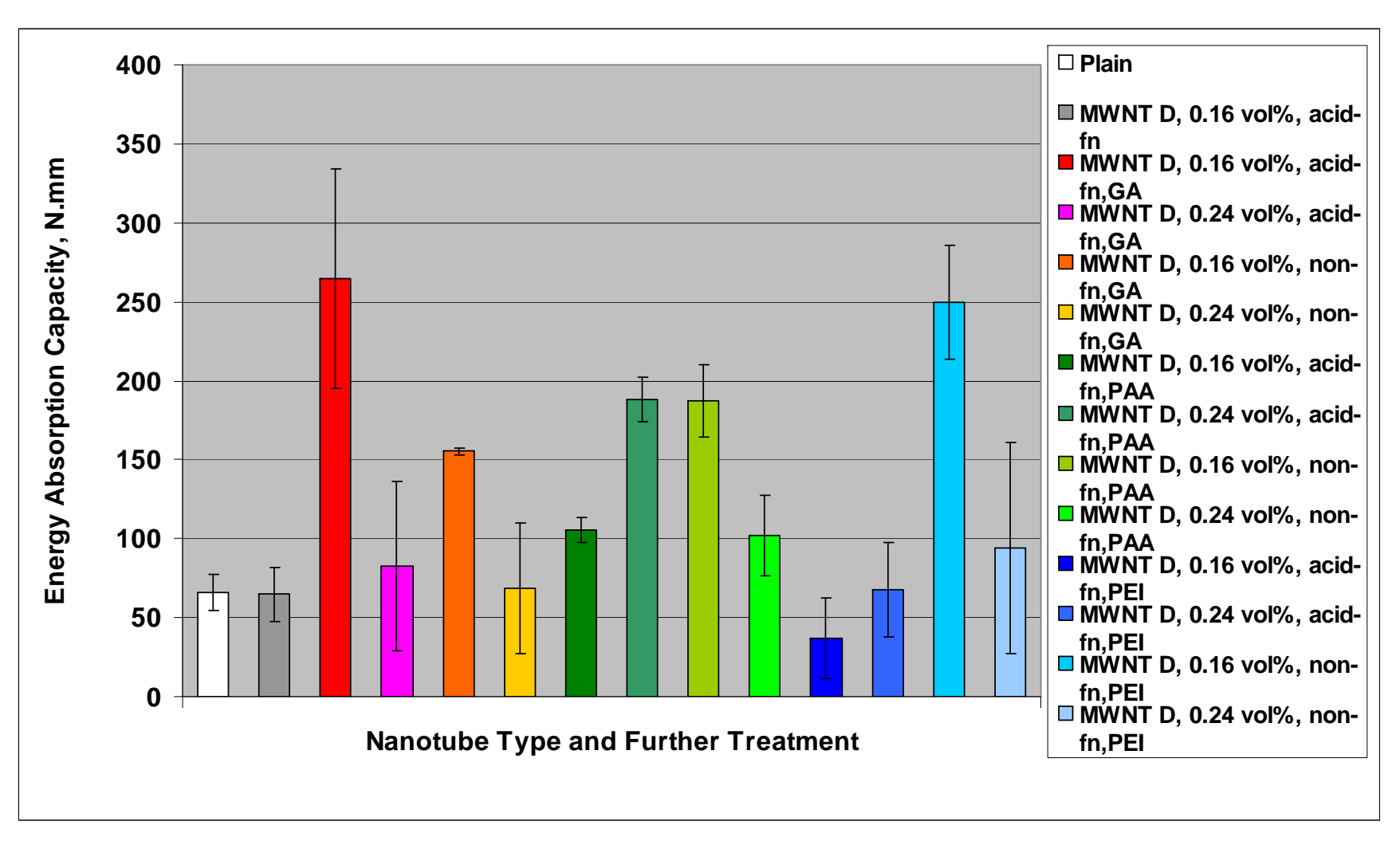
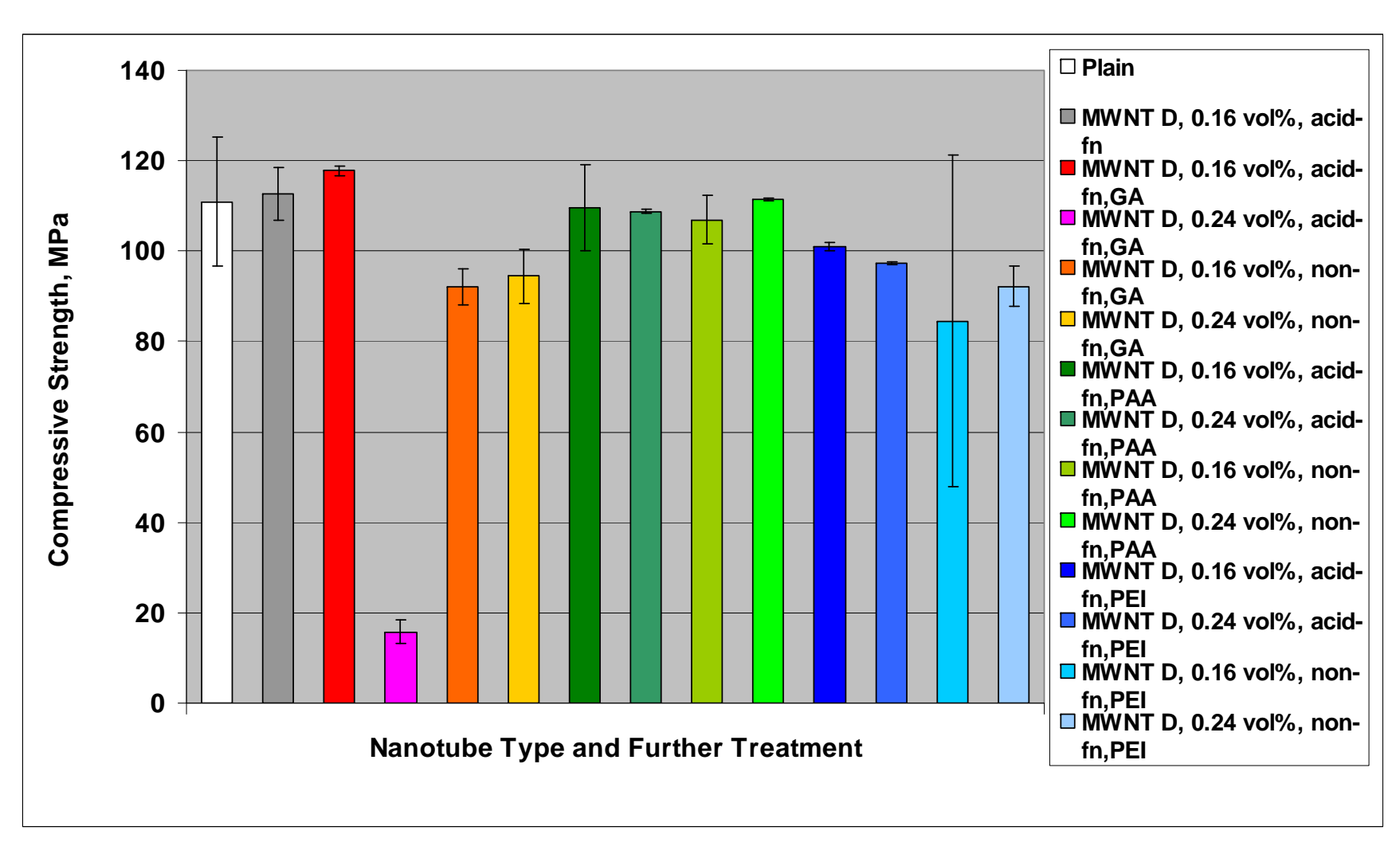


Figure 4.12- Mean values and standard errors of the flexural attributes and compressive strength of DSP paste reinforced with 0%, 0.16% and 0.24% volume fractions of acid-functionalized and non-functionalized MWNT D with different further treatments.



(d) Energy absorption capacity



(c) Compressive strength

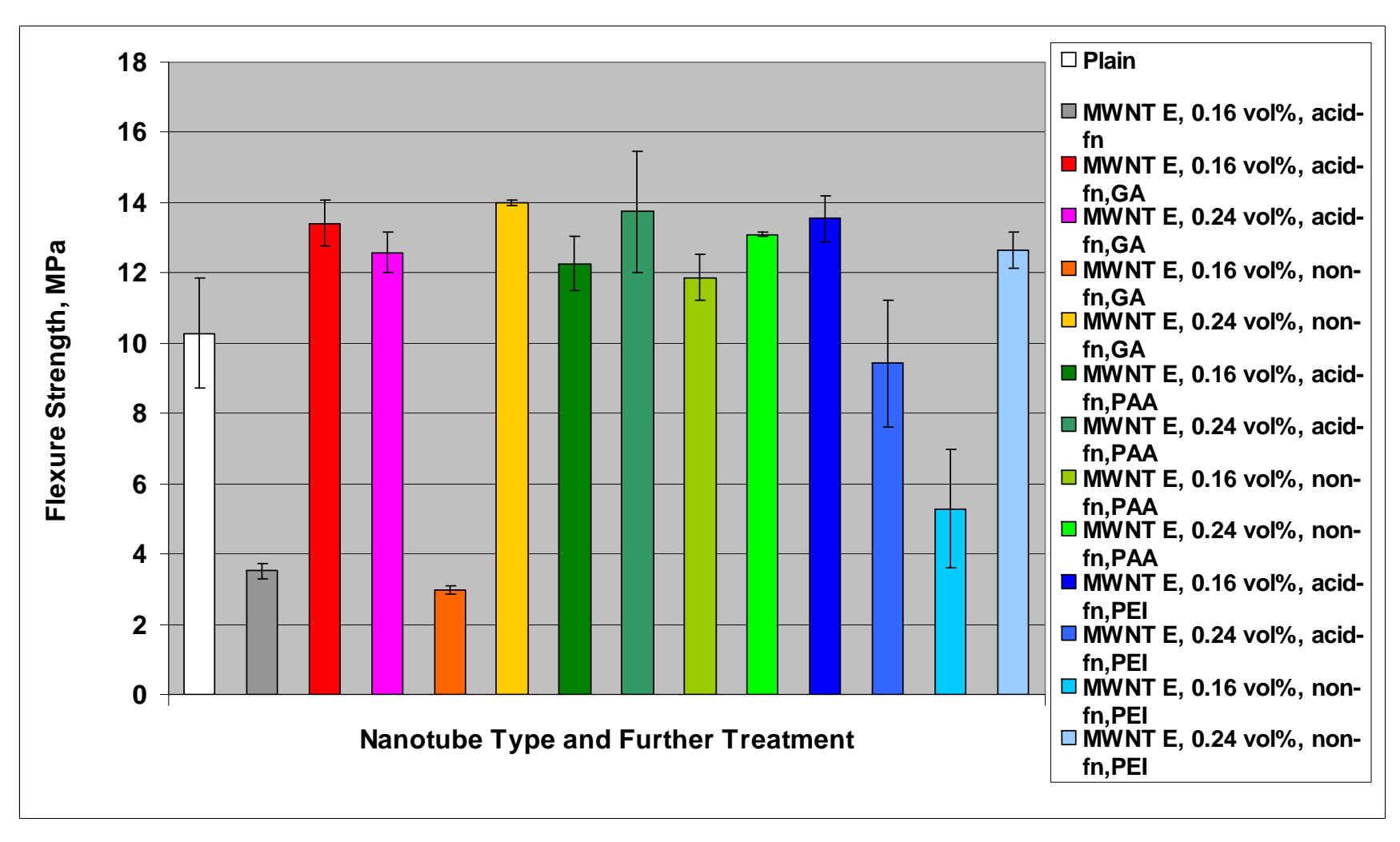
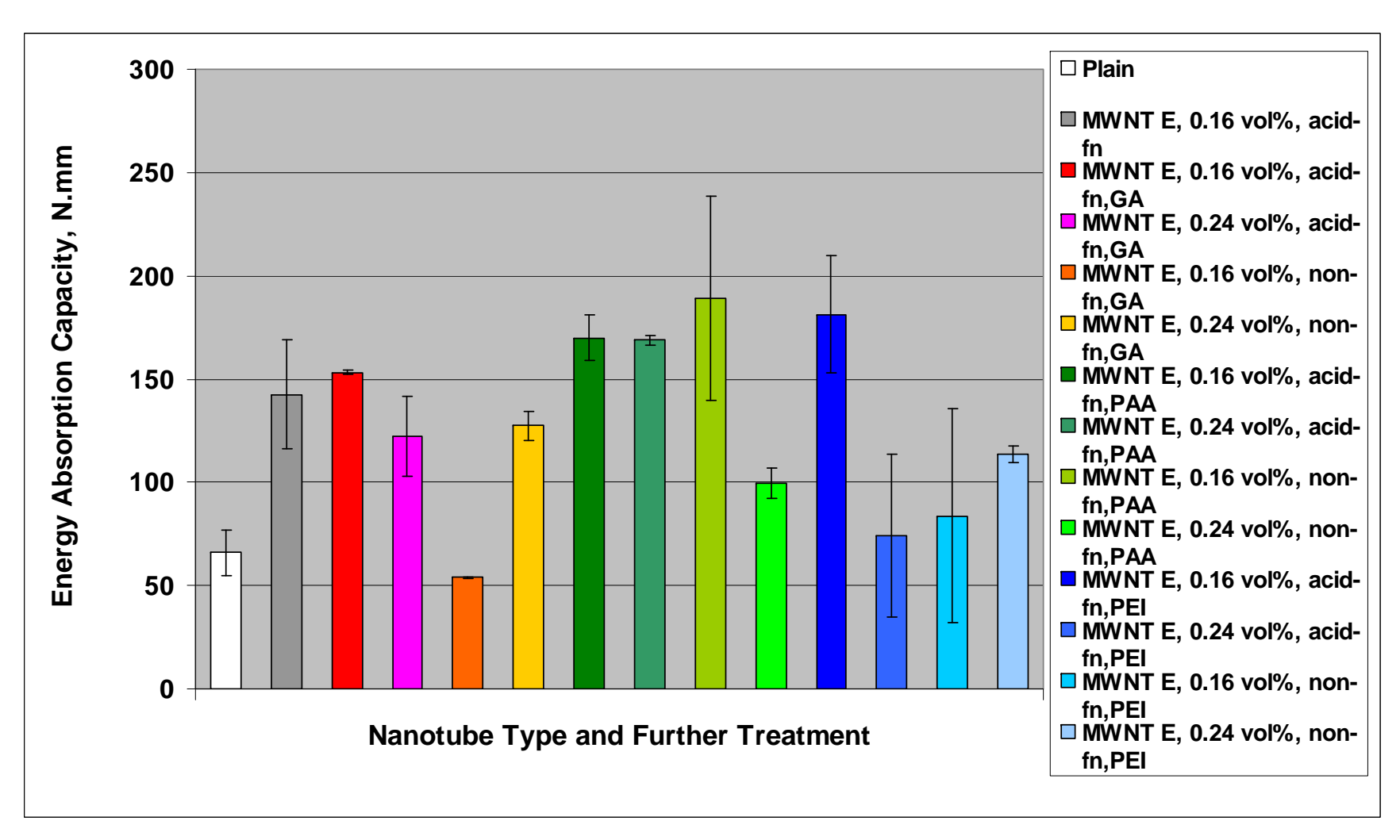
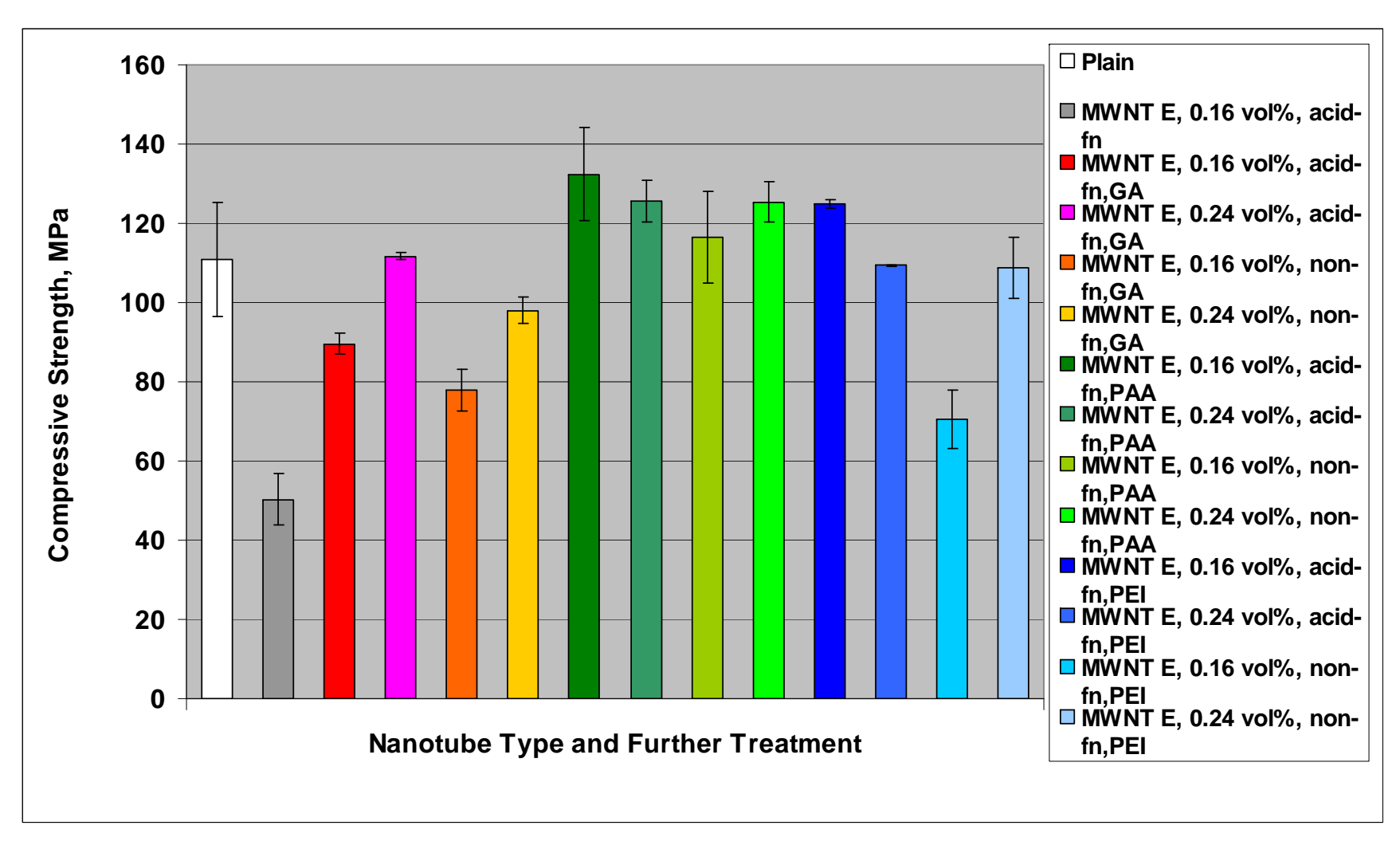


Figure 4.13- Mean values and standard errors of the flexural attributes and compressive strength of cementitious (DSP) pastes reinforced with 0%, 0.16% and 0.24% volume fractions of acid-functionalized and non-functionalized MWNT E with different further treatments.



(b) Energy absorption capacity



(c) Compressive strength

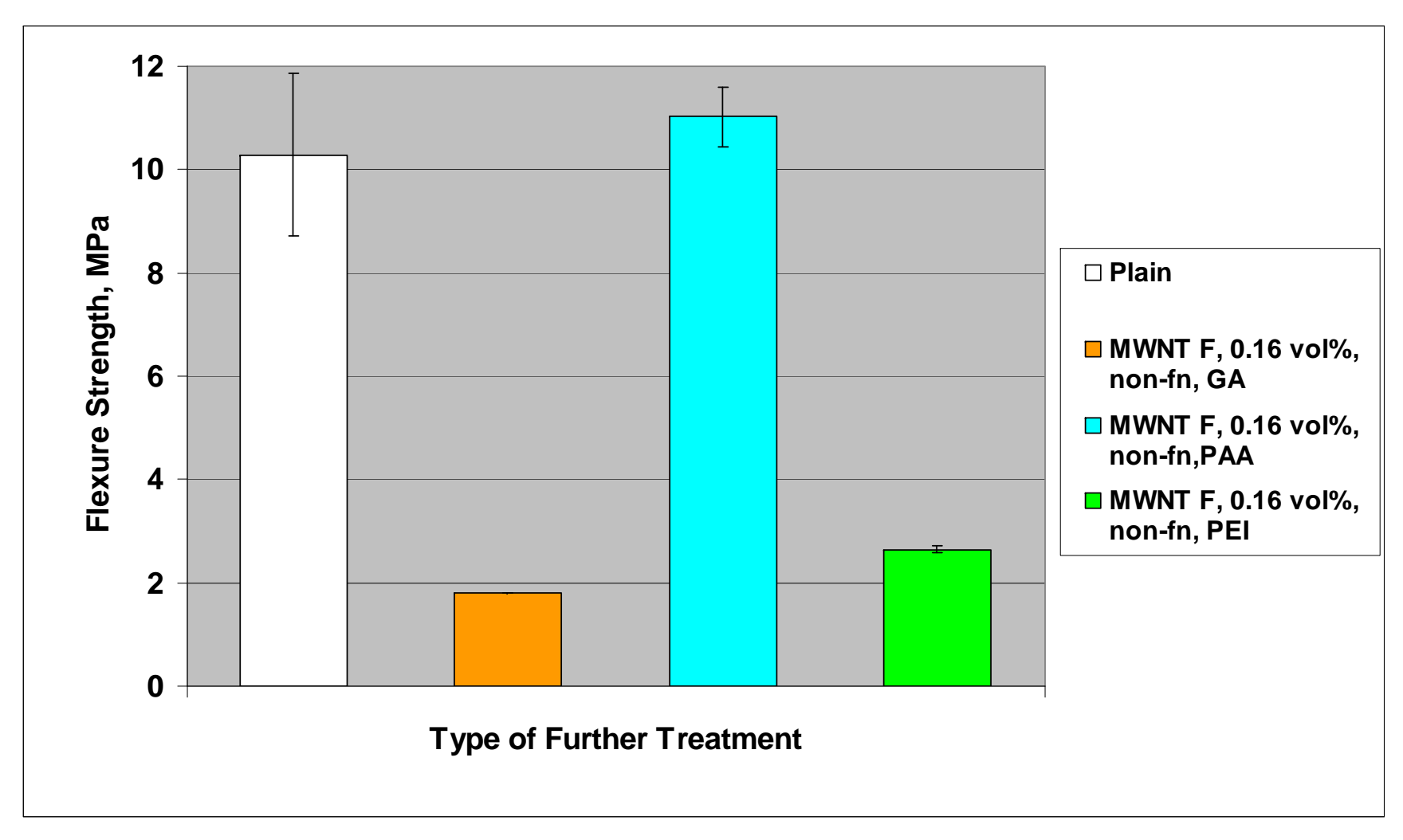
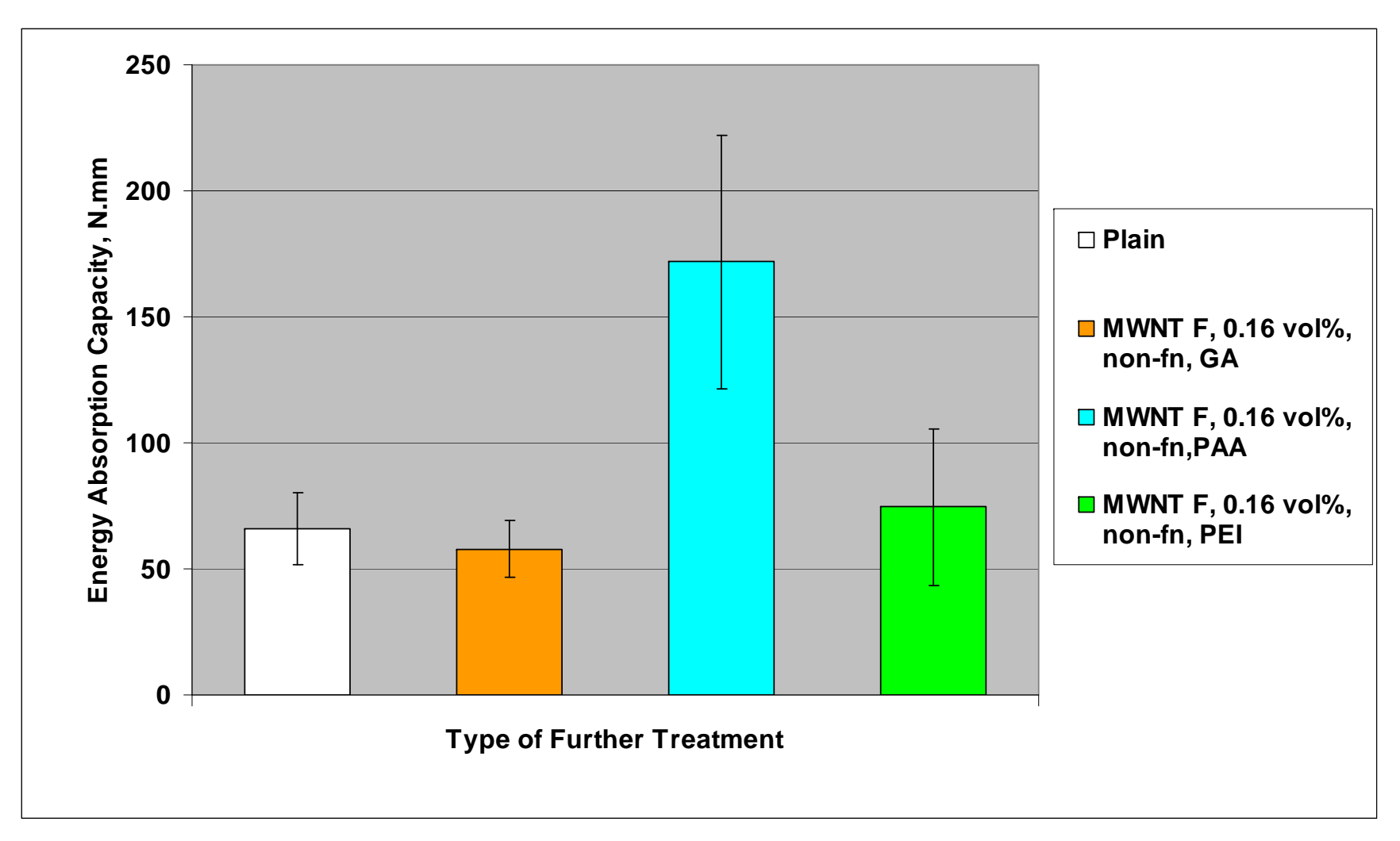


Figure 4.14- Mean values and standard deviations of the flexural strength and energy absorption capacity test results for cementitious (DSP) pastes reinforced with 0% and 0.16% volume fractions of non-functionalized MWNT F with different polymer treatments.



(b) Energy absorption capacity

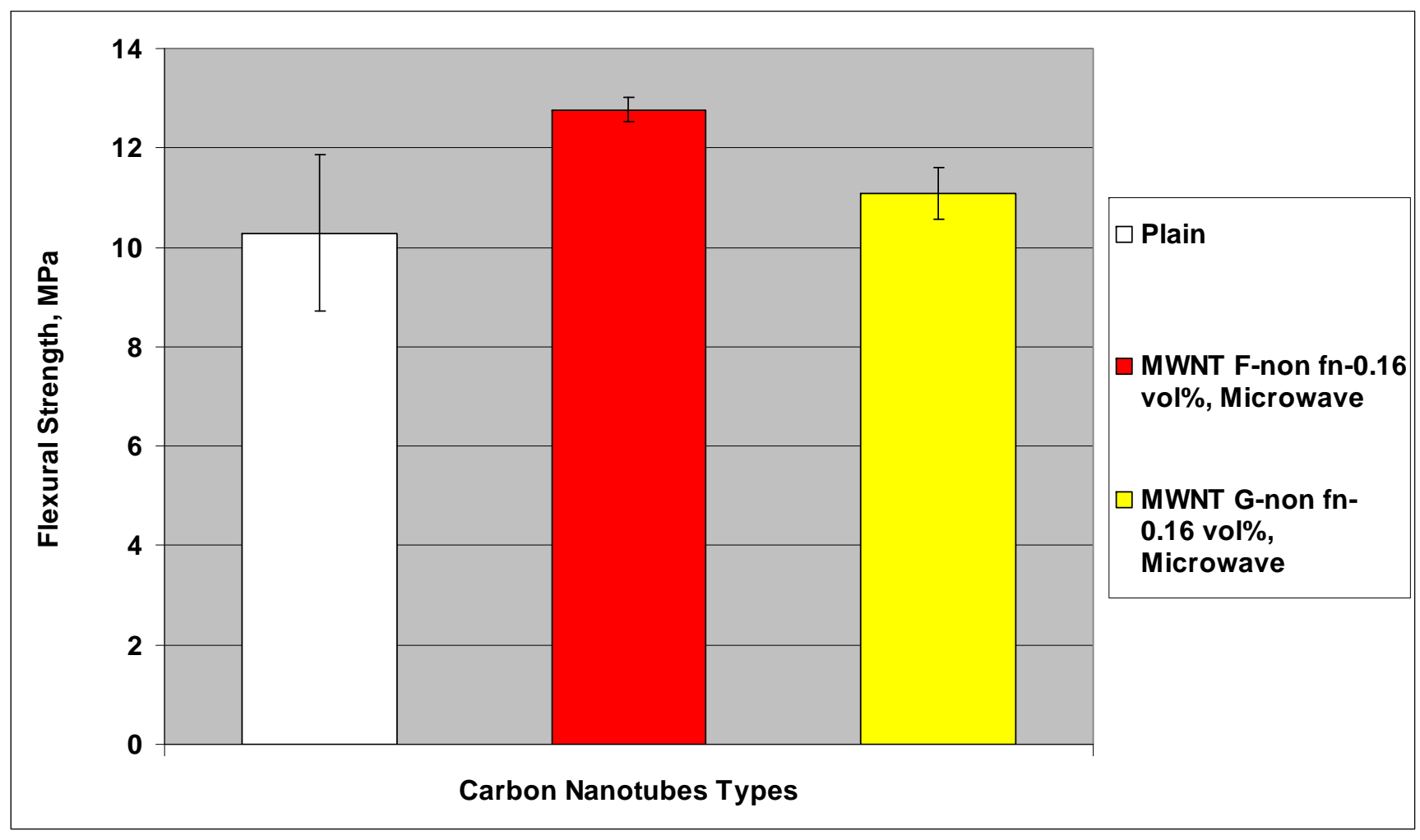
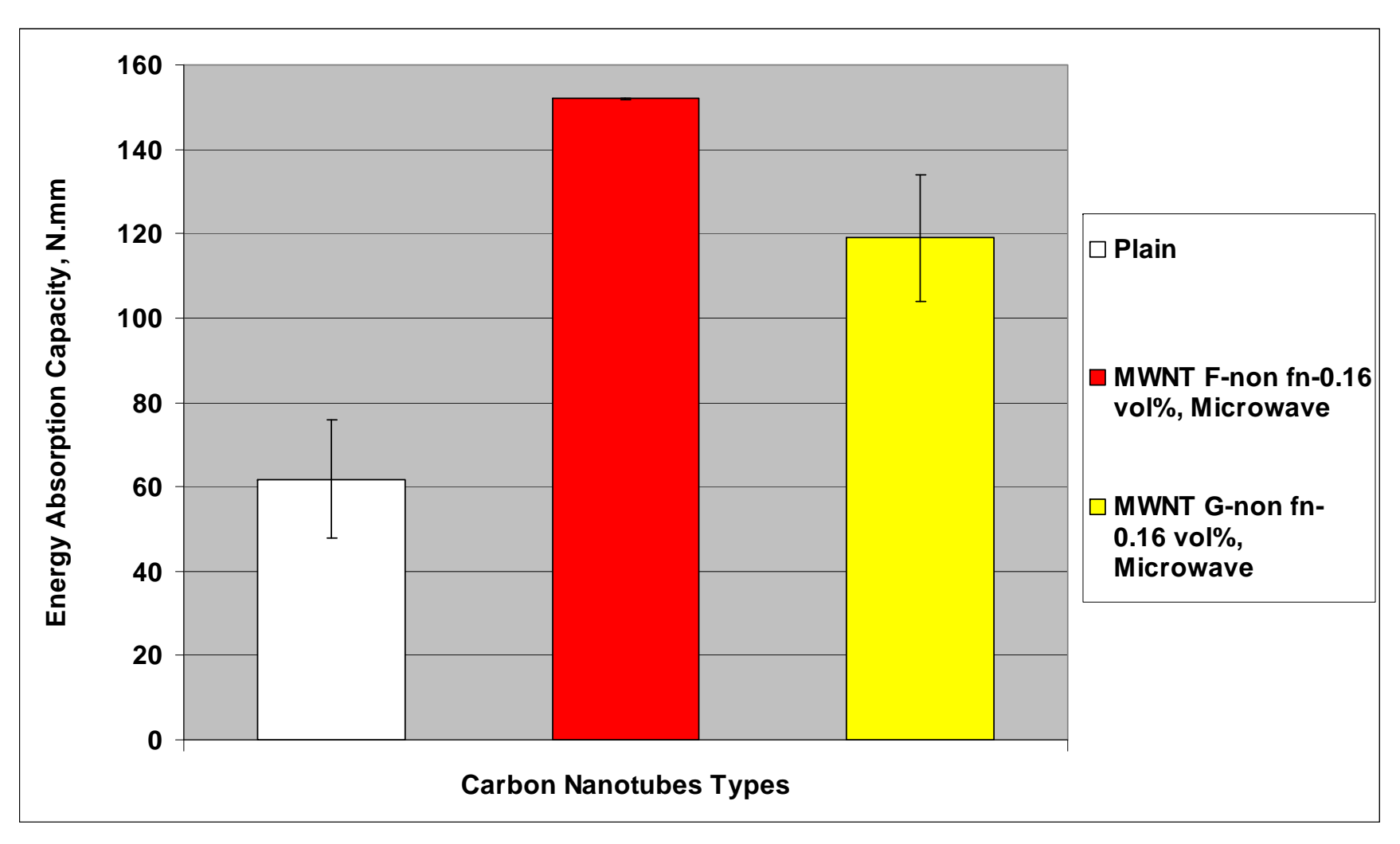


Figure 4.15- Flexural strength and energy absorption capacity of DSP cement pastes reinforced with 0% and 0.16% volume fractions of microwave treated MWNTs F and G.



(b) Energy Absorption Capacity

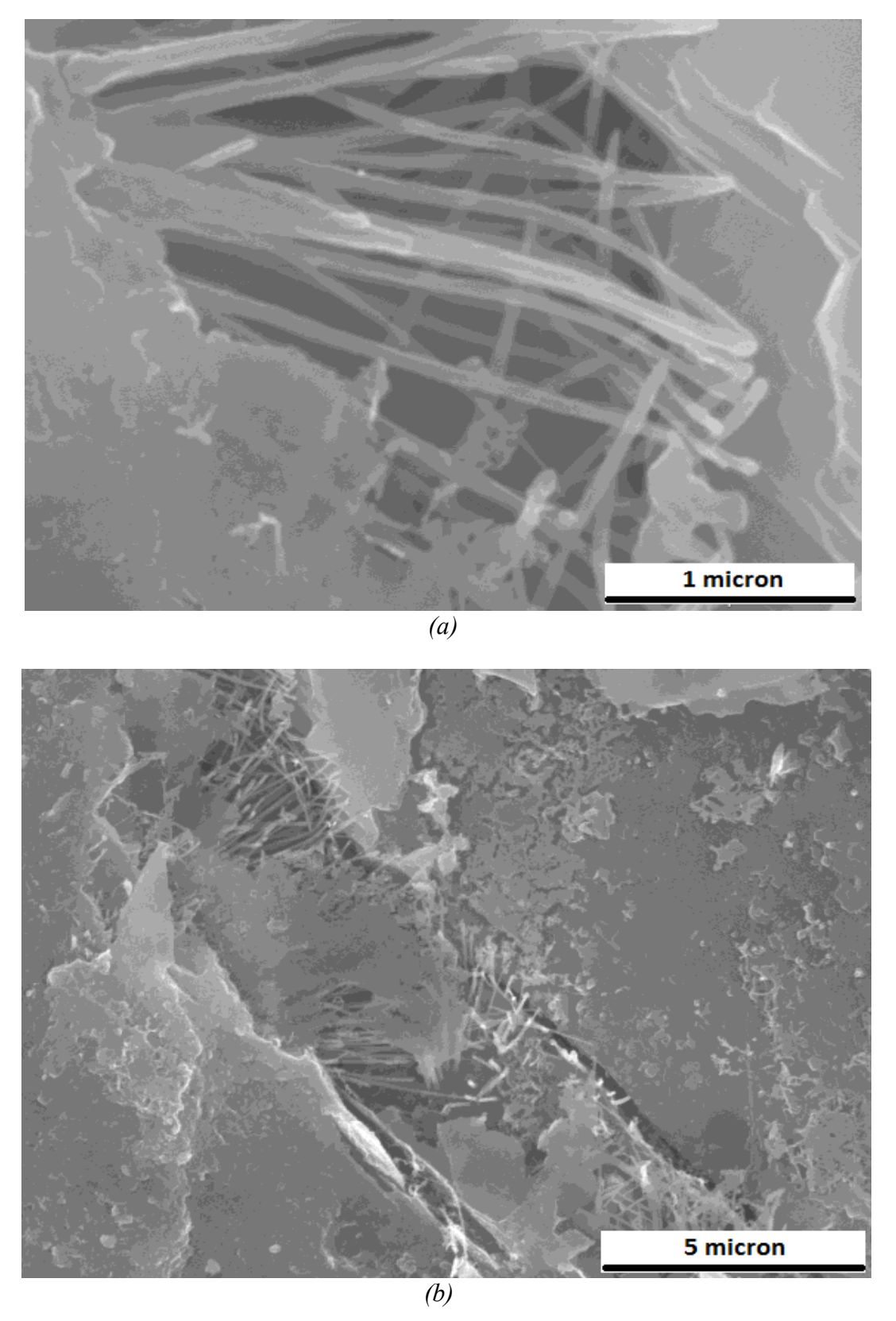
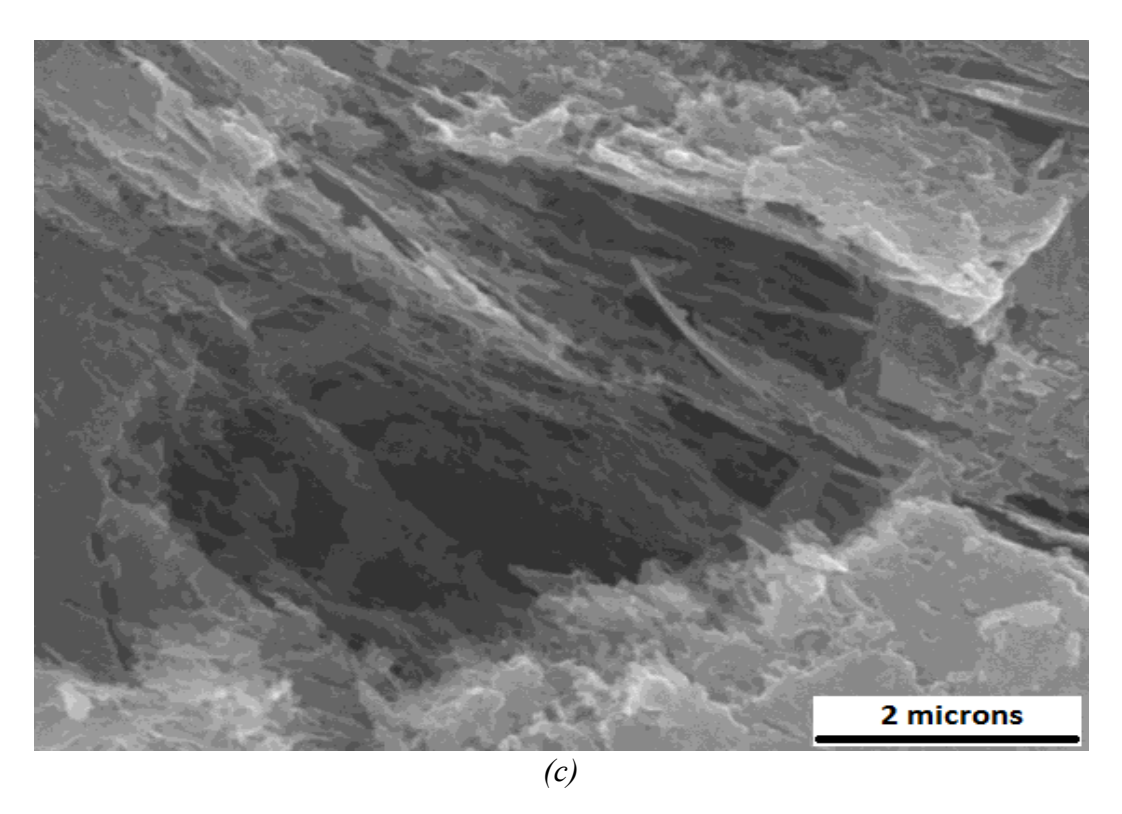
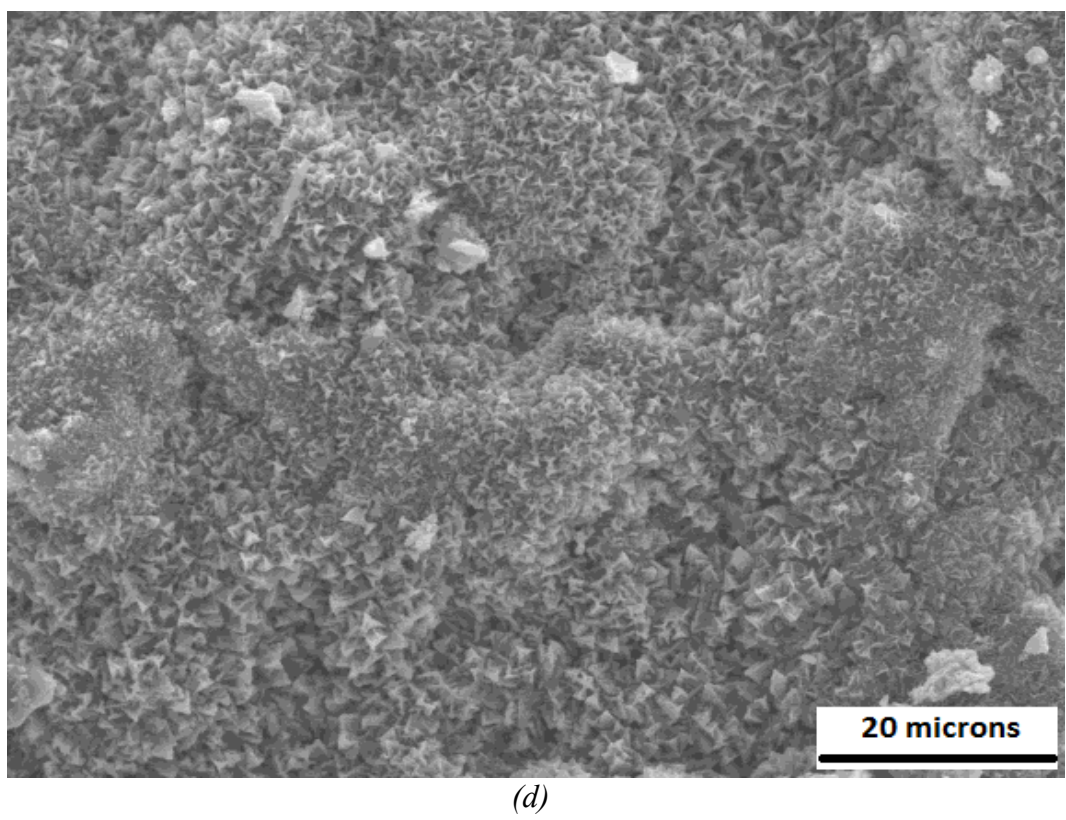


Figure 4.16- Scanning electron microscope images of the cementitious DSP paste with different volume fractions of surface-modified carbon nanotubes.

Figure 4.16 (cont'd)





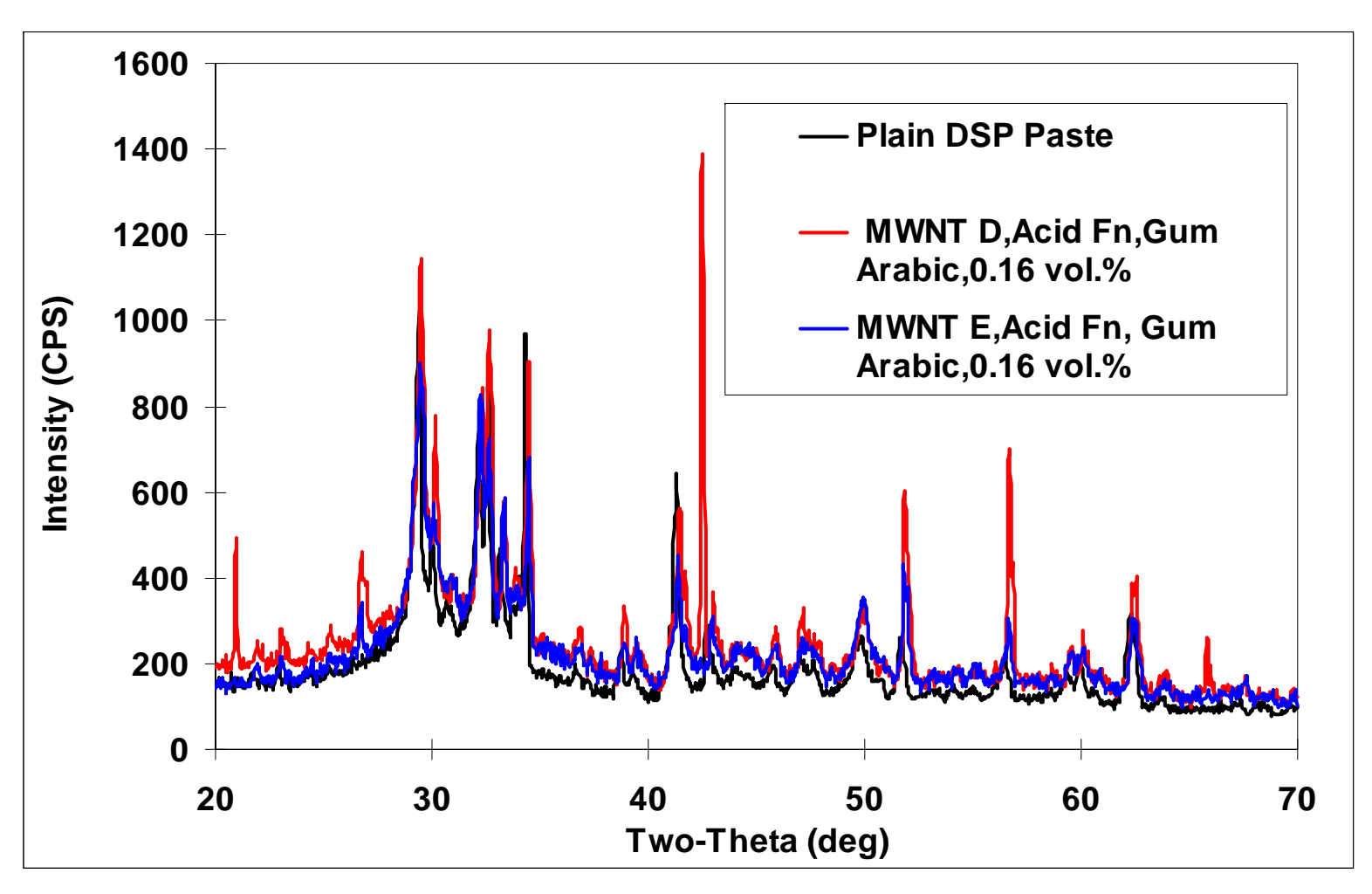


Figure 4.17- XRD spectrographs of DSP pastes with 0% and 0.16% volume fractions of acid-functionalized MWNT D and MWNT E, that are further modified with Gum Arabic.

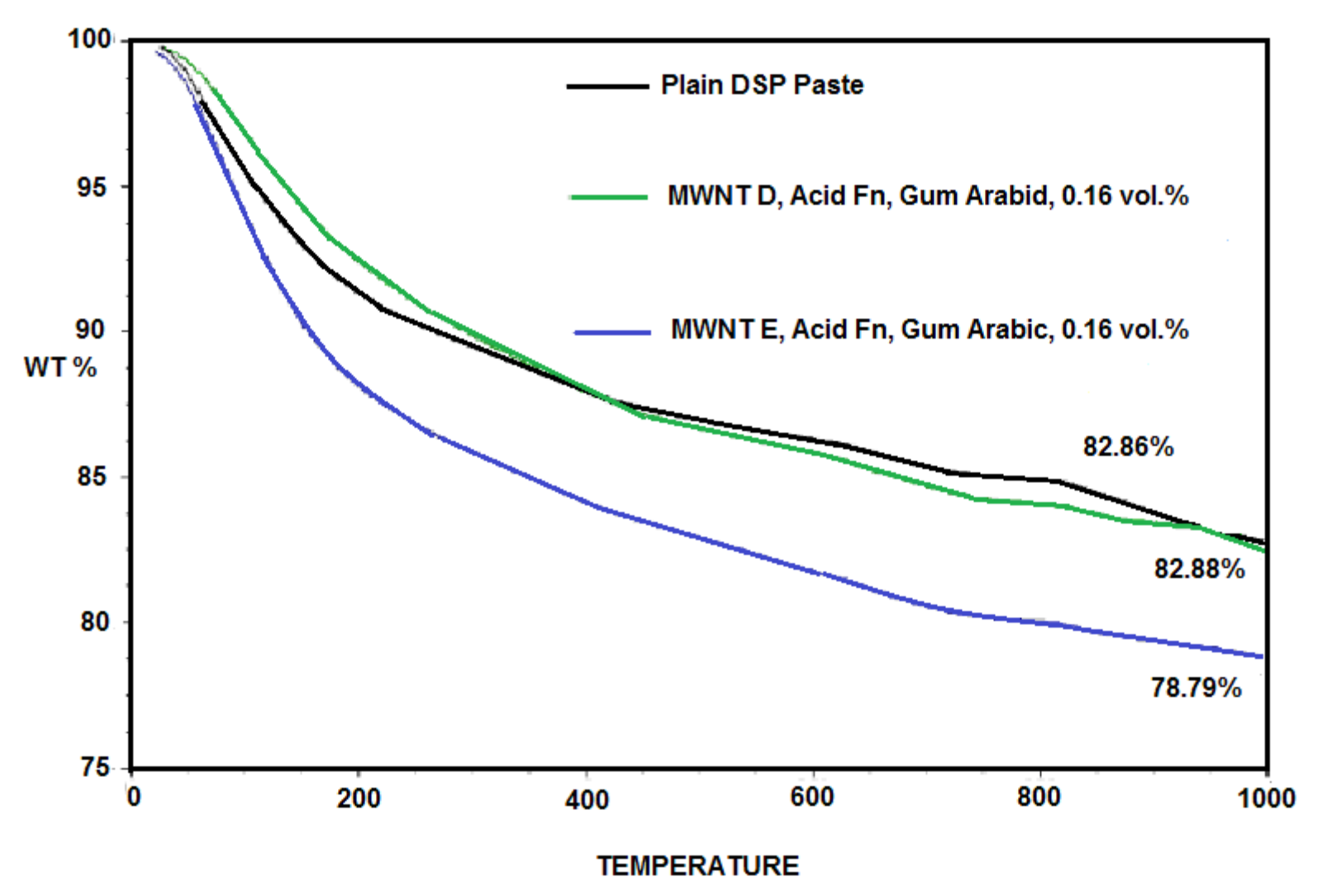


Figure 4.18- Results of thermogravimetric analysis showing weight loss versus temperature.

5 REINFORCING EFFECTS OF MULTIWALLED CARBON NANOTUBES AND FIBERS IN HIGH-PERFORMANCE CEMENTITIOUS MATERIALS

5.1 General

The effects of surface functionalization of multiwalled carbon nanotubes (MWNTs) through introduction of carboxyl groups and use of refined dispersion techniques on the reinforcement efficiency of nanotubes at different volume fractions within a high-performance cementitious Two types of surface-functionalization and intense (DSP) matrix were evaluated. stirring/sonication techniques were employed for improving the reinforcement efficiency of carbon nanotubes at volume fractions as high as 0.48 vol.% (volume percent of dry cementitious materials). SEM observations of fractured surfaces pointed at successful dispersion of nanotubes within the cement-based matrix. Cementitious nanocomposites with increased volume fractions of functionalized nanotubes provided superior flexural strength and energy absorption capacity. The effects of the degree of nanotube functionalization as well as the nanotube length and diameter on their reinforcing effects in the high-performance cement-based matrix were also investigated. An investigation of hybrid reinforcement systems comprising multiwalled carbon nanotubes and micro-scale fibers indicated that selected hybrid systems offer a cost-effective approach for realizing balanced gains in performance characteristics of high-performance cementitious matrices.

5.2 Materials and Methods

5.2.1 Graphite Nanomaterials and Microfibers

Different types of acid-functionalized and non-functionalized multiwalled carbon nanotubes as well as chopped (micro-scale) carbon fibers were evaluated for use in cement-based nanocomposites. These graphite nanomaterials and microfibers have been introduced in detail in Chapter 2, Section 2.4, Fig. 2.3 and Table 2.3. Multiwalled carbon nanotubes (MWNT D and MWNT E) and carbon microfibers (CMF) were used in high-performance cement-based paste and mortar matrices.

5.2.2 Cementitious Matrices, Mixing and Curing Procedure

Dense cementitious matrix selected has been introduced in detail in Chapter 2, Section 2.5. DSP paste was used to evaluate the reinforcement efficiency of both graphite nanomaterials and carbon microfibers at relatively low volume fractions.

Cementitious materials with and without functionalized and non-functionalized graphite nanomaterials dispersed in the mixing water via sonication, described in detail in Chapter 2, Section 2.5.2, and/or carbon microfibers were prepared and cured following ASTM procedures described in the same section.

5.2.3 Experimental Methods

The test procedures employed to determine the engineering properties of high-performance cement-based materials with and without nano- and/ or micro-scale reinforcements include *Compression* tests (ASTM C 109), *Flexure* tests (ASTM C 1185), *Impact* tests (ASTM D 7136) and *Abrasion* tests (ASTM C 944). The following experimental methods were also employed to gain further insight into the structure and failure mechanisms of cement-based nanocomposites:

(i) SEM; (ii) EDS; (iii) XRD; and (iv) DT/TGA. The experimental results were subjected to the ANOVA (Analysis of Variance) and PWC (Pair-Wise Comparison) statistical analyses.

5.3 Experimental Results and Discussion

5.3.1 Multiwalled Carbon Nanotube Aspect Ratio and Volume Fraction

5.3.1.1 Flexural Performance

The flexural strength of cementitious nanocomposites was higher with the longer/smallerdiameter (higher-aspect-ratio) MWNT D when compared with MWNT E. Non-functionalized and acid-functionalized MWNT D generated (at 0.24 vol.%) 72% and 43% gains in flexural strength, and 264% and 161% gains in flexural energy absorption capacity, respectively. In the case of MWNT D (Figure 5.1 and Table 5.1), the adverse shortening effects of acidfunctionalization overshadowed the contributions associated with the improved interfacial interactions in the presence of carboxyl functional groups. Non-functionalized and acidfunctionalized MWNT E (at 0.24 vol.%) generated 16% and 20% gains in flexural strength, and 67% and 95% gains in flexural energy absorption capacity, respectively (see Figure 5.1 and Table 5.1). In the case of MWNT E, the benefits of carboxyl functional groups to interfacial interactions (upon acid-functionalization) more than compensated for the shortening effects of acid-functionalization. It should be noted that the acid-functionalized MWNT E had a lower degree of functionalization (1.2% COOH groups) when compared with functionalized MWNT D (2.5% COOH groups). This difference (which is caused by the smaller diameter of MWNT D), together with the observation that the maximum lengths of both nanotubes were reduced to about half upon functionalization, can be used to explain the overall negative and positive effects of acid-functionalization on MWNT D and MWNT E, respectively. In spite of these differences,

one can conclude that longer and smaller-diameter (i.e., higher-aspect-ratio) multi-walled carbon nanotubes offer (as predicted theoretically) higher reinforcement efficiencies in cement-based matrices. Another theoretical prediction verified experimentally is that the flexural energy absorption capacity of cement-based matrices benefit more than their flexural strength from introduction of multi-walled carbon nanotubes. The contributions of carbon nanotubes to the flexural energy absorption capacity and strength of cementitious materials were confirmed through statistical analysis (ANOVA) of test results at significance levels of 0.001 and 0.050, respectively. At 0.48 vol.% nanotube volume fraction, drops in flexural strength were observed (see Figure 5.1 and Table 5.1), with gains in energy absorption capacity experienced in most conditions. For the cementitious nanocomposite materials and processing conditions considered here, a nanotube volume fraction of 0.48 vol.% seems to be excessive; the sonication and mixing procedures employed here may not be capable of effectively dispersing the nanotubes at this volume fraction. SEM observations of cementitious nanocomposites with 0.48 vol.% nanotube volume fraction confirmed excess clumping of nanotubes (Figure 5.2). The adverse effects of 0.48% nanotube volume fraction could also result from the excess superplasticizer dosage required to maintain the fresh mix workability of this cementitious material; at such high dosage, the superplasticizer molecules covering cement particles (and later cement hydrates) could mitigate their effective interactions with water for thorough hydration of cement. More extensive steam curing or extended moist curing periods could help overcome this obstacle and advance the hydration process of cement. Statistical analysis (of variance) of test results indicated that the (adverse) effects of 0.48 vol.% MWNT D and MWNT E on flexural strength were not statistically significant (at 0.05 significance level); the corresponding (positive) effects of nanotubes on flexural energy absorption, however, were statistically significant.

5.3.1.2 Compressive Strength

The compressive strength test data (means and standard deviations) are summarized in Table 5.2. The increase in carbon nanotube volume fraction occasionally resulted in a slight drop in compressive strength (especially for non-functionalized nanotubes). This slight loss of compressive strength with introduction of nanotubes (which is also observed with micro-scale fibers) generally results from the loss of fresh mix workability and thus the reduced compaction of matrix in the presence of discrete (nano- or micro-scale) reinforcement systems. This effect is highly dependent on the specifics of mix composition and processing conditions. Another factor influencing this trend can be the increased amount of superplasticizer used for (partially) restoring the fresh mix workability at higher nanotube volume fractions. The excess superplasticizer dosage could coat cement particles and their hydrates, delaying the hydration process. In order to study this trend, control specimens with higher amounts of superplasticizer were prepared and tested. The results showed that higher amounts of superplasticizer produced losses of compressive strength (without adding nanotubes). With the high superplasticizer dosage, mixes with and without nanotubes provided statistically comparable (at 0.05 significance level) compressive strengths.

5.3.1.3 Impact Resistance

The impact resistance of the high-performance (DSP) cementitious matrix increased with introduction of 0.24 vol.% non-functionalized or acid-functionalized MWNT D. However, non-functionalized MWNT E produced a drop in impact resistance (see Table 5.3). The two types of functionalized nanotubes considered here (MWNT D & E), at 0.24 vol.%, produced about 70% gain in impact resistance. The impact resistance of the cementitious matrix increased further with increasing the nanotube volume fraction to 0.48 vol.% for both non-functionalized and acid-

functionalized MWNT D. Test results indicated that functionalization of carbon nanotubes benefits their contributions to the impact resistance of the high-performance cementitious matrix. The two types of functionalized nanotubes considered here (MWNT D & E), at 0.48 vol.%, produced about 75% and 58% gains, respectively, in impact resistance, which can be attributed to arrest and deflection of microcracks by nanotubes, frictional pullout of nanotubes, and the multiple cracking induced by nanotubes. Statistical analysis (of variance) of impact test results indicated that the impact resistance of the DSP cementitious matrix experienced statistically significant gains (at 0.027 significance level) with increasing nanotube volume fractions. Acid-functionalized nanotubes provided somewhat better reinforcement efficiency (0.010 significance level) as compared to their non-functionalized counterparts, which could be attributed to improved interfacial interactions of functionalized nanotubes with the cementitious matrix. In general, MWNT D produced greater improvements in impact resistance when compared with MWNT E (which was generally the case with different engineering properties).

5.3.1.4 Abrasion Resistance

The control specimen without nanotube experienced a mean weight loss of 0.28 grams upon abrasion, compared to only 0.1 gram or less weight loss for the cementitious material with 0.24 vol.% acid-functionalized MWNT D & E. The contributions of functionalized nanotubes to abrasion resistance may be attributed to the corresponding gains in fracture toughness and the control of surface (restrained shrinkage) microcracking by nanotubes. However, mixes with 0.48 vol.% acid-functionalized and non-functionalized MWNT D & E provided less abrasion resistance than those with 0.24 vol.% nanotube, as shown in Table 5.4. As noted earlier, for the mix designs and processing conditions considered here, 0.48 vol.% seems to exceed the maximum limit for effective dispersion of nanotubes. Clumping of nanotubes at this excess

volume fraction compromises their reinforcement efficiency in the cementitious matrix. The relatively high dosage of superplasticizer required for restoring the fresh mix workability in the presence of high nanotube volume fractions further compromises the quality of these cementitious nanocomposites. Statistical analysis (of variance) of abrasion test results pointed at a statistically significant improvement in abrasion resistance (at 0.05 significance level) with 0.24 vol.% carbon nanotube. The gains in abrasion resistance would, however, be statistically insignificant at the higher nanotube volume fraction of 0.48 vol.%).

5.3.1.5 Scanning Electron Microscope Evaluation

The SEM images presented in Figure 5.3 indicate that the refined sonication and mixing steps developed in the project were successful in dispersion of individual nanotubes within the cementitious matrix at 0.24 vol.% volume fraction. These images also point at the low porosity of the high-performance cement-based matrix; the introduction of nanotubes does not seem to have compromised the high density (low porosity) of this matrix. SEM observations provided ample evidence for uniform dispersion of both types of nanotubes; evidences of crack suppression and crack bridging were also found in all specimens examined under SEM. Functionalized nanotubes, which provided higher levels of reinforcement efficiency, were found to produce a more uniform dispersion within the cementitious matrix.

5.3.1.6 Thermogravimetric Analysis (TGA)

Results of thermogravimetric analysis for DSP pastes with different volume fractions of MWNT D and E (Figure 5.4) point at some improvements in the matrix structure resulting from the addition of nanotubes. Figure 5.4 suggests that the rates of mass loss with increasing temperature are less steep for cementitious nanocomposites when compared with the plain matrix.

5.3.1.7 Energy Dispersive Spectroscopy (EDS)

Elemental analyses were performed on 2.54x12x12 mm samples of DSP Paste with 0 and 0.24 vol.% non-functionalized and acid-functionalized MWNT D & E. Elemental and Quantitative analysis of these samples indicated that all cementitious materials exhibit similar elemental compositions, except for the (expected) higher carbon content in materials incorporating carbon nanotubes. This further confirms the findings of thermogravimetry analyses, indicating that graphite nanomaterials do not significantly alter the chemistry of cement hydration for the reinforcement conditions considered here.

5.3.2 Effects of Hybrid (nano- and micro-scale) Reinforcement Systems

Hybrid reinforcement systems comprising multiwalled carbon nanotubes and carbon fibers with micro-scale diameter were evaluated in DSP paste. Exploratory studies with MWNT D or E multiwalled carbon nanotube reinforcement and carbon fiber indicated that, for the cementitious matrix and processing conditions considered here, the nanotube volume fraction should be lowered below 0.24 vol.% before benefits can be realized from introduction of carbon fibers. Hence, a nanotube volume fraction of 0.16 vol.% was considered for development of hybrid reinforcement systems. The nanotubes considered here were either non-functionalized MWNT D or PAA-physisorbed MWNT D.

5.3.2.1 Flexural Performance

The flexural strength and energy absorption capacity test results for the high-performance (DSP) cementitious paste with different reinforcement systems are summarized in Table 5.5. When carbon nanotube and/or microfiber reinforcement were used in DSP paste, the highest values of flexural strength, maximum deflection and energy absorption capacity were obtained with hybrid

reinforcement. The improvements brought about by hybrid reinforcement in flexural strength, maximum deflection and energy absorption capacity were 61%, 260% and 365%, respectively. These results point at the synergy of the reinforcement mechanisms at nano and micro scales in a high-performance cementitious matrix. Statistical analysis (of variance) of test results confirmed the statistical significance of the gains in flexural performance upon hybrid reinforcement of the DSP cementitious paste (at significance level of 0.001).

5.3.2.2 Compressive Strength

While there are minor gains in compressive strength with micro-scale and hybrid reinforcement systems (Table 5.6), the hybrid reinforcement effects on compressive strength were found to be statistically insignificant (at 0.05 significance level). Past experience with micro-scale fibers indicates that fibers generally lower the compressive strength of cementitious composites by lowering the fresh mix workability and introducing fiber clumps which act as defects within matrix. Hence, the fact that the compressive strength of the matrix is retained with nano-scale and hybrid reinforcement systems points at the benefits of nano-scale reinforcement to the structure of cementitious matrix.

5.3.2.3 Impact Resistance

The improvements in impact resistance of DSP paste upon hybrid reinforcement are summarized in Table 5.7. Statistical analysis of the impact test results indicated that nano- and/or micro-scale reinforcement of DSP paste led to statistically significant gains in impact resistance (0.038 significance level).

5.3.2.4 Abrasion Resistance

The mean values of abrasion weight loss are presented in Table 5.8. The hybrid reinforcement system reduces the abrasion weight loss of DSP cementitious paste by 60%, which was found to be statistically significant (at 0.000 significance level).

5.3.2.5 Scanning Electron Microscope Evaluation

Figure 5.5 shows the SEM images indicating the uniform distribution of nanotubes and the failure mechanism of carbon fibers (involving rupture within the paste and pullout at fracture surfaces. One may observe in Figure 5.5 the individually dispersed multiwalled carbon nanotubes within the paste matrix at the fracture surface. The investigation, Figure 5.5b, also reveals the pullout behavior of carbon microfibers which adds to the flexural strength of the matrix.

5.3.2.6 Thermogravimetric Analysis (TGA)

Thermogravimetric analysis of DSP paste with microfiber and hybrid (nanotube/microfiber) reinforcement systems as well as that for a conventional cementitious mortar (Figure 5.6) indicated that:

The mass loss between 100°C to 400°C was considered in order to assess, with a certain degree of approximation, the chemically bound water in calcium silicate hydrate (C-S-H). This approximation helps avoid the errors caused by the possible presence of CaCO₃ and the mass loss associated with its decomposition at higher temperatures (around 800°C), and by the presence of free water below 100°C. The maximum weight loss of 9.65% occurs for DSP Paste containing hybrid reinforcement, followed by 7.54% for that

incorporating carbon microfiber as compared with 6.87% for plain DSP paste. In conventional mortar, the total weight loss was 3.93%. These results indicate that more water is chemically bound with C-S-H in the high-performance cementitious material (DSP paste) when compared with conventional mortar.

Total weight loss is greater for the high-performance cementitious material (DSP paste), at 20.2% with hybrid reinforcement, 18.5% with carbon microfiber and 17.9% for plain DSP matrix, versus 10.2% for the conventional mortar. This reflects the higher concentration of hydration products in DSP paste when compared with conventional mortar.

5.4 Summary

The experimental results generated for cementitious pastes reinforced with different non-functionalized and functionalized multiwalled carbon nanotubes and also their hybrids with carbon microfibers yield some conclusions that the length, diameter and surface functionalization (as well as mechanical attributes) of carbon nanotubes all have critical effects on their reinforcement efficiency in cement-based matrices. Functionalization of nanotubes could introduce new defects or reduce the length of nanotubes. These adverse effects of functionalization may overshadow its positive contributions to interfacial bonding and thus the reinforcement efficiency of nanotubes. Use of polymer-wrapped (PAA physisorbed) multiwalled carbon nanotubes addresses this issue by enhancing the dispersion/interfacial interactions of nanotubes within cementitious matrix without introducing defects or shortening the nanotubes.

Table 5.1- Mean values of flexural strength, maximum deflection and energy absorption capacity of DPS paste matrix reinforced with 0%, 0.24% and 0.48% volume fractions of non-functionalized and acid-functionalized MWNT D & E.

Reinforcement Condition	Mean Flexure	Deflection	Energy
	Strength (MPa)	(mm)	Absorption(N.mm)
Plain	10.29	0.40	61.84
MWNT D, acid-fn, 0.24	14.73	0.69	161.45
vol.%			
MWNT D, non-fn, 0.24	15.81	0.78	225.71
vol.%			
MWNT E, acid-fn, 0.24	12.36	0.54	120.79
vol.%			
MWNT E, non-fn, 0.24	11.90	0.44	103.53
vol.%			
MWNT D, acid-fn, 0.48	12.14	0.75	172.99
vol.%			
MWNT D, non-fn, 0.48	12.78	0.85	237.32
vol.%			
MWNT E, acid-fn, 0.48	9.54	0.60	138.89
vol.%			
MWNT E, non-fn, 0.48	8.68	0.44	95.34
vol.%			

Table 5.2- Mean values of compressive strength test results for DSP paste matrix reinforced with 0%, 0.24% and 0.48% volume fractions of non-functionalized and acid-functionalized carbon nanotubes.

Reinforcement Condition	Mean Compressive Strength (MPa)	Standard Deviation (MPa)
Plain	110.92	14.27
MWNT D, acid-fn, 0.24 vol.%	107.96	19.26
MWNT D, non-fn, 0.24 vol.%	111.65	8.48
MWNT E, acid-fn, 0.24 vol.%	103.63	11.69
MWNT E, non-fn, 0.24 vol.%	112.56	16.92
MWNT D, acid-fn, 0.48 vol.%	112.89	19.03
MWNT D, non-fn, 0.48 vol.%	100.14	9.51
MWNT E, acid-fn, 0.48 vol.%	111.39	4.48
MWNT E, non-fn, 0.48 vol.%	100.37	6.62

Table 5.3- Mean values of impact resistance test results for DSP paste reinforced with 0%, 0.24% and 0.48% volume fractions of non-functionalized and acid-functionalized carbon nanotubes MWNT D & E.

Reinforcement Condition	Impact Resistance, θ (mm/mm)
Plain	0.36
MWNT D, acid-fn, 0.24 vol.%	0.57
MWNT D, non-fn, 0.24 vol.%	0.42
MWNT E, acid-fn, 0.24 vol.%	0.52
MWNT E, non-fn, 0.24 vol.%	0.26
MWNT D, acid-fn, 0.48 vol.%	0.63
MWNT D, non-fn, 0.48 vol.%	0.47
MWNT E, acid-fn, 0.48 vol.%	0.57
MWNT E, non-fn, 0.48 vol.%	0.36

Table 5.4- Mean weight loss test results after abrasion for DSP paste reinforced with 0%, 0.24% and 0.48% volume fractions of non-functionalized and acid-functionalized carbon nanotubes MWNT D & E.

Reinforcement Condition	Mean Weight Loss (grams)
Plain	0.28
MWNT D, acid-fn, 0.24 vol.%	0.10
MWNT D, non-fn, 0.24 vol.%	0.15
MWNT E, acid-fn, 0.24 vol.%	0.10
MWNT E, non-fn, 0.24 vol.%	0.25
MWNT D, acid-fn, 0.48 vol.%	0.18
MWNT D, non-fn, 0.48 vol.%	0.23
MWNT E, acid-fn, 0.48 vol.%	0.20
MWNT E, non-fn, 0.48 vol.%	0.28

Table 5.5- Mean values of flexural strength, maximum deflection and energy absorption capacity of DSP paste reinforced different vol. fractions of micro- and/or nano-scale reinforcement.

Reinforcement Condition	Flexural Strength (MPa)	Maximum Deflection (mm)	Energy Absorption(N.mm)
Plain	10.29	0.40	61.84
CMF (TT 143), 0.24 vol.%	16.06	1.13	251.12
MWNT D (PAA-fn), 0.16 vol.%	13.90	0.49	105.62
CMF (TT 143), 0.24 vol.% and MWNT D (PAA-fn), 0.16 vol.%	16.64	1.46	287.98

Table 5.6- Compressive strength test results for the DSP paste matrix reinforced with different volume fractions of nano and micro-scale reinforcements.

Reinforcement Condition	Mean Compressive Strength (MPa)	Standard Deviation (MPa)
Plain	110.92	14.27
CMF (TT 143), 0.24 vol.%	116.68	18.01
MWNT D (PAA-fn), 0.16 vol.%	109.64	9.43
CMF (TT 143), 0.24 vol.% and MWNT D (PAA-fn), 0.16 vol.%	122.76	12.12

Table 5.7- Impact resistance test results of DSP pastes with nano- and/or micro-scale reinforcement.

Reinforcement Condition	Impact Resistance (mm/mm)
Plain	0.365
CMF (TT 143), 0.24 vol.%	0.521
MWNT D (PAA-fn), 0.16 vol.%	0.625
CMF (TT 143), 0.24 vol.% and MWNT D (PAA-fn), 0.16 vol.%	0.729

 ${\it Table~5.8-Abrasion~weight~losses~of~DSP~pastes~with~nano-~and/or~micro-scale~reinforcement.}$

Reinforcement Condition	Loss of Mass (grams)
Plain	0.275
CMF (TT 143), 0.24 vol.%	0.150
MWNT D (PAA-fn), 0.16 vol.%	0.110
CMF (TT 143), 0.24 vol.% and MWNT D (PAA-fn), 0.16 vol.%	0.125

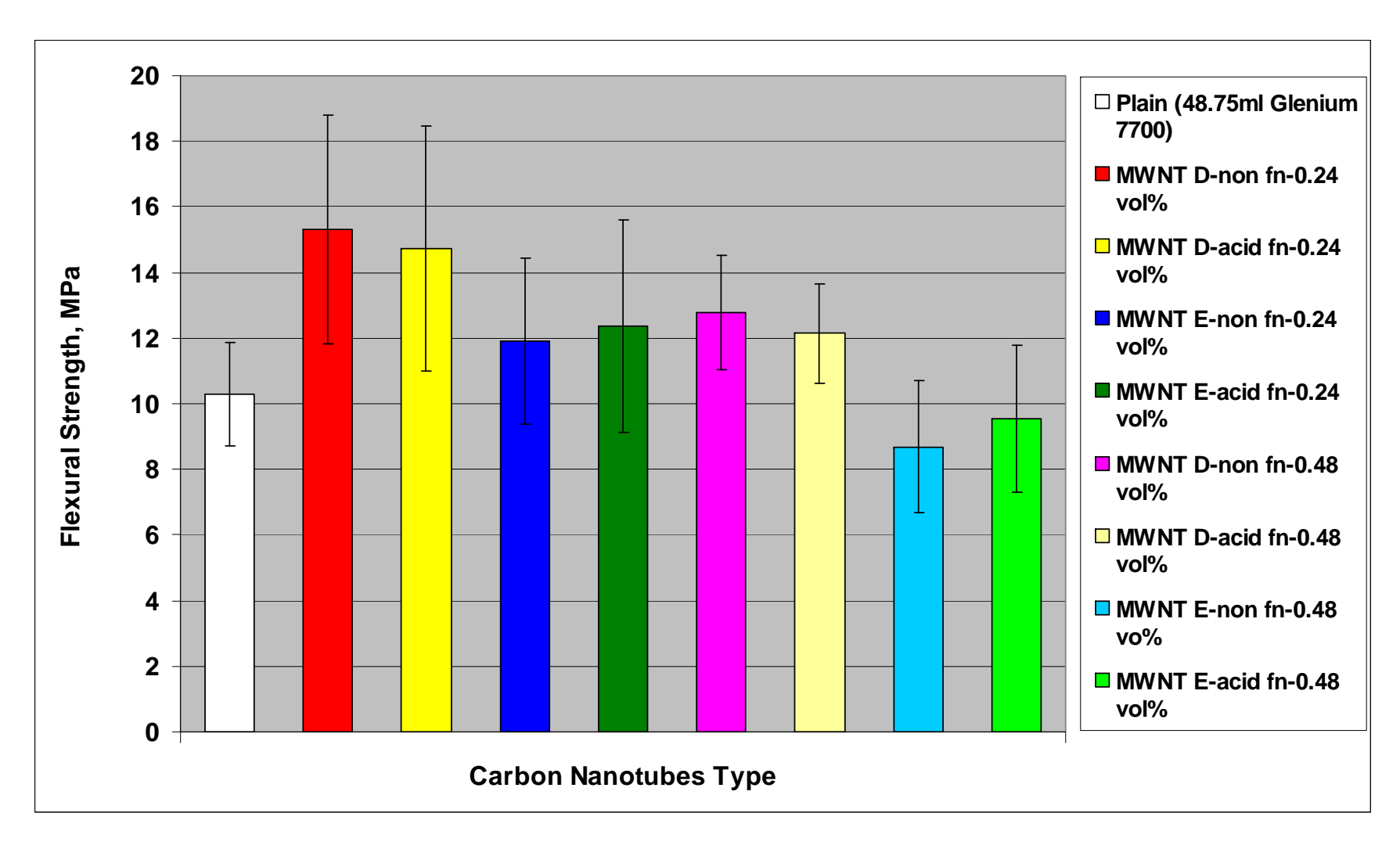
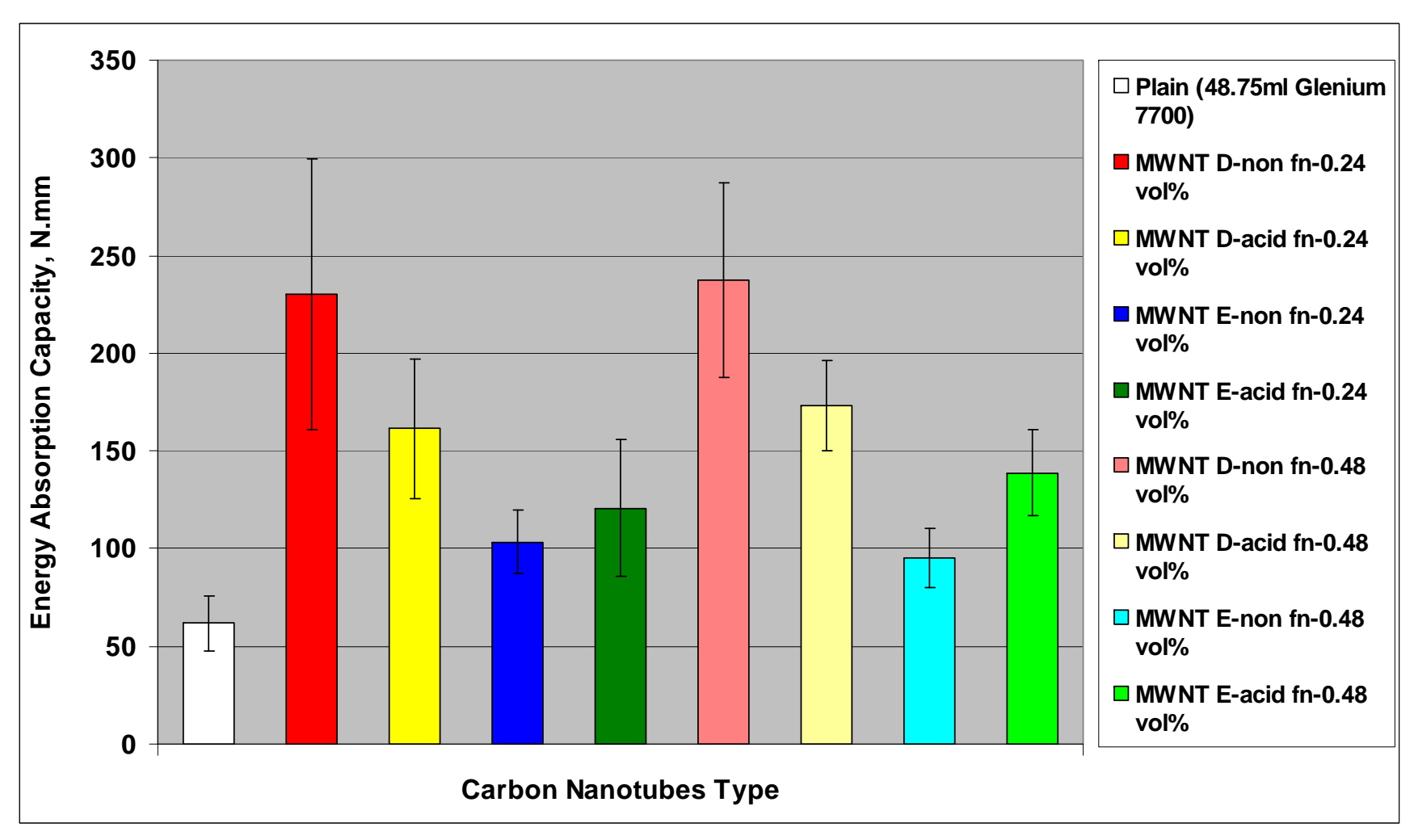


Figure 5.1- Flexural strength and energy absorption capacity of DSP cement pastes with 0.24 and 0.48 vol.% non-functionalized and acid-functionalized MWNT D & E.



(b) Energy absorption capacity

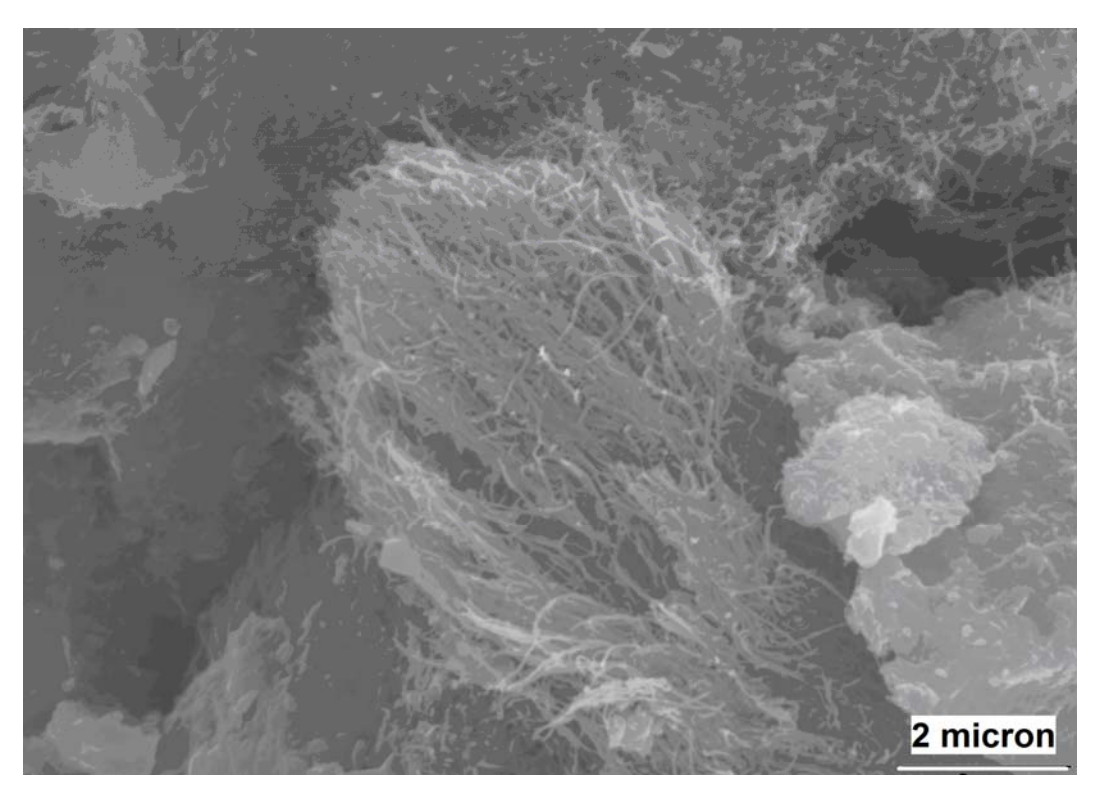
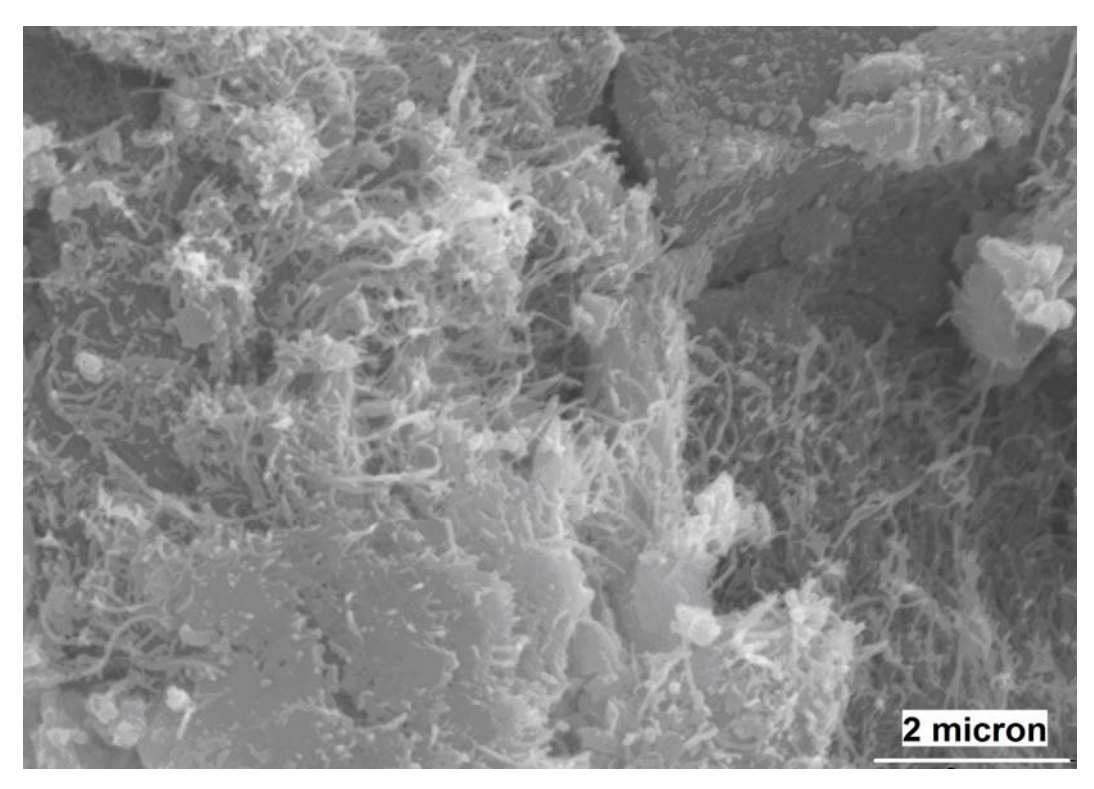
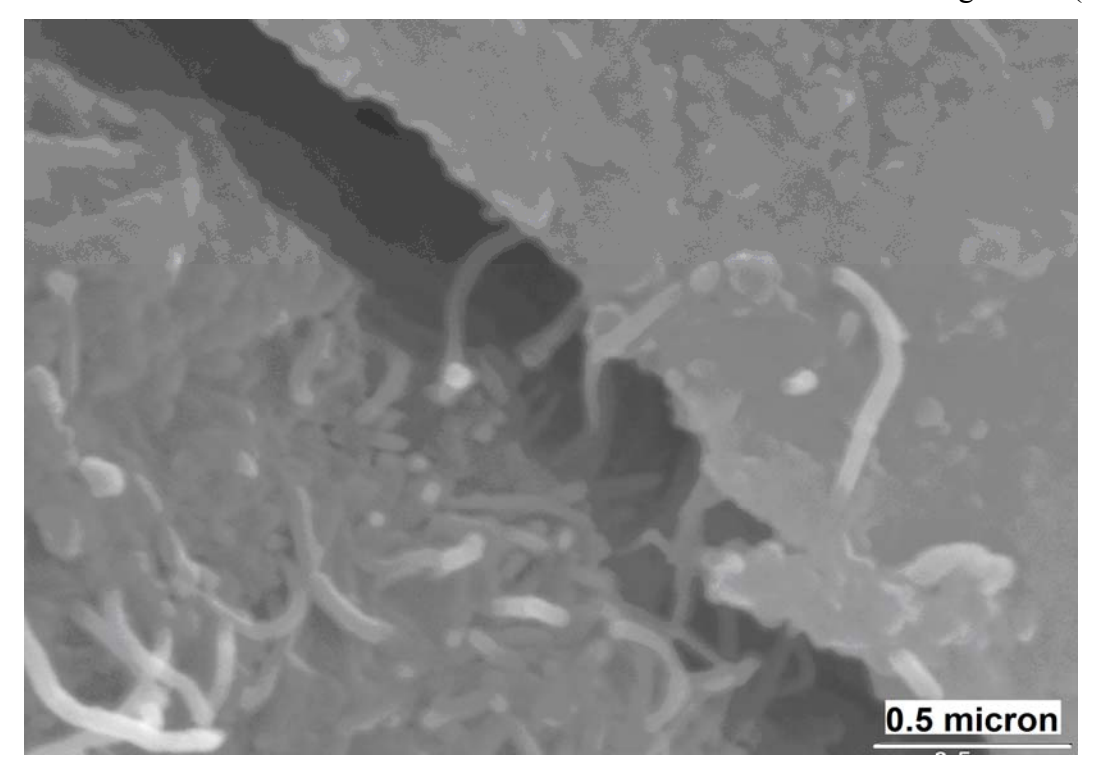


Figure 5.2- Excessive clumping of carbon nanotubes in DSP paste at 0.48% volume fraction.

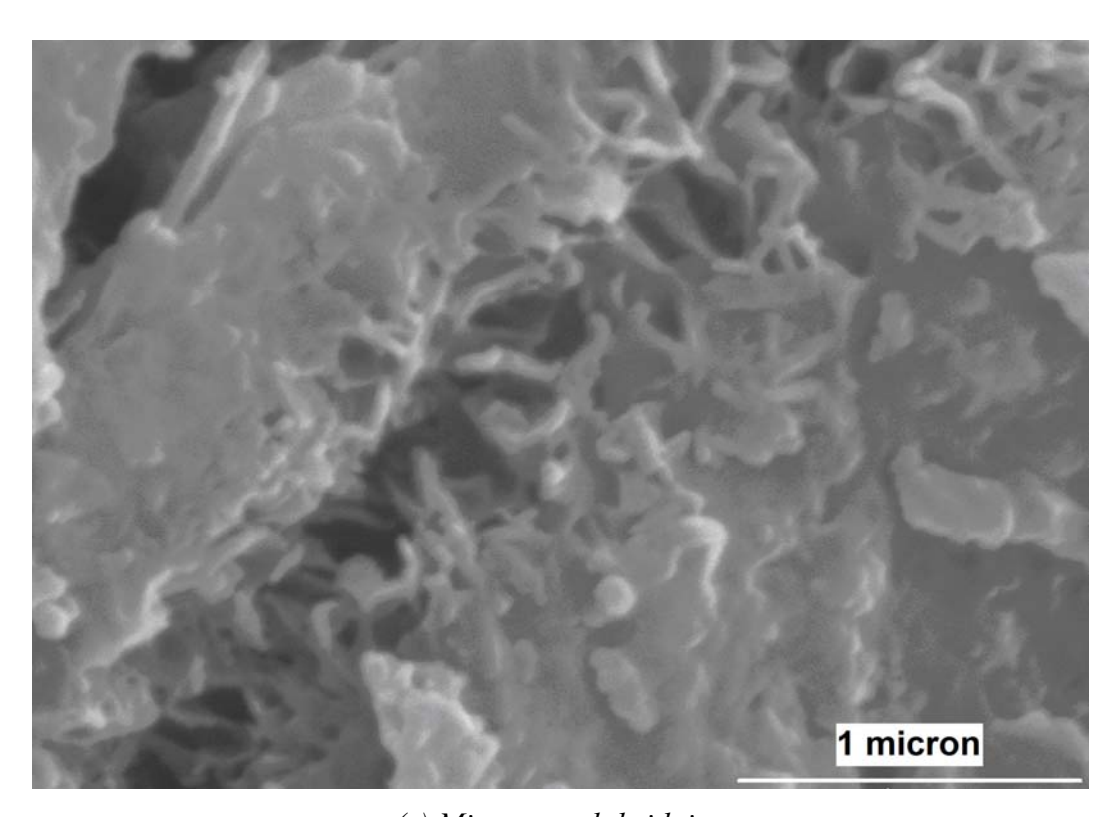


(a) Uniform distribution of nanotubes in the matrix Figure 5.3- Typical SEM images of DSP paste.

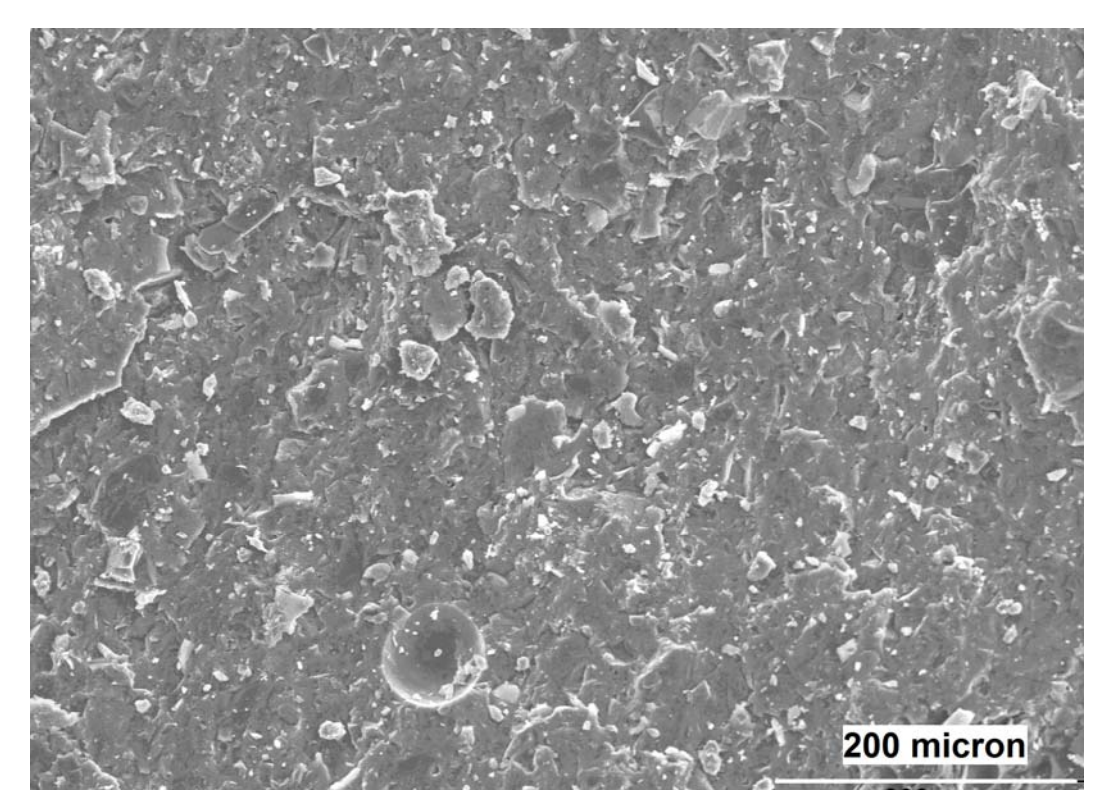
Figure 5.3 (cont'd)



(b) Micro- crack-bridging



(c) Micro- crack-bridging



(d) Dense DSP matrix

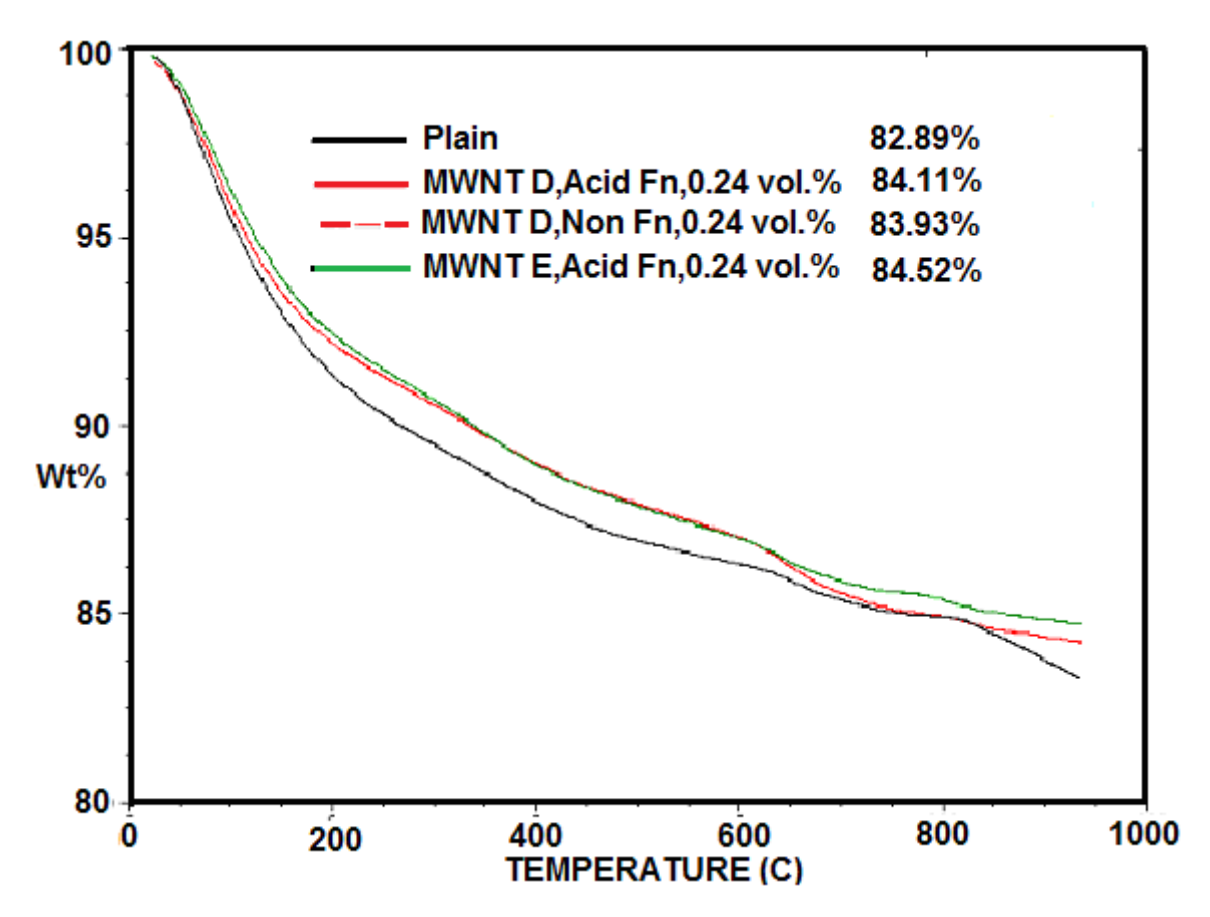


Figure 5.4- The results of thermogravimetric analysis of DSP cement paste with 0% and 0.24% volume fractions of functionalized multi-walled carbon nanotubes MWNT D & E.

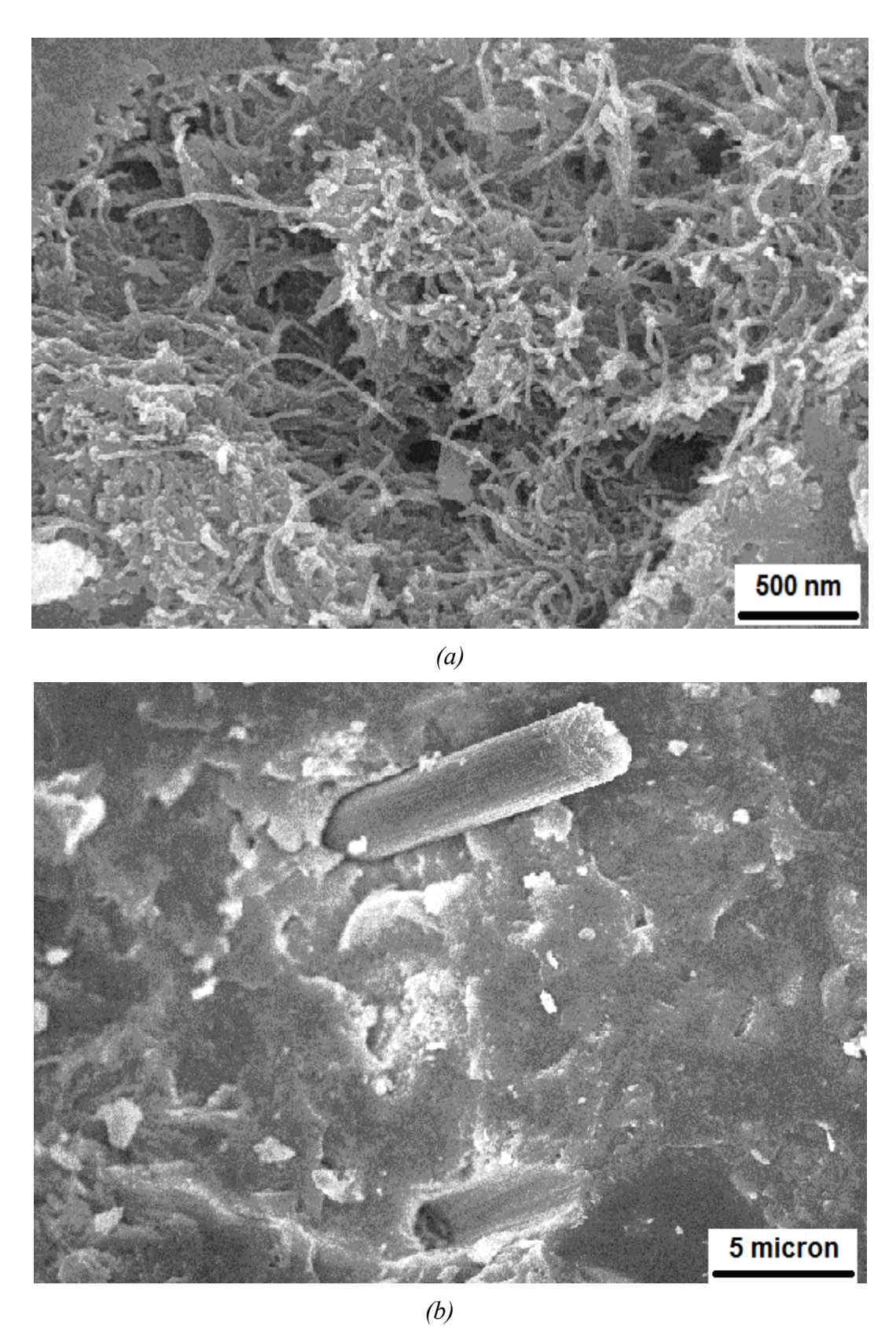


Figure 5.5- Typical SEM mages of DSP paste reinforced with 0.16 vol.% of MWNT D-PAA and 0.24 vol.% of CMF: (a) dispersed MWNTs; and (b) failure mechanism of micro-scale fibers.

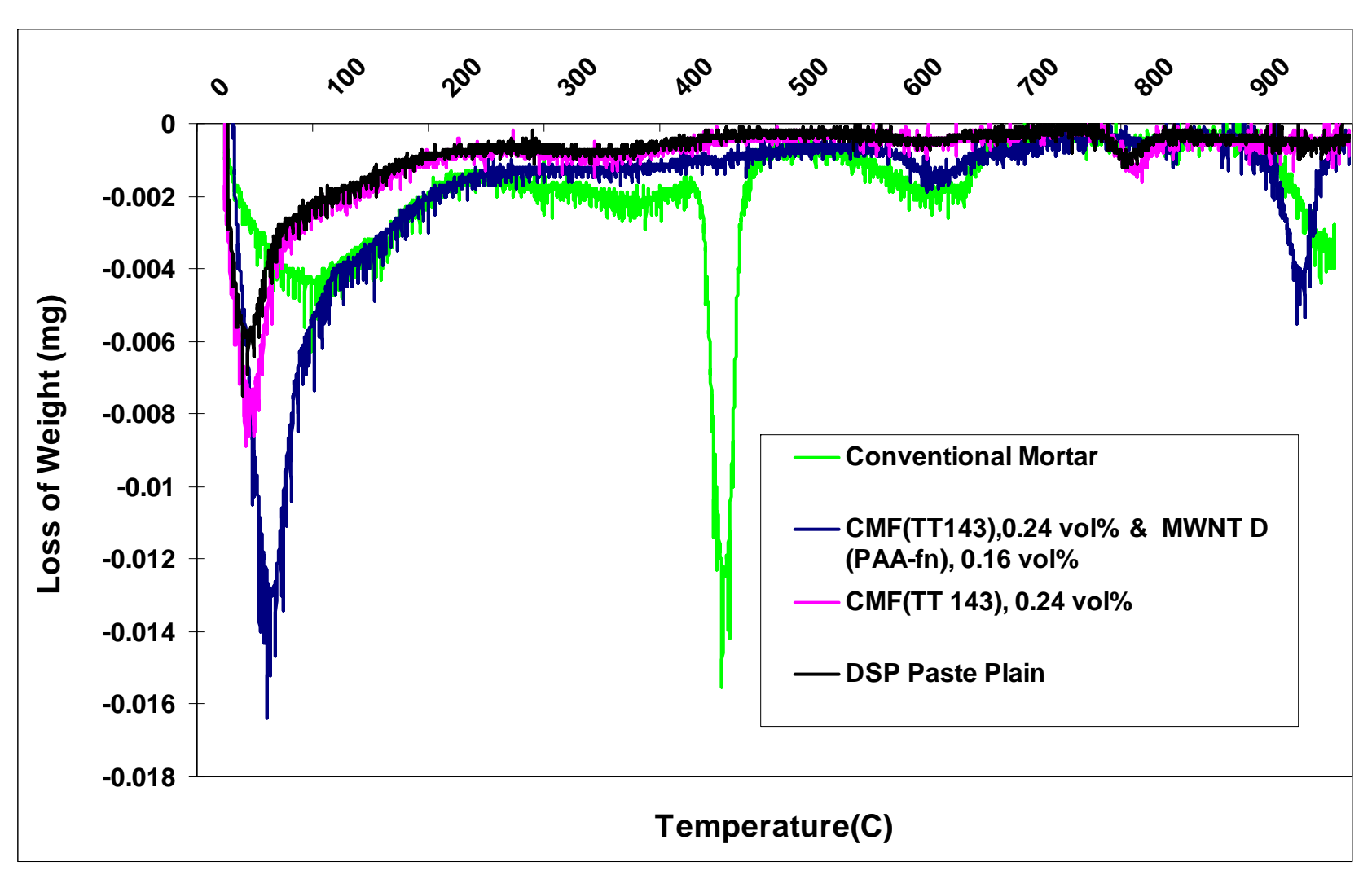


Figure 5.6- Results of thermogravimetric analysis (weight loss vs. temperature) for the high-performance cementitious matrix (DSP paste) with different volume fractions of micro and nano reinforcements.

6 REINFORCING EFFECTS OF MULTIWALLED CARBON NANOTUBES AT DIFFERENT VOLUME FRACTIONS IN CEMENTITIOUS PASTES

6.1 General

Multiwalled carbon nanotubes would realize their reinforcement potential within cement-based materials as far as they are thoroughly dispersed within cementitious matrix, and effectively bonded to cement hydrates. Superplasticizers, which are commonly used in high-performance cementitious materials, can facilitate the dispersion of nanotubes. Carboxylate-based superplasticizers have assumed a prominent position among concrete admixtures; various proprietary formulations of these superplasticizers are available commercially. Two carboxylate-based superplasticizers were evaluated in the experimental work reported here. Multiwalled carbon nanotubes were introduced into cementitious pastes at different volume fractions. A high-performance cementitious paste (densified with small particles – DSP) was considered in this investigation.

It is challenging to disperse nanotubes in water at relatively high concentrations. Nanotubes were thus dispersed in the whole mixing water of cementitious paste, which can complicate large-scale production of cementitious nanocomposites. This investigation evaluated the potential for increasing the concentration nanotube dispersions in water. Cementitious nanocomposites were thus prepared with nanotubes dispersed in different fractions of mixing water, and the effects on performance characteristics of cementitious nanocomposites were evaluated. The minimum

fraction of mixing water required for effective dispersion of nanotubes was identified through this experimental program.

6.2 Materials and Methods

6.2.1 Graphite Nanomaterials

Multiwalled carbon nanotubes (MWNT D) were used in non-functionalized, carboxylic acid-functionalized, and polyacrylic acid-physisorbed conditions. MWNT D has been introduced in detail in Chapter 2, Section 2.4, Fig. 2.3 and Table 2.3 and was used in high-performance cement-based paste matrix.

6.2.2 Cementitious Matrices, Mixing and Curing Procedure

Dense cementitious matrix selected has been introduced in detail in Chapter 2, Section 2.5. DSP (Densified with Small Particles) paste was used to evaluate the reinforcement efficiency of MWNT D at different volume fractions.

Cementitious materials (with and without functionalized and non-functionalized multiwalled carbon nanotubes dispersed in the mixing water via sonication) were prepared and cured following ASTM procedures described in the same section.

6.2.3 Experimental Methods

Compression tests (ASTM C 109) and *flexure* tests (ASTM C 1185) were performed as well as SEM was also employed to gain further insight into the structure and failure mechanisms of cement-based nanocomposites. The experimental results were subjected to the ANOVA and PWC statistical analyses.

6.3 Experimental Results and Discussion

6.3.1 Effects of MWNT D Volume Fraction and Superplasticizer Type

6.3.1.1 Flexural Performance

The flexure test data are summarized in Table 6.1. Both functionalized (MWNT D FN) and nonfunctionalized MWNT D (MWNT D NF) produced more pronounced gains in flexural attributes when used with the ADVA® Cast 575 superplasticizer. ADVA® Cast 575 enabled better dispersion of non-functionalized and functionalized nanotubes, and seemed to enhance their interactions with the cementitious matrix when compared with the Glenium® 7700 superplasticizer. The improvements in flexural attributes were more pronounced with nonfunctionalized nanotubes (due to improved dispersion of nanotubes with the ADVA® Cast 575 superplasticizer). ADVA® Cast 575, when compared with Glenium® 7700, was found to be more effective in improving all flexural attributes as well as the compressive strength of the high-performance cementitious paste with either MWNT D FN or MWNT D NF at 0.24 and 0.48 vol.%. The gains in flexural strength, maximum deflection and energy absorption capacity of cementitious nanocomposites incorporating MWNT D FN at 0.24 vol.% (0.48 vol.%) prepared using ADVA® Cast 575 were 9.23% (59.5%), 127% (137%) and 25.3% (116%), respectively. The corresponding gains at 0.24 vol.% (0.48 vol.%) for MWNT D NF were 28.5% (60.9%), 128% (146%) and 62.6% (73%), respectively.

Outcomes of statistical analysis of test results, using the analysis of variance and pair-wise comparison techniques, verified the improved performance of cementitious nanocomposites with different volume fractions of functionalized or non-functionalized nanotubes realized with ADVA® Cast 575 versus Glenium® 7700 superplasticizer. Pair-wise comparisons of flexure test

data indicated that the gains in flexural strength with 0.24 vol.% acid-functionalized nanotubes were not statistically significant (0.128 significance level) with the ADVA® Cast 575 superplasticizer. At 0.48 vol.%, however, acid-functionalized nanotubes produced statistically significant gains (at 0.000 significance level) in the flexural strength of high-performance cementitious paste. It should be noted that statistical significance levels below 0.05 are generally considered as indicative of statistically significant effects. In the case of flexural energy absorption capacity and maximum deflection, the effects of acid-functionalized nanotubes were found to be statistically significant at both 0.24 and 0.48 vol.% (significance levels ≤0.03) with the ADVA® Cast 575 superplasticizer. For non-functionalized nanotubes, the gains in flexural strength, energy absorption capacity and maximum deflection were all statistically significant (at 0.000 significance level). Pair-wise comparisons of experimental results indicated that the distinctions between the flexural attributes of cementitious nanocomposites incorporating 0.24 vol.% versus 0.48 vol.% nanotubes were not statistically significant.

6.3.1.2 Compressive Strength

The compressive strength test results for high-performance pastes with both acid-functionalized and non-functionalized MWNT D, at 0.24 vol.% and 0.48 vol.%, prepared using the two polycarboxylate-based superplasticizers are summarized in Table 6.2. When ADVA® Cast 575 superplasticizer was used, the addition of non-functionalized and functionalized carbon nanotubes at 0.24 vol.% and especially 0.48 vol.% produced some increase in compressive strength. The superplasticizer type greatly influenced the effects of nanotubes on compressive strength. Functionalized MWNT D, at 0.24 vol.% (0.48 vol.%), prepared using the ADVA® Cast 575 superplasticizer increased the compressive strength by 4.62% (11.5%) when compared with similar nanocomposites prepared with the Glenium® 7700 superplasticizer; these gains were

found to be statistically significant at 0.005 (0.000) significance level. The corresponding improvements in the case of non-functionalized nanotube were 8.88% (31.0%) with 0.087 (0.000) significance levels.

6.3.1.3 Scanning Electron Microscope Evaluation

Fig. 6.1 shows SEM images of cementitious nanocomposites with MWNT D prepared with the ADVA® Cast 575 superplasticizer. Multiwalled carbon nanotubes were uniformly distributed within the dense matrix. This uniform dispersion of the reinforcement system is essential for realizing the observed gains in the engineering properties of cementitious matrices. Figure 6.6c indicates that carbon nanotubes were pulled out of the matrix during the fracture process. This pull-out behavior benefits the ductility and energy absorption capacity of cementitious materials.

6.3.2 Effect of Dispersing Multiwalled Carbon Nanotubes in Different Fractions of Mixing Water

In order to facilitate industrial-scale production of cementitious nanocomposites, one needs to minimize the fraction of mixing water used for dispersion of the required quantities of nanomaterials. Comparative studies were conducted involving dispersion of nanomaterials in different fractions of the mixing water followed by preparation of cementitious nanocomposites. Polymer-wrapped multiwalled carbon nanotubes (CNTD-FN) and non-functionalized multiwalled carbon nanotubes (CNTD-NF) were used as reinforcement in the high-performance (DSP) cementitious paste at 0.24 vol.%. Multiwalled carbon nanotubes were dispersed, following the procedures described earlier, in 30%, 20% and 10% of the total mixing water of the cementitious paste. All mixes were prepared using the ADVA® Cast-575 superplasticizer.

6.3.2.1 Flexural Performance

The flexural strength, maximum deflection and energy absorption capacity test results for the high-performance (DSP) cementitious paste reinforced with 0.24 vol.% of CNTD-NF and CNTD-FN dispersed in different fractions of mixing water are shown in Table 6.3. These results indicate that the maximum improvements in flexural performance were realized by dispersing CNTD-FN in the full quantity of mixing water; the corresponding improvements in flexural strength, energy absorption capacity and maximum deflection were 41.0%, 249% and 160%, respectively. The test data also suggest that reducing the fraction of mixing water used for dispersion of both functionalized and non-functionalized nanotubes reduced the reinforcement efficiency of nanotubes. This trend could be attributed to the reduced thoroughness of nanotube dispersion resulting from the use of smaller quantities of water during dispersion. The least gains in the DSP paste flexural performance with nanotube reinforcement were observed when only 10% of mixing water was used for dispersion of CNTD-NF; the corresponding improvements in flexural strength, energy absorption capacity and maximum deflection were 3.6%, 136% and 20%, respectively. Desired gains in flexural qualities were realized when 30% of the mixing water was used for dispersion of both CNTD-FN and CNTD-NF.

Analysis of variance followed by pair-wise comparison of test results indicated that reducing the fraction of mixing water used for dispersion of nanotubes from 100% to 30% did not produce statistically significant drops in the reinforcement efficiency of the CNTD-FN and CNTD-NF multiwalled carbon nanotubes. A statistically significant effect was, however, observed for both flexural strength and energy absorption capacity when the fraction of mixing water used for dispersion of nanotubes was reduced to 20% or 10% for CNTD-NF. In the case of CNTD-FN, a statistically significant effect was observed only for flexural strength when 10% of the mixing

water was used for dispersion of nanotubes. This implies that, with CNTD-FN, the fraction of mixing water required for dispersion of nanotube can be reduced to 20%.

6.3.2.2 Compressive Strength

The compressive strength test results (mean values and standard errors) for high-performance (DSP) cementitious pastes with 0.24 vol.% of CNTD-FN and CNTD-NF reinforcement dispersed in different fractions of mixing water are presented in Table 6.4. Analysis of variance of the compression test results followed by pair-wise comparisons indicated that 0.24 vol.% of CNTD-FN or CNTD-NF, dispersed in different fractions of mixing water, did not produce a statistically significant drop in compressive strength (at 0.05 significance level). While with CNTD-NF the mean value of compressive strength dropped with decreasing fractions of mixing water used for dispersion of nanotubes, in the case of CNTD-FN, compressive strength did remained practically unchanged as decreasing fractions of the mixing water used for dispersion of multiwalled carbon nanotubes.

6.4 Summary

The reinforcement efficiency of functionalized, non-functionalized and polymer-wrapped multiwalled carbon nanotubes were evaluated in a high-performance cementitious paste. Two different polycarboxylate-based superplasticizers were used to enhance dispersion of nanotubes and workability of fresh cementitious nanocomposites. The results showed that different polycarboxylate-based superplasticizers produce cementitious nanocomposites with significant differences in performance characteristics. Scanning electron microscope observations of fractured surfaces of cementitious nanocomposites indicated that multiwalled carbon nanotubes were uniformly distributed within the dense matrix. This uniform dispersion of the reinforcement

system is essential for realizing the observed gains in the engineering properties of cementitious matrices. Some carbon nanotubes were observed to have pulled out of the cementitious matrix during the fracture process. This pull-out behavior benefits the ductility and energy absorption capacity of cementitious materials.

Polymer-wrapped as well as non-functionalized multiwalled carbon nanotubes were added as reinforcement to the high-performance cementitious paste after dispersion in reduced quantities of water. While the reinforcing effects of nanotubes decreased with decreasing fraction of the mixing water used for their dispersion, reasonable results were obtained when nanotubes were dispersed in 30% of the total mixing water, which benefits scaled-up production of cementitious nanocomposites. For polymer wrapped nanotubes, the quantity of mixing water could be reduced to 20% without having a statistically significant drop in the various engineering properties evaluated.

Table 6.1- Mean values of the flexural properties of DSP pastes with functionalized and non-functionalized MWNT D at 0.24 vol.% and 0.48vol.%, prepared using different carboxylic-based superplasticizers.

Reinforcement Condition	Mean Flexure Strength	Deflection (mm)	Energy Absorption
	(MPa)	(111111)	(N.mm)
Plain, Glenium 7700	10.3	0.40	61.8
Plain, ADVA CAST 575	13.9	0.71	155
MWNT D, acid-fn, 0.24 vol%, Glenium	14.7	0.69	162
7700			
MWNT D, non-fn, 0.24 vol%, Glenium	15.8	0.86	226
7700			
MWNT D, acid-fn, 0.24 vol%, ADVA	16.1	1.57	202
CAST 575			
MWNT D, non-fn, 0.24 vol%, ADVA	20.3	1.96	367
CAST 575			
MWNT D, acid-fn, 0.48 vol%, Glenium	12.1	0.75	173
7700			
MWNT D, non-fn, 0.48 vol%, Glenium	12.8	0.85	237
7700			
MWNT D, acid-fn, 0.48 vol%, ADVA	19.3	1.78	373
CAST 575			
MWNT D, non-fn, 0.48 vol%, ADVA	20.6	2.09	411
CAST 575			

Table 6.2- Mean values and standard errors of the compressive strength test results for DSP pastes with functionalized and non-functionalized MWNT D at 0.24 vol.% and 0.48 vol.%, prepared using different poly carboxylate-based superplasticizers.

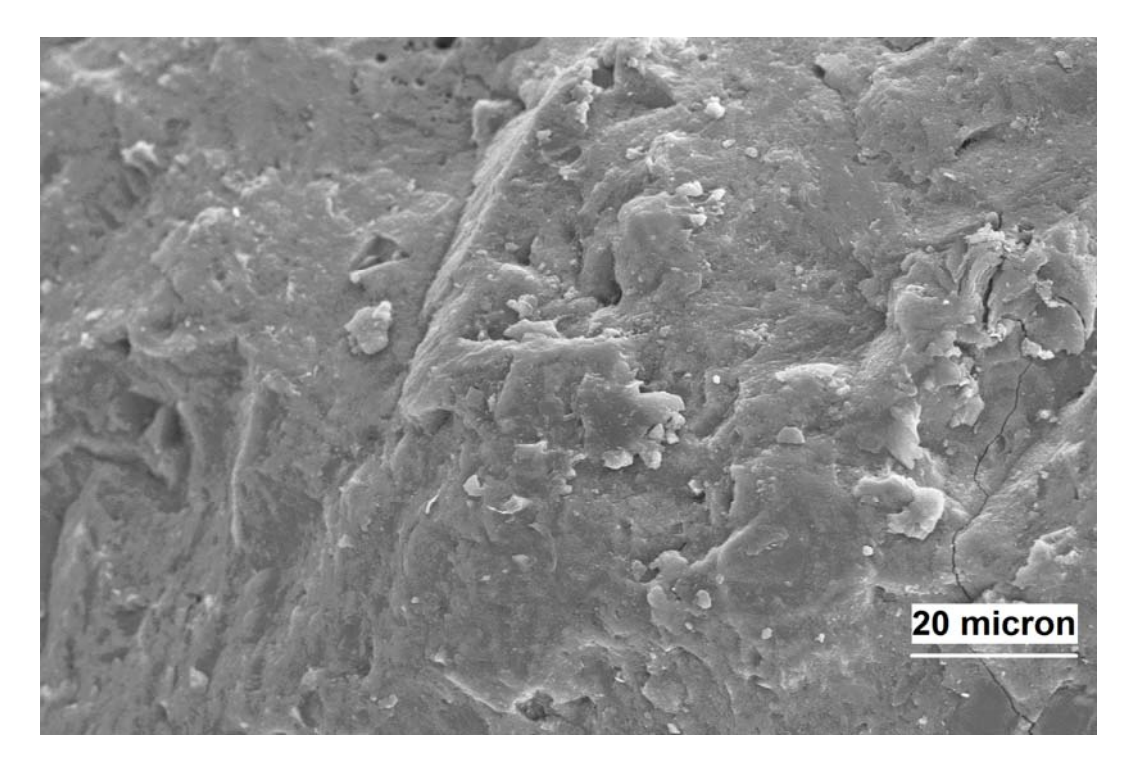
Reinforcement Condition	Mean	Standard
	Compressive Strength (MPa)	Error (MPa)
Plain, Glenium 7700	111	14.3
Plain, ADVA CAST 575	120	7.09
MWNT D, acid-fn, 0.24 vol%, Glenium 7700	108	16.3
MWNT D, non-fn, 0.24 vol%, Glenium 7700	112	8.48
MWNT D, acid-fn, 0.24 vol%, ADVA CAST 575	113	7.96
MWNT D, non-fn, 0.24 vol%, ADVA CAST 575	123	9.54
MWNT D, acid-fn, 0.48 vol%, Glenium 7700	113	15.7
MWNT D, non-fn, 0.48 vol%, Glenium 7700	100	9.51
MWNT D, acid-fn, 0.48 vol%, ADVA CAST 575	126	7.15
MWNT D, non-fn, 0.48 vol%, ADVA CAST 575	133	11.9

Table 6.3- Mean values of flexural strength, maximum deflection and energy absorption capacity of DSP paste with and without 0.24 vol.% of polymer-wrapped and non-functionalized MWNT D dispersed in different fractions of mixing water.

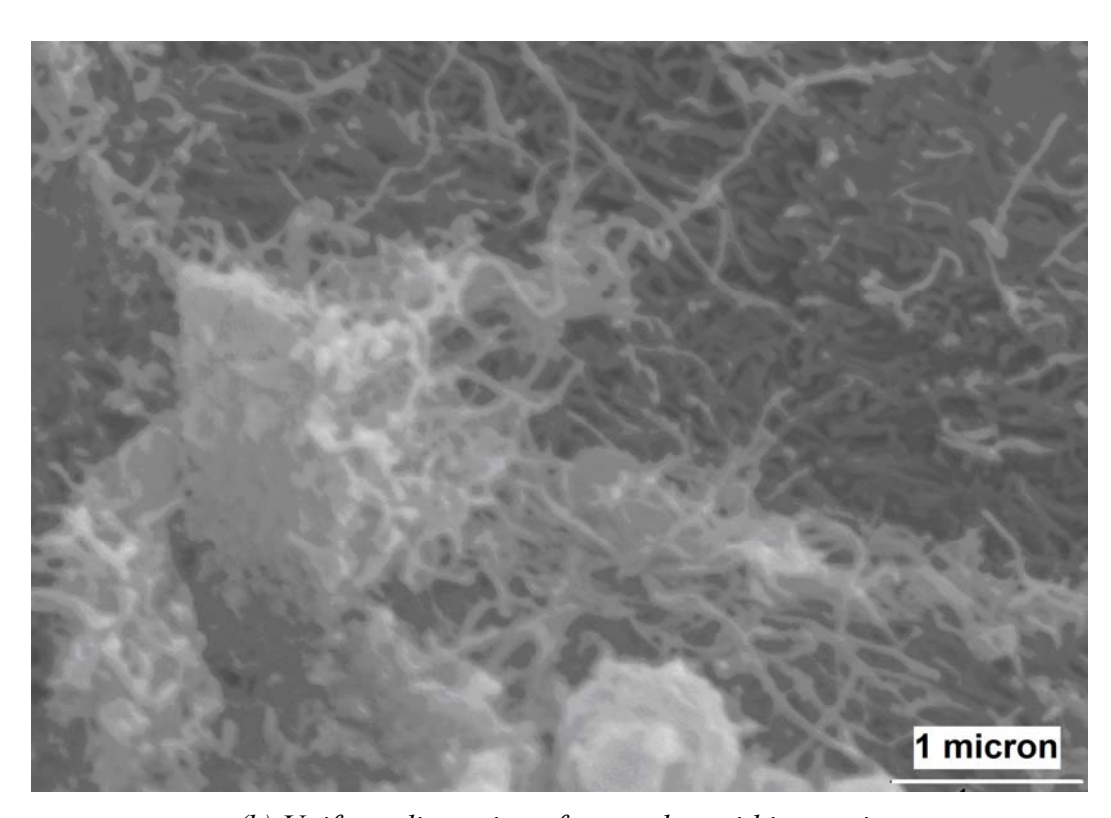
Reinforcement Condition	Mean Flexure	Deflection (mm)	Energy Absorption
	Strength	(111111)	(N.mm)
	(MPa)		
Plain, ADVA CAST 575	13.9	0.71	155
MWNT D, non-fn, 0.24 vol%, ADVA CAST 575	20.3	1.96	367
MWNT D, poly-fn, 0.24 vol%, ADVA CAST 575	23.6	2.48	404
MWNT D, non-fn, 0.24 vol%, ADVA CAST 575,	18.4	1.96	315
30% water			
MWNT D, non-fn, 0.24 vol%, ADVA CAST 575,	15.6	1.81	217
20% water			
MWNT D, non-fn, 0.24 vol%, ADVA CAST 575,	14.4	1.68	186
10% water			
MWNT D, poly-fn, 0.24 vol%, ADVA CAST 575,	21.5	2.15	375
30% water			
MWNT D, poly-fn, 0.24 vol%, ADVA CAST 575,	19.3	1.91	325
20% water			
MWNT D, poly-fn, 0.24 vol%, ADVA CAST 575,	16.6	1.82	265
10% water			

Table 6.4- Mean values and standard errors of the compressive strength test results for DSP paste with and without 0.24 vol.% polymer-wrapped and non-functionalized MWNT D dispersed in different fractions of the mixing water.

Reinforcement Condition	Mean Compressive Strength	Standard Error (MPa)
Plain, ADVA CAST 575	(MPa) 120	5.89
MWNT D, non-fn, 0.24 vol%, ADVA CAST 575	123	9.54
MWNT D, poly-fn, 0.24 vol%, ADVA CAST 575	125	5.00
MWNT D, non-fn, 0.24 vol%, ADVA CAST 575, 30% water	125	6.71
MWNT D, non-fn, 0.24 vol%, ADVA CAST 575, 20% water	121	11.9
MWNT D, non-fn, 0.24 vol%, ADVA CAST 575, 10% water	109	10.3
MWNT D, poly-fn, 0.24 vol%, ADVA CAST 575, 30% water	121	6.09
MWNT D, poly-fn, 0.24 vol%, ADVA CAST 575, 20% water	121	9.24
MWNT D, poly-fn, 0.24 vol%, ADVA CAST 575, 10% water	120	5.79

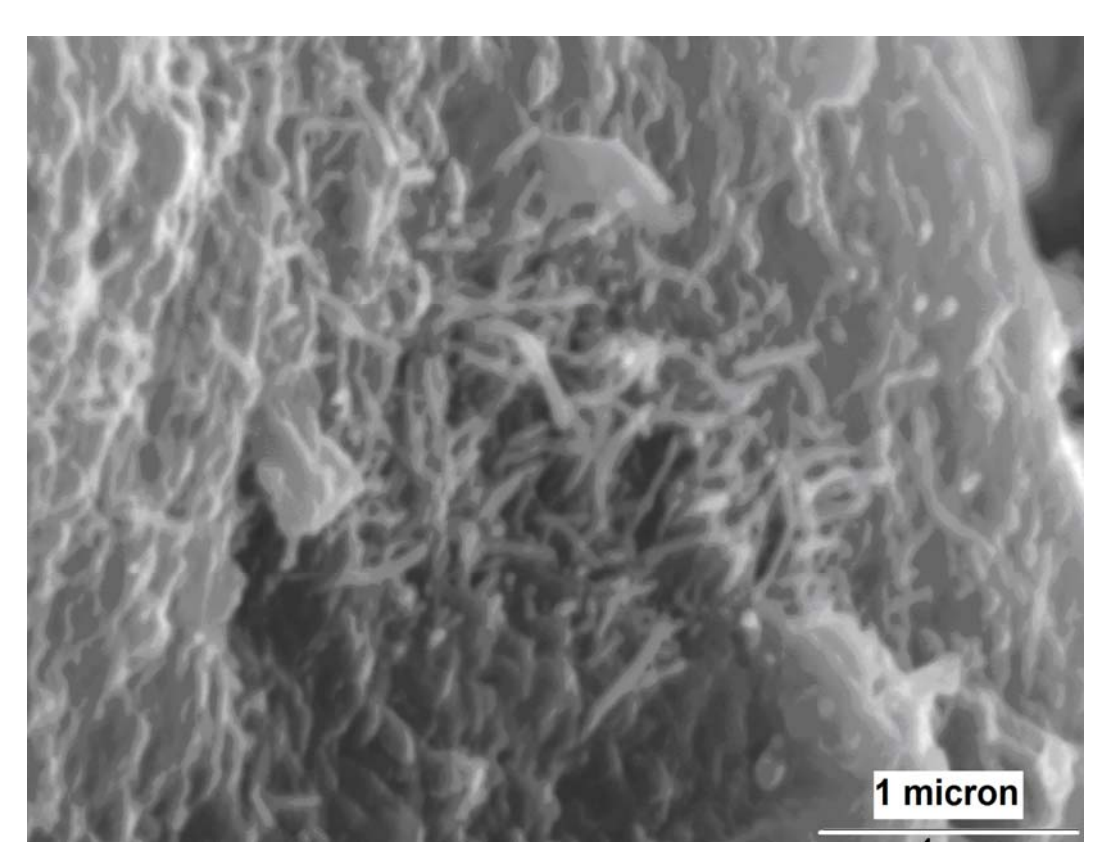


(a) Dense DSP matrix



(b) Uniform dispersion of nanotubes within matrix

Figure 6.1- SEM mages of DSP paste reinforced with 0.24 vol.% of MWNT D casted with ADVA® Cast 575 superplasticizer.



(c) Pulled-out nanotubes at a fractured surface

7 NANO- AND/OR MICRO-SCALE REINFORCEMENTS OF HIGH-PERFORMANCE CEMENTITIOUS MORTAR

7.1 General

Multiwalled carbon nanotubes provide major advantages over (micro-scale) carbon fibers in terms of mechanical, physical and geometric attributes. The geometric features of graphite nanomaterials (including high aspect ratio and specific surface area, and close spacing within matrix) benefit: (i) control of defect size and propagation within composites; (ii) energy dissipation via frictional pullout; and (iii) tortuosity of the diffusion and crack propagation paths. When effectively dispersed, the spacing of typical multi-walled nanotubes within matrix is three orders of magnitude smaller than that of typical carbon fibers at similar volume fractions; the surface area of multiwalled nanotubes available for energy dissipation through frictional pullout is two orders of magnitude greater than that of carbon fiber.

Successful use of graphite nanomaterials in concrete requires: (i) thorough dispersion of individual nanomaterials within the aqueous fresh mix; and (ii) adequate bonding of cement hydrates to nanomaterial surfaces for effective stress transfer. Modification of the MWNT surfaces for improved compatibility with aqueous media and cement hydrates can effectively mobilize the distinct qualities of graphite nanomaterials towards reinforcement of cementitious matrices. As aggressive acid-functionalization (Figure 1.11) for introduction of a high concentration of functional groups on MWNTs has not produced the highest reinforcement efficiency in cementitious matrices as shown in Chapter 4. Physisorption (wrapping) of

polyacrylic acid (PAA) onto nanotube surfaces (Figure 4.1) was evaluated in the work reported herein as a means of improving the reinforcement efficiency of nanotubes in cementitious matrices. Figure 7.1 shows an example SEM image of a fracture surface of a cementitious nanocomposite produced in this work. This image shows the uniform dispersion of nanotubes achieved through surface modification of nanotube and proper selection of the nanotube dispersion methods and the nanocomposite mixing procedures.

Earlier results have shown that functionalized nanotubes, at relatively low (~0.1%) volume fraction, can bring about balanced gains in diverse engineering properties of high-performance cementitious matrices (Konsta-Gdoutos, Metaxa et al. 2010; Konsta-Gdoutos, Metaxa et al. 2010). Carbon nanotubes effectively arrest the initiation and propagation of cracks at the nanoscale. The effectiveness of nano-scale reinforcement diminishes as the crack width increases. Given the effectiveness of micro-scale fibers in arresting larger cracks, nano- and micro-scale (hybrid) reinforcement systems can render synergistic effects in cementitious matrices. Control of crack growth by hybrid reinforcement at different scales benefits the mechanical performance and durability of cementitious materials. The concept of hybridization of fibers has been explored using micro-scale fibers of different types and dimensions (Lawler, Zampini et al. 2005; Banthia and Sappakittipakorn 2007).

7.2 Materials and Methods

7.2.1 Materials, Graphite Nanomaterials and Microfibers

Multiwalled carbon nanotubes (MWNT) and/or carbon microfibers (CMF) were used as reinforcement in high-performance (DSP) mortar at different volume fractions. These graphite nanomaterials and microfibers have been introduced in detail in Chapter 2, Section 2.4, Fig. 2.3

and Table 2.3. In the course of dispersing the nanotubes in water PAA was physisorbed upon multiwalled carbon nanotubes. PAA with average molecular weight (M_w) of about 100,000 at 35 wt.% concentration in water, was purchased from Sigma-Aldrich. Figure 7.2 shows a transmission electron micrograph PAA-physisorbed nanotube (CNTD-PAA), which exhibited improved dispersion in aqueous media and interfacial interactions with cement hydrates.

7.2.2 Cementitious Matrices, Mixing and Curing Procedure

Dense cementitious matrix selected has been introduced in detail in Chapter 2, Section 2.5. DSP mortar was used to evaluate the reinforcement efficiency of both multiwalled carbon nanotubes and carbon microfibers at different volume fractions.

Cementitious materials (with and without functionalized graphite nanomaterials dispersed in the mixing water via sonication) and/or microfibers were prepared and cured following ASTM procedures described in the same section.

7.2.3 Experimental Methods

The test procedures employed to determine the engineering properties of high-performance mortar included compression tests (ASTM C 109), flexure tests (ASTM C 1185), impact tests (ASTM D 7136) and Abrasion tests (ASTM C 944). SEM was also employed to gain further insight into the structure and failure mechanisms of cement-based nanocomposites. Experimental results were evaluated using ANOVA and PWC techniques. Response Surface Analysis (RSA) of test results was used to identify the optimum reinforcement condition which yields balanced gains in various engineering properties of the cementitious matrix.

7.3 Experimental Results and Discussion

7.3.1 Carbon Nanotubes and/ or Carbon Microfibers at Different Volume Fractions and with Different Superplasticizers

7.3.1.1 Flexural Performance

The flexure test results for the high-performance (DSP) cementitious mortar reinforced with different volume fractions of PAA-physisorbed multiwalled carbon nanotube (CNT D-PAA) and/or carbon microfiber (CMF) are summarized in Table 7.1. These test results indicate that all the reinforcement conditions considered here bring about improvements in all aspects of flexural performance with both superplasticizer types used in the experimental program. The ADVA® Cast 575 superplasticizer (when compared Glenium® 7700) was particularly effective in enhancing the flexural attributes of the plain and reinforced high-performance cementitious mortar, confirming the preliminary findings with high-performance cementitious paste (Sadiq, Soroushian et al. 2012). The flexural strength, energy absorption capacity and maximum deflection of plain matrix improved by 12.7%, 39.4% and 27.3%, respectively, when the ADVA® Cast 575 superplasticizer was used in lieu of Glenium® 7700 superplasticizer.

With the Glenium® 7700 superplasticizer, 0.16 vol.% (volume percent of dry cementitious materials) modified multiwalled carbon nanotube (CNT D-PAA) was found to be optimum, producing 37.9%, 106% and 141% gains in flexural strength, energy absorption capacity and maximum deflection, respectively. At 0.96 vol.% carbon microfiber (CMF), these improvements were 39.0%, 119% and 156%, respectively (with the Glenium® 7700 superplasticizer).

With the ADVA® Cast 575 superplasticizer, the optimum nanotube (CNT D-PAA) volume fraction was 0.24%, yielding 35.3%, 58.2% and 86.9% gains in flexural strength, energy absorption capacity and maximum deflection, respectively, of plain matrix with the same superplasticizer. The corresponding improvements brought about by 0.96 vol.% CMF were

27.8%, 74.9% and 84.8%, respectively. These results indicate that the reinforcing effects, normalized with respect to volume fractions, are greater with the modified multiwalled carbon nanotube (CNT D-PAA) when compared with carbon microfiber (CMF).

With both superplasticizers, the most balanced improvements in flexural performance characteristics of the high-performance cementitious mortar were realized with the hybrid reinforcement comprising both carbon nanotube and carbon fiber. With the ADVA® Cast 575 (Glenium® 7700) superplasticizer, the gains in flexural strength, energy absorption capacity and maximum deflection were 13.4% (18.7%), 65.0% (105%) and 53.8% (84.0%), respectively, noting that these improvements are versus a plain matrix made with the same superplasticizer.

Analysis of variance and pair-wise comparisons of test results indicated that (i) the gains in flexural attributes of the high-performance cementitious mortars with the nano- and/or microscale reinforcement systems considered here were statistically significant (at 0.05 significance level) with both superplasticizers; and (ii) the improvements in the flexural performance of cementitious mortar brought about by the use of ADVA® Cast 575 superplasticizer in lieu of Glenium® 7700 were also statistically significant.

7.3.1.2 Compressive Strength

The compressive strength test results (mean values and standard errors) for the high-performance cementitious mortars with nano- and/or micro-scale reinforcement systems and the two superplasticizers are presented in Table 7.2. The effects of carbon nano- and/or micro-scale reinforcement systems on the compressive strength of the high-performance cementitious mortar were relatively small and statistically insignificant (per outcomes of the analysis of variance of test results), confirming the observations made with cementitious paste presented earlier.

7.3.1.3 Impact Resistance

The impact test data are summarized in Table 7.3. With the ADVA® Cast 575 superplasticizer, PAA-physisorbed carbon nanotubes (CNT D-PAA) at 0.16 and 0.24 vol.% produced 58.2% and 66.7% gains, respectively, in the impact resistance of high-performance cementitious mortar. Micro-scale carbon fibers (CMF) at 0.24, 0.48 and 0.96 vol.% increased the impact resistance of the high-performance cementitious mortar by 33.3%, 46.5% and 50.1%, respectively. Hybrid (nano- and micro-scale) reinforcement produced further gains in impact resistance over those achieved with micro-scale reinforcement used alone. Analysis of variance and pair-wise comparisons of the impact test results confirmed the statistical significance of the gains in impact resistance of the high-performance cementitious mortar with hybrid reinforcement. The ADVA® Cast 575 superplasticizer was found to be more effective in improving the impact resistance of the high-performance cementitious mortar in plain form and also with nano- and/or micro-scale reinforcement systems. Comparisons with preliminary test results produced with highperformance cementitious paste indicated that the high-performance mortar (plain or with different reinforcement systems) provided higher levels of impact resistance. This finding points at the benefits rendered by sand particles to the impact resistance of the high-performance cementitious matrix.

7.3.1.4 Abrasion Resistance

The abrasion test results performed on the high-performance cementitious mortar with carbon nano- and/or micro-scale reinforcement and different superplasticizers are summarized in Table 7.4. With the ADVA® Cast 575 superplasticizer, PAA-physisorbed carbon nanotubes (CNT D-PAA) at different volume fractions (and the hybrid reinforcement system) produced the greatest improvement (34.9% - 39.0%) gains in the abrasion resistance of the high-performance

cementitious mortar. The benefits of all reinforcement systems to the abrasion resistance of the high-performance cementitious mortar were found to be statistically significant.

7.3.1.5 Scanning Electron Microscope Evaluation

Figures 7.1, 7.3 and 7.4 show SEM images of the high-performance cementitious mortars. The damaging effects of mechanical loads and aging are generally manifested in cementitious materials as inception and growth of microcracks, which tend to be concentrated initially at the aggregate-paste interfaces. The close (nano-scale) spacing and high specific surface of carbon nanotubes seem to make them effective in suppression of microcrack inception (and initial growth) (Figs 7.3a, b & c) and control of microcrack propagation by effectively interacting with the microcrack tips (Figures 7.3a & c). Longer micro-scale fibers, on the other hand, are particularly effective in bridging across wider cracks, and mitigating their further opening (Figures 7.3c & f).

The relatively dense structure of the high-performance cementitious mortar is apparent in Figure 7.4a. The uniform dispersion of nanotubes and their bridging/pullout actions across a fine (nanoscale) crack within the cementitious matrix are depicted in Figures 7.1, 7.3b and 7.4b. Indications of micro-fiber pullout from the matrix are provided in Figures 7.3b, 7.4b and 7.4c. Scanning electron microscope (SEM) observations of the high-performance cementitious mortar with hybrid reinforcement (comprising carbon nanotubes and micro-fibers) indicate that the presence of nanotubes in the matrix around micro-fibers could have benefited the interaction of matrix with micro-fibers (Figures 7.4b & c), thus benefiting the performance gains associated with hybrid reinforcement. This strong interaction of matrix with micro-fibers was not observed when the micro-fiber reinforcement was used alone (Figure 7.4d). Finally, although calcium hydroxide crystals (C-H) were rarely found in the high-performance cementitious mortar, their

deleterious effects were reduced by nanotubes bridging across the weak zones formed by C-H crystals (Fig. 7.4e). These observations provide some insight into the synergistic action of nano-and micro-scale reinforcement systems in cementitious matrices.

7.3.2 Enhanced Hybrid Reinforcement of High-Performance Cementitious Mortar

Response surface analysis of the test results presented above, with carbon nanotube and carbon microfiber volume fractions used as input variables, led to selection of the following two optimum hybrid reinforcement conditions: (i) 0.06 vol.% carbon nanotube (CNT D-PAA) & 0.30 vol.% carbon microfiber (CMF); and (ii) 0.08 vol.% carbon nanotube (CNT D-PAA) & 0.40 vol.% carbon microfiber (CMF). The simple fact that optimum reinforcement conditions comprise both nano- and micro-scale systems points at the synergistic action of the two in enhancing the performance characteristics of high-performance cementitious mortars.

The materials, and processing and testing methods introduced earlier were employed for producing and characterizing high-performance cementitious mortars with the two optimum reinforcement conditions introduced above (using the ADVA® Cast 575 superplasticizer). The performance characteristics of these cementitious nanocomposites are reviewed in the following, and compared against those of the high-performance cementitious mortar in plain form and also with some preferred nano- and/or micro-scale reinforcement systems evaluated earlier.

7.3.2.1 Flexural Performance

The flexural strength, maximum deflection and energy absorption capacity test results for the high-performance (DSP) cementitious mortar reinforced with different volume fractions of PAA-physisorbed multiwalled carbon nanotube (CNT D-PAA) and/or carbon microfiber (CMF) are presented in Table 7.5. These results indicate that all the reinforcement conditions considered

here enhance the flexural performance characteristics of the high-performance cementitious mortar. With a single reinforcement type, maximum improvements in flexural characteristics were realized with 0.16 vol.% carbon nanotube (CNT D-PAA). This reinforcement condition yielded 31.6%, 70.9% and 82.6% improvements (versus plain mortar) in flexural strength, energy absorption capacity and maximum deflection, respectively. Carbon nanotube offered higher reinforcement efficiency per unit volume when compared with carbon microfiber. The experimental results presented in Table 6 indicate that the hybrid reinforcement systems provide particularly high reinforcing effects, confirming the value rendered by the synergistic actions of nano- and micro-scale reinforcement in high-performance cementitious mortar, confirming the preliminary results produced with high-performance cementitious paste. The hybrid reinforcement comprising 0.08 vol.% carbon nanotube and 0.40 vol.% carbon microfiber produced the maximum improvements in flexural attributes, yielding 16.6%, 66.2% and 70.3% improvements in flexural strength, energy absorption capacity and maximum deflection, respectively. Lowering the nanotube volume fraction would reduce the flexural performance characteristics of the high-performance cementitious mortar with hybrid reinforcement. Analysis of variance and pair-wise comparison of test results indicated that: (i) carbon nanotube and hybrid reinforcement systems produce statistically significant gains (at 0.05 significance level) in all aspects of the flexural performance of the high-performance cementitious mortar. Carbon microfiber, however, produced statistically significant gains in the flexural energy absorption capacity (but not the flexural strength and maximum deflection) of the high-performance cementitious mortar. This finding further confirms the desired reinforcing effects of nano-scale and hybrid reinforcement systems, when compared with micro-scale fibers, in high-performance cementitious mortar.

7.3.2.2 Compressive Strength

The compressive strength test results (mean values and standard errors) for high-performance (DSP) cementitious mortars with carbon nanotube and/or microfiber reinforcement systems are presented in Table 7.6. The mean values of compressive strength dropped slightly with the addition of 0.24 vol.% carbon microfiber. The effects of carbon nanotube and/or microfiber on the compressive strength of high-performance cementitious mortar, however, were not statistically significant.

7.3.2.3 Impact Resistance

The impact test data are summarized in Table 7.7. The two (optimum) hybrid reinforcement systems are observed to be effective in enhancing the impact resistance of DSP mortar (by 50-65%). The hybrid reinforcement comprising 0.08 vol.% carbon nanotube (CNT D-PAA) and 0.40 vol.% carbon microfiber (CMF) produced the highest improvement in impact resistance of the high-performance cementitious mortar. The contributions of carbon nanotube and/or carbon microfiber to impact resistance were found to be statistically significant (at 0.05 significance level).

7.4 Summary

Effects of reinforcement with multiwalled carbon nanotubes modified through physisorption of a polyelectrolyte (PAA) and/or carbon microfiber on the flexural and compressive performance, abrasion resistance, and the structure and failure modes of a high-performance fiber reinforced cementitious mortar were evaluated. Desired dispersion and interfacial interactions of carbon nanotubes in cementitious matrix were realized through modification of nanotubes (via PAA physisorption on their surfaces) and sonication of nanotubes in water resulting in substantial

increase in all engineering properties of the high performance matrix. As was seen in high-performance paste matrix the selection of the superplasticizer type can significantly impact the to reinforcement efficiency of carbon nanotubes in high-performance cementitious mortars. The results were also substantiated by SEM observations. The use of response surface analysis (RSA) of experimental results identified optimum hybrid reinforcement condition for high-performance mortar matrix.

Table 7.1- Mean values of the flexural attributes high-performance cementitious mortars with nano- and/or micro-scale reinforcement systems.

Reinforcement Condition - Superplasticizer	Flexural	Deflection	Energy
	Strength (MPa)	(mm)	Absorption (N.mm)
Plain – Gl	16.6	0.99	216
Plain - Adva	18.7	1.38	275
Carbon microfiber, 0.24 vol% (CMF-0.24) - Gl	19.3	1.37	319
Carbon microfiber, 0.24 vol% (CMF-0.24) - Adva	19.6	1.42	344
Carbon microfiber, 0.48 vol% (CMF-0.48) - Gl	22.5	2.31	424
Carbon microfiber, 0.48 vol% (CMF-0.48) - Adva	23.0	2.35	459
Carbon microfiber, 0.96 vol% (CMF-0.96) - Gl	23.1	2.54	474
Carbon microfiber, 0.96 vol% (CMF-0.96) - Adva	23.9	2.55	481
Carbon nanotube D, PAA-physisorbed, 0.16 vol%	22.9	2.39	445
(CNT D-PAA-0.16) - Gl			
Carbon nanotube D, PA- physisorbed, 0.16 vol%	24.6	2.52	470
(CNT D-PAA-0.16) - Adva			
Carbon nanotube D, PAA-physisorbed, 0.24 vol%	22.6	2.48	404
(CNTD-PAA-0.24) - Gl			
Carbon nanotube D, PAA-physisorbed, 0.24 vol%	25.3	2.58	435
(CNTD-PAA-0.24) - Adva			
Carbon microfiber, 0.24 vol%, & Carbon nanotube	19.7	2.03	398
D, PAA-physisorbed, 0.16 vol% (HYCNT1) - Gl			
Carbon microfiber, 0.24 vol%, & Carbon nanotubes	21.2	2.28	423
D, PAA physisorbed, 0.16 vol% (HYCNT1) - Adva			

Table 7.2- Mean values and standard errors of the compressive strength of the high-performance cementitious mortar matrices with nano- and/or micro-scale reinforcement systems.

Reinforcement Condition	Mean Compressive Strength (MPa)	Standard Error (MPa)
Plain – Gl	125	17.0
Plain - Adva	129	9.42
Carbon microfiber, 0.24 vol%-(CMF-0.24) - Gl	119	5.69
Carbon microfiber, 0.24 vol%-(CMF-0.24) - Adva	121	10.4
Carbon microfiber, 0.48 vol%-(CMF-0.48) - Gl	138	8.45
Carbon microfiber, 0.48 vol%-(CMF-0.48) - Adva	137	5.44
Carbon microfiber, 0.96 vol%-(CMF-0.96) - Gl	127	17.6
Carbon microfiber, 0.96 vol%-(CMF-0.96) - Adva	128	6.57
Carbon nanotubes D, PAA physisorbed, 0.16 vol%-(CNT D-PAA-0.16) - Gl	132	6.21
Carbon nanotubes D, PAA physisorbed, 0.16 vol%-(CNT D-PAA-0.16) - Adva	135	4.59
Carbon nanotubes D, PAA physisorbed, 0.24 vol%-(CNTD-PAA-0.24) - Gl	125	3.18
Carbon nanotubes D, PAA physisorbed, 0.24 vol%-(CNTD-PAA-0.24) - Adva	130	3.58
Carbon microfiber, 0.24 vol%, & Carbon nanotubes D, PAA physisorbed, 0.16 vol%-(HYCNT1) - Gl	126	17.4
Carbon microfiber, 0.24 vol%, & Carbon nanotubes D, PAA physisorbed, 0.16 vol%-(HYCNT1) - Adva	131	12.8

Table 7.3- Mean values of the impact resistance test results for high-performance cementitious mortars reinforced with nano- and/or micro-scale reinforcement systems.

Reinforcement Condition	Impact Resistance, mm/mm
Plain – Gl	0.573
Plain - Adva	0.625
Carbon microfiber, 0.24 vol% (CMF-0.24) - Gl	0.781
Carbon microfiber, 0.24 vol% (CMF-0.24) - Adva	0.833
Carbon microfiber, 0.48 vol% (CMF-0.48) - Gl	0.833
Carbon microfiber, 0.48 vol% (CMF-0.48) - Adva	0.885
Carbon microfiber, 0.96 vol% (CMF-0.96) - Gl	0.938
Carbon microfiber, 0.96 vol%-(CMF-0.96) - Adva	0.938
Carbon nanotubes D, PAA physisorbed, 0.16 vol% (CNT D-PAA-0.16) - Gl	0.938
Carbon nanotubes D, PAA physisorbed, 0.16 vol% (CNT D-PAA-0.16) - Adva	0.989
Carbon nanotubes D, PAA physisorbed, 0.24 vol% (CNTD-PAA-0.24) - Gl	0.990
Carbon nanotubes D, PAA-physisorbed, 0.24 vol% (CNTD-PAA-0.24) - Adva	1.042
Carbon microfiber, 0.24 vol% & Carbon nanotube D, PAA-physisorbed, 0.16 vol% (HYCNT1) - Gl	0.938
Carbon microfiber, 0.24 vol% & Carbon nanotube D, PAA-physisorbed, 0.16 vol% (HYCNT1) - Adva	0.989

Table 7.4- Mean values of the abrasion resistance test results for high-performance cementitious mortars reinforced with nano- and/or micro-scale reinforcement systems.

Reinforcement Condition	Loss of Mass (gr)
Plain – Gl	1.38
Plain - Adva	1.23
Carbon microfiber, 0.24 vol%-(CMF-0.24) - Gl	0.98
Carbon microfiber, 0.24 vol%-(CMF-0.24) - Adva	0.93
Carbon microfiber, 0.48 vol%-(CMF-0.48) - Gl	0.93
Carbon microfiber, 0.48 vol%-(CMF-0.48) - Adva	0.93
Carbon microfiber, 0.96 vol%-(CMF-0.96) - Gl	0.85
Carbon microfiber, 0.96 vol%-(CMF-0.96) - Adva	0.83
Carbon nanotubes D, PAA physisorbed, 0.16 vol%-(CNT D-PAA-0.16) - Gl	0.83
Carbon nanotubes D, PAA physisorbed, 0.16 vol%-(CNT D-PAA-0.16) - Adva	0.80
Carbon nanotubes D, PAA physisorbed, 0.24 vol%-(CNTD-PAA-0.24) - Gl	0.80
Carbon nanotubes D, PAA physisorbed, 0.24 vol%-(CNTD-PAA-0.24) - Adva	0.75
Carbon microfiber, 0.24 vol%, & Carbon nanotubes D, PAA physisorbed, 0.16 vol%-(HYCNT1) - Gl	0.80
Carbon microfiber, 0.24 vol%, & Carbon nanotubes D, PAA physisorbed, 0.16 vol%-(HYCNT1) - Adva	0.80

Table 7.5- Mean values of flexural strength, maximum deflection and energy absorption capacity of high-performance cementitious mortars with nano- and/or micro-scale reinforcement systems.

Reinforcement Condition	Mean Flexure Strength (MPa)	Deflection (mm)	Energy Absorption (N.mm)
Plain - Adva	18.7	1.38	275
Carbon microfiber, 0.24 vol%-(CMF-0.24) - Adva	19.6	1.42	344
Carbon nanotubes D, PAA physisorbed, 0.16 vol%-(CNTD-PAA-0.16) - Adva	24.6	2.52	470
Carbon microfiber, 0.24 vol%, & Carbon nanotubes D, PAA physisorbed, 0.16 vol%-(HYCNT1) - Adva	21.2	2.28	423
Carbon microfiber, 0.30 vol%, & Carbon nanotubes D, PAA physisorbed, 0.06 vol%-(HYCNT2) - Adva	21.0	2.29	441
Carbon microfiber, 0.40 vol%, & Carbon nanotubes D, PAA physisorbed, 0.08 vol%-(HYCNT3) - Adva	21.8	2.35	457

Table 7.6- Mean values and standard errors of the compressive strength test results for high – performance cementitious mortars with nano- and/or micro-scale reinforcement systems.

Reinforcement Condition	Mean Compressive Strength (MPa)	Standard Error (MPa)
Plain - Adva	129	9.42
Carbon microfiber, 0.24 vol%-(CMF-0.24) - Adva	121	10.4
Carbon nanotubes D, PAA physisorbed, 0.16 vol%-(CNTD-PAA-0.16) - Adva	135	4.59
Carbon microfiber, 0.24 vol%, & Carbon nanotubes D, PAA physisorbed, 0.16 vol%-(HYCNT1) - Adva	131	12.8
Carbon microfiber, 0.30 vol%, & Carbon nanotubes D, PAA physisorbed, 0.06 vol%-(HYCNT2) - Adva	133	4.83
Carbon microfiber, 0.40 vol%, & Carbon nanotubes D, PAA physisorbed, 0.08 vol%-(HYCNT3) - Adva	130	7.99

Table 7.7- Mean values of the impact resistance test results for high-performance cementitious mortars with nano- and/or micro-scale reinforcement.

Reinforcement Condition	Impact Resistance (mm/mm)
Plain - Adva	0.63
Carbon microfiber, 0.24 vol%-(CMF-0.24) - Adva	0.83
Carbon nanotubes D, PAA physisorbed, 0.16 vol%-(CNTD-PAA-0.16) - Adva	0.99
Carbon microfiber, 0.24 vol%, & Carbon nanotubes D, PAA physisorbed, 0.16 vol%-(HYCNT1) - Adva	0.99
Carbon microfiber, 0.30 vol%, & Carbon nanotubes D, PAA physisorbed, 0.06 vol%-(HYCNT2) - Adva	0.95
Carbon microfiber, 0.40 vol%, & Carbon nanotubes D, PAA physisorbed, 0.08 vol%-(HYCNT3) - Adva	1.04

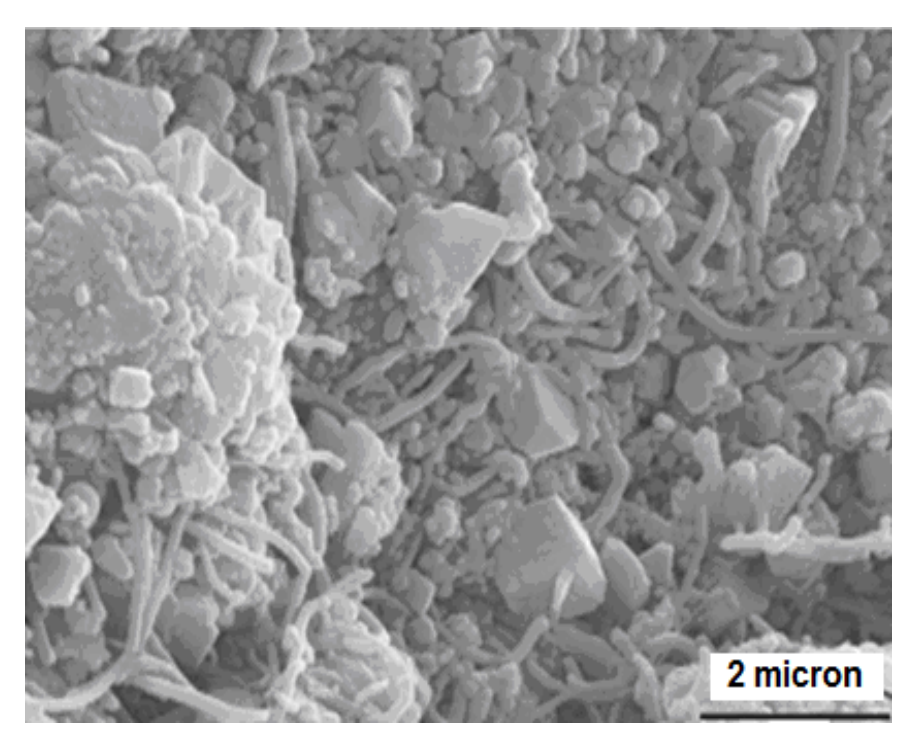


Figure 7.1- SEM image of a cement-based material incorporating well dispersed PAA-physisorbed multiwalled carbon nanotubes (CNT D-PAA).

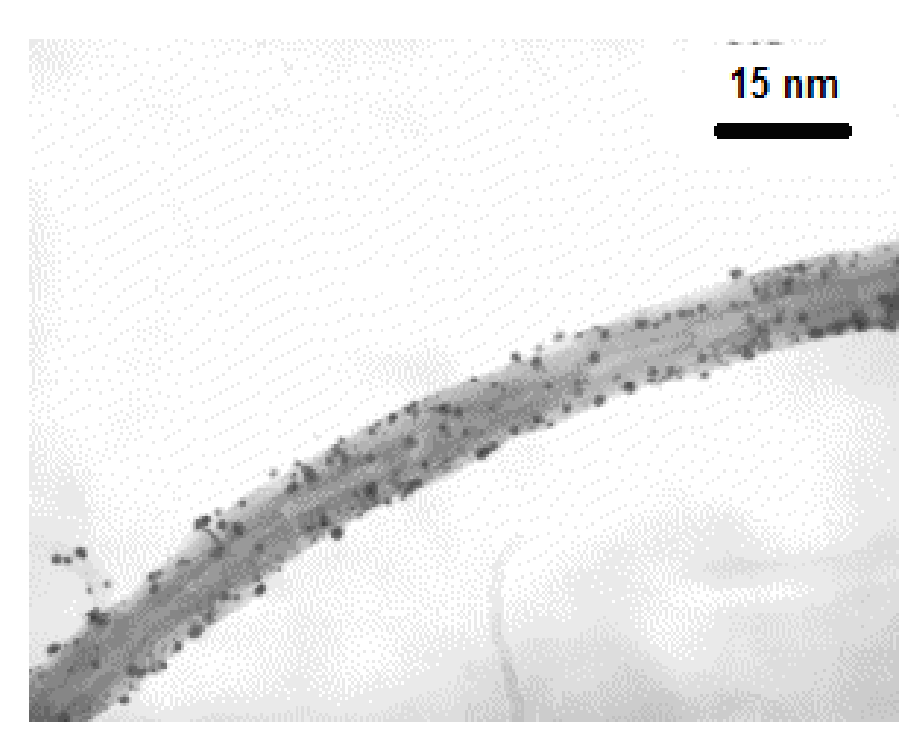
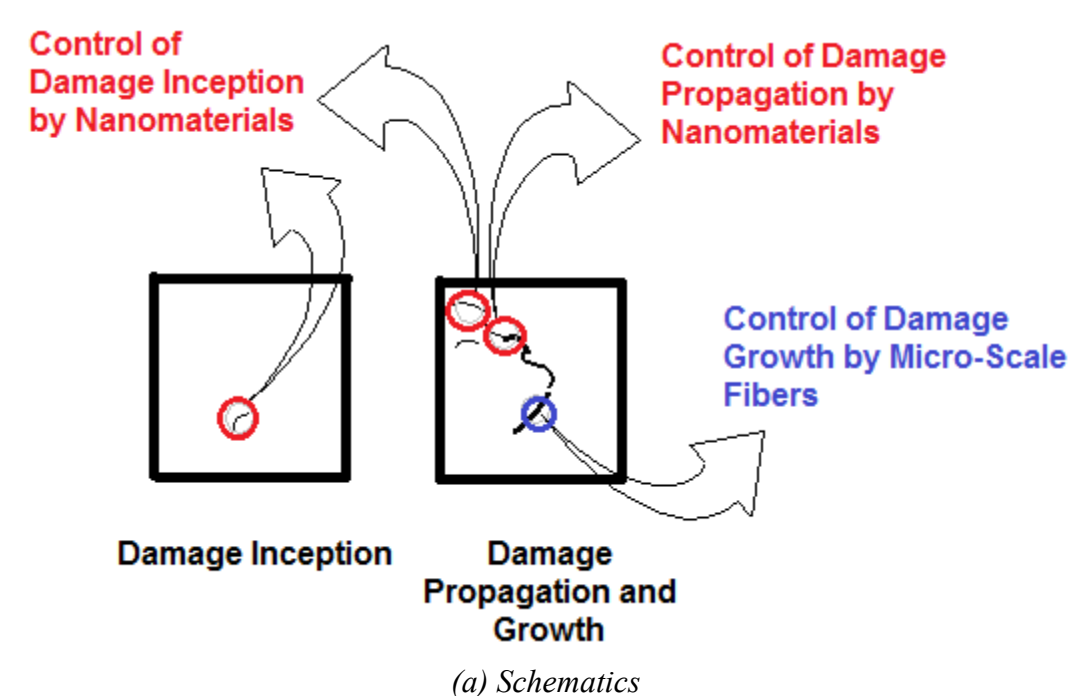


Figure 7.2- Transmission electron microscope image of PAA physisorbed multiwalled carbon nanotube Type D.



(u) senematics

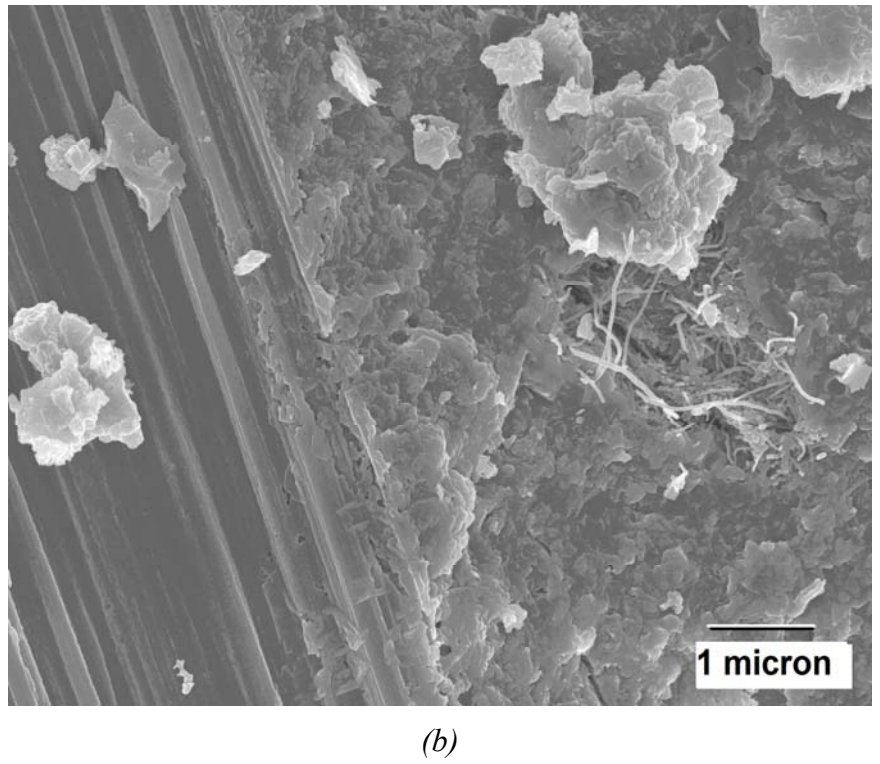
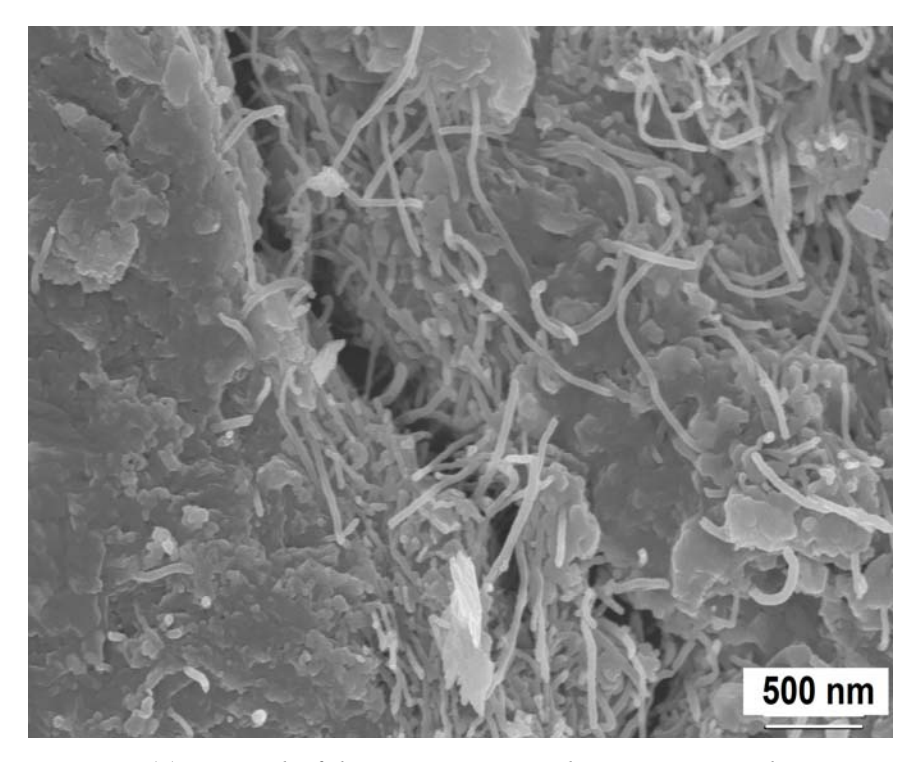
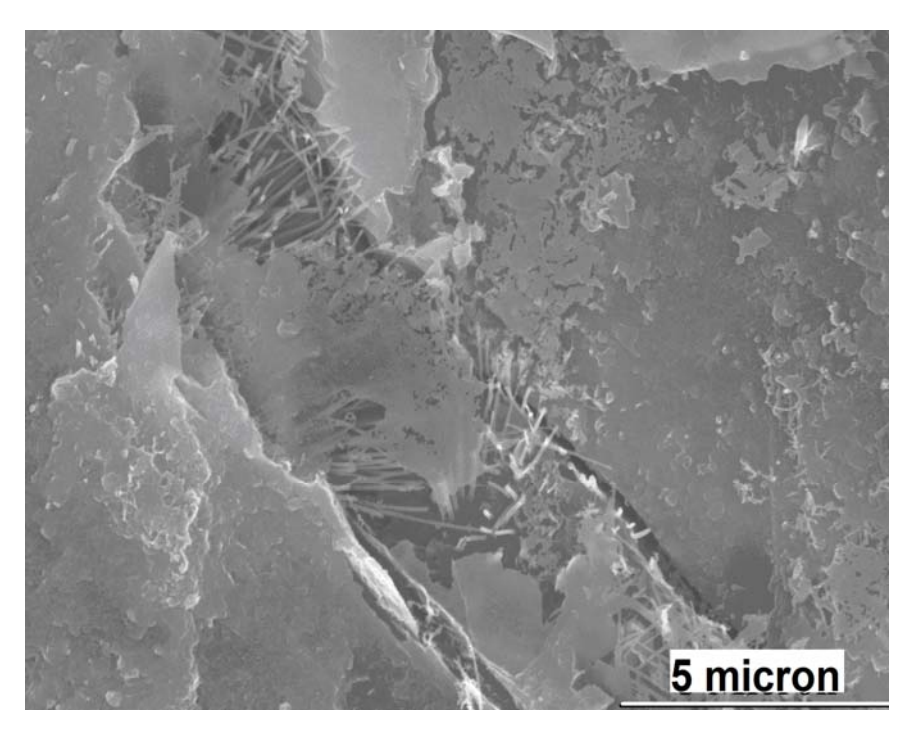


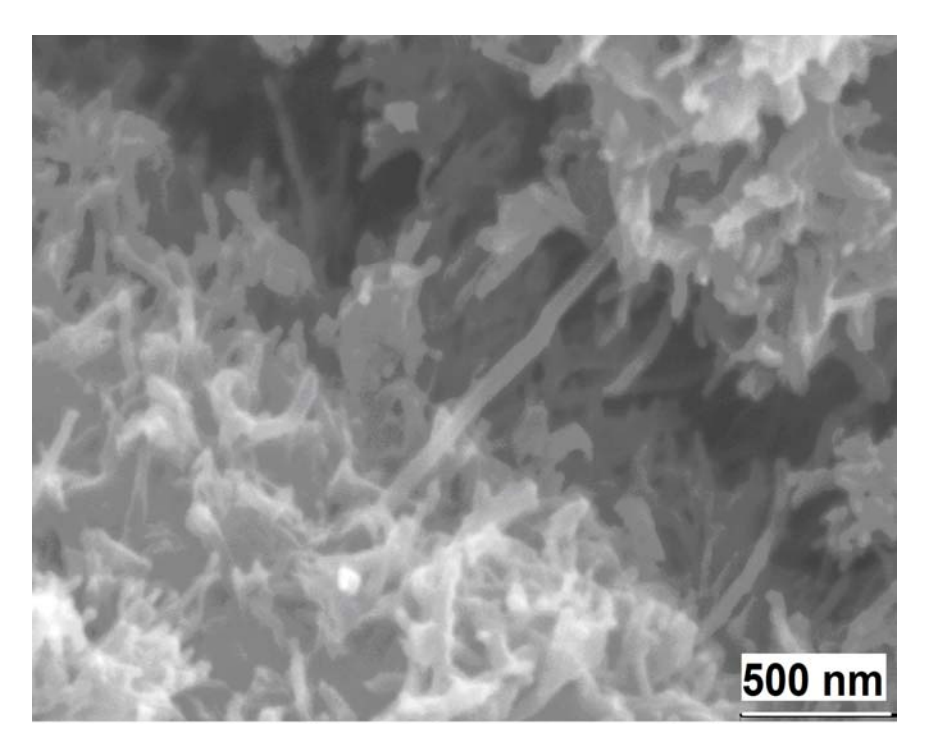
Figure 7.3- Complementary roles of nano- and micro-scale reinforcement in damage control by suppression of micro-crack inception and control of microcrack growth.



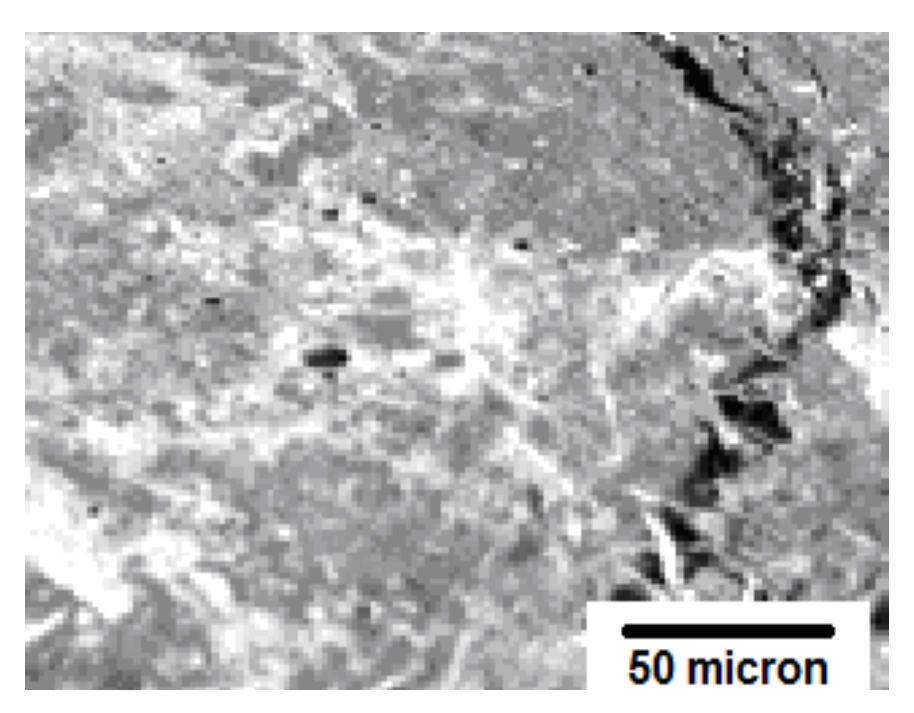
(c) Control of damage inception by nanomaterials



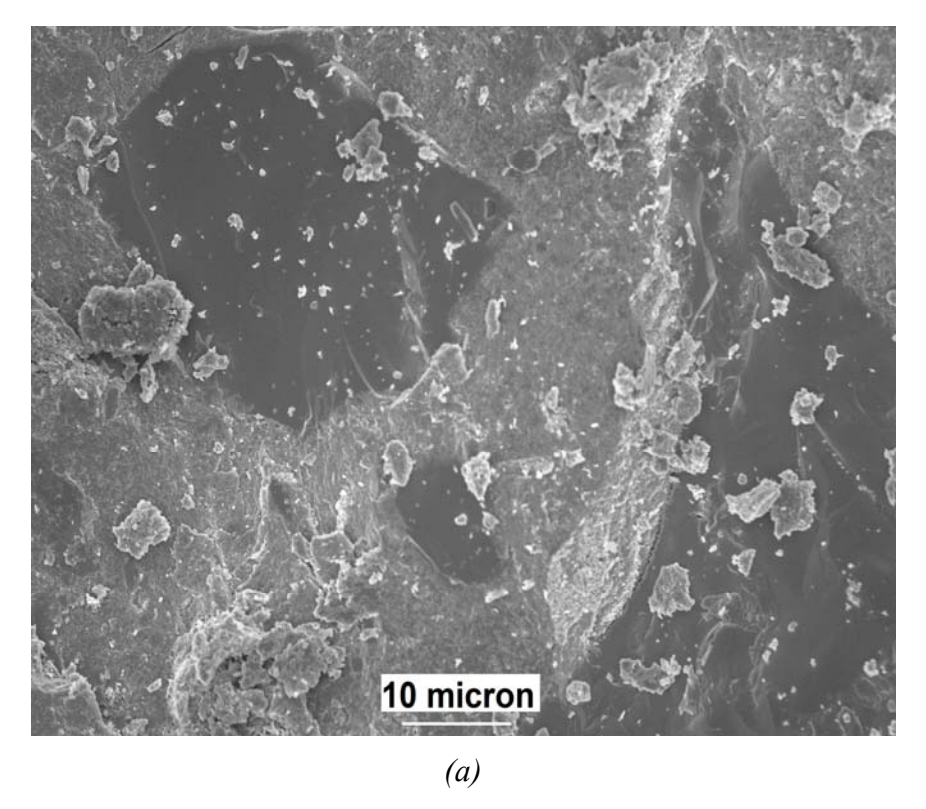
(d)



(e) Control of Damage propagation by nanomaterials



(f) Control of damage growth by micro-scale fibers



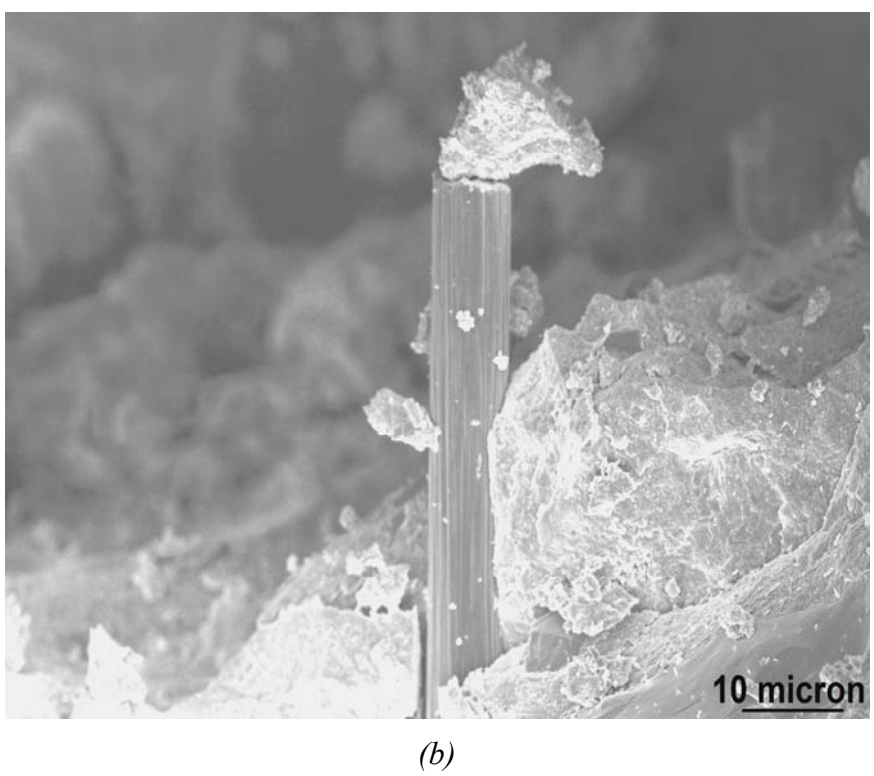
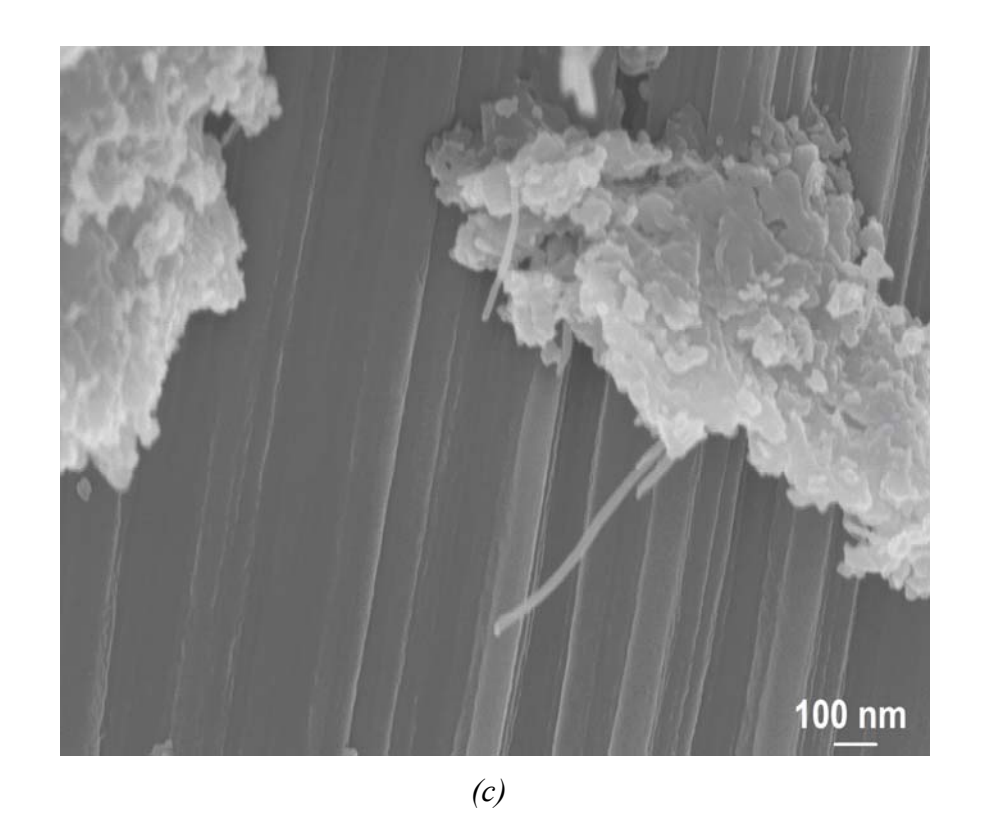


Figure 7.4- Typical SEM images of the fractured surfaces of high-performance cementitious mortars with nano- and micro-scale reinforcement systems.



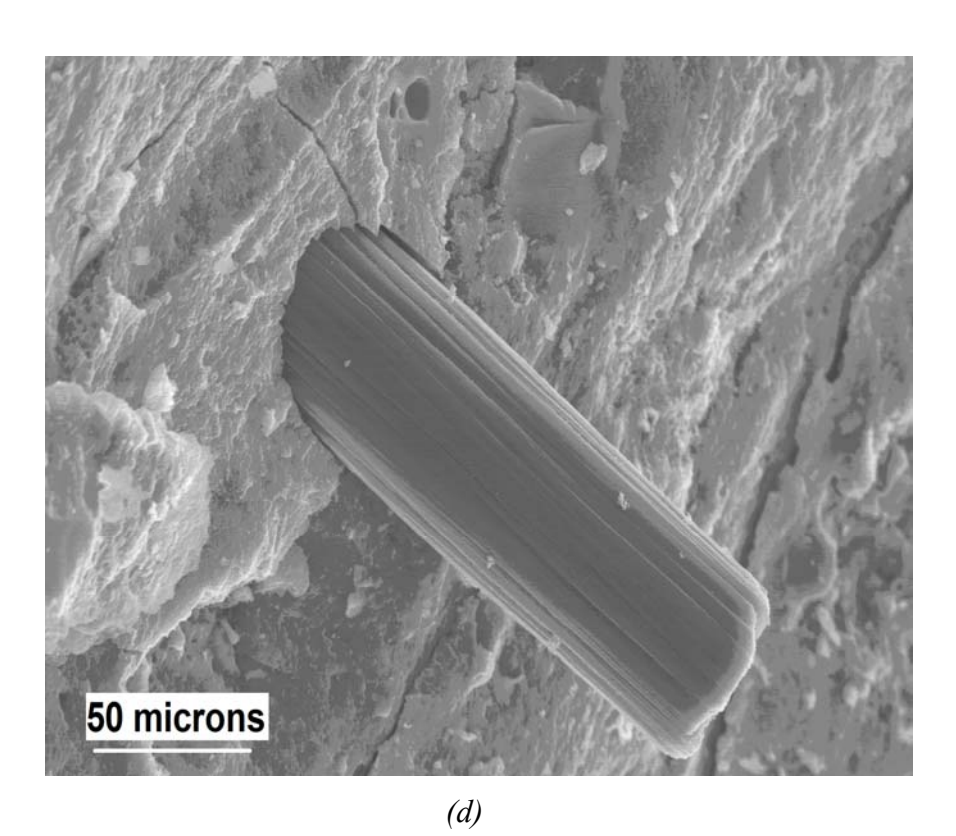
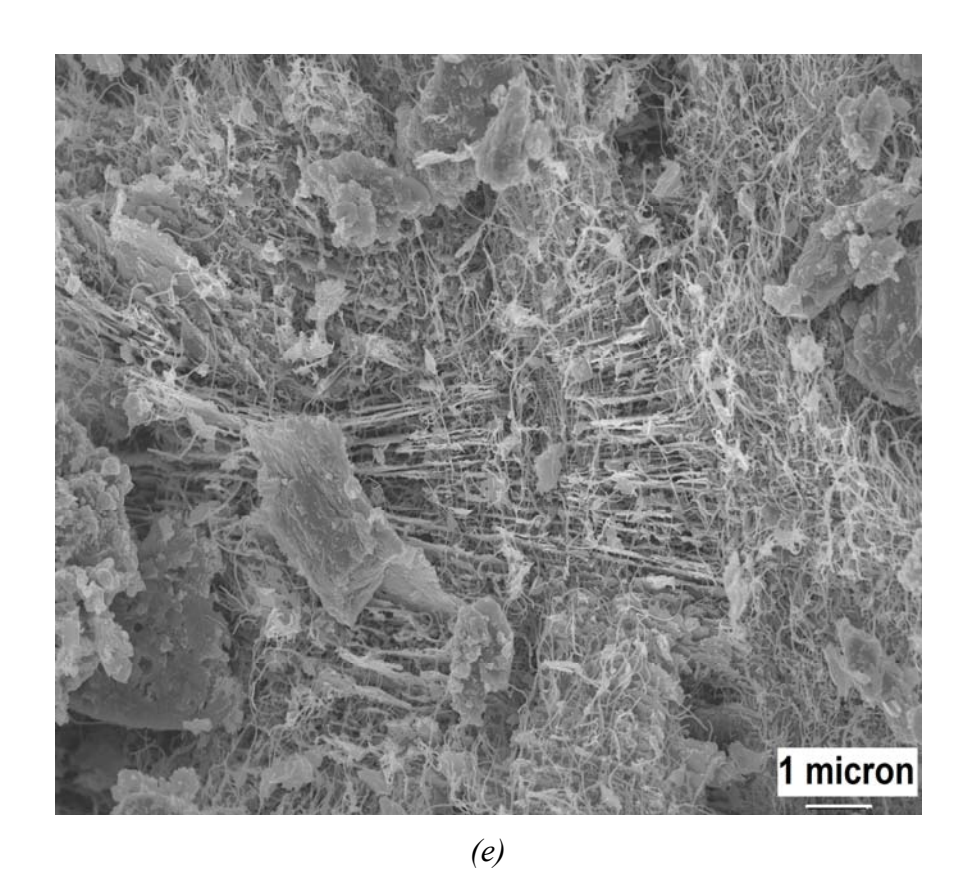


Figure 7.4 (cont'd)



8 DAMAGE-SENSITIVE ELECTRICAL CONDUCTIVITY OF HIGH-PERFORMACNE MORTARS REINFORCED WITH MULTIWALLED CARBON NANOTUBES

8.1 General

Carbon nanotubes, when properly functionalized and thoroughly dispersed in well-graded cementitious materials, bring about balanced gains in diverse engineering properties of highperformance concrete. These properties include fracture toughness, impact resistance, strength, barrier qualities, abrasion resistance, fatigue life, and weathering resistance (Metaxa, Konsta-Gdoutos et al. 2009; Metaxa, Konsta-Gdoutos et al. 2010; Metaxa, Konsta-Gdoutos et al. 2010). In addition, multiwalled carbon nanotubes offer distinctly high thermal and electrical conductivity. They can thus significantly increase the conductivity attributes of cement-based materials when a percolated (networked) structure of nanomaterials forms within cement-based matrices (Figure 8.1). The distinctly high aspect ratio of nanomaterials substantially lowers the "threshold" volume fraction at which the percolation phenomenon occurs. Percolated nanomaterials provide continuous paths for transport of electricity and heat; given the relatively high aspect (length-to-diameter) ratio of carbon nanotubes, well-dispersed nanotubes percolate at relatively low volume fractions. Break-up of the percolated network under damaging effects such as microcracks and large strains could disrupt the continuous conduction path, and thus lower the conductivity of cementitious nanocomposites. The damage-sensitivity of electrical conductivity

offers a convenient basis for health monitoring of cementitious nanocomposites (and concrete-based infrastructure systems incorporating them).

Applications of carbon nanotubes towards development of self-sensing, self-monitoring materials have generally employed the piezo-resistive qualities of carbon nanotubes in polymer matrices (Sandlar, Shaffer et al. 1999; Hu, Zhao et al. 2006); limited work has been reported on the use of carbon nanotubes in cement paste (Li, Wang et al. 2007; Han, Yu et al. 2009; Han, Yu et al. 2011). The available data point at the potential of carbon nanotubes to yield nanocomposites with inherent structural health monitoring attributes. The work reported uses carbon nanotubes in a high-performance cementitious mortar (incorporating fine aggregates), and relies upon the disturbance of the percolation conditions of carbon nanotubes as the matrix experiences damage to enable health monitoring via measurement of electrical conductivity.

8.2 Materials and Methods

8.2.1 Materials and Graphite Nanomaterials

Modified multiwalled carbon nanotubes, modified by physisorption of PAA (polyacrylic acid), were used in a high-performance (DSP) cementitious mortar matrix. These graphite nanomaterials have been introduced in detail in Chapter 2, Fig. 2.3 and Table 2.3. In the course of dispersing the nanotubes in water PAA was physisorbed upon multiwalled carbon nanotubes. PAA with average molecular weight (M_w) of about 100,000 at 35 wt.% concentration in water, was purchased from Sigma-Aldrich. Figure 7.4 shows a transmission electron micrograph PAA-physisorbed nanotube (CNTD-PAA), which exhibited improved dispersion in aqueous media and interfacial interactions with cement hydrates.

8.2.2 Cementitious Matrices, Mixing and Curing Procedure

Dense cementitious matrix selected has been introduced in detail in Chapter 2, Section 2.5. DSP mortar was used to evaluate the pressure-sensitive properties of both graphite nanomaterials at different volume fractions.

Cementitious materials (with and without functionalized graphite nanomaterials dispersed in the mixing water via sonication) were prepared and cured following ASTM procedures described in the same section.

8.2.3 Experimental Methods

The electrical conductivity of high-performance cementitious mortar specimens (75 x 50 x 12.5 mm) with different fractions of MWNTs modified by PAA physisorption, prepared using two different superplasticizers, was measured in dry condition using Gamry Electro-Chemical Spectrometer following the procedures of ASTM D991, D 4496 and D 257. The experimental setup is shown in Figure 8.2. PELCO® Conductive Silver paint was applied, and copper tapes were firmly attached to the opposite faces of the specimen. Electrodes were connected to copper tapes, and electrical conductivity was measured in dry condition in longitudinal direction. In order to determine the damage-sensitivity of the electrical conductivity of nanocomposites, conductivity tests were also conducted after subjecting cube (50 x 50 x 50 mm) specimens of the high-performance cementitious mortars with or without nanotubes to 60% and 80% of their mean compressive strength. The means (standard errors) of the compressive strength test results for the high-performance cementitious mortars with 0, 0.16 and 0.24 vol.% (volume percent of dry cementitious materials) of modified carbon nanotubes, prepared using the Glenium® 7700 superplasticizer, were 125 (17.0), 132 (6.21) and 125 (3.18) MPa, respectively. The corresponding values for cementitious materials prepared with the ADVA® Cast 575

superplasticizer were 129 (9.42), 135 (4.59) and 130 (3.58) MPa, respectively. For each specimen, three resistance measurements were made in each (longitudinal and transverse) direction, and the average was recorded. Electrical conductivity was calculated as inverse of the measure value of resistance. The specimens were also subjected to SEM in order to gain further insight into their structure and failure mechanisms. Experimental results were evaluated using the analysis of variance (ANOVA) and pair-wise comparison techniques.

8.3 Experimental Results and Discussion

8.3.1 Effects of Modified Multiwalled Carbon Nanotubes on the Electrical Conductivity of High-Performance Cementitious Mortars

The mean values of electrical conductivity for high-performance cementitious mortars with different volume fractions of modified multiwalled carbon nanotubes (prepared using two different superplasticizers) are presented in Table 8.1. Depending on the superplasticizer type, the addition of 0.16 vol.% modified carbon nanotube increased the electrical conductivity of the high-performance cementitious mortar by two to three orders of magnitude. Increasing the dosage of modified nanotube from 0.16 to 0.24 vol.% further increased the electrical conductivity of cementitious mortar by an order of magnitude. The significant rise in electrical conductivity of cementitious mortars with the addition of 0.16 and 0.24 vol.% modified carbon nanotubes indicates that a percolated network of nanotubes is formed at either volume fraction. The experimental results indicate that the selection of superplasticizer can significantly impact the effects of nanotubes on the electrical conductivity of high-performance cementitious mortars. This could be attributed to the differences in the thoroughness of nanotube dispersion realized with different superplasticizers and/or the differences in (nanotube-to-nanotube) interfacial electrical resistance when different superplasticizers are used.

8.3.2 Damage-Sensitivity of the Electrical Conductivity of High-Performance Cementitious Mortars Incorporating Modified Carbon Nanotubes

The mean values of electrical conductivity for high-performance cementitious mortars with 0.16 and 0.24 vol.% modified multiwalled carbon nanotubes prepared with the ADVA® Cast 575 superplasticizer are presented in Table 8.2. The results clearly indicate establishment of conductive percolated network of carbon nanotubes at both 0.16 and 0.24 vol.% nanotube additions. The test results presented in Tables 8.2 and 8.3 were produced using specimens of different dimensions prepared using different batches of cementitious materials, which can be used to explain the differences between electrical conductivity measurements for specimens prepared using the same (ADVA® Cast 575) superplasticizer.

All specimens containing nanotubes, when subjected to increasing compressive stress levels, experienced a sharp drop in electrical conductivity, which can be attributed to breakdown of the percolated nanotube network under the damaging effects (e.g., microcracking and large permanent strains) of compression loading. After application of 60% of compressive strength, electrical conductivity dropped by one order of magnitude. Application of 80% of compressive strength produced two orders of magnitude drop in electrical conductivity. The higher conductivity levels in the presence of 0.24 vol.% carbon nanotubes simplify the conductivity measurements. The significant damage sensitivity of electrical conductivity in cementitious materials incorporating carbon nanotubes points at the inherent health monitoring qualities of the material.

8.3.3 Scanning Electron Microscope Observations

Failed surfaces of compression test specimens were evaluated under a high-precision scanning electron microscope (JOEL 7500F). All samples were coated with Osmium (using Osmium

Coater Neoc-AN, Meiwa Shoji) prior to SEM observations. The scanning electron microscope images depicted in Figure 8.3 point at a dense cementitious matrix incorporating uniformly dispersed carbon nanotubes which seem to form a percolated network.

8.4 Summary

Multiwalled carbon nanotubes were modified through physisorption of a polyelectrolyte, and were dispersed within a high-performance cementitious mortar at relatively low (0.16-0.24 vol.%) volume fractions. The effects of nanotubes on the electrical conductivity of the cementitious mortar were evaluated, and the damage-sensitivity of electrical conductivity was evaluated by making conductivity measurements prior to and after application of different fractions of compressive strength. The results show that functionalized carbon nanotubes form percolation networks within the matrix thus increasing the conductivity of the matrix. The pressure sensitive properties of the matrix can be effectively utilized in self-sensing, self-monitoring and smart structures.

Table 8.1- Mean values of the electrical conductivity test results for high-performance cementitious mortars with different volume fractions of modified multiwalled carbon nanotubes prepared using two different superplasticizers.

Reinforcement Condition	Electrical Conductivity, 1/Ω m
Plain	1.09 x 10 ⁻⁶
CNT D-PAA, 0.16 vol% - Gl [#]	1.19 x 10 ⁻⁴
CNT D-PAA, 0.16 vol% - Ad*	1.72 x 10 ⁻³
CNT D-PAA, 0.24 vol% - Gl	4.72 x 10 ⁻³
CNT D-PAA, 0.24 vol% - Ad	2.07 x 10 ⁻²

[#]Glenium® 7700; *ADVA® Cast 575

Table 8.2- Mean values of the electrical conductivity of high-performance cementitious mortar specimens with different volume fractions of functionalized multiwalled carbon nanotubes after application of different compressive stress levels.

Reinforcement Condition	Electrical Conductivity- longitudinal direction, 1/ Ω m	Electrical Conductivity- transverse direction, 1/Ω m
CNT D-PAA, 0.16 vol%	1.92 x 10 ⁻³	2.25 x 10 ⁻³
CNT D-PAA, 0.16 vol%, 60% ultimate	4.14 x 10 ⁻⁴	4.72 x 10 ⁻⁴
CNT D-PAA, 0.16 vol%, 80% ultimate	1.05×10^{-5}	1.12 x 10 ⁻⁴
CNT D-PAA, 0.24 vol%	2.07×10^{-2}	2.80 x 10 ⁻²
CNT D-PAA, 0.24 vol%, 60% ultimate	3.15×10^{-3}	4.05 x 10 ⁻³
CNT D-PAA, 0.24 vol%, 80% ultimate	4.23 x 10 ⁻⁴	4.15 x 10 ⁻⁴

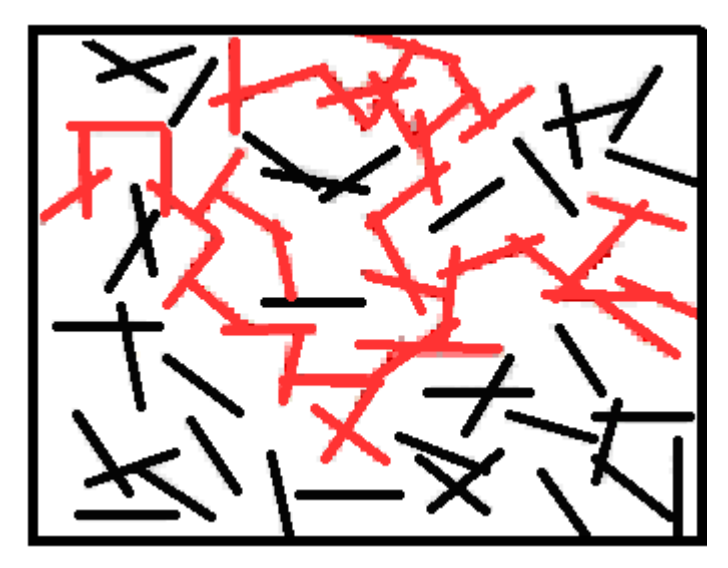


Figure 8.1- Percolated network.



(a) Experimental Setup

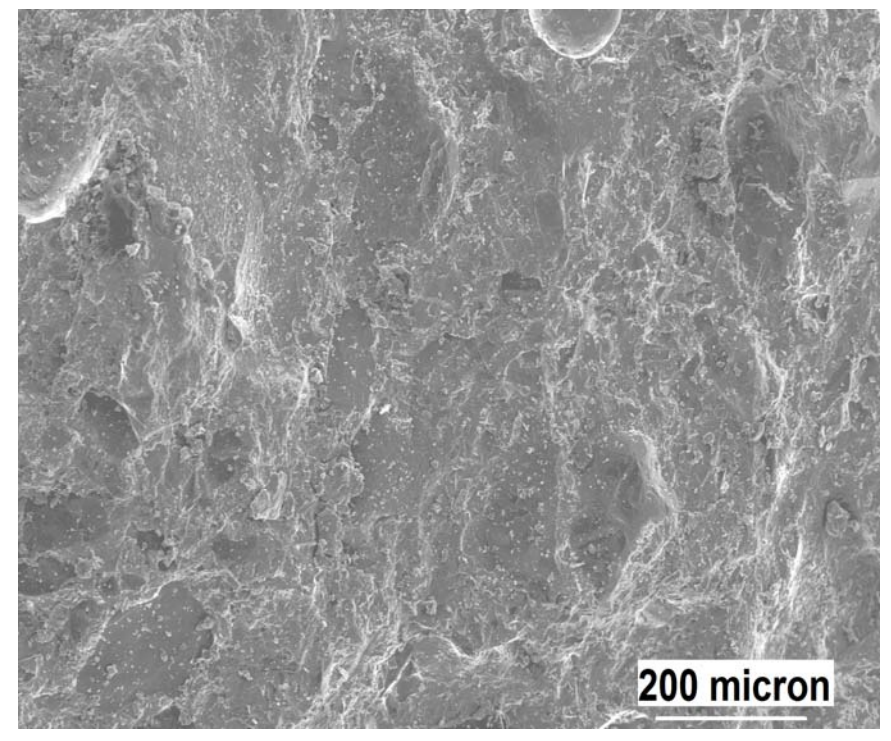
Figure 8.2- Electrical conductivity test setup and specimens.



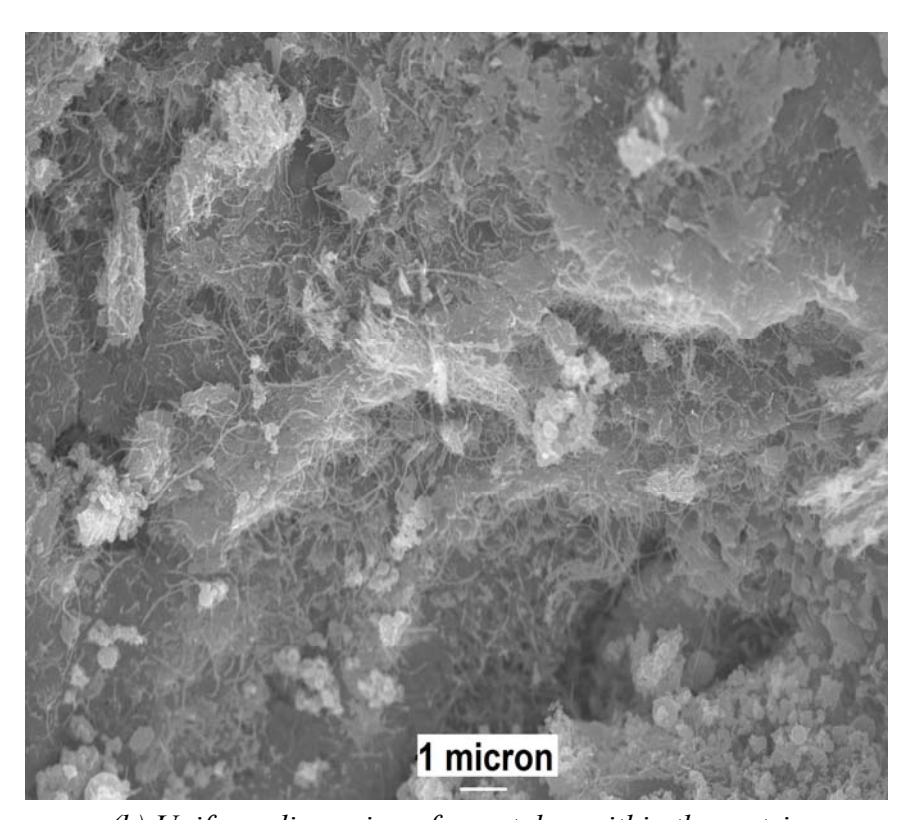
(b) Prepared specimens prior to test



(c) Specimen surfaces coated with silver paint

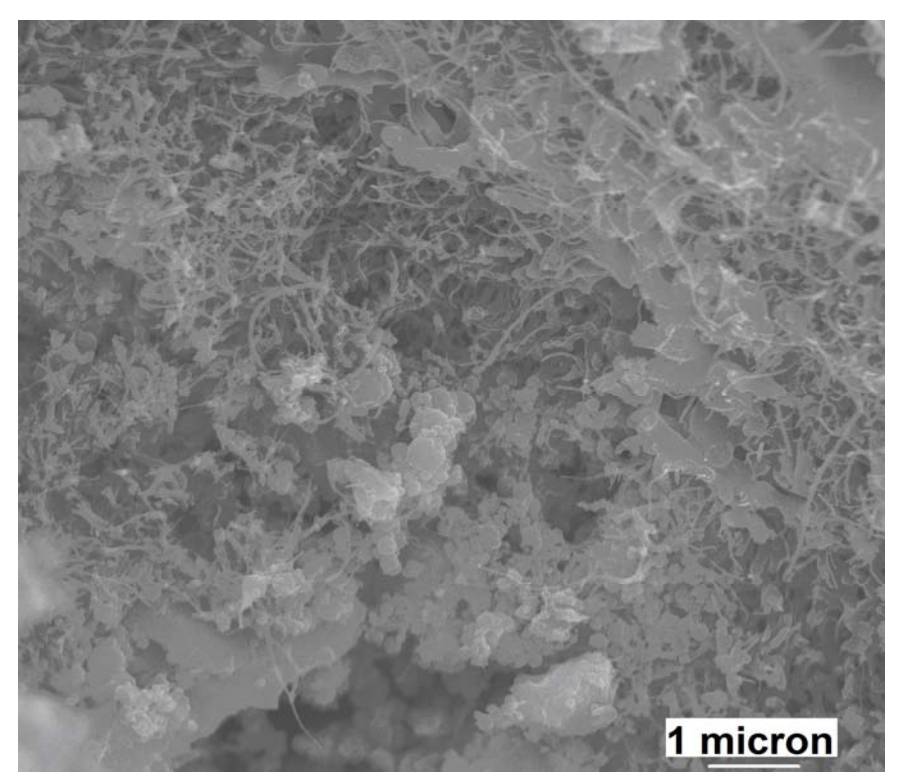


(a) Dense matrix



(b) Uniform dispersion of nanotubes within the matrix

Figure 8.3- Typical SEM mages of high-performance cementitious mortar reinforced with modified multiwalled carbon nanotube.



(c) Percolation of nanotubes within the matrix

9 EVALUATION OF HYBRID (NANO- AND MICRO-SCALE) REINFORCEMET EFFECTS ON THE ENGINEERING OF HIGH-PERFORMANCE CONCRETE

9.1 General

High-performance cementitious materials are subject of intense development efforts. Given the brittle nature of high-strength cementitious materials, discrete reinforcement systems (fibers) are used to render toughening and crack control effects. The reinforcing fibers commonly used in high-performance cementitious materials have diameters in micrometer to millimeter scales. Their primary reinforcing effect involves bridging across cracks to control their growth and dissipate energy via frictional pullout.

Carbon nanotubes (CNTs) present several distinct advantages over conventional fibers as reinforcement for high-performance cementitious materials. These advantages include: (i) high strength, modulus and aspect ratio which benefit their crack-arrest and toughening effects; (ii) high specific surface area and close spacing, which intensify their interactions with cement hydrates and microcracks at their inception. These advantages can be realized as far as the nanotubes are uniformly dispersed within the cementitious matrix, and develop strong bonds to cement hydrates.

The reinforcement efficiency of carbon nanotubes has been evaluated primarily in cementitious pastes (without the addition of any aggregates), and occasionally in cementitious mortars with relatively fine aggregates; modest gains in some engineering properties have been reported with

the addition of relatively low volume fractions of nanotubes (Makar and Beaudoin 2004; Cwirzen, Habermehl-Cwirzen et al. 2008; Cwirzen, Habermehl-Cwirzen et al. 2009; Makar and Chan 2009; Metaxa, Konsta-Gdoutos et al. 2009; Metaxa, Konsta-Gdoutos et al. 2010; Li, Wang et al. 2005). The work reported herein is part of a comprehensive investigation on the use of modified carbon nanotubes in high-performance cementitious paste, mortar and concrete. Proper selections of the nanotube modification and dispersion methods, and the cementitious matrix mix designs have led to significant gains in performance characteristics of high-performance cementitious materials with the addition of relatively low nanotube volume fractions. Results of these background studies have been shown in earlier chapters.

The work reported herein focused on the use of hybrid (nano- and micro-scale) discrete reinforcement systems in high-performance (DSP) concrete. The experience gained with the use of nano-scale reinforcement in cementitious materials has largely avoided the use of coarse aggregates in the matrix. The use of coarse aggregates in this work adds to the complexity of the structure and failure modes of the cementitious matrix. The presence of coarse aggregates limits the volume of paste available for dispersion of nano-scale reinforcement. Formation of an interfacial zone around aggregates, which is more porous, has a higher concentration of coarser crystals, and is prone to shrinkage microcracking, are some key effects of coarse aggregates in cementitious matrix. A key objective of this investigation was to assess the contributions of functionalized multiwalled carbon nanotubes, alone or in combination with micro-scale fibers, to the performance characteristics of high-performance concrete incorporating coarse aggregate.

Cementitious materials are essentially particulate composites, which are rarely used without aggregates (particulates). Given the micro- to millimeter-scale dimensions of the sand and gravel particles used in high-performance (DSP) concrete (Figure 9.1), hybrid reinforcement which

renders reinforcing effects at different scales could produce particularly positive effects. In the past, the concept of using hybrid (micro- and millimeter-scale) reinforcement has been explored for achieving balanced gains in material properties (Moranville-Regourd 2001; O'Connell, Boul et al. 2001; Lawler, Zampini et al. 2005; Banthia and Sappakittipakorn 2007). The work reported herein has extended this background work by making complementary use of reinforcement at micro- and nano-scales.

9.2 Materials and Methods

9.2.1 Graphite Nanomaterials and Microfibers

PAA (Polyacrylic acid) physisorbed MWNTs and/or carbon microfibers (CMF) and polypropylene microfibers (PP) were used as reinforcement in high-performance (DSP) concrete at different volume fractions. These graphite nanomaterials and microfibers have been introduced in detail in Chapter 2, Section 2.4, Fig. 2.3 and Table 2.3. In the course of dispersing the nanotubes in water PAA was physisorbed upon multiwalled carbon nanotubes.

9.2.2 Cementitious Matrices, Mixing and Curing Procedure

Dense cementitious matrix selected has been introduced in detail in Chapter 2, Section 2.5.1.

DSP concrete was used to evaluate the reinforcement efficiency of both graphite nanomaterials and microfibers at different volume fractions.

Cementitious materials (with and without functionalized graphite nanomaterials dispersed in the mixing water via sonication) and/ or different microfibers were prepared and cured following ASTM procedures described in the same section.

9.2.3 Experimental Methods

The test procedures employed to determine the engineering properties of high-performance concrete included compression tests (ASTM C 109), flexure tests (ASTM C 1185), impact tests (ASTM D 7136) and Abrasion tests (ASTM C 944). SEM was also employed to gain further insight into the structure and failure mechanisms of cement-based nanocomposites. Experimental results were evaluated using the analysis of variance (ANOVA) and pair-wise comparison techniques. Response Surface Analysis (RSA) of test results was used to identify the optimum reinforcement condition which yields balanced gains in various engineering properties of the cementitious matrix.

9.3 Experimental Results and Discussion

9.3.1 Carbon Nanotubes and/ or Carbon Microfibers at Different Volume Fractions and with Different Superplasticizers

9.3.1.1 Flexural Performance

The flexure test results for high-performance concrete reinforced with multiwalled carbon nanotubes and/or microfibers are summarized in Table 9.1. These test results indicate that all reinforcement systems produced gains in the flexural strength, maximum deformation (ductility) and energy absorption capacity of the high-performance concrete, except for the two microfibers which lowered the flexural strength of concrete when used alone. The most desired balance of flexural properties for a single reinforcement system was realized by the addition of 0.16 vol.% (volume percent of dry cementitious materials) of CNTD-PAA. The corresponding improvements in flexural strength, energy absorption capacity and maximum deflection with respect to plain concrete were 23.0%, 151% and 123%, respectively. Test results also indicate

that the addition of each of the microfibers to this (relatively brittle) high-strength concrete produced important gains in two out of the three flexural attributes considered here (maximum deflection and energy absorption capacity), while causing a relatively small drop in flexural strength. Polypropylene microfiber produced the maximum rise in energy absorption capacity (315%) and maximum deflection (550%).

The test presented in earlier chapters for cementitious paste and mortar matrices have pointed at the positive effects of hybrid (nano- and micro-scale) reinforcement systems in highperformance cementitious materials. The test data presented in Table 9.1 suggest that polypropylene microfibers of lower modulus and lower cost (when compared with carbon microfibers) could effectively complement the reinforcing effects of nanomaterials in highperformance concrete. Hybrid reinforcement systems comprising polypropylene microfibers and multiwalled carbon nanotubes produced balanced gains in the flexural performance characteristics of high-performance concrete by interacting with and arresting cracks which developed in matrix at different scales. The hybrid reinforcement comprising 0.16 vol.% PAAphysisorbed multiwalled carbon nanotube and 0.24 vol.% polypropylene microfiber produced 41.8%, 648% and 352% rise in flexural strength, maximum deflection and energy absorption capacity, respectively. Hybrid reinforcement systems also overcame the adverse effects of microfibers on flexural strength. The synergistic reinforcement actions of nano- and micro-scale reinforcement systems point at the merits of multi-scale reinforcement in high-performance concrete. This effectiveness of hybrid reinforcement was also evident in the case of highmodulus carbon microfibers used together with multiwalled carbon nanotube. This hybrid reinforcement produced improvements in flexural performance of high-performance concrete when compared with plain concrete and also that reinforced with carbon microfiber alone.

Statistical analysis (of variance) of flexure test results indicated that there are statistically significant (at 0.05 significance level) improvements in all flexural attributes of highperformance concrete due to the addition of nano-scale and hybrid reinforcement systems. Pairwise comparisons were carried out in order to assess the statistical significance of the effects associated with the addition of nano- and/or micro-scale reinforcement systems. These results indicated that nano-scale reinforcement at 0.16 vol.% produced statistically significant improvements in all flexural attributes of the plain concrete at 0.05 significance level. Both microfibers produced statistically insignificant drops in flexural strength (0.297 and 0.481 significance levels for carbon and polypropylene microfibers, respectively). Pair-wise analysis also pointed at statistically insignificant gains in energy absorption capacity (0.502 significance level) and maximum deflection (0.402 significance level) realized with 0.24 vol.% carbon microfiber. Combined use of carbon nanotube with any of the two microfibers (low-modulus polypropylene or high-modulus carbon microfiber) exhibited synergistic effects of nano- and micro-scale reinforcement, producing balanced gains in different flexural attributes of highperformance concrete at significance levels varying from 0.000 to 0.047.

9.3.1.2 Compressive Strength

The compressive strength test results (mean values and standard errors) for high-performance concretes with nano- and/or micro-scale reinforcement systems are presented in Table 9.2. As earlier results with high-performance paste and mortar indicates, PAA-physisorbed multiwalled carbon nanotubes as well as polypropylene or carbon microfibers produced relatively small and statistically insignificant (at 0.05 significance level) effects on the compressive strength of high-performance concrete. The use of hybrid reinforcement systems comprising carbon or polypropylene microfiber and carbon nanotube restored the compressive strengths of the high-

performance concrete by inducing interactions with matrix and its cracks at different scales. The hybrid reinforcement system comprising PAA-physisorbed multiwalled carbon nanotube and micro-scale polypropylene fibers produced a small rise in the compressive strength of high-performance concrete.

9.3.1.3 Impact Resistance

The impact test data are summarized in Table 9.3. All nano- and/or micro-scale reinforcement systems produced improvements in the impact resistance of high-performance concrete. The maximum rise in impact resistance achieved with a single reinforcement (73%) was for 0.16 vol.% of CNTD-PAA. In the case of micro-scale fibers, polypropylene produced a higher gain (60%) than carbon in the impact resistance of high-performance concrete.

All hybrid reinforcement systems produced further gains in the impact resistance of high-performance concrete when compared with individual (nano-or micro-scale) reinforcement used alone. The maximum rise in the impact resistance of high-performance concrete (120%) was produced by the hybrid reinforcement comprising 0.24 vol.% polypropylene microfiber and 0.16 vol.% multiwalled carbon nanotube; this gain in impact resistance was found to be statistically significant (at 0.000 significance level). Outcomes of the analysis of variance and pair-wise comparisons of the impact test data pointed at the statistical significant (at 0.000 to 0.012 significance levels) of nano- and/or micro-scale reinforcement effects on the impact resistance of high-performance concrete. When compared with the test data presented in earlier chapters on the impact resistance of high-performance cementitious paste and mortar (with nano-scale reinforcement), concrete (with nano-scale reinforcement) provides higher levels of impact resistance; this observation points at the well-known contributions of aggregates (in concrete) to the toughness of the cementitious matrix.

9.3.1.4 Abrasion Resistance

The abrasion test results produced for high-performance concrete with different reinforcement conditions are summarized in Table 9.4. Multiwalled carbon nanotube at 0.16 vol.% produced the greatest improvement (40.0%) in the abrasion resistance of high-performance concrete. All nano- and/or micro-scale reinforcement systems produced marked gains in the abrasion resistance of the high-performance concrete, which were statistically significant at 0.05 significance level. Outcomes of pair-wise comparisons confirmed that each of the reinforcement conditions considered here produced statistically significant improvements in the abrasion resistance of high-performance concrete (with significance levels ranging from 0.006 to 0.000).

9.3.1.5 Response Surface Analysis of Test Results

The test data on high-performance concrete with nano- and/or micro-scale reinforcement systems was subjected to response surface analysis. The objective of this analysis was to identify optimum reinforcement conditions of high-performance concrete which maximize the benefits to specific engineering properties or a combination of such properties.

Response surface analysis (RSA) of the test data was conducted considering the volume fractions of nano- and micro-scale reinforcement systems as input variables. Flexural strength, energy absorption capacity, maximum deflection and impact resistance were used as response variables. The response surface analysis process started with evaluating the effects of input variables on response variables, and was followed by desirability analyses; two methods of response surface analysis (canonical and ridge) were used in this investigation.

Response Surface analyses performed separately for the flexural strength, energy absorption capacity, maximum deflection and impact resistance test data (Figure 9.1) indicated that an

optimum reinforcement system comprising 0.15 vol.% CNTD-PAA and 0.23 vol.% PP microfiber maximizes subject properties. Optimal mean values (95% confidence intervals) for flexural strength, energy absorption capacity, maximum deflection and impact resistance were 15.6 (15.0 - 16.2) MPa, 282.8 (256.7 - 308.9 N/mm), 3.10 (2.79 - 3.41) mm and 2.50 mm/mm (2.38 - 2.63) mm/mm, respectively. Outcomes of Ridge analysis, which can be used to further refine the reinforcement condition, indicated that the optimum hybrid reinforcement identified in this investigation is reasonable for the performance characteristics considered here.

Desirability analysis of test data was conducted in order to identify reinforcement conditions which yield a desired balance of all the engineering properties considered here. Desirability analysis was conducted using the mean values obtained through both canonical and ridge analyses. These outputs indicate that a desired balance of all response variables can be achieved with 0.14 (or 0.15) vol.% CNTD-PAA carbon nanotube and 0.19 (or 0.20) vol.% PP microfiber.

9.3.1.6 Scanning Electron Microscope Evaluation

Figure 9.2 shows SEM images of the high-performance concrete samples. Figures 9.2a and 9.2b point at the relatively dense structure of the high-performance concrete material considered here. Figure 9.2a depicts an aggregate-paste interfacial crack that has propagated into the cementitious matrix. Figures 9.2c through 9.2e are indicative of the uniform dispersion of nanotubes within cementitious matrix, and their bridging/pullout actions across fine cracks developing within matrix. Figures 9.2f and 9.2g depict pullout of microfibers from the cementitious matrix. The scanning electron microscope observations presented in Figure 9.2 indicate that nano- and microscale reinforcement systems interact with cracks at different scales, which partly explains their complementary reinforcement effects in high-performance concrete. The nano-scale reinforcement also seems to benefit the interfacial interactions of micro-scale fibers with the

cementitious matrix, which can further explain their complementary effects on cementitious matrix. These observations rationalize the finding that optimum reinforcement systems for high-performance concrete comprise both nano- and micro-scale reinforcement systems.

9.4 Summary

The effects of reinforcement with MWNTs modified by physisorption of a polyelectrolyte (PAA) and/or polypropylene and carbon microfibers on the engineering properties of a high-performance concrete were evaluated. Proper use of nano-scale reinforcement in high-performance concrete can yield improvements in mechanical properties which surpass those realized with similar dosages of micro-scale fibers. Nano- and micro-scale reinforcements render complementary reinforcing effects in high-performance concrete; optimum reinforcement systems thus incorporate both carbon nanotubes and microfibers.

The synergistic actions of nano- and micro-scale reinforcement systems in high-performance concrete can be explained by their interactions with cracks developing in the cementitious matrix at different scales, and also by the positive effects of nanotubes on the interfacial interactions of micro-scale fibers with the high-performance cementitious matrix. These synergistic actions of nano- and micro-scale reinforcement were realized with nanotubes that were uniformly dispersed within the matrix.

Table 9.1- Mean values of flexural attributes of high-performance concrete with and without different nano- and/ or micro-scale reinforcement systems.

Reinforcement Condition	Flexural Strength (MPa)	Deflection (mm)	Energy Absorption (N.mm)
Plain	13.4	0.71	92
CMF-0.24	12.8	1.01	111
PP-0.24	13.0	4.55	383
CNT D-0.16	16.5	1.58	231
CNT D-PAA+PP	19.7	5.31	416
CNT D-PAA+CMF	19.0	1.78	316

Table 9.2- Mean values and standard errors of the compressive strength test results for high-performance concrete with and without nano- and/ or micro-scale reinforcement systems.

Reinforcement Condition	Mean Compressive Strength (MPa)	Standard Error (MPa)
Plain	151	7.75
CMF-0.24	139	13.5
PP-0.24	137	18.4
CNT D-0.16	143	5.55
CNT D-PAA+PP	153	11.0
CNT D-PAA+CMF	150	7.53

Table 9.3- Impact resistance test results for high-performance concrete with and without nano-and/or micro-scale reinforcement.

Reinforcement Condition	Impact Resistance (mm/mm)
Plain	1.50
CMF-0.24	1.98
PP-0.24	2.40
CNT D-0.16	2.60
CNT D-PAA+PP	3.30
CNT D-PAA+CMF	2.65

Table 9.4- Mean abrasion weight losses of high-performance concretes with and without nano-and/ or micro-scale reinforcement systems.

Reinforcement Condition	Loss of Mass (grams)
Plain	1.50
CMF-0.24	1.15
PP-0.24	1.05
CNT D-0.16	0.90
CNT D-PAA+PP	0.92
CNT D-PAA+CMF	0.90

Table 9.5- Outcomes of Ridge analysis of the flexural attributes and impact resistance test data for high performance concrete with nano- and/or micro-scale reinforcement.

(a) Flexural Strength

Ridge Analysis for Maximizing Flexural Strength					
Coded Ra		95.00% C	onfidence Inte	rval Uncoded Facto	or Values
	Response	Upper	Lower	CNT D-PAA	PP
0.000	15.604	15.024	16.183	0.080	0.120
0.100	15.847	15.264	16.429	0.088	0.123
0.200	16.093	15.502	16.684	0.095	0.127
0.300	16.344	15.739	16.949	0.103	0.131
0.400	16.600	15.976	17.225	0.110	0.136
0.500	16.861	16.212	17.511	0.117	0.141
0.600	17.128	16.449	17.807	0.125	0.147
0.700	17.400	16.686	18.115	0.132	0.152
0.800	17.678	16.924	18.433	0.139	0.158
0.900	17.963	17.164	18.762	0.146	0.165
1.000	18.253	17.404	19.103	0.152	0.171

(b) Energy Absorption Capacity

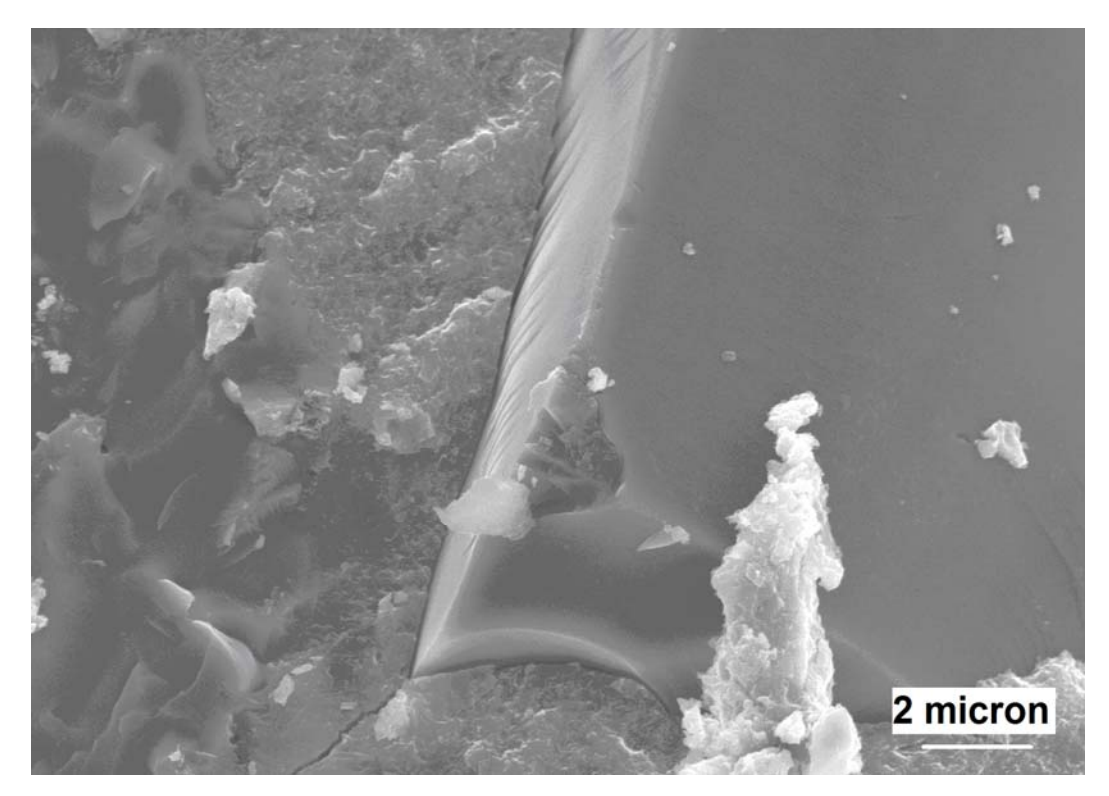
Ridge Analysis for Maximizing Energy Absorption Capacity						
Coded Rad	dius Estimated Response	95.00% Co	onfidence Inter	val Uncoded Facto	or Values	
	Response	Upper	Lower	CNT D-PAA	PP	
0.000	282.779	256.693	308.865	0.080	0.120	
0.100	295.584	269.367	321.800	0.082	0.132	
0.200	308.239	281.635	334.843	0.084	0.143	
0.300	320.761	293.521	348.000	0.086	0.155	
0.400	333.167	305.059	361.276	0.087	0.167	
0.500	345.477	316.288	374.667	0.087	0.179	
0.600	357.712	327.254	388.171	0.088	0.191	
0.700	369.893	338.003	401.783	0.088	0.203	
0.800	382.042	348.582	415.501	0.087	0.215	
0.900	394.181	359.037	429.326	0.086	0.228	
1.000	406.334	369.406	443.263	0.085	0.240	

(c) Maximum Deflection

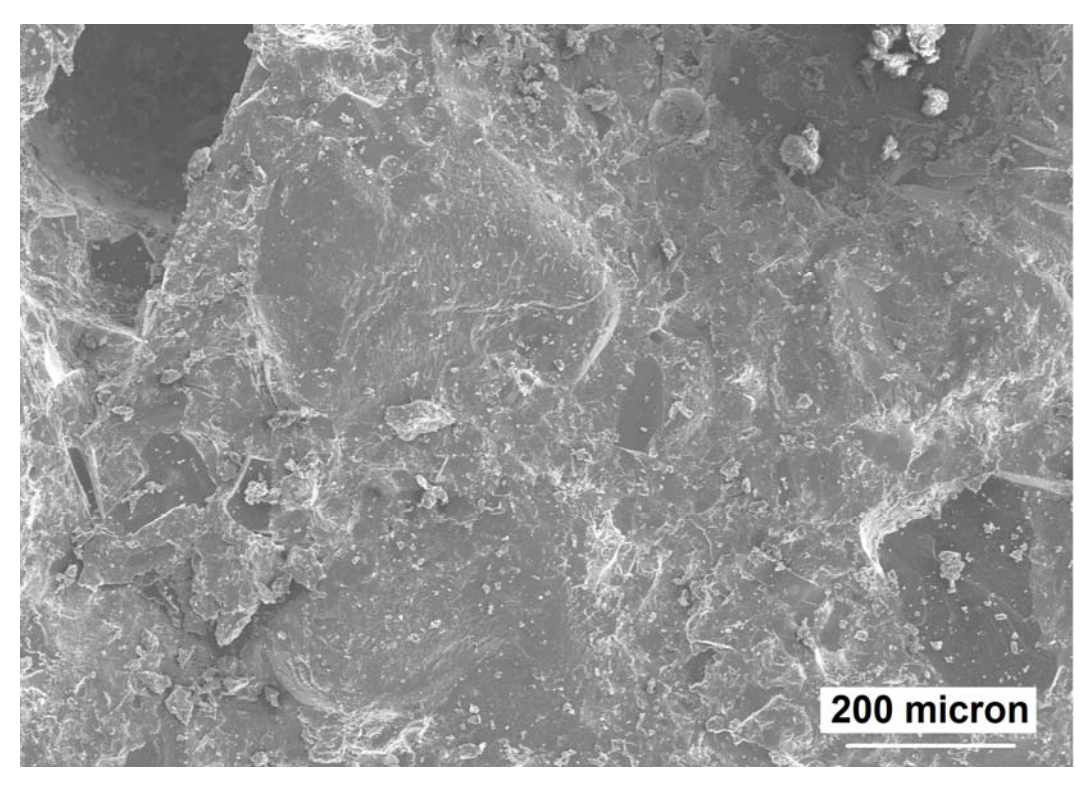
Ridge Analysis for Maximizing Maximum Deflection					
Coded Ra	dius Estimated Response	95.00% C	onfidence Inte	rval Uncoded Facto	or Values
	Kesponse	Upper	Lower	CNT D-PAA	PP
0.000	3.101	2.793	3.408	0.080	0.120
0.100	3.296	2.987	3.605	0.082	0.132
0.200	3.492	3.178	3.805	0.083	0.143
0.300	3.687	3.366	4.008	0.085	0.155
0.400	3.882	3.551	4.213	0.086	0.167
0.500	4.076	3.733	4.420	0.088	0.179
0.600	4.271	3.912	4.630	0.089	0.191
0.700	4.465	4.089	4.841	0.091	0.202
0.800	4.659	4.264	5.054	0.092	0.214
0.900	4.853	4.437	5.268	0.093	0.226
1.000	5.046	4.608	5.484	0.094	0.238

(d) Impact Resistance

Ridge A	Ridge Analysis for Maximizing Impact Resistance					
	Estimated Response	95.00% Confidence Interval Uncoded Factor Val				
	response	Upper	Lower	CNT D-PAA	PP	
0.000	2.500	2.375	2.625	0.080	0.120	
0.100	2.567	2.441	2.693	0.086	0.127	
0.200	2.633	2.506	2.761	0.092	0.135	
0.300	2.700	2.569	2.831	0.099	0.142	
0.400	2.767	2.631	2.902	0.105	0.150	
0.500	2.833	2.693	2.974	0.111	0.157	
0.600	2.900	2.752	3.048	0.117	0.165	
0.700	2.967	2.811	3.123	0.124	0.172	
0.800	3.034	2.868	3.199	0.130	0.180	
0.900	3.100	2.925	3.276	0.136	0.187	
1.000	3.167	2.979	3.355	0.142	0.195	



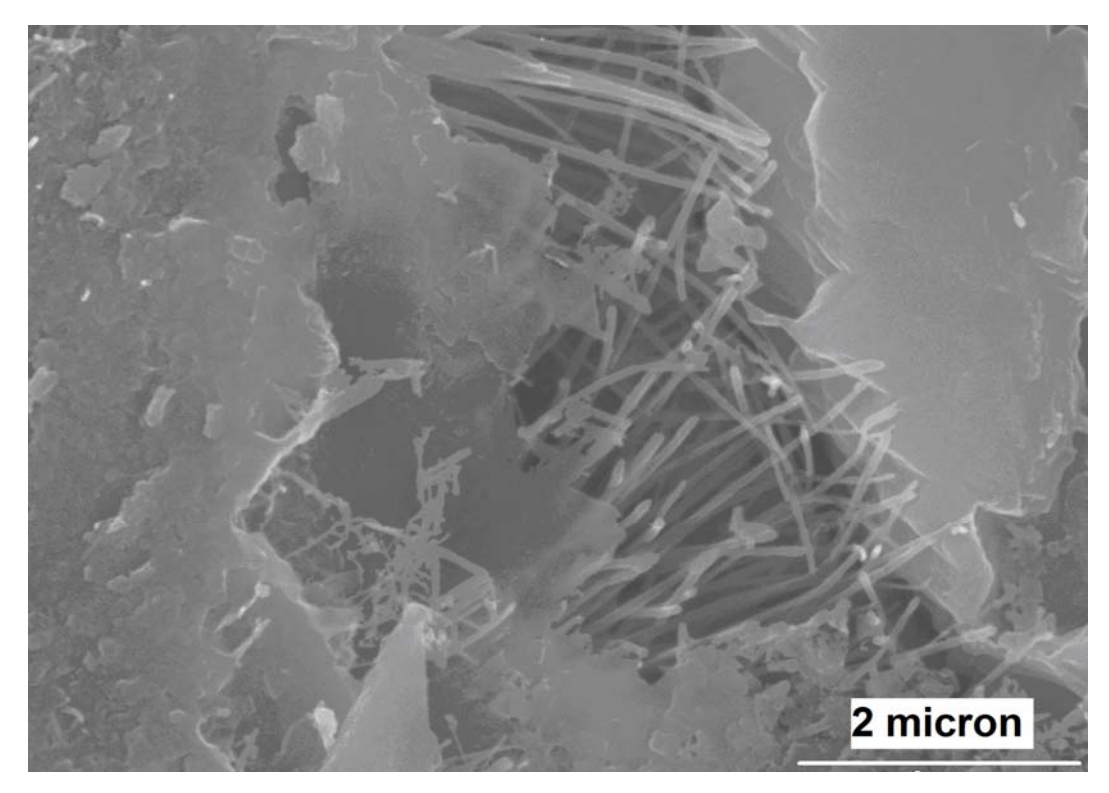
(a) Crack deflection around sand particle



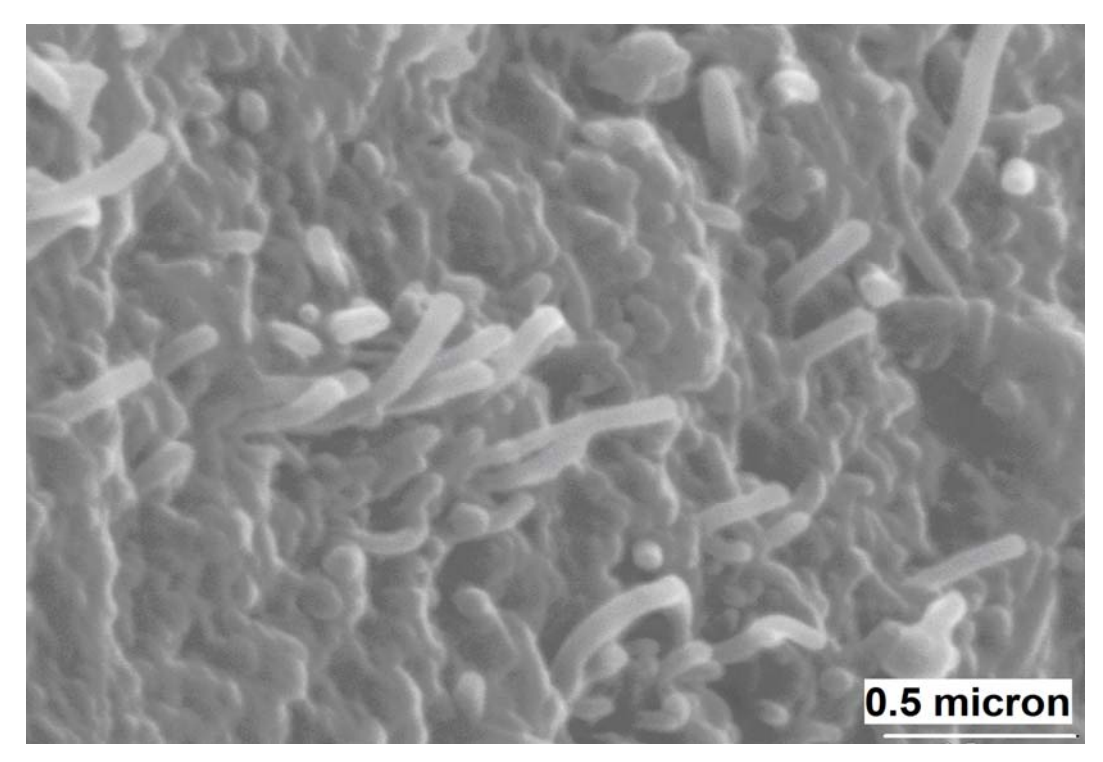
(b) Dense structure of paste

Figure 9.1- SEM images of fractured surfaces of high performance concrete.

Figure 9.1 (cont'd)

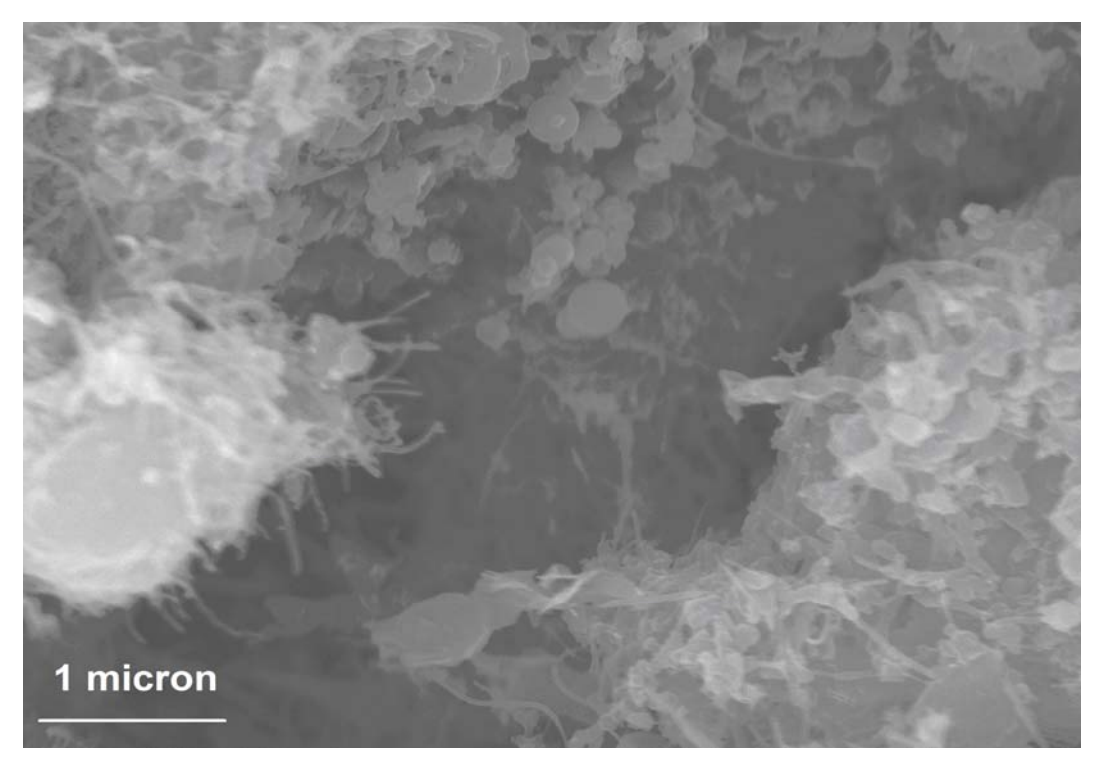


(c) Pulled out nanotubes at fractured surface

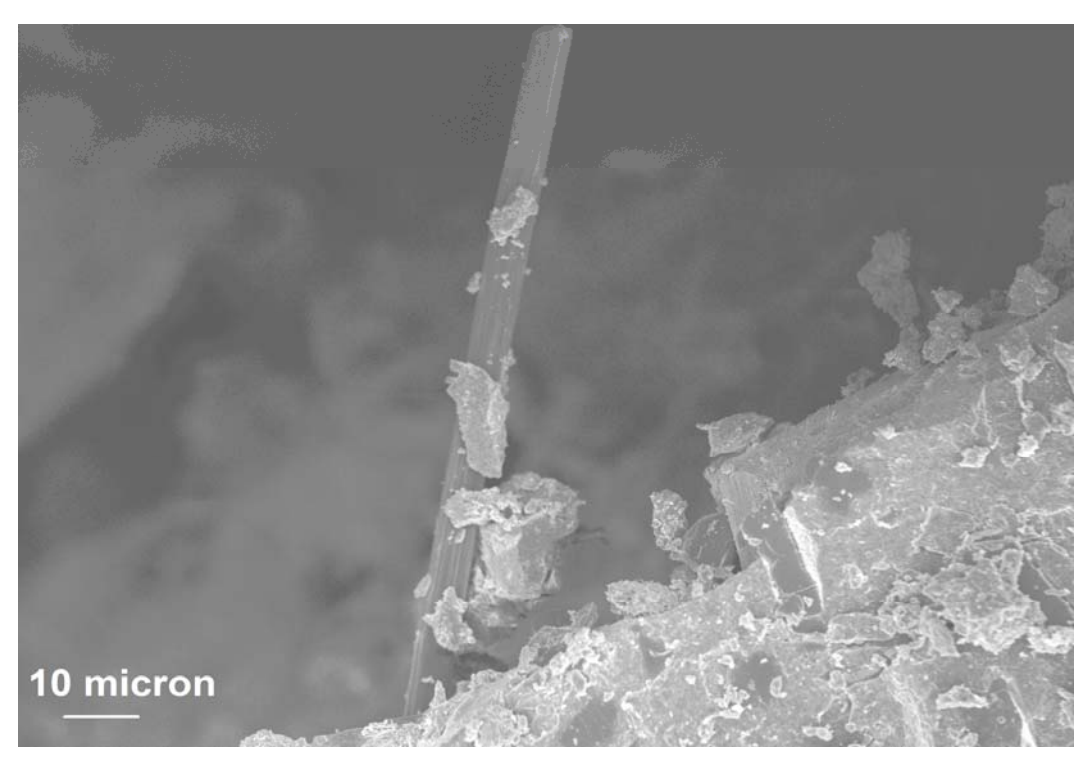


(d) Pulled out nanotubes at fractured surface

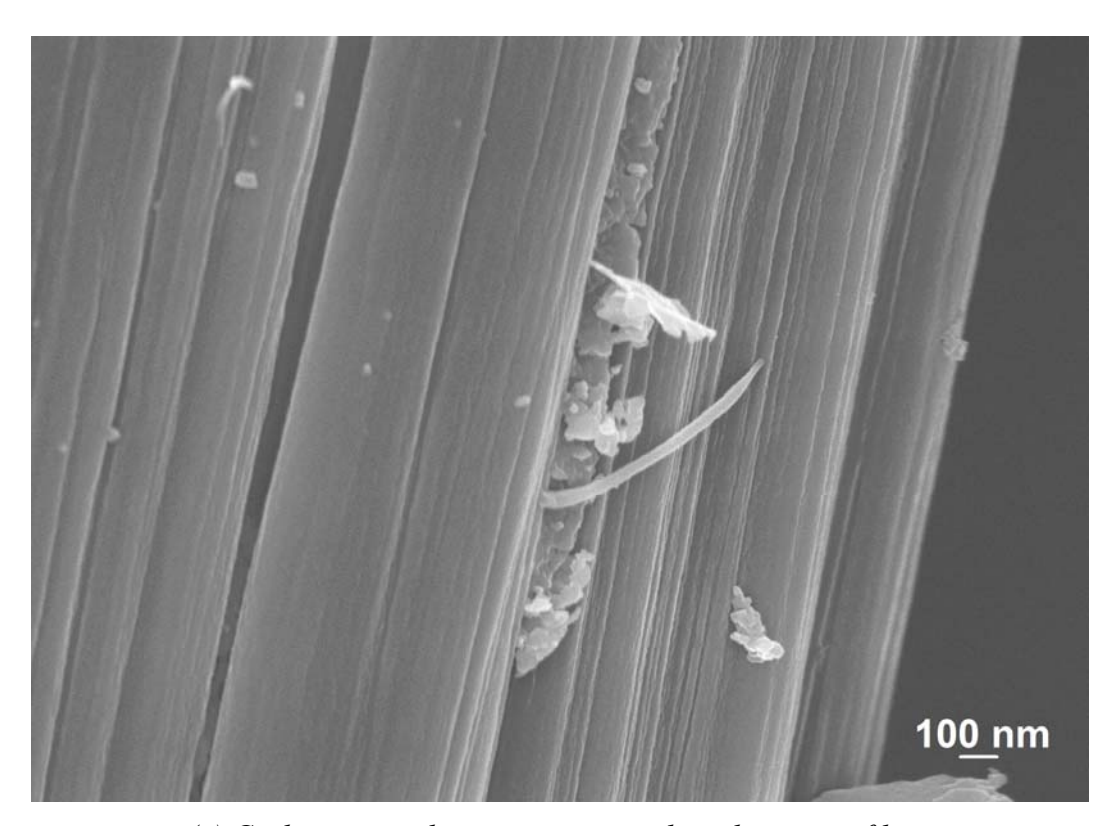
Figure 9.1 (cont'd)



(e) Distribution of nanotubes within the matrix



(f) Pulled out carbon microfibers



(g) Carbon nanotubes interacting with carbon microfibers

10 EVALUATION OF CARBON NANO AND/ OR MICRO-SCALE REINFORCEMENTS ON THE ENGINEERING PROPERTIES OF HIGH STRENGTH CONCRETE AND COMPARISON WITH HIGH-PERFORMANCE CONCRETE

10.1 General

Most of the works involving use of graphite nanomaterials, especially multiwalled carbon nanotubes, in cementitious matrices have used very fine matrices to evaluate the efficiency of their reinforcement and reported modest gains in some of the engineering properties (Makar and Beaudoin 2004; Cwirzen, Habermehl-Cwirzen et al. 2008; Cwirzen, Habermehl-Cwirzen et al. 2009; Makar and Chan 2009; Metaxa, Konsta-Gdoutos et al. 2009; Metaxa, Konsta-Gdoutos et al. 2010; Li, Wang et al. 2005). A comprehensive approach was taken to evaluate functionalized graphite nanomaterials in both high-strength and high-performance cementitious matrices of higher complexity.

The focus of this research is on the use of high-strength concrete, normally cured as the matrix in which the reinforcement efficiency of optimally functionalized multiwalled carbon nanotubes and/ or microfibers is evaluated. The larger aggregate size and content in concrete, when compared with mortar and paste, adds to complexity of behavior and failure modes by introducing an interfacial zone, generating interactions between aggregates and propagating microcracks, and the need to disperse nanomaterials in the space between aggregates. The results

are compared with same reinforcement conditions used in high-performance (DSP) concrete matrix.

10.2 Materials and Methods

10.2.1 Graphite Nanomaterials and Microfibers

Polyacrylic acid physisorbed multiwalled carbon nanotubes (CNTD-PAA) and carbon microfibers (CMF) at different volume fractions were used in a high-strength, normally cured, concrete matrix. These graphite nanomaterials and microfibers have been introduced in detail in Chapter 2, Section 2.4, Fig. 2.3 and Table 2.3. In the course of dispersing the nanotubes in water PAA was physisorbed upon multiwalled carbon nanotubes.

10.2.2 Cementitious Matrices, Mixing and Curing Procedure

High-Performance (DSP) concrete matrix has been described in detailed in Chapter 2, Section 2.5.1. For this experimental regimen, a more practical high-strength concrete matrix was selected with a targeted compressive strength of 15,000 psi (104 MPa). Most of the materials used are the same as were used for high-performance matrix but with different proportions. Table 10.1 gives the composition of both high-performance (DSP) and high-strength concrete matrix. The mixes included a plain without any reinforcement, one with CNT D-PAA, one with CNT D-PAA and CMF; and with CMF microfibers alone. CNT D-PAA were used at 0.16 vol.% (volume percent of the dry *cementitious materials* or *binder* (cement plus silica fume)) and CMF were used at 0.24 vol.% of binder both individually and when used as hybrid reinforcement.

Cementitious materials (with and without functionalized graphite nanomaterials dispersed in the mixing water via sonication, described in detail in Chapter 2, Section 2.5.2) and/ or different microfibers were prepared and cured following ASTM procedures described in the same section.

For high-strength concrete the samples were cured in fresh water for 9 days. At least two batches were casted with at least four specimens for each test condition in each batch for all reinforcement conditions and engineering properties.

10.2.3 Experimental Methods

The test procedures employed to determine the engineering properties of this high-strength concrete matrix included compression tests (ASTM C 109), flexure tests (ASTM C 1185) and impact tests (ASTM D 7136) and Abrasion tests (ASTM C 944). Experimental results were evaluated using the analysis of variance (ANOVA) and pair-wise comparison techniques.

10.3 Experimental Results and Discussion

Poly-acrylic acid physisorbed multiwalled carbon nanotubes Type D (CNT D-PAA) were used as reinforcement at 0.16 vol.% and carbon microfibers(CMF) were used at 0.24 vol.%. Combination of carbon microfibers with multiwalled carbon nanotubes were also used as hybrid reinforcement for concrete, with CMF and CNT D-PAA used at 0.24 vol.% and 0.16 vol.%, respectively.

10.3.1 Flexural Performance

The flexural attributes test results for the both high-strength and high-performance concrete reinforced with different volume fractions of multiwalled carbon nanotubes and/or carbon microfibers is summarized in Table 10.2. These test results indicate that all reinforcement systems produced gains in all flexural attributes considered here, for the high-strength concrete matrix considered here. Due to relatively lesser brittle nature, the plain high-strength matrix showed some increase in both maximum (25%) deflection and energy absorption capacity (17%) but a significant (30.6%) drop in flexural strength with respect to plain DSP concrete matrix.

For high-strength concrete, the most desired balance of properties for a single reinforcement was realized by the addition of 0.16 vol.% of CNT D-PAA. The corresponding improvements in flexural strength, energy absorption capacity and maximum deflection with respect to plain concrete were 24.7%, 17% and 53.7%, respectively. Test results also indicate that the addition of microfibers alone at 0.24 vol.% to this high-strength concrete produced important gains in all flexural attributes considered here. The most significant gain was realized for maximum deflection (51.7%) with respect to plain high-strength matrix.

As was the case for high-performance concrete matrix, the test data generated in the past pointed at the positive effects of hybrid (nano- and micro-scale) reinforcement systems in high-strength concrete matrix. Carbon microfibers (CMF), when used together with CNT D-PAA as hybrid reinforcement, produced balanced gains in the flexural performance characteristics of high-strength concrete by interacting with and arresting cracks which developed in matrix at different scales. Overall, the best balance of flexural attributes was produced by the hybrid reinforcement comprising CNT D-PAA (0.16 vol.%) and CMF (0.24 vol.%), which produced a 38.7%, 59.6% and 41.7% rise in flexural strength, maximum deflection and energy absorption capacity, respectively. The synergistic reinforcement actions of nano- and micro-scale reinforcement systems point at the merits of multi-scale reinforcement in high-strength concrete. Although the reinforcement efficiency of CNT D-PAA and/ or CMF in high-strength concrete is lower than in high-performance DSP concrete matrix. Still they point to the superior reinforcement efficiency of both nanomaterials and microfibers, especially when used in hybrid.

The experimental results were subjected to statistical analysis of variance (ANOVA). Due to the large number of observations, ANOVA only gives the general trends in test results. The ANOVA outcomes indicate that there are statistically significant (at 0.05 significance level) improvements

in all flexural attributes of high-strength concrete due to the addition of nano-scale and hybrid reinforcement systems. Pair-wise comparisons were carried out in order to assess the statistical significance of the effects associated with the addition of nano- and/or micro-scale reinforcement systems. These results indicate that nano-scale reinforcement systems at 0.16 vol.% produced statistically significant improvements in all flexural attributes of the plain matrix at 0.05 significance level when compared with plain concrete. Use of high-modulus carbon microfiber in conjunction with CNT D-PAA produced balanced gains in the engineering properties of high-strength concrete at significance levels varying from 0.000 to 0.047.

10.3.2 Compressive Strength

The compressive strength test results (mean values and standard errors) for high-strength concretes with nano- and/or micro-scale reinforcement systems and compared with high-performance DSP concrete, are presented in Table 10.3. As was the case with DSP paste and mortar and concrete, PAA physisorbed multiwalled carbon nanotubes as well as its hybrid with CMF microfibers produced small increase in the mean value of compressive strength. However, CMF when used alone showed a small drop in compressive strength.

Outcomes of pair-wise comparisons also indicate the effects of nano- and/ or micro-scale reinforcement systems on compressive strength are not statistically significant (at 0.05 significance level). The use of hybrid reinforcement systems comprising of CNT D-PAA and CMF restored the compressive strengths of high-strength concrete by inducing interactions with matrix and its cracks at different scales. This effect was also evident in the results of high-performance DSP concrete.

10.3.3 Impact Resistance

The impact test data are summarized in Table 10.4. All nano- and/or micro-scale reinforcement systems produced improvements in the impact resistance of high-strength concrete. The maximum rise in impact resistance realized with a single reinforcement (87%) was for 0.16 vol.% of CNT D-PAA. In the case of micro-scale fibers alone, CMF produced a gain 34.8% in the impact resistance of high-performance (DSP) concrete.

The hybrid nano- and micro-scale reinforcement systems produced further rise in the impact resistance (104%) of high-strength concrete when compared with individual (nano-or micro-scale) reinforcement used alone. A significant (0.000 significance level) increase in impact resistance was observed for the hybrid reinforcement comprising CMF with CNT D-PAA, which confirms the effectiveness of hybrid reinforcement.

Outcomes of ANOVA and pair-wise comparisons point at the statistical significant (0.000 to 0.012 significance levels) of nano- and/ or micro-scale reinforcement effects on the impact resistance of high-strength concrete. When compared with high-performance concrete (with nano-scale reinforcement), high-strength concrete (with nano-scale reinforcement) provides lower levels of impact resistance; this observation points at the weakening of matrix due to higher volume fraction of coarse aggregates in the high-strength.

10.3.4 Abrasion Resistance

The abrasion test results produced for high-strength concrete with different volume fractions of graphite nanomaterials and/ or microfiber reinforcement and its comparison with high-performance concrete are summarized in Table 10.5.

Overall high-strength concrete matrix showed lower value of abrasion resistance both plain and with all reinforcement conditions when compared with high-performance DSP concrete matrix. As was the case for high-performance concrete, for a single reinforcement, CNT D-PAA at 0.16 vol.% produced the greatest improvement (35%) in the abrasion resistance of high-strength concrete. All nano- and/or micro-scale reinforcement systems, produced gains in the abrasion resistance of this high-strength concrete matrix, which were statistically significant at 0.05 significance level. Hybrid reinforcement of CNT D-PAA and CMF produced the maximum gain of 37% in the abrasion resistance of high-performance concrete matrix. Outcomes of pair-wise comparisons confirmed that each of the reinforcement conditions considered here produced statistically significant improvements in the abrasion resistance of high-performance concrete (with significance levels ranging from 0.006 to 0.000).

10.4 Summary

The experimental results generated for high strength concrete reinforced with PAA physisorbed multiwalled carbon nanotubes (CNT D-PAA), carbon microfibers (CMF) and their hybrids casted at optimum volume fractions and with carboxyl-based superplasticizers indicated that proper use of nano-scale reinforcement can produce improvements in high-strength concrete mechanical properties which surpass those realized with micro-scale reinforcement. However, the level of reinforcement efficiency is reduced as we move down from a high-performance to a high-strength concrete matrix. This is obvious due to normally curing of concrete versus steam curing of high-performance concrete matrix which makes it denser thus the interaction of the matrix at with the nano-reinforcement is more for high-performance matrices.

Table 10.1- Starting material selections and mix proportions (weight ratios) of high-performance and high-strength concrete matrix.

Ingredient	DSP Concrete	High Strength
		Concrete
Silica Fume/Binder	0.20	0.20
Water/Binder	0.20	0.35
Superplasticizer/Binder	Adjusted for diff	Adjusted for diff
	reinforcement	reinforcement
Silica Sand (0 – 0.18 mm) / Binder	0.36	0.36
Silica Sand (0.18 -0.6 mm) / Binder	0.86	0.86
Granite Gravel (1 mm – 9 mm)/	0.5	1.1
Binder		

Table 10.2- Mean values of flexural attributes of high-strength concrete with and without nanoand/or micro-scale reinforcement systems and comparison with high-performance concrete.

Reinforcement Condition	Flexural Strength (MPa)	Deflection (mm)	Energy Absorption (N.mm)
Plain DSP	13.4	0.71	92
Plain HSC	9.3	0.89	108
CMF-0.24-DSP	12.8	1.01	111
CMF-0.24-HSC	10.9	1.35	129
CNT D-PAA-0.16-DSP	16.5	1.58	231
CNT D-PAA-0.16-HSC	11.6	1.06	166
CNT D-PAA+CMF-DSP	19.0	1.78	316
CNT D-PAA+CMF-HSC	12.9	1.42	153

Table 10.3- Compressive strength values of high-strength concrete with and without nano- and/ or micro-scale reinforcement systems and comparison with high-performance concrete.

Reinforcement Condition	Mean Compressive Strength (MPa)	Standard Error (MPa)
Plain DSP	151	7.75
Plain HSC	112	7.60
CMF-0.24-DSP	139	13.5
CMF-0.24-HSC	108	6.95
CNT D-PAA-0.16-DSP	143	5.55
CNT D-PAA-0.16-HSC	118	8.26
CNT D-PAA+CMF-DSP	150	7.53
CNT D-PAA+CMF-HSC	113	5.95

Table 10.4- Impact resistance test results for high-strength concretes with and without nano-and/or micro-scale reinforcement systems and comparison with high-performance concrete.

Reinforcement Condition	Impact Resistance (mm/mm)
Plain DSP	1.50
Plain HSC	1.15
CMF-0.24-DSP	1.98
CMF-0.24-HSC	1.55
CNT D-PAA-0.16-DSP	2.60
CNT D-PAA-0.16-HSC	2.15
CNT D-PAA+CMF-DSP	2.65
CNT D-PAA+CMF-HSC	2.35

Table 10.5- Mean abrasion weight losses of high-strength concretes with and without nano- and/ or micro-scale reinforcement systems and comparison with high-performance concrete.

Reinforcement Condition	Loss of Mass (grams)
Plain DSP	1.50
Plain HSC	3.75
CMF-0.24-DSP	1.15
CMF-0.24-HSC	3.45
CNT D-PAA-0.16-DSP	0.90
CNT D-PAA-0.16-HSC	2.43
CNT D-PAA+CMF-DSP	0.90
CNT D-PAA+CMF-HSC	2.35

CHAPTER 11

11 EVALUATION OF REINFORCEMENT EFFICIENCY OF CARBON NANO AND MICRO-FIBERS IN HIGH-PERFORMANCE CEMENTITIOUS PASTE

11.1 General

Cementitious materials are generally characterized as brittle materials with relatively low tensile strength and strain capacity, which are susceptible to early-age cracking due to restraint of shrinkage movements. These problems tend to be more pronounced in the case of highperformance cementitious materials with high compressive strengths. Fibers (with micro-scale diameters) are incorporated into cementitious matrices to overcome these drawbacks. The microscale diameters and relatively low aspect (length-to-diameter) ratios of these fibers, and their viable volume fractions in cementitious materials, however, yield relatively large fiber-to-fiber spacing and relatively small specific surface area of fibers. These features limit the effectiveness of micro-scale fibers in controlling the flaw (microcrack) size and propagation in cementitious materials. Slender nanomaterials (e.g. CNFs) with nano-scale diameters and relatively high aspect ratios offer the potential to overcome these drawbacks of micro-scale fibers in cementitious materials. The relatively close spacing and high specific surface area of nanomaterials provide them with the potential to effectively control the flaw size and propagation in cementitious materials. The close spacing of nanomaterials could also enhance the moisture barrier qualities and thus the durability characteristics of cementitious materials by

forcing tortuous diffusion paths of moisture (and aggressive solutions) into cementitious materials.

Previous research on high-performance cementitious materials reinforced with multiwall carbon nanotubes (MWNT) has shown that, as far as the uniform dispersion and effective interfacial interactions of nanotubes within cementitious paste are achieved, important gains in diverse engineering properties of cementitious materials can be realized at nanotube volume fractions below 0.1% of the cementitious paste. The work reported herein examines the potential of carbon nanofibers (CNFs), which are of substantially lower cost when compared with carbon nanotubes, to bring about balanced gains in engineering properties of high-performance cementitious materials.

CNFs have a unique hybrid grapheme sheet structure based on conical and tubular elements. Their diameters range from 50 to 200 nm (which are greater than typical nanotube diameters). CNFs provide high mechanical properties (e.g., 25 to 200 GPa elastic modulus depending on their diameter) (Cwirzen and Penttala 2005), specific surface areas and aspect ratios, which are below those of carbon nanotubes. Their electrical and thermal conductivity as well as thermal and chemical stability are also relatively high. When compared to carbon nanotubes, CNFs provide more active sites on their surfaces for bonding to cementitious materials. The desired combination of performance and cost of CNFs suits applications in the field of nanocomposites. Past research efforts have primarily focused on development of carbon nanofiber–polymer nanocomposites (Ping, Beaudoin et al. 1991; Song, Jang et al. 2007; Pfeifer, Moeser et al. 2009). Limited work has been conducted on the use of CNFs in cementitious matrices. The prerequisites for successful use of CNFs in cementitious materials include thorough dispersion and effective interfacial interactions of CNFs within the cementitious matrix (Ahlborn, Harris et al. 2011).

Past research efforts have examined the effects of 0.005%, 0.02%, 0.05%, 0.5% and 2% CNF by weight of cementitious materials on the microstructure and mechanical properties of a cementitious matrix with 10% of cement replaced with silica fume (Bentz 2000; Bentz, Jensen et al. 2000). The effects of surface treatment of CNF with nitric acid on their reinforcement efficiency (at 0.5% by weight of cementitious materials) were also evaluated. It was found that the use of silica fume and surface treatment of CNF facilitated their dispersion, and improved their interfacial interactions with the cementitious paste. The gains in engineering properties (splitting tensile strength and compressive strength) of cementitious matrix with introduction of CNFs were, however, insignificant. Other investigations involving microscopic observations have indicated that CNFs can control cracking in cementitious materials by bridging across fine cracks, yielding improvements in flexural strength of cementitious materials at weight fractions of about 0.048% (Metaxa, Konsta-Gdoutos et al. 2010).

In this study, the effects of surface functionalization of carbon nanofibers (CNFs) through introduction of carboxyl groups and use of refined dispersion techniques on the reinforcement efficiency of nanotubes at different volume fractions within a high-performance cementitious (DSP) matrix were evaluated. Scanning electron microscope observations of fractured surfaces pointed at successful dispersion of nanofibers within the cement-based matrix. An investigation of hybrid reinforcement systems comprising CNFs and micro-scale fibers (CMFs) indicated that selected hybrid systems offer a cost-effective approach to realizing balanced gains in performance characteristics of high-performance cementitious matrices.

11.2 Materials and Methods

11.2.1 Graphite Nanomaterials and Microfibers

Different types of acid-functionalized and non-functionalized CNFs as well as chopped CMFs were evaluated for use in cement-based nanocomposites. These graphite nanomaterials and microfibers have been introduced in detail in Chapter 2, Section 2.4, Fig. 2.3 and Table 2.3. Acid-functionalized and non-functionalized carbon nanofibers (CNF-OX and CNF) and carbon microfibers (CMF) were used in high-performance cement-based paste matrix.

11.2.2 Cementitious Matrices, Mixing and Curing Procedure

Dense cementitious matrix selected has been introduced in detail in Chapter 2, Section 2.5. DSP paste was used to evaluate the reinforcement efficiency of both carbon nanofibers and/or carbon microfibers at different volume fractions.

Cementitious materials (with and without functionalized graphite nanomaterials dispersed in the mixing water via sonication) and/ or carbon microfibers were prepared and cured following ASTM procedures described in the same section.

11.2.3 Experimental Methods

The test procedures employed to determine the engineering properties of high-performance paste included compression tests (ASTM C 109), flexure tests (ASTM C 1185), impact tests (ASTM D 7136) and Abrasion tests (ASTM C 944). SEM and EDS were also employed to gain further insight into the structure and failure mechanisms of cement-based nanocomposites. The experimental results were subjected to statistical analysis using the analysis of variance (ANOVA) and pair-wise comparison methods.

11.3 Experimental Results and Discussion

11.3.1 Effects of Carbon Nanofiber Surface Functionalization on Engineering Properties

11.3.1.1 Flexural Performance

Typical flexural load-deflection curves for cementitious (DSP paste) matrices reinforced with 0% and 0.24 vol.% of acid-functionalized and non-functionalized nanofibers are shown in Fig. 11.1. Volume fraction is calculated here with respect to the volume of cement and silica fume. The mean values of flexural strength, maximum deflection and energy absorption capacity (area underneath the flexural load-deflection curve) are summarized in Table 11.1. The mean values and standard deviations of the flexural strength and energy absorption capacity test results are presented in Figs. 11.2a and 11.2b, respectively.

Acid-oxidized nanofibers produced significant gains in the flexural strength and especially energy absorption capacity of the cementitious matrix. The improvements in flexural strength and energy absorption capacity were 52% and 296%, respectively. The relatively large length of CNFs benefits their contributions to energy absorption capacity via extended frictional pullout at cracks. The contributions of oxidized CNFs to the flexural energy absorption capacity and strength of the high-performance cementitious paste were confirmed through statistical analysis (ANOVA) of test results at 0.001 significance level. Non-oxidized nanofibers produced a drop in flexural strength, although they contributed to the flexural energy absorption capacity and maximum deflection of the cementitious matrix. The drop in flexural strength can be attributed to the potential for clumping of non-functionalized nanofibers in the cementitious matrix. This observation was confirmed by SEM observations, Fig 11.3. The contributions of CNFs to the

flexural performance characteristics of high-performance cementitious materials are attractive, given their relatively low cost when compared with other nanomaterials.

11.3.1.2 Compressive Strength

The compressive strength test results (means and standard deviations) are summarized in Fig. 11.4. The compressive strength of the high-performance cementitious matrix is observed to be either preserved or improved with the addition of nanofibers. Analysis of variance of test results indicated that, at 0.05 significance level, the high compressive strength of the cementitious matrix was preserved after introduction of nanofibers.

11.3.1.3 Impact Resistance

Examples of failed impact test specimens are shown in Fig. 11.5. The mean values of impact test results are presented in Fig. 11.6. The impact resistance of cementitious materials is observed to increases with introduction of 0.24 vol.% of both non-functionalized and acid-functionalized nanofibers. The test results suggest that functionalization of nanofibers benefits their contributions to the impact resistance of the cement-based matrix. The functionalized and non-functionalized nanofibers, at 0.24 vol.%, yielded about 73.6% and 44.7% gains, respectively, in impact resistance, which can be attributed to the arrest and deflection of microcracks, pullout of nanofibers, and multiple cracking phenomena in the presence of nanofibers. Cementitious materials reinforced with oxidized nanofibers exhibited more pronounced multiple cracking as compared to those with pristine nanofibers (see Fig. 11.5).

11.3.1.4 Abrasion Resistance

Examples of abrasion test specimens after performance of abrasion tests are shown in Fig. 11.7. The abrasion test results presented in Fig. 11.8 indicate that cementitious materials with oxidized

and pristine nanofibers, 0.24 vol.% showed superior abrasion resistance when compared when compared with the plain cementitious matrix. The significant increase in abrasion resistance with oxidized nanofibers can be attributed to their thorough dispersion and effective interfacial interactions in the high-performance cementitious matrix. Analysis of variance of test results indicated that the contributions of nanofibers to the abrasion resistance of high-performance cementitious matrix were statistically significant at 0.05 significance level.

11.3.1.5 Scanning Electron Microscope Evaluation

The SEM images presented in Fig. 11.9 indicate that the refined sonication and mixing steps developed in the project were successful in dispersion of individual oxidized nanofibers within the cementitious matrix at 0.24 vol.%. These images also point at the low porosity of the high-performance cementitious matrix used here; the introduction of nanofibers does not seem to have compromised the high density (low porosity) of this matrix. SEM observations verified the uniform dispersion of oxidized nanofibers; evidences of crack suppression and crack bridging were also found in all specimens examined under SEM. Oxidized nanofibers, which provided higher levels of reinforcement efficiency, were found to be more uniformly dispersed within the cementitious matrix, as some clumping was found for pristine nanofibers.

11.3.1.6 Energy Dispersive Spectroscopy (EDS)

Elemental and Quantitative analyses of these samples indicated that all cementitious materials exhibit similar elemental compositions, except for the (expected) higher carbon content in materials incorporating CNFs.

11.3.2 Effects of Hybrid (Nano- and Micro-scale) Reinforcement Systems

Hybrid reinforcement systems comprising oxidized carbon nanofibers (CNF-OX) and carbon fibers with micro-scale diameter (CMF) were evaluated in DSP paste. Exploratory studies of carbon nanofiber and carbon microfiber reinforcement indicated that, for the cementitious matrix and processing conditions considered here, the nanofiber volume fraction (of cement plus silica fume) should be lowered below 0.24 vol.% before benefits can be realized from introduction of carbon microfibers. Hence, a nanofiber volume that was 0.16 vol.% that of cement plus silica fume was considered for development of hybrid reinforcement systems, which also incorporated carbon microfiber at 0.24 vol.% of cement plus silica fume.

11.3.2.1 Flexural Performance

The flexural strength, maximum deflection and energy absorption capacity test results for the high-performance (DSP) cementitious paste reinforced with different volume fractions of CNFs and CMFs are shown in Table 11.2. CNFs and CMFs, and especially their combination, are observed to yield important gains in the flexural strength, energy absorption capacity and maximum deflection of DSP cementitious paste. The hybrid (carbon nanofiber and microfiber) reinforcement system produced 64.9%, 356% and 288% gains in the flexural strength, energy absorption capacity and maximum deflection, respectively, of DSP paste. These benefits could be attributed to the multi-scale reinforcing action of the hybrid reinforcement system. ANOVA and pair-wise comparison of flexure test data confirm, at 0.00 significance level, that the contributions of nano- and/or micro-scale reinforcement effects to the flexural performance of this high-performance cementitious paste are statistically significant.

11.3.2.2 Compressive Strength

While micro-fiber reinforcement tends to lower the compressive strength of concrete, mainly due to the introduction of interfacial stress rise and structural defects, nano-scale (and hybrid) reinforcement systems are observed in Table 11.3 to produce a slight rise in the compressive strength of the high-performance cementitious paste. This effect, however, is not statistically significant. The somewhat positive effects of nano-scale reinforcement on compressive strength could be attributed to: (i) the reduced interfacial stress concentration and structural defects due to the nano-scale dimensions and spacing of the reinforcement; and (ii) effective arrest of microcrack propagation by the closely space nanofibers.

11.3.2.3 Impact Resistance

The impact resistance test results presented in Table 11.4 indicate that carbon microfibers, CNFs and the hybrid reinforcement systems enhance the impact resistance of DSP paste by 42.7%, 71.2% and 92.9%, respectively, which can be attributed to the arrest and deflection of microcracks by nanofibers, frictional pullout of nanofibers, the multiple cracking induced by nanofibers, and control of microcrack size by the closely spaced nanofibers. The particularly significant contribution of the hybrid reinforcement to impact resistance could be attributed to the multi-scale interaction of the nano- and micro-scale reinforcement within the matrix with microcracks. The contribution of nano- and/or micro-scale reinforcement to the impact resistance of the high-performance cementitious paste was found to be statistically significant (at 0.01 significance level).

11.3.2.4 Abrasion Resistance

The abrasion test results presented in Table 11.5 indicate that carbon microfibers and especially hybrid reinforcement, and (to a lesser extent) CNFs enhance the abrasion resistance of the high-performance (DSP) cementitious paste. These benefits were found to be statistically significant at 0.000 significance level.

11.3.2.5 Scanning Electron Microscope Evaluation

Fig. 11.11 shows SEM images which are indicative of the uniform dispersion of nanofibers within the cementitious paste (Fig. 11.10a), and a combination of carbon fiber rupture and pullout at fracture surfaces (Fig. 11.10b & c).

11.4 Summary

Results of experiments conducted on cementitious pastes reinforced with non-functionalized and functionalized CNFs as well as their hybrids with carbon microfibers yielded that acid-oxidization of CNFs benefited their dispersion and reinforcement efficiency in a high-performance cementitious matrix. A hybrid reinforcement comprising CNFs and CMFs at 0.16% and 0.24% of the volume of cementitious materials produced distinct gains in the engineering properties of the high-performance cementitious paste, which could not be matched by nano- or micro-scale reinforcement used alone. This finding points at the synergistic effects offered by nano- and micro-scale reinforcement systems.

Table 11.1- Mean values of the flexural strength, maximum deflection and energy absorption capacity test results for high-performance cementitious pastes with 0% and 0.24% (by volume of cement plus silica fume) of non-functionalized and acid-functionalized CNFs.

Reinforcement Condition	Flexural Strength (MPa)	Maximum Deflection (mm)	Energy Absorption (N.mm)
Plain	10.3	0.40	62.0
Acid-functionalized nanofiber (CNF-OX), 0.24 vol.%	15.7	1.18	245
Non-functionalized nanofiber (CNF), 0.24 vol.%	9.09	0.79	102

Table 11.2- Mean values of the flexural strength, maximum deflection and energy absorption capacity test results for high-performance cementitious paste with carbon nanofiber and/or microfiber reinforcement systems.

Reinforcement Condition	Flexural Strength (MPa)	Maximum Deflection (mm)	Energy Absorption (N.mm)
Plain	10.3	0.40	61.8
Carbon microfiber, 0.24 vol%	16.1	1.13	251
Carbon nanofiber, 0.16 vol%	14.9	1.05	213
Carbon microfiber, 0.24 vol%, & Carbon nanofiber, 0.16 vol%	17.0	1.55	282

Table 11.3- Mean values and standard errors of the compressive strength test results for high-performance cementitious paste reinforced with CNFs and/or microfibers.

Reinforcement Condition	Mean (MPa)	Standard Error (MPa)
Plain	111	14.3
Carbon microfiber, 0.24 vol%	117	28.0
Carbon nanofiber, 0.16 vol%	113	17.9
Carbon microfiber, 0.24 vol%, & Carbon nanofiber, 0.16 vol%	117	15.3

Table 11.4- Mean values of the impact resistance test results for high-performance cementitious pastes with carbon nanofiber and/or microfiber reinforcement systems.

Reinforcement Condition	Impact Resistance
	(mm/mm)
Plain	0.365
Carbon microfiber, 0.24 vol%	0.521
Carbon nanofiber, 0.16 vol%	0.625
Carbon microfiber, 0.24 vol% & Carbon nanofiber, 0.16 vol%	0.704

Table 11.5- Mean values and standard errors of the abrasion test results for high-performance cementitious pastes with carbon nanofiber and/or microfiber reinforcement systems.

Reinforcement Condition	Loss of Mass
	(grams)
Plain	0.275
Carbon microfiber, 0.24 vol%	0.150
Carbon nanofiber, 0.16 vol%	0.250
Carbon microfiber, 0.24 vol% & carbon nanofiber, 0.16 vol%	0.125

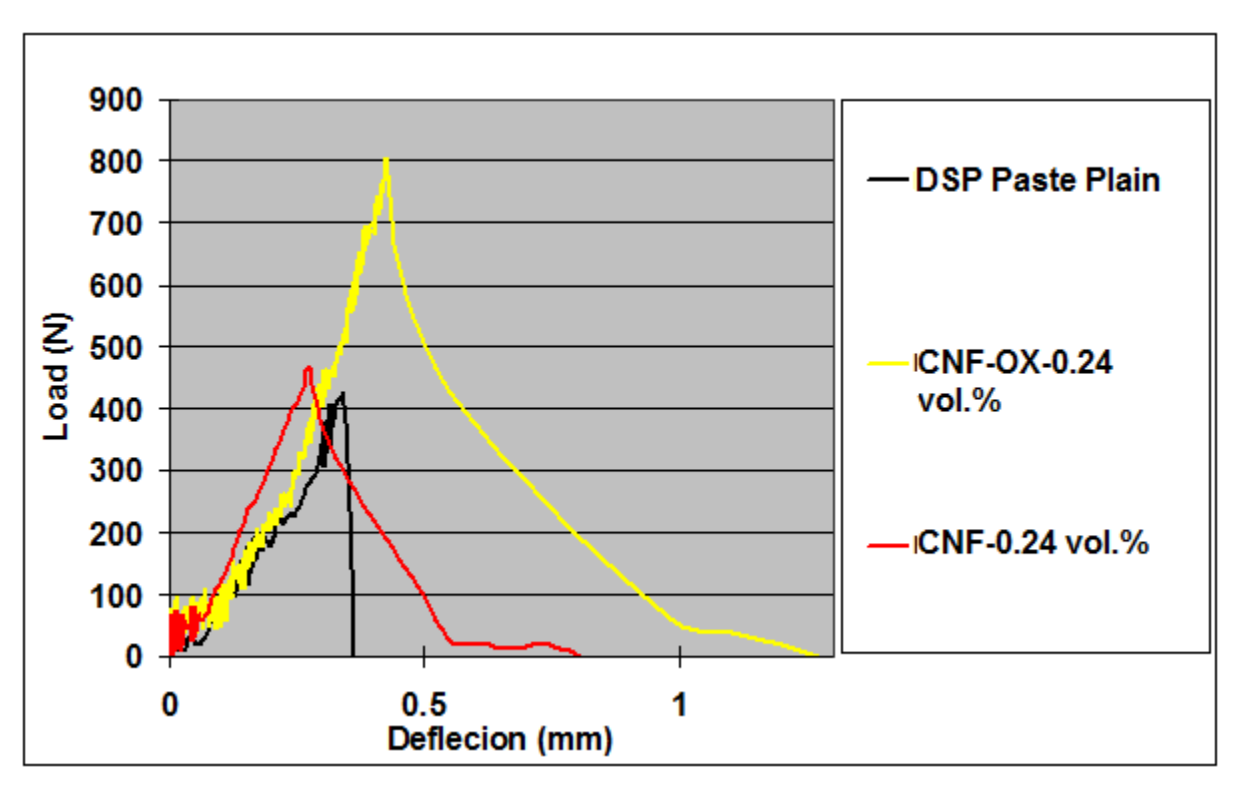


Figure 11.1- Representative flexural load-deflection curves of high-performance cementitious pastes with 0 and 0.24 vol.% of non-functionalized and oxidized nanofibers.

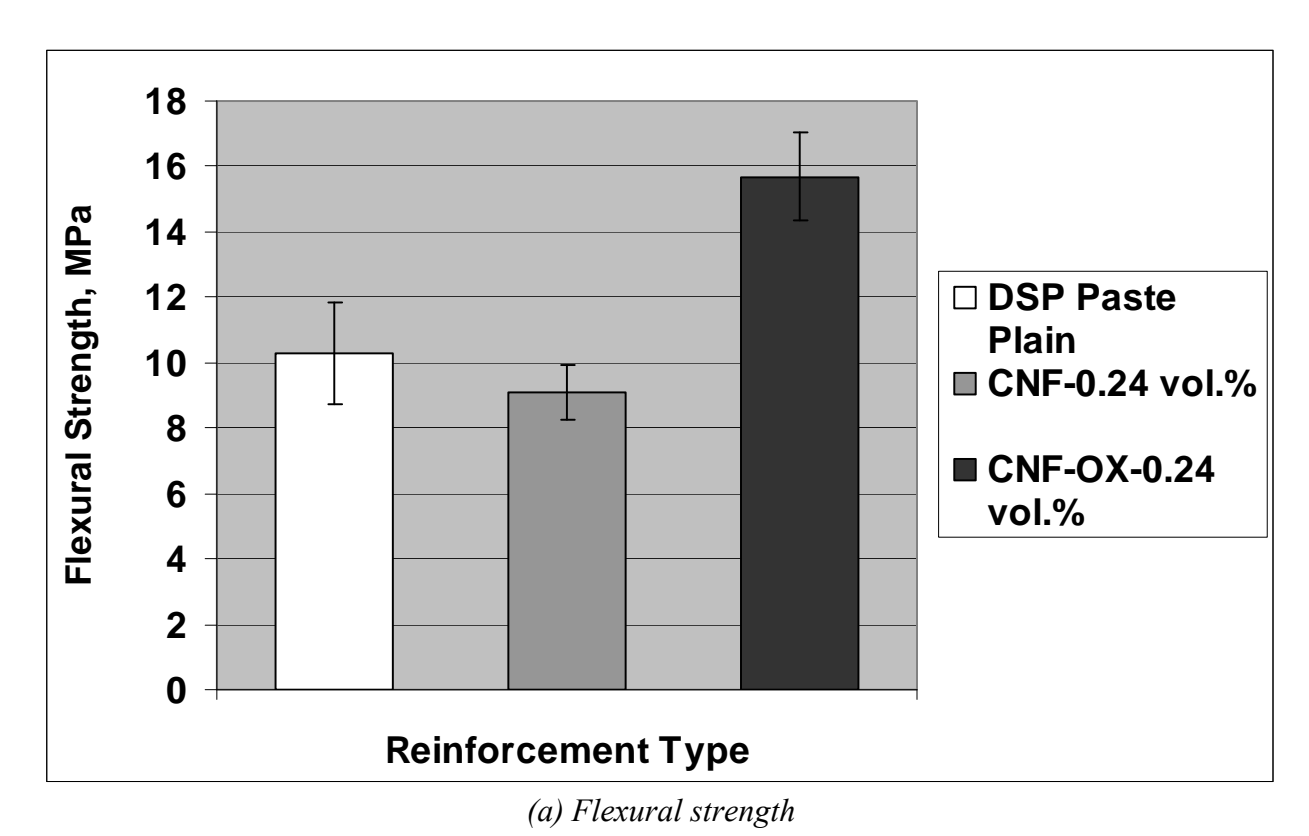
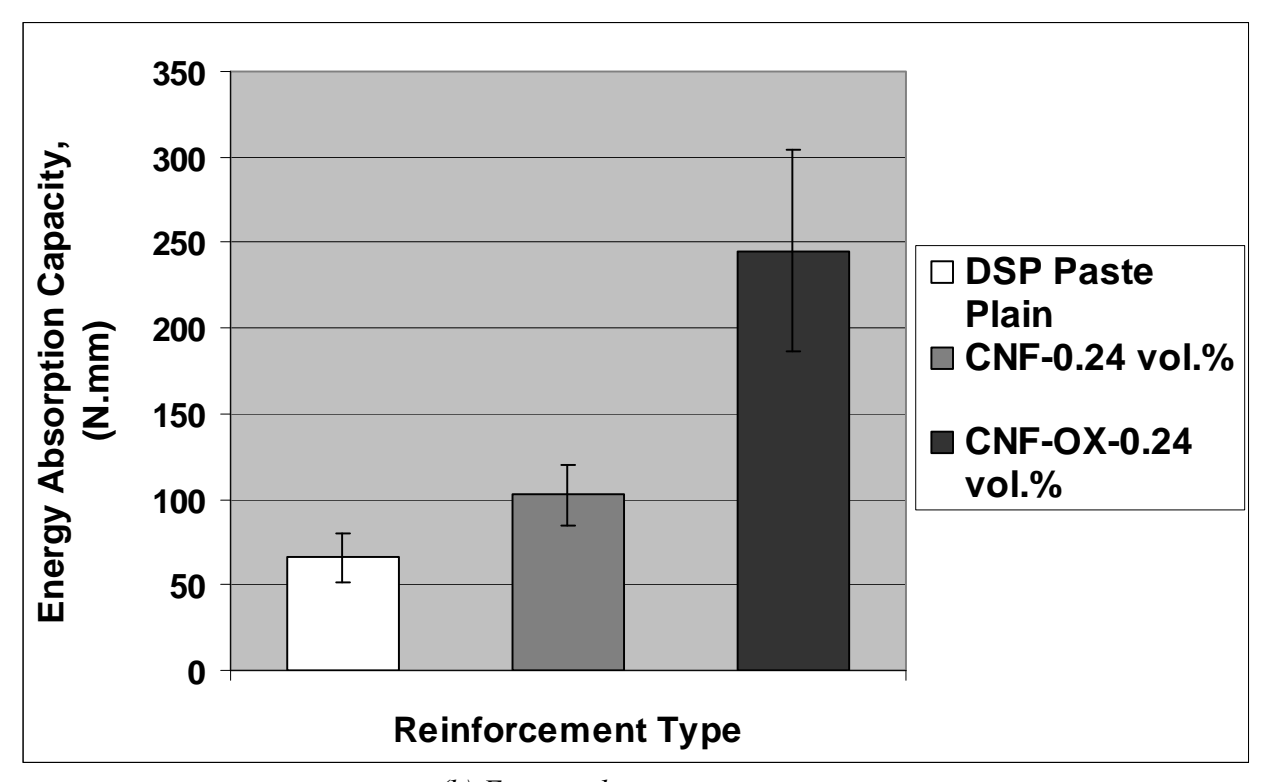


Figure 11.2- Flexural attributes of high-performance cementitious pastes.



(b) Energy absorption capacity

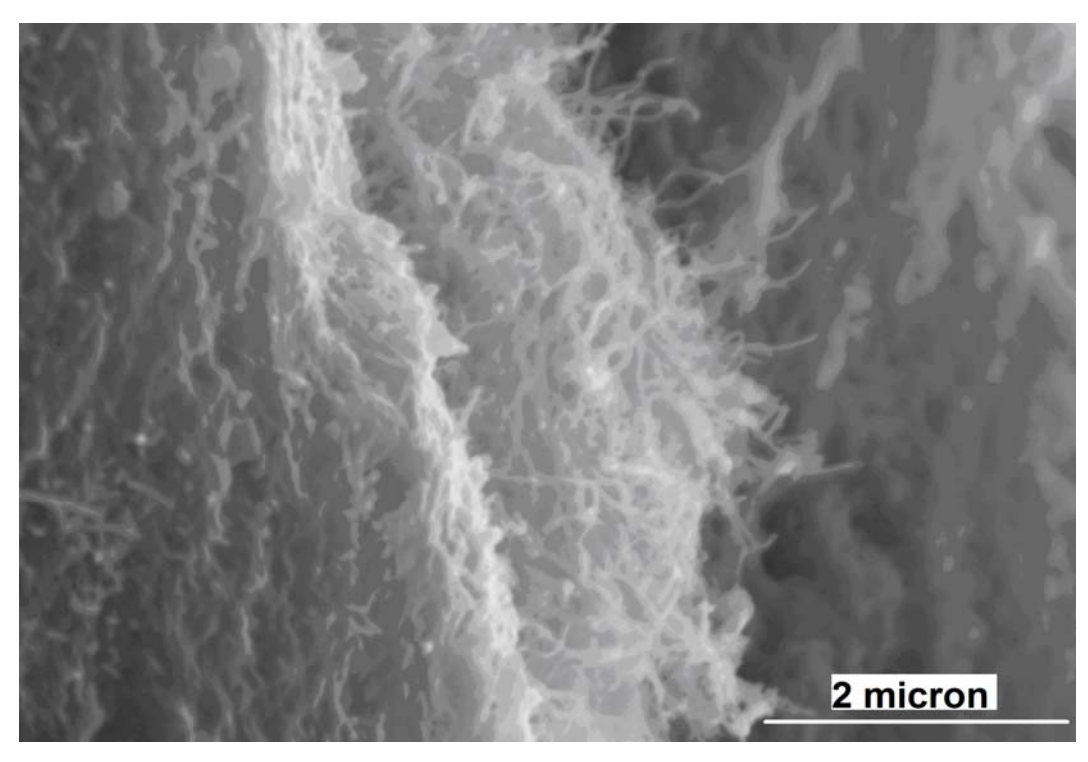


Figure 11.3- Clumping of non-functionalized CNFs in the high-performance cementitious paste at 0.24% by volume of cement plus silica fume.

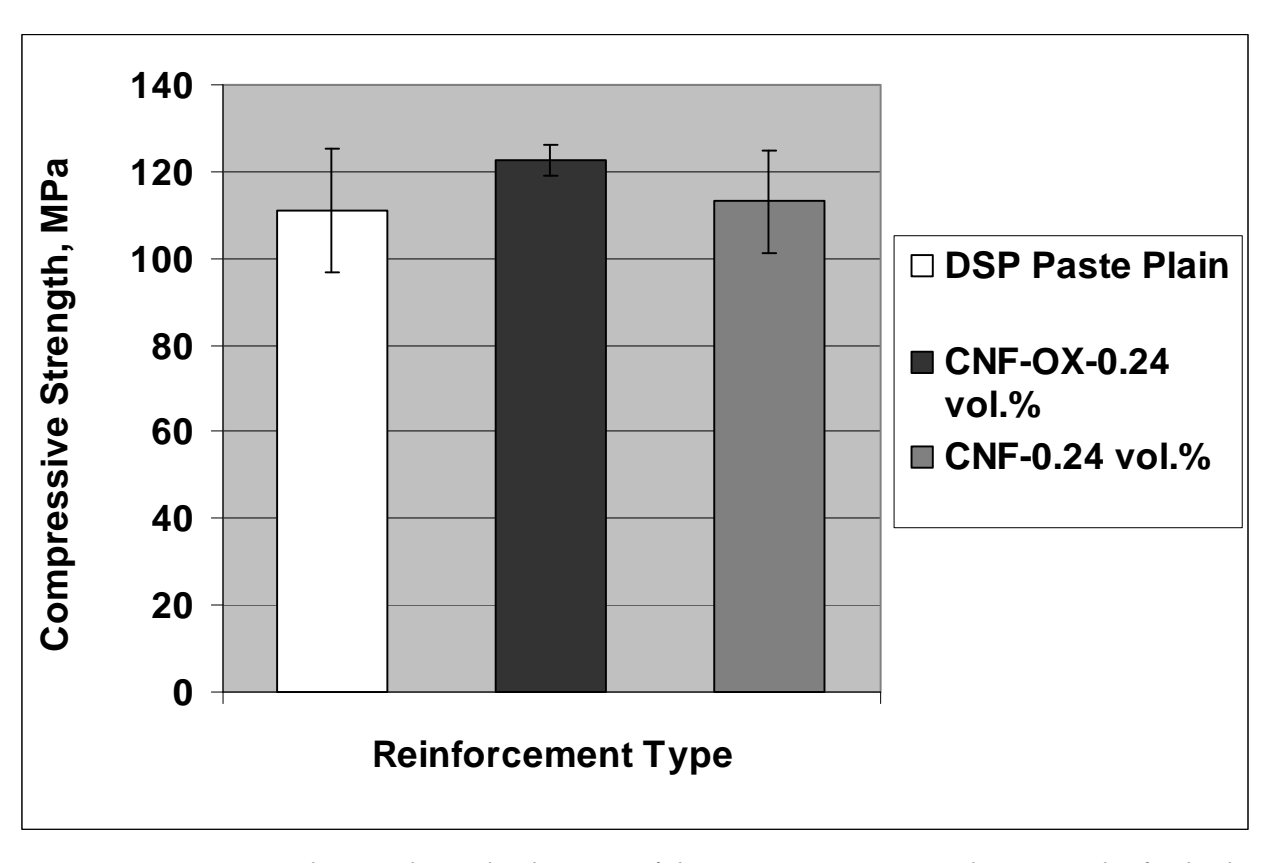


Figure 11.4- Mean values and standard errors of the compressive strength test results for highperformance cementitious paste reinforced with 0 and 0.24 vol.% of non-functionalized and acid-functionalized CNFs.

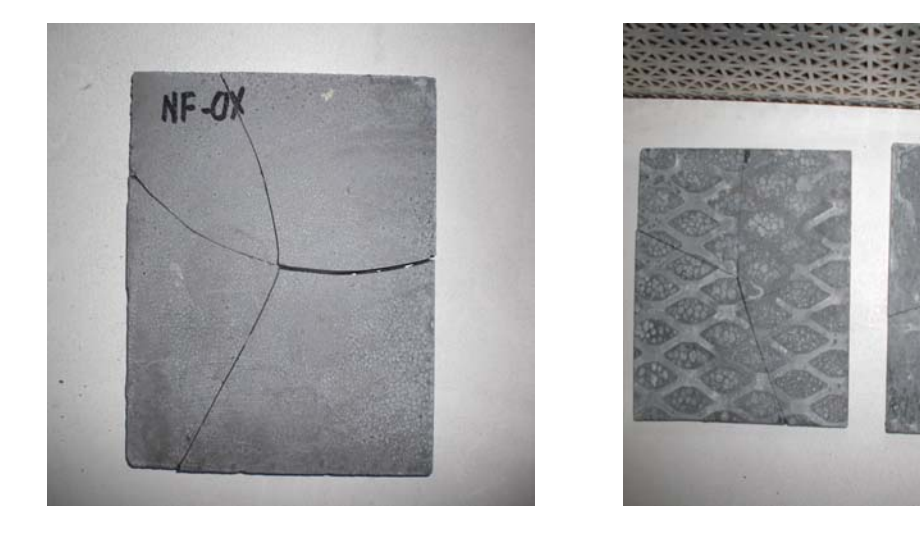


Figure 11.5- Failed impact test specimens.

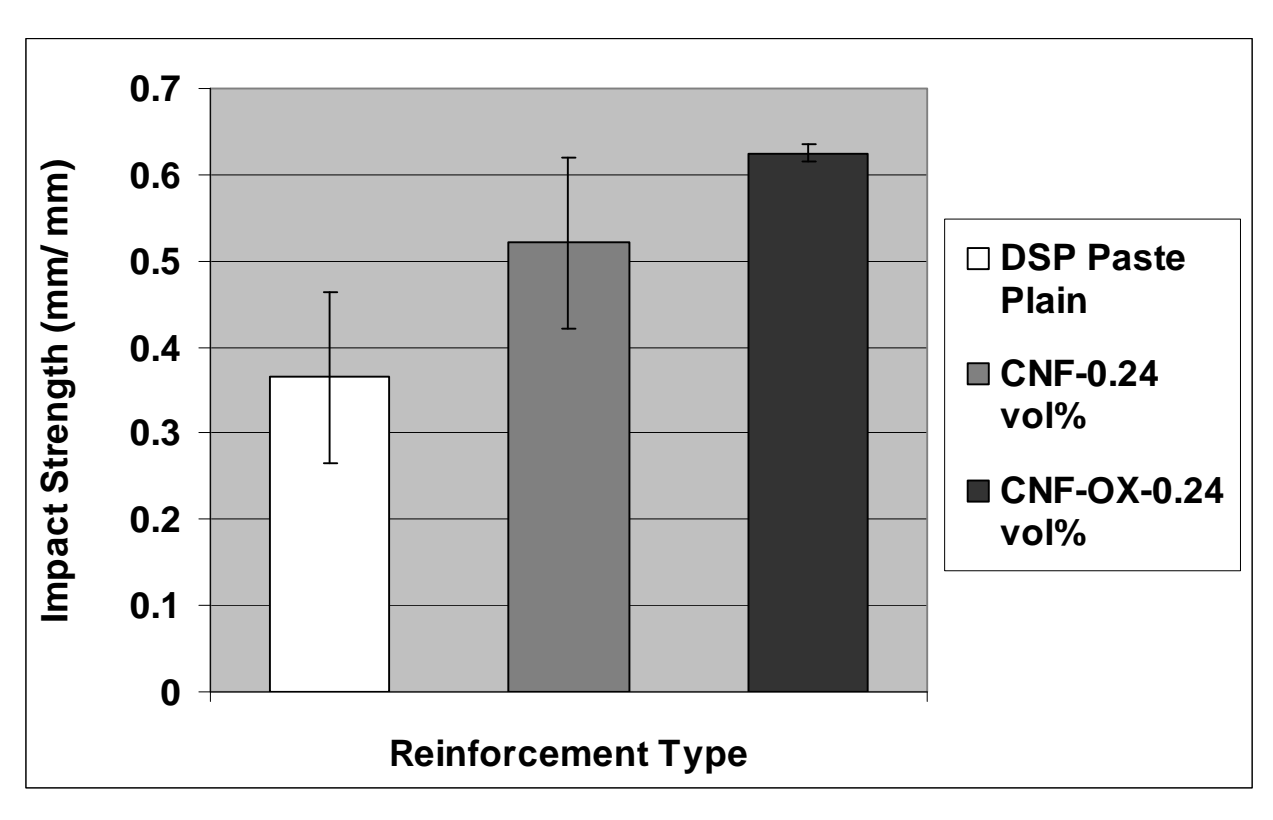


Figure 11.6- Mean values and standard errors of the impact resistance test results for high-performance cementitious paste reinforced with 0 and 0.24 vol.% of non-functionalized and acid-functionalized CNFs.

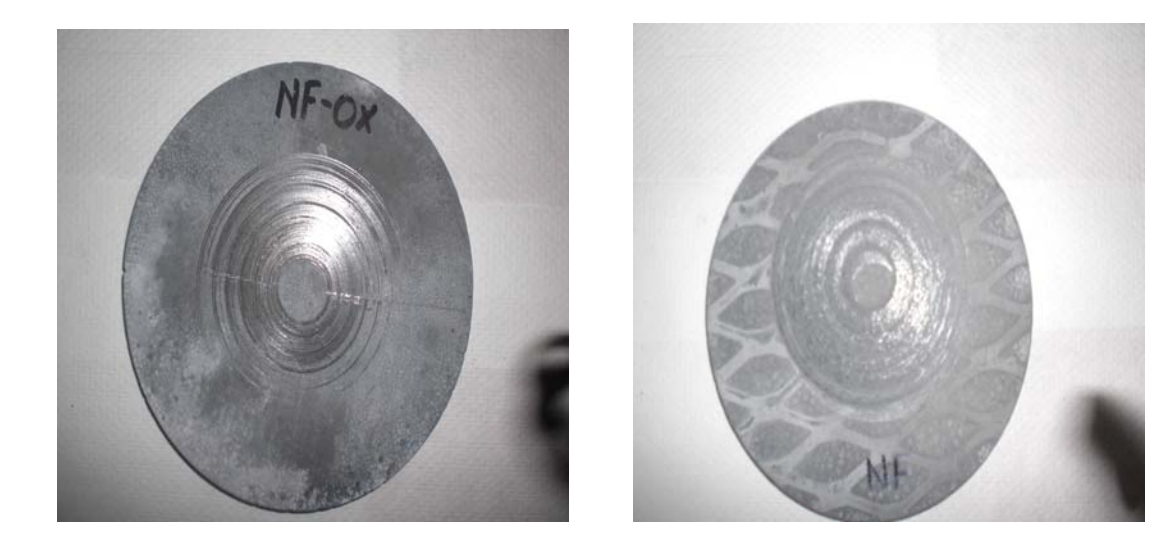


Figure 11.7- Abrasion test specimens after test.

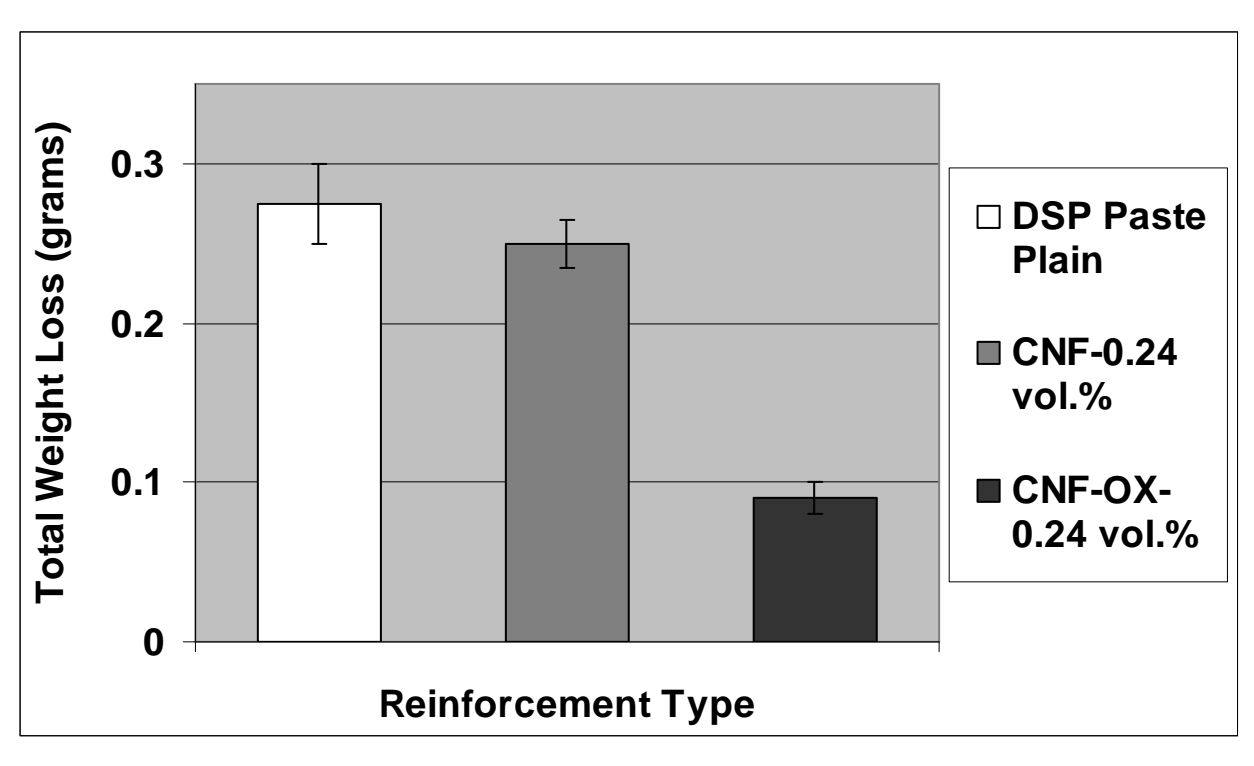
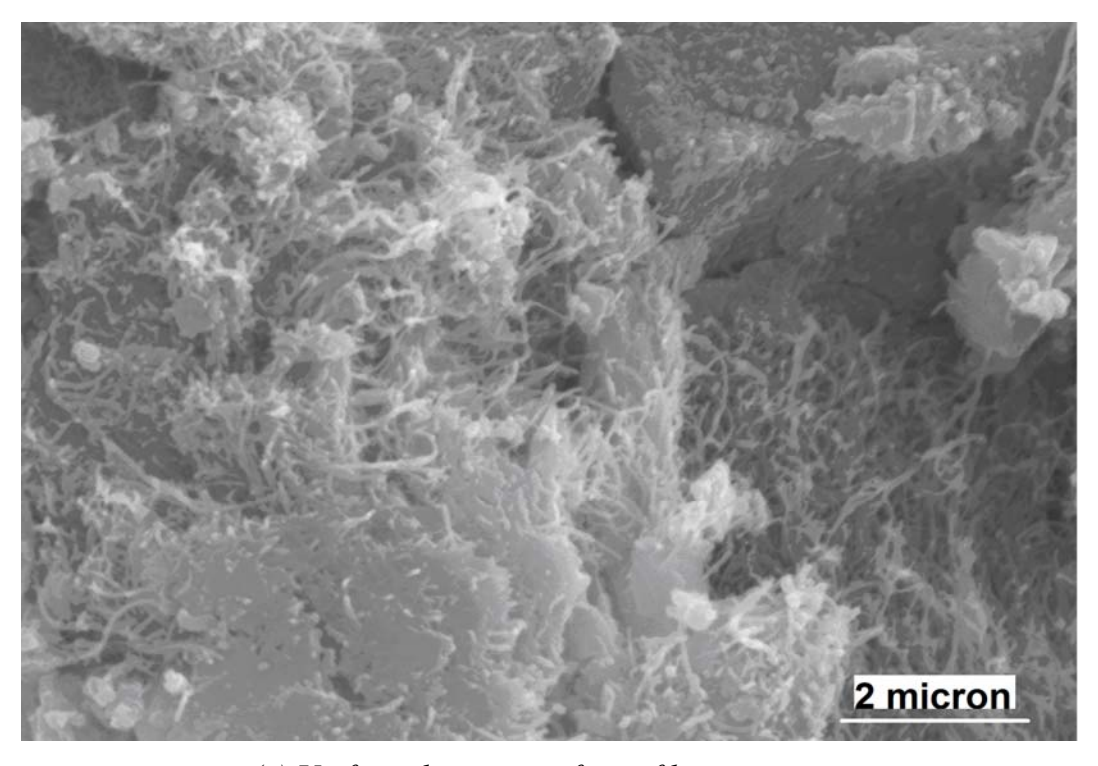
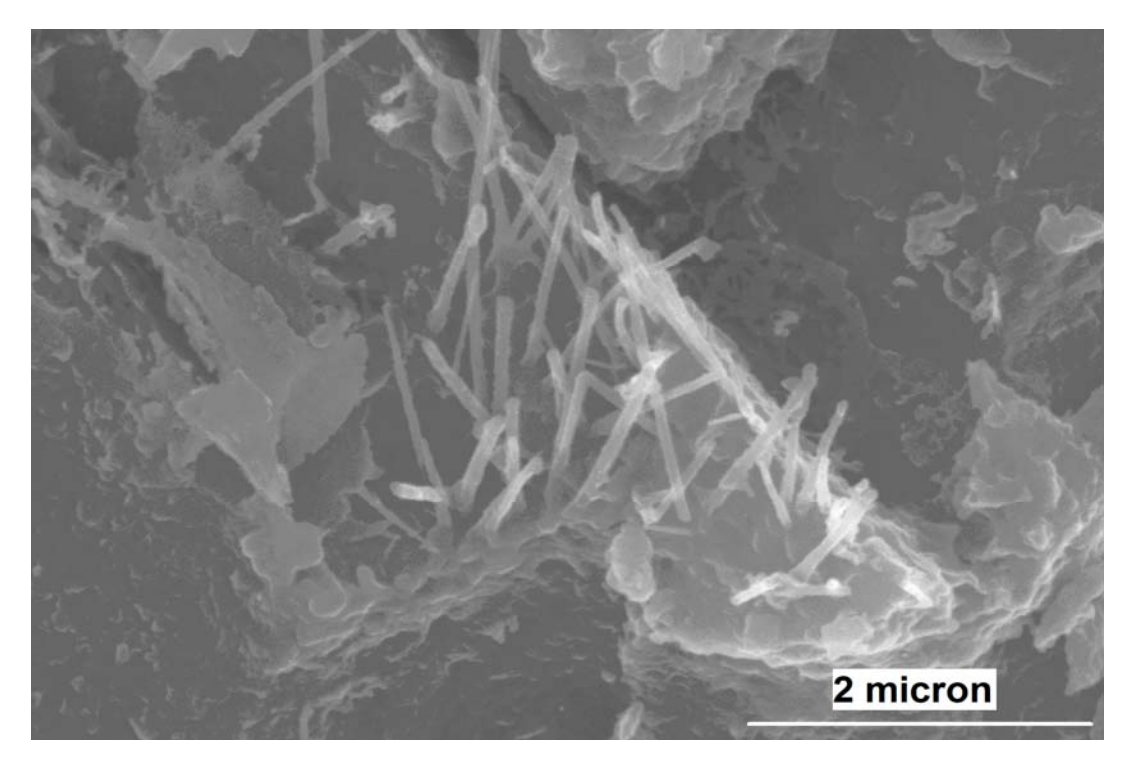


Figure 11.8- Mean values of abrasion weight loss for high-performance cementitious pastes reinforced with 0% and 0.24% of non-functionalized and acid-functionalized CNFs.

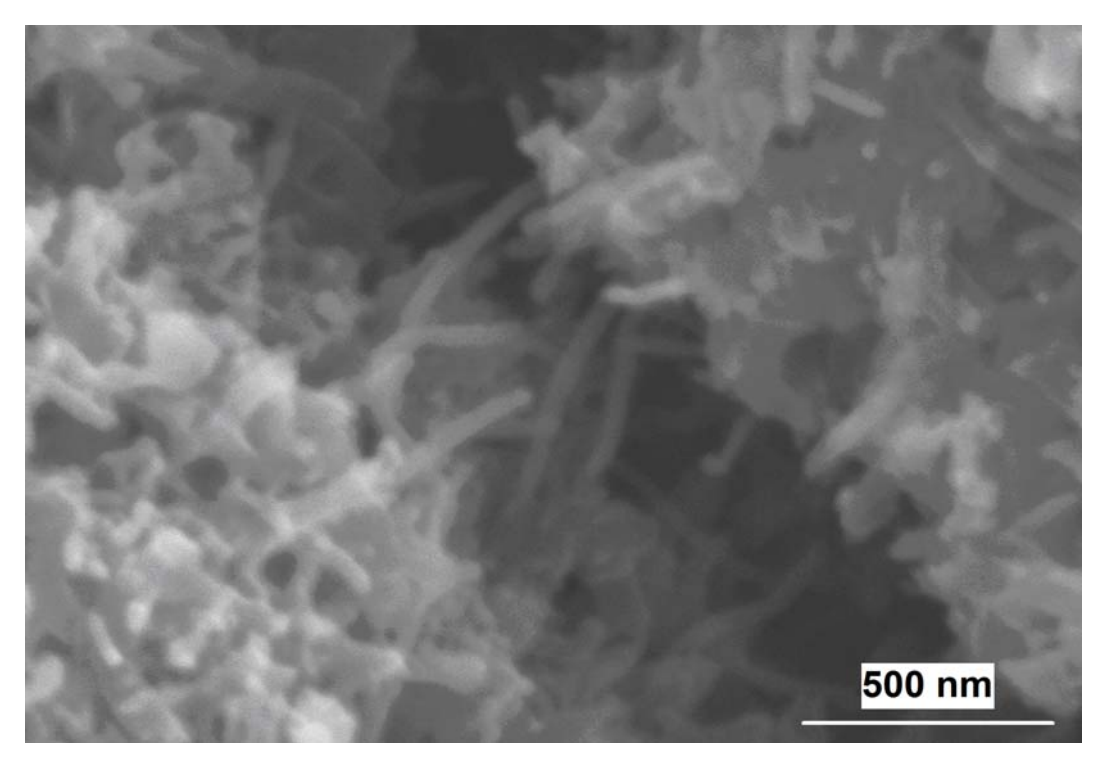


(a) Uniform dispersion of nanofibers in matrix

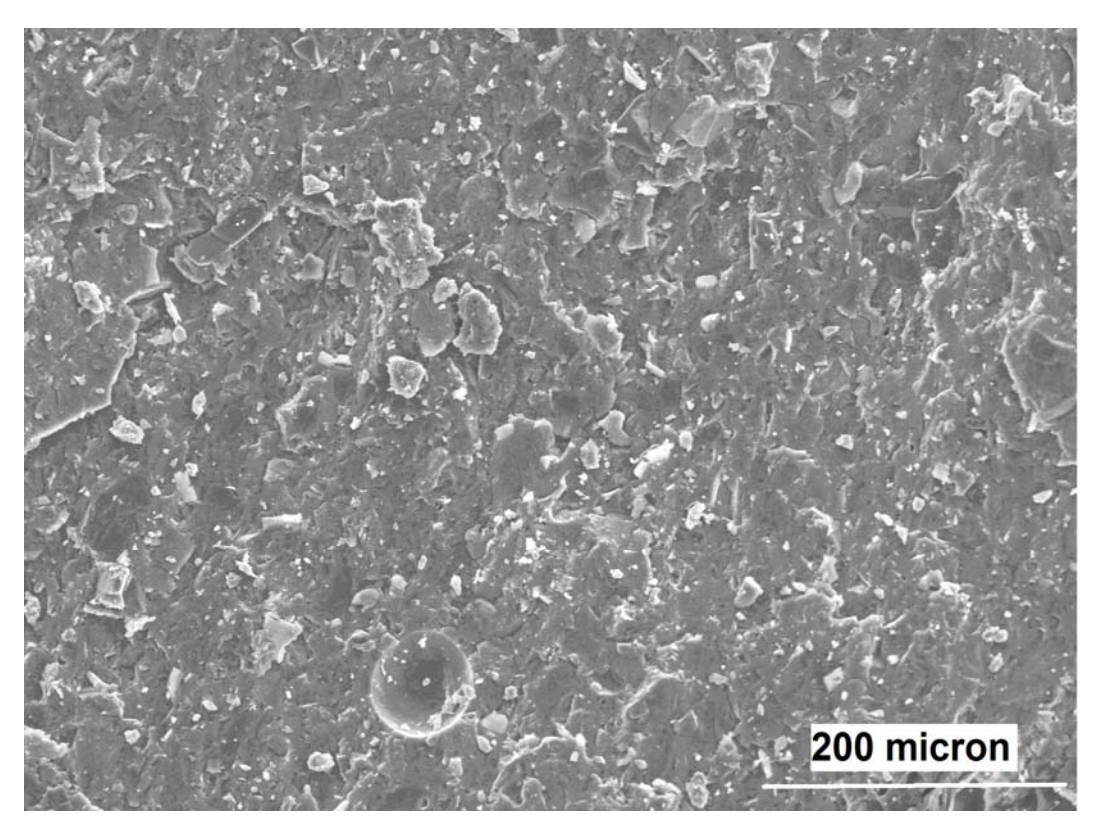
Figure 11.9- Typical SEM images of high-performance pastes reinforced with 0.24 vol.% of CNFs.



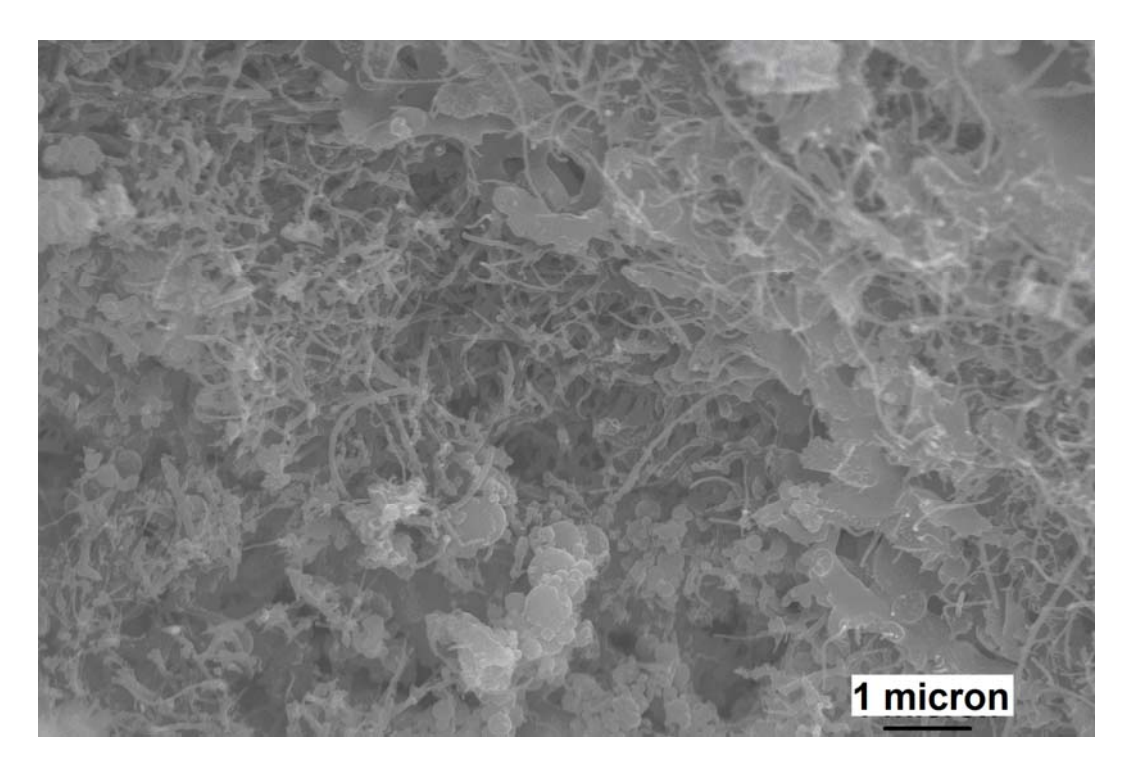
(b) Micro- crack-bridging action of nanofibers



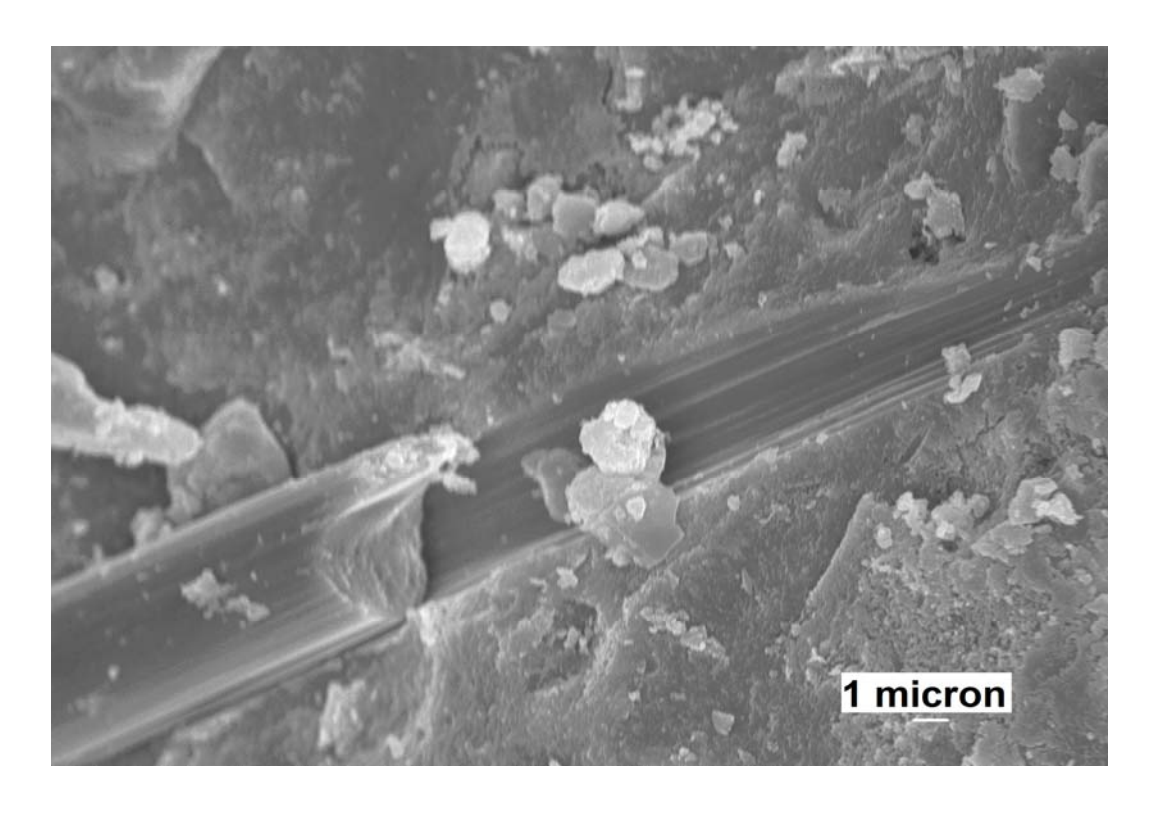
(c) Micro- crack-bridging action of nanofibers



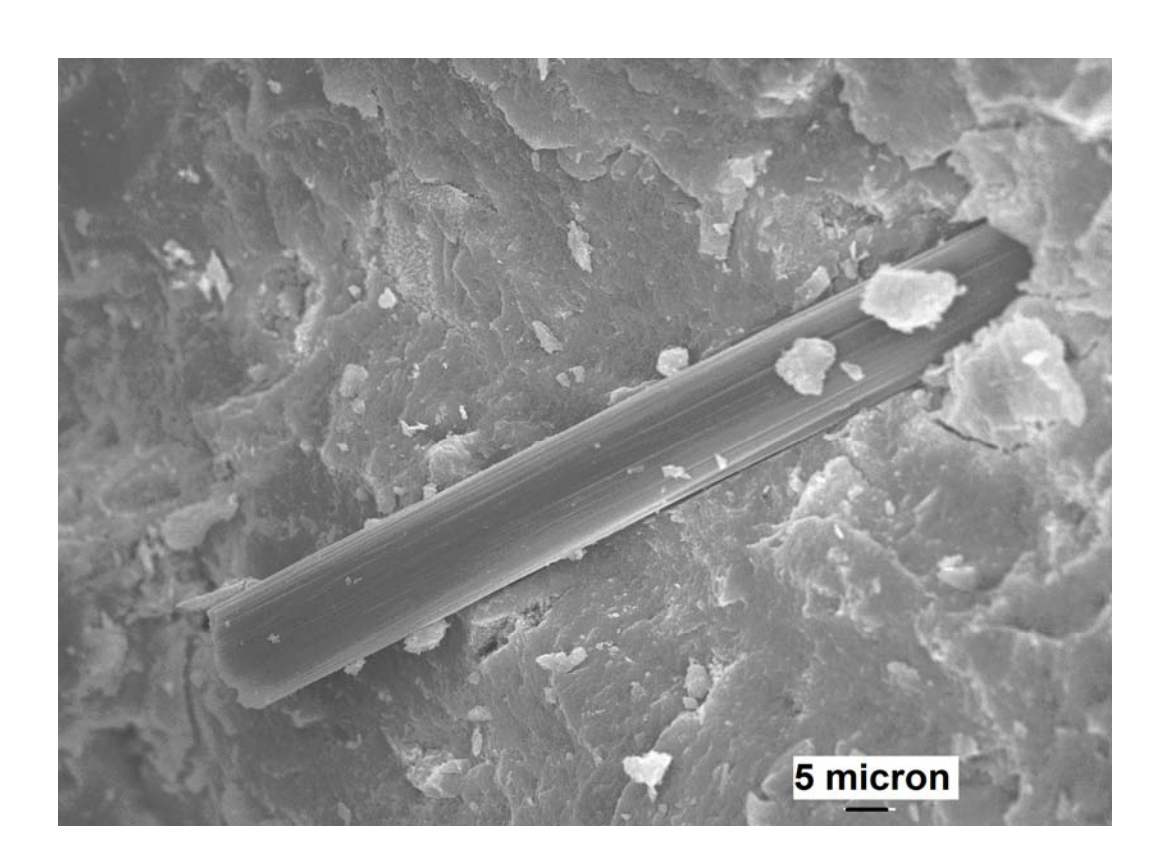
(d) Dense DSP matrix



(a) Dispersion of oxidized CNFs within the matrix



(b) Failure mechanism of micro-scale fibers at fracture surfaces
Figure 11.10- Typical SEM mages of DSP cementitious paste reinforced with carbon microfibers
and/or oxidized CNFs.



(c) Failure mechanism of micro-scale fibers at fracture surfaces

12 EVALUATION OF REINFORCEMENT EFFICIENCY OF CARBON NANO- AND MICRO-FIBERS IN HIGH-PERFORMANCE CEMENTITIOUS MORTAR

12.1 General

Fibers are incorporated into cementitious matrices to enhance their toughness, tensile strength and ductility, and crack resistance. Cracks initiate in cementitious materials at fine scales, as a result of local restraint of the past shrinkage; conventional (micro-scale) fibers are not effective in controlling the development and size of such fine cracks. The relatively close spacing and high surface area of nanofibers, on the other hand, could limit the concentration and size of such "microcracks", and their propagation in cementitious materials. Thorough dispersion and effective interfacial interactions of nanofibers are critical to their effectiveness in cementitious materials. The relatively short lengths of nanofibers, however, limit their ability to bridge across wider cracks, and provide for substantial energy dissipation via extended frictional pullout. Longer micro-scale fibers can complement the action of nanofibers at fine scale with crack control and toughening effects at advanced stages of damage development. Earlier results on use of nano-scale (primarily multi-walled carbon nanotubes) reinforcement of high-performance cementitious materials have indicated that major gains in engineering properties of cementitious materials can be realized with relative low dosages (as small as 0.04 vol.% by weight of cement). One objective of the work reported herein was to assess the effectiveness of CNFs as relatively low-cost nano-scale reinforcement in high-performance cementitious mortars. The other objective was to validate the synergic action of a multi-scale reinforcement comprising CNFs and microfibers as reinforcement in high-performance cementitious mortars.

Carbon nanofibers (CNFs) are made of grapheme sheets formed into cones, which are stacked to assume a tubular geometry with 50-200 nm outer diameter. The elastic modulus of individual nanofibers ranges from 25 to 200 GPa, depending on their diameter (Cwirzen and Penttala 2005). Given their relatively low cost compared to carbon nanotubes, development of carbon nanofiber reinforced polymer nanocomposites is actively pursued (Ping, Beaudoin et al. 1991; Song, Jang et al. 2007; Pfeifer, Moeser et al. 2009). Efforts to assess the value of CNFs to inorganic (including cementitious) matrices have also been initiated; uniform dispersion and effective interfacial interactions are key to their reinforcement efficiency in cementitious materials (Ahlborn, Harris et al. 2011). Past experimental evaluations of the reinforcement efficiency of CNFs in cementitious matrices have yielded mixed results, which could be partly attributed to the extent of dispersion and interfacial interactions of nanofibers in cementitious materials, and also to the qualities (e.g., density, pore system characteristics and strength) of the cementitious matrix. In a series of tests, the introduction of silica fume (with nano-scale particle size) to cement (with micro-scale particle size) as well as acid treatment of nanofibers were found to benefit dispersion of CNFs in cementitious matrices; the addition of nanofibers at 0.005% to 2% by weight of cement, however, did not benefit the mechanical properties of cementitious materials (Bentz 2000; Bentz, Jensen et al. 2000). Metaxa et al. also investigated the nanostructure and the mechanical properties of cementitious nanocomposites reinforced with CNF at low volume fractions. Another experimental work (Metaxa, Konsta-Gdoutos et al. 2010), on the other hand, showed improvements in the flexural strength of cementitious materials

realized by introduction of CNFs at 0.048 wt.%. Scanning electron microscope images showed that CNFs bridge across fine cracks, and control their propagation.

In this study, the gains in reinforcement efficiency of CNFs, alone or in combination with carbon microfibers, resulting from oxidation of nanofibers and also the use of refined methods for dispersion of nanofibers were investigated. A high-performance cementitious matrix (DSP) was considered here, and different nanofiber volume fractions were evaluated. Two alternative polycarboxylate-based superplasticizers were used for preparation of cementitious matrices. One of these superplasticizers, which performed better in cementitious nanocomposites, was used throughout the investigation.

12.2 Materials and Methods

12.2.1 Graphite Nanomaterials and Microfibers

Different types of functionalized and non-functionalized carbon nanofibers as well as chopped (micro-scale) carbon fibers were evaluated for use in cement-based nanocomposites. These graphite nanomaterials and microfibers have been introduced in detail in Chapter 2, Section 2.4, Fig. 2.3 and Table 2.3. Acid-functionalized and polymer wrapped carbon nanofibers (CNF-OX and CNF-PAA) and carbon microfibers (CMF) were used in high-performance cement-based mortar matrix.

12.2.2 Cementitious Matrices, Mixing and Curing Procedure

Dense cementitious matrix selected has been introduced in detail in Chapter 2, Section 2.5. DSP mortar was used to evaluate the reinforcement efficiency of both graphite nanomaterials and/or carbon microfibers at different volume fractions.

Cementitious materials (with and without functionalized graphite nanomaterials dispersed in the mixing water via sonication) and/ or carbon microfibers were prepared and cured following ASTM procedures described in the same section.

12.2.3 Experimental Methods

The test procedures employed to determine the engineering properties of high-performance mortar included compression tests (ASTM C 109), flexure tests (ASTM C 1185), impact tests (ASTM D 7136) and Abrasion tests (ASTM C 944). SEM and EDS were also employed to gain further insight into the structure and failure mechanisms of cement-based nanocomposites. The experimental results were subjected to statistical analysis using the analysis of variance (ANOVA) and pair-wise comparison methods. RSA (Response Surface Analysis) was used to identify reinforcement volume fractions which yield optimum gains in various engineering properties of the cementitious matrix.

12.3 Experimental Results and Discussion

12.3.1 Effects of Carbon Nano- and/or Micro-fibers Used at Different Volume Fraction and with Different Superplasticizers

12.3.1.1 Flexural Performance

The flexural strength, maximum deflection and energy absorption capacity (area underneath the flexural load-deflection curves) were determined for the high-performance (DSP) cementitious mortar reinforced with different volume fractions of oxidized or PAA-physisorbed CNFs and/or microfibers, prepared using two different carboxylate-based superplasticizers. The flexure test data are summarized in Table 12.1. The experimental results indicate that all reinforcement conditions considered here produced improvements in the flexural attributes of high-performance

cementitious mortar. Maximum improvements were realized with PAA-physisorbed carbon nanofiber (CNF-PAA) and its hybrid combination with carbon microfibers. The maximum gain in flexural strength versus plain mortar (21.4%) was achieved at 0.16 vol.% CNF-PAA, which was 4.3% greater than that achieved with a similar volume fraction of CNFs used without polymer wrapping. It should be noted that the volume fraction of CNFs is calculated here with respect to the volume of dry cementitious materials (cement and silica fume). The maximum improvements in energy absorption capacity and maximum deflection versus plain mortar (62.2% and 52.9%, respectively) were realized with 0.24 vol.% CNF-PAA. The gains in these flexural attributes were also higher with polymer-wrapped CNFs (CNF-PAA) when compared with CNFs used without polymer wrapping. Hybrid reinforcement systems comprising both nano-scale CNF-PAA and micro-scale carbon fibers brought about balanced improvements in the engineering properties of high-performance cementitious mortars, which surpassed those achieved with nano- or micro-scale reinforcement used alone. Polymer wrapping of CNFs consistently improved the reinforcement efficiency of nanofibers in high-performance (DSP) mortar. ADVA® Cast 575 polycarboxylate-based superplasticizer produced better results when compared with Glenium® 7700.

Per unit volume fraction, carbon nanofiber was more effective than carbon microfiber in enhancing the flexural performance characteristics of DSP cementitious mortar. Hybrid (nano-and micro-scale) reinforcement systems comprising 0.16 vol.% CNF-PAA and 0.24 vol.% CMF produced highly desired, balanced gains in the flexural performance characteristics of high-performance DSP cementitious mortar at a relatively low total reinforcement volume fraction.

Analysis of variance of test results indicated that the reinforcement conditions considered here produced statistically significant (at 0.05 significance level) improvements in all flexural

attributes of the high-performance cementitious mortar. Subsequent pair-wise comparisons of test results indicated that all nano- and/or micro-scale reinforcement conditions produced statistically significant gains (at 0.05 significance level) in the flexural performance characteristics of the high performance (DSP) mortar. Distinct improvements (at 0.00 significance level) in all flexural attributes were realized with the addition of CNF-PAA and/or CMF reinforcement.

12.3.1.2 Compressive Strength

The compressive strength test results (mean values and standard errors) for high-performance cementitious mortars with nano- and/or micro-scale reinforcement systems are presented in Table 12.2. PAA- physisorbed as well as oxidized or pristine CNFs, when used alone or in combination with carbon microfibers produced statistically insignificant effects on the compressive strength of the high-performance cementitious mortar (0.76 significance level). Pair-wise comparisons indicated that the difference between no pair of compressive strength test results was statistically significant (at 0.05 significance level).

12.3.1.3 Impact Resistance

The impact test data are summarized in Table 12.3. Nanofiber reinforcement at 0.24 vol.% as well as hybrid reinforcement of DSP mortar produced more than 50% gain in impact resistance. At equal volume fractions, nanofibers were more effective than microfibers in enhancing the impact resistance of the high-performance cementitious mortar with both superplasticizers. The hybrid (nano- and micro-scale) reinforcement was more effective than micro-scale reinforcement alone in improving the impact resistance of DSP mortar. The analysis of variance and pair-wise comparisons of impact test results indicated that the gains in impact resistance with nano- and/or

micro-scale reinforcement of DSP mortar were statistically significant (at 0.05 significance level).

12.3.1.4 Abrasion Resistance

The abrasion test results for DSP mortars with different volume fractions of carbon nanofiber and/or microfiber reinforcement are summarized in Table 12.4. With ADVA® Cast 575 superplasticizer, carbon nanofiber (0.24 vol.%) and its hybrid combination with carbon microfiber produced the greatest improvement (34.7%) in the abrasion resistance of DSP mortar. Nano- and/or micro-scale reinforcement of DSP mortar produced marked improvements in abrasion resistance, which were statistically significant at 0.05 significance level. Outcomes of pair-wise comparisons confirmed that each of the reinforcement conditions considered here produced statistically significant gains in the abrasion resistance of the DSP cementitious mortar.

12.3.1.5 Scanning Electron Microscope Evaluation

The SEM images presented in Fig. 12.1 indicate that the refined sonication and mixing steps developed in the project were successful in dispersion of individual nanofibers within the cementitious matrix. These images also point at the low porosity of the high-performance cement-based matrix; the introduction of nanofibers does not seem to have compromised the high density (low porosity) of this matrix. SEM observations also provided evidence for the crack suppression and crack bridging actions of the nanofibers in cementitious matrix. PAA-physisorbed nanofibers, which provided higher levels of reinforcement efficiency, were found to produce a more uniform dispersion within the cementitious matrix, as some clumping was found for pristine nanofibers, Fig. 12.2.

12.3.2 Energy-Dispersive Spectroscopy (EDS)

Elemental and Quantitative analysis of these samples indicated that all cementitious materials exhibit similar elemental compositions, except for the (expected) higher carbon content in materials incorporating carbon reinforcement. These results indicate that graphite nanomaterials do not significantly alter the chemistry of cement hydration for the reinforcement conditions considered here.

12.3.3 Response Surface Analysis of High-Performance Cementitious Mortar

The test data on high-performance cementitious mortar with nano- and/or micro-scale reinforcement systems prepared with two different superplasticizers were subjected to response surface analysis. The objective of this analysis was to identify optimum reinforcement conditions which maximize: (i) benefits to specific engineering properties of the high-performance mortar; and (ii) simultaneous benefits to several engineering properties.

Response surface analysis (RSA) of the test data was conducted considering the volume fractions of nano- and micro-scale reinforcement systems as input variables. Flexural strength, energy absorption capacity and maximum deflection, and impact resistance were used as response variables. The RSA process started with evaluating the effects of input variables on response variables, and was followed by desirability analyses considering means of response variables, using both canonical and ridge analysis methods.

Response Surface analyses conducted for each of the flexural strength, energy absorption capacity, maximum deflection and impact resistance test data indicated that an optimum reinforcement system comprising 0.09-0.13 vol.% PAA-physisorbed carbon nanofiber and 0.21-0.23 vol.% carbon microfiber maximized subject properties. Optimal Responses for flexural

strength, energy absorption and maximum deflection were calculated at 21.6 MPa, 429 N.mm and 2.61 mm mean values, respectively, with 95% confidence Interval of 20.4-22.8 MPa, 390-467 N.mm and 1.67–3.56 mm, respectively. The optimal response for impact resistance was calculated at 0.945 mm/mm mean value with 95% Confidence Interval of 0.767-1.12 mm/mm. All stationary points were found to be saddle points, which do not give a maximum but a general direction to follow in which the targeted properties can be maximized, Fig. 12.3. Outcomes of ridge analysis can be used to adjust the reinforcement condition for achieving further gains in engineering properties. The analyses for flexural attributes and impact resistance show that the hybrid reinforcement systems considered here occur within the range of optimal reinforcement conditions.

The test data were also subjected to desirability analyses in order to identify reinforcement conditions which yield a desired balance of all the engineering properties considered here. Desirability analyses were conducted using mean values obtained through both canonical and ridge analyses. These outputs indicate that maximum values of all response variables can be achieved with CNT-PAA/CMF volume fractions 0.13/0.22 or 0.15/0.26 vol.% (calculated with respect to the volume of dry cementitious materials). These optimum reinforcement systems do not differ significantly from those considered in this investigation.

12.4 Summary

Comprehensive experimental evaluations of high-performance cementitious mortar with nanoscale (pristine, polymer-wrapped or oxidized CNFs) and/or micro-scale (carbon microfiber) reinforcement were conducted using two polycarboxylate-based superplasticizers. As was the case for carbon nanotubes the experimental results indicated that for similar reinforcement conditions, the gains in performance characteristics of the cementitious matrix depended upon the specific polycarboxylate-based superplasticizer used. The gains in flexural performance characteristics per unit volume of reinforcement were more significant with carbon nanofiber when compared with carbon microfiber.

Similarly, the experimental results also pointed at the merits of hybrid (nano- and micro-scale) reinforcement towards achieving balanced gains in the flexural performance characteristics and impact resistance of high-performance cementitious materials. Response surface analysis of experimental results indicated that optimum reinforcement conditions comprised both nano- and micro-scale reinforcement systems. The reinforcement conditions considered here produced minor (and statistically insignificant) changes in the compressive strength of high-performance cementitious materials.

Table 12.1- Mean values of the flexural attributes of high-performance (DSP) cementitious mortar with nano- and/or micro-scale reinforcement systems.

Reinforcement Condition	Flexural Strength	Maximum Deflection	Energy Absorption
NI-:- CI	(MPa)	(mm)	(N.mm)
Plain – Gl	16.6	0.99	216
Plain - Adva	18.7	1.38	275
Carbon microfiber, 0.24 vol%-(CMF-0.24) - Gl	19.3	1.37	319
Carbon microfiber, 0.24 vol%-(CMF-0.24) - Adva	19.6	1.42	344
Carbon microfiber, 0.48 vol%-(CMF-0.48) - Gl	22.5	2.31	424
Carbon microfiber, 0.48 vol%-(CMF-0.48) - Adva	23.0	2.35	459
Carbon microfiber, 0.96 vol%-(CMF-0.96) - Gl	23.1	2.54	474
Carbon microfiber, 0.96 vol%-(CMF-0.96) - Adva	23.9	2.55	481
Carbon nanofiber, 0.16 vol%-(CNF-OX-0.16) - Gl	21.6	1.76	405
Carbon nanofiber, 0.16 vol%-(CNF-OX-0.16) - Adva	21.9	1.87	430
Carbon nanofiber, 0.16 vol%-(CNF-PAA-0.16) - Adva	22.7	2.02	443
Carbon nanofiber, 0.24 vol%-(CNF-OX-0.24) - Gl	20.9	1.87	410
Carbon nanofiber, 0.24 vol%-(CNF-OX-0.24) - Adva	21.2	1.95	435
Carbon nanofiber, 0.24 vol%-(CNF-PAA-0.24) - Adva	22.2	2.11	446
Carbon microfiber, 0.24 vol%, & Carbon nanofiber, 0.16 vol%-(CMF;CNF-OX) - Gl	20.4	2.13	375
Carbon microfiber, 0.24 vol%, & Carbon nanofiber, 0.16 vol%-(CMF;CNF-OX) - Adva	20.9	2.17	423
Carbon microfiber, 0.24 vol%, & Carbon nanofiber, 0.16 vol%-(CMF;CNF-PAA) - Adva	21.4	2.18	425

Table 12.2- Mean values and standard errors of the compressive strength test results for DSP mortar with nano- and/or micro-scale reinforcement systems.

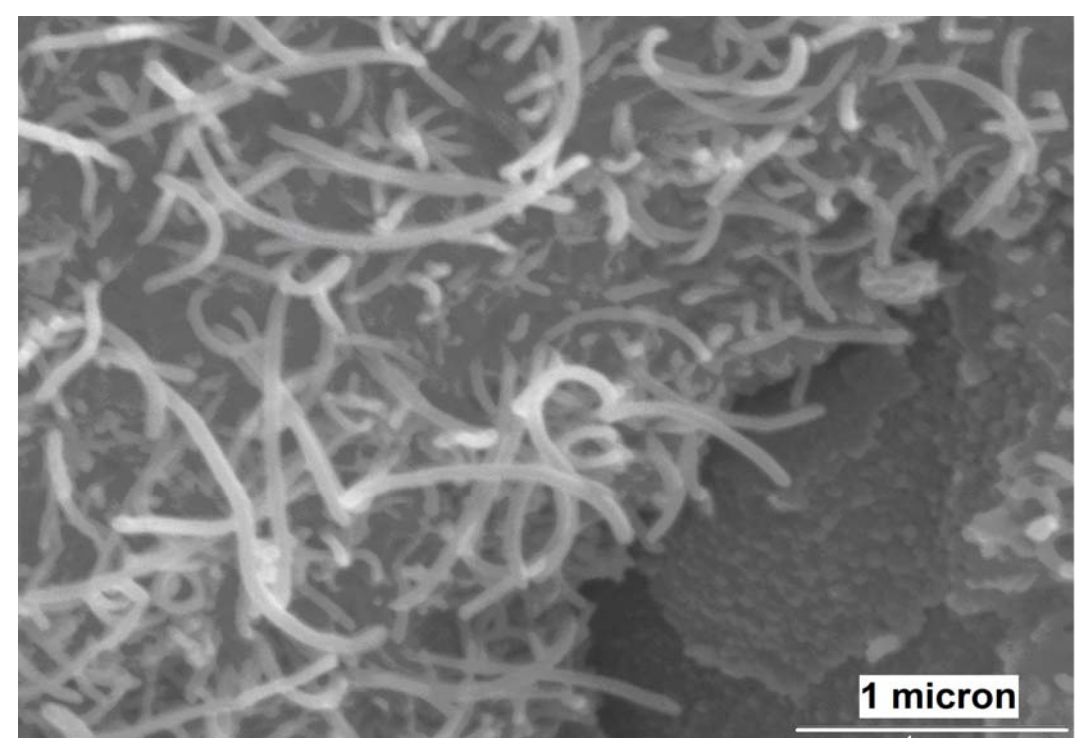
Reinforcement Condition	Mean Compressive Strength (MPa)	Standard Error (MPa)
Plain – Gl	125	17.0
Plain - Adva	129	9.42
Carbon microfiber, 0.24 vol%-(CMF-0.24) - Gl	119	5.69
Carbon microfiber, 0.24 vol%-(CMF-0.24) - Adva	121	10.4
Carbon microfiber, 0.48 vol%-(CMF-0.48) - Gl	138	8.45
Carbon microfiber, 0.48 vol%-(CMF-0.48) - Adva	137	5.44
Carbon microfiber, 0.96 vol%-(CMF-0.96) - Gl	127	17.6
Carbon microfiber, 0.96 vol%-(CMF-0.96) - Adva	128	6.57
Carbon nanofiber, 0.16 vol%-(CNF-OX-0.16) - Gl	129	9.57
Carbon nanofiber, 0.16 vol%-(CNF-OX-0.16) - Adva	129	7.57
Carbon nanofiber, 0.16 vol%-(CNF-PAA-0.16) - Adva	131	7.72
Carbon nanofiber, 0.24 vol%-(CNF-OX-0.24) - Gl	122	15.5
Carbon nanofiber, 0.24 vol%-(CNF-OX-0.24) - Adva	126	5.56
Carbon nanofiber, 0.24 vol%-(CNF-PAA-0.24) - Adva	127	4.75
Carbon microfiber, 0.24 vol%, & Carbon nanofiber, 0.16 vol%-(CMF;CNF-OX) - Gl	132	7.96
Carbon microfiber, 0.24 vol%, & Carbon nanofiber, 0.16 vol%-(CMF;CNF-OX) - Adva	131	1.21
Carbon microfiber, 0.24 vol%, & Carbon nanofiber, 0.16 vol%-(CMF;CNF-PAA) - Adva	133	1.77

Table 12.3- Impact resistance test results for high-performance (DSP) cementitious mortar with nano- and/or micro-scale reinforcement systems.

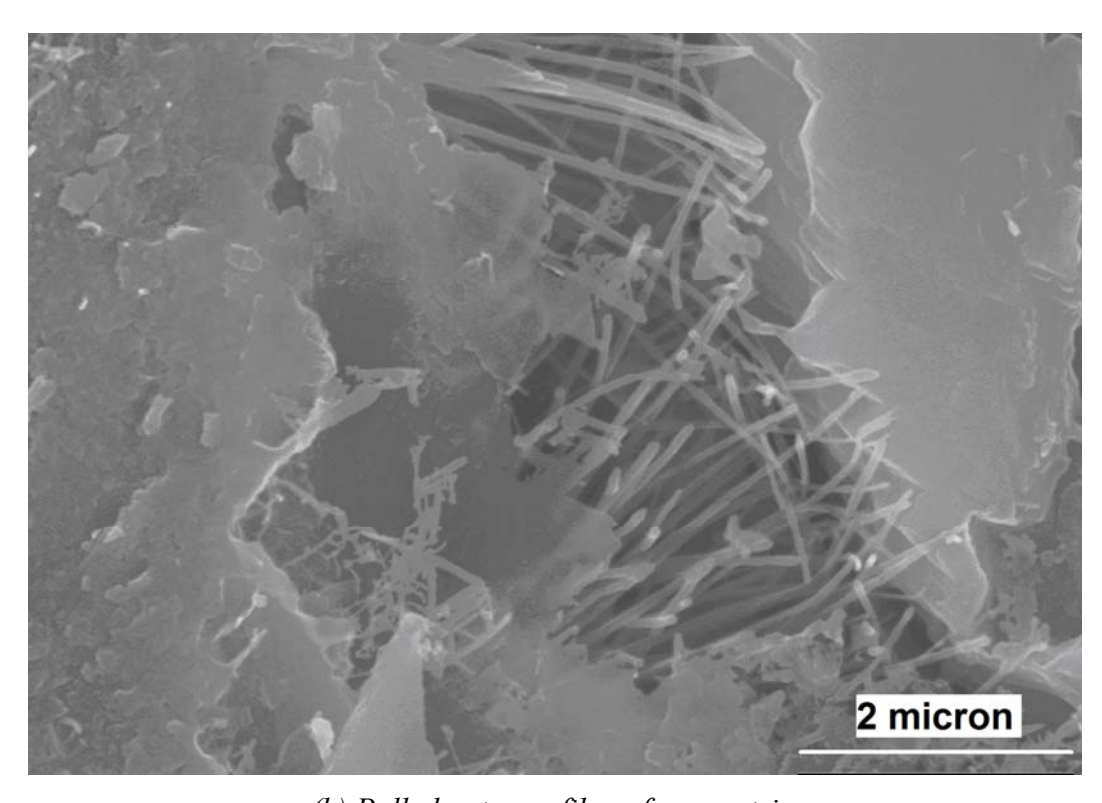
Reinforcement Condition	Impact Resistance
	(mm/mm)
Plain – Gl	0.57
Plain - Adva	0.63
Carbon microfiber, 0.24 vol%-(CMF-0.24) - Gl	0.78
Carbon microfiber, 0.24 vol%-(CMF-0.24) - Adva	0.83
Carbon microfiber, 0.48 vol%-(CMF-0.48) - Gl	0.83
Carbon microfiber, 0.48 vol%-(CMF-0.48) - Adva	0.89
Carbon microfiber, 0.96 vol%-(CMF-0.96) - Gl	0.94
Carbon microfiber, 0.96 vol%-(CMF-0.96) - Adva	0.94
Carbon nanofiber, 0.16 vol%-(CNF-OX-0.16) - Gl	0.89
Carbon nanofiber, 0.16 vol%-(CNF-OX-0.16) - Adva	0.94
Carbon nanofiber, 0.24 vol%-(CNF-OX-0.24) - Gl	0.94
Carbon nanofiber, 0.24 vol%-(CNF-OX-0.24) - Adva	0.99
Carbon microfiber, 0.24 vol%, & Carbon nanofiber, 0.16 vol%-	0.94
(CMF;CNF-OX) - Gl	
Carbon microfiber, 0.24 vol%, & Carbon nanofiber, 0.16 vol%-(CMF;CNF-OX) - Adva	0.99

Table 12.4 - Mean abrasion weight losses of high-performance DSP cementitious mortars with nano- and/or micro-scale reinforcement.

Reinforcement Condition	Loss of Mass
	(grams)
Plain – Gl	1.38
Plain - Adva	1.23
Carbon microfiber, 0.24 vol%-(CMF-0.24) - Gl	0.98
Carbon microfiber, 0.24 vol%-(CMF-0.24) - Adva	0.93
Carbon microfiber, 0.48 vol%-(CMF-0.48) - Gl	0.93
Carbon microfiber, 0.48 vol%-(CMF-0.48) - Adva	0.92
Carbon microfiber, 0.96 vol%-(CMF-0.96) - Gl	0.85
Carbon microfiber, 0.96 vol%-(CMF-0.96) - Adva	0.83
Carbon nanofiber, 0.16 vol%-(CNF-OX-0.16) - Gl	0.88
Carbon nanofiber, 0.16 vol%-(CNF-OX-0.16) - Adva	0.85
Carbon nanofiber, 0.24 vol%-(CNF-OX-0.24) - Gl	0.83
Carbon nanofiber, 0.24 vol%-(CNF-OX-0.24) - Adva	0.80
Carbon microfiber, 0.24 vol%, & Carbon nanofiber, 0.16 vol%-	0.88
(CMF;CNF-OX) - Gl	
Carbon microfiber, 0.24 vol%, & Carbon nanofiber, 0.16 vol%-(CMF;CNF-OX) - Adva	0.80

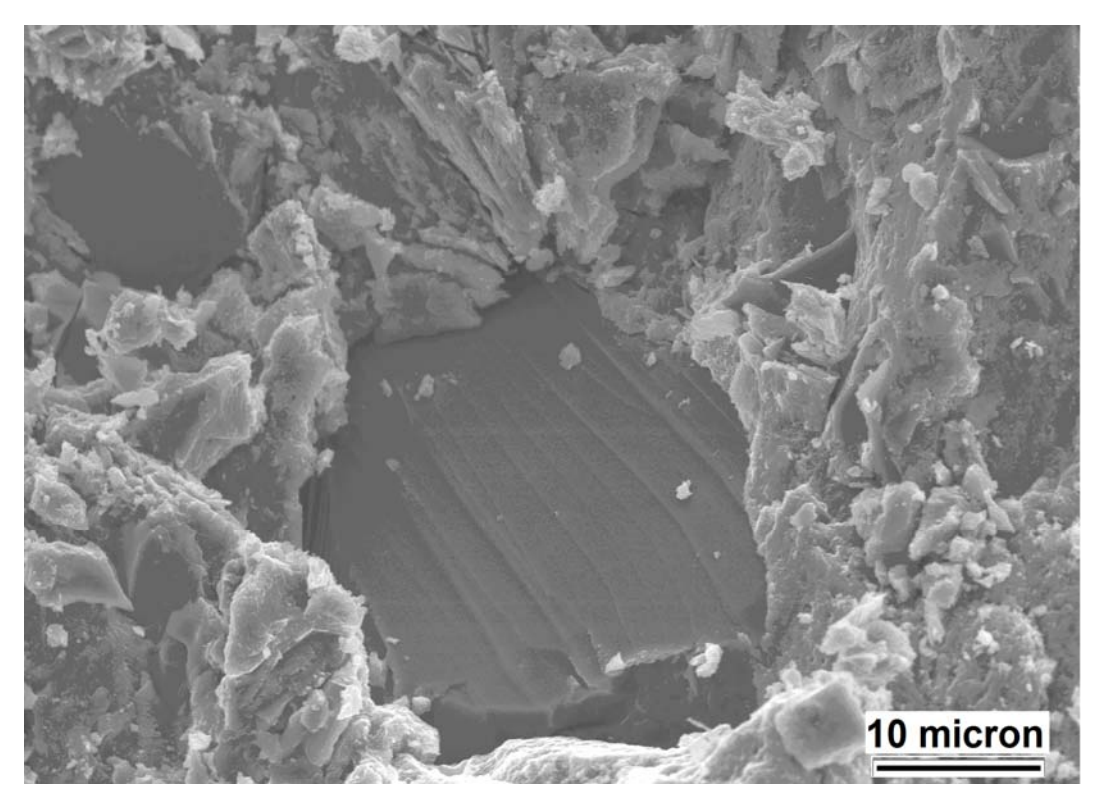


(a) Uniform distribution of nanofibers in the matrix

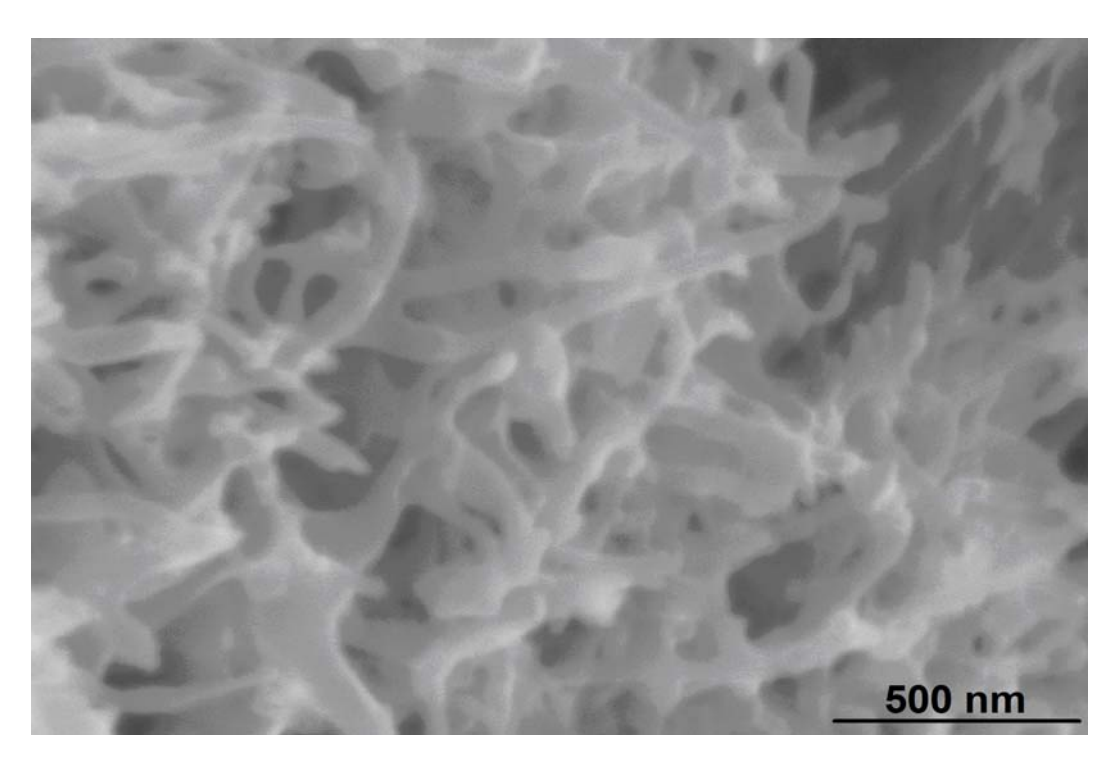


(b) Pulled out nanofibers from matrix

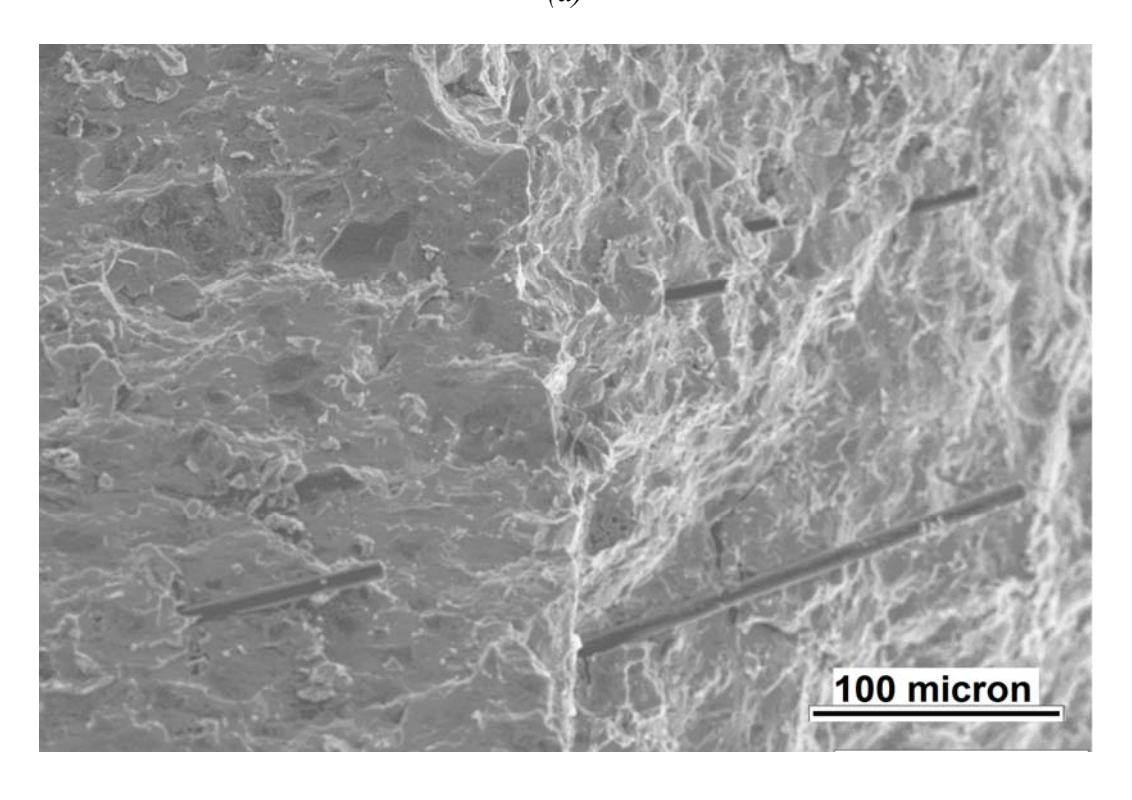
Figure 12.1- Typical SEM images of high-performance cementitious mortar reinforced with different contents of polymer-wrapped or acid-functionalized CNFs.



(c) DSP mortar matrix with embedded sand grain



(a)



(b)

Figure 12.2- Typical SEM images of DSP cementitious materials reinforced with CNFs and/or CMFs.

CHAPTER 13

13 EVALUATION OF REINFORCEMENT EFFICIENCY OF CARBON NANO- AND MICRO-FIBERS IN HIGH-PERFORMANCE CEMENTITIOUS CONCRETE

13.1 General

Advanced technological aspects of cement based materials have recently focused on developing high-performance cementitious composites, which exhibit high compressive strengths. Such composites however, exhibit also extremely brittle failure, low tensile capacity and appear sensitive to early age microcracking as a result of volumetric changes due to high autogenous shrinkage stresses. These characteristics of cement based materials are serious shortcomings that not only impose constrains in structural design, but also affect the long term durability of structures. To overcome the aforementioned disadvantages reinforcement of cementitious materials is typically provided at the millimeter and/or the micro scale using macro-fibers and microfibers, respectively. Cementitious matrices however, exhibit flaws at the nano-scale, where traditional reinforcement is not effective. Graphite Nanomaterials, including carbon nanofibers distinct advantages as a reinforcing material for (CNFs), present several strength/performance cementitious composites as compared to more traditional fibers. First, they exhibit significant greater strength and stiffness than conventional fibers, which should improve overall mechanical behavior. Second, their higher aspect ratio is expected to effectively arrest the nano-cracks and demand significantly higher energy for crack propagation. Thirdly, provided that CNFs are uniformly dispersed, and due to their nano-scale diameter, fiber spacing is

reduced. This has opened a new field for nano-sized reinforcements that should theoretically hinder the formation and later propagation of microcracks at the very beginning. Few attempts have been made to add different graphite nanomaterials as reinforcement in cementitious matrices.

Most of the works involving use of graphite nanomaterials in cementitious matrices have used very fine matrices to evaluate the efficiency of their reinforcement and reported modest gains in some of the engineering properties (Makar and Beaudoin 2004; Cwirzen, Habermehl-Cwirzen et al. 2008; Cwirzen, Habermehl-Cwirzen et al. 2009; Makar and Chan 2009; Metaxa, Konsta-Gdoutos et al. 2009; Metaxa, Konsta-Gdoutos et al. 2010; Li, Wang et al. 2005). A comprehensive approach was taken to evaluate suitably functionalized CNFs in high-performance concrete of higher complexity.

The focus of this research paper is on the use of high-performance (DSP) concrete as the matrix in which the reinforcement efficiency of suitably functionalized CNFs and/ or different microfibers is evaluated. The larger aggregate size and content in concrete, when compared with mortar and paste, adds to complexity of behavior and failure modes by introducing an interfacial zone, generating interactions between aggregates and propagating microcracks, and the need to disperse nanomaterials in the space between aggregates.

Evaluation of the reinforcement efficiency of CNFs in a coarser cementitious matrix, high-performance concrete, was undertaken to see the effect of increased particle size on the interaction of nano-reinforcements with the relatively coarser matrix. This has also highlighted the filler effect and dimensional stability brought about by use coarser aggregates in a well graded matrix. Furthermore, micro-scale fibers along with their hybrid combination with CNFs were evaluated to achieve desired balance of performance and cost efficiency.

Cementitious materials are essentially particulate composites, which are rarely used without aggregates (particulates). Given the micro- to millimeter-scale dimensions of the sand and gravel particles used in DSP concrete, hybrid reinforcements which complement the reinforcing and dimensional stabilizing actions of particulates with multi-scale reinforcement mechanisms could produce particularly positive effects. In the past, the concept of using hybrid (micro- and millimeter-scale) reinforcement has been explored by the concrete industry for achieving balanced gains in material properties (Moranville-Regourd 2001; O'Connell, Boul et al. 2001; Lawler, Zampini et al. 2005; Banthia and Sappakittipakorn 2007).

13.2 Materials and Methods

13.2.1 Graphite Nanomaterials and Microfibers

Different types of acid-functionalized and polyacrylic acid (PAA) physisorbed carbon nanofibers as well as (micro-scale) carbon and polypropylene fibers were evaluated for use in cement-based nanocomposites. These graphite nanomaterials and microfibers have been introduced in detail in Chapter 2, Section 2.4, Fig. 2.3 and Table 2.3. Acid-functionalized and PAA physisorbed CNFs (CNF-OX and CNF-PAA), carbon microfibers (CMF) and polypropylene microfibers (PP) were used in high-performance cement-based concrete matrix.

13.2.2 Cementitious Matrices, Mixing and Curing Procedure

Dense cementitious matrix selected has been introduced in detail in Chapter 2, Section 2.5. DSP concrete was used to evaluate the reinforcement efficiency of both graphite nanomaterials and/ or carbon or polypropylene microfibers at different volume fractions.

Cementitious materials (with and without functionalized graphite nanomaterials dispersed in the mixing water via sonication) and/ or carbon; polypropylene microfibers were prepared and cured following ASTM procedures described in the same section.

13.2.3 Experimental Methods

The test procedures employed to determine the engineering properties of high-performance concrete included compression tests (ASTM C 109), flexure tests (ASTM C 1185), impact tests (ASTM D 7136) and Abrasion tests (ASTM C 944). SEM and EDS were also employed to gain further insight into the structure and failure mechanisms of cement-based nanocomposites. The experimental results were subjected to statistical analysis using the analysis of variance (ANOVA) and pair-wise comparison methods. RSA (Response Surface Analysis) was used to identify reinforcement volume fractions which yield optimum gains in various engineering properties of the cementitious matrix.

13.3 Experimental Results and Discussion

Acid-oxidized (CNF-OX) and Poly-acrylic acid physisorbed (CNF-PAA) CNFs were used as reinforcement at 0.16 vol.%; polypropylene (PP) and carbon microfibers(CMF) were used at 0.24 vol.%. Combinations of polypropylene and carbon microfibers with PAA physisorbed CNFs were also used as hybrid reinforcement for concrete, with PP/ CMF microfibers and CNF-PAA used at 0.24 vol.% and 0.16 vol.%, respectively.

13.3.1 Flexural Performance

The flexural attributes test results for the high-performance concrete reinforced with different volume fractions of CNFs and/or microfibers are summarized in Table 13.1. Significant gains in all flexural performance characteristics of concrete are observed with carbon nanofiber

reinforcement used alone or in combination with microfibers. Polymer wrapping of nanofibers improves their reinforcement efficiency in concrete. The most desired balance of properties for a single reinforcement system was realized with 0.16 vol.% of PAA-physisorbed CNFs (CNF-PAA). The corresponding improvements in flexural strength, energy absorption capacity and maximum deflection versus plain concrete were 20.9%, 134% and 120%, respectively.

The experimental data generated in the past pointed at the positive effects of hybrid (nano- and micro-scale) reinforcement systems in high-performance cementitious materials [Banthia, 2007]. The test data presented here suggest that micro-scale fibers of lower modulus and lower cost (when compared with high-modulus carbon microfiber) could effectively complement the reinforcing effects of polymer-wrapped CNFs in high-performance (DSP) concrete. These lower-modulus microfibers, when used as hybrid reinforcement together with both treated and untreated carbon microfibers, produced balanced gains in the flexural performance attributes of the high-performance (DSP) concrete by interacting with and arresting the cracks developing in matrix at different scales. The hybrid reinforcement of low-modulus polypropylene microfibers with nanofibers produced particularly pronounced gains in the mechanical properties of DSP concrete. The best balance of flexural attributes was realized with the hybrid reinforcement comprising PAA-physisorbed CNFs (0.16 vol.%) and polypropylene microfiber (0.24 vol.%), which produced 35.8%, 644% and 371% rise in the flexural strength, maximum deflection and energy absorption capacity of the high-performance concrete, respectively.

The hybrid reinforcement systems also overcame the adverse effects of microfibers on flexural strength, as reported earlier. The synergistic reinforcing action of nano- and micro-scale reinforcement was further enhanced by polymer wrapping of CNFs. The effectiveness of hybrid reinforcement was also evident for high-modulus carbon microfibers when used with different

PAA-physisorbed CNFs. This hybrid reinforcement resulted in improvement of all engineering properties versus plain matrix and also versus a similar hybrid reinforced materials incorporating untreated CNFs.

The experimental results were subjected to statistical analysis of variance (ANOVA). Due to the large number of observations, ANOVA only gives the general trends in test results. The ANOVA outcomes indicate that there are statistically significant (at 0.05 significance level) improvements in all flexural attributes of high-performance concrete due to the addition of nano-scale and hybrid reinforcement systems. Pair-wise comparisons were carried out in order to assess the statistical significance of the effects associated with the addition of nano- and/or micro-scale reinforcement systems. These results indicate that nano-scale reinforcement systems at 0.16 vol.% produced statistically significant improvements in all flexural attributes of the plain matrix at 0.05 significance level when compared with plain concrete. Both microfibers produced statistically insignificant drops in flexural strength (0.297 and 0.481 significance levels for carbon and polypropylene microfibers, respectively). Pair-wise analysis also pointed at statistically insignificant gains in energy absorption capacity (0.502 significance level) and maximum deflection (0.402 significance level) realized with 0.24 vol.% carbon microfiber. Use of low-modulus polypropylene microfiber as well as high-modulus carbon microfiber in conjunction with different surface functionalized CNFs reversed any negative trends in the effects of individual reinforcement, producing balanced gains in the engineering properties of high-performance (DSP) concrete at significance levels varying form 0.000 to 0.047. The lower values of significance level were only for maximum deflection when carbon microfibers were used in conjunction with CNFs.

13.3.2 Compressive Strength

The compressive strength test results (mean values and standard errors) for high-performance concretes with nano- and/or micro-scale reinforcement systems are presented in Table 13.2. As was the case with DSP paste and mortar, PAA physisorbed CNFs as well as both microfibers produced relatively small and statistically insignificant (at 0.05 significance level) effects on the compressive strength of high-performance concrete.

Outcomes of pair-wise comparisons also indicate the effects of nano- and micro-scale reinforcement systems on compressive strength are not statistically significant (at 0.05 significance level). The use of hybrid reinforcement systems comprising carbon or polypropylene microfiber and carbon nanotubes restored the compressive strengths of DSP concrete by inducing interactions with matrix and its cracks at different scales. The hybrid reinforcement system comprising functionalized CNFs and micro-scale polypropylene fiber produced a small rise in the compressive strength of high-performance concrete.

13.3.3 Impact Resistance

The impact test data are summarized in Table 13.3. All nano- and/or micro-scale reinforcement systems produced improvements in the impact resistance of high-performance concrete. The maximum rise in impact resistance realized with a single reinforcement (69%) was for 0.16 vol.% of CNF-PAA. In the case of micro-scale fibers, polypropylene produced a higher gain (60%) in the impact resistance of high-performance (DSP) concrete.

All hybrid nano- and micro-scale reinforcement systems produced further rise in the mechanical properties of high-performance concrete when compared with individual (nano-or micro-scale) reinforcement used alone. A significant (0.000 significance level) increase in impact resistance

was observed for the hybrid reinforcement comprising polypropylene microfiber with CNF-PAA, which confirms the effectiveness of hybrid reinforcement. The maximum increase in impact resistance (115%) was brought about by hybrid use of 0.16 vol.% of CNF-PAA and 0.24 vol.% of PP microfiber. Outcomes of ANOVA and pair-wise comparisons point at the statistical significant (0.000 to 0.012 significance levels) of nano- and/ or micro-scale reinforcement effects on the impact resistance of high-performance concrete. When compared with high-performance cement paste and mortar (with nano-scale reinforcement), concrete (with nano-scale reinforcement) provides higher levels of impact resistance; this observation points at the well-known contributions of aggregates (in concrete) to the toughness of cementitious matrices.

13.3.4 Abrasion Resistance

The abrasion test results produced for high-performance concrete with different volume fractions of graphite nanomaterials and/ or microfiber reinforcement are summarized in Table 13. 4.

CNF-PAA at 0.16 vol.% produced the greatest improvement (40.0%) in the abrasion resistance of high-performance (DSP) concrete. All nano- and/or micro-scale reinforcement systems produced marked gains in the abrasion resistance of this high-performance concrete matrix, which were statistically significant at 0.05 significance level. Outcomes of pair-wise comparisons confirmed that each of the reinforcement conditions considered here produced statistically significant improvements in the abrasion resistance of high-performance concrete (with significance levels ranging from 0.006 to 0.000).

13.3.5 Response Surface Analysis

The test data on high-performance concrete with nano- and/or micro-scale reinforcement systems was subjected to response surface analysis. The objective of this analysis was to identify

optimum reinforcement conditions which maximize the benefits to specific engineering properties of high-performance concrete. This section presents optimization of concrete nanocomposites for enhancing specific engineering properties, and also for simultaneous enhancement of several engineering properties.

Response surface analysis (RSA) of the test data was conducted considering the volume fractions of nano- and micro-scale reinforcement systems as input variables. Flexural strength, energy absorption capacity, maximum deflection and impact resistance were used as response variables. The RSA process started with evaluating the effects of input variables on response variables, and was followed with desirability analyses considering means of response variables, using both canonical and ridge analyses.

Response Surface analyses conducted for each of the flexural strength, energy absorption capacity, maximum deflection and impact resistance test data indicated that an optimum reinforcement system comprising 0.12 vol.% CNF-PAA and 0.24 vol.% PP microfiber maximizes subject properties. Optimal Response for flexural strength as calculated to be 17.20 MPa with 95% Confidence Interval (16.02, 18.18 MPa), Optimal Response for energy absorption capacity is 482.78 N/mm with 95% Confidence Interval (336.69, 508.86 N.mm), Optimal Response for maximum deflection is 5.101 mm with 95% Confidence Interval (4.79, 5.41 mm), and Optimal Response for maximum impact resistance is 2.90 mm/mm with 95% Confidence Interval (2.75, 3.63 mm/ mm). All stationary points are saddle points which do not give a maximum but a general direction to follow in which targeted properties can be maximized.

The ridge analysis outcomes can be used to adjust the reinforcement condition for achieving further gains in engineering properties, Table 13.5. The analyses for flexural attributes and

impact resistance show that the current hybrid reinforcement is the appropriate combination to maximize these properties of the matrix.

Desirability analysis of test data was also conducted in order to identify reinforcement conditions which yield a desired balance of all the engineering properties considered here. Desirability analyses were conducted using mean values obtained through both canonical and ridge analyses. These outputs indicate that maximum values of all response variables can be achieved with 0.11; 0.12 vol.% CNF-PAA and 0.26; 0.24 vol.% PP microfiber. These values are closer to what is being used as hybrid reinforcement in this high-performance concrete matrix.

13.3.6 Scanning Electron Microscope Observations

Fig. 13.1, shows SEM images of DSP concrete samples. The density of the DSP matrix is apparent in Fig. 13.1a and 13.1b. Fig 13.1a also highlights the positive effective of coarser particles in the matrix like sand and gravel. Fig. 13.1c and 13.1d points at the uniform dispersion of nanotubes and their bridging/pullout actions across a fine (nano-scale) crack within the cementitious matrix. Figs. 13.1e and 13.1f, present evidence of micro-fiber pullout from the matrix. SEM observations of cementitious concrete matrices reinforced with hybrid reinforcement (CNFs and micro-fibers) also indicated that the presence of nanofibers in the matrix around micro-fibers enhanced the interaction of matrix with micro-fibers, (Fig. 13.1f), thus benefiting the gains in matrix performance with hybrid reinforcement. This strong interaction of matrix with micro-fibers was not observed in samples reinforced with only micro-fiber reinforcement. These observations provide some insight into the synergistic action of nanoand micro-scale reinforcement systems in cementitious matrices. All these observations support the results of various engineering properties mentioned in earlier.

13.4 Summary

The experimental results generated for high performance cementitious concrete reinforced with both oxidized and (CNF-OX) PAA physisorbed carbon nanofibers (CNF-PAA), polypropylene (PP) microfibers, carbon microfibers (CMF) and their hybrids casted at various/ optimum volume fractions and with carboxyl-based superplasticizers yield that proper use of nano-scale reinforcement can produce improvements in high-performance concrete mechanical properties which surpass those realized with micro-scale reinforcement. Nano- and micro-scale reinforcement renders complementary reinforcing effects in high-performance concrete; optimum reinforcement systems thus incorporate both nano- and micro-scale reinforcement systems. The experimental results produced using the refined hybrid reinforcement condition, identified through RSA, point at the effectiveness of response surface analysis in identifying the desired reinforcement condition for improving the targeted attributes of a matrix.

Table 13.1- Mean values of flexural attributes of plain high-performance concrete and those reinforced with different nano- and/ or micro-scale reinforcement systems.

Reinforcement Condition	Flexural Strength (MPa)	Deflection (mm)	Energy Absorption (N.mm)
Plain	13.4	0.71	92
Carbon microfiber, 0.24 vol.% (CMF-0.24)	12.8	1.01	111
Polypropylene microfiber, 0.24 vol.% (PP-0.24)	13.0	4.55	383
Carbon nanofiber, 0.16 vol.% (CNF-OX-0.16)	15.4	1.52	193
Carbon nanofiber, 0.16 vol.% (CNF-PAA-0.16)	16.2	1.56	215
Polypropylene microfiber, 0.24 vol.% and Carbon nanofiber, 0.16 vol.% (CNF-OX+PP)	17.4	5.30	400
Polypropylene microfiber, 0.24 vol.% and Carbon nanofiber, 0.16 vol.% (CNF-PAA+PP)	18.2	5.28	433
Carbon microfiber, 0.24 vol.% and Carbon nanofiber, 0.16 vol.% (CNF-OX+CMF)	17.2	1.55	274
Carbon microfiber, 0.24 vol.% and Carbon nanofiber, 0.16 vol.% (CNF-PAA+CMF)	17.5	1.65	269

Table 13.2- Mean values and standard errors of the compressive strength test results for plain DSP concrete and those reinforced with nano- and/ or micro-scale reinforcement systems.

Reinforcement Condition	Mean Compressive Strength (MPa)	Standard Error (MPa)
Plain	151	7.75
Carbon microfiber, 0.24 vol.% (CMF-0.24)	139	13.5
Polypropylene microfiber, 0.24 vol.% (PP-0.24)	137	18.4
Carbon nanofiber, 0.16 vol.% (CNF-OX-0.16)	140	8.75
Carbon nanofiber, 0.16 vol.% (CNF-PAA-0.16)	144	8.23
Polypropylene microfiber, 0.24 vol.% and Carbon	148	12.3
nanofiber, 0.16 vol.% (CNF-OX+PP)		
Polypropylene microfiber, 0.24 vol.% and Carbon	148	4.33
nanofiber, 0.16 vol.% (CNF-PAA+PP)		
Carbon microfiber, 0.24 vol.% and Carbon nanofiber,	150	9.87
0.16 vol.% (CNF-OX+CMF)		
Carbon microfiber, 0.24 vol.% and Carbon nanofiber,	151	13.1
0.16 vol.% (CNF-PAA+CMF)		

Table 13.3- Impact resistance test results for high-performance concrete with and without nano-and/or micro-scale reinforcement.

Reinforcement Condition	Impact Resistance (mm/mm)
Plain	1.50
Carbon microfiber, 0.24 vol.% (CMF-0.24)	1.98
Polypropylene microfiber, 0.24 vol.% (PP-0.24)	2.40
Carbon nanofiber, 0.16 vol.% (CNF-OX-0.16)	2.29
Carbon nanofiber, 0.16 vol.% (CNF-PAA-0.16)	2.32
Polypropylene microfiber, 0.24 vol.% and Carbon nanofiber, 0.16 vol.% (CNF-OX+PP)	3.25
Polypropylene microfiber, 0.24 vol.% and Carbon nanofiber, 0.16 vol.% (CNF-PAA+PP)	3.26
Carbon microfiber, 0.24 vol.% and Carbon nanofiber, 0.16 vol.% (CNF-OX+CMF)	2.35
Carbon microfiber, 0.24 vol.% and Carbon nanofiber, 0.16 vol.% (CNF-PAA+CMF)	2.35

Table 13.4- Mean abrasion weight losses of DSP concretes with and without nano- and/ or micro-scale reinforcement systems.

Reinforcement Condition	Loss of
	Mass
	(grams)
Plain	1.50
Carbon microfiber, 0.24 vol.% (CMF-0.24)	1.15
Polypropylene microfiber, 0.24 vol.% (PP-0.24)	1.05
Carbon nanofiber, 0.16 vol.% (CNF-OX-0.16)	0.97
Carbon nanofiber, 0.16 vol.% (CNF-PAA-0.16)	0.98
Polypropylene microfiber, 0.24 vol.% and Carbon nanofiber, 0.16 vol.% (CNF-OX+PP)	0.99
Polypropylene microfiber, 0.24 vol.% and Carbon nanofiber, 0.16 vol.% (CNF-PAA+PP)	0.99
Carbon microfiber, 0.24 vol.% and Carbon nanofiber, 0.16 vol.% (CNF-OX+CMF)	1.00
Carbon microfiber, 0.24 vol.% and Carbon nanofiber, 0.16 vol.% (CNF-PAA+CMF)	1.01

Table 13.5- Outcomes of Ridge analysis of the flexural attributes and impact resistance test data for high performance concrete with nano- and/or micro-scale reinforcement.

(a) Flexural Strength

Coded Radius	Estimated	95.00% Co	onfidence Inter	val Uncoded Fac	tor Value
	Response	Upper	Lower	CNF-PAA	PP
0.000	15.604	15.024	16.183	0.080	0.120
0.100	15.847	15.264	16.429	0.088	0.123
0.200	16.093	15.502	16.684	0.095	0.127
0.300	16.344	15.739	16.949	0.103	0.131
0.400	16.600	15.976	17.225	0.110	0.136
0.500	16.861	16.212	17.511	0.111	0.141
0.600	17.128	16.449	17.807	0.112	0.147
0.700	17.400	16.686	18.115	0.113	0.152
0.800	17.678	16.924	18.433	0.116	0.208
0.900	17.963	17.164	18.762	0.118	0.225
1.000	18.253	17.404	19.103	0.120	0.240

(b) Energy Absorption Capacity

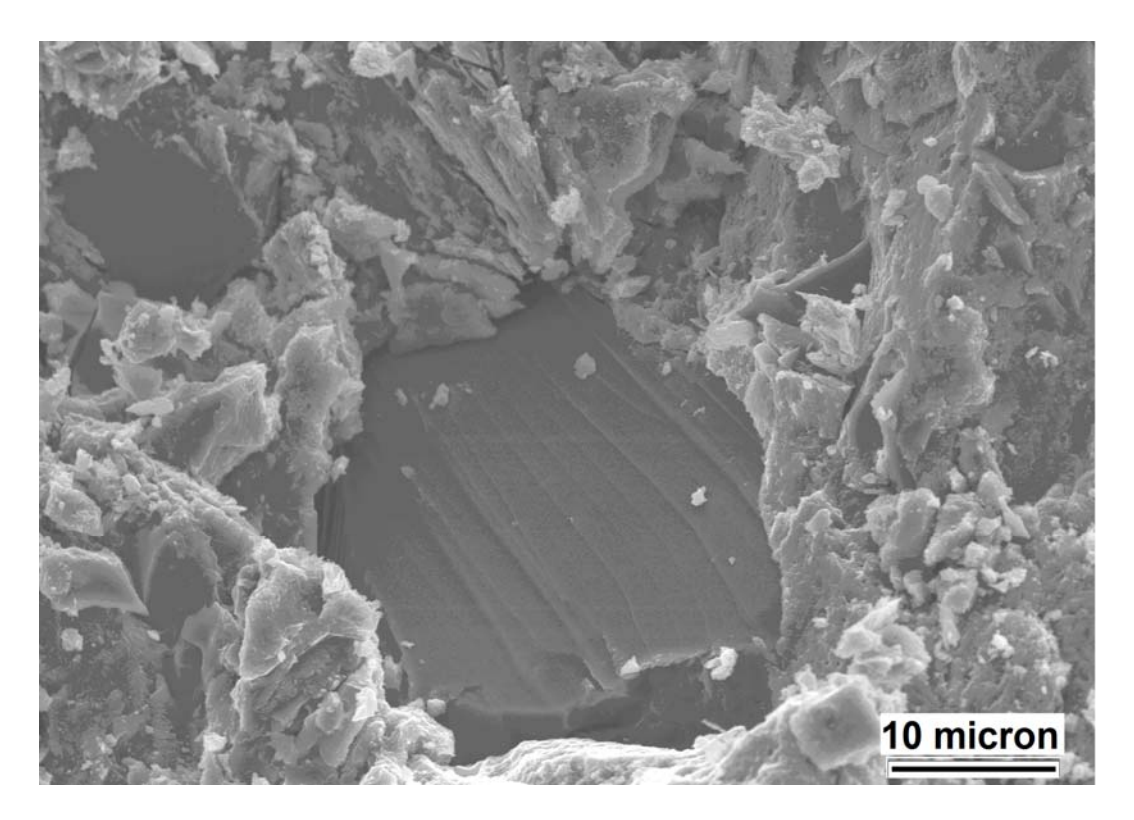
Coded Radius	Estimated	95.00% Co	nfidence Inter	val Uncoded Fac	tor Values
	Response	Upper	Lower	CNF-PAA	PP
0.000	282.779	256.693	308.865	0.080	0.120
0.100	295.584	269.367	321.800	0.082	0.132
0.200	308.239	281.635	334.843	0.084	0.143
0.300	320.761	293.521	348.000	0.086	0.155
0.400	333.167	305.059	361.276	0.087	0.167
0.500	345.477	316.288	374.667	0.087	0.179
0.600	357.712	327.254	388.171	0.098	0.191
0.700	369.893	338.003	401.783	0.108	0.203
0.800	382.042	348.582	415.501	0.117	0.215
0.900	394.181	359.037	429.326	0.0119	0.228
1.000	406.334	369.406	443.263	0.120	0.240

(c) Maximum Deflection

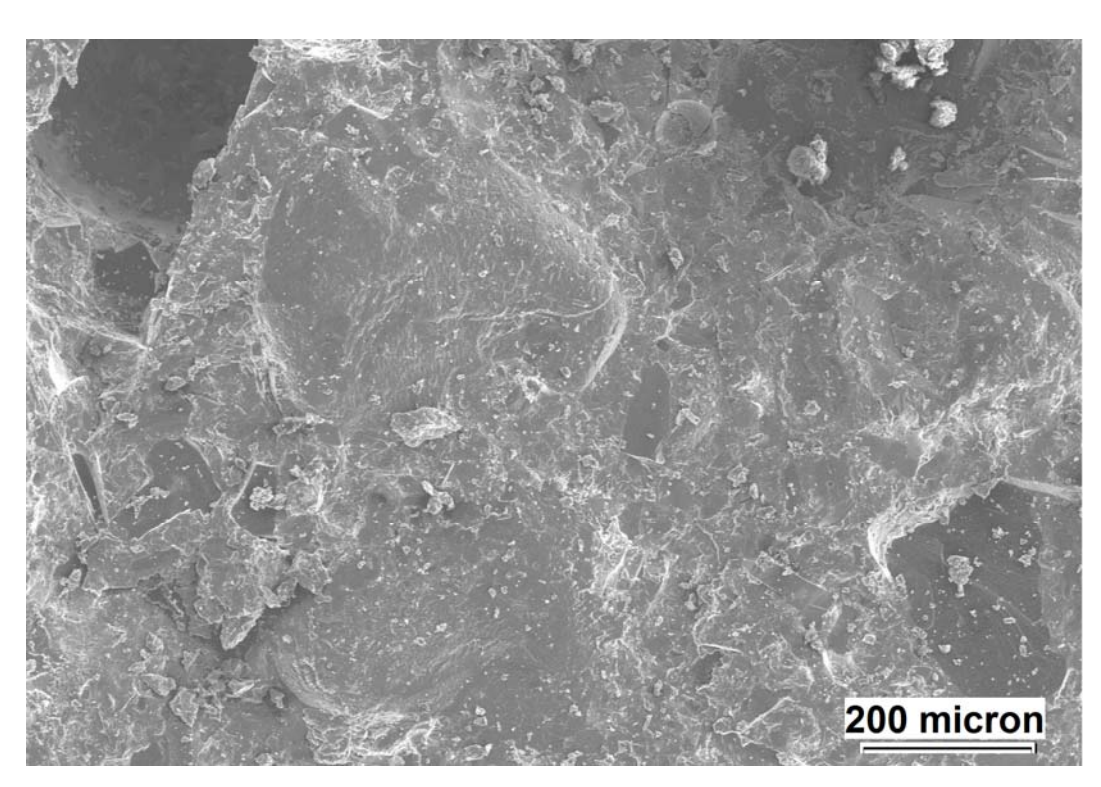
Ridge Analysis for Maximizing Maximum Deflection Coded Radius Estimated 95.00% Confidence Interval Uncoded Factor Values Response Upper Lower **CNF-PAA** PP 2.793 3.101 0.0003.408 0.080 0.120 0.100 3.296 2.987 3.605 0.082 0.132 0.200 3.492 3.178 3.805 0.083 0.143 0.300 3.687 0.085 0.155 3.366 4.008 4.213 0.167 0.400 3.882 3.551 0.086 0.500 4.076 3.733 4.420 0.088 0.179 0.089 0.191 0.6004.271 3.912 4.630 0.700 4.089 0.091 0.202 4.465 4.841 0.800 4.659 5.054 0.092 0.214 4.264 0.900 4.853 4.437 0.109 0.226 5.268 1.000 0.119 0.238 5.046 4.608 5.484

(d) Impact Resistance

Ridge Analysis for Maximizing Impact Resistance					
Coded Radiu	s Estimated	95.00% Conf	idence Interval	Uncoded Factor	· Values
	Response	Upper	Lower	CNTF-PAA	PP
0.000	2.500	2.375	2.625	0.080	0.120
0.100	2.567	2.441	2.693	0.086	0.127
0.200	2.633	2.506	2.761	0.092	0.135
0.300	2.700	2.569	2.831	0.099	0.142
0.400	2.767	2.631	2.902	0.105	0.150
0.500	2.833	2.693	2.974	0.111	0.157
0.600	2.900	2.752	3.048	0.117	0.165
0.700	2.967	2.811	3.123	0.124	0.172
0.800	3.034	2.868	3.199	0.130	0.180
0.900	3.100	2.925	3.276	0.136	0.227
1.000	3.167	2.979	3.355	0.120	0.240

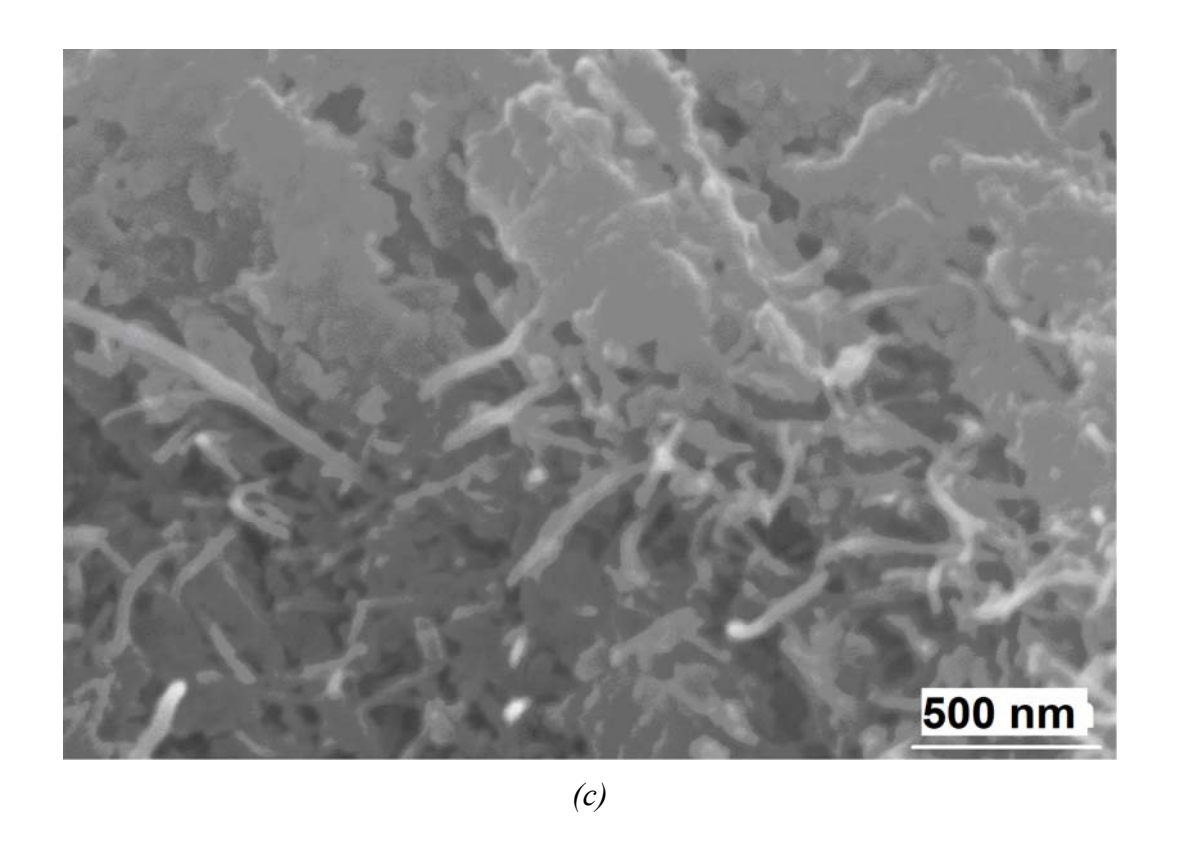


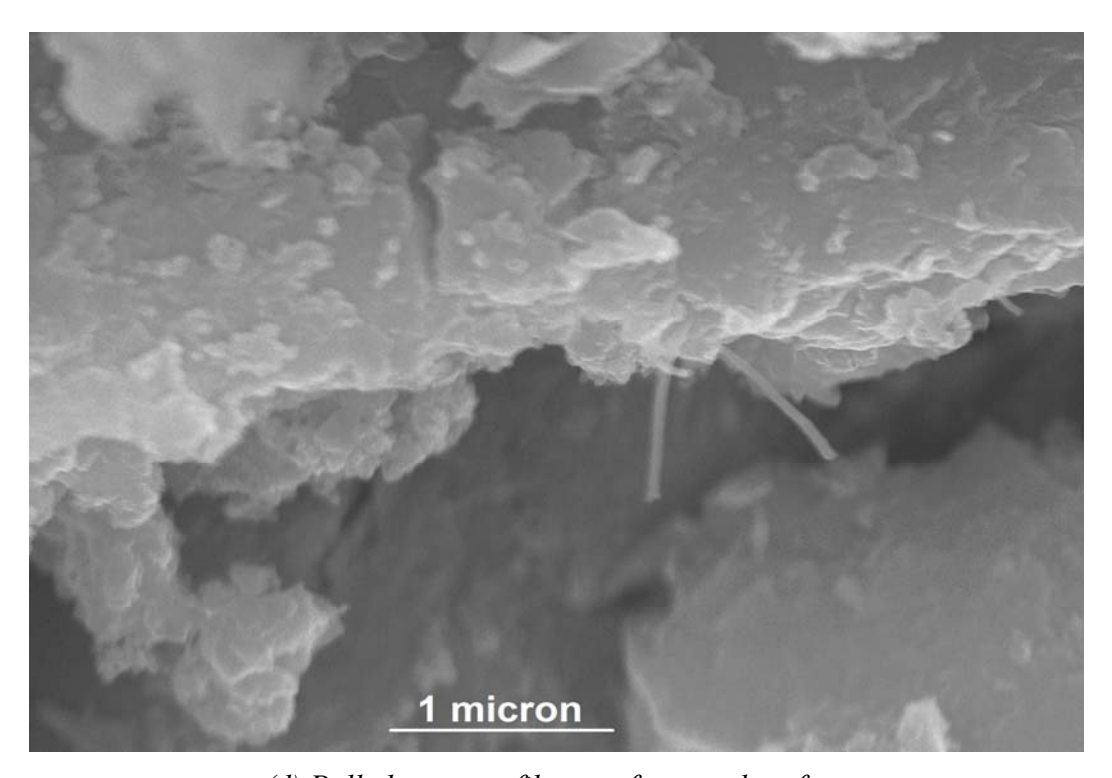
(a) Crack deflection around sand particle



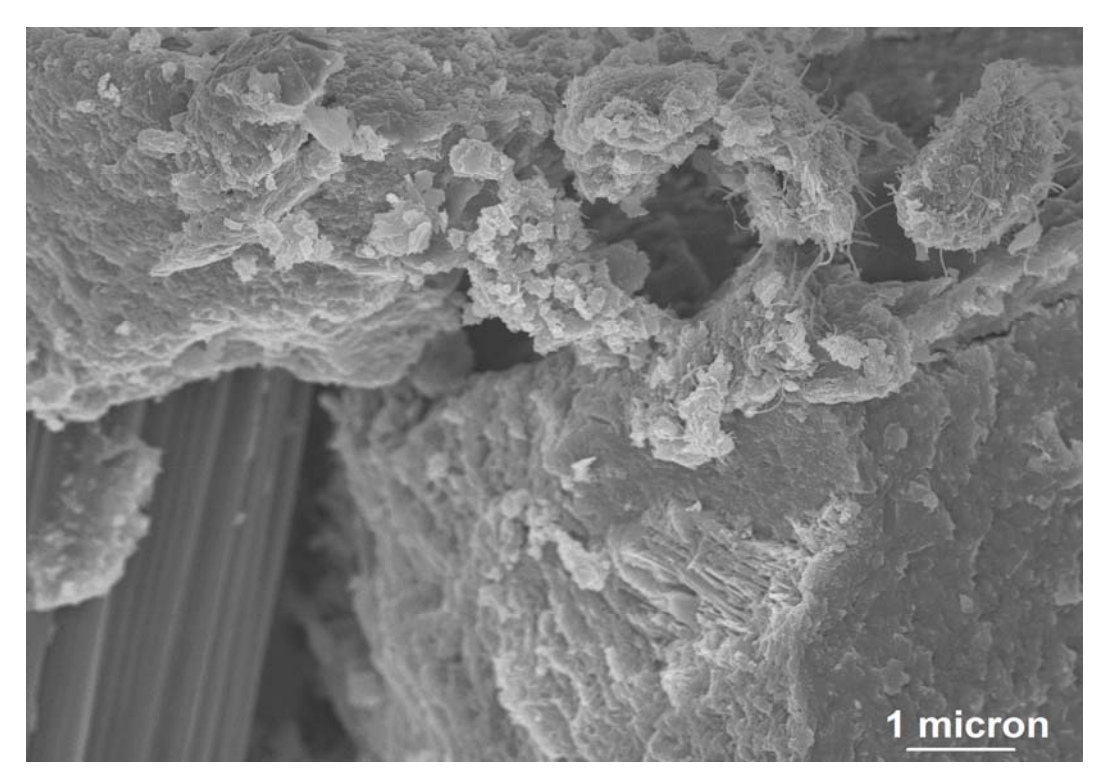
(b) Dense structure of paste

Figure 13.1- SEM images of fractured surfaces of high performance concrete.

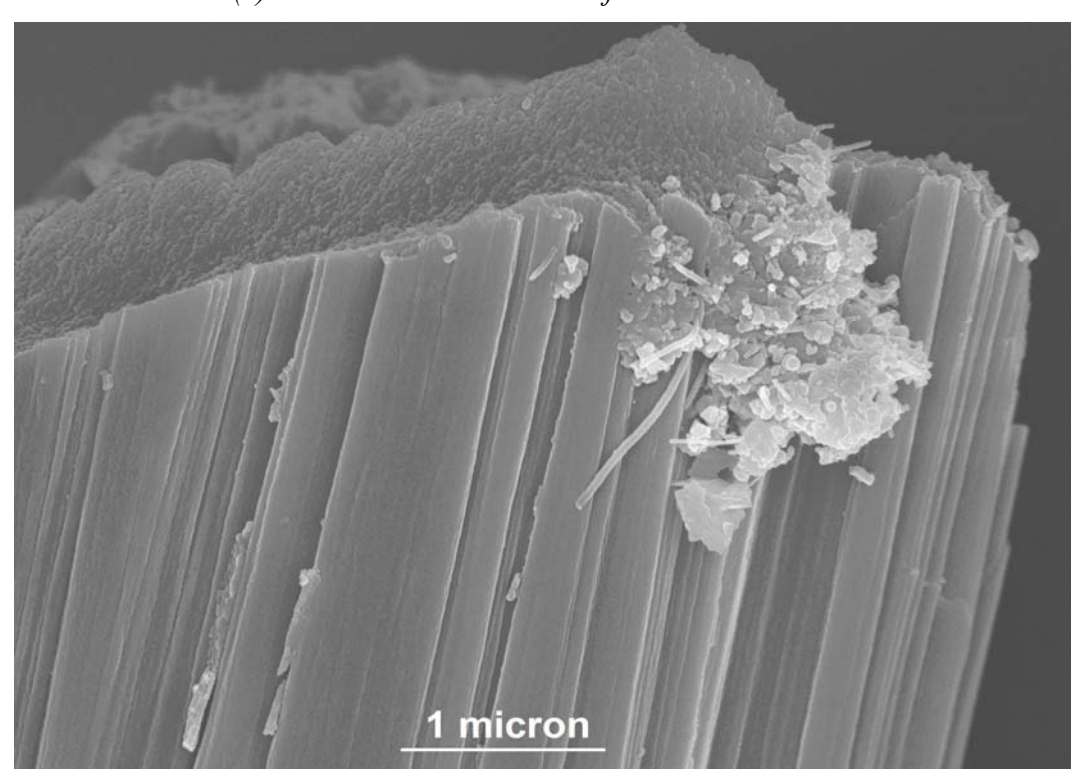




(d) Pulled out nanofibers at fractured surface



(e) Carbon nano- and micro-fibers in the matrix



(f) CNFs interacting with carbon microfibers

CHAPTER 14

14 GRAPHITE NANOPLATELETS IN HIGH PERFORMANCE MATRICES

14.1 General

Fibers are incorporated into cementitious matrices to overcome these weaknesses, producing materials with increased tensile strength, ductility, and toughness and improved durability. However, cracking in cement-based materials starts at the nano-scale level, where traditional reinforcement is not effective. The introduction of graphite nanomaterials has opened a new field for nano-sized reinforcement that should hinder the formation and propagation of nano-cracks and improve abrasion and impact resistance of the matrix. Previous research by the authors of this work on reinforcing cementitious materials with multiwall carbon nanotubes (MWNTs) and carbon nanofibers (CNFs) has shown that all major engineering properties as well as durability of high-performance cementitious matrices can be significantly increased by adding very low concentrations of homogeneously dispersed carbon nanotubes and carbon nanofibers (as little as 0.04% by weight of cement). However, higher costs of these nanomaterials sometimes become a hindrance in their effective use in cement-based matrices. One objective of this study is to examine whether exfoliated graphite nanoplatelets (GP) can have similar beneficial effects as a reinforcing material for cementitious matrices.

Graphite nanoplatelets (Fig. 2.3g) are obtained by exfoliation of natural graphite; their thickness can be controlled in a range from 1 to 25 nm (with about 0.5 nm thickness of each grapheme layer), and their diameter from the sub-micron level to tens of microns. Graphite, in its basal

plane, offers elastic modulus of 1,060 GPa, thermal conductivity of 250 W/m.K, and electrical resistivity of $4x10^{-5}$ Ω .cm (Kalaitzidou, Fukushima et al. 2007; Kalaitzidou, Fukushima et al. 2007; Li, Sham et al. 2007). Stress concentrations at the rough edges of graphite nanoplatelets lower their tensile strength below that of carbon nanotubes.

GP appear extremely promising in opening new avenues in the field of nanocomposites. Research efforts have concentrated on developing GP–polymer composites (Ping, Beaudoin et al. 1991; Song, Jang et al. 2007; Pfeifer, Moeser et al. 2009). The investigation of graphite nanomaterials/concrete composites is at a relatively novel stage, and no authentic work regarding the effectiveness of GP in enhancing the engineering properties of concrete has been published. To develop high-performance nanoplatelet–cement nanocomposites, a homogeneous dispersion of the nanoplatelets in cementitious matrices must be achieved (Ahlborn, Harris et al. 2011). In addition, a strong bond between the nano-reinforcement and the matrix will allow efficient load transfer.

In this study, the effects of pristine graphite nanoplatelets (GP) and PAA physisorbed graphite nanoplatelets (GP-PAA) are use of refined dispersion techniques on the reinforcement efficiency of nanotubes at different volume fractions within a high-performance cementitious (DSP) matrices were evaluated. Scanning electron microscope observations of fractured surfaces pointed at successful dispersion of nanofibers within the cement-based matrix. An investigation of hybrid reinforcement systems comprising GP and micro-scale fibers carbon (CMF) and polypropylene (PP) indicated that selected hybrid systems offer a cost-effective approach for realizing balanced gains in performance characteristics of high-performance cementitious matrices.

14.2 Materials and Methods

14.2.1 Graphite Nanomaterials and Microfibers

Both pristine (GP) and Polyacrylic acid physisorbed graphite nanoplatelets (GP-PAA), carbon microfibers (CMF) and polypropylene microfibers (PP) at different volume fractions were used in different DSP matrices. These graphite nanomaterials and microfibers have been introduced in detail in Chapter 2, Section 2.4, Fig. 2.3 and Table 2.3.

14.2.2 Cementitious Matrices, Mixing and Curing Procedure

Dense cementitious matrices selected have been introduced in detail in Chapter 2, Section 2.5.1 and Table 2.4. DSP paste, mortar and concrete were used to evaluate the reinforcement efficiency of both graphite nanoplatelets and different microfibers at different volume fractions.

Cementitious materials (with and without functionalized graphite nanomaterials dispersed in the mixing water via sonication) and/ or carbon and polypropylene microfibers were prepared and cured following ASTM procedures described in Chapter 2, Section 2.5.2.

14.2.3 Experimental Methods

The test procedures employed to determine the engineering properties of high-performance matrices included compression tests (ASTM C 109), flexure tests (ASTM C 1185), impact tests (ASTM D 7136) and Abrasion tests (ASTM C 944). SEM and EDS were also employed to gain further insight into the structure and failure mechanisms of cement-based nanocomposites. The experimental results were subjected to statistical analysis using the analysis of variance (ANOVA) and pair-wise comparison methods.

14.3 Experimental Results and Discussion

14.3.1 Effects of Graphite Platelets and Carbon Microfibers on Engineering Properties of DSP Paste

14.3.1.1 Flexural Performance

The flexure test data are summarized in Table 14.1. GPs, CMFs, and especially their combination (hybrid reinforcement) produce important gains in the flexural strength, energy absorption capacity and maximum deflection of DSP cementitious pastes. The hybrid reinforcement system yields 61.7%, 366% and 264% gains in flexural strength, energy absorption capacity and maximum deflection of cementitious pastes. The ANOVA outcomes confirm the statistical significance (at significance level, p, of 0.000) of the contributions of nanoplatelet and microfiber reinforcement to the flexural performance of DSP pastes.

14.3.1.2 Compressive Strength

The compressive strength test results for DSP pastes with graphite nanoplatelet and/or carbon microfiber reinforcement are summarized in Table 14.2. GPs seem to produce a minor (statistically insignificant) loss of compressive strength. This could be attributed to their planar (flaky) geometry and micro-scale planar dimension, which could produce local stress rise. The ANOVA outputs indicate that reinforcement with graphite nanoplatelet and/or carbon microfiber has statistically insignificant effects (significant level, p, of 0.482).

14.3.1.3 Impact Resistance

The impact resistance test results presented in Table 14.3 and point at the desirable effects of carbon microfibers and especially graphite nanoplatelets and hybrid reinforcement systems. The impact resistance of DSP paste increases by 42.7%, 114% and 158% with carbon microfiber,

graphite nanoplatelet and hybrid reinforcement. The ANOVA outcomes also point at the statistical significance of the graphite nanoplatelet and/or carbon microfiber reinforcement effects on the impact resistance of DSP paste (at a significance level, p, of 0.001). The high effectiveness of graphite nanoplatelets in enhancing the impact resistance of cementitious paste is somewhat surprising given their flaky geometry. Fig. 14.1 shows scanning electron microscope images of the failed surfaces of impact specimens reinforced with graphite nanoplatelets. It seems that the layered structure of nanoplatelets have undergone some level of delamination while their exterior surfaces interacting with microcracks propagating in the cementitious matrix under impact loads.

14.3.1.4 Abrasion Resistance

The abrasion resistance test results presented in Table 14.4 and indicate that graphite nanoplatelet and/or carbon microfiber reinforcement of cementitious pastes produce improvements in the abrasion resistance of plain DSP paste. The abrasion resistance of DSP paste increases by 45.5%, 58.9% and 56.4% with carbon microfiber, graphite nanoplatelet and hybrid reinforcement.

The ANOVA outcomes point at the statistical significance of the contributions of graphite nanoplatelet and/or carbon microfiber reinforcement to the abrasion resistance of DSP cementitious pastes.

14.3.2 Effects of Graphite Platelets and Carbon Microfibers on Engineering Properties of DSP Mortar

Different reinforcement systems comprising PAA-physisorbed graphite nanoplatelets (GP-PAA) and carbon fibers (CMF) with micro-scale diameter were evaluated in DSP mortar. Exploratory

studies with different graphite nanomaterial reinforcement indicated that, for the cementitious matrix and processing conditions considered here, the GP-PAA volume fraction should be lowered below 0.24 vol.% before benefits can be realized from introduction of carbon microfibers. Hence, a graphite nanoplatelet volume fraction of 0.16 vol.% was considered for development of hybrid reinforcement systems.

14.3.2.1 Flexural Performance

The flexural strength, maximum deflection and energy absorption capacity test results for the high-performance (DSP) cementitious mortar reinforced with different volume fractions of PAAphysisorbed graphite nanoplatelets and/ or microfibers are presented in Table 14.5. These results indicate that all the reinforcement conditions considered here produce improvements in flexural strength, maximum deflection and energy absorption capacity of the high-performance (DSP) cementitious plain mortar matrix. For single reinforcement condition, a highly desired balance of flexural qualities was produced at 0.16 vol. % of GP-PAA and 0.96 vol.% of CMF. The improvements in the flexural strength, energy absorption capacity and maximum deflection of DSP mortar realized with 0.16 vol.% of GP-PAA were 3.6%, 13% and 64%), respectively. The improvements in flexural strength, maximum deflection and energy absorption capacity with addition of 0.96 vol.% of carbon microfibers were 39%, 119% and 156%, respectively. The comparatively lesser improvement in all flexural attributes with use of GP-PAA is expected due to morphology and physical characteristics of GP-PAA. The experimental results also indicate that hybrid (nano- and micro-scale) reinforcement systems produce desired effects, which point at the complementary role of reinforcement systems operating at different length scales.

Due to large number of observations, application of analysis of variance (ANOVA) to test results only reveals general trends. The analysis of variance of test results was followed by pair-wise

comparisons. The key findings of pair-wise comparisons are summarized below. The comparisons indicate that reinforcement systems using GP-PAA alone or with CMF did not produce improvement in all flexural attributes of the plain matrix. However CMF, when used alone, did produce improvements in all flexural attributes at a high significance (p) levels ranging from 0.042 to 0.000, at different volume fractions.

14.3.2.2 Compressive Strength

The compressive strength test results (mean values and standard errors) for DSP cementitious mortars with nano- and/or micro-scale reinforcement systems are presented in Table 14.6. As was the case with DSP paste, carbon nano- and/or micro-scale reinforcement of DSP mortar produces small and statistically insignificant (0.755 significance level) effects on compressive strength; pair-wise comparisons, however, indicate GP-PAA (and hybrid reinforcement systems incorporating GP-PAA/ CMF) tend to have statistically significant (but still small) adverse effects on the compressive strength of DSP mortar, varying from 0.051 to 0.07.

14.3.2.3 Impact Resistance

The impact resistance test data are summarized in Table 14.8. GP-PAA at 0.16 and 0.24 vol.% improve the impact resistance of DSP mortar by 99%; 109%. Micro-scale carbon fibers reinforcement at 0.24, 0.48 and 0.96 vol% increases the impact resistance of DSP mortar by 36%, 46% and 64%, respectively. All hybrid (nano- and micro-scale) reinforcement systems also produced improvements in impact resistance when compared with their corresponding case with micro-scale reinforcement alone. ANOVA outcomes and pair wise comparison point at the statistical significance (p=0.002) of nano- and/or micro-scale reinforcement effects on the impact resistance of DSP mortar. When compared with DSP paste with nano-scale reinforcement, DSP mortar with nano-scale reinforcement provides higher levels of impact resistance. DSP mortars

reinforced with different volume fractions of GP-PAA generally provided particularly high levels of impact resistance due to their platy morphology and physical attributes (which was not the case for flexural performance and compressive strength).

14.3.2.4 Abrasion Resistance

The abrasion test results performed on DSP mortar with different carbon nano- and/or microscale reinforcement are summarized in Table 14.8. At equal volume fractions, GP-PAA and its hybrid combination with carbon microfiber produced the lesser improvement in the abrasion resistance of DSP mortar when compared with CMF. However, all nano- and/or micro-scale reinforcement conditions produced marked improvements in the abrasion resistance of DSP mortar, which were statistically significant (p = 0.007). Detailed pair-wise comparisons of test results confirmed that improvements in abrasion resistance with nano- and/or micro-scale reinforcement (versus plain DSP mortar) were statistically significant at 0.042 to 0.000 significance levels.

14.3.3 Effects of Graphite Platelets and Different Microfibers on Engineering Properties of DSP Concrete

Different reinforcement systems comprising PAA-physisorbed graphite nanoplatelets (GP-PAA), carbon fibers (CMF) and polypropylene fibers (PP) with micro-scale diameter were evaluated in DSP concrete, at different volume fractions.

14.3.3.1 Flexural Performance

The flexural strength, maximum deflection and energy absorption capacity test results for the high-performance (DSP) concrete reinforced with different volume fractions of PAA-physisorbed graphite nanoplatelets and/or microfibers, prepared using ADVA® Cast 575

superplasticizer, are summarized in Table 14.9. These test results indicate that all reinforcement systems produced gains in all flexural attributes considered here, except for the two microfibers which lowered the flexural strength of concrete when used alone. The most desired balance of properties for a single reinforcement was realized by the addition of 0.16 vol.% of GP-PAA. The corresponding improvements in flexural strength, energy absorption capacity and maximum deflection with respect to plain concrete were 10.5%, 97% and 76%, respectively. Test results also indicate that the addition of each of the microfibers to this (relatively brittle) high-performance (DSP) concrete produced important gains in two out of the three flexural attributes considered here (maximum deflection and energy absorption capacity), while causing a relatively small drop in the flexural strength. PP microfiber produced the maximum rise in energy absorption capacity (315%) and maximum deflection (550%).

The test data generated in the past pointed at the positive effects of hybrid (nano- and micro-scale) reinforcement systems in high-performance cementitious materials. The test data presented here suggest that micro-scale fibers of lower modulus and lower cost (when compared with carbon microfiber) could effectively complement the beneficial effects of graphite nanoplatelets in high-performance (DSP) concrete. These lower-modulus microfibers, when used together with different graphite nanoplatelets as hybrid reinforcement, produced balanced gains in the flexural performance characteristics of high-performance (DSP) concrete by interacting with and arresting cracks which developed in matrix at different scales. The hybrid reinforcement comprising low-modulus polypropylene microfibers with different graphite nanomaterials produced particularly pronounced gains in the mechanical properties of DSP concrete. The best balance of flexural attributes was produced by the hybrid reinforcement comprising GP-PAA (0.16 vol.%) and PP (0.24 vol.%), which produced a 15%, 573% and

329% rise in flexural strength, maximum deflection and energy absorption capacity, respectively. Hybrid reinforcement systems also overcame the adverse effects of microfibers on flexural strength. The synergistic reinforcement actions of nano- and micro-scale reinforcement systems point at the merits of multi-scale reinforcement in high-performance concrete. This effectiveness of hybrid reinforcement was also evident in the case of high-modulus carbon microfibers used together with different graphite nanomaterials. This hybrid reinforcement produced improvements in all the engineering properties of high-performance concrete when compared with plain concrete and also that reinforced with CMFs alone.

The experimental results were subjected to statistical analysis of variance (ANOVA). Due to the large number of observations, ANOVA only gives the general trends in test results. Pair-wise comparisons were carried out in order to assess the statistical significance of the effects associated with the addition of GP-PAA- and/or micro-scale reinforcement systems. These results indicate that GP-PAA only produced statistically insignificant gains in maximum deflection (0.158 significance level) when compared with plain concrete. Both microfibers produced statistically insignificant drops in flexural Strength (0.297 and 0.481 significance levels for carbon and polypropylene microfibers, respectively). Pair-wise analysis also pointed at statistically insignificant gains in energy absorption capacity (0.502 significance level) and maximum deflection (0.402 significance level) realized with 0.24 vol.% carbon microfiber. Use of low-modulus PP microfiber as well as high-modulus CMFs in conjunction with GP-PAA reversed any negative trends in the effects of individual reinforcement, producing balanced gains in the engineering properties of high-performance (DSP) concrete at significance levels varying form0.000 to 0.047. The lower values of significance level were only for maximum deflection when CMFs were used in conjunction with GP-PAA.

14.3.3.2 Compressive Strength

The compressive strength test results (mean values and standard errors) for high-performance (DSP) concretes with GP-PAA- and/or different micro-scale reinforcement systems are presented in Table 14.10. As was the case with DSP paste and mortar, GP-PAA as well as both microfibers produced relatively small and statistically insignificant (at 0.05 significance level) effects on the compressive strength of DSP concrete.

Outcomes of pair-wise comparisons also indicate that, except for GP-PAA (0.003 significance level), the effects of micro-scale reinforcement systems on compressive strength are not statistically significant (at 0.05 significance level). The adverse effects of GP-PAA on compressive strength were also observed in DSP paste and mortar, and can be attributed to the planar geometry and probably agglomeration of graphite nanoplatelets. The combination of GP-PAA and PP or CMF mitigated this adverse effect. This is due to interactions of reinforcements with matrix and its cracks at different scales.

14.3.3.3 Impact Resistance

The impact test data are summarized in Table 14.11. All GP-PAA- and/or micro-scale reinforcement systems produced improvements in the impact resistance of plain high-performance concrete matrix. The maximum rise in impact resistance realized with GP-PAA reinforcement (46%) was for 0.16 vol.% of GP-PAA. In the case of micro-scale fibers, PP produced a gain of 60% in the impact resistance of high-performance (DSP) concrete at 0.24 vol.%.

All hybrid GP-PAA- and micro-scale reinforcement systems produced further rise in the mechanical properties of high-performance concrete when compared with individual (nano-or

micro-scale) reinforcement used alone. A significant (0.000 significance level) increase in impact resistance was observed for the hybrid reinforcement comprising PP microfiber with GP-PAA, which confirms the effectiveness of hybrid reinforcement. The maximum increase in impact resistance (106%) was brought about by 0.16 vol.% of GP-PAA and 0.24 vol.% of PP microfiber. Outcomes of ANOVA and pair-wise comparisons point at statistical significant (0.000 to 0.012 significance levels) effects on the impact resistance of high-performance concrete due to addition of GP-PAA- and/ or micro-scale reinforcements. When compared with high-performance cement paste and mortar (with nano-scale reinforcement), concrete (with nano-scale reinforcement) provides higher levels of impact resistance; this observation points at the well-known contributions of aggregates (in concrete) to the toughness of cementitious pastes.

14.3.3.4 Abrasion Resistance

The abrasion test results produced for DSP concrete with different volume fractions of GP-PAA and/ or different microfiber reinforcement are summarized in Table 14.12.

All GP-PAA- and/or micro-scale reinforcement systems, using in conjunction with the ADVA® Cast 575 superplasticizer, produced marked gains in the abrasion resistance of DSP concrete, which were statistically significant at 0.05 significance level. GP-PAA at 0.16 vol.% produced the greatest improvement (38%) in the abrasion resistance of high-performance (DSP) concrete. Outcomes of pair-wise comparisons confirmed that each of the reinforcement conditions considered here produced statistically significant improvements in the abrasion resistance of high-performance (DSP) concrete (with significance levels ranging from 0.006 to 0.000).

14.4 Summary

The experimental results generated for cementitious pastes reinforced with pristine and PAA-physisorbed graphite nanoplatelets and also their hybrids with carbon microfibers/ polypropylene microfibers in increasingly coarser high-performance matrices indicated that the test results of all engineering properties indicate that all the reinforcement conditions considered here produce improvements in flexural attributes, impact and abrasion resistance of the all high-performance (DSP) cementitious plain matrices.

In all DSP matrices, GP-PAA, CMF, and especially their combination (hybrid reinforcement) produce important gains in the flexural strength, energy absorption capacity and maximum deflection of DSP cementitious pastes. The most important contribution of GP-PAA was to the impact resistance of DSP paste and mortar. This significant increase is due to flaky geometry which tends to be very effective under sudden loads.

In DSP concrete matrix because of a coarser matrix. GP-PAA effectively reinforced the paste portion of the matrix. Thus improvements were observed flexural strength, energy absorption capacity and maximum deflection with respect to plain concrete. Whereas the addition of both CMF and PP microfibers high-performance (DSP) concrete produced important gains in only two out of the three flexural attributes considered here (maximum deflection and energy absorption capacity), while causing a relatively small drop in the flexural strength. The hybrid reinforcement comprising low-modulus polypropylene microfibers with different graphite nanomaterials produced particularly pronounced gains in the mechanical properties of DSP concrete.

Table 14.1- Mean values of the flexural properties of DSP pastes with graphite nanoplatelet and/or carbon microfiber reinforcement.

Reinforcement Condition	Mean Flexure Strength (MPa)	Deflection (mm)	Energy Absorption (N.mm)
Plain	10.3	0.401	61.8
Carbon microfiber, 0.24 vol% (CMF-0.24)	16.1	1.13	251
Graphite nanoplatelet, 0.16 vol% (GP-0.16)	13.2	0.835	156
Carbon microfiber, 0.24 vol% & Graphite nanoplatelet, 0.16 vol% (CMF; GP)	16.6	1.46	288

Table 14.2- Mean values and standard errors of the compressive strength test results for DSP pastes with graphite nanoplatelet and/or carbon microfiber reinforcement.

Reinforcement Condition	Mean Compressive Strength (MPa)	Standard Error (MPa)
Plain	111	14.3
Carbon microfiber, 0.24 vol% (CMF-0.24)	117	28.0
Graphite nanoplatelet, 0.16 vol% (GP-0.16)	99.9	8.77
Carbon microfiber, 0.24 vol% & Graphite	106	7.97
nanoplatelet, 0.16 vol% (CMF; GP)		

Table 14.3- Mean values and standard errors of the impact resistance test results for DSP pastes with graphite nanoplatelet and/or carbon microfiber reinforcement.

Reinforcement Condition	Impact Resistance (mm/mm)
Plain	0.365
Carbon microfiber, 0.24 vol% (CMF-0.24)	0.521
Graphite nanoplatelet, 0.16 vol% (GP-0.16)	0.781
Carbon microfiber, 0.24 vol% & Graphite nanoplatelet,	0.937
0.16 vol% (CMF; GP)	

Table 14.4- Mean values and standard errors of the abrasion weight loss test results for DSP pastes with graphite nanoplatelet and/or carbon microfiber reinforcement.

Reinforcement Condition	Loss of Mass
	(grams)
Plain	0.275
Carbon microfiber, 0.24 vol% (CMF-0.24)	0.150
Graphite nanoplatelet, 0.16 vol% (GP-0.16)	0.113
Carbon microfiber, 0.24 vol% & Graphite nanoplatelet, 0.16 vol%	0.120
(CMF; GP)	

Table 14.5- Mean values of flexural strength, maximum deflection and energy absorption capacity of DSP mortar with nano- and/or micro-scale reinforcement systems.

Reinforcement Condition	Mean Flexure	Deflection	Energy
	Strength	(mm)	Absorption
	(MPa)		(N.mm)
Plain	16.6	0.99	216
Carbon microfiber, 0.24 vol% (CMF-0.24)	19.3	1.37	319
Carbon microfiber, 0.48 vol% (CMF-0.48)	22.5	2.31	424
Carbon microfiber, 0.96 vol% (CMF-0.96)	23.1	2.54	474
Graphite nanoplatelets, 0.16 vol% (GP-PAA-	17.2	1.62	243
0.16)			
Graphite nanoplatelets, 0.24 vol% (GP-PAA-	14.7	1.13	201
0.24)			
Carbon microfiber, 0.24 vol%, & Graphite	18.3	1.68	261
nanoplatelets, 0.16 vol% (CMF; GP-PAA)			

Table 14.6- Mean values and standard errors of compressive strength test results for DSP mortar with nano- and/or micro-scale reinforcement systems.

Reinforcement Condition	Mean (MPa)	Std. Error (MPa)
Plain	125	17.0
Carbon microfiber, 0.24 vol% (CMF-0.24)	119	5.69
Carbon microfiber, 0.48 vol% (CMF-0.48)	138	8.45
Carbon microfiber, 0.96 vol% (CMF-0.96)	127	17.6
Graphite nanoplatelets, 0.16 vol% (GP-PAA-0.16)	119	14.2
Graphite nanoplatelets, 0.24 vol% (GP-PAA-0.24)	111	6.10
Carbon microfiber, 0.24 vol%, & Graphite nanoplatelets,	118	6.18
0.16 vol% (CMF; GP-PAA)		

Table 14.7- Mean values of impact resistance test results for DSP mortar reinforced with nanoand/or micro-scale reinforcement systems.

Reinforcement Condition	Impact Resistance (mm/mm)
Plain	0.57
Carbon microfiber, 0.24 vol% (CMF-0.24)	0.78
Carbon microfiber, 0.48 vol% (CMF-0.48)	0.83
Carbon microfiber, 0.96 vol% (CMF-0.96)	0.94
Graphite nanoplatelets, 0.16 vol% (GP-PAA-0.16)	1.15
Graphite nanoplatelets, 0.24 vol% (GP-PAA-0.24)	1.20
Carbon microfiber, 0.24 vol%, & Graphite nanoplatelets, 0.16	0.99
vol% (CMF; GP-PAA)	

Table 14.8- Mean values of abrasion resistance test results for DSP mortar reinforced with nano- and/or micro-scale reinforcement systems.

Reinforcement Condition	Loss of Mass (grams)
Plain	1.38
Carbon microfiber, 0.24 vol% (CMF-0.24)	0.98
Carbon microfiber, 0.48 vol% (CMF-0.48)	0.93
Carbon microfiber, 0.96 vol% (CMF-0.96)	0.85
Graphite nanoplatelets, 0.16 vol% (GP-PAA-0.16)	0.95
Graphite nanoplatelets, 0.24 vol% (GP-PAA-0.24)	1.01
Carbon microfiber, 0.24 vol%, & Graphite nanoplatelets, 0.16	0.93
vol% (CMF; GP-PAA)	

Table 14.9- Mean values of flexural attributes of plain DSP concrete and those reinforced with different nano- and/ or micro-scale reinforcement systems.

Reinforcement Condition	Flexural	Deflection	Energy
	Strength	(mm)	Absorption
	(MPa)		(N.mm)
Plain	13.4	0.71	92
Carbon microfiber, 0.24 vol.% (CMF-0.24)	12.8	1.01	111
Polypropylene microfiber, 0.24 vol.% (PP-	13.0	4.55	383
0.24)			
Graphite Nanoplatelet, 0.16 vol.% (GP-PAA-	14.8	1.25	181
0.16)			
Polypropylene microfiber, 0.24 vol.% and	16.4	4.78	395
Graphite Nanoplatelet, 0.16 vol.% (PP;GP-			
PAA)			
Carbon microfiber, 0.24 vol.% and Graphite	16.7	1.37	219
Nanoplatelet, 0.16 vol.% (CMF;GP-PAA)			

Table 14.10- Mean values and standard errors of the compressive strength test results for plain DSP concrete and those reinforced with nano- and/ or micro-scale reinforcement systems.

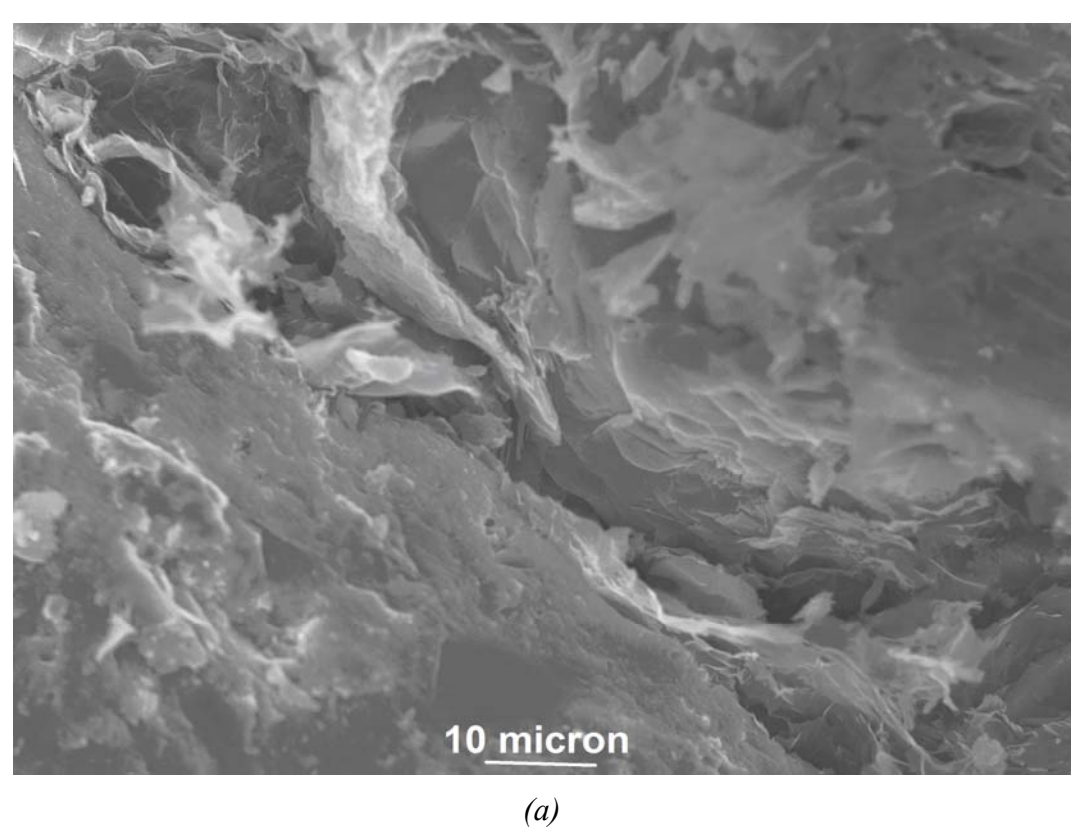
Reinforcement Condition	Mean Compressive	Standard Error (MPa)
Disim	Strength (MPa)	7.75
Plain	151	7.75
Carbon microfiber, 0.24 vol.% (CMF-0.24)	139	13.5
Polypropylene microfiber, 0.24 vol.% (PP-0.24)	137	18.4
Graphite Nanoplatelet, 0.16 vol.% (GP-PAA-	131	8.32
0.16)		
Polypropylene microfiber, 0.24 vol.% and	146	10.4
Graphite Nanoplatelet, 0.16 vol.% (PP;GP-PAA)		
Carbon microfiber, 0.24 vol.% and Graphite	148	7.85
Nanoplatelet, 0.16 vol.% (CMF;GP-PAA)		

Table 14.11- Impact resistance test results for DSP concrete with and without nano- and/or micro-scale reinforcement.

Reinforcement Condition	Impact Resistance (mm/mm)
Plain	1.50
Carbon microfiber, 0.24 vol.% (CMF-0.24)	1.98
Polypropylene microfiber, 0.24 vol.% (PP-0.24)	2.40
Graphite Nanoplatelet, 0.16 vol.% (GP-PAA-0.16)	2.19
Polypropylene microfiber, 0.24 vol.% and Graphite Nanoplatelet, 0.16 vol.% (PP;GP-PAA)	3.10
Carbon microfiber, 0.24 vol.% and Graphite Nanoplatelet, 0.16 vol.% (CMF;GP-PAA)	2.20

Table 14.12- Mean abrasion weight losses of DSP concretes with and without nano- and/ or micro-scale reinforcement systems.

Reinforcement Condition	Loss of Mass
	(grams)
Plain	1.50
Carbon microfiber, 0.24 vol.% (CMF-0.24)	1.15
Polypropylene microfiber, 0.24 vol.% (PP-0.24)	1.05
Graphite Nanoplatelet, 0.16 vol.% (GP-PAA-0.16)	0.93
Polypropylene microfiber, 0.24 vol.% and Graphite Nanoplatelet, 0.16 vol.% (PP;GP-PAA)	0.97
Carbon microfiber, 0.24 vol.% and Graphite Nanoplatelet, 0.16 vol.% (CMF;GP-PAA)	0.96



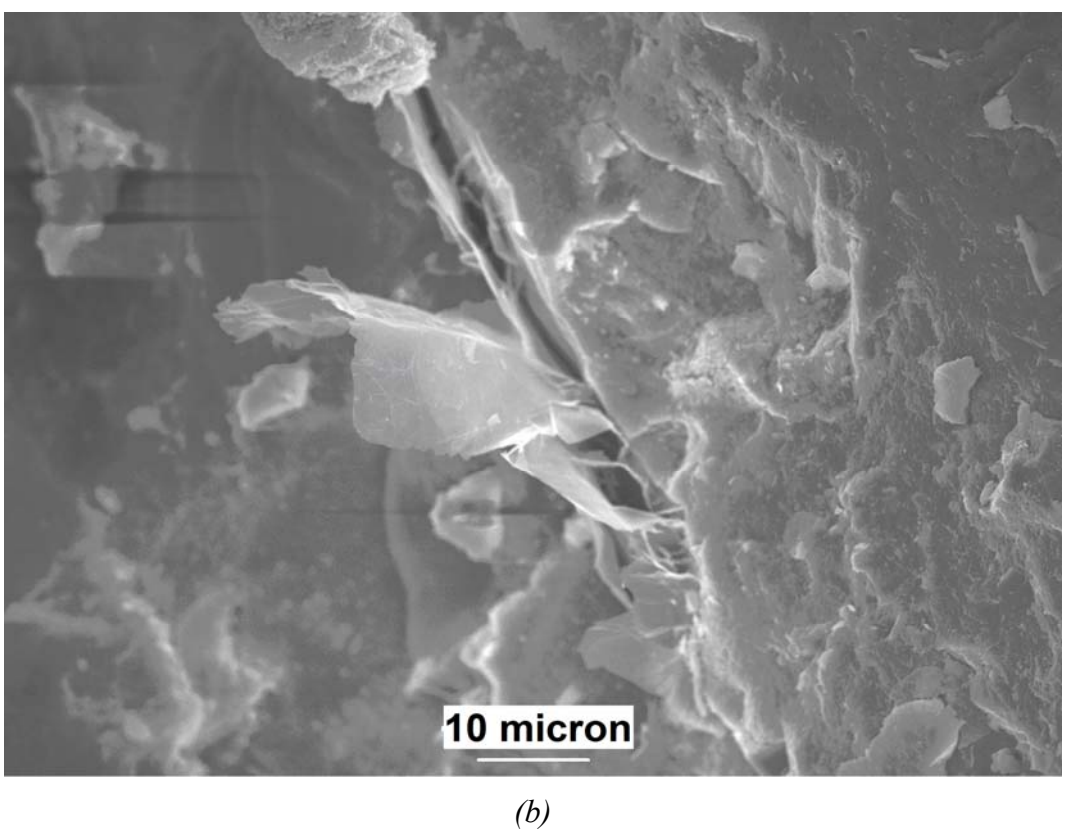


Figure 14.1- SEM images of failed specimens of DSP paste reinforced with GP, providing indications of the graphite nanoplatelet delamination and their interactions with microcracks.

15 DURABILITY CHARACTERISTICS OF HIGH-PERFORMANCE CEMENTITIOUS MATRIX REINFORCED WITH NANO AND/ OR MICRO REINFORCMENTS

15.1 General

Unlike micro-scale fibers which do not benefit the barrier qualities of concrete, the closely spaced nanomaterials force tortuous diffusion paths into concrete, which enhance the barrier qualities (impermeability and diffusion/sorption resistance) of concrete (Fig. 15.1). Nano- and micro-scale reinforcement controls the growth of defects at different scales; nano-scale reinforcement could also reduce the rate of diffusion of moisture and aggressive chemicals into cementitious matrices. These effects can potentially enhance the durability characteristics of cement-based materials.

Degradation of cementitious materials with hybrid reinforcement systems could be influenced by degradation of the reinforcement under chemical attack, fiber-matrix physical and chemical interfacial interactions, and volume instability and cracking of the matrix under various severe exposures and long-term environmental effects. The chemical attack on nano- and micro-scale reinforcement can occur by either the highly alkaline (pH>13) nature of pore water, or the diffusion of aggressive solutions into the cementitious matrix. In conventional fiber cement composites, the ITZ (Interfacial Transition Zone) tends to be more porous initially, and subject to continued hydration and densification over time. With dense matrices such as DSP, however, SEM observations have not indicated the presence of a definite ITZ in matrix. While this

observation supports the assumption of a homogenous cement matrix (neglecting any ITZ effect), aging of these composites seem to enhance fiber-matrix interaction upon normal aging. This phenomenon causes an increase in the flexural strength of composites reinforced with high-modulus nano- and micro-scale reinforcement. The tailored structure of interface upon aging would also alter the performance (bending and pullout) of fibers (and nanofibers) at cracks, thereby refining the mechanical performance of composites (Katz and Bentur 1994; Katz and Bentur 1995; Katz, Li et al. 1995; Katz and Bentur 1996). Depending on the nature of accelerated aging, dimensional (and differential dimensional) movements under moisture and temperature effects are also among the key aging mechanisms of cementitious composites. Temperature and moisture gradients across the thickness aggravate damage mechanisms caused by differential dimensional movements.

15.2 Materials and Methods

15.2.1 Graphite Nanomaterials and Microfibers

Polyacrylic acid (PAA) physisorbed carbon nanotubes, graphite nanoplatelets as well as (microscale) carbon and polypropylene fibers were evaluated for use in cement-based nanocomposites. These graphite nanomaterials and microfibers have been introduced in detail in Chapter 2, Section 2.4, Fig. 2.3 and Table 2.3. PAA physisorbed CNFs (CNT D-PAA), graphite nanoplatelets (GP), carbon microfibers (CMF) and polypropylene microfibers (PAA) were used in high-performance mortar and cement-based concrete matrix.

15.2.2 Cementitious Matrices, Mixing and Curing Procedure

Dense cementitious matrix selected has been introduced in detail in Chapter 2, Section 2.5. DSP mortar and concrete was used to evaluate the reinforcement efficiency of both graphite nanomaterials and/ or carbon or polypropylene microfibers at different volume fractions.

Cementitious materials (with and without functionalized graphite nanomaterials dispersed in the mixing water via sonication) and/ or carbon; polypropylene microfibers were prepared and cured following ASTM procedures described in Chapter 2, Section 2.5.2.

15.2.3 Experimental Methods

In order to evaluate the durability and stability of DSP matrix with different nano- and/or microscale reinforcement, accelerated aging tests were conducted and introduced in detail in Chapter 2, Section 2.6. *Freeze-Thaw* tests (ASTM C666), *Wet-dry* tests (ASTM C1185), *Hot Water Immersion* (ASTM C1185) and The *Elevated Temperature* tests were carried out in an electric furnace.

During long-term exposures to different severe environments, the specimen degradation over the course of exposure was monitored by nondestructive evaluation of the dynamic elastic modulus using a sonometer in accordance with ASTM C215. The flexural attributes of different specimens were also evaluated after half and full exposure in accordance with ASTM C 1185. Experimental results were evaluated using the analysis of variance (ANOVA) and pair-wise comparison techniques.

15.3 Test Results and Discussion of DSP Mortar Matrix

15.3.1 DSP Mortar with Different Nano and/or Micro Reinforcements

15.3.1.1 Exposure to Elevated Temperature

The high-temperature exposure conditions used in our experiments simulated exposure to fire, and subjected the specimens to high (thermal and vapor pressure) stresses. The specimens exhibited severe spalling, disintegration and strength loss. Plain DSP mortar specimens as well as those with graphite nanoplatelets and microfibers together with graphite nanoplatelets did not survive this severe exposure (Fig. 15.2a-c). However, two samples each, Fig. 15.2d, of DSP mortar reinforced with hybrid reinforcement (HYCNT1) of CNTD-PAA and CMF as well as CMF alone survived the exposure to elevated temperature. The chances of survival of a dense matrix like DSP at elevated temperature are very slim because of its relatively high impermeability (which increases the internal vapor pressure upon temperature rise) and brittleness. The fact that half of DSP mortars with microfiber and hybrid (microfiber and nanotube) reinforcement survives exposure to elevated temperature reflects upon: (i) the gains in DSP mortar toughness with reinforcement; (ii) increased thermal conductivity in the presence of graphite micro- and nano-scale reinforcement, which could reduce the temperature gradient within cementitious specimens; and (iii) combustion of graphite microfibers and nano-scale reinforcement which could open space within cementitious matrices for release of vapor pressure at elevated temperature.

The specimens that survived exposure to elevated temperature were saturated by immersion in water for 24 hours, and then tested in flexure. The results are given in Table 15.1. DSP mortar with CMF reinforcement experienced 62.3%, 61.8% and 83.0% loss of flexural strength, maximum deflection and energy absorption capacity after exposure to high temperature. DSP mortar with hybrid (HYCNT1) reinforcement provided improved thermal stability, experiencing

26.4%, 49.3% and 65.3% losses of flexural strength, maximum deflection and energy absorption capacity, respectively. This finding reflects upon the positive effects of reinforcement at microand nano-scale upon the stability of cementitious materials under severe exposure conditions.

15.3.1.2 Freeze-Thaw Cycles

The relative dynamic elastic moduli of specimens with different reinforcement conditions after exposure to different freeze-thaw cycles are shown in Fig. 15.3. The flexural performance characteristics of unaged and aged specimens are summarized in Table 15.2. The dynamic moduli test results presented in Fig. 15.3 indicate that any adverse effects of freeze-thaw cycles on dynamic modulus is overshadowed by the positive effects associated with continued hydration of the cementitious matrix in the presence of moisture. Similar trends are observed as far as freeze-thaw effects on flexural performance are concerned. The gains in properties are particularly pronounced in the case of DSP mortar with hybrid reinforcement (HYCNT1) comprising CNTD-PAA and carbon CMF. This system experienced 14.2%, 44.5% and 36.5% gains in flexural strength, energy absorption capacity and maximum deflection, respectively, after freeze-thaw cycles. It is worth mentioning that the high-performance (plain) DSP mortar, due to its desired combination of impermeability and mechanical performance, exhibits a desired resistance to freeze-thaw attack. The benefits of nano-scale and hybrid reinforcement systems to the barrier and mechanical qualities of DSP mortar further enhance its freeze-thaw durability. Analysis of variance (ANOVA) and pair-wise comparison of test results indicate that, at significance level of 0.05, only DSP mortar with hybrid reinforcement (HYCNT1) reinforcement

experiences statistically significant gains in all flexural attributes after exposure to freeze-thaw

cycles. Mortars with CMF alone and with HYGP (graphite nanoplatelet/carbon microfiber)

reinforcement experience statistically significant gains in flexural energy sorption capacity and maximum deflection (but not flexural strength) after exposure to freeze-thaw cycles.

15.3.1.3 Wet-Dry Cycles

The relative dynamic elastic moduli of mortars with different reinforcement conditions after exposure to different wet-dry cycles are shown in Fig. 15.4. The flexural performance characteristics prior to and after exposure to freeze-thaw cycles are summarized in Table 15.3. As was the case with freeze-thaw cycles, the elastic moduli and flexural performance characteristics of DSP mortars (plain or with different reinforcement conditions) improve under exposure to wet-dry cycles. This finding implies that any damage associated with wet-dry cycles is overshadowed by the positive effects of continuous hydration of the cementitious material in the presence of moisture. The DSP mortar with hybrid (HYCNT1) reinforcement benefits the most from exposure to wet-dry cycles (which was also the case for freeze-thaw cycles). Mortar with this hybrid reinforcement system experiences 7.6%, 24% and 40% gains in flexural strength, energy absorption capacity and maximum deflection, respectively, after exposure to 300 wet-dry cycles.

ANOVA and pair-wise comparison of test results indicate that, at 0.05 significance level, only DSP mortar with hybrid reinforcement (HYCNT1) experiences statistically significant gains in all flexural attributes after exposure to repeated wet-dry cycles. In the case of mortar with CMF reinforcement alone, flexural energy absorption capacity and maximum deflection (but not flexural strength) experience statistically significant gains upon exposure to wet-dry cycles. As far as the plain and matrix with HYGP is concerned, only the gains in maximum deflection under wet-dry cycles are statistically significant.

15.3.1.4 Hot Water Immersion

The relative dynamic elastic moduli of DSP mortars with different nano- and/or micro-scale reinforcement, after different intervals of immersion in hot water at 60°C, are summarized in Fig. 15.5. The flexural performance characteristics of these mortars prior to and after immersion in hot water are presented in Table 15.4. The trends observed here are different to those observed for tests involving exposure to freeze-thaw and wet-dry cycles. All DSP mortar whether plain or containing micro and/ or nano reinforcements experienced a drop in flexural strength after 56 days of hot water immersion. The other two flexural attributes were relatively not effected for matrix containing reinforcements. Both maximum mean deflection and energy absorption capacity showed increase in mean value. The minimum drop in flexural strength (3%) and maximum increase in deflection (7%) and energy absorption capacity (8%) was shown by specimens containing hybrid reinforcement (HYCNT1), containing both CNTD-PAA and CMF and the maximum drop in flexural strength was shown by plain DSP matrix which was about 29%. At 0.05 level of significance the ANOVA and pair-wise comparison results point at a statistically significant drop in flexural strength of plain DSP matrix and matrix containing GP only.

15.3.2 DSP Mortar with Refined Nano and/or Micro Reinforcements

The preferred hybrid reinforcement systems identified through response surface analysis (RSA) based on extensive test results conducted earlier were considered here. The preferred hybrid reinforcement systems identified through RSA, comprising CNTD-PAA and CMF included one with 0.06 vol.% CNTD-PAA and 0.3 vol.% CMF (HYCNT2) and another with 0.08 vol.% CNTD-PAA and 0.4 vol.% CMF (HYCNT3). The preferred hybrid reinforcement system

comprising GP and CMF comprised either 0.01 vol.% GP and 0.8 vol.% CMF (HYGP2), or 0.2 vol.% GP and 0.4 vol.% CMF (HYGP3).

To evaluate the durability characteristics, two conditions were selected for evaluation of high-performance (DSP) cementitious mortar with nano- and/or micro-scale reinforcement systems under extreme exposure/accelerated aging effects: (i) exposure to elevated temperature; and (ii) extended immersion in hot water. The test procedures have been described earlier. Given the high qualities of DSP cementitious materials, these conditions were found in our earlier work to produce some detectable damage to the material.

15.3.2.1 Exposure to Elevated Temperature

Specimens reinforced with the preferred hybrid reinforcement systems comprising CNTD-PAA and CMF, three specimens with HYCNT3 reinforcement one specimen with HYCNT2 reinforcement survived exposure to elevated temperature (Fig. 15.6b). As pointed earlier, the chances of survival of a dense matrix like DSP at elevated temperature is very slim because of its relatively high impermeability (which increases the internal vapor pressure upon temperature rise) and brittleness. The fact that some DSP mortars with hybrid reinforcement survived exposure to elevated temperature reflects upon the enhancement of durability by hybrid reinforcement. By tailoring these hybrid reinforcements through RSA can give higher performance characteristics at suitable cost. Specimens that survived exposure to elevated temperature were saturated by immersion in water for 24 hours, and then tested in flexure. The results are summarized in Table 15.5. DSP mortar specimens with hybrid reinforcement systems HYCNT2 (HYCNT3) experienced 42.5% (32.6%), 59.2% (51.5%) and 79.1% (69.0%) losses of flexural strength, maximum deflection and energy absorption capacity, respectively. This finding reflects upon the positive effects of hybrid (nano- and micro-scale) reinforcement on the fire

resistance of high-performance cementitious (DSP) mortar. When compared to the values of DSP mortar reinforced with either CMF alone and HYCNT1, the results clearly indicate the positive effect of CNTD-PAA presence in the matrix. The loss in the flexural attributes is less with increased volume fraction of carbon nanotubes in the cementitious matrix.

15.3.2.2 Hot Water Immersion

After 56 days of hot water immersion a slight rise in elastic modulus occurs initially, Fig. 15.7, which reverses after about 14 days. The rise tends to be greater in the case of DSP mortar specimens with hybrid reinforcement systems comprising carbon nanotube and carbon microfiber. The test data summarized in Table 15.6 indicate that a drop in mean flexural strength occurs for all samples after 28 days of immersion in hot water. This drop is relatively small (4.9% and 9%) for DSP mortar with hybrid reinforcement systems HYCNT3 and HYCNT2, respectively. It tends to be greater (12% and 19%) for hybrid reinforcement systems (HYGP2 and HYGP3, respectively) comprising GP and carbon microfiber CMF. Other flexural attributes were less affected by hot water immersion; maximum deflection increased in all samples, and flexural energy absorption capacity increased in most samples after hot water immersion.

At 0.05 level of significance the ANOVA and pair-wise comparison results point at a statistically significant drop in flexural strength and energy absorption capacity of both DSP mortars with hybrid reinforcement comprising GP and CMF. The corresponding effects on DSP mortars with hybrid reinforcement systems comprising CNTD-PAA and CMF, however, were not statistically significant. This further augments that hybrid reinforcements involving carbon nanotubes augment the durability characteristics of DSP cementitious matrix.

15.4 Test Results and Discussion of DSP Concrete Matrix

To assess the durability characteristics of DSP concrete matrix, plain matrix as well as matrix containing CNTD-PAA were used at 0.16 vol.% and/ or the low modulus polypropylene (PP) microfibers at 0.24 vol.%. Same mixing, curing and accelerated aging conditions were used as described in Chapter 2, Section 2.5.2.

15.4.1 Exposure to Elevated Temperature

After exposure the specimens exhibited fracture, disintegration and strength loss. Plain DSP concrete specimens as well as some specimens with PP microfibers showed severe spalling and broke into pieces, Fig. 15.8c. However, two samples of DSP concrete containing PP microfibers and all samples containing functionalized carbon nanotubes (CNTD-PAA) and hybrid reinforcement (PPCNTD), Fig. 15.8b, survived the exposure to elevated temperature. The fact that almost all DSP concrete samples with microfiber and/or hybrid (microfiber and nanotube) reinforcement survives exposure to elevated temperature reflects upon in addition to the factors mentioned earlier to combustion of PP microfibers reinforcement which opens space within cementitious matrices for release of vapor pressure at elevated temperature.

The specimens that survived exposure to elevated temperature were saturated by immersion in water for 24 hours, and then tested in flexure. The results are given in Table 15.7. DSP concrete with polypropylene microfiber reinforcement experienced 39.1%, 74.0% and 71.0% loss of flexural strength, maximum deflection and energy absorption capacity after exposure to high temperature. DSP concrete with nano and hybrid (PPCNTD) reinforcement provided improved thermal stability, experiencing 25.4%; 27.6% and 4.32%; 61.6% loss in flexural strength, maximum deflection and energy absorption capacity, respectively. Whereas, specimens with

nano reinforcement observed on an average 22.8% increase in mean maximum deflection. This finding reflects upon the positive effects of reinforcement at nano- and micro- (when used in hybrid) scale upon the stability of cementitious materials under severe exposure conditions.

15.4.2 Freeze-Thaw Cycles

As was the case for DSP mortar, Fig. 15.9 shows no effect on the values of relative dynamic modulus after repeated exposure to freeze thaw on plain specimen and specimens containing CNTD-PAA. The values of relative dynamic modulus increase with time due to continuation of hydration in wet state. However, the relative dynamic modulus for specimens containing PP microfibers or hybrid (PPCNTD) of CNTD-PAA and PP started showing drop in value of relative dynamic modulus. Although the value is not yet below 100 but the overall curve starts showing a negative slope.

Table 15.8 also shows no effect of freeze-thaw cycles and an increase in all flexure attributes of all plain as well as samples containing CNTD-PAA. This points out to the superior durability of DSP concrete matrix and its further reinforcement by nanomaterials. The increase in flexure attributes is the most for matrix reinforced with 0.16 vol.% CNTD-PAA. The increase in flexural strength, energy absorption capacity and maximum deflection for this matrix is 4.8%, 0.7% and 33.3%, respectively. However, there was a drop observed in the mean values of all flexural attributes of all the samples containing both PP microfibers and hybrid reinforcement (PP; CNTD-PAA). The ANOVA results show a little different picture. At 95% confidence or for values of p less than or equal to 0.05, no DSP concrete matrix whether plain or reinforced with nano and/or micro reinforcement showed any change in flexural strength. However for matrices containing PP microfibers and PP; CNTD, the loss in maximum deflection is statistically significant. But the loss in energy absorption capacity is significant for DSP concrete matrix

containing hybrid reinforcement (PPCNTD). The main reason that matrices containing PP microfibers showed drop in some of the flexural attributes is due to the well-known fact of fiber-matrix degradation due to long-term exposure to severe freeze-thaw conditions.

15.4.3 Wet-Dry Cycles

As was the case for freeze-thaw, Fig. 15.10 shows no effect on the values of relative dynamic modulus after repeated exposure to wet-dry cycles on plain specimen and specimens containing CNTD-PAA. The values of relative dynamic modulus increase with time due to continuation of hydration in wet state. However, the relative dynamic modulus for specimens containing PP microfibers and hybrid reinforcement (PPCNTD) started showing drop in value of relative dynamic modulus. Although the value is not yet below 100 but the overall curve starts showing a negative slope.

Similarly, Table 15.9 show no effect of wet-dry cycles and an increase in all flexure attributes of all plain as well as samples containing CNTD-PAA. The increase in flexure attributes is the most for matrix reinforced with 0.16 vol.% CNTD-PAA. The increase in flexural strength, energy absorption capacity and maximum deflection for this matrix is 9.4%, 38.3% and 39.1%, respectively. However, there was a drop observed in the mean values of flexural strength and energy absorption capacity of all the samples containing both PP microfibers and hybrid reinforcement (PPCNTD). The ANOVA results show that at 95% confidence, no DSP concrete matrix plain or reinforced showed any increase/ decrease in any of the flexural attributes evaluated.

15.4.4 Hot Water Immersion

Fig. 15.11 shows no effect on the values of relative dynamic modulus after hot water immersion for 56 days on DSP concrete plain specimen and specimens containing CNTD-PAA. The values of relative dynamic modulus increase with time due to continuation of hydration in wet state, especially for samples containing CNTD-PAA at 0.16 vol.%. However, the relative dynamic modulus for specimens containing PP microfibers or with hybrid reinforcement (PPCNTD) started showing drop in value of relative dynamic modulus. Although the value is not yet below 100 but the overall curve starts showing a negative slope.

Table 15.10 shows no effect of hot water immersion after 56 days and an increase in all flexure attributes of all plain as well as samples containing CNTD-PAA. The increase in flexural attributes is more pronounced for matrix reinforced with 0.16 vol.% CNTD-PAA. The increase in flexural strength, energy absorption capacity and maximum deflection for this matrix is 17.1%, 4.3% and 20.3%,, respectively. However, there was a drop observed in the mean values of all flexural attributes of all the samples containing both PP microfibers and hybrid reinforcement (PPCNTD). The ANOVA results show that at 95% confidence level, no DSP concrete matrix whether plain or reinforced with nano and/or micro reinforcement showed any change in flexure strength. However for matrices containing PP microfibers and hybrid reinforcement (PPCNTD), the loss in maximum deflection is statistically significant. But the loss in energy absorption capacity is significant for DSP concrete matrix containing hybrid reinforcement only.

15.5 Summary

The durability characteristics of high-performance (DSP) cementitious mortars and concrete were evaluated under different accelerated aging effects. The results indicated indicate that the DSP mortars provide desirable durability characteristics, which tend to be enhanced through reinforcement with nano-scale and especially hybrid (nano- and micro-scale) reinforcement systems. Hybrid reinforcement of DSP cementitious mortar, when used at appropriate volume fractions, proved very effective in improving key durability characteristics of the matrix through barrier qualities and synergistic reinforcement at different scales.

For DSP concrete as well the accelerated aging test results showed no effect on the flexural attributes and dynamic elastic modulus of plain DSP concrete matrix and matrix containing CNTD-PAA after 300 cycles of freeze-thaw and wet-dry and 56 days immersion in hot water. However, matrices containing PP microfibers and hybrid (PPCNTD) of CNT-PAA and PP, showed drop in the mean values of almost all flexural attributes when exposed to above mentioned accelerated aging test.

Table 15.1- Mean values of flexural attributes of DSP mortar reinforced with micro- and/or nano-scale reinforcement prior to and after exposure to elevated temperature (ET).

Reinforcement Condition	Mean Flexural Strength(MPa)	Deflection (mm)	Energy Absorption(N.mm)
CMF (0.24 vol%)	19.3	1.37	319
CMF (0.24 vol%), ET	7.29	0.52	54.1
HYCNT1- (CMF 0.24 vol% &	19.7	2.03	398
MWNTD-PAA, 0.16 vol%)			
HYCNT1-(CMF, 0.24 vol% &	14.5	1.03	138
MWNTD-PAA, 0.16 vol%), ET			

Table 15.2 - Mean values of the flexural attributes of DSP mortar samples with micro- and/or nano-scale reinforcement before and after exposure to 300 cycles of freeze-thaw (FT).

Reinforcement Condition	Mean Flexural Strength(MPa)	Deflection (mm)	Energy Absorption(N.mm)
Plain, unaged	16.6	0.99	216
Plain, FT	17.0	1.15	272
CMF (0.24 vol%), unaged	19.3	1.37	319
CMF(0.24 vol%), FT	19.9	1.77	435
HYCNT1-(CMF, 0.24 vol% &	19.7	2.03	398
MWNTD-PAA, 0.16 vol%), unaged			
HYCNT1-(CMF, 0.24 vol% &	22.5	2.77	575
MWNTD-PAA, 0.16 vol%), FT			
GP (0.16 vol%), unaged	17.2	1.62	244
GP (0.16 vol%), FT	17.8	1.83	305
HYGP1-(CMF, 0.24 vol% & GP, 0.16	18.3	1.68	261
vol%), unaged			
HYGP1-(CMF, 0.24 vol% & GP, 0.16	19.6	2.07	355
vol%), FT			

Table 15.3- Mean values of the flexural attributes of DSP mortars with micro- and/or nano-scale reinforcement prior to and after exposure to 300 wet-dry (WD) cycles.

Reinforcement Condition	Mean Flexural	Deflection	Energy
	Strength(MPa)	(mm)	Absorption(N.mm)
Plain, unaged	16.6	0.99	216
Plain, WD	17.1	1.15	275
CMF (0.24 vol%), unaged	19.3	1.37	319
CMF(0.24 vol%), WD	20.3	1.91	430
HYCNT1-(CMF, 0.24 vol% &	19.7	2.03	398
MWNTD-PAA, 0.16 vol%), unaged			
HYCNT1-(CMF, 0.24 vol% &	21.2	2.85	495
MWNTD-PAA, 0.16 vol%), WD			
GP (0.16 vol%), unaged	17.2	1.62	244
GP (0.16 vol%), WD	18.1	1.88	301
HYGP1-(CMF, 0.24 vol% & GP, 0.16	18.3	1.68	261
vol%), unaged			
HYGP1-(CMF, 0.24 vol% & GP, 0.16	19.9	2.04	335
vol%), WD			

Table 15.4- Mean values of the flexural attributes of DSP mortars with micro- and/or nano-scale reinforcement prior to and after 56 days of hot water (HW) immersion.

Reinforcement Condition	Mean Flexural	Deflection	Energy
	Strength(MPa)	(mm)	Absorption(N.mm)
Plain, unaged	16.6	0.99	216
Plain, HW	11.8	1.05	220
CMF (0.24 vol%), unaged	19.3	1.37	319
CMF(0.24 vol%), HW	17.2	1.40	328
HYCNT1-(CMF, 0.24 vol% &	19.7	2.10	398
MWNTD-PAA, 0.16 vol%), unaged			
HYCNT1-(CMF, 0.24 vol% &	19.1	2.05	430
MWNTD-PAA, 0.16 vol%), HW			
GP (0.16 vol%), unaged	17.2	1.62	244
GP (0.16 vol%), HW	13.8	1.65	250
HYGP1-(CMF, 0.24 vol% & GP, 0.16	18.3	1.68	261
vol%), unaged			
HYGP1-(CMF, 0.24 vol% & GP, 0.16	15.5	1.69	270
vol%), HW			

Table 15.5- Mean values of flexural attributes of DSP mortar reinforced with preferred hybrid reinforcement systems prior to and after exposure to elevated temperature (ET).

Reinforcement Condition	Mean Flexural	Deflection	Energy
	Strength(MPa)	(mm)	Absorption(N.mm)
HYCNT2-(CMF, 0.30 vol%, &	21.0	2.29	441
MWNTD-PAA, 0.06 vol%),			
unaged			
HYCNT2-(CMF, 0.30 vol%, &	12.1	0.93	92
MWNTD-PAA, 0.06 vol%), ET			
HYCNT3-(CMF, 0.40 vol%, &	21.8	2.35	457
MWNTD-PAA, 0.08 vol%),			
unaged			
HYCNT3-(CMF, 0.40 vol%, &	14.7	1.14	142
MWNTD-PAA, 0.08 vol%), ET			

Table 15.6- Mean values of the flexural attributes of DSP mortar specimens with preferred hybrid reinforcement systems prior to and after 56 days of immersion in hot water (HW).

Reinforcement Condition	Mean Flexural	Deflection	Energy
	Strength(MPa)	(mm)	Absorption(N.mm)
HYCNT2-(CMF, 0.30 vol%, &	21.0	2.29	441
MWNTD-PAA, 0.06 vol%), unaged			
HYCNT2-(CMF, 0.30 vol%, &	19.2	2.31	450
MWNTD-PAA, 0.06 vol%), HW			
HYCNT3-(CMF, 0.40 vol%, &	21.8	2.35	457
MWNTD-PAA, 0.08 vol%), unaged			
HYCNT3-(CMF, 0.40 vol%, &	20.7	2.39	473
MWNTD-PAA, 0.08 vol%)- HW			
HYGP2-(CMF, 0.80 vol%, & GP,	22.7	2.36	477
0.01 vol%)			
HYGP2-(CMF, 0.80 vol%, & GP,	19.9	2.38	403
0.01 vol%)- HW			
HYGP3-(CMF, 0.40 vol%, & GP,	19.2	1.83	401
0.20 vol%)			
HYGP3-(CMF, 0.40 vol%, & GP,	15.5	1.86	298
0.20 vol%)- HW			

Table 15.7- Mean values of flexural attributes of DSP concrete reinforced with micro- and/or nano-scale reinforcement prior to and after exposure to elevated temperature (ET).

Reinforcement Condition	Mean Flexural	Deflection	Energy
	Strength(MPa)	(mm)	Absorption(N.mm)
PP(0.24 vol%)	9.50	4.54	383
PP(0.24 vol%) -ET	5.79	1.18	111
CNTD-PAA(0.16 vol%)	13.4	1.40	139
CNTD-PAA(0.16 vol%)-ET	9.99	1.72	133
PPCNTD-(PP, 0.24 vol% &	13.6	4.77	420
CNTD-PAA, 0.16 vol%)			
PPCNTD-(PP, 0.24 vol% &	9.84	1.83	153
CNTD-PAA, 0.16 vol%)-ET			

Table 15.8- Mean values of the flexural properties of DSP concrete samples with micro- and/or nano-scale reinforcement before and after exposure to 300 cycles of freeze-thaw (FT).

Reinforcement Condition	Mean Flexural	Deflection	Energy
	Strength(MPa)	(mm)	Absorption(N.mm)
Plain	9.89	1.04	98
Plain -FT	10.19	1.10	90
CNTD-PAA(0.16 vol%)	13.38	1.41	138
CNTD-PAA(0.16 vol%)-FT	14.02	1.42	184
PP(0.24 vol%)	9.50	4.54	383
PP(0.24 vol%) -FT	8.08	3.19	278
PPCNTD-(PP, 0.24 vol% & CNTD-	13.61	4.77	420
PAA, 0.16 vol%)			
PPCNTD-(PP, 0.24 vol% & CNTD-	12.13	3.41	211
PAA, 0.16 vol%)-FT			

Table 15.9- Mean values of the flexural properties of DSP concrete samples with micro- and/or nano-scale reinforcement before and after exposure to 300 wet-dry cycles (WD).

Reinforcement Condition	Mean Flexural	Deflection	Energy
	Strength(MPa)	(mm)	Absorption(N.mm)
Plain	9.89	1.04	98
Plain -WD	10.03	1.16	124
CNTD-PAA(0.16 vol%)	13.38	1.41	138
CNTD-PAA(0.16 vol%)-WD	14.64	1.95	192
PP(0.24 vol%)	9.50	4.54	383
PP(0.24 vol%) -WD	8.88	4.84	330
PPCNTD-(PP, 0.24 vol% & CNTD-	13.61	4.77	420
PAA, 0.16 vol%)			
PPCNTD-(PP, 0.24 vol% & CNTD-	31.42	5.86	355
PAA, 0.16 vol%)-WD			

Table 15.10- Mean values of the flexural properties of DSP concrete samples with micro- and/or nano-scale reinforcement before and after exposure to 56 days in hot water (HW).

Reinforcement Condition	Mean Flexural	Deflection	Energy
	Strength(MPa)	(mm)	Absorption(N.mm)
Plain	9.89	1.04	98
Plain -WD	12.02	1.10	111
CNTD-PAA(0.16 vol%)	13.38	1.41	138
CNTD-PAA(0.16 vol%)-WD	15.67	1.47	166
PP(0.24 vol%)	9.50	4.54	383
PP(0.24 vol%) -WD	8.47	3.04	273
PPCNTD-(PP, 0.24 vol% & CNTD-	13.61	4.77	420
PAA, 0.16 vol%)			
PPCNTD-(PP, 0.24 vol% & CNTD-	12.71	3.30	218
PAA, 0.16 vol%)-WD			

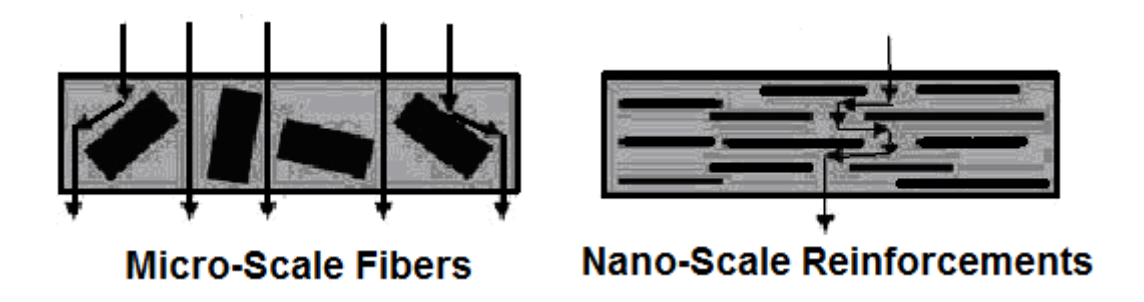


Figure 15.1- Tortuous diffusion paths forced by nano-scale reinforcement.



(a) Failed plain DSP mortar specimens

Figure 15.2- DSP mortar specimens with different reinforcement conditions after exposure to elevated temperature.



(b) Failed DSP mortar with hybrid reinforcement



(c) Survived DSP mortar with hybrid reinforcement

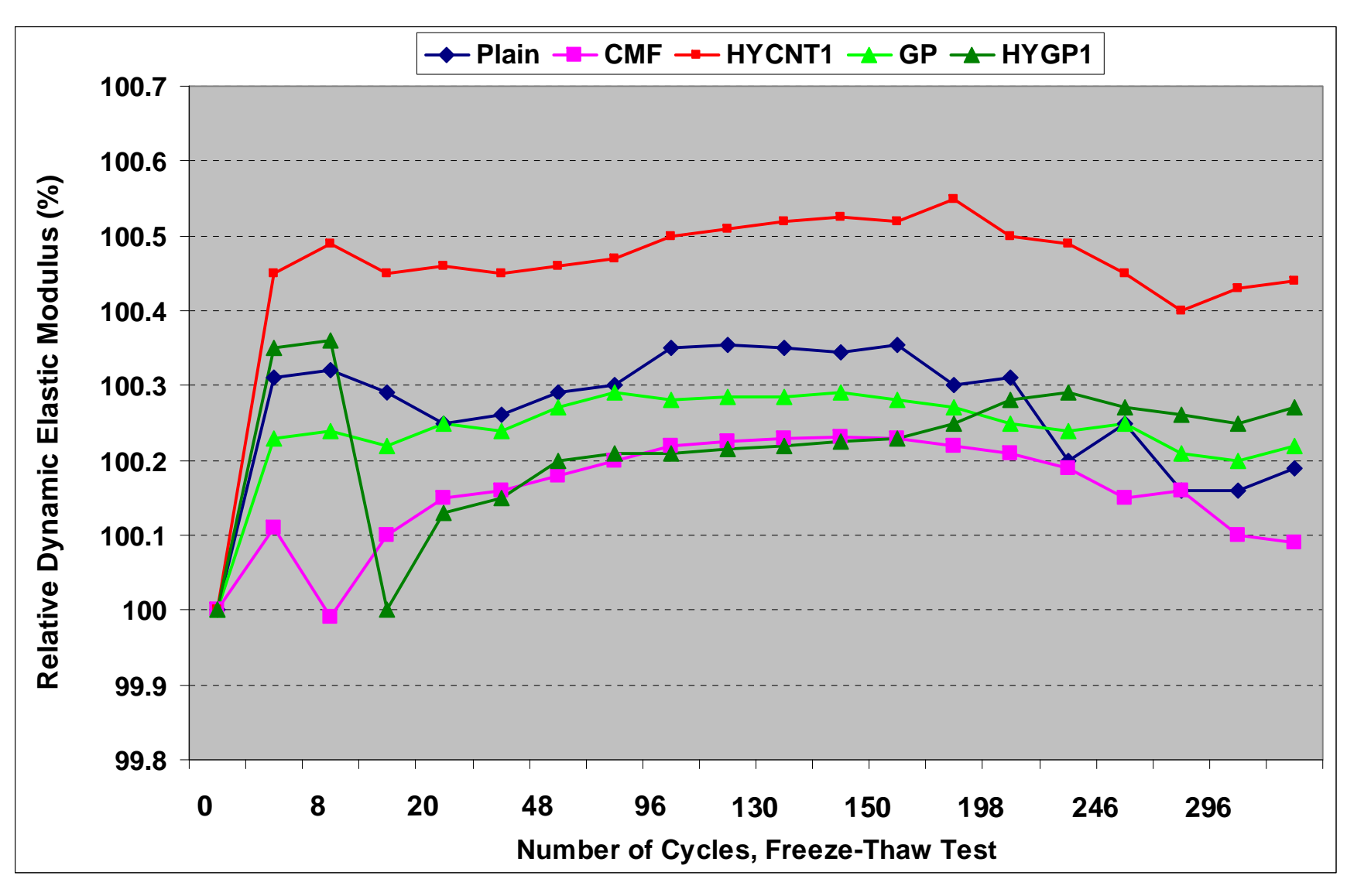


Figure 15.3- Effects of exposure to freeze-thaw on the dynamic modulus of DSP mortars with micro- and/or nano-scale reinforcement after 300 cycles.

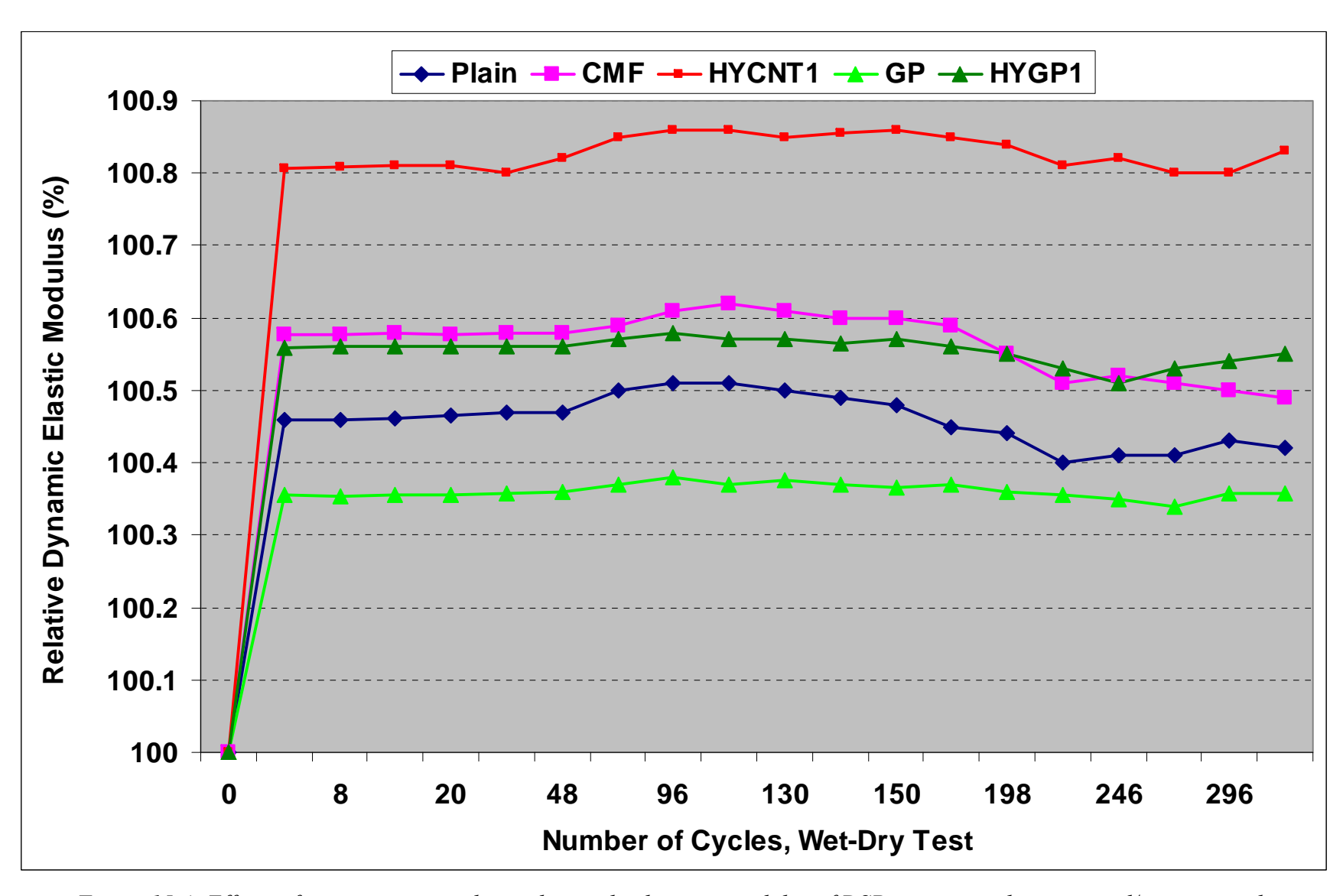


Figure 15.4- Effects of exposure to wet-dry cycles on the dynamic modulus of DSP mortars with micro- and/or nano-scale reinforcement.

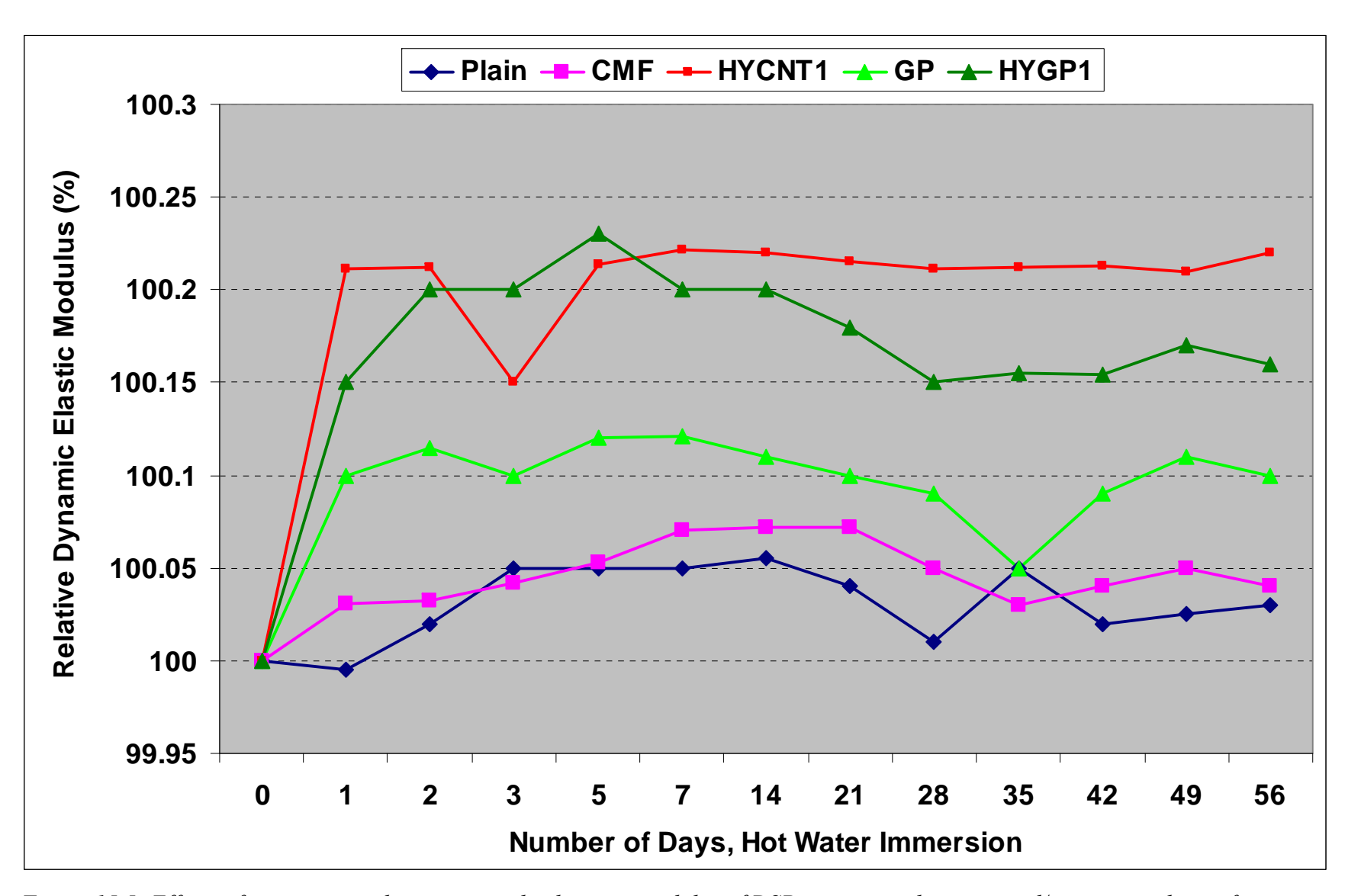


Figure 15.5- Effects of immersion in hot water on the dynamic modulus of DSP mortars with micro- and/or nano-scale reinforcement.



(a) Failed DSP mortar with hybrid reinforcement



(b) Survived DSP mortar with hybrid reinforcement

Figure 15.6- High-performance (DSP) mortar specimens with different reinforcement conditions after exposure to elevated temperature.

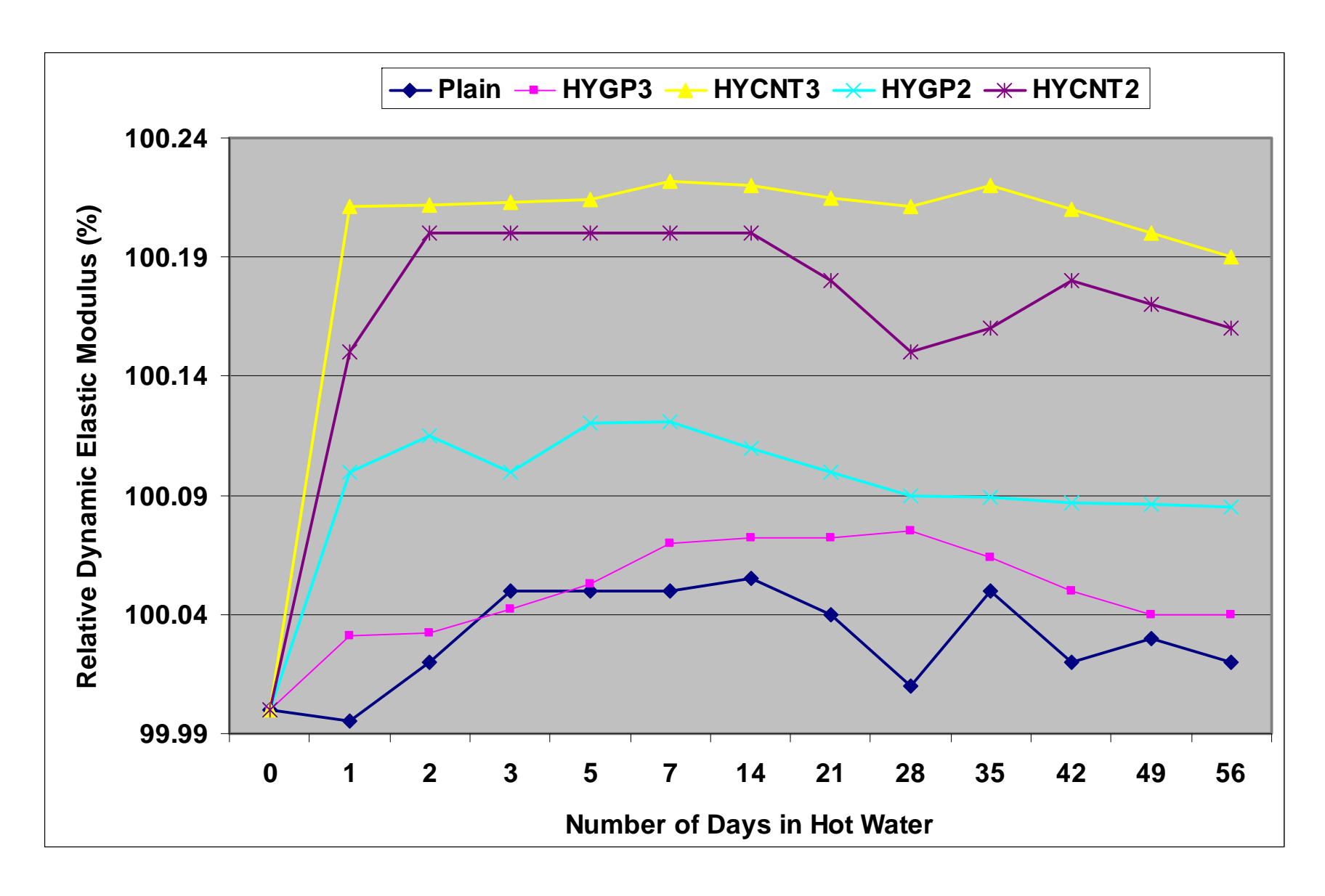


Figure 15.7- Effects of immersion in hot water on the dynamic modulus of DSP mortars with preferred hybrid reinforcement systems after 56 days.



(a) DSP concrete specimens before exposure



 $(b) \ Survived \ samples \ with \ nano \ and/or \ micro \ reinforcement$

Figure 15.8- DSP concrete specimens with different reinforcement conditions after exposure to elevated temperature.

Figure 15.8 (cont'd)



(c) Failed samples without any and with micro reinforcement

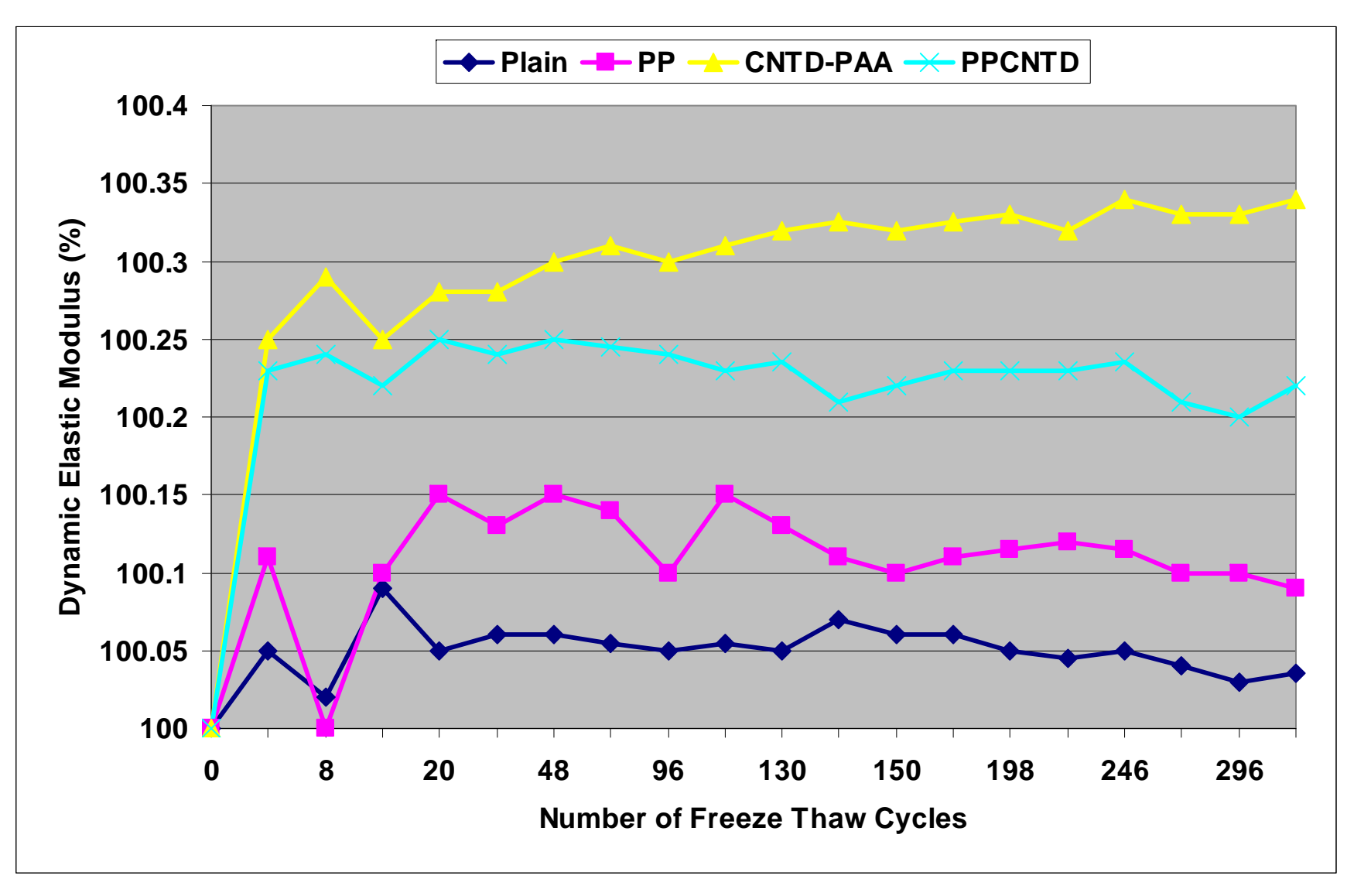


Figure 15.9- Effects of exposure to freeze-thaw on the dynamic modulus of DSP concrete with micro- and/or nano-scale reinforcement after 300 cycles.

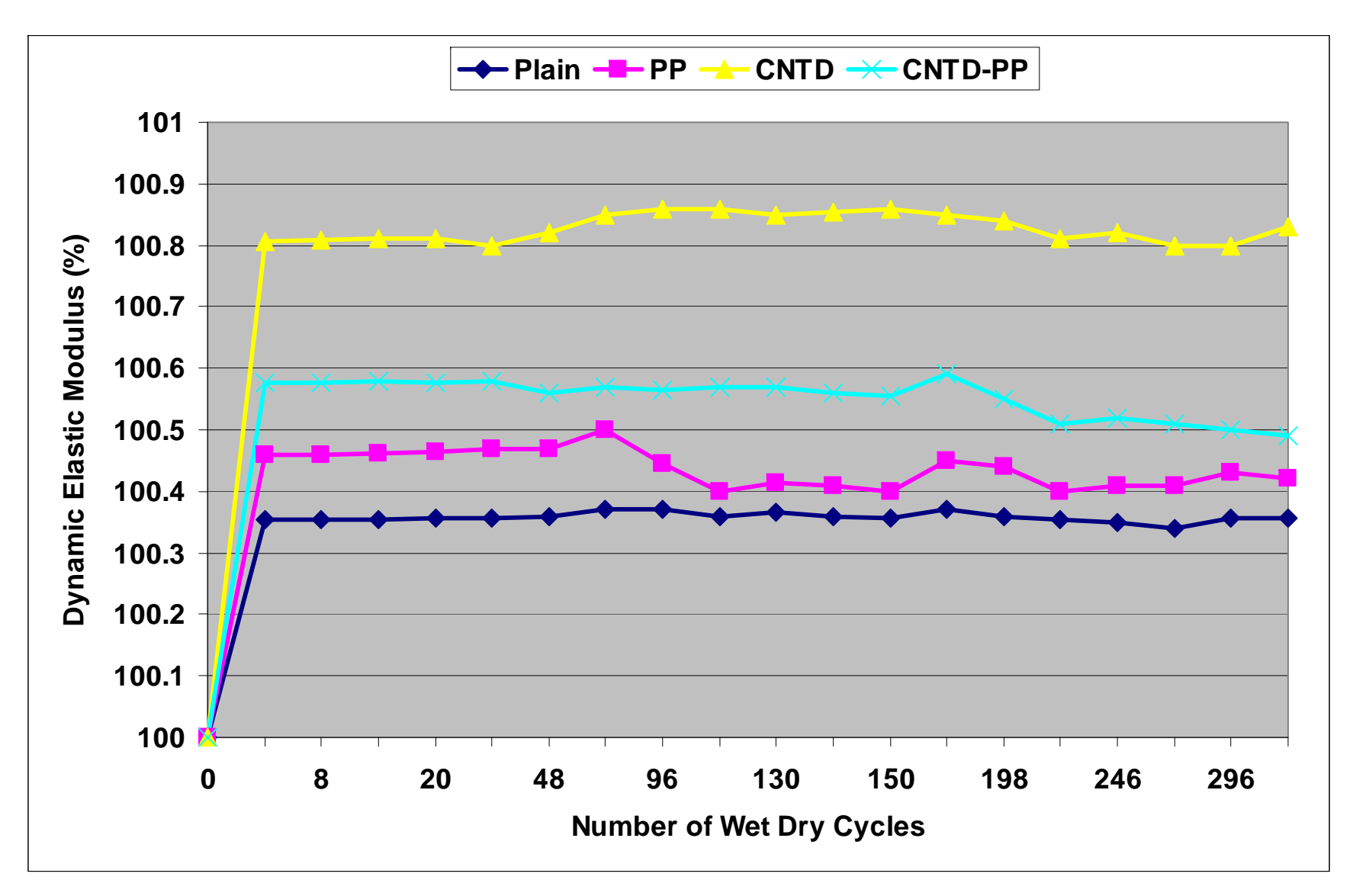


Figure 15.10- Effects of exposure to wet-dry on the dynamic modulus of DSP concrete with micro- and/or nano-scale reinforcement.

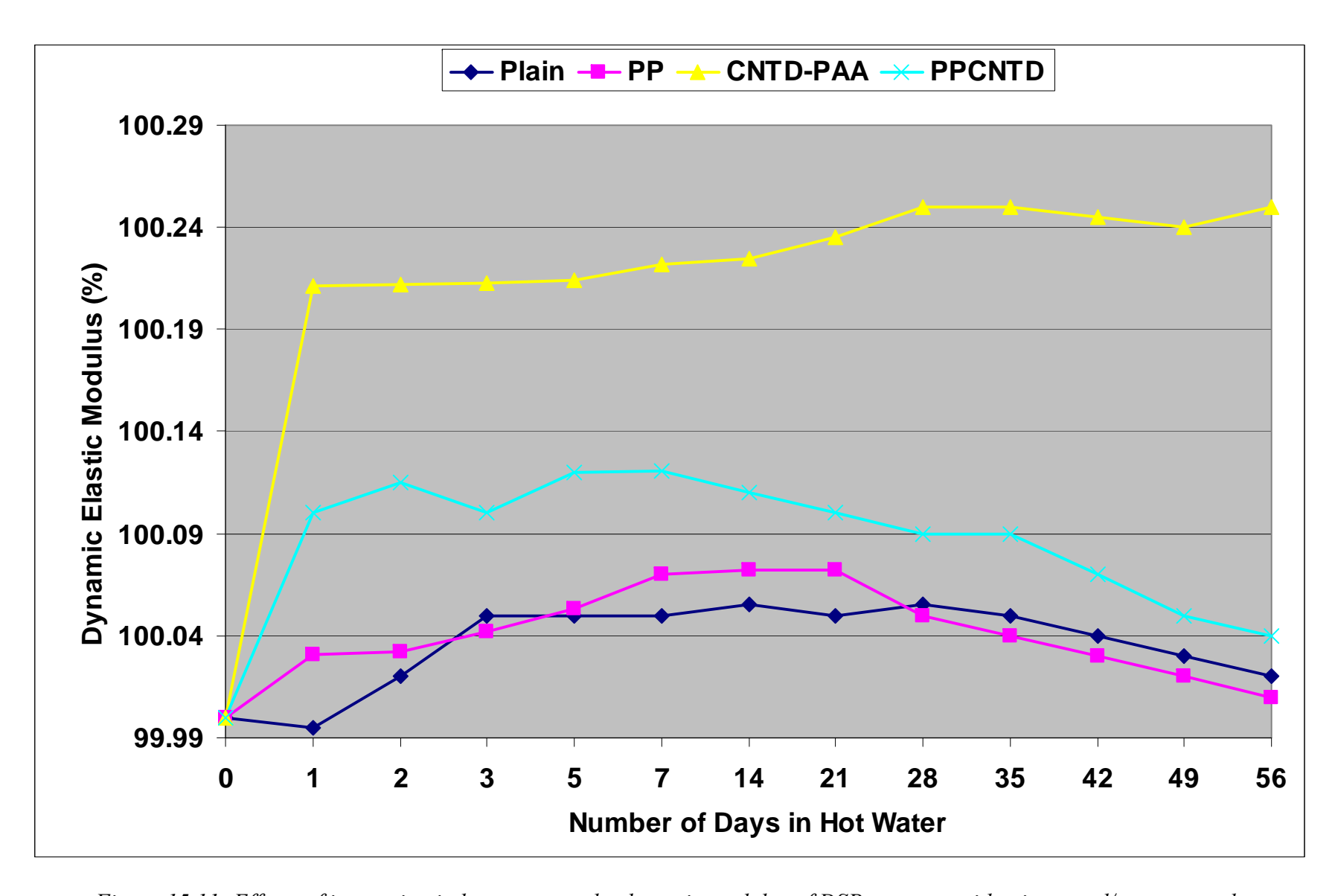


Figure 15.11- Effects of immersion in hot water on the dynamic modulus of DSP concrete with micro- and/or nano-scale reinforcement.

16 EFFECTS OF MODIFIED GRAPHITE NANOMATERIALS ON THE MOISTURE SORPTION CHARACTERISTICS OF HIGH-PERFORMANCE CEMENTITIOUS MATERIALS

16.1 General

Realizing balanced gains in diverse engineering properties of concrete is a challenging undertaking. Lowering the water-to-cementitious ratio of concrete to improve its strength, for example, compromises the toughness of concrete. Fiber reinforcement of concrete (using conventional fibers with micro-scale diameter) for achieving improved toughness does not necessarily benefit the strength of concrete. Another example is latex modification of concrete for enhancing its barrier attributes, which would not necessarily benefit the strength of concrete. Among the additives considered so far for use in concrete, nanomaterials provide unique qualities for bringing about balanced gains in diverse engineering properties of concrete. The geometric, physical and mechanical properties of nanomaterials offer the potential to realize balanced improvements in such diverse qualities of concrete as toughness, strength, barrier attributes, abrasion resistance, thermal/electrical conductivity, and fire resistance. The investigation reported herein evaluated the effects of graphite nanomaterials on the moisture sorption characteristics of a high-performance concrete. These effects of nanomaterials were compared against the corresponding effects of fibers with micro-scale diameter.

The durability of concrete in aggressive environments depends largely upon its transport qualities (Ping, Beaudoin et al. 1991; Cwirzen and Penttala 2005). Among the primary transport

mechanisms (capillary sorption, permeation and diffusion), sorption of moisture via capillary action is probably the one with the greatest impact on concrete durability (Poon, Lam et al. 1999; Bentz 2000; Bentz, Jensen et al. 2000; Pfeifer, Moeser et al. 2009). A large fraction of concrete in service is only partly saturated, which is due to the drying action of sun and wind. The initial ingress of water and dissolved salts in concrete thus involves, at least partly, capillary sorption which involves suction of water into empty capillary cavities within hydrated cement paste (Song, Jang et al. 2007; Ahlborn, Harris et al. 2011).

The resistance of concrete to moisture sorption can be enhanced by the use of supplementary cementitious materials (e.g., fly ash and silica fume) which tend to block capillary pores by products of pozzolanic reactions; other measures such as reduction of water-to-cementitious ratio, use of water-repellents or latex polymers can also lower the moisture sorption of concrete (Sahmaran and Li 2009). Graphite nanomaterials, some of which have reached industrial-scale production and offer viable cost structures, provide an alternative means of lowering the moisture sorption rate of concrete by forcing water molecules to travel tortuous paths within the hydrated cementitious paste.

16.2 Materials and Methods

16.2.1 Graphite Nanomaterials and Microfibers

Polyacrylic acid (PAA) physisorbed carbon nanotubes and graphite nanoplatelets as well as (micro-scale) carbon and polypropylene fibers were evaluated for use in cement-based nanocomposites. These graphite nanomaterials and microfibers have been introduced in detail in Chapter 2, Section 2.4, Fig. 2.3 and Table 2.3. PAA physisorbed carbon nanotubes (CNT D-PAA), graphite nanoplatelets (GP-PAA), carbon microfibers (CMF) and polypropylene

microfibers (PP) were used in high-performance paste, mortar and cement-based concrete matrix.

16.2.2 Cementitious Matrices, Mixing and Curing Procedure

Dense cementitious matrices selected have been introduced in detail in Chapter 2, Section 2.5. DSP paste, mortar and concrete were used to evaluate the water sorption characteristics of both graphite nanomaterials and/ or carbon or polypropylene microfibers at different volume fractions.

Cementitious materials (with and without functionalized graphite nanomaterials dispersed in the mixing water via sonication) and/ or carbon; polypropylene microfibers were prepared and cured following ASTM procedures as described in Chapter 2, Section 2.5.2.

16.2.3 Experimental Methods

The moisture sorption characteristics (capillary rise) of high-performance cement-based materials were assessed using ASTM C1585 procedures (Fig. 2.8f). In this test (Hall 1989), cylindrical samples with 4 in (102 mm) diameter are pre-conditioned (over 18 days) to a known moisture content; their bottom surfaces are then exposed to liquid water, and the increase in mass due to moisture sorption is measured. Measurement of mass during the sorption test is performed more frequently during the first six hours after contact with water, with subsequent measurements made daily up to fifteen days. The rate of moisture sorption and the total moisture sorption are two key outcomes of this test method.

For the test the sides and top surface of the specimens were covered with impermeable adhesive sheets. The bottom surface was immersed in water (1-3 mm depth), and the mass gain of the specimen over time (due to capillary sorption of water) was measured frequently (with the tested

surface patted dry prior to weight measurement). Absorption, I (mm), is mass change divided by both the cross-section area of the specimen and the density of water. The initial rate of absorption is defined as the slope of the line that is the best fit to I plotted against the square root of time (minute) from 1 minute to 6 hours or until the plot shows a clear change of slope (Nick point time). The later-age rate of water absorption (mm/min) is the slope of the line that is the best fit to I plotted against the square root of time (min $\frac{1}{2}$) from 1 to 7 days.

The experimental results were subjected to statistical analysis using the analysis of variance (ANOVA) and pair-wise comparison techniques in order to assess the statistical significance of the effects of different reinforcement systems on the moisture sorption characteristics of high-performance cementitious materials. Insight into the structure of the cementitious nanocomposites was gained through scanning electron microscope observations of the specimens.

16.3 Experimental Results and Discussion

Poly-acrylic acid physisorbed CNFs (CNT D-PAA) and graphite platelets (GP-PAA) were used as reinforcement at 0.16 vol.% (volume percent of dry cementitious materials); polypropylene (PP) and carbon microfibers(CMF) were used at 0.24 vol.%. Combinations of polypropylene and carbon microfibers with PAA physisorbed carbon nanotubes and graphite nanoplatelets were also used as hybrid reinforcement for different high-performance matrices, with PP/ CMF microfibers and CNT D-PAA/ GP-PAA used at 0.24 vol.% and 0.16 vol.%, respectively.

16.3.1 Rate of Moisture Absorption of DSP Paste Matrix

The mean rate of moisture absorption (ROMS) and total amount of water absorbed over a 15 days period for the high-performance paste reinforced with different volume fractions of graphite

nanomaterials and microfibers are shown in Fig. 16.1 and Fig. 16.2, respectively. The proper proportioning of cement and silica fume particles, contribution of silica fume in forming C-S-H by reaction with calcium hydroxide (C-H) in the matrix through pozzolanic reaction combined with steamed curing results in a very dense high-performance paste matrix, Fig. 16.4, which reduce the transport of moisture by capillary rise due to presence of very fine and discontinuous pours. The introduction of graphite nanomaterials further reduces the sorption rate and total moisture sorption of the high-performance cementitious pastes.

The addition of Poly-acrylic acid (PAA) physisorbed graphite nanomaterials at different volume fractions results in almost impermeable matrix. The rise in diffusion resistance with respect to plain matrix varies form 63.7% for 0.16 vol.% CNT D-PAA to 74.3% for 0.24 vol.% of GP-PAA. Unlike conventional (micro-scale) fibers, graphite nanomaterials significantly enhance the diffusion resistance of cement-based materials. This could be attributed to the close spacing and large surface area of graphite nanomaterials (Fig. 16.4), which significantly increase the tortuosity of diffusion paths within the cement-based matrix. Also the presence of graphite nanomaterials in the matrix refine the existing pore structure by providing discontinuity in a pore at nano-scale which decreases the permeability of a cement-based matrix.

Li et.al (Li, Wang et al. 2005) also found that addition of 0.5 weight percent of MWNTs refined the pore structure by mercury intrusion porosimetry (MIP). Konsta-Gdoutos et.al (Konsta-Gdoutos, Metaxa et al. 2010) also indicated that when compared to plain cement matrix, the nanocomposites appear to have a higher amount of high stiffness C–S–H and reduced nanoporosity.

Due to their small diameter MWNTs appear to specifically reduce the amount of fine pores. These results are in accordance with the results found here. On the other hand, CMF at 0.24

vol% produced a very small improvement in diffusion resistance of about 11.7%. The mean value of total amount of water absorbed by capillary rise after exposure of one surface to water for 15 days also showed similar trend which were observed for the rate of moisture absorption.

The experimental results were subjected to ANOVA followed by pair-wise comparison. The statistical analyses clearly suggested a sharp decrease in the permeability of high-performance DSP paste matrix with addition of different volume fractions of both graphite nanomaterials, at 0.05 significance level. However, the increase in diffusion resistance of the matrix due to CMF alone was not found to be statistically significant.

16.3.2 Rate of Moisture Absorption of DSP Mortar Matrix

The mean ROMS and total amount of water absorbed over a 15 days period for the high-performance mortar reinforced with different volume fractions of graphite nanomaterials and/ or microfibers are shown in Fig. 16.5 and Fig. 16.6, respectively. The proper proportioning of cement, silica fume and fine silica sand particles, combined with the factors mentioned earlier results in a very dense matrix, Fig 16.7a and 16.7b, which reduce the transport of moisture by capillary rise due to presence of fine and discontinuous pours. The resulting mean rate of moisture absorption by capillary rise in the plain matrix is 0.002967 mm/min which results in a very dense matrix. When compared to a normal mortar with out silica fume and a w/c ratio of 0.45, the increase in diffusion resistance is about 79.3%.

However, due to the addition of silica sand the increase in rate of moisture sorption due to capillary rise with respect to plain DSP paste is 63.3%. This increase is primarily due to addition of silica sand and the porosity is increased due to bigger sand grains (500 microns), Fig. 16.8a. The ITZ around these grains seems more porous and a likely path for crack to progress under load, Fig. 16.8b. However, as was shown for DSP paste matrix, the addition of both

functionalized graphite nanomaterials as well as their hybrid combination with CMF resulted in drop of both rate of moisture sorption rate as well as the total water absorbed. The maximum increase was recorded with use of 0.24 vol.% GP-PAA (66.9%). This increase in diffusion resistance is due to the reinforcement of graphite nanomaterials of the paste portion of the matrix as well as the ITZ with sand grains, Fig 16.7c. These results show a lot of promise for use of such material for repair and rehabilitation work. On the other hand, CMF at 0.24 vol% produced a very small improvement in diffusion resistance of about 5.6%.

The experimental results were subjected to ANOVA followed by pair-wise comparison. The statistical analyses clearly suggested a sharp decrease in the permeability of high-performance DSP mortar matrix with addition of different volume fractions of both graphite nanomaterials and their hybrid combination with CMF, at 0.05 significance level. However, the increase in diffusion resistance of the matrix due to CMF alone was not found to be statistically significant.

16.3.3 Rate of Moisture Absorption of DSP Concrete Matrix

The mean ROMS and total amount of water absorbed over a 15 days period for the high-performance concrete reinforced with different volume fractions of graphite nanomaterials and/ or microfibers are shown in Fig. 16.8 and Fig. 16.9, respectively. The proper proportioning of cement, silica fume, fine silica sand particles and granite gravel, combined with the factors mentioned earlier results in a very dense matrix, which reduce the transport of moisture by capillary rise due to presence of fine and discontinuous pours. The resulting mean rate of moisture absorption by capillary rise in the plain matrix is 0.009919 mm/min which results in a very dense matrix. When compared to a high strength concrete matrix with silica fume (10,000 psi; 69 MPa) and a w/c ratio of 0.35, the increase in diffusion resistance is about 49.2%. This is much superior to 0.19 mm/min for normal concrete with a W/C ratio of 0.4 which is suggested

by (Neville A.M. 1995)and other research suggested that ordinary Portland cement concrete with W/C ratio of 0.4–0.5 would have sorptivity of about 0.23 mm/min (Tsivilis, Tsantilas et al. 2003; Chindaprasirt, Jaturapitakkul et al. 2005). The reason for the lower sorptivity of different DSP matrices samples may be attributed to significantly lower water to cementitious material (w/cm) ratio, high silica fume content and absence of classic coarse aggregate. The use of silica fume results in a denser matrix, by reducing the pore size and thickness of transition zone between aggregate particles/ microfiber and surrounding cementitious matrix. According to the Mehta and Monteiro (Mehta 1993), the existence of microcracks in the interfacial transition zone at the interface with coarse aggregate is the primary reason that concrete is more permeable than the corresponding hydrated cement paste and mortar. Also in general, everything else being the same, the larger the aggregate size the higher the local water–cement ratio in the interfacial transition zone and, consequently, the weaker and more permeable would be the concrete.

However, due to the addition of granite gravel the increase in rate of moisture sorption due to capillary rise with respect to plain DSP mortar is 70%. This increase is primarily due to addition of much bigger inclusions which are relatively more porous than the bulk past and the porosity is increased due to bigger gravel particles (9 mm). The ITZ around these gravel particles is much more pronounced and porous. Being weaker than the bulk paste these gravel particles are and the ITZ around them are the likely paths for crack to progress under load. However, as was shown for DSP paste and mortar matrix, the addition of both PAA physisorbed graphite nanomaterials as well as their hybrid combination with PP microfibers resulted in drop of both moisture sorption rate as well as the total water absorbed. The maximum increase was recorded with use of 0.24 vol.% GP-PAA (63.9%). This increase in diffusion resistance is due to the reinforcement of graphite nanomaterials of the paste portion of the matrix as well as the ITZ with sand and

gravel particles. These results show a lot of promise for use of such material for repair and rehabilitation work as well as when combined with appropriate microfibers these nanocomposites can be used in structural members with superior engineering and durability properties. On the other hand, PP microfibers at 0.24 vol% produced a very small improvement in diffusion resistance of about 5.7%.

The experimental results were subjected to ANOVA followed by pair-wise comparison. The statistical analyses clearly suggested a sharp decrease in the permeability of high-performance DSP concrete matrix with addition of different volume fractions of both graphite nanomaterials and their hybrid combination with PP microfibers, at 0.05 significance level. However, the increase in diffusion resistance of the matrix due to PP microfibers alone was not found to be statistically significant.

16.4 Comparison of Graphite Nanomaterials with other Methods of Reducing Permeability of Concrete

The durability of concrete structures is intimately related to the rate at which water is able to penetrate the concrete. This is because concrete is susceptible to degradation through leaching, sulfate attack, freezing-and-thawing damage, and other mechanisms such as steel corrosion in reinforced concrete structures that depend on the ingress of water. Because cracks significantly modify the transport properties of concrete, their presence greatly accelerates the deterioration process. To solve this serious problem, many ways can be adopted i.e. adding water repellant agents to the concrete, treating the top with latex modified impermeable concrete and using high strength matrices with secondary supplementary materials like silica fume and fly ash.

However, all these agents have a certain service life till they are effective. A first possibility for the improvement of the life span of concrete structures can be realized by impregnation of the covercrete with water repellent agents (Ahlborn, Harris et al. 2011). In this method the properties of the covercrete are optimized in a rational way. The most important parameter controlling the effectiveness of impregnating water repellent admixtures as means of protecting concrete from aggressive ions to cause concrete deterioration is the depth of penetration of the water repellent agents. However, when concrete structures experience cracking in field conditions, the depth of cracking can easily reach or exceed the full depth of penetration.

Another possibility to reduce water transportation is to modify the structural concrete properties by adding a water repellent agent directly to the fresh mixture (Katz and Bentur 1996). Using a water-soluble silicone based water repellent chemical admixture (Dow Corning IE-6683). This water repellent chemical admixture is supplied by the manufacturer in liquid form with a solid content of 40%. This type of admixture does not provide an impenetrable physical barrier, but rather induces a chemical repulsion/repellency of the concrete to water (Sahmaran and Li 2009). This water repellent admixture is usually used at a medium dosage of 13.6 kg/m³ (about 0.80% by weight of total dry materials) recommended by the manufacturer and is directly added to the fresh mixture during the mixing process. However, these chemical agents have limited life varying form 2-5 years and are neutralized by the action different weathering agents.

Water based polymer systems are often used for improvement in the properties of plain cement mortar or concrete. Presently, latexes of a single or combinations of polymers like polyvinyl acetate, copolymers of vinyl acetate–ethylene, styrene– butadiene, styrene–acrylic, and acrylic and styrene butadiene rubber emulsions are generally used. One of the limitations of these polymer systems is that they may re-emulsify in humid alkaline conditions.

A effective solution to address this problem is to add graphite nanomaterials which interact with the matrix at the nano level and increase the durability and reduce transport of the moisture through the matrix by increasing the tortousity of the diffusion path as well as increasing the density of the CSH phase of the matrix (Konsta-Gdoutos, Metaxa et al. 2010). When comparing with the above solution to make concrete impermeable, graphite nanomaterials have inherent advantage of being present in the matrix as inclusion and there effectiveness is not reduced by different weathering agents. When comparing from price to performance ratio functionalized graphite nanoplatelets (\$10/kg) at a dosage rate of 3 to 4 lbs/cubic meter of concrete is a very viable solution to be used as a repair material. Also when combined with appropriate microfibers these nanocomposites can be used in structural concrete with superior engineering and durability properties.

16.5 Summary

The durability results generated for different high performance cementitious matrices reinforced with different volume fractions of graphite nanomaterials and/ or microfibers indicated proper gradation of matrix materials results in a dense high-performance matrix with much lower porosity.

Addition of both PAA physisorbed graphite nanomaterials as well as their hybrid combination with both microfibers resulted in drop of both moisture sorption rate as well as the total water absorbed. Due to inherent advantages of being present in the matrix as an inclusion and being relatively inert to all weathering agents, graphite nanomaterials, especially graphite nanomaterials, provide a cost-effective solution for durable repair materials. When appropriately combined with microfibers these nanocomposites can be using in structural concrete with superior engineering and durability properties.

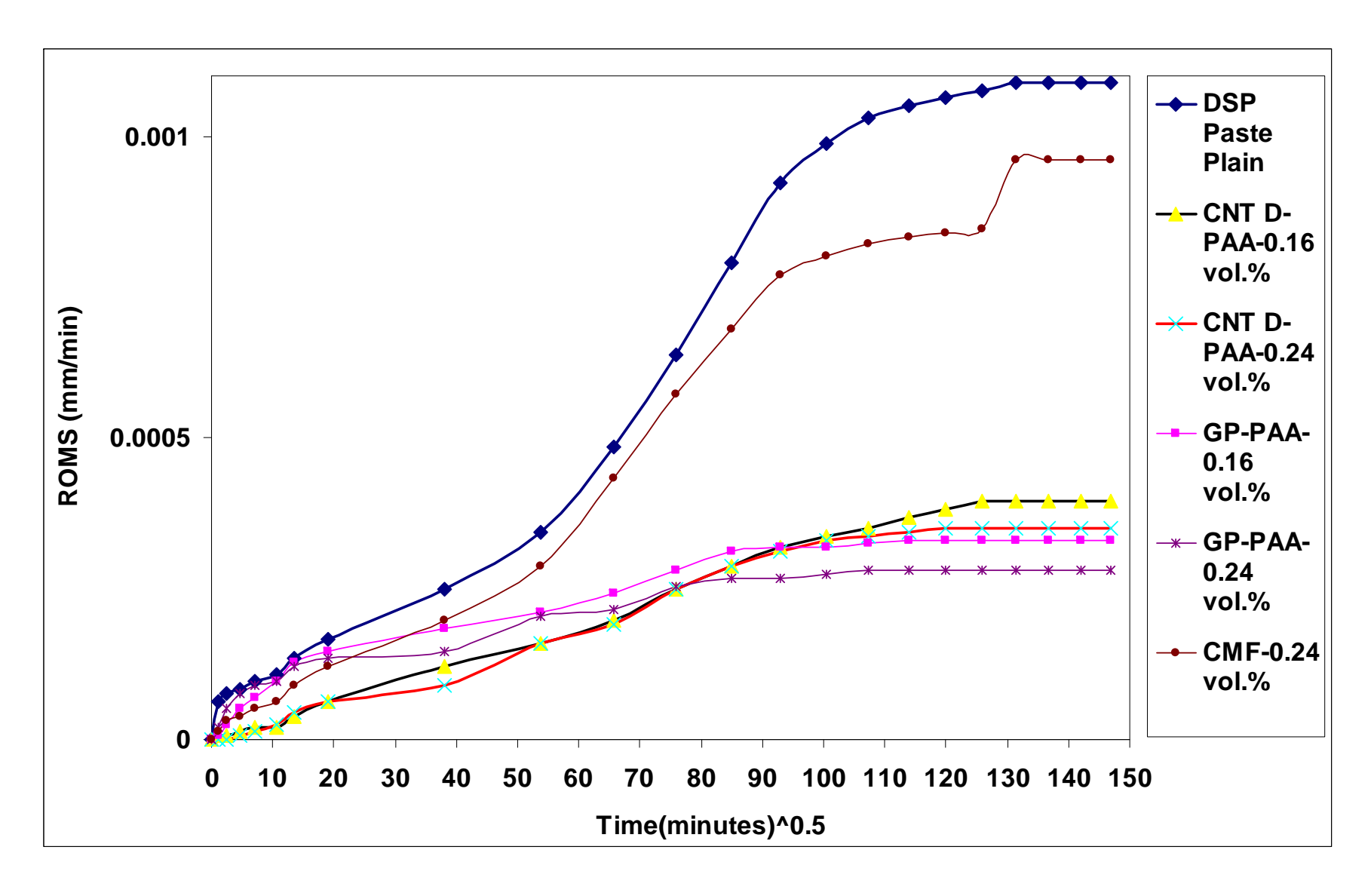


Figure 16.1- Mean ROMS by capillary rise in high-performance DSP paste matrix reinforced with and without different volume fraction of graphite nanomaterials and microfibers.

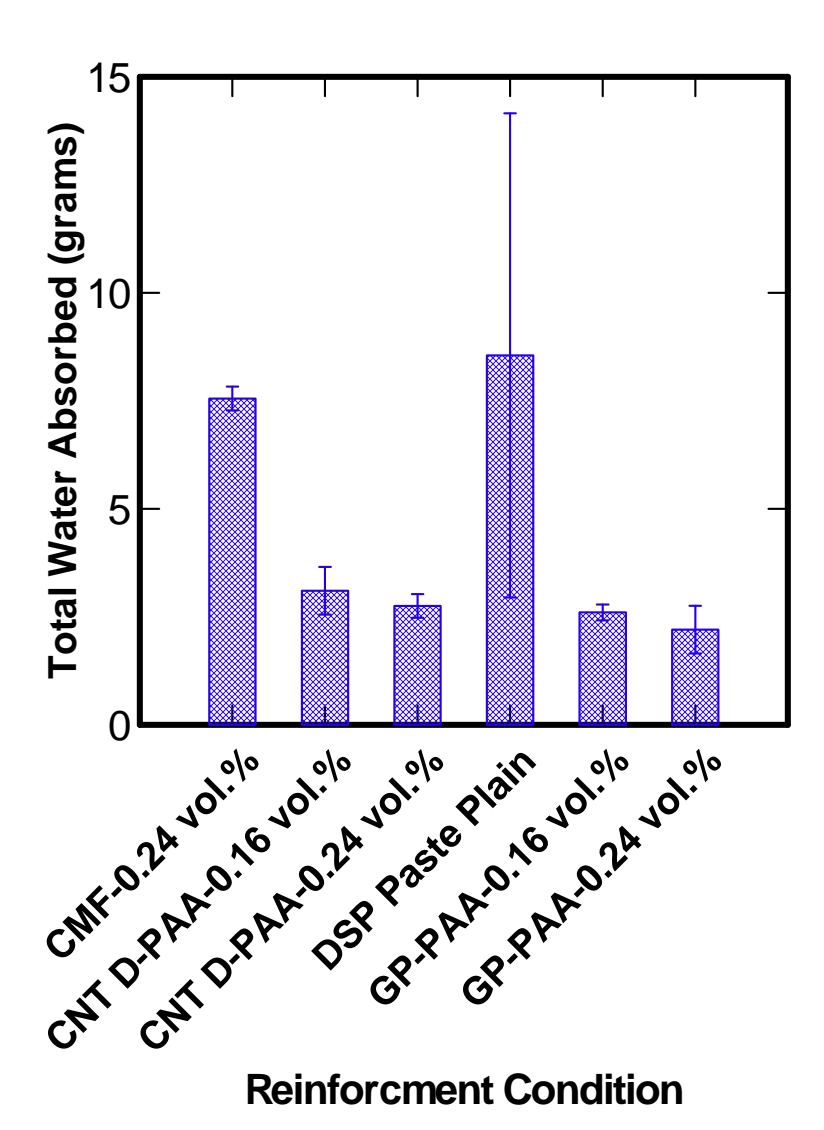


Figure 16.2- Mean total water absorbed after 15 days in high-performance DSP paste matrix reinforced with and without different volume fraction of graphite nanomaterials and microfibers.

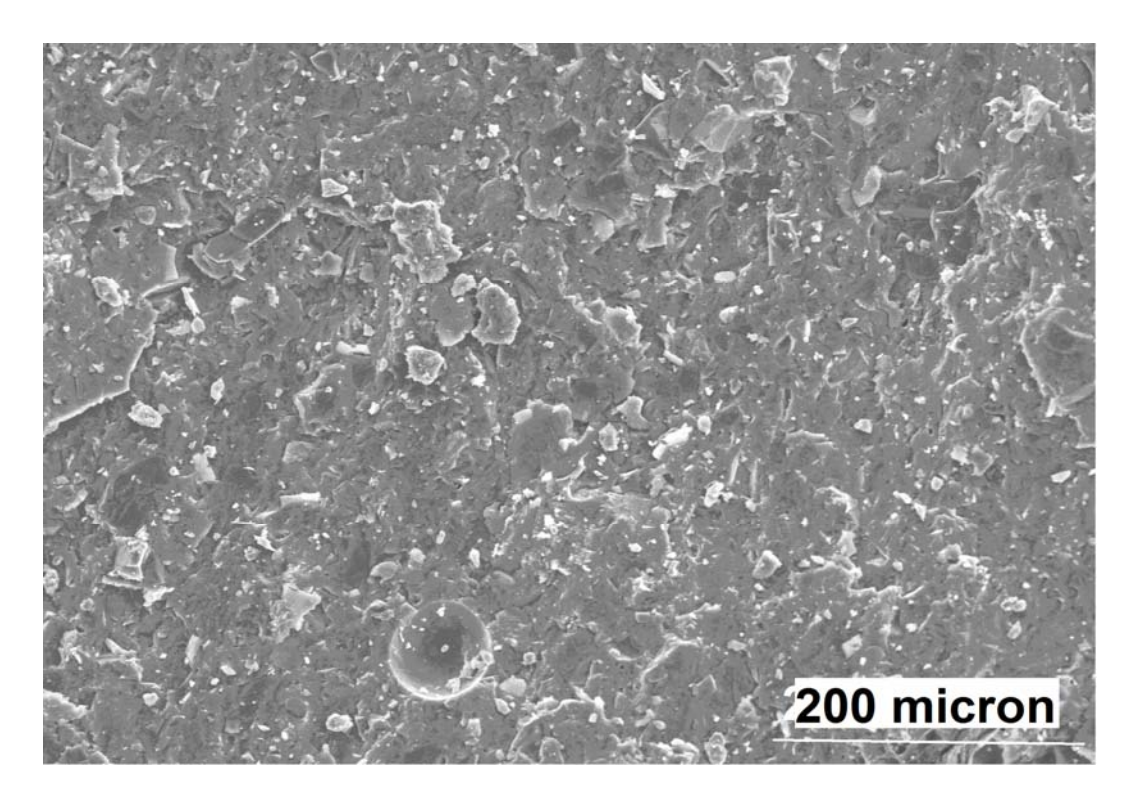


Figure 16.3- SEM images of fractured surfaces of high performance paste matrix showing dense structure of the matrix.

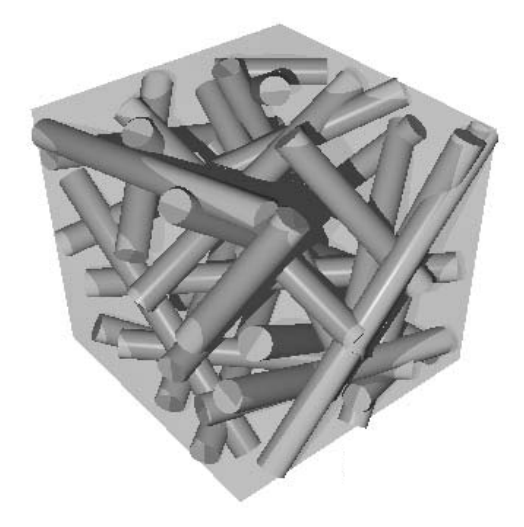


Figure 16.4- Three-dimensional assembly of carbon nanotubes within a cement-based matrix.

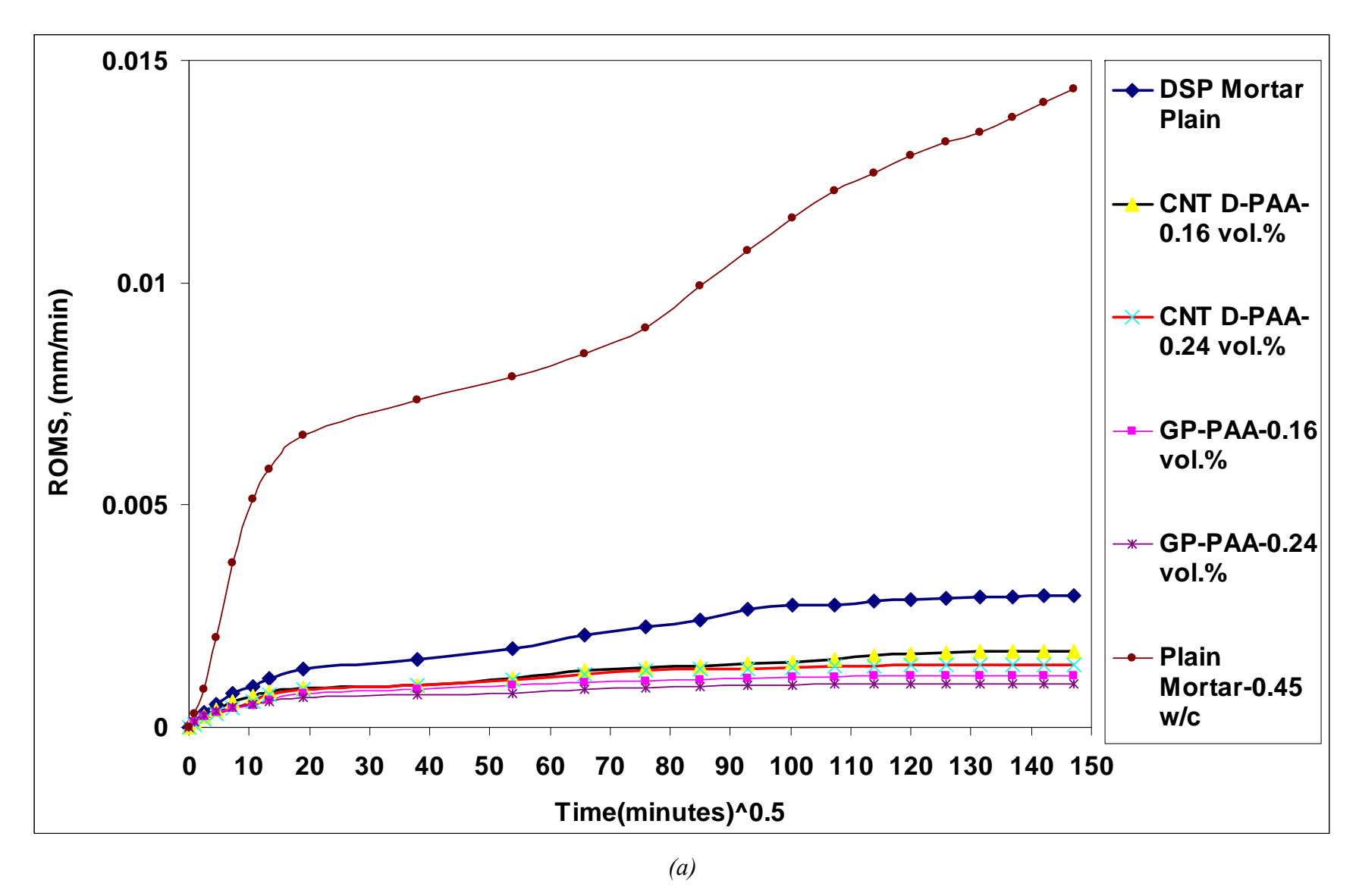
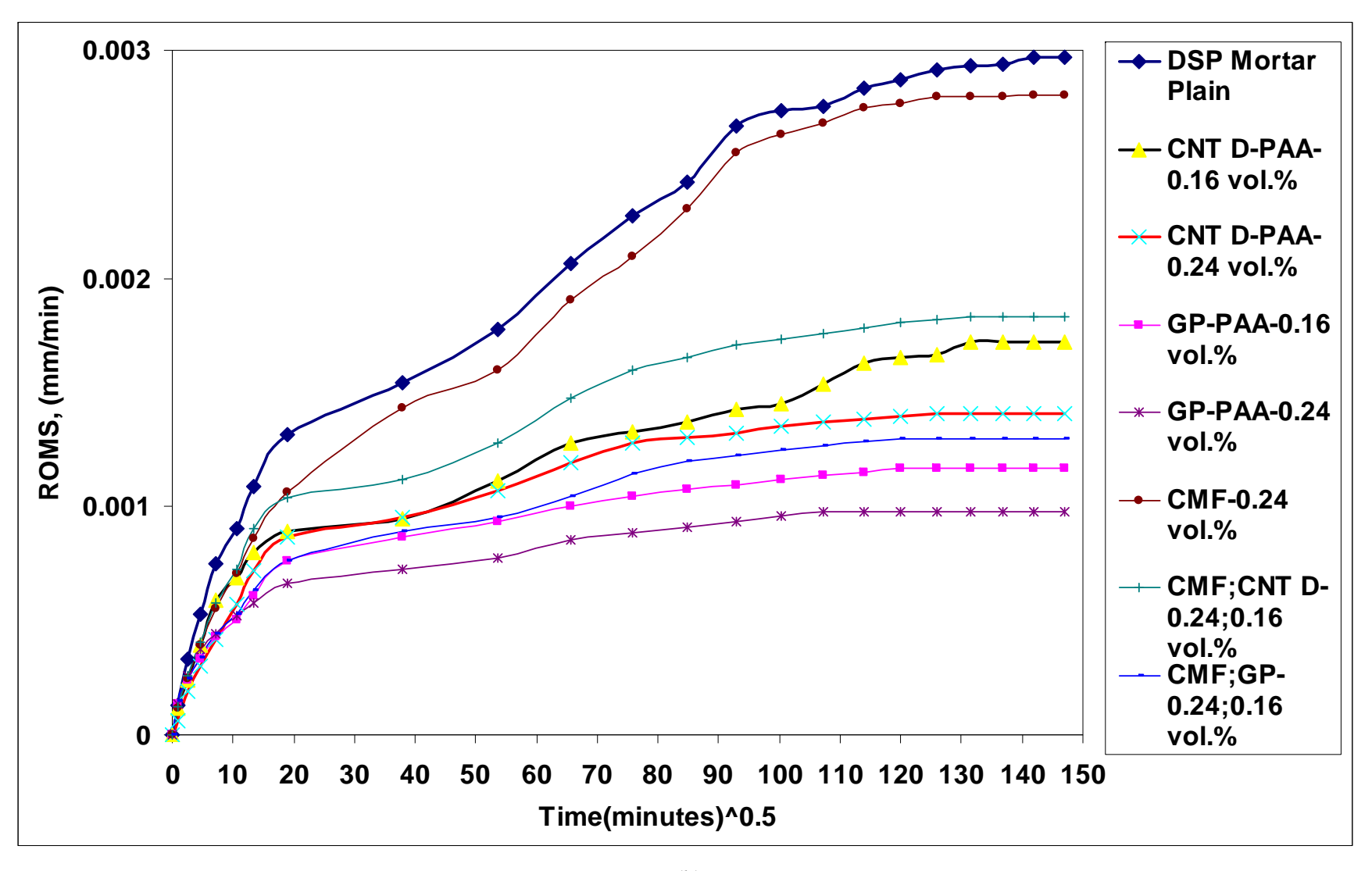


Figure 16.5- Mean ROMS by capillary rise in high-performance DSP mortar matrix reinforced with and without different volume fraction of graphite nanomaterials and/or microfibers.

Figure 16.5 (cont'd)



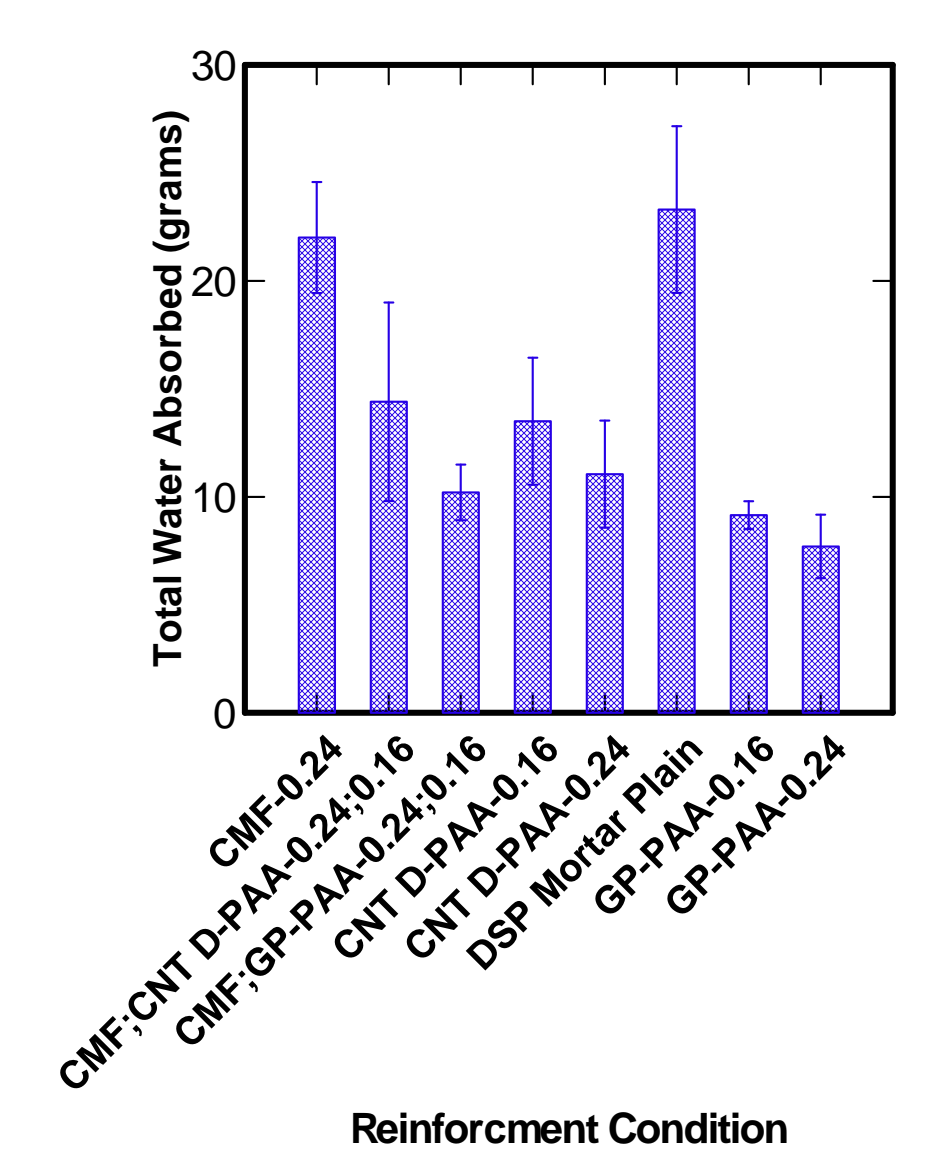
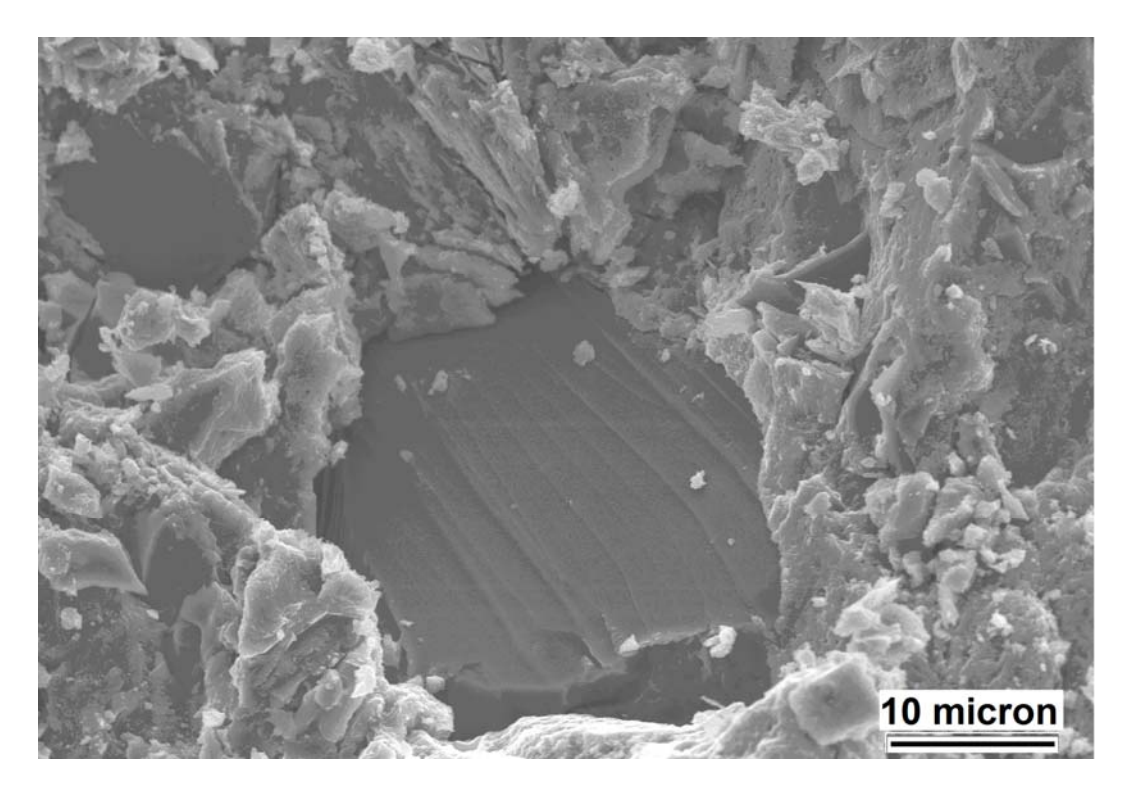
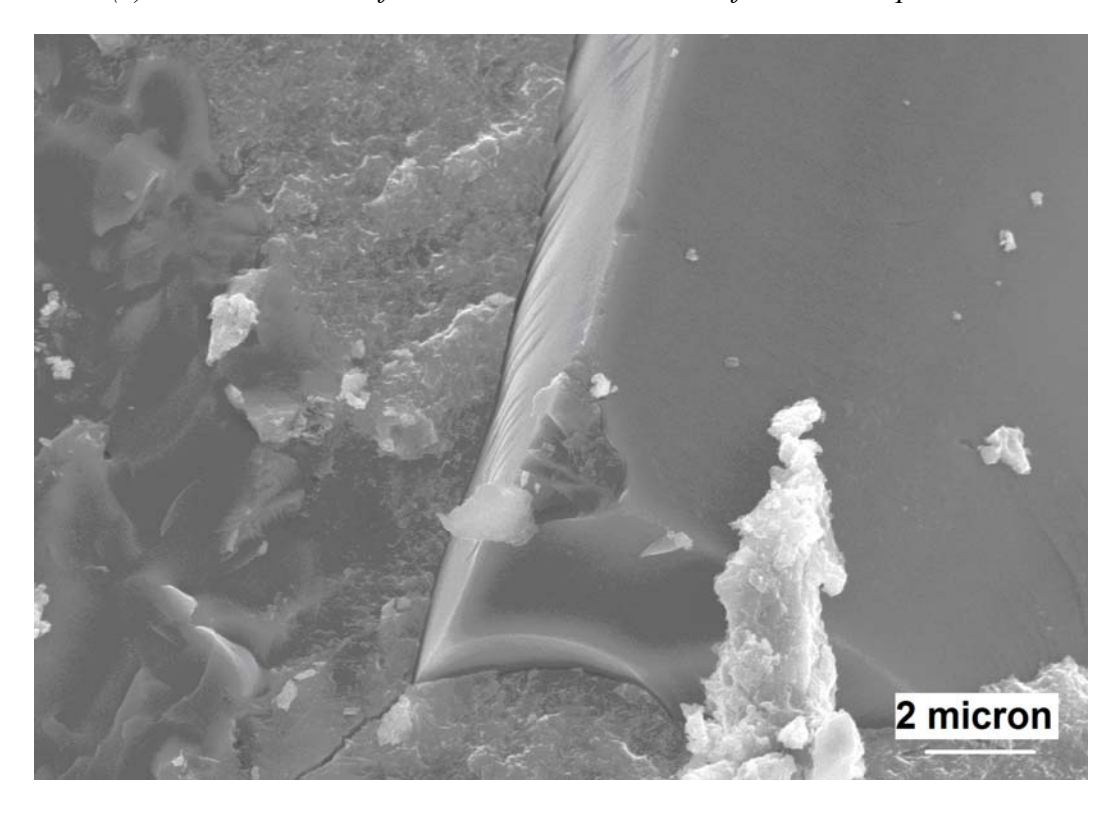


Figure 16.6- Mean total water absorbed after 15 days in high-performance DSP mortar matrix reinforced with and without different volume fraction of graphite nanomaterials and microfibers.



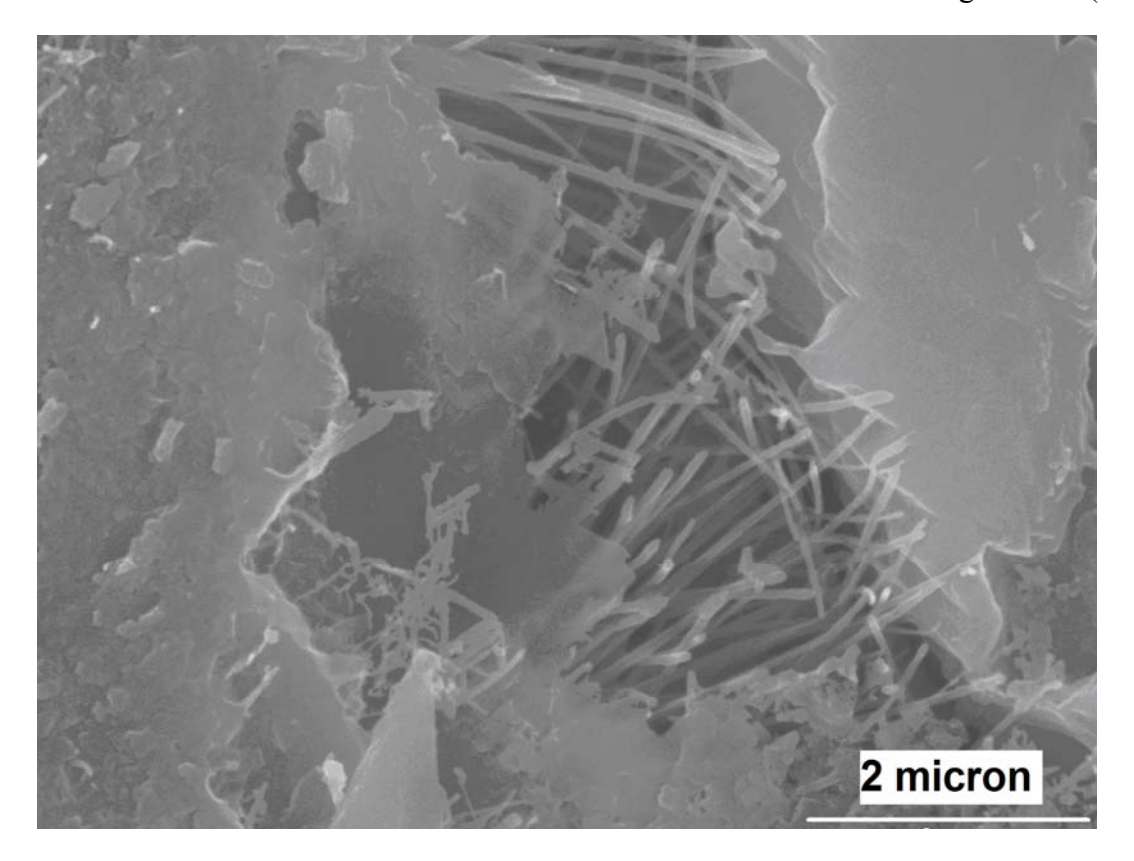
(a) Dense structure of the matrix and inclusion of silica sand particles



(b) Diversion of crack around sand particle

Figure 16.7- SEM images of fractured surfaces of high performance mortar matrix.

Figure 16.8 (cont'd)



(c) Close spacing of nanomaterials within the matrix

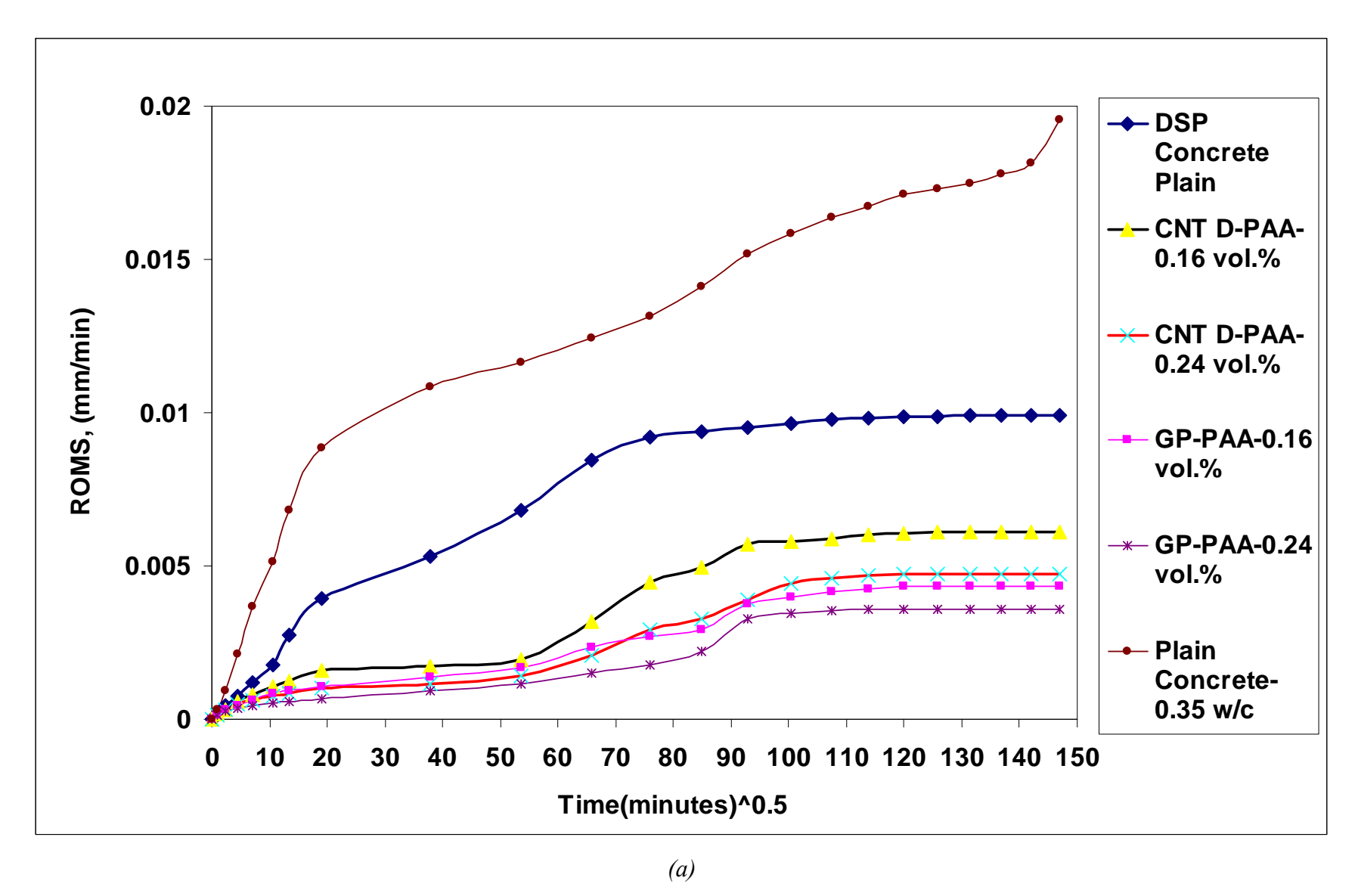
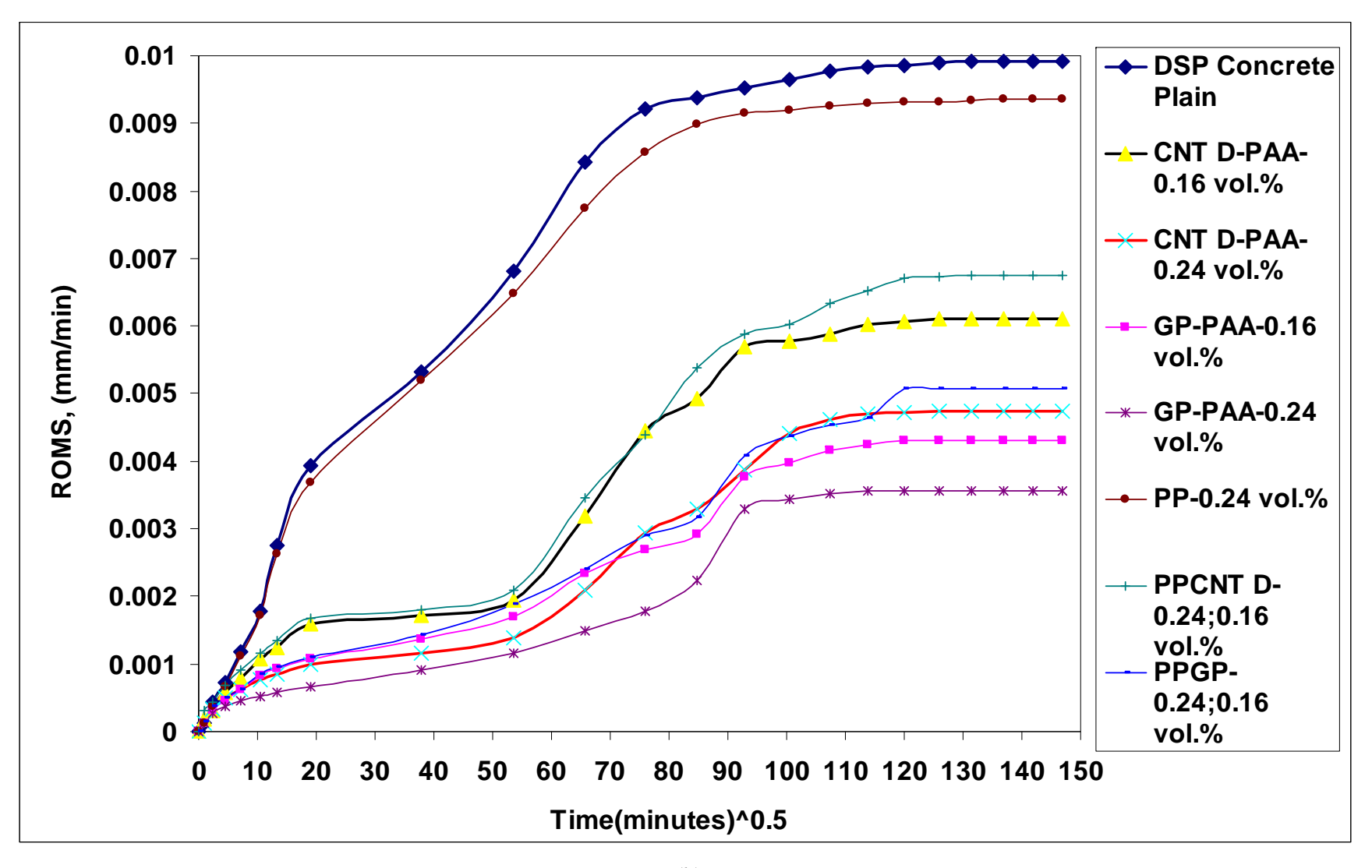
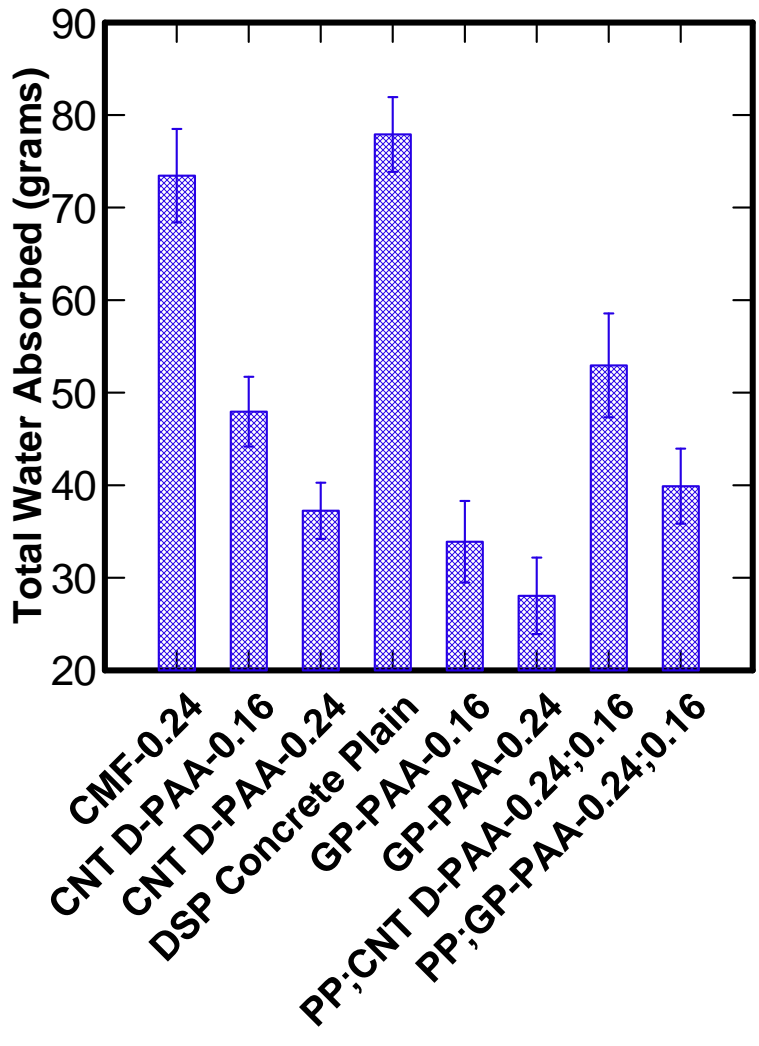


Figure 16.8- Mean ROMS by capillary rise in DSP concrete matrix reinforced with and without different volume fraction of graphite nanomaterials and/or microfibers.





Reinforcment Condition

Figure 16.9- Average values of total water absorbed by capillary rise after 15 days in high-performance DSP concrete matrix reinforced with and without different volume fraction of graphite nanomaterials and microfibers.

17 PLANT PRODUCTION AND PLACEMENT OF NANOCOMPOSITES – CHALLENGES AND RESULTS

17.1 General

To overcome extremely brittle failure, low tensile capacity and sensitivity to early age microcracking high strength concrete matrices are typically provided with fiber reinforcements at the millimeter and/or the micro scale using macro-fibers and microfibers, respectively. These matrices however, exhibit flaws at the nano-scale, where traditional reinforcement is not effective. Graphite Nanomaterials, including relatively low cost carbon nanofibers (CNF) and graphite nanoplatelets (GP), present several distinct advantages as a reinforcing material for high strength/performance cementitious composites as compared to more traditional fibers. First, they exhibit significant greater strength and stiffness than conventional fibers, which should improve overall mechanical behavior. Second, their higher aspect ratio is expected to effectively arrest the nano-cracks and demand significantly higher energy for crack propagation. Thirdly, provided these nanomaterials are uniformly dispersed, and due to their nano-scale diameter, fiber spacing is reduced. This has opened a new field for nano-sized reinforcements that should theoretically hinder the formation and later propagation of microcracks at the very beginning. Few attempts have been made to add different graphite nanomaterials as reinforcement in cementitious matrices.

Most of the works involving use of graphite nanomaterials in cementitious matrices have used very fine matrices to evaluate the efficiency of their reinforcement and reported modest gains in

some of the engineering properties (Makar and Beaudoin 2004; Cwirzen, Habermehl-Cwirzen et al. 2008; Cwirzen, Habermehl-Cwirzen et al. 2009; Makar and Chan 2009; Metaxa, Konsta-Gdoutos et al. 2010; Li, Wang et al. 2005). A comprehensive approach was taken to evaluate suitably functionalized CNFs and GPs in high-performance cementitious materials of higher complexity, especially concrete. The results of functionalized and non-functionalized graphite nanomaterials in different high performance DSP matrices have presented in detail in earlier chapters. However, all the work done in the field of cement-based nanocomposites is confined to laboratory evaluation.

The focus of this part of research is to take the laboratory experience and scale up the production of these cement-based nanocomposites by tailoring their use to practical situation. In this research a HSC (High-Strength Concrete) matrix was selected using the materials commonly used in plant production of concrete. The matrix was suitably reinforced with polyacrylic acid (PAA) physisorbed CNFs/ GPs and polypropylene (PP) microfibers. The larger aggregate size and content in concrete, when compared with mortar and paste, adds to complexity of behavior and failure modes by introducing an interfacial zone, generating interactions between aggregates and propagating microcracks, and the need to disperse nanomaterials in the space between aggregates.

Evaluation of the reinforcement efficiency of CNFs and GPs in a coarser cementitious matrix, high-strength concrete, was undertaken to see the effect of increased particle size on the interaction of nano reinforcements with the relatively coarser matrix during and after plant production. Furthermore, micro-scale PP fibers along with their hybrid combination with CNFs and GPs were evaluated to achieve desired balance of performance and cost efficiency. Parallel

laboratory specimens were also casted to compare the efficiency of mixing procedures adopted during concrete plant production.

Cementitious materials are essentially particulate composites, which are rarely used without aggregates (particulates). Given the micro- to millimeter-scale dimensions of the sand and gravel particles used in HSC, hybrid reinforcements which complement the reinforcing and dimensional stabilizing actions of particulates with multi-scale reinforcement mechanisms could produce particularly positive effects. In the past, the concept of using hybrid (micro- and millimeter-scale) reinforcement has been explored by the concrete industry for achieving balanced gains in material properties (Moranville-Regourd 2001; O'Connell, Boul et al. 2001; Lawler, Zampini et al. 2005; Banthia and Sappakittipakorn 2007).

17.2 Materials and Methods

17.2.1 Graphite Nanomaterials and Microfibers

Polyacrylic acid (PAA) physisorbed carbon nanofibers and graphite nanoplatelets as well as (micro-scale) polypropylene fibers were evaluated for use in high-strength cement-based nanocomposites. These graphite nanomaterials and microfibers have been introduced in detail in Chapter 2, Section 2.4, Fig. 2.3 and Table 2.3. PAA physisorbed CNFs (CNF-PAA), graphite nanoplatelets (GP-PAA) and polypropylene microfibers (PP) were used in high-performance cement-based concrete matrix.

17.2.2 Cementitious Matrices, Dispersion, Mixing and Curing Procedure

A more practical HSC matrix was selected with a targeted compressive strength of 10,000 psi (69 MPa). Most of the materials used are commonly used in concrete manufacturing at any major concrete plant. Table 17.1 gives the composition of the high-strength concrete matrix as well as

the composition of different mixes selected and casted for evaluation of the merits of graphite nanomaterials and microfibers in cement-based materials. Four mixes were casted at High Grade Materials, Inc concrete plant located at Lansing, MI. The mixes included a plain without any reinforcement, one with CNF-PAA and PP, one with GP-PAA and PP; and with PP microfibers alone. CNF-PAA and GP-PAA nano-reinforcements were used at 0.16 volume percent (vol.%) of the dry cementitious materials or binder (cement plus silica fume) and PP microfibers were used at 0.24 vol.% of binder. The plant mixes were made in 1 cubic yd batches and were laid as over lay of an existing slab. Specimens were taken from these batches to evaluate various engineering and durability properties. Commensurate laboratory mixes were also casted using same materials and reinforcement conditions to evaluate different engineering properties and compare with the values of plant produced specimens. In the initial laboratory evaluation it was ascertained that dispersing the graphite nanomaterials in up to 20% of the mixing water does not effect the dispersion and reinforcement efficiency of the nanomaterials. Therefore, only 20% of the initial mixing water was used for dispersion of nanomaterials in the laboratory. The nanomaterials were provided in dispersed condition when mixing was done at the concrete plant. The materials selected for use in cement-based matrices included Type I Portland cement (Illinois Cement Company), densified silica fume (Elkem Materials, Inc.) with ~200 nm average particle size, ~15 m²/g specific surface area and minimum 7-day pozzolanic activity index of 105%, 2NS river sand (High Grade Materials, Inc), gravel ranging in size from 1 mm to less than 9.5 mm, with average particle size of 3.55 mm (High Grade Materials, Inc), Polychem SPC a polycarboxylate-based Type F ASTM C 494 complete range water reducing admixture procured from General Resource Technology, Inc.

Cementitious materials (with and without functionalized graphite nanomaterials dispersed in the mixing water via sonication as described in Chapter 2, Section 2.5.2) and/ or polypropylene microfibers were prepared following ASTM C 192 and C 305 procedures. The specimens were moist-cured inside molds after casting (ASTM C 192) over a 24-hour period, and then demolded and subjected to curing in water for 27 days before testing.

17.2.3 Challenges Associated with Plant Production

In order to scale up there are different challenges involved with control on the quality including the batch weights of mix ingredients, mixing procedure and dispersion of reinforcements within the matrix. Some of the challenges which were faced during the plant production of these high-strength cement based nanocomposite are listed below:

- The increase in the quantity of mix ingredients decreases the control on the quality and quantity of mix ingredients during plant production. Most of the concrete plants produce batches of 10 to 15 cubic yards where the rounding off of different ingredient weights does not cause a major change in the engineering properties, especially for normal strength concrete. But for high-strength concrete when using low water to cement ratio and high cement content this rounding can have a major effect, especially when a one cubic yard batch is prepared. A lot of care must be taken to weigh the matrix materials as close to the calculated materials as possible and variation between the batches must be avoided.
- Most of the concrete producing plants do not handle supplementary cementitious materials, especially silica fume, in large quantities. The required amount if required is usually added directly to the mixing truck. This although allows control of weight of material to be added but becomes cumbersome for large volume concrete jobs.

- Sonication and dispersion of graphite nanomaterials in the mixing water at larger scale present a major challenge. Thus in our laboratory work initial evaluation was done to evaluate the minimum quantity (20% of mix water) of mix water that can be used without effecting the dispersion and subsequent reinforcement efficiency of graphite nanomaterials in the matrix. PAA physisorption also prove effective in dispersion of nanomaterials in lesser quantity of mix water.
- The procedure for mixing the dry ingredients and introduction of fiber reinforcements, especially graphite nanomaterials, in to the matrix should be carefully considered. As at most of the concrete plants the mixing is done by the mixing truck, therefore, the pre-dispersed graphite nanomaterials were introduced into the mixing drum with 50% of the remaining mixing water. The matrix materials including all-purpose water reducer and remaining water were introduced into the drum slowly with the drum of the mix truck rotating. The ingredients were mixed for 15 minutes at maximum rotation. Microfibers were added to the mix when the ingredients have turned in to slurry and the concrete mix was rotated for another 5 minutes before moving to lay-down site. For laboratory specimen the procedure followed in plant production was roughly followed.
- Due to large capacity of the mixing drum and small volume of the mixing batch a lot of matrix material was attached to the central mixing shaft. One way to address this issue is to reverse rotate the drum in a controlled fashion so that any material attached to the mixing shaft is mixed with the main ingredients.
- The specimens from the testing must be taken from the main batch both form the starting, middle and end part of the pouring to get statistically reliable results.

17.2.4 Experimental Methods

The test procedures employed to determine the engineering properties of HSC included compression tests (ASTM C 109), flexure tests (ASTM C 1185), impact tests (ASTM D 7136), abrasion tests (ASTM C 944) and moisture absorption rate tests (ASTM C 1585). Experimental results were evaluated using the analysis of variance (ANOVA) and pair-wise comparison techniques to reach statistically viable conclusions.

17.3 Experimental Results and Discussion

Hybrid combination of poly-acrylic acid physisorbed carbon nanofibers (CNF-PAA) / graphite nanoplatelets (GP-PAA) were used as reinforcement at 0.16 vol.% and polypropylene (PP) microfibers were used at 0.24 vol.% of binder. PP microfibers were also casted alone at 0.24 vol.% of binder to assess the beneficial effects of nano-reinforcements when added to the matrix.

17.3.1 Flexural Performance

The flexural attributes test results for the HSC reinforced with different volume fractions of graphite nanomaterials and polypropylene microfibers produced at a concrete plant and in laboratory are summarized in Table 17.2.

A drop in the mean values of all flexural attributes was observed in samples casted from plant mixed batches when compared with those casted in the laboratory. This is expected due to large quantity of material mixed in a plant as compared to lab casting, rounding up or down of weight of matrix materials during bathing and mixing in the truck mixer and improper dispersion of fibers within the matrix. However, it was observed that all hybrid reinforcements, whether casted in laboratory or mixed in concrete plant, produced increase in the mean values of all flexural attributes when compared with respective plain matrices. However, samples containing

polypropylene microfibers when used alone showed a small drop in the mean flexural strength both for laboratory and plant produced specimens.

Both in laboratory and plant production, the most desired balance of properties was realized with hybrid reinforcement consisting of 0.16 vol.% CNF-PAA and 0.24 vol.% of PP microfibers. The corresponding improvements in flexural strength, energy absorption capacity and maximum deflection for laboratory and plant produced specimens versus respective plain concrete were 23.4; 22.4%, 252; 356% and 532; 591%, respectively. This points out that hybrid reinforcement of brittle high-strength concrete matrices can effectively improve all the flexural attributes, thus bringing about balanced improved at competitive cost.

The experimental data presented earlier pointed at the positive effects of hybrid (nano- and micro-scale) reinforcement systems in high-performance concrete materials. The test data presented here suggest that micro-scale fibers of lower modulus and lower cost could effectively complement the reinforcing effects of polymer-wrapped CNFs and GPs in high-strength concrete. The hybrid reinforcement systems also overcame the adverse effects of microfibers on flexural strength. The synergistic reinforcing action of nano- and micro-scale reinforcement was further enhanced by polymer wrapping of graphite nanomaterials.

The experimental results were subjected to statistical analysis of variance (ANOVA) followed by pair-wise comparison. The statistical analyses indicated that statically significant improvement in all flexural attributes was observed for all samples reinforced with CNF-PAA and PP, whether casted in laboratory or in a concrete plant, with respect to their plain matrices at 95% confidence level. Other reinforcement systems considered here only showed improvements in energy absorption capacity and maximum deflection at this level. The pair-wise comparison also points out that the drop in mean values of flexural attributes of specimens casted from the plant mix

with respect to those casted in a laboratory is not statistically significant. The detailed statistical analysis points out to the effectiveness of procedures adopted during plant production and paves the way for effective production of high-strength nanocomposites.

17.3.2 Compressive Strength

The compressive strength test results (mean values and standard errors) for HSC with different volume fractions of graphite nanomaterials and polypropylene microfibers produced at a concrete plant and in laboratory are summarized in Table 17.3. As was seen for all flexural attributes a small drop in the mean values of compressive strength was also observed in samples casted from plant mixed batches when compared with those casted in the laboratory. This is expected due to the reasons given earlier. However, it was observed that all hybrid reinforcements, whether casted in laboratory or mixed in concrete plant, produced increase in the mean values of compressive strength when compared with respective plain matrices. However, samples containing polypropylene microfibers when used alone showed a drop in the mean compressive strength both for both laboratory and plant produced specimens. This drop in compressive strength and flexural strength is commonly seen in cement-based matrices reinforced with micro and macro fibers while increasing the post-peak deflection and energy absorption capacity.

Outcomes of pair-wise comparisons indicate that the small drop in compressive strength observed between plant produced specimens and laboratory specimens was not found statistically significant (at 0.05 significance level). The outcome of pair-wise comparisons also revealed that the increase in compressive strength due to addition of hybrid reinforcement is also not statistically significant at 0.05 significance level. This shows the positive contribution of nano-reinforcement in maintaining the desired compressive strength.

17.3.3 Impact Resistance

The mean values of impact resistance test results for HSC with different volume fractions of graphite nanomaterials and polypropylene microfibers produced at a concrete plant and in laboratory are summarized in Table 17.4. As was seen for other engineering properties a small drop in the mean values of impact resistance was also observed in samples casted from plant mixed batches when compared with those casted in the laboratory. This is expected due to the reasons explained earlier. However, it was observed that all hybrid reinforcements as well as polypropylene microfibers when used alone, whether casted in laboratory or mixed in concrete plant, produced increase in the mean values of impact resistance when compared with respective plain matrices. The maximum rise in impact resistance was realized with hybrid reinforcement (87.5; 95.5%) containing 0.16 vol.% of GP-PAA and 0.24 vol.% of PP microfibers both for laboratory and plant produced specimens. In the case of micro-scale fibers, polypropylene produced a gain (56.6; 65.5%) in the impact resistance of high-strength concrete.

Both hybrid nano- and micro-scale reinforcement systems produced better increase in the mechanical properties of high-strength concrete when compared with individual micro-scale reinforcement used alone. A significant (0.000 significance level) increase in impact resistance was observed for the hybrid reinforcement comprising polypropylene microfiber with CNF-PAA, which confirms the effectiveness of hybrid reinforcement. The maximum increase in impact resistance (115%) was brought about by hybrid use of 0.16 vol.% of CNF-PAA and 0.24 vol.% of PP microfiber. Outcomes of ANOVA and pair-wise comparisons point at the statistical significant (0.000 to 0.012 significance levels) of nano- and/ or micro-scale reinforcement effects on the impact resistance of high-performance concrete. When compared with high-performance cement paste and mortar (with nano-scale reinforcement), concrete (with nano-scale

reinforcement) provides higher levels of impact resistance; this observation points at the well-known contributions of aggregates (in concrete) to the toughness of cementitious matrices.

17.3.4 Abrasion Resistance

The mean values of abrasion resistance for the HSC reinforced with different volume fractions of graphite nanomaterials and polypropylene microfibers produced at a concrete plant and in laboratory are summarized in Table 17.5.

As was observed with other engineering properties a drop in the mean values of abrasion resistance was also observed in samples casted from plant mixed batches when compared with those casted in the laboratory. Detailed statistical analysis indicated that this drop in mean values was not statistically significant at 0.05 significance level. However, it was observed that both hybrid reinforcements, whether casted in laboratory or mixed in concrete plant, produced increase in the mean values of abrasion resistance when compared with respective plain matrices. The increase ranged from 8.7% for GP-PAA and PP hybrid mixed in concrete plant to 29.5% for CNF-PAA and PP hybrid high-strength concrete samples casted in the laboratory. However, samples containing polypropylene microfibers when used alone showed a small drop in the mean abrasion resistance both for laboratory and plant produced test specimens. But ANOVA followed by pair-wise comparison indicated that this drop is statistically insignificant at 95% confidence level.

As was the case for all flexural attributes and compressive strength for both in laboratory and plant production, the most significant increase in abrasion resistance, with respect to their respective plain concrete, was realized in specimens with hybrid reinforcement consisting of 0.16 vol.% CNF-PAA and 0.24 vol.% of PP microfibers whether casted in field or mixed in the concrete plant and was found to be statistically significant. The results of abrasion resistance

further point to the benefits of adding graphite nano-reinforcements to high-strength concrete matrices.

17.3.5 Rate of Moisture Absorption by Capillary Rise

The mean ROMS (Rate of Moisture Absorption) and TWA (Total Water Absorbed) over a 15 days period for the high-strength concrete reinforced with different volume fractions of graphite nanomaterials and/ or microfibers are shown in Fig. 17.1 and Fig. 17.2, respectively. As was the case with other engineering properties the plant specimens showed a decrease in diffusion resistance of the concrete matrix with respect to the specimens casted in the laboratory. However, resulting mean rate of moisture absorption by capillary rise in the plain concrete matrix is 0.0195/ 0.0161 mm/min for plant and laboratory produced specimens. This is much superior to 0.19 mm/min for normal concrete with a W/C (water to cement) ratio of 0.4 which is suggested by (Neville A.M. 1995)and other research suggested that ordinary Portland cement concrete with W/C ratio of 0.4-0.5 would have sorptivity of about 0.23 mm/min 1/2 (Tsivilis, Tsantilas et al. 2003; Chindaprasirt, Jaturapitakkul et al. 2005). The reason for the lower sorptivity of different high strength concrete matrices samples may be attributed to lower water to cementitious material (w/cm) ratio, high silica fume content and absence of classic coarse aggregate. The use of silica fume results in a denser matrix, by reducing the pore size and thickness of transition zone between aggregate particles/ microfiber and surrounding cementitious matrix. According to the Mehta and Monteiro (Mehta 1993), the existence of microcracks in the interfacial transition zone at the interface with coarse aggregate is the primary reason that concrete is more permeable than the corresponding hydrated cement paste and mortar. Also in general, everything else being the same, the larger the aggregate size the higher

the local water-cement ratio in the ITZ (Interfacial Transition Zone) and, consequently, the weaker and more permeable would be the concrete.

However, due to the addition of normal gravel the increase in rate of moisture sorption due to capillary rise with respect to plain DSP concrete is 70%. This increase is primarily due to addition of weaker inclusions which are relatively more porous than the bulk past. The ITZ around these gravel particles is much more pronounced and porous. Being weaker than the bulk paste these gravel particles are and the ITZ around them are the likely paths for crack to progress under load. However, as was shown for DSP concrete matrix, the addition of both PAA physisorbed graphite nanomaterials as hybrid combination with PP microfibers resulted in drop of both moisture sorption rate as well as the total water absorbed. The maximum increase was recorded with use of 0.16 vol.% GP-PAA and 0.24 vol.% PP microfibers. The increase is 55; 57% for plant and laboratory produced specimens with respect to their plain matrices. This increase in diffusion resistance is due to the reinforcement of graphite nanomaterials of the paste portion of the matrix as well as the ITZ with sand and gravel particles. These results show a lot of promise for use of such material for repair and rehabilitation work as well as when combined with appropriate microfibers these nanocomposites can be used in structural members with superior engineering and durability properties. On the other hand, PP microfibers at 0.24 vol% produced a very small improvement in diffusion resistance of about 4.5; 10% for plant and laboratory produced specimens, respectively.

The mean value of total amount of water absorbed by capillary rise after exposure of one surface to water for 15 days also showed similar trend which were observed for the rate of moisture absorption for the high-strength concrete matrix.

The experimental results were subjected to ANOVA followed by pair-wise comparison. The statistical analyses clearly suggested a sharp decrease in the permeability of high-strength concrete matrix with addition of different volume fractions of both graphite nanomaterials as hybrid combination with PP microfibers, at 0.05 significance level. However, the increase in diffusion resistance of the matrix due to PP microfibers alone was not found to be statistically significant.

17.3.6 General Observations

All the batches of cement-based nanocomposite produced in plant were produced with a slump of 10 to 13 inches. The final product was quite fluid and was easily laid, Fig. 17.3b. The high-strength plain matrix and those reinforced with nano and micro-reinforcements set will in Michigan weather during the month of March. No surface cracking or other detrimental effects were recorded, Fig. 17.3g and 17.3h. No finish treatment was applied to the slab overlay. These segments are being watched for their behavior to Michigan weather.

17.4 Summary

The plant casting and field project highlights the challenges associated with scale up plant production of HSC nanocomposites and points out that many procedures have to be streamlined before scaling up the production of concrete nanocomposites from laboratory to concrete plant production. Issues like dispersion of larger quantities of graphite nanomaterials, their introduction into the plant batching and mixing process and due diligence to ensure proper dispersion of both nano and micro-reinforcements must be well thought out and executed. A small drop in mean values of all engineering properties was observed in plant produced specimens when compared to those casted in laboratory. The most balanced and significant

increase in all engineering properties was observed with use of hybrid reinforcement system including both nano and micro-scale fiber reinforcements. Nano- and micro-scale reinforcement renders complementary reinforcing effects in high-strength concrete; optimum reinforcement systems thus incorporate both nano- and micro-scale reinforcement systems.

Table 17.1- Starting material selections and mix proportions of high-strength concrete matrix for plant production.

Ingredient (lb/yd ³)	Design	Plain	PP	CNF-	GP-
	Composition			PAA+PP	PAA+PP
Cement Type I	1013	1040	1030	1060	1030
Silica Fume	253	253	250	256	250
Water	443	440	445	450	446
Superplasticizer - oz. cwt	300	306	305	310	305
River Sand (2NS)	786	789	790	790	785
#67 Aggregate	320	325	325	330	320
Polypropylene Microfibers	4.5	-	4.50	4.5	4.5
Carbon Nanofibers	3	-	-	3	-
Graphite Nanoplatelets	3		-	-	3

Table 17.2- Mean values of flexural attributes of plain high-performance concrete and those reinforced with different nano- and/ or micro-scale reinforcement systems.

Reinforcement Condition	Flexural Strength (MPa)	Deflection (mm)	Energy Absorption (N.mm)
Plain-Lab	10.7	1.00	168
Plain-Plant	9.56	0.89	120
Polypropylene microfiber, 0.24 vol.%-Lab (PP-0.24-Lab)	10.6	6.29	534
Polypropylene microfiber, 0.24 vol.%-Plant (PP-0.24-Plant)	9.37	6.05	505
Polypropylene microfiber, 0.24 vol.% and Carbon nanofiber, 0.16 vol.%-Lab (CNF-PAA+PP-Lab)	13.2	6.32	591
Polypropylene microfiber, 0.24 vol.% and Carbon nanofiber, 0.16 vol.%-Plant (CNF-PAA+PP-Plant)	11.7	6.15	548
Polypropylene microfiber, 0.24 vol.% and Graphite nanoplatelet, 0.16 vol.%-Lab (GP-PAA+PP-Lab)	11.1	6.22	521
Polypropylene microfiber, 0.24 vol.% and Graphite nanoplatelet, 0.16 vol.%-Plant (GP-PAA+PP-Plant)	10.2	6.00	493

Table 17.3- Mean values and standard errors of the compressive strength test results for plain DSP concrete and those reinforced with nano- and/ or micro-scale reinforcement systems.

Reinforcement Condition	Mean Compressive	Standard Error (MPa)
	Strength (MPa)	
Plain-Lab	77.6	7.8
Plain-Plant	71.6	7.1
Polypropylene microfiber, 0.24 vol.%-Lab	69.9	10.7
(PP-0.24-Lab)		
Polypropylene microfiber, 0.24 vol.%-Plant	60.5	7.5
(PP-0.24-Plant)		
Polypropylene microfiber, 0.24 vol.% and	94.1	8.1
Carbon nanofiber, 0.16 vol.%-Lab (CNF-		
PAA+PP-Lab)		
Polypropylene microfiber, 0.24 vol.% and	85.5	8.8
Carbon nanofiber, 0.16 vol.%-Plant (CNF-		
PAA+PP-Plant)		
Polypropylene microfiber, 0.24 vol.% and	77.8	7.7
Graphite nanoplatelet, 0.16 vol.%-Lab (GP-		
PAA+PP-Lab)		
Polypropylene microfiber, 0.24 vol.% and	72.2	11.1
Graphite nanoplatelet, 0.16 vol.%-Plant (GP-		
PAA+PP-Plant)		

Table 17.4- Impact resistance test results for high-performance concrete with and without nano-and/or micro-scale reinforcement.

Reinforcement Condition	Impact Resistance
DI: I I	(mm/mm)
Plain-Lab	1.20
Plain-Plant	1.10
Polypropylene microfiber, 0.24 vol.%-Lab (PP-0.24-Lab)	1.88
Polypropylene microfiber, 0.24 vol.%-Plant (PP-0.24-Plant)	1.82
Polypropylene microfiber, 0.24 vol.% and Carbon nanofiber, 0.16 vol.%-Lab (CNF-PAA+PP-Lab)	2.10
Polypropylene microfiber, 0.24 vol.% and Carbon nanofiber, 0.16 vol.%-Plant (CNF-PAA+PP-Plant)	2.05
Polypropylene microfiber, 0.24 vol.% and Graphite nanoplatelet, 0.16 vol.%-Lab (GP-PAA+PP-Lab)	2.25
Polypropylene microfiber, 0.24 vol.% and Graphite nanoplatelet, 0.16 vol.%-Plant (GP-PAA+PP-Plant)	2.15

Table 17.5- Mean abrasion weight losses of DSP concretes with and without nano- and/ or micro-scale reinforcement systems.

Reinforcement Condition	Loss of
	Mass (grams)
	(grams)
Plain-Lab	3.90
Plain-Plant	4.25
Polypropylene microfiber, 0.24 vol.%-Lab (PP-0.24-Lab)	3.94
Polypropylene microfiber, 0.24 vol.%-Plant (PP-0.24-Plant)	4.29
Polypropylene microfiber, 0.24 vol.% and Carbon nanofiber, 0.16	2.75
vol.%-Lab (CNF-PAA+PP-Lab)	
Polypropylene microfiber, 0.24 vol.% and Carbon nanofiber, 0.16	3.31
vol.%-Plant (CNF-PAA+PP-Plant)	
Polypropylene microfiber, 0.24 vol.% and Graphite nanoplatelet, 0.16	3.38
vol.%-Lab (GP-PAA+PP-Lab)	
Polypropylene microfiber, 0.24 vol.% and Graphite nanoplatelet, 0.16	3.88
vol.%-Plant (GP-PAA+PP-Plant)	

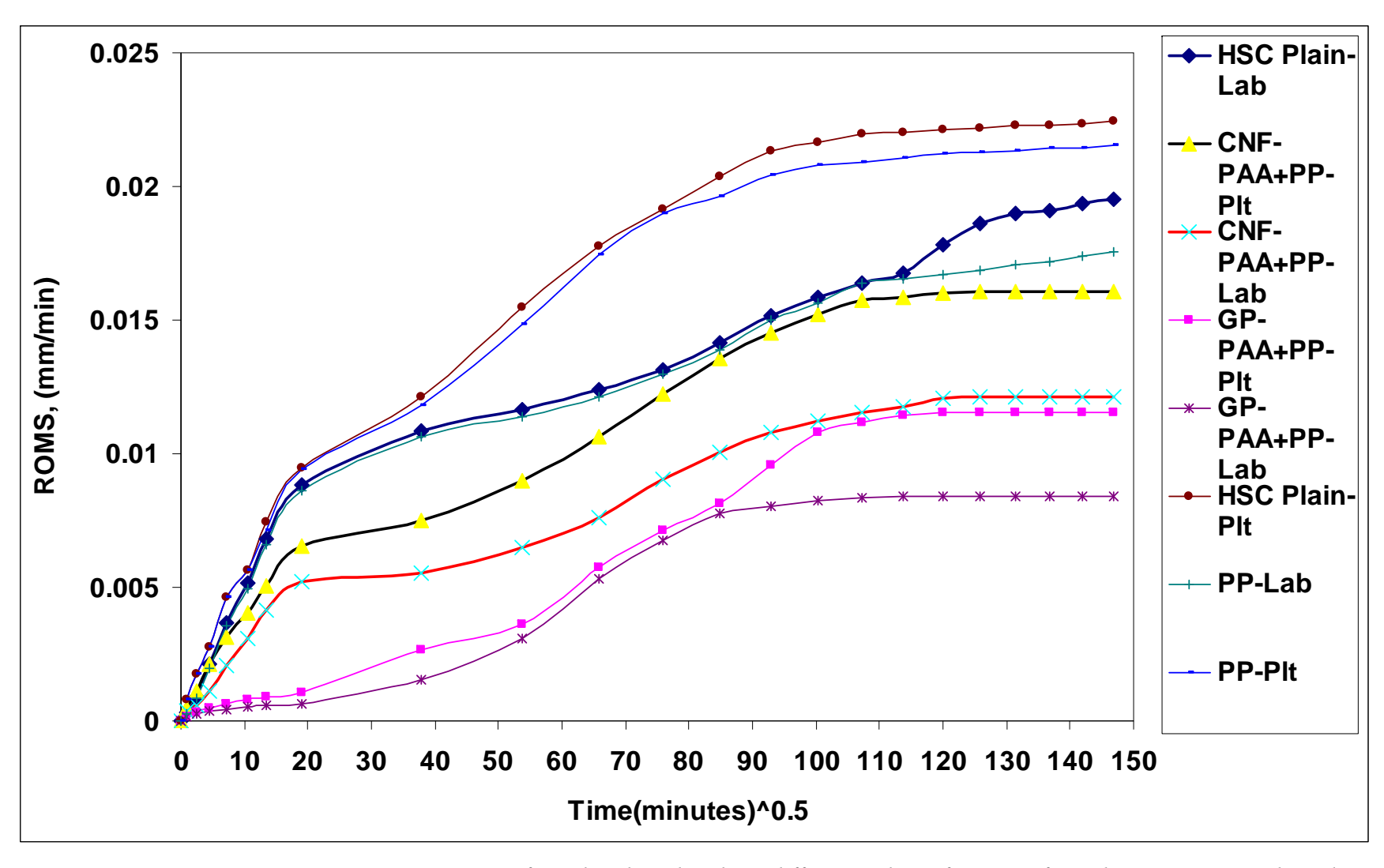
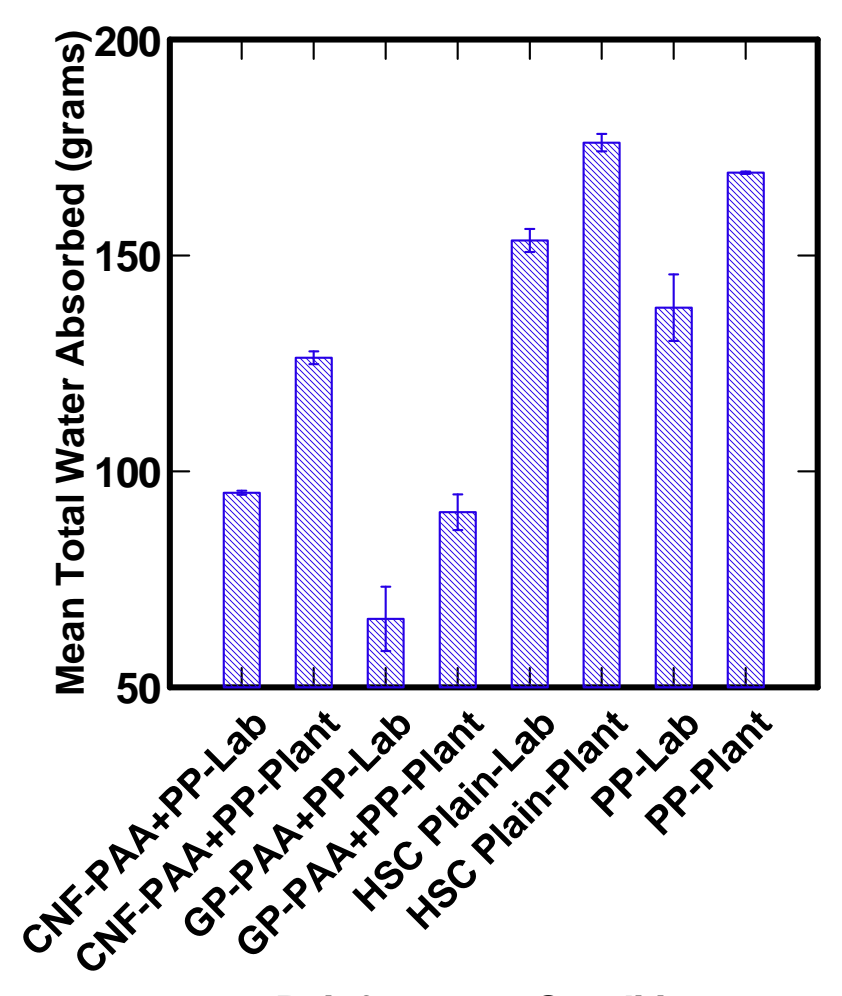


Figure 17.1- Mean ROMS in HSC matrix reinforced with and without different volume fraction of graphite nanomaterials and microfibers produced in laboratory and concrete mixing plant.



Reinforcment Condition

Figure 17.2- Average TWA in HSC matrix reinforced with and without different volume fraction of graphite nanomaterials and microfibers produced in laboratory and concrete mixing plant.



(a) Preparation of old slab for an overlay



(b) Pouring of concrete for slab

Figure 17.3- Photos of Plant Production and laying of slab overlay.



(c) Overlay outlook of high-strength concrete after being laid



(d) Overlay outlook of high-strength concrete after being laid



(e) Casting of specimens for evaluation



(f) Laboratory and plant specimens being cured in water baths



(g) Finished look of HSC nanocomposites after 3 months



(h) Finished look of HSC nanocomposites after 3 months

18 THEORATICAL STUDIES AND PERFORMANCE TO COST ANALYSIS OF DSP MATRICES REINFORCED WITH GRAPHITE NANOMATERIALS

18.1 General

Various UHPC (Ultra-High-Performance Concrete) materials have been developed over the past two decades, with properties which approach those of lower-quality ceramics. These UHPC materials are divided into different categories, including MDF (Macro-Defect-Free), DSP (Densified with Small Particles), and RPC (Reactive Powder Concrete) (Cheyrezy, Maret et al. 1995; Bonneau, Vernet et al. 2000; Chan and Chu 2004). These emerging concrete materials are distinguished by a very dense microstructure, high compressive strengths of about 150 [22 ksi] and as high as 840 MPa [122 ksi], and superior barrier attributes and durability characteristics. The experimental work in project focused on DSP cementitious pastes, mortars and concretes. The compositions of DSP matrices considered in this investigation are introduced in Table 2.4, and schematically depicted in Fig. 18.1. DSP cementitious materials offer distinct advantage in a variety of engineering applications such as blast shelters, impact-resistant structures, nuclear structures, skyscrapers, corrosion-proof structures and pavements. In order to improve the strength, deformability and toughness of DSP, fibers of micro-scale diameter (e.g., relatively short steel fibers) are used to restrain cracks in the matrix (Hu, Fang et al. 1999; Shannag and Hansen 2000; Collepardi, Corinaldesi et al. 2002; Badanoiu, Georgescu et al. 2003).

Fibers enhance the mechanical characteristics of cement-based materials, especially after the matrix has cracked, by bridging across cracks and providing some post-cracking ductility; they benefit the fracture toughness and impact resistance of cement-based materials. Fibers of microscale diameter do not generally enhance the flexural strength of cement-based materials, especially at common volume fractions which are below 1%; they tend to slightly lower the compressive strength and occasionally the flexural strength of concrete.

Cementitious materials incorporate flaws at different scales; conventional fibers with micro-scale diameter cannot interact effectively with finer flaws with nano-scale size and spacing; these finer flaws can form and grow in the relatively large space between microfibers. The use of discrete reinforcement with smaller dimensions in nano-scale (and nano-scale spacing) can hinder the formation and growth of fiber flaws in cementitious materials.

This research was based upon the hypothesis that *properly functionalized graphite* nanomaterials, when used in an appropriately graded matrix, can bring about substantial gains in diverse engineering properties of high-performance cementitious materials.

Properly functionalized and thoroughly dispersed graphite nanomaterials, including multiwalled carbon nanotubes, are used in dense DSP matrices to hinder the formation and growth of finer flaws/cracks. These effects of nanomaterials can benefit the flexural strength of high-performance cementitious materials. Nanomaterials can also benefit the toughness and impact resistance of cementitious materials by bridging across microcracks, energy dissipation via frictional pullout, microcrack arrest and deflection, and blunting of crack tips. The nano-scale spacing of graphite nanomaterials can also force tortuous diffusion paths within cementitious pastes, thus benefiting the barrier and durability characteristics of cement-based materials. The typically high aspect (length-to-diameter) ratios of nanomaterials also allows for their

percolation at relatively low volume fractions. The percolated network of nanomaterials could raise the (thermal and electrical) conductivity and fire resistance of cementitious materials. In short, graphite nanomaterials can be distinguished from conventional fibers (with micro-scale diameter) by their ability to bring about balanced improvements in diverse engineering properties of cement-based materials.

18.2 Merits of Graphite Nanomaterials

Graphite nanomaterials would play multi-faceted roles towards enhancing the mechanical, physical and functional attributes of cementitious materials. As far mechanical attributes are concerned, a comprehensive view of the contributions of graphite nanomaterials can be developed by considering their spacing, debonding and frictional pullout characteristics, and the implications for the mechanical performance of nanocomposites. Theoretical treatments of these topics (presented below) can be used as guides toward judicious use of graphite nanomaterials in cementitious matrices.

18.2.1 Average Spacing and Specific Surface Area of Nanomaterials in Cementitious Matrices

For nanomaterials uniformly dispersed (with different orientation conditions) within a matrix, the average nanomaterial spacing can be expressed as follows:

$$S=K.d/V_f^{0.5}$$

where, S is the average nanomaterial (or fiber) spacing, d is the nanomaterial diameter, V_f is the nanomaterial volume fraction, and K is a constant which ranges from 0.8 to 1.38 depending on the nanomaterial orientation(1-, 2- or 3-D) and the assumptions made in the calculation.

At 0.1% volume fraction, for the typical diameters introduced in Table 1.2, the average reinforcement spacing within composites, calculated using the above equation (with K=1), are 632, 3160 and 221,200 nm for multi-walled carbon nanotube, carbon nanofiber and carbon fiber, respectively. The average spacing of carbon fiber is thus about **350 times** that of multi-walled carbon nanotube at similar volume fractions. This provides nanotubes with superior capabilities for control of defect size and propagation within cementitious materials.

Fig. 18.2 plots the average spacing of carbon nanotubes versus nanotube diameter for different nanotube volume fractions (ranging from 0.1% to 1%). For typical carbon nanotube diameters of about 10 nm or less, the nanotube spacing (at less than 1% volume fraction) fall within the nanoscale range (i.e., less than about 100 nm). This extremely close spacing of nanomaterials can be used, with proper functionalization of graphite nanomaterials, to refine the structure and thus properties of the hydrated cement paste.

The specific surface area (A_s) , that is the surface area of reinforcement per unit volume of composite, can be calculated as follows:

$$A_s = 4 V_f / d$$

where, V_f is the nanomaterial volume fraction and d is the nanomaterial diameter. The graphical depiction of this expression in Fig. 18.3 highlights the substantial gains in the specific surface area of nanotubes within matrix realized with decreasing the nanotube diameter to typical values of about 10 nm (for multiwalled carbon nanotubes).

The close spacing of nanotubes in the cementitious matrix would have important implications in terms of microcrack suppression and control of diffusion. The crack suppression action of nanomaterials is schematically depicted in Fig. 18.4. Closer spacing of nanotubes would reduce

the flaw (microcrack) size within the matrix (size would be limited to nanotube spacing as far as interfacial defects are controlled), and nanotubes occurring in close vicinity of microcracks would effectively control the intensity of stress system near the microcrack tip, thus delaying the propagation and joining of microcracks which lead to formation of larger cracks within cementitious nanocomposites. Fig. 18.5 schematically depicts the rise in first-crack stress with reduction of nanotube spacing.

The high specific surface area of nanomaterials would, upon proper functionalization of nanomaterials, offer opportunities to refine the structure of hydrated cementitious paste by providing numerous sites for nucleation of hydration products.

The potentials to control defects (microcracks) and to refine the structure of cementitious paste with nano-scaled inclusions point at the unique capabilities of nanomaterials to render direct reinforcing effects and also to improve the structure of the cementitious matrix.

18.3 Reinforcement Efficiency of Multiwalled Carbon Nanotubes

18.3.1 Optimum Volume Fraction of MWNTs

The effects of MWNTs D & E at different volume fractions on the flexural strength of DSP paste were determined. MWNTs D & E, in functionalized and non-functionalized forms, were introduced into the cementitious paste at 0.24 vol.% and 0.48 vol.%. Flexural strengths were measured using 12.5x50x150 mm specimens under center-point loading over a span of 125 mm in accordance with ASTM C 293 procedures. The trends in measured values of flexural strength with increasing volume fractions of MWNTs D & E are shown in Fig. 18.6. It is clear from Fig. 18.6 that 0.24 vol.% of various nanotubes produced higher flexural strengths. However, the longer length (100 micrometer) and higher aspect ratio of non-functionalized MWNT D

compensates for its inferior interfacial interactions due to lack of functionalization, producing superior flexural strength test results when compared with its functionalized counterpart with half the length (50 micrometer).

MWNT E, which has a larger diameter, provides less improvement in flexural strength at similar volume fractions. The 0.48 vol.% was found to be excessive for the material compositions and processing conditions considered here. Flexural strength generally decreases as the nanotube volume fraction increases from 0.24% to 0.48%. It should be emphasized that volume fraction of nanotubes is calculated here with respect to the volume of cementitious materials (cement and silica fume). The nanotube dispersion and mixing techniques considered here cannot ensure thorough dispersion of nanotubes beyond a certain volume fraction, causing excess nanotube agglomeration, especially for nanotubes of smaller diameter and longer length. Scanning electron microscope images of agglomerated MWNT E at higher volume fraction are shown in Fig. 18.7 Agglomeration greatly reduces the reinforcement efficiency of carbon nanotubes in cement-based matrices.

Larger-diameter nanotubes yield a smaller number of nanotubes per unit cross-section area of cement nanocomposites, which is not favorable to their reinforcement efficiency in cement-based materials. Furthermore, the comparatively shorter length of both functionalized and non-functionalized MWNT E, and agglomeration of nanotubes at higher volume fractions negatively impact the flexural strength of cementitious nanocomposites. Similar trends have been observed with flexural energy absorption capacity and ductility.

For the material selections and compositions, and the nanotube dispersion and mixing procedures considered in this investigation, 0.24 vol.% of nanotubes seems to be the optimum, beyond which a downtrend in the measured values of engineering properties is generally observed.

Similar trends were observed for the other two categories of graphite nanomaterials. Based on the experience gained with the use of nanomaterials, alone or in combination with microfibers, in cementitious materials, graphite nanomaterials were used at 0.24 vol.% and 0.16 vol.% in cementitious materials without and with microfiber reinforcement. The volume fraction is expressed here with respect to the volume of cementitious materials (cement and silica fume).

18.4 Analysis of the Debonding Process of Functionalized Carbon Nanotubes, and Their Contribution to Tensile Strength

18.4.1 DSP Paste

SEM observations have indicated that debonding of functionalized carbon nanotubes occurs away from the interface within the cementitious matrix. This observation suggests that the fracture energy of the cementitious matrix is lower than that of the interface. There are close to $38x10^{18}$ carbon atoms per square meter of carbon nanotube surface area, and the covalent bond energy is of the order of $5x10^{-19}$ J (Joules). With f representing the fraction of surface carbon atoms functionalized (and capable of developing chemical bonds with the cement matrix), the debonding energy per unit area of nanotubes (G_{db}) would be:

$$G_{dh} = (f).(38 \times 10^{18}).(5 \times 10^{-19}) = 19 f \text{ J/m}^2$$

The compact cementitious pastes considered in our investigation are relatively brittle (due to the fine microstructure comprising largely of nanostructured calcium silicate hydrate). Considering the percent of COOH (carboxyl) groups on MWNT D and E, their fracture energy is estimated at about 0.475 J/m² and 0.228 J/m², respectively.

With debonding occurring by fracture of a brittle cementitious matrix, the nanotube (average) tensile stress (σ) associated with catastrophic debonding (neglecting any frictional shear resistance) can be calculated as follows (see Fig. 18.8):

$$\sigma = (8 \text{ E.G}_{db} / d)^{0.5} = 12 (\text{f.E/d})^{0.5}$$

where, E and d are the elastic modulus and diameter of the nanotube, and G_{db} is the energy required to debond a unit surface area of the nanotube (estimated at 0.475 J/m^2 and 0.228 J/m^2 for MWNT D and E, respectively, noting that debonding actually occurs within the compact matrix).

The tensile strength and elastic modulus of multi-walled carbon nanotubes are about 300 GPa and 1 TPa, respectively. In the context of a composite, where stress is transferred via interfacial bonds to the outer wall of the multi-walled carbon nanotube, one may conservatively assume that the transferred load is carried by the outer wall alone (with minimal contributions from the inner walls which interact via weak van der Waals bonds). With a 0.34 nm thickness of each nanotube wall, the effective (apparent) strength and elastic modulus of multi-walled nanotube would be $300 (1.36 \times 10^{-9})$ GPa and 1 (1.36×10^{-9}) TPa, respectively (where d is the nanotube diameter in meter).

Based on discussions with manufacturers of multi-walled carbon nanotubes and reviews of the relevant literature, it is ascertained that the ranges of nanotube length and diameter stated earlier are applicable to the nanotubes in a particular batch, with a greater probability of occurrence of nanotubes with the shorter lengths and larger diameters within the corresponding range. It has been noted that if the aspect ratio distribution is not symmetric and/or the aspect ratio is not very high, the predictions of reinforcement contributions based on the distribution of aspect ratio

could differ from those based on the mean aspect ratio by as much as 30% (Jiang, Liu et al. 2007).

Based on the above considerations, diameters of MWNT D and E were taken as 15 nm and 25 nm, respectively. For these diameters, the effective values of strength and elastic modulus would be 27.2, 16.32 GPa, and 90.6 and 54.4 GPa, respectively. Therefore, the debonding stress can be calculated as follows:

$$\sigma_{\text{MWNTD}} = 4.74 \text{ GPa}$$

$$\sigma_{MWNTE} = 1.99 \text{ GPa}$$

For nanotubes that are uniformly dispersed and randomly oriented within matrix, the number of nanotubes per unit area, N_1 , can be calculated as follows:

$$N_1 = 0.53 \ V_f / d^2$$

where, V_f is the nanotube volume fraction, and d is the nanotube diameter.

Functionalized MWNT D and E at 0.24% volume fraction thus represent 2.82×10^{12} /m² and 2.04×10^{12} /m² nanotubes per unit area, respectively. With 3.8×10^{-6} N force developed in each nanotube, assuming that all nanotubes crossing a crack are mobilized simultaneously, this force per nanotube generates a tensile stress of 3.8×10^{-6} x N₁. Hence, the contribution of MWNT D and E to tensile strength can be estimated at **10.74 MPa and 7.73 MPa** at 0.24 vol.%, respectively.

The above predicted contributions are more than the actual increase observed in experiments. The SEM observations as well as the findings of other researchers indicate that factors such as lesser than ideal distribution of nanotubes in the brittle matrix, waviness of nanotubes, their tendency to cluster, and deficient bonding to the cement-based matrix tend to lower the actual reinforcement efficiency of carbon nanotubes (Zhang, Picu et al. 2008).

Hence, reduction factors need to be incorporated into theoretical models in order to produce more realistic predictions of the nanotube reinforcement efficiency. Considering the greater tendency of higher-aspect-ratio nanotubes towards coiling and clustering, an aspect ratio reduction factor (F) of 0.45 was introduced into our models in light of experimental observations. The contribution of MWNTs D and E to tensile strength can now be estimated at:

MWNT D =
$$0.45 \times 10.74 = 4.83 \text{ MPa}$$
 (at 0.24 vol.\%)

MWNT E =
$$0.45 \times 7.73 = 2.31 \text{ MPa}$$
 (at 0.24 vol.\%)

These, results are within 10-15% of the flexural strength test results, which can be used as approximate measures for tensile strength.

18.5 Analysis of the Frictional Pullout of Carbon Nanotubes, and their Contribution to Fracture Energy

With longer nanotubes used in later stages of the research program, which were modified by polymer physisorption, one may estimate the interfacial friction based on the estimated frictional shear stress (τ_{fu}) of 10 MPa developed with the cementitious matrix (Zhang, Sun et al. 2008). For a frictional (linear) shear stress transfer, the critical nanotube length l_c (defined as the

minimum nanotube length required for buildup of a stress in nanotube which is equal to its strength (as shown in Fig. 18.9) can be calculated as:

$$l_{\rm c} = \sigma_{\rm u} \cdot d/(2 \tau_{\rm fu})$$

where, σ_u is the effective tensile strength of nanotubes, which was calculated earlier.

For MWNT D and E, the above equation yields a critical nanotube length of $l_c = 24$ micrometer.

For $l < l_{\rm C}$, nanotube pullout dominates, and a fraction (but not all) of the nanotube tensile strength would be mobilized during frictional pullout.

In case of PAA-physisorbed, non-functionalized MWNT D and E, average lengths are 24 micrometer and 16 micrometer, respectively, compared to critical length of 24 micrometer. Frictional pullout would thus be an important factor, with an average pullout length of l/4. The average nanotube tensile force at the beginning of frictional pullout for MWNT D and E would be: $\tau_{\text{fu}} \cdot \pi \cdot d \cdot l/4 = 2.82 \times 10^{-6} \text{ N}$ and $3.14 \times 10^{-6} \text{ N}$, respectively.

The average frictional energy dissipation per nanotube for MWNT D and E would be: (2.36×10^{-6}) /2).(l/4)=1.69×10⁻¹¹ J and 1.25×10⁻¹¹ J, respectively.

The debonding energy over the average pullout length of l/4 for MWNT D and E would be: $G_{db}.\pi.d.l/4 = 1.34x10^{-13}$ J and $6.28x10^{-13}$ J, respectively. The **debonding** and **frictional pullout** energies of MWNT D and E thus add up to $1.70x10^{-11}$ J and $1.31x10^{-11}$ J, respectively.

According to the Dugdale-Barenblatt model, a nanomaterial bridging zone can be assumed, which may be the major source of energy dissipation. The contribution of nanotube debonding

and frictional pullout to the energy dissipation of cement nanocomposites can be estimated at 47.94 J/m² and 26.65 J/m² for MWNT D and E, respectively, at 0.24 vol.%. The bulk (about 90%) of the nanotube contribution to fracture energy is attributed to the frictional pullout of nanotubes from the matrix, and the rest (about 10%) to the debonding process. These values constitute significant contributions to the fracture energy (2 J/m²) of the brittle (DSP) cementitious paste.

Besides their direct contributions (via debonding and frictional pullout) to the fracture energy of cement-based materials, carbon nanotubes can further benefit the fracture process through *control of defect size*, as explained earlier.

Closely spaced and effectively bonded carbon nanotubes would benefit the fracture process through yet another mechanism – *suppression of flaw propagation under stress*. Nanotubes occurring in the close vicinity of microcracks would control the intensity of stress system near the microcrack tip, thus delaying the propagation and joining of microcracks which lead to crack formation within nanocomposites.

18.6 Elastic Modulus and Tensile Strength Based on the Composite Materials Approach

The composite materials approach yields the following expression for the elastic modulus of carbon nanotube/cementitious matrix nanocomposites:

$$E_c = E_m.(1-V_f) + F_l.F_o.E_n.V_f$$

where, E_c , E_m and E_n are the nanocomposite, cementitious matrix and nanotube elastic moduli, respectively, F_l and F_o are the length and orientation efficiency factors, respectively, and V_f is the nanotube volume fraction.

For low-porosity (DSP) cementitious pastes and mortars with elastic moduli of 15 and 50 GPa, respectively (Guerrini 2000), with an effective nanotube elastic modulus of 160 GPa, and length and orientation efficiency factors of 0.9 and 0.2, respectively, there would be minimal effects of carbon nanotubes (at volume fractions below 1%) on elastic modulus of cementitious nanocomposites per composite materials approach.

In the post-cracking range of behavior, the composite materials approach predicts the **tensile** strength of cementitious nanocomposites (σ_{cu}) as follows:

$$\sigma_{cu} = F_o.V_f.\tau_{fu}.1/d$$

where, τ_{fu} is the frictional shear resistance of nanotubes in the low-porosity matrix (~10 MPa), and F_o is the orientation factor. For MWNT D and E, assuming a post-crack orientation efficiency factor of 0.12 and 0.135, respectively, the tensile strength of the cementitious nanocomposite using MWNT D and E can be calculated as **4.60 MPa and 2.07 MPa**, respectively, at 0.24% nanotube volume fraction. With MWNT D at 0.16 vol.%, the tensile strength of DSP paste was **3.07 MPa**.

18.7 Theoretical Predictions versus Experimental Results for High-Performance Cementitious Paste, Mortar and Concrete

18.7.1 High-Performance Paste

The theoretical models provided a basis to predict the gains in mechanical properties of the high-performance (DSP) cementitious matrix with introduction of 0.24 vol.% acid-functionalized MWNT D and E. These theoretically predicted values were compared with experimental results. The debonding stress (σ) of carbon nanotubes was expressed earlier as:

$$\sigma = (8 \text{ E.G}_{db} / d)^{0.5}$$

With MWNT D and E, the cumulative contributions of nanotube debonding stresses at a section to the tensile strength of matrix add up to **4.83 MPa** and **2.31 MPa**, respectively. Since tension tests were not performed, we relied on the flexural strength test results to approximately verify the theoretical predictions. It should, however, be noted that flexural strength depends not only on tensile strength but also on the ductility and toughness of the material.

Experimental results suggest that the mean flexural strength of the high-performance cementitious paste increased by **4.4 and 2.1 MPa** (from 10.3 MPa at 0 vol.% to 14.7 MPa and 12.4 MPa at 0.24 vol.% of MWNT D and E, respectively). The measured gains in flexural strength are somewhat less than, but still within the range of, the theoretically predicted gains in tensile strength. The deviations of experimental results from theoretical predictions could have been caused by imperfect dispersion and interfacial bonding of nanotubes in cementitious paste. The composite materials approach, assuming an orientation efficiency factor of 0.12 and 0.135 for MWNT D and E, respectively, predicts gains of **4.60 MPa** and **2.07 MPa** in tensile strength. Both these results are within 10% of the mean experimental gains. For MWNT D at 0.16 vol.%,

the tensile strength of DSP paste was **3.07 MPa**. This value is closer to but still lower than the actual value of **3.2 MPa** for DSP paste reinforced with 0.16 vol.% of MWNT D. This trend could be explained by the improved dispersion of nanotubes, using the stirring, sonication and mixing procedure used in the project, at reduced nanotube concentrations.

18.7.2 High Performance Mortar and Concrete

Given its superior reinforcing attributes, MWNT D was evaluated in high-performance cementitious mortar and concrete. As graphite nanomaterials act within the paste portion of the matrix, contributions of nanotubes at 0.16 and 0.24 vol.% to the tensile strength of high-performance DSP mortar can be estimated to be proportional to the volume of paste within cementitious matrix. This approach yields **7.16 MPa** and **10.74 MPa** contributions of nanotubes to tensile strength at 0.16 and 0.24 vol.%, respectively. Application of reduction factors yields the following anticipated contributions of nanotubes to the tensile strength of mortar:

MWNT D =
$$0.90 \times 7.16 = 6.44 \text{ MPa}$$
 (at 0.16 vol.\%)

MWNT D =
$$0.55 \times 10.74 = 5.91 \text{ MPa}$$
 (at 0.24 vol.\%)

The above values are within 10% to 15% of the experimental results produced in the project. The value of the reduction factor was reduced to reflect the effects of sand particles on dispersion of nanotubes and formation of interfacial transition zones. Furthermore, the reduction factors reflect the magnified dispersion problems at volume fractions beyond 0.16%. At 0.16 vol.%, the contribution of carbon nanotubes to tensile strength is very close to the theoretical value.

Due to economic considerations, and also for improving the dimensional stability of the cementitious matrix, coarser aggregates were introduced into the high-performance matrix. Although the coarser aggregate used here (granite) offers high mechanical attributes, it

introduces interfacial transition zones which tend to be weaker than the bulk matrix, and are also prone to cracking. The transition zones represent preferred routes of crack propagation under load. The contributions of nanotubes to high-performance concrete result from their reinforcing action within the matrix and also at the ITZ. Theoretically, at 0.16 vol.%, the contribution of nanotubes to the tensile strength of high-performance DSP concrete can be estimated at **7.16** MPa. Application of the reduction factors yields:

MWNT D =
$$0.5 \times 7.16 = 3.58 \text{ MPa}$$
 (at 0.16 vol.\%)

The reduction factor accounts for the inclusion of coarser aggregate in the high-performance matrix and formation of microcracks in the interfacial transition zone.

18.8 Synergistic Role of Nano- and Micro-scale Reinforcement

An important finding of the project concern the synergistic role that nano- and conventional micro-scale reinforcement systems can play in enhancement of concrete properties. The damaging effects of mechanical loads and aging are generally manifested in concrete as inception and growth of micro-cracks within the aggregate-paste interfacial transition zones and the bulk cementitious paste. Closely spaced graphite nanomaterials exhibit a strong presence within the bulk paste and at interfacial zones in concrete. Their close (nano-scale) spacing and high specific surface are make them highly effective in suppression of microcrack inception (and initial growth) (Figures 7.9a&b) and control of microcrack propagation by effectively interacting with their tips (Figures 7.9a&c). Longer micro-scale fibers, on the other hand, are particularly effective in bridging across wider cracks, and mitigating their further opening (Figures 7.9a&d). Unlike micro-scale fibers which do not benefit the barrier qualities of concrete, the closely

spaced nanomaterials force tortuous diffusion paths into concrete, which enhance the barrier qualities (impermeability and diffusion/sorption resistance) of concrete.

The theoretical studies presented earlier and the experimental evidence produced in the project yield the following conclusions:

For viable lengths of multiwalled carbon nanotubes, and the types and degrees of functionalization considered in this investigation, debonding of nanotubes occurs at a smaller interfacial (adhesional) shear stress (τ_{au}) when compared with frictional shear stress (τ_{fu}). This implies that the nanotube pull-out load-deflection behavior would follow the diagram of Fig. 18.10a (in lieu of those in Figs. 18.10b & c). In this type of behavior, after the maximum interfacial shear stress has been exceeded, debonding will initiate and gradually develop along the entire length of the reinforcement, without catastrophic failure. The maximum pull-out load can be calculated as:

$$P_{max} = 2\pi r. \, \tau_{fin}$$

The pull-out load decreases linearly form the maximum load. It is assumed that the frictional resistances before and after sliding (i.e. static and dynamic) are the same. Nanotubes mainly reinforce the matrix by increasing the first-crack load through crack-blunting, crack-arrest and crack-bridging. Evidences for these effects were produced in the experimental phases of the research and SEM observations.

• Microfibers are effective in cement-based matrices at relatively high volume fraction of about 2%, below which their contribution to the flexural attributes of the matrix are relatively small. Ultra-high-performance (DSP, RPC and DUCTAL®) concrete materials

generally incorporate microfiber volume fractions of about 2% and higher. Furthermore, in a brittle cementitious matrix, much of the fiber contribution is made at a stage where the matrix has cracked and fibers are bridging across cracks. Carbon nanotubes can complement this action of microcracks by enhancing pre-crack performance, which mainly results in an increase in flexural strength and, to some extent, toughness.

• By using both nano- and micro-scale reinforcements at much lower volume fractions, a load-deflection behavior similar to that shown in Fig. 18.10b can be achieved, with improvements realized in both flexural strength and toughness. This condition promises to yield superior flexural performance at reduced reinforcement volume fractions.

Figure 18.11 presents examples of experimental results which reflect the gains in performance characteristics of high-performance concrete realized by the addition of 0.16 vol.% functionalized carbon nanotube and/or 0.24 vol.% carbon (micro)fiber. These results point at the superior reinforcement efficiency of functionalized carbon nanotube over carbon (micro)fiber, and the synergistic action of the two in high-performance concrete at lower volume fractions than those commonly used in fiber reinforced concrete.

Table 18.1 summarizes the gains in engineering properties of high-performance cementitious paste, mortar and concrete resulting from reinforcement with 0.16 vol.% functionalized carbon nanotube (CNT) and/or 0.24 vol.% carbon microfiber (CMF), or 0.16 vol.% of functionalized graphite nanoplatelet or carbon nanofiber. Nano-scale reinforcement brings about balanced improvements in engineering properties of cement-based materials, surpassing those offered by micro-scale fibers. The (optimized) hybrid reinforcement comprising multiwalled carbon nanotube and carbon (micro) fiber produces particularly large gains in engineering properties of cement-based materials. Similar trends are observed for broader aspects of engineering

properties, including impermeability, fire resistance, and durability under aggressive exposures. It should be emphasized that micro-scale fibers alone can improve the toughness and impact resistance of concrete; their contributions to strength, abrasion resistance, impermeability and durability are, however, limited.

The high reinforcement efficiency of nanomaterials in concrete can be explained by their effectiveness in micro-crack suppression, control of microcrack propagation, frictional energy dissipation during pullout, and imposition of tortuous diffusion paths within concrete.

18.9 Diffusion Resistance of Cement-Based Nanocomposites

Moisture sorption is a primary factor governing the weathering resistance and long-term durability of cement- and concrete-based infrastructure systems. Unlike conventional (microscale) fibers, carbon nanotubes were found to significantly enhance the diffusion resistance of cement-based materials. This could be attributed to the close spacing and large surface area of nanotubes (Fig. 18.12), which significantly increase the tortuosity of diffusion paths within the cement-based matrix (Fig. 18.13).

It has been suggested that the diffusivity of a random 3D fiber (or nanotube) structure is equivalent to that of a cubical lattice of cylinders. This approach implies (Tomadakis and Robertson 2005) that diffusivity is proportional to:

$$(0.0375 \text{ d}^2/\text{V}_f)$$
.[-ln V_f - 0.931 + (ln V_f)⁻¹]

where, d and V_f are the nanotube (or fiber) diameter and volume fraction, respectively. Fig. 18.14 presents this diffusivity factor (as a function of nanotube/fiber diameter) for 0.24% nanotube (or fiber) volume fraction. The range of reinforcement diameter in this figure includes

those of multi-walled carbon nanotubes (few to several nanometers) and conventional microscale fibers (7 to $10 \mu m$). Multi-walled carbon nanotubes are observed to offer diffusivity factors which are about five orders of magnitude smaller than those of conventional micro-scale fibers. In other words, reduction of reinforcement diameter to the nano-scale range makes them quite effective in lowering the diffusivity of cement-based matrices.

The relative drops in rate of moisture sorption and total water absorbed, Fig 18.15, indicate that properly functionalize carbon nanotubes and graphite nanoplatelets can reduce these values by more than 2 to 3 times and 2.7 to 3.9 times, respectively.

Another approach is to define a tortuosity factor (t), that is the ratio of the actual distance that a penetrant (or crack) must travel (for avoiding the reinforcement) to the shortest distance that would be traveled in the absence of reinforcement, and can be expressed (for reinforcement with nanoplatelet geometry, length L, and thickness T) as:

$$t = 1 + V_{f} \cdot L/(2T)$$

This equation can be strictly applied only to graphite nanoplatelets; we assume that it would also be applicable to carbon nanotubes, nanofibers and microfibers. The tortuosity factor for carbon nanotubes, graphite nanoplatelets and carbon microfibers at 0.24% volume fraction are (for the typical geometric attributes of these reinforcement systems used in the project) 3.08, 4.60 and 1.07, respectively. This rise in tortuosity factor is very close to the relative drops in rate of moisture sorption and total water absorbed in the presence of these reinforcement systems, Fig 18.15.

18.10 Electric Conductivity and Its Damage Sensitivity

Multiwalled carbon nanotubes offer distinctly high thermal and electrical conductivity. They can thus increase the conductivity of cement-based materials when a percolated (networked) structure of nanomaterials forms within cement-based matrices (Fig. 18.16). The distinctly high aspect ratio of nanomaterials substantially lowers the "threshold" volume fraction at which the percolation phenomenon occurs. Percolated nanomaterials provide continuous paths for transport of electricity and heat; given the relatively high aspect (length-to-diameter) ratio of carbon nanotubes, well-dispersed nanotubes percolate at relatively low volume fractions. Break-up of the percolated network upon cracking and development of large strains could disrupt the continuous conduction path, and thus lower the conductivity of cementitious nanocomposites. The damage-sensitivity of electrical conductivity offers a convenient basis for health monitoring of cementitious nanocomposites (and concrete-based infrastructure systems incorporating them). It is a common practice to add conductive fillers (e.g., carbon black) to insulating matrices (e.g., polymers) in order to increase their electrical conductivity and thus prevent electrostatic charge buildup (by enabling continuous discharge). Upon percolation, conductive fillers provide conduction paths within matrix (Fig. 18.17a), causing a sharp rise in conductivity of the composite (Fig. 18.17b). In the case of conductive fillers of relatively low aspect (length-todiameter) ratio, the percolation threshold (volume fraction) is relatively high. The percolation volume fraction can be reduced by choosing conductive inclusions of high aspect ratio (Fig. 18.16) (Farriss, Kelley et al. 1995).

The experimental results generated in the project indicated that lower nanotube dosages of about 0.04 vol.%, especially for nanotubes of shorter lengths (5-15 µm), no increase in electric conductivity was observed in high-performance DSP paste and mortar matrices. However, 0.16

vol.% of modified multiwalled carbon nanotubes with longer lengths (50-100 μm) produced to two to three orders of magnitude rise in electrical conductivity of high-performance cementitious mortar (depending upon the superplasticizer type). Increasing the nanotube volume fraction from 0.16 to 0.24% produced another order of magnitude rise in electrical conductivity, Table 18.2.

A first-level approximation of electric conductivity can be based on the classical percolation theory, according to which the electrical conductivity of a filled composite follows a power law relationship (Hu, Zhao et al. 2006)

$$\sigma \alpha (v-v_c)^{\beta}$$

where, σ is the nanocomposite conductivity, v is the nanowire volume fraction, v_c is the percolation threshold, and β is the critical exponent which relates to system dimension. Theoretical predictions of β range from 1.6 to 2.0 for three-dimensional percolating systems; in the case of nanocomposites incorporating carbon nanotubes, the experimental values of β (in polymer matrices) range from 0.7 to 3.1 (Hu, Zhao et al. 2006).

The values of electrical conductivity of cementitious nanocomposites are plotted using different values of β in Fig. 18.18. The graph shows that at 0.16 vol.% of PAA-physisorbed MWNT D, the values of β range form 0.9 to 1.2. With increase in dosage of PAA-physisorbed MWNT D to 0.24 vol.%, the value of β drops to a range of 0.6 - 0.85. This reduction in value of β applies to longer, suitably functionalized carbon nanotubes which effectively form a percolated network within the insulative cementitious matrix as shown in Fig. 18.19 and explained in Chapter 8.

The damaging effects (microcracking and permanent strains) induced by compressive stresses lower the electrical conductivity of high-performance cementitious materials incorporating carbon nanotubes at 0.24 vol.% (Table 18.3). After application of compressive stresses

corresponding to 60% and 80% of compressive strength, electrical conductivity is observed to drop by one and two orders of magnitude, respectively. The damage-sensitivity of the electrical conductivity of high-performance cementitious materials incorporating carbon nanotubes provides these materials with inherent health monitoring qualities (Fig 18.20) (Baoguo, Xun et al. 2009).

18.11 Cost versus Performance of Cementitious Nanocomposites

Large-scale availability of functionalized graphite nanomaterials is a pre-requisite for their transition to concrete markets. Fortunately, there is an explosive growth in supply of carbon nanotubes and other graphite nanomaterials. The mid-term price targets for carbon nanotubes has been reducing consistently, benefiting their competitive market position.

Fiber reinforcement of cement and concrete products has enjoyed commercial success over the past two decades, with an annual growth rate of 15%. The benefits of functionalized graphite nanomaterials to cement-based materials surpass those of conventional (e.g., polypropylene, steel and glass) fibers in terms of both the extent of improvements and the range of properties impacted at relatively low volume fractions of the reinforcement system. Table 18.5 compares typical performance gains associated with the introduction (at specified volume fractions) of functionalized carbon nanotube versus discrete steel, polypropylene and glass fibers (Bentur and Mindess 1990; Balaguru and Shah 1992). Functionalized carbon nanotube is observed to be distinguished from other discrete reinforcement systems by the extent and the balance of improvements it brings about per vol.% addition to cement-based materials.

The breadth of material properties improved by functionalized graphite nanomaterials suggests that markets for nanomaterials in cement and concrete applications can go beyond those for

conventional fiber reinforcement systems. While the understanding of the benefits of functionalized graphite nanomaterials to cement- and concrete-based products is just emerging, the trends established in the project indicate that functionalized graphite nanomaterials could have a strong impact on the \$10 billion/year markets (with 10% annual growth rate) of cement and concrete admixtures (including fibers). According to reports prepared by BCC Associates, the total global consumption of all types of nanomaterials reached 10.3 million tons or \$20.5 billion in 2010, with an AAGR (average annual growth rate) of 9.3% in value terms. Multiwalled carbon nanotubes are now sold in million-pound plus quantities for modifying polymers. Nanotubes are finding growing applications in military, consumer and industrial products. Long-term applications of nanotubes can easily exceed several billion dollars, but when, is debatable.

The unique value of functionalized graphite nanomaterials to cement- and concrete-based materials should be evaluated in light of their current and projected future costs. Over the past two years, scale-up of multi-walled carbon nanotube production (by Arkema, Bayer Material Science, Showa Dendo, etc.) has led to a sharp price reduction, down from thousands of dollar per kg to \$150/kg for semi-industrial applications. The run for industrial carbon nanotube production plants has started in order to develop a sustainable business around commercialization of nanotubes in different fields of application, with a mid-term price target of \$45/kg.

Typical sales prices (in 2008) of steel, polypropylene and alkali-resistant glass fibers are \$2.5, \$6 and \$5.25 per kg. The specific gravity of steel, polypropylene and AR glass are 7.8, 0.91 and 2.7, respectively. At 1% by volume of cementitious materials, the purchase price of fibers accounts for approximately 71, 20 and 52 dollars per ton of concrete. With functionalized carbon nanotubes at 1% volume fraction (which is for calculation purposes, and far exceeds their

optimum volume fraction), the purchase price of nanotubes per ton of concrete would be \$300. The normalized values of performance gains per vol.% of reinforcement were further normalized with respect to the price (at 1 vol.%) per ton of concrete, and the results are summarized in Table 18.5. Noting that the long-term cost of multi-walled carbon nanotubes is expected to experience significant drops below the mid-term cost used here, their high reinforcement efficiency makes them quite cost-competitive against competing fibers even with the conservative mid-term costs used here. It should be noted the range of properties improved by carbon nanotubes far exceeds those improved by conventional (micro-scale) fibers.

The global markets for fibers in cement-based materials account for about \$2 billion annual sales. A fraction (about 25%) of this market makes secondary use of fibers for plastic shrinkage crack control. The targeted markets for functionalized carbon nanotubes as primary reinforcement in cement-based materials thus account for \$1.5 billion annual sales (with growing market penetration). Since functionalized carbon nanotubes, when compared with conventional microfibers, benefit a broader range of concrete properties, they could compete with other admixtures (e.g., water-repelling agents and latex polymers) for a share of the \$10 billion markets for concrete admixtures. Based on performance considerations, the fractions of fiber and admixture markets within which functionalized carbon nanotubes are competitive can amount to more than \$2 billion annual sales (with an anticipated annual growth rate of about 10%).

18.12 Targeted Applications

Cement- and concrete-based products which could benefit from introduction of functionalized carbon nanotubes account for nearly 11% of the U.S. construction market value (\$110 billion). Cement consumption (normalized with respect to the construction market value) has, in recent years, experienced an annual growth rate of about 5% (Klemens 2005). The markets for fiber

reinforced cement and concrete, which are the primary targets for use of functionalized graphite nanomaterials, have experienced an annual growth rate of 15% prior to the economic recession during the first decade of 21st century (Li 2002). The growing market share of fibers in concrete markets can be attributed to the rapid evolution of cement- and concrete-based materials into complex composites which increasingly incorporate various mineral and chemical admixtures as well as reinforcing fibers to meet the growing demands for improved performance (Aitcin 2000). The worldwide markets for concrete admixtures and fibers are estimated at \$10 billion, with an annual growth rate of 10%, which is twice the growth rate of cement consumption. Functionalized graphite nanomaterials surpass today's fiber reinforcement systems in terms of the range of properties they improve. They would thus compete not only with fiber reinforcement systems but also with other admixtures in broader fields of application. For example, functionalized graphite nanomaterials greatly improve the moisture barrier (and durability) characteristics of cement-based materials, and can compete with water-repelling admixtures and polymer emulsions in applications involving aggressive exposure conditions.

The decisions concerning the use of functionalized carbon nanotubes in consultation with designers, contractors and materials suppliers have to rely on technical data and specifications. Some technical specifications impacting the transition of functionalized graphite nanomaterials to markets for cement- and concrete-based products include: (i) ASTM C 1116: Standard Specification for Fiber-Reinforced Concrete; (ii) ASTM C 1399: Standard Test Method for Obtaining Average Residual Strength of Fiber Reinforced Concrete; (iii) ASTM C 1550: Standard Test Method for Flexural Toughness of Fiber Reinforced Concrete; (iv) ATM C 1609: Standard Test Method for Flexural Performance of Fiber Reinforced Concrete; (v) ASTM C 1186: Standard Specification for Flat Non-Asbestos Fiber Cement Sheets; (vi) ASTM C 1288:

Standard Specification for Discrete Non-Asbestos Fiber Cement Interior Substrate Sheets; and (vii) JCI-SF4: Method of Test for Flexural Strength and Flexural Toughness of Fiber Reinforced Concrete. The trend away from recipe-based towards performance-based specifications within the concrete industry has created a favorable environment for expedited introduction of new materials based on their performance merits.

The targeted applications are of value to both the military and civilian infrastructure systems. Applications of functionalized carbon nanotubes towards development of explosion-resistant infrastructure represent a priority topic actively pursued by the U.S. Army (Survivability Branch). The benefits of graphite nanomaterials to concrete-based infrastructure systems would be of direct relevance to this program. Existing fiber cement and fiber concrete applications, especially those with greater demands for structural performance, durability and safety, represent viable entry points for market introduction of functionalized carbon nanotubes. These applications are introduced in Table 1.1 together with the relevant performance considerations and the competing fibers.

In the course of implementing this project, a pilot-scale project involving mixing in ready-mix concrete plant and field placement of high-performance concrete nanocomposites was performed with the assistance of High Grade Materials, a leading concrete supplier in Mid-Michigan. This project was quite helpful towards identifying major issues related to scaled-up production of concrete nanocomposites. Some key issues towards industrial-scale production and use of concrete nanocomposites relate to scaled-up dispersion of graphite nanomaterials for addition to industrial concrete mixers, control of variability in concrete nanocomposite production at large scale, and satisfaction of broad aspects of fresh mix workability requirements.

18.13 Summary

Theoretical studies were conducted in conjunction with micro-structural, chemical and crystalline analyses in order to develop insight into the reinforcement mechanisms of properly functionalized graphite nanomaterials. The results suggested that functionalized graphite nanomaterials improve the mechanical performance of cement-based matrices primarily through dissipation of substantial energy by debonding and frictional pullout phenomena over their enormous surface areas, and also through effective suppression of micro-crack size and propagation by closely spaced nanomaterials. The gains in barrier qualities of cement-based materials with introduction of functionalized graphite nanomaterials could be attributed to the increased tortuosity of diffusion paths in the presence of closely spaced nanomaterials.

Uniformly dispersed graphite nanomaterials percolate within concrete at relatively low volume fractions, producing a rise in electrical conductivity. Damage-dependence of the electrical conductivity of concrete nanocomposites provides a convenient basis for health monitoring of concrete-based infrastructure systems. The electrical conductivity of concrete nanocomposites was found to be sensitive to damaging effects imposed on concrete. Concrete nanocomposites thus offer the potential to offer inherent health monitoring qualities.

Theoretical explanations were also presented for the synergistic role of carbon nanotubes and conventional (micro-scale) fibers towards achieving balanced gains in diverse engineering properties of concrete.

Table 18.1- Typical improvements in properties of high-performance cement-based materials (concrete/mortar/paste) with 0.16 vol.% graphite nanomaterials, 0.24 vol.% carbon microfibers, or hybrid reinforcement comprising 0.16 vol.% functionalized carbon nanotube and 0.24 vol.% carbon microfibers.

Reinforcement System	Flexural Strength	Toughness	Abrasion Resistance	Impact Resistance
Multiwalled Carbon Nanotube (CNT)	23% / 43% / 53%	151% / 165% / 260%	40% / 64% / 45%	73% / 58% / 20%
Carbon Nanofiber (CNF)	15% / 38%	110% /	32% / 50%	62% / 53% /
	/40%	145% /215%	/36%	19%
Graphite Nanoplatelet (GP)	10% /13% /	96% / 73% /	30% / 36% /	59% /100% /
	28%	90%	54%	114%
Carbon Microfiber (CMF)	1% / 14% /	21% / 48% /	23% / 30% /	32% / 36% /
	10%	55%	19%	20%
Hybrid (CNT & CMF)	45% / 51% /	215% / 85% /	36% / 40% /	84% / 64% /
	62%	365%	55%	99%

Table 18.2- Mean values of the electrical conductivity test results for high-performance cementitious mortars with different volume fractions of modified multiwalled carbon nanotubes prepared using two different superplasticizers.

Reinforcement Condition	Electrical Conductivity, 1/Ω m
Plain	1.09 x 10 ⁻⁶
CNT D-PAA, 0.16 vol% - Gl [#]	1.19 x 10 ⁻⁴
CNT D-PAA, 0.16 vol% - Ad*	1.72 x 10 ⁻³
CNT D-PAA, 0.24 vol% - Gl	4.72×10^{-3}
CNT D-PAA, 0.24 vol% - Ad	2.07 x 10 ⁻²

^{*}Glenium® 7700; *ADVA® Cast 575

Table 18.3- Mean values of the electrical conductivity of high-performance cementitious mortar specimens with different volume fractions of functionalized multiwalled carbon nanotubes after application of different compressive stress levels.

Reinforcement Condition	Electrical Conductivity- longitudinal direction, 1/ Ω m	Electrical Conductivity- transverse direction, 1/Ω m
CNT D-PAA, 0.16 vol%	1.92 x 10 ⁻³	2.25 x 10 ⁻³
CNT D-PAA, 0.16 vol%, 60% ultimate	4.14 x 10 ⁻⁴	4.72 x 10 ⁻⁴
CNT D-PAA, 0.16 vol%, 80% ultimate	1.05×10^{-5}	1.12 x 10 ⁻⁴
CNT D-PAA, 0.24 vol%	2.07×10^{-2}	2.80×10^{-2}
CNT D-PAA, 0.24 vol%, 60% ultimate	3.15×10^{-3}	4.05 x 10 ⁻³
CNT D-PAA, 0.24 vol%, 80% ultimate	4.23 x 10 ⁻⁴	4.15 x 10 ⁻⁴

Table 18.4- Performance gains of high-performance concrete per vol.% of reinforcement, normalized with respect to the reinforcement cost.

Reinforcement	Flexural Strength	Toughness	Abrasion Resistance	Moisture Diffusion Resistance	Impact Resistance
Carbon Nanotube	1.9	8.4	2.1	2.9	2.5
Steel Fiber	0.18	5.6	0.035	0.035	2.1
Polypropylene Fiber	1.2	8.5	0	0	2.7

Table 18.5- Typical performance gains of cement-based materials with introduction of the specified volume fractions of functionalized carbon nanotube, and steel, polypropylene and glass fibers.

Reinf. Type	Reinf. Vol.%	% Improvement in Properties (Normalized Value with respect to Vol.%)				
		Flex. Strength	Flex. Energy	Abrasion Res.	Mois.Diff.Res.	Impact Res.
Carbon Nanotube	0.24	50 (625)	200 (2,500)	50 (625)	70 (875)	60 (750)
Steel Fiber	2	25 (12.5)	800 (400)	5 (2.5)	5 (2.5)	300 (150)
Polypropylene Fiber	0.5	20 (40)	100 (200)	0 (0)	0 (0)	250 (500)
Glass Fiber	5	50 (10)	1000 (200)	0 (0)	0 (0)	260 (52)

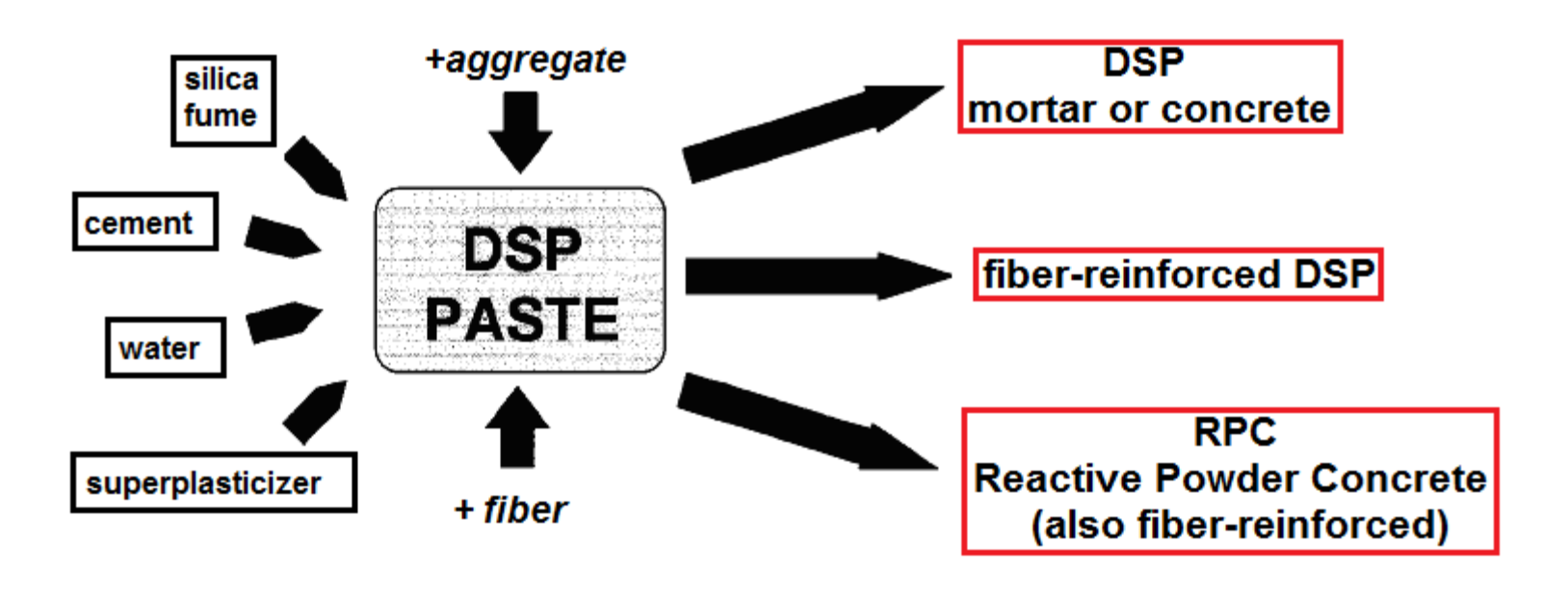


Figure 18.1- Evolution of DSP paste into DSP mortar and RPC cementitious products (Guerrini 2000).

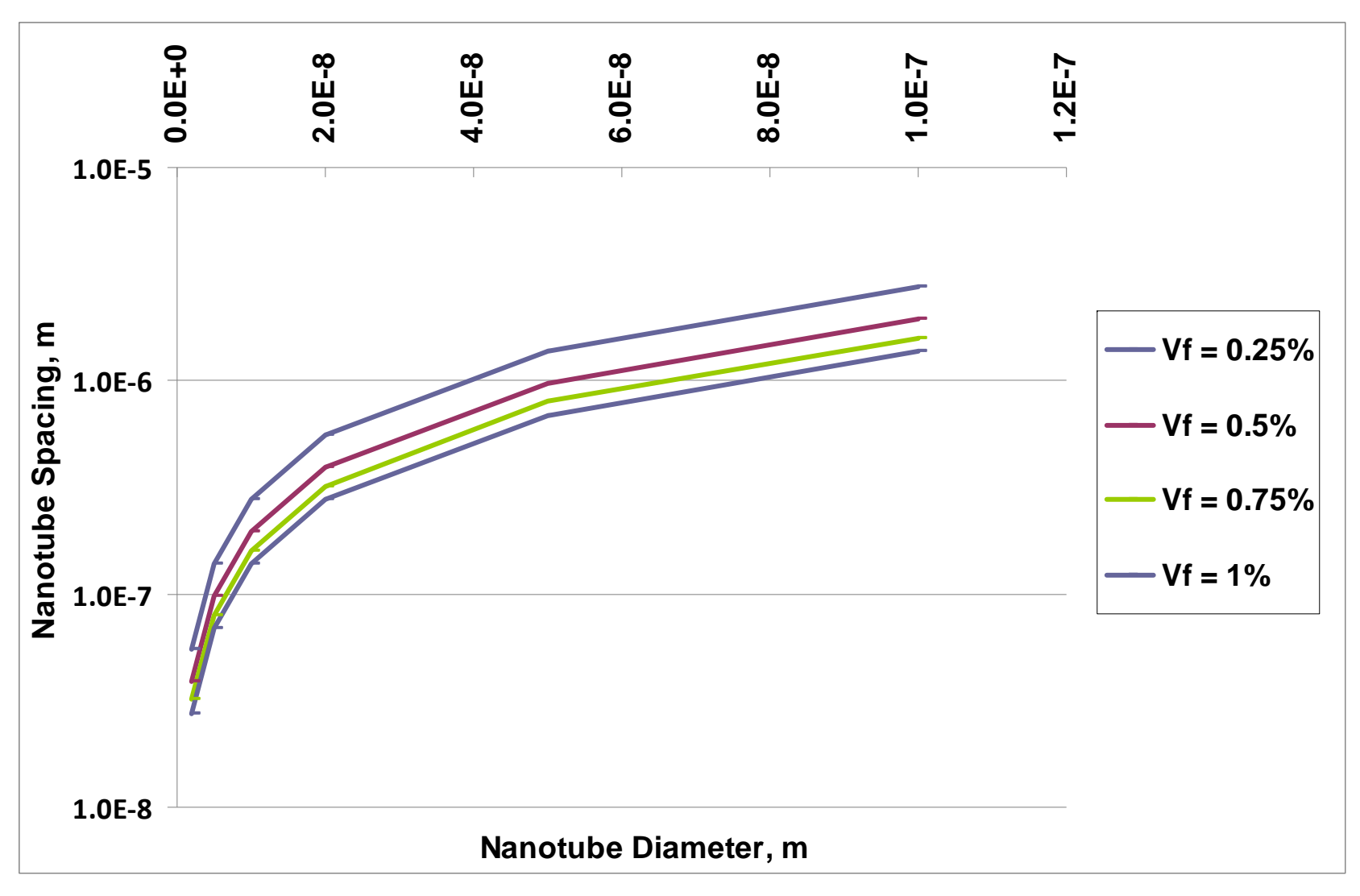


Figure 18.2- Average nanotube spacing versus nanotube diameter at different nanotube volume fractions ranging from 0.1% to 1% (K=1.38 for 3-D random orientation of nanotubes).

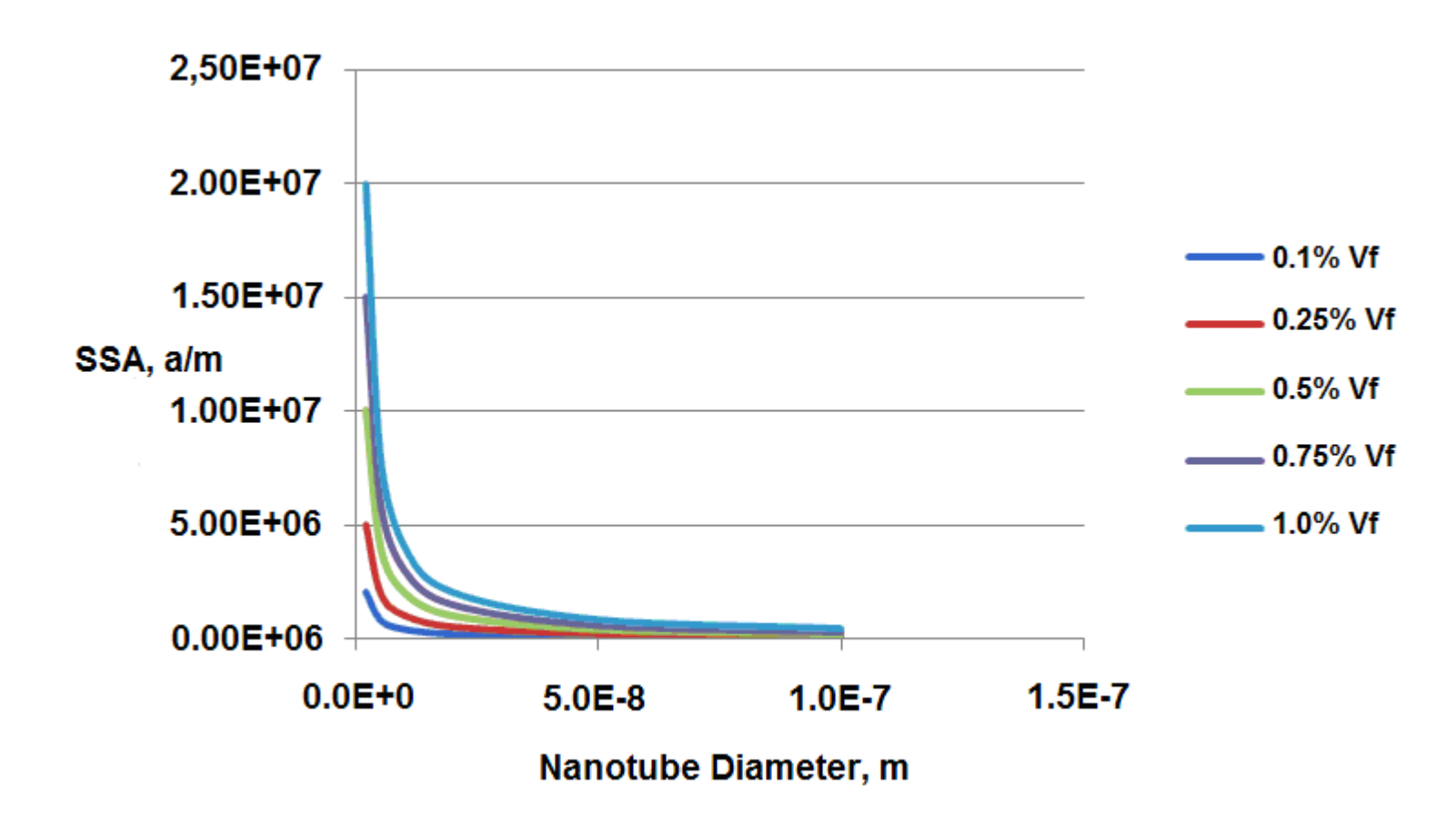


Figure 18.3- The specific surface area of nanotubes versus nanotube diameter for different nanotube volume fractions.

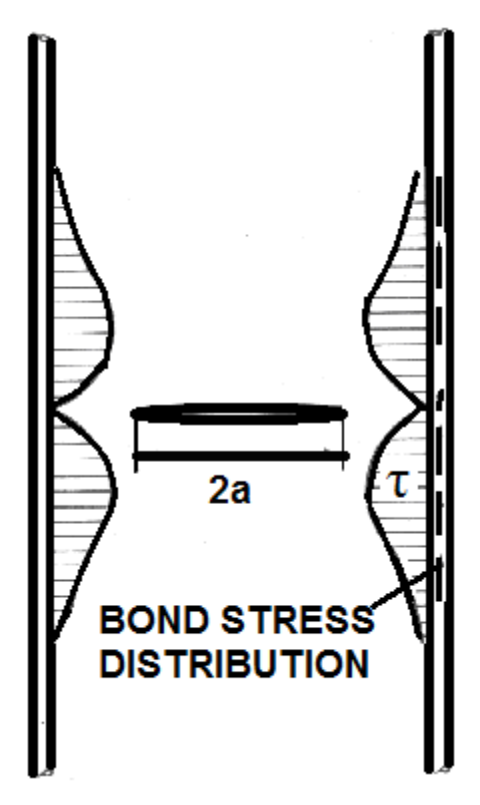


Figure 18.4- The crack suppression effect of closely spaced nanotubes.

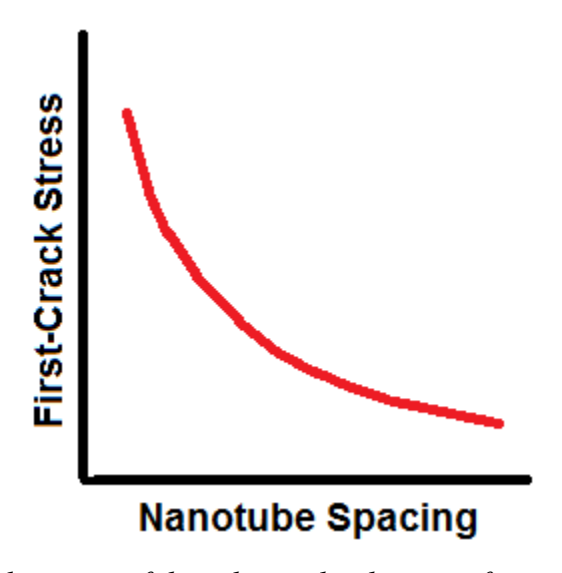


Figure 18.5- Schematic depiction of the relationship between first-crack stress and nanotube spacing.

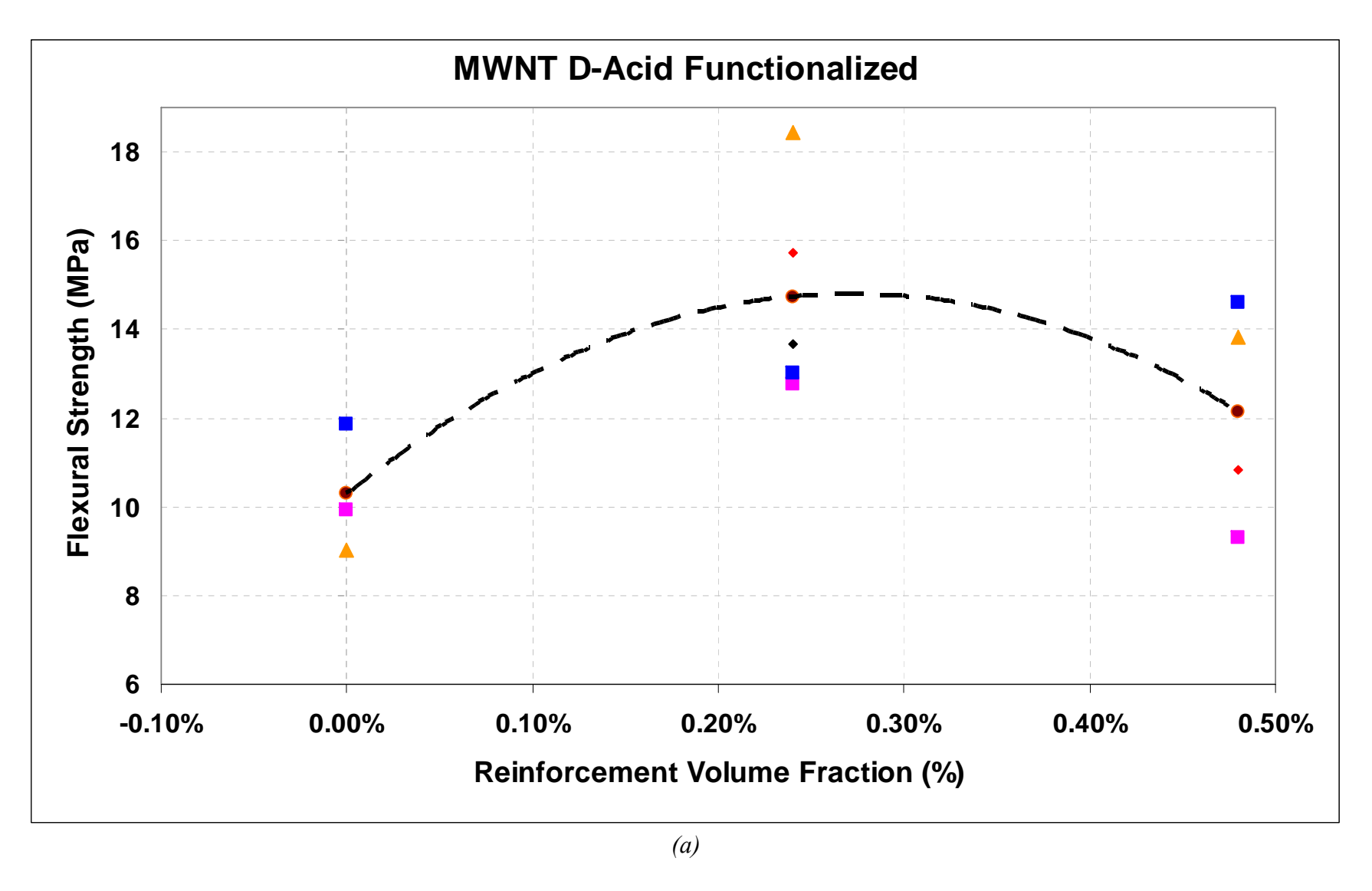


Figure 18.6- The trends in measured values of flexural strength at different volume fractions of MWNTs.

Figure 18.6 (cont'd)

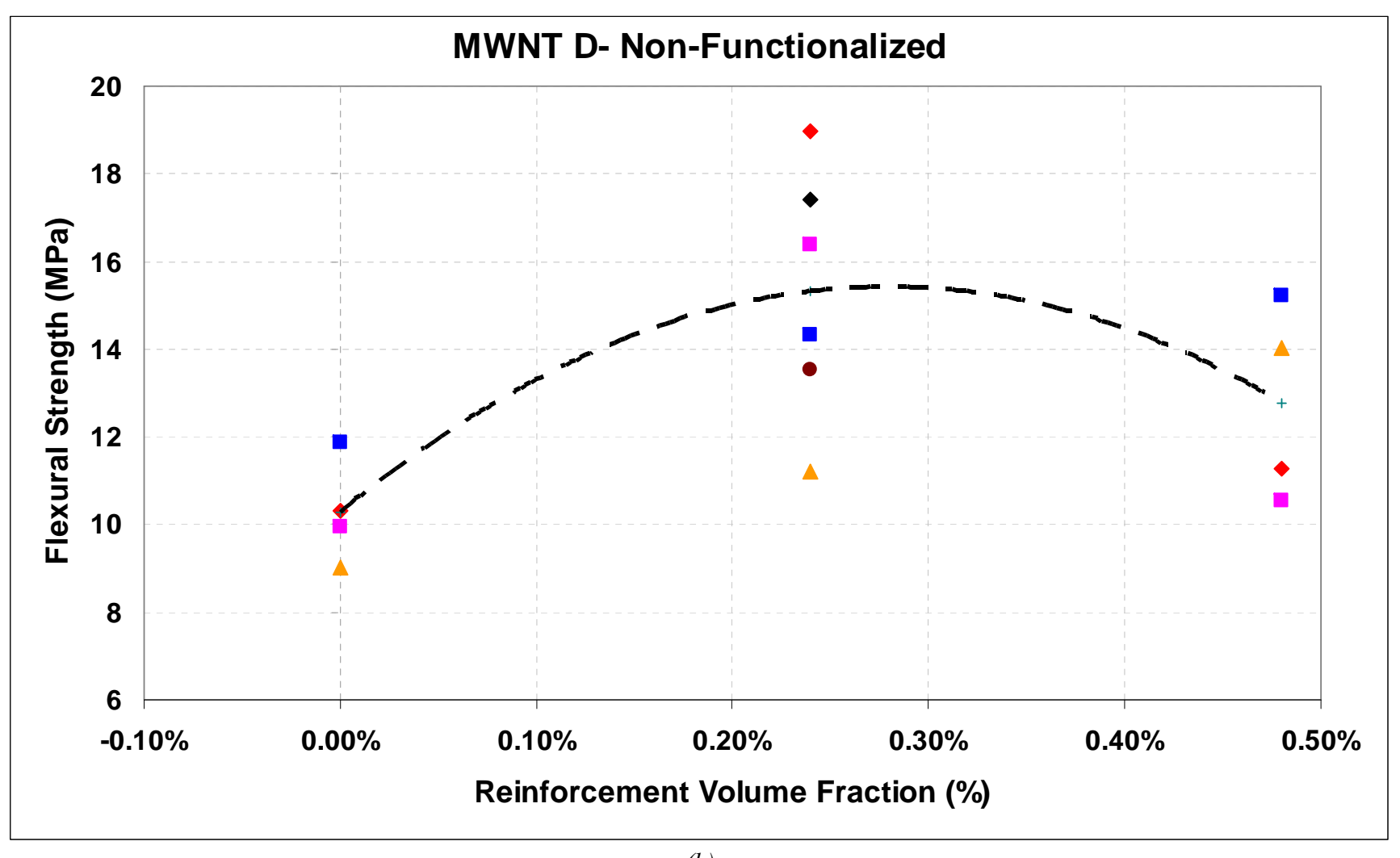
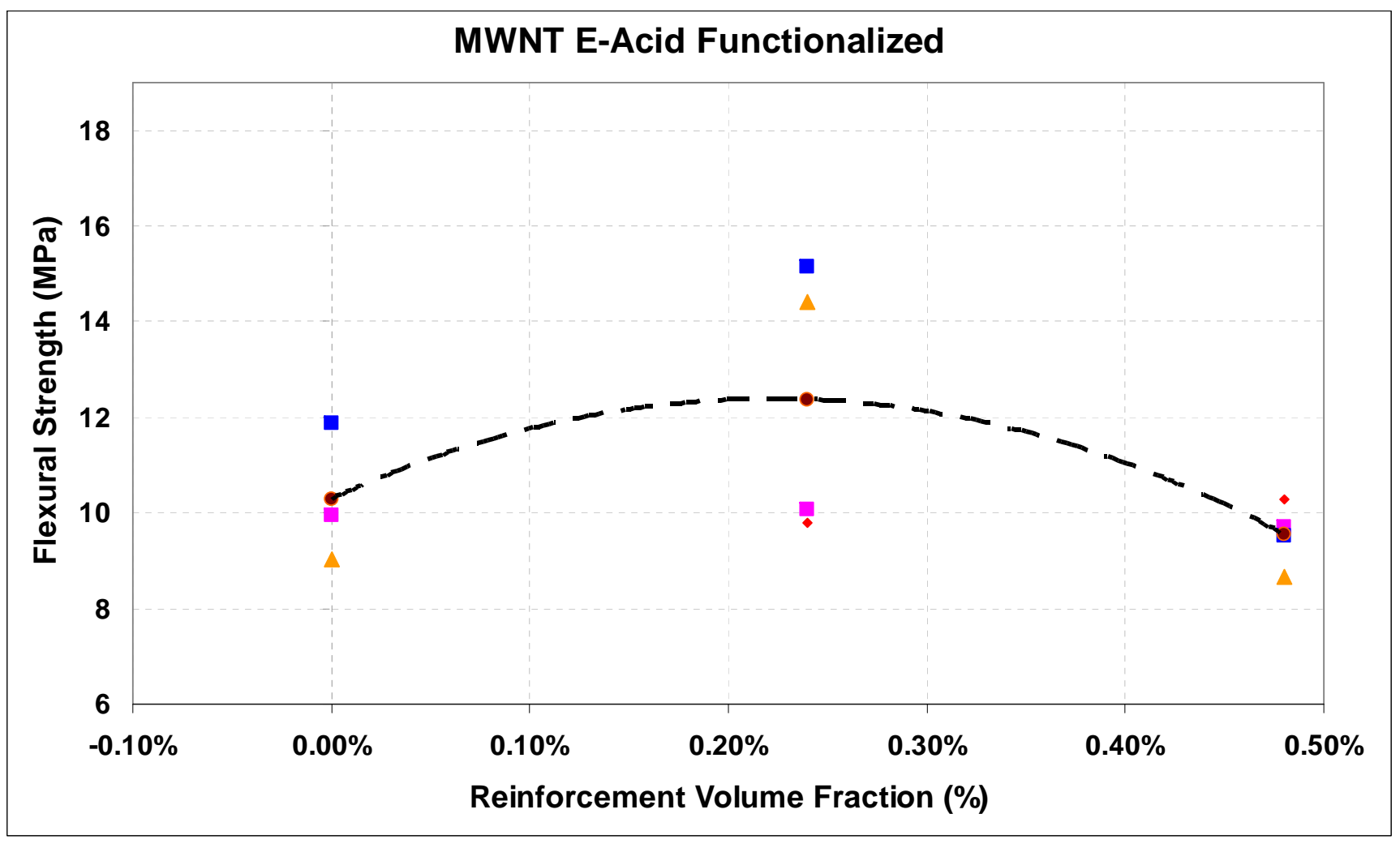
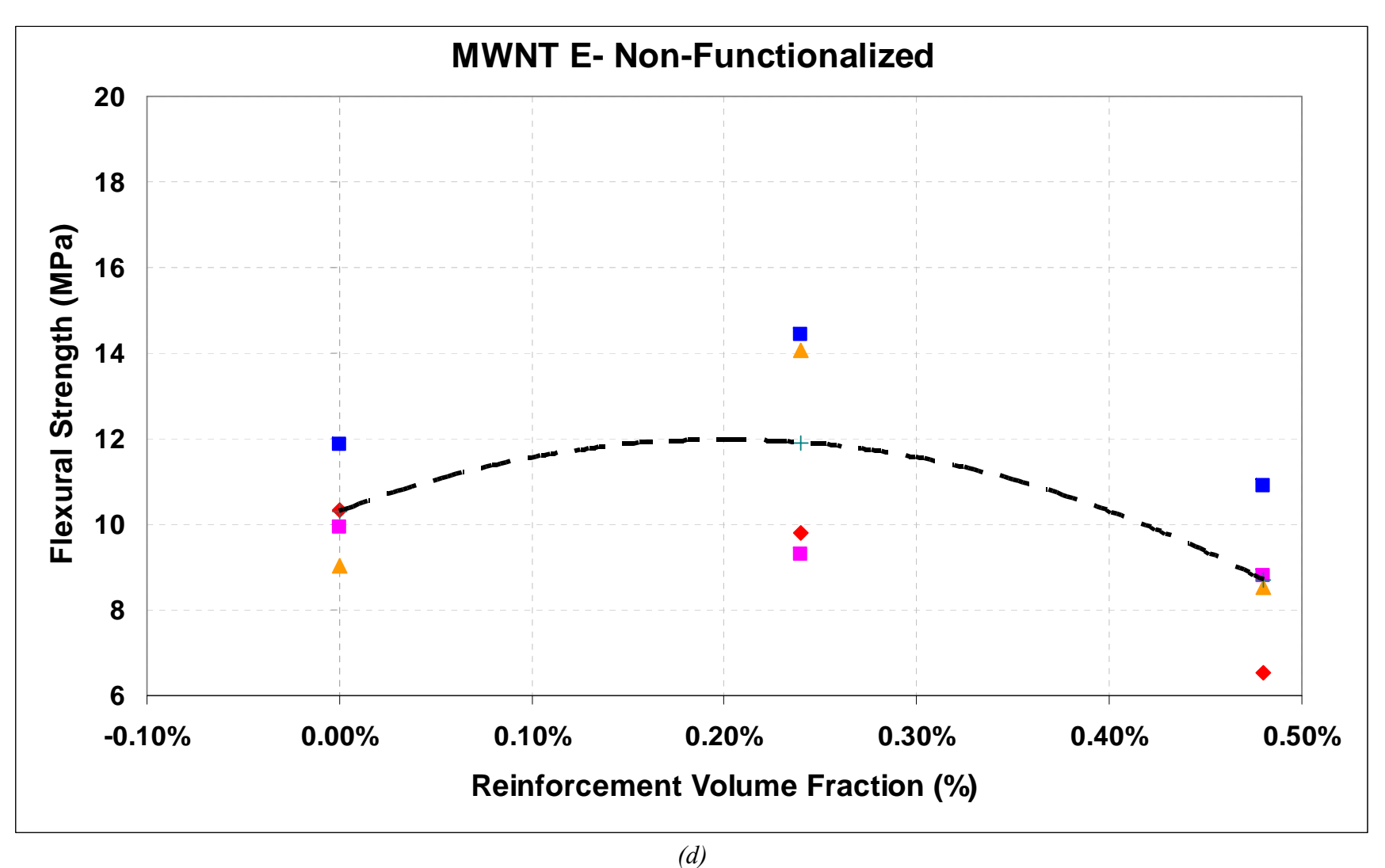
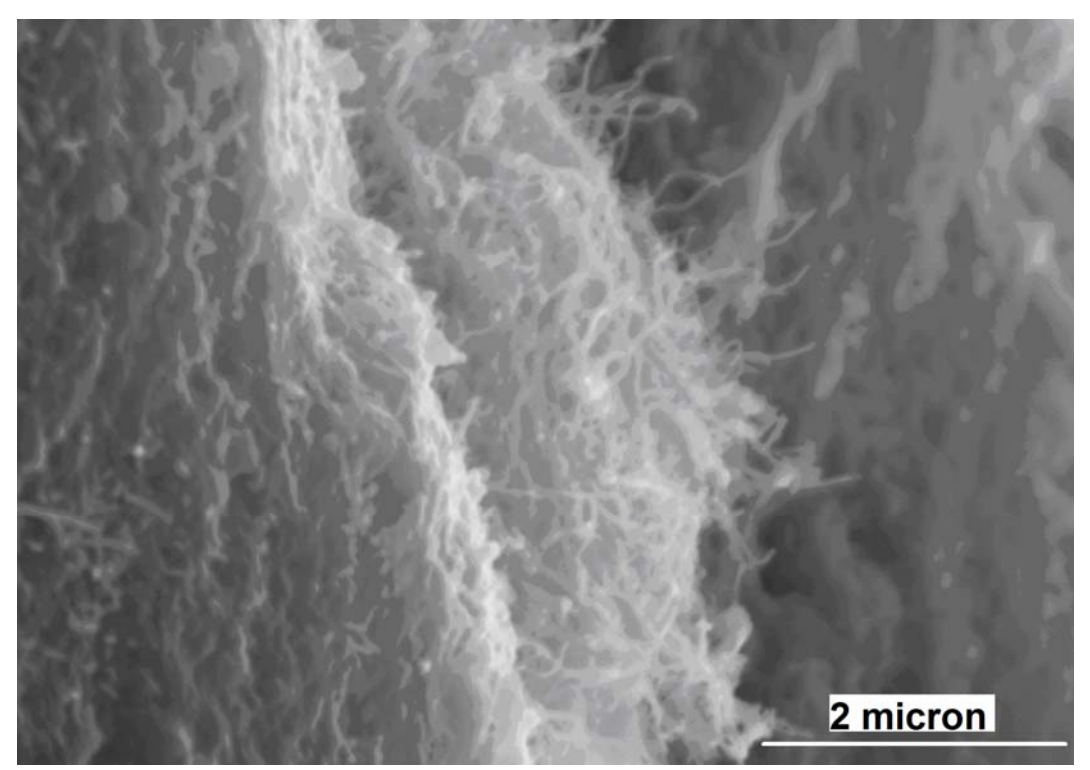


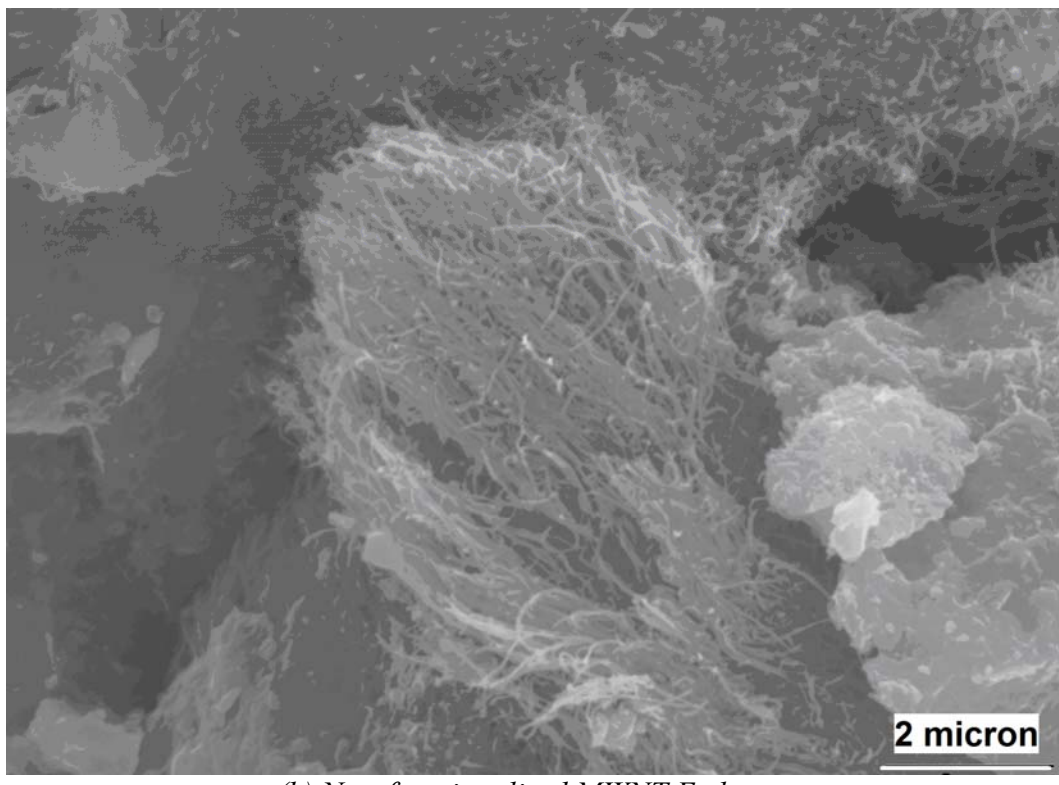
Figure 18.6 (cont'd)







(a) Clustering of functionalized MWNT E



(b) Non-functionalized MWNT E cluster

Figure 18.7- Typical SEM mages of the fractured surfaces of DSP paste reinforced with 0.48% volume fraction of acid-functionalized and non-functionalized MWNT E.

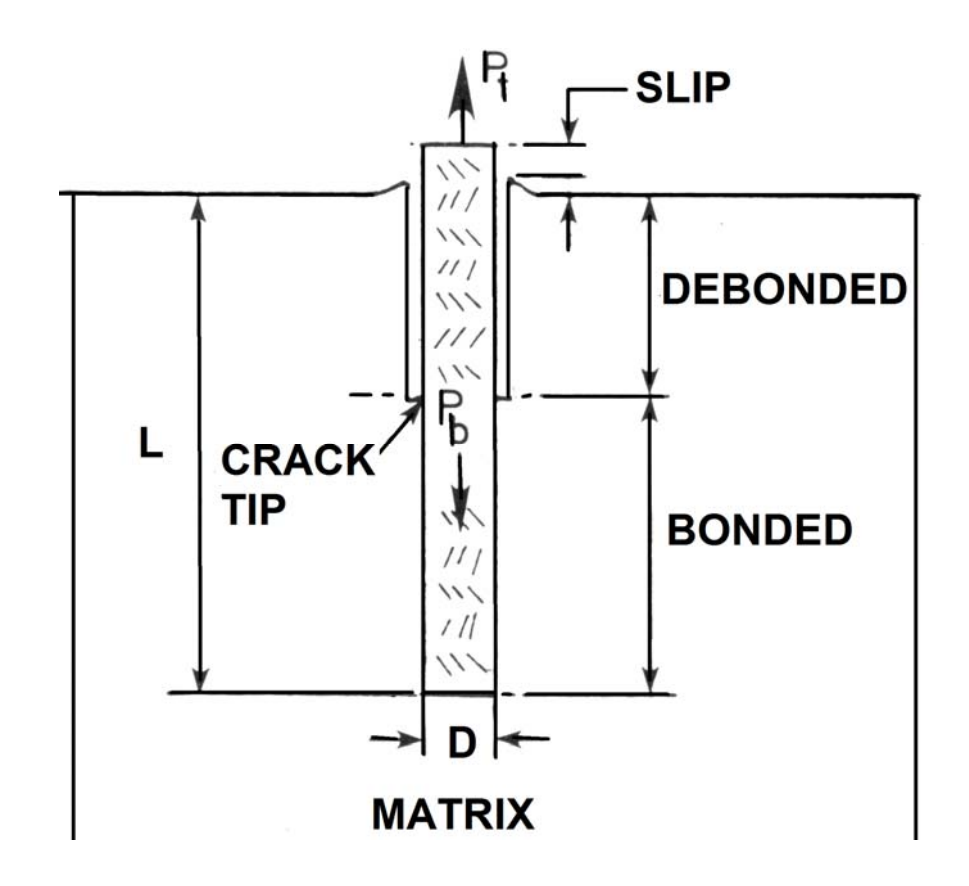


Figure 18.8- The debonding model.

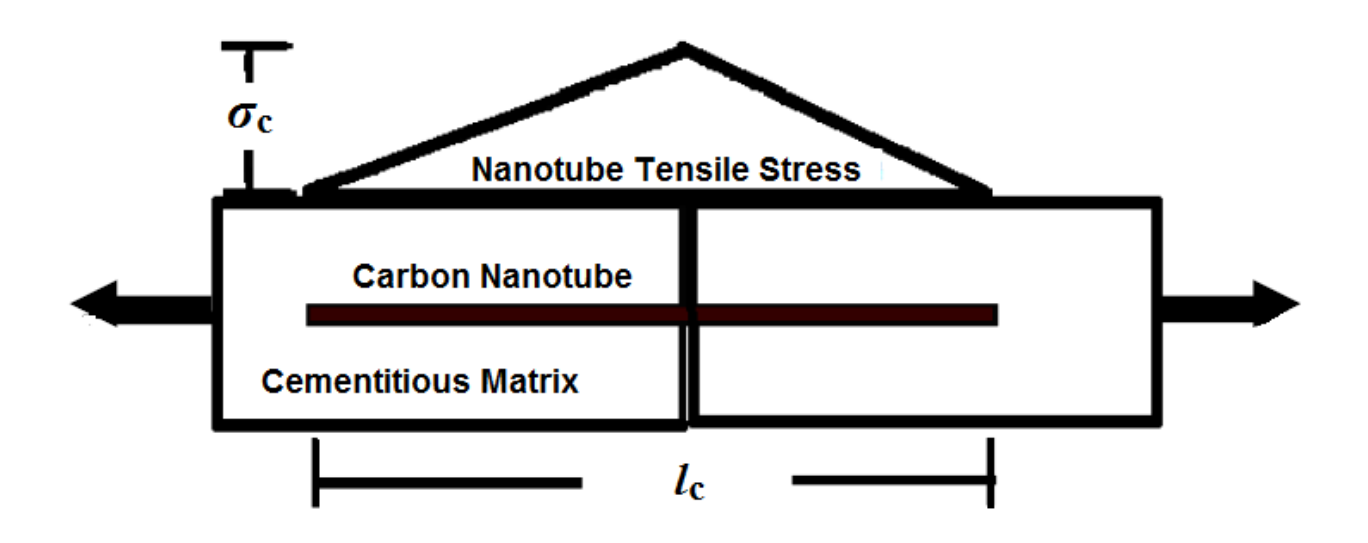


Figure 18.9- Interfacial shear stress distribution for critical length (l_c) calculation.

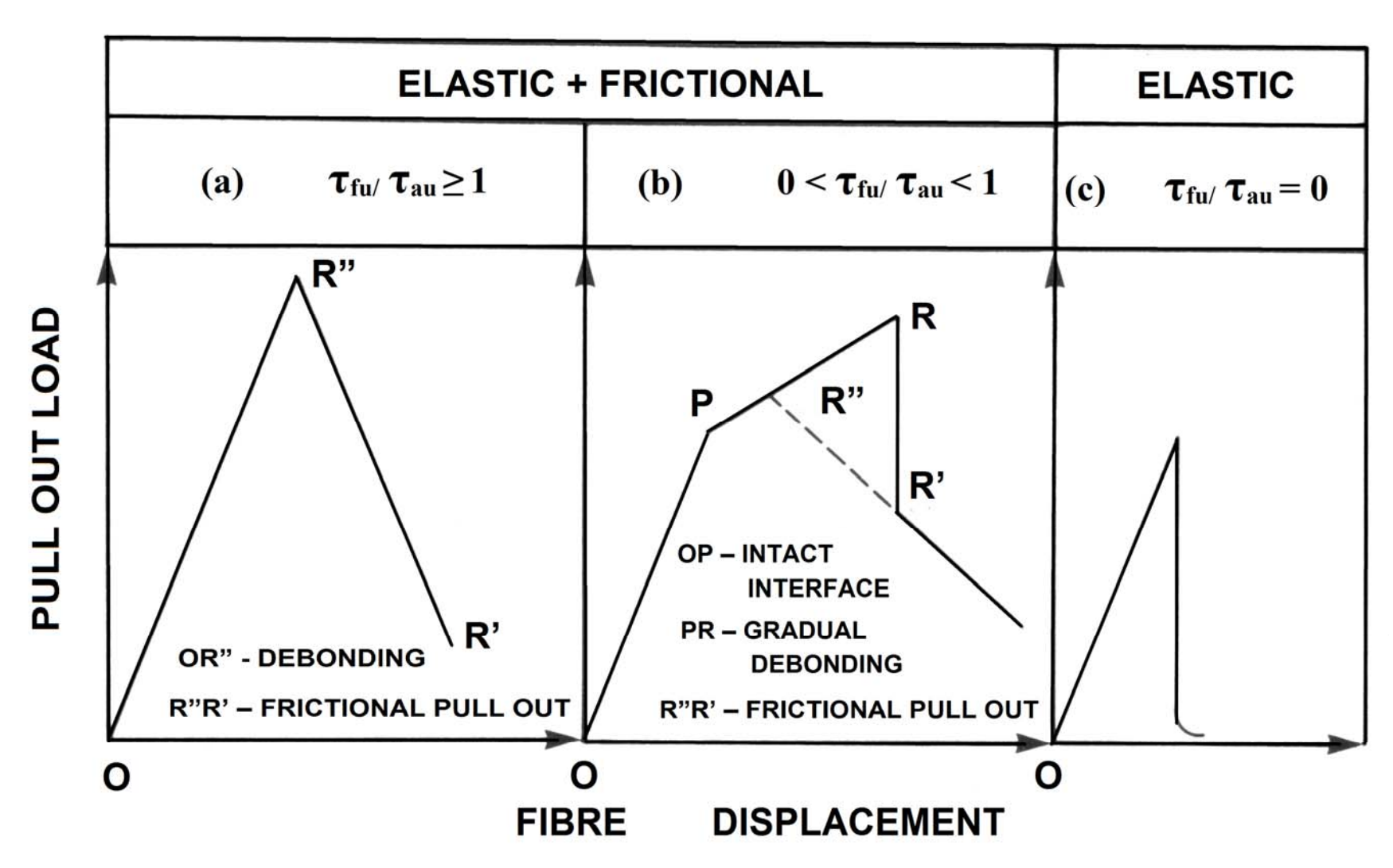


Figure 18.10- Pullout load versus displacement for various ratios of adhesion shear to interfacial friction resistance.

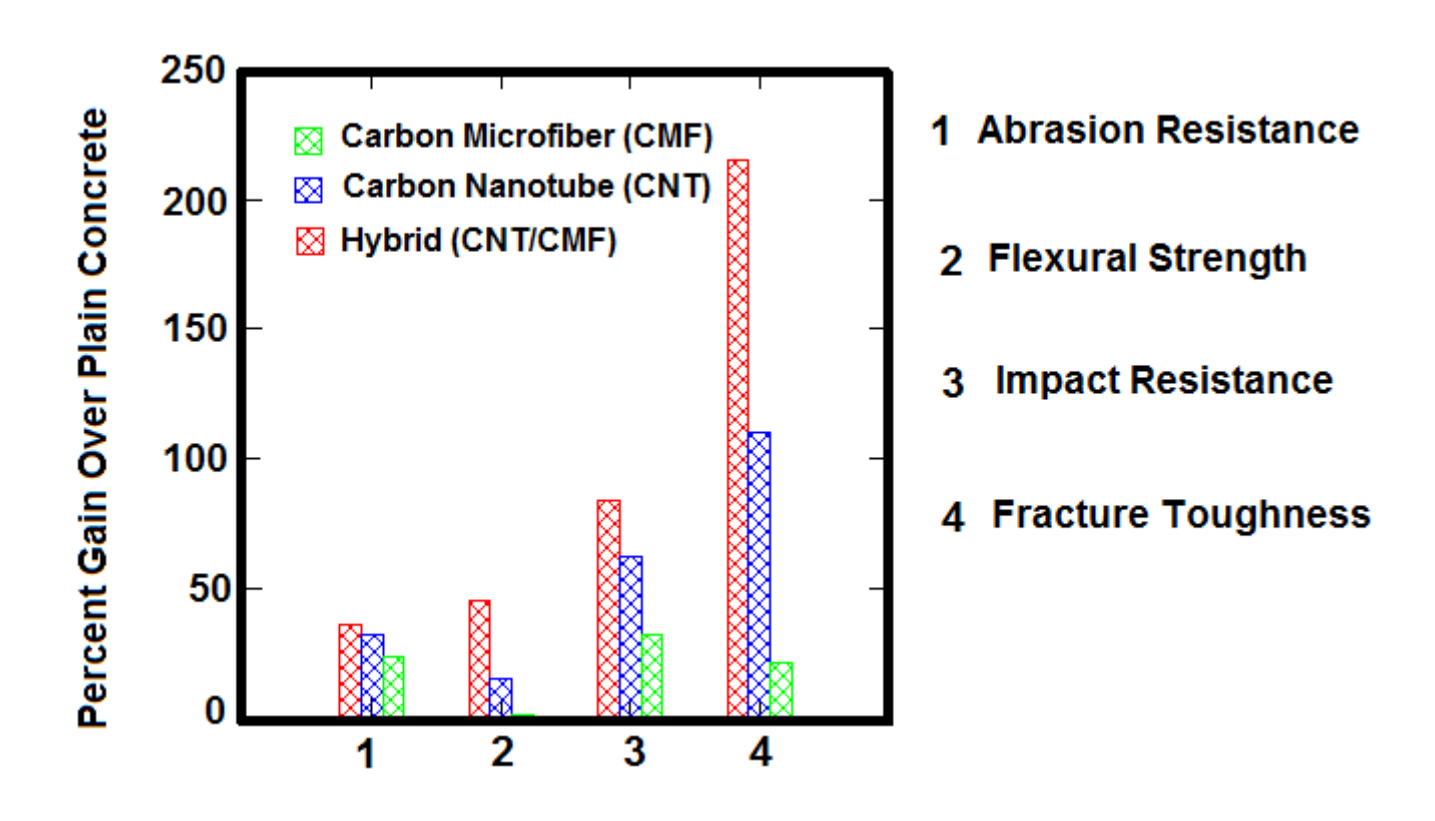


Figure 18.11- Gains in engineering properties of high-performance concrete brought about by 0.16 vol.% functionalized carbon nanotube and/or 0.24 vol.% carbon (micro)fiber.

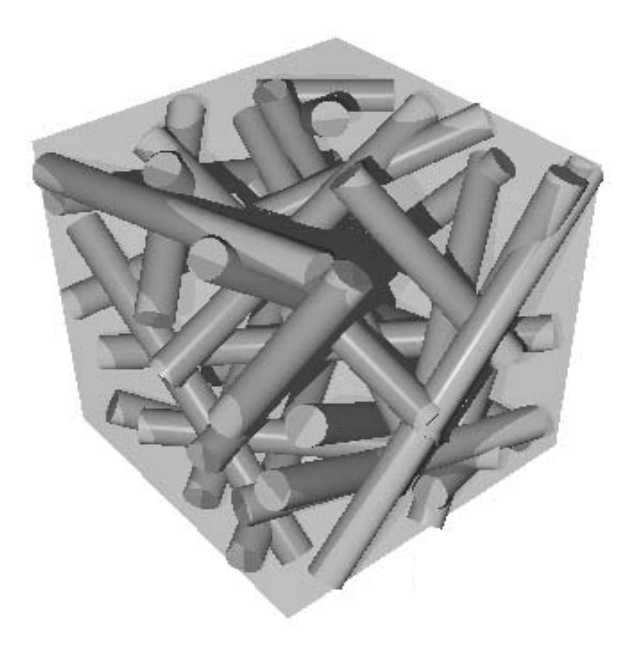


Figure 18.12- Three-dimensional assembly of carbon nanotubes within a cement-based matrix.

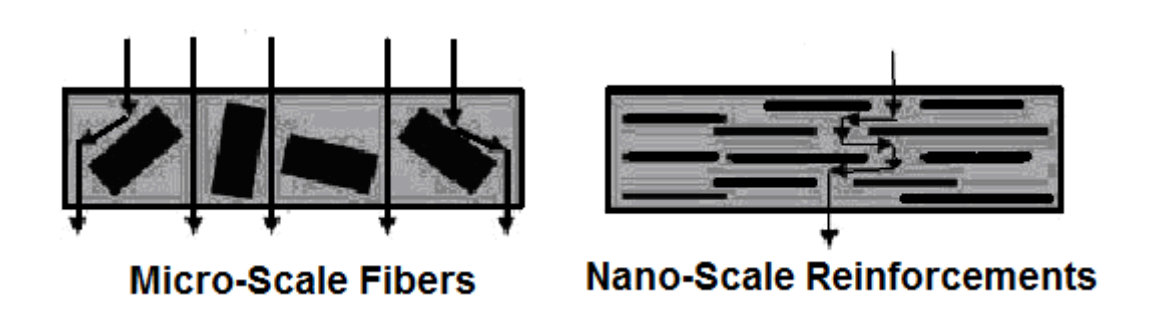


Figure 18.13- Tortuous diffusion paths forced by nano-scale reinforcement.

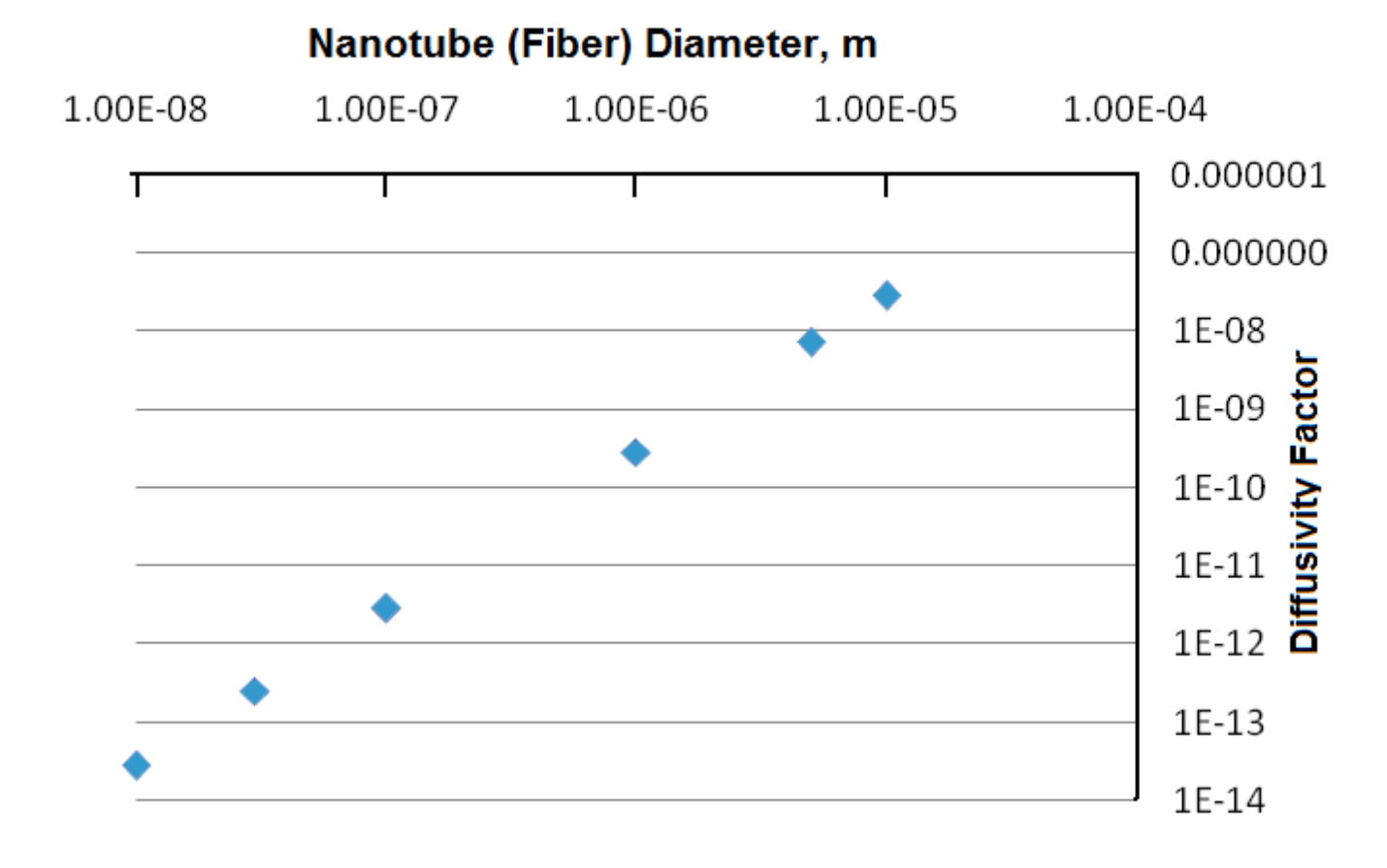
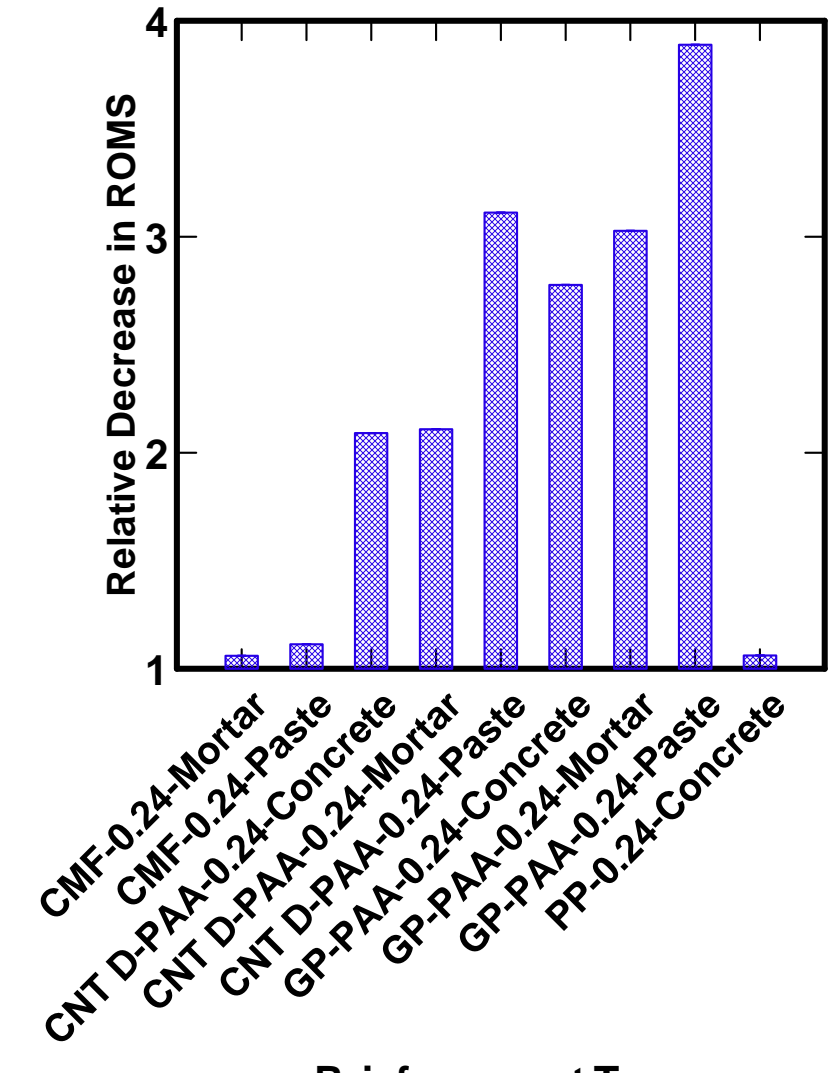


Figure 18.14- Diffusivity factor versus the reinforcement diameter at 0.24% volume fraction for a diameter range covering multiwalled carbon nanotubes and conventional micro-scale fibers.



Reinforcement Type

Figure 18.15- Relative decrease in rate of moisture sorption for different high-performance matrices incorporating 0.24 vol.% of different nano and micro-scale reinforcements.

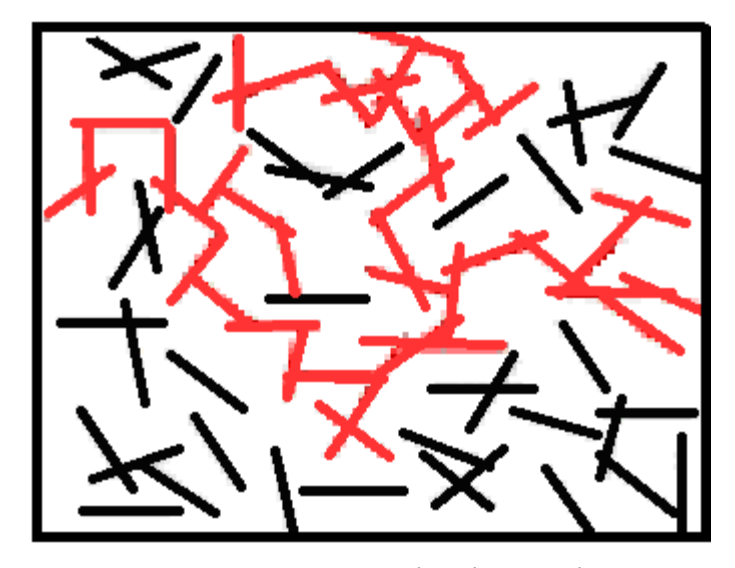


Figure 18.16- Percolated network.

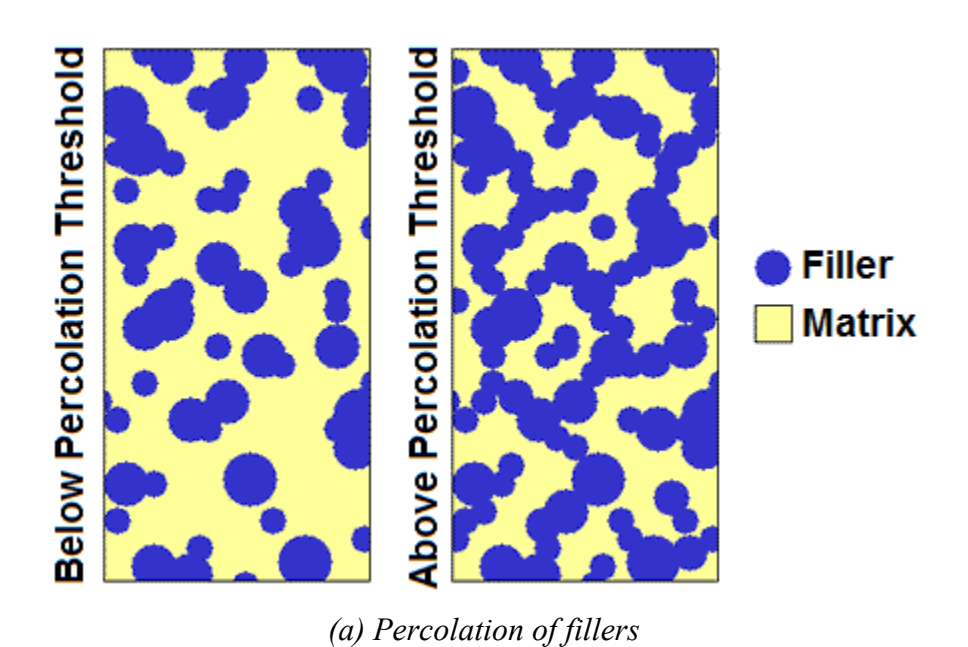
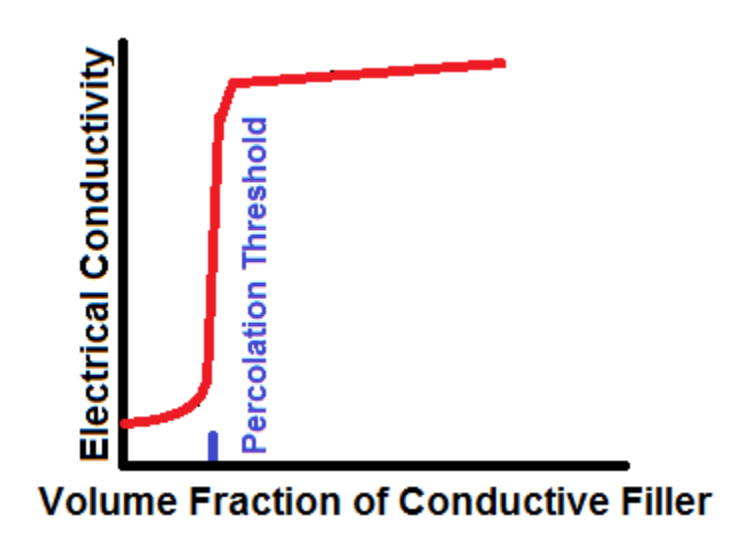


Figure 18.17- Percolation of conductive inclusions within a matrix.



(b) Conductivity vs. volume fraction

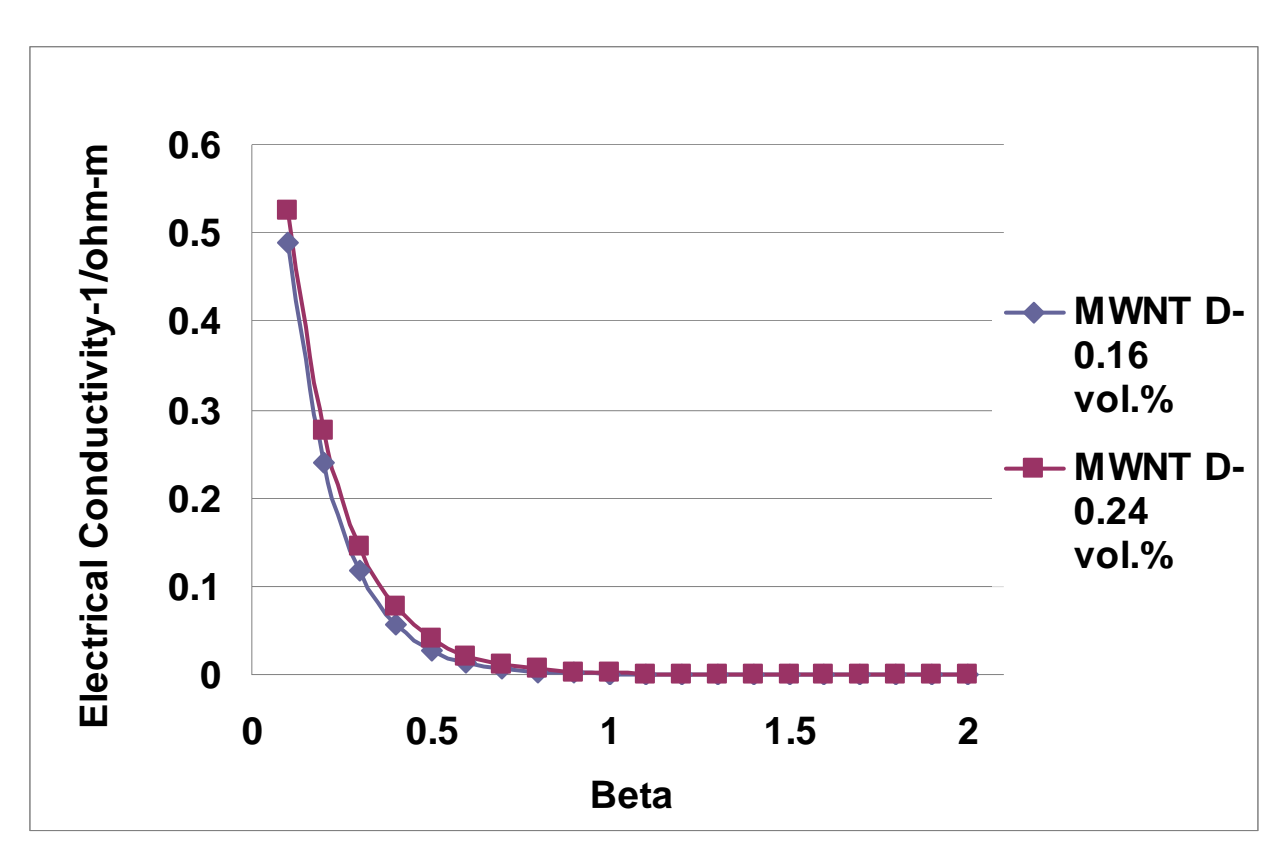


Figure 18.18- Electrical conductivity values plotted for different volume fractions of PAA-physisorbed MWNT D using different β values.

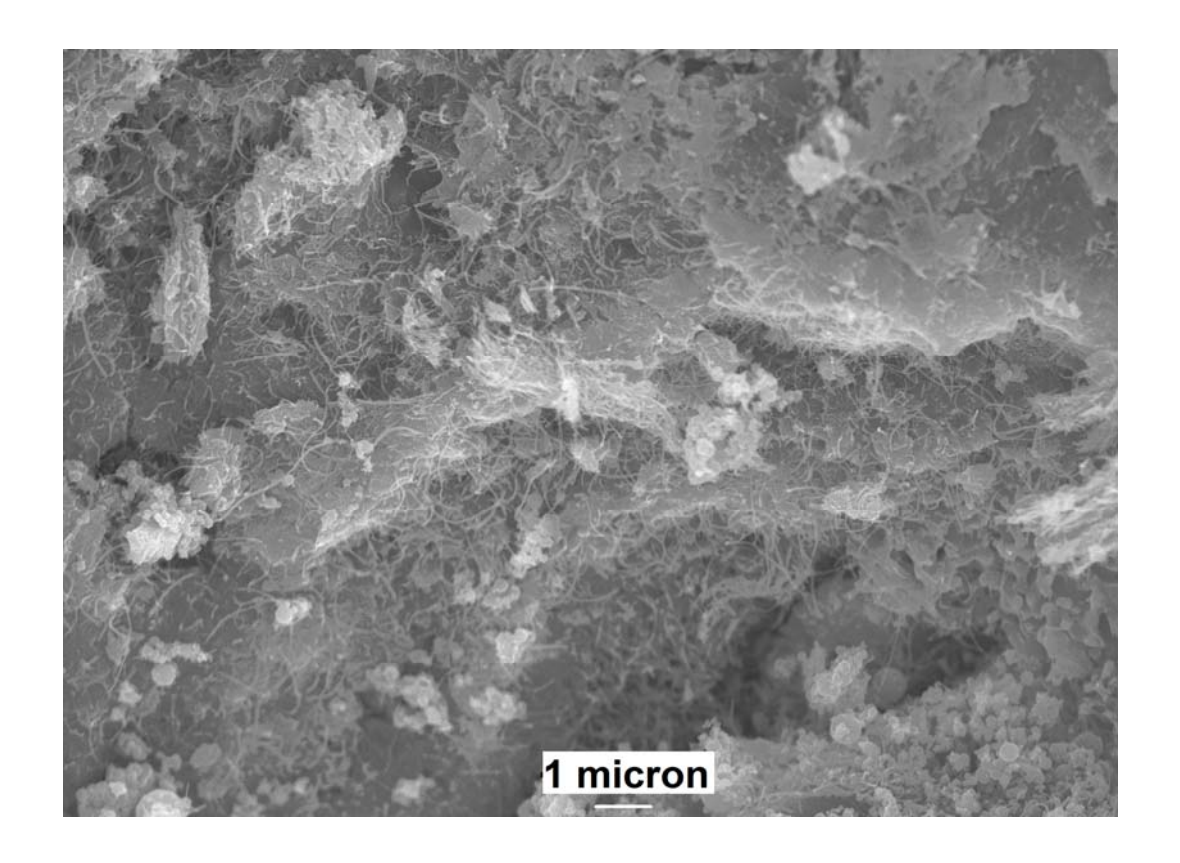


Figure 18.19- Typical SEM image of high-performance cementitious mortar reinforced with modified MWNTs showing uniform dispersion and percolation of nanotubes within the matrix.

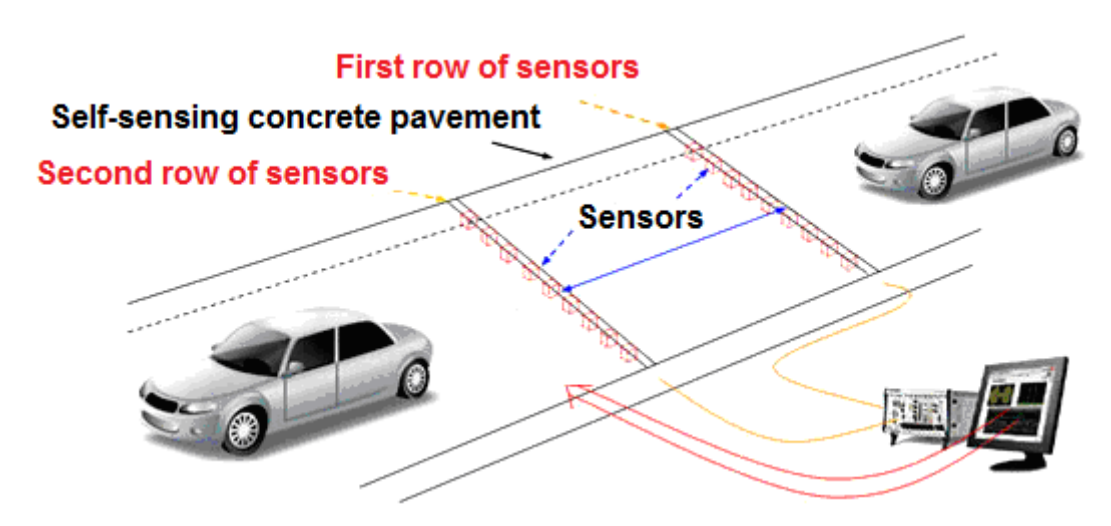


Figure 18.20- Self-sensing smart concrete (Baoguo, Xun et al. 2009).

CHAPTER 19

19 CONCLUSIONS

19.1 General

Advances in concrete additives have played enabling roles towards development of high-strength concrete materials. The rise in concrete compressive strength, however, tends to lower the toughness and tensile-to-compressive strength ratio of concrete, and make it more prone to early-age microcracking under restrained (drying / autogeneous) shrinkage and thermal stresses. These issues have been addresses through introduction of discrete fibers with micrometer- to millimeter-scale diameters. Concrete, however, incorporates flaws at different scales; finer flaws with nano-scale size and spacing challenge the effectiveness of conventional reinforcing fibers; these flaws can form and grow within the cementitious matrix in between fibers without encountering them. The use of nano-scale reinforcement (with nano-scale spacing) in high-performance cementitious materials can overcome this drawback of conventional reinforcing fibers.

Graphite Nanomaterials, including carbon nanotubes, present several distinct advantages over conventional (micro-scale) fibers as reinforcement in high-performance cementitious materials. Graphite nanomaterials generally provide significantly higher strength and modulus than conventional fibers. These nanomaterials also provide distinctly high specific surface areas and aspect ratios, which benefit their interactions with the cementitious matrix and effectiveness in control of crack formation and propagation. Provided that nanomaterials are uniformly dispersed

within the cementitious matrix, due to their nano-scale cross-sectional dimensions and high aspect ratios, the spacing between nanomaterials tends to be very small. The inception and propagation of microcracks in the space between nano-scale reinforcement would thus be effectively hindered.

Experimental studies were conducted on the reinforcement efficiency of multiwalled carbon nanotubes with different aspect ratios and surface modification conditions in high-performance cementitious materials. While the focus of the project was on multiwalled carbon nanotubes, graphite nanoplatelets and carbon nanofibers were also evaluated. The surface modification conditions considered involved (acid) functionalization of carbon nanotubes and/or anchoring different polymers via chemical bonding or physical adsorption as well as microwave irradiation. Comparative evaluations of different surface modification conditions led to the development of an effective nanotube surface modification procedure which favored the dispersion and interfacial interactions of nanotubes in cement-based materials. With proper surface modification, nanotubes of higher aspect ratios could be dispersed within cementitious materials at larger dosages for achieving pronounced, balanced gains in diverse engineering properties. This research has laid a solid foundation for development of a new class of high-performance concrete materials with a unique balance of engineering properties at competitive cost.

Comprehensive experimental studies were conducted to tailor the selection and proportioning of concrete-making materials for effective mobilization of the distinct qualities of modified multiwalled carbon nanotubes towards achieving balanced gains in engineering properties. Smooth gradation of cementitious particles was considered to benefit the dispersion of nanomaterials; this measure, together with pozzolanic reactions, produced dense cement hydrates which effectively interacted with the modified nanotube surfaces.

Experimental investigations were undertaken in order to identify optimum (nano- and microscale) reinforcement systems for high-performance concrete. A comprehensive experimental data
base was developed on the mechanical, physical and durability characteristics as well as the
structure and failure mechanisms of high-performance cementitious nanocomposites reinforced
with modified graphite nanomaterials. Thorough dispersion and effective interfacial interactions
of graphite nanomaterials within concrete, enabled by proper surface modification of
nanomaterials, led to major gains in the engineering properties of high-performance concrete at
relatively low dosages of nanomaterials. Another unique feature of modified nanomaterials was
their ability to bring about balanced gains in diverse engineering properties of high-performance
concrete. Significant gains in fracture toughness and impact resistance were accompanied with
major rise in strength, barrier qualities, abrasion and weathering resistance, fatigue life and
weathering resistance of high-performance concrete.

Graphite nanomaterials percolate within concrete at relatively low volume fractions, causing a rise in electrical conductivity. Damage-sensitivity of the electrical conductivity of concrete nanocomposites provides a convenient basis for health monitoring of concrete-based infrastructure systems. The significant gains in diverse aspects of concrete properties brought about by low dosages of nanomaterials, combined with the growth in their industrial-scale production at reduced costs; enable development of a new class of high-performance concrete materials with unique balance of qualities at competitive cost. A highly desired synergism was found between the contributions of nano- and micro-scale reinforcement to different engineering properties of concrete.

19.2 Key Findings

The following key conclusions are drawn based on the work conducted in the project:

- Past investigations on the use of graphite nanomaterials in cement-based matrices have been conducted mostly in cementitious pastes, and the test results do not provide a consistent view of the reinforcement efficiency of nanomaterials in cement-based matrices.
- The initial **feasibility studies** conducted in the project indicated that:
 - Surface modification is a critical step towards enhancement of the reinforcement efficiency of graphite nanomaterials in cement-based matrices by improving the dispersion and interfacial interactions of nanomaterials within matrix.
 - o Modified graphite nanomaterials at relatively low volume fractions (<0.1 vol.%) offer superior reinforcement efficiency when compared with micro-scale (carbon) fibers and unmodified nanomaterials.
 - Modified graphite nanomaterials yield uniquely balanced gains in the engineering properties of cement-based matrices; these properties range from flexural strength, energy absorption capacity and impact resistance to abrasion resistance and moisture barrier qualities, which cannot be matched by micro-scale fiber reinforcement systems.
 - The improvements in mechanical properties of cement-based matrices with introduction of graphite nanomaterials can be attributed to:
 - Significant energy dissipation associated with debonding and frictional
 pullout over the enormous surface area of nanomaterials; and

- Effective suppression of micro-crack size and propagation by the closely spaced nanomaterials.
- The gains in moisture barrier qualities (against capillary sorption) of cement-based matrices with introduction of modified graphite nanomaterials can be attributed to the tortuous diffusion paths in the presence of closely spaced nanomaterials.
- The introduction of modified (and unmodified) graphite nanomaterials at <0.1 vol.% does not fundamentally alter the structure of cement hydration products.
- The **surface modification** conditions and the aspect ratio of multiwalled carbon nanotubes determine their reinforcement efficiency in high-performance cementitious matrices.
 - O Among the surface modification conditions considered, physisorption of poly(acrylic acid) (PAA) on multiwalled carbon nanotubes produced the most consistent favorable effects.
 - The best balance of mechanical properties was realized when longer multiwalled carbon nanotubes were modified through PAA physisorption without acid-functionalization of nanotubes prior to introduction of PAA; it seems that any benefits of acid-functionalization prior to PAA-physisorption are more than compensated for by their damaging effects (e.g., shortening of carbon nanotubes).
 - o Increased nanotube length and aspect ratio benefited their reinforcement efficiency in high-performance cementitious matrices; excess nanotube lengths,

however, complicate their dispersion in the mixing water of cementitious matrix at required concentrations.

- O The benefits realized by proper surface modification of nanotubes can be explained by their contributions towards uniform dispersion in aqueous media, and improved interfacial interactions with cement hydrates.
- The extent of surface modification as well as the concentration of nanotubes in cementitious matrix should be optimized, depending upon the composition and processing conditions of cementitious nanocomposites, in order to avoid agglomeration of nanotubes and their potential interferences with the hydration process of cement.
- The experimental results generated for **cementitious pastes** reinforced with different unmodified and modified multiwalled carbon nanotubes, and also their hybrids with carbon microfibers at higher volume fractions, yielded the following conclusions:
 - The length, diameter and surface modification conditions (as well as the mechanical attributes) of carbon nanotubes all have critical effects on their reinforcement efficiency in cement-based matrices.
 - Acid functionalization of nanotubes could introduce new defects, and reduce the length of nanotubes. These adverse effects of functionalization may overshadow its positive contributions to the dispersion and interfacial bonding and thus the reinforcement efficiency of nanotubes.
 - Use of polymer-wrapped (PAA physisorbed) multiwalled carbon
 nanotubes enhances the dispersion and interfacial interactions of

nanotubes within cementitious matrix without introducing defects or shortening the nanotubes.

- Upon acid-functionalization, the larger-diameter multiwalled carbon nanotubes considered here provided a lower degree of functionalization (1.2% COOH groups) when compared with the smaller-diameter nanotubes (2.5% COOH groups). The finer, higher-aspect-ratio nanotubes, in both functionalized and non-functionalized conditions, produced (at 0.24% by volume of dry cementitious materials) more pronounced gains in the engineering properties of the high-performance cementitious (densified with small particles DSP) paste considered in the project. The high specific surface area and the nano-scale spacing of dispersed nanotubes benefit their microcrack arrest action, which explains their reinforcement efficiency in the cementitious matrix. Well-dispersed multiwalled carbon nanotubes with desired interfacial interactions brought about balanced gains in the flexural strength, energy absorption capacity and ductility, impact and abrasion resistance of high-performance cementitious paste, while preserving its high compressive strength.
- Relatively high nanotube contents (0.48 vol.% by volume of dry cementitious materials) led, for the cementitious matrix composition and processing conditions considered here, to clumping of nanotubes which compromised their reinforcement efficiency.
- O Hybrid (combined nano- and micro-scale) reinforcement of the high-performance cementitious paste, when used at appropriate volume fractions, provided distinct gains in diverse engineering properties, which could not be realized by nano- or

micro-scale reinforcement alone; this point at the synergistic beneficial effects offered by nano- and micro-scale reinforcement systems.

- The reinforcement efficiencies of **functionalized**, **non-functionalized** and **polymer-wrapped multiwalled carbon nanotubes** were evaluated in a high-performance cementitious **paste** prepared using two different commercially available polycarboxylate-based superplasticizers. It should be noted that the role of superplasticizers in high-performance cementitious nanocomposites was expanded to also cover that of a nanomaterial dispersant. Experimental results indicated that:
 - O Different polycarboxylate-based superplasticizers produce cementitious nanocomposites with significant differences in performance characteristics.

 Hence, the specifics of polycarboxylate-based superplasticizer formulation impact its effectiveness towards dispersion, interfacial interactions and reinforcement efficiency of multiwalled carbon nanotubes in high-performance cementitious matrices.
 - Nanotubes were dispersed in the mixing water of cementitious paste as a first step towards preparation of cementitious nanocomposites. This step employed a specific ultra-sonication schedule to ensure thorough dispersion of modified nanotubes in the mixing water incorporating superplasticizer. Subsequent mixing and casting steps for preparation of cementitious nanocomposites followed the procedures used commonly with plain high-performance cementitious pastes.
 - The gains in flexural strength, maximum deflection and energy absorption capacity of high-performance cementitious pastes resulting from reinforcement with modified (PAA-physisorbed) multiwalled carbon nanotubes at 0.24 vol.%

(0.48 vol.%) by volume of dry cementitious materials prepared using the preferred superplasticizer were 46.0% (48.2%), 176% (194%) and 136% (165%), respectively. The preferred superplasticizer (ADVA® Cast 575) produced gains in all flexural attributes with increasing nanotube volume fraction contrary to the other superplasticizer (Glenium® 7700) which caused a drop in flexural strength at higher volume fraction of both modified and unmodified multiwalled carbon nanotubes of higher aspect ratios.

- Modified and unmodified multiwalled carbon nanotubes, when used at 0.24 vol.% and especially 0.48 vol.%, produced some increase in compressive strength of the high-performance cementitious paste when prepared with the preferred superplasticizer (ADVA® Cast 575). Selection of superplasticizer had a major influence on the effects of nanotubes on the compressive strength of cementitious paste.
- SEM observations of the fractured surfaces of cementitious nanocomposites indicated that multiwalled carbon nanotubes were uniformly dispersed within the dense matrix. This uniform dispersion of the reinforcement system is essential for realizing the observed gains in the engineering properties of the cementitious paste. Some carbon nanotubes were observed to have pulled out of the cementitious matrix during the fracture process. This pull-out behavior benefits the ductility and energy absorption capacity of cementitious materials.
- Modification by polymer wrapping (PAA-physisorption) of multiwalled carbon nanotubes significantly benefited their reinforcement efficiency in high-performance cementitious pastes. The improvements in flexural strength, energy

absorption capacity and maximum deflection of cementitious paste with addition of 0.24 vol.% polymer-wrapped nanotubes were 41.0%, 249% and 160%, respectively.

- Polymer-wrapped as well as unmodified multiwalled carbon nanotubes were added as reinforcement to the high-performance cementitious paste after dispersion in reduced quantities of mixing water. While the reinforcing effects of nanotubes decreased with decreasing fraction of the mixing water used for their dispersion, reasonable results were obtained when nanotubes were dispersed in as low as 30% of the total mixing water, which benefits scaled-up production of cementitious nanocomposites. For polymer wrapped nanotubes, the quantity of mixing water could be reduced to as low as 20% for dispersion of nanotubes without producing a statistically significant drop in the various engineering properties of cementitious nanocomposites evaluated.
- Experimental evaluation of reinforcement with multiwalled carbon nanotubes modified through physisorption of a polyelectrolyte (PAA) and/or carbon microfiber on the flexural and compressive performance, abrasion resistance, and the structure and failure modes of a high-performance fiber reinforced **cementitious mortar** incorporating silica sand yielded the following conclusions:
 - Reinforcement of high-performance cementitious mortars with different volume fractions of modified carbon nanotube and/or carbon microfiber produced important gains in its flexural strength, ductility and energy absorption capacity, impact resistance and abrasion resistance. At equal volume fractions, carbon nanotubes produced more pronounced gains in performance characteristics of

high-performance cementitious mortar when compared with carbon microfibers.

Hybrid reinforcement systems comprising both carbon nanotubes and carbon microfibers produced particularly favorable results.

- Selection of the superplasticizer type can significantly impact the reinforcement efficiency of carbon nanotubes (modified via PAA physisorption) in high-performance cementitious mortars, which can be attributed to the corresponding impacts on the dispersion and interfacial interactions of nanotubes in the cementitious matrix.
- Response surface analysis of experimental results identified an optimum reinforcement condition comprising 0.08% modified carbon nanotube and 0.40% carbon microfiber (by volume of dry cementitious materials), which produced balanced gains in the performance characteristics of the high-performance cementitious mortar considered in the project. This finding confirms the synergistic actions of nano- and micro-scale reinforcement systems in cementitious materials.
- SEM observations of the fractured surfaces of high-performance cementitious (mortar) nanocomposites confirmed uniform dispersion of modified carbon nanotubes within the dense matrix. The contributions of nanomaterials towards restraint of microcracks by bridging action and crack arrest were also evident. Thermogravimetric analyses pointed at increased production of hydration products with the addition of carbon nano- and micro-scale reinforcement system.
- The effects of nanotubes on the **electrical conductivity** of the cementitious mortar were evaluated, and the damage-sensitivity of electrical conductivity was assessed by making

conductivity measurements prior to and after application of compressive stress (up to different fractions of the ultimate strength of the cementitious mortar). Experimental results indicated that:

- Dispersion of 0.16 vol.% modified multiwalled carbon nanotubes (by volume of dry cementitious materials) into high-performance cementitious mortar led to two to three orders of magnitude rise in electrical conductivity (depending upon the superplasticizer type). Increasing the nanotube volume fraction from 0.16 to 0.24 vol.% produced another order of magnitude rise in electrical conductivity.
- The damaging effects (microcracking and permanent strains) induced by increasing compressive stress levels lowered the electrical conductivity of high-performance cementitious mortars incorporating carbon nanotubes. After application of 60% and 80% of compressive strength, electrical conductivity dropped by one and two orders of magnitude, respectively. The higher conductivity levels in the presence of 0.24 vol.% (versus 0.16 vol.%) carbon nanotubes (by volume of dry cementitious materials) simplify measurement of electrical conductivity. Damage-sensitivity of the electrical conductivity of high-performance cementitious materials incorporating carbon nanotubes provides these materials with inherent health monitoring qualities.
- SEM images confirmed successful dispersion of carbon nanotubes in a dense, high-performance cementitious matrix, with nanotubes forming a percolated network within matrix which benefits their contributions to electrical conductivity.

- Experimental results were generated for high-performance **concrete** (incorporating silica sand and granite coarse aggregate) reinforced with modified (PAA-physisorbed) multiwalled carbon nanotubes, polypropylene microfibers, carbon microfibers and their hybrids prepared at various/optimum volume fractions with carboxyl-based superplasticizers. Test results indicated that:
 - o Proper use of nano-scale reinforcement can produce improvements in highperformance concrete mechanical properties which surpass those realized with micro-scale reinforcement at equal volume fractions.
 - Nano- and micro-scale reinforcement renders complementary reinforcing effects in high-performance concrete; optimum reinforcement systems thus incorporate both nano- and micro-scale reinforcement.
 - Among the single reinforcement conditions evaluated in high-performance concrete, PAA-physisorbed multiwalled carbon nanotubes produced particularly significant improvements in the mechanical properties of high-performance concrete.
 - o PAA-physisorbed multiwalled carbon nanotubes act synergistically with microscale reinforcement towards enhancement of the mechanical properties of high-performance concrete; the synergistic effects of nano- and micro-scale reinforcement are reflected in the fact that hybrid (nano- and micro-scale) reinforcement overcomes any drawbacks associated with the use of each (nano- or micro-scale) reinforcement used alone.

- The experimental results produced using the optimu hybrid reinforcement condition identified through RSA (response surface analysis) pointed at the effectiveness of RSA in identifying the desired reinforcement condition for improving the targeted attributes of high-performance concrete. The refined hybrid reinforcement produced results which further demonstrated the synergetic actions of nano- and micro-scale reinforcement systems. For the hybrid reinforcement comprising polymer-wrapped multiwalled carbon nanotubes at 0.15% and polypropylene microfiber at 0.23% by volume of dry cementitious materials, pronounced and balanced gains in performance characteristics were realized when compared with systems where either nano- or micro-scale reinforcement was used alone.
- Experimental results generated for **high-strength concrete materials with lower performance characteristics** than those considered throughout the project, reinforced with PAA physisorbed multiwalled carbon nanotubes, carbon microfibers and their optimum hybrid system, prepared with carboxyl-based superplasticizer, indicated that:
 - o Proper use of nano-scale reinforcement can produce improvements in highstrength concrete mechanical properties which surpass those realized with microscale reinforcement at equal volume fractions. However, the reinforcement efficiency is reduced with reduction of concrete matrix performance (which accompanied lowering of the cementitious paste content). The higherperformance concrete (which was steam cured) exhibited a denser microstructure when compared with the concrete considered at this stage of investigation (which

was moist cured). The increased density of cementitious matrix benefits its interactions with nanomaterials.

- The hybrid (nano- and micro-scale) reinforcement produces complementary reinforcing effects in high-strength concrete (as it did in the higher-performance concrete considered earlier); optimum reinforcement systems for this concrete would also incorporate both nano- and micro-scale reinforcement.
- Among the nano- and micro-scale reinforcement systems considered, PAAphysisorbed multiwalled carbon nanotubes produced balanced gains in
 engineering properties of high-strength concrete when compared with micro-scale
 reinforcement.
- Experimental results on **cementitious pastes** reinforced with non-functionalized and functionalized **carbon nanofibers** as well as their hybrids with carbon microfibers indicated that:
 - Acid-oxidization of CNFs benefited their dispersion and reinforcement efficiency in the high-performance cementitious matrix. The high specific surface area and the nano-scale spacing of dispersed nanofibers benefit their control of defect (microcrack) size and mitigation of microcrack growth, thus improving the nanofiber contributions to the strength, energy absorption capacity and ductility of high-performance cementitious materials. Properly functionalized and well-dispersed CNFs with desired interfacial interactions brought about balanced gains in the flexural strength, energy absorption and ductility, impact and abrasion resistance of high-performance cementitious paste, while preserving its high compressive strength.

- For the cementitious matrix and processing conditions considered in this investigation, the nanofiber dosage should be lowered below 0.24% (by volume of dry cementitious materials) before benefits can be realized from introduction of carbon microfibers. Hence, a nanofiber volume fraction of 0.16% was considered for development of hybrid reinforcement systems.
- A hybrid reinforcement comprising CNFs and microfibers at 0.16% and 0.24% by volume of dry cementitious materials produced distinct gains in the engineering properties of the high-performance cementitious paste, which could not be matched by the nano- or micro-scale reinforcement used alone. This finding points at the synergistic effects of nano- and micro-scale reinforcement systems.
- Results of comprehensive experimental evaluations of high-performance **cementitious**mortar with nano-scale (pristine, polymer-wrapped or oxidized **carbon nanofibers**)

 and/or micro-scale (carbon microfiber) reinforcement using two polycarboxylate-based superplasticizers indicated that:
 - As was the case with carbon nanotubes for similar reinforcement conditions, the gains in performance characteristics of the cementitious matrix depended upon the specific polycarboxylate-based superplasticizer used. The gains in flexural performance characteristics per unit volume of reinforcement were more significant with CNFs when compared with carbon microfibers.
 - The high-performance cementitious mortar experienced important (and statistically significant) gains in all flexural attributes (strength, energy absorption capacity and maximum deflection), impact and abrasion resistance with introduction of different volume fractions of polymer-wrapped CNFs (used alone

or in combination with microfibers) versus plain mortar or those with similar volume fractions of pristine or oxidized CNFs.

- O Hybrid reinforcement systems comprising CNFs and microfibers produced particularly significant gains in the flexural performance characteristics and impact resistance of high-performance cementitious mortar. Response surface analysis of experimental results indicated that optimum reinforcement conditions comprised both CNFs and microfibers. The reinforcement conditions considered here produced minor (and statistically insignificant) changes in the compressive strength of high-performance cementitious mortar.
- The experimental results generated for high performance **concrete** reinforced with both oxidized and PAA physisorbed **carbon nanofibers**, polypropylene microfibers, carbon microfibers and their hybrids, prepared at various/optimum volume fractions and with carboxyl-based superplasticizers, indicated that:
 - o Proper use of CNFs can produce improvements in high-performance concrete mechanical properties which surpass those realized with micro-scale reinforcement.
 - O CNFs and micro-scale reinforcement render complementary reinforcing effects in high-performance concrete; optimum reinforcement systems thus incorporate both nano- and micro-scale reinforcement.
 - O Among the individual reinforcement conditions evaluated in high-performance concrete, PAA-physisorbed CNFs produced particularly high and balanced improvements in the mechanical properties of high-performance concrete.

- O PAA-physisorbed CNFs act synergistically with micro-scale reinforcement towards enhancement of the mechanical properties of high-performance concrete; the synergistic effects of CNFs and micro-scale reinforcement are reflected in the fact that hybrid (nano- and micro-scale) reinforcement overcomes any drawbacks associated with the use of each (nano- or micro-scale) reinforcement used alone.
- The optimized hybrid reinforcement system, identified through response surface analysis (RSA) of experimental results, point at the effectiveness of RSA in identifying desired reinforcement conditions for improving the targeted attributes of high-performance concrete. The refined hybrid reinforcement produced results which further demonstrated the synergetic actions of CNFs and micro-scale reinforcement. The hybrid reinforcement system comprising polymer-wrapped CNFs at 0.12% and polypropylene microfibers at 0.24% (by volume of dry cementitious materials) produced more pronounced and balanced gains in performance characteristics versus conditions with either nano- or micro-scale reinforcement used alone.
- Experimental results generated for high-performance **cementitious paste**, **mortar and concrete** reinforced with pristine and PAA-physisorbed **graphite nanoplatelets** and also
 their hybrids with carbon or polypropylene microfibers indicated that:
 - All the reinforcement conditions considered produced improvements in flexural attributes, impact and abrasion resistance of high-performance (DSP) cementitious paste, mortar and concrete.
 - o In DSP paste, graphite nanoplatelets, carbon microfibers and especially their combination (hybrid reinforcement) produced important gains in the flexural

strength, energy absorption capacity and maximum deflection. The hybrid reinforcement system yielded 61.7%, 366% and 264% gains in flexural strength, energy absorption capacity and maximum deflection, respectively, of cementitious paste. Graphite nanoplatelets seem to produce a minor (statistically insignificant) loss of compressive strength. This could be attributed to their planar (flaky) geometry and micro-scale planar dimension, which could produce local stress rise. The most important contribution of graphite nanoplatelets was to the impact resistance of DSP paste, which increased by 42.7%, 114% and 158% with introduction of carbon microfiber, graphite nanoplatelet and hybrid reinforcement. The abrasion resistance of DSP paste increased by 45.5%, 58.9% and 56.4% with carbon microfiber, graphite nanoplatelet and hybrid reinforcement.

Similar trends in all engineering properties were observed in the case of the DSP mortar matrix. The comparatively smaller and statistically insignificant improvement in flexural attributes with the use of PAA-physisorbed graphite nanoplatelets can be attributed to the morphology and physical characteristics of nanoplatelets. The experimental results also indicate that hybrid (nano- and micro-scale) reinforcement systems produce more pronounced and balanced benefits, which point at the complementary role of reinforcement systems operating at different length scales. In mortar matrix, pair-wise comparisons indicated that PAA-physisorbed graphite nanoplatelets (and their hybrid with carbon microfiber) produce statistically significant (but still small) adverse effects on the compressive strength of DSP mortar. As was the case with DSP paste, the most significant effect of PAA-physisorbed graphite nanoplatelet was on the

0

impact resistance of DSP mortar. PAA-physisorbed graphite nanoplatelet at 0.16 and 0.24% by volume of dry cementitious materials improved the impact resistance of DSP mortar by 99% and 109%, respectively. This significant increase is due to flaky geometry which tends to be more effective under dynamic loads.

In DSP concrete incorporating coarse aggregates, PAA-physisorbed graphite 0 nanoplatelets effectively reinforced the paste portion of the matrix. The improvements in flexural strength, energy absorption capacity and maximum deflection with respect to plain concrete were 10.5%, 97% and 76%, respectively. The addition of carbon or polypropylene microfibers to high-performance (DSP) concrete produced important gains in only two out of the three flexural attributes considered here (maximum deflection and energy absorption capacity), while causing a relatively small drop in the flexural strength. The hybrid reinforcement comprising low-modulus polypropylene microfibers with graphite nanoplatelets produced particularly pronounced gains in the mechanical properties of DSP concrete. The best balance of flexural attributes was produced by the hybrid reinforcement comprising PAA graphite nanoplatelet (0.16 vol.%) and polypropylene microfiber (0.24 vol.%), which produced 15%, 573% and 329% rise in flexural strength, maximum deflection and energy absorption capacity, respectively. As was the case with DSP paste and mortar, PAA-physisorbed graphite nanoplatelets as well as carbon or polypropylene microfibers, produced relatively small and statistically insignificant effects on the compressive strength of DSP concrete. The modified graphite nanoplatelet and/or micro-scale reinforcement systems produced improvements in the impact resistance of the high-performance concrete matrix. However, due to addition of coarse aggregates, the contribution of PAA-physisorbed graphite nanoplatelet was not that significant. The modified graphite nanoplatelet at 0.16% by volume of dry cementitious materials produced the greatest improvement (38%) in the abrasion resistance of high-performance (DSP) concrete when compared with the two microfibers.

- Experimental results on the **durability characteristics** of high-performance (DSP) cementitious **mortar and concrete** indicated that:
 - DSP mortars provide desirable durability characteristics, which tend to be enhanced through reinforcement with nano-scale and especially hybrid (nano- and micro-scale) reinforcement systems. Hybrid reinforcement of DSP cementitious mortar, when used at appropriate volume fractions, proved very effective in improving key durability characteristics of the matrix through enhancement of barrier qualities and synergistic reinforcement at different scales.
 - Plain DSP mortars as well as those with hybrid graphite nanoplatelet/carbon microfiber reinforcement did not survive exposure to elevated temperatures. DSP mortars with hybrid PAA-physisorbed multiwalled carbon nanotube and carbon microfiber reinforcement, however, survived exposure to extreme temperatures. This was attributed to the high toughness, tensile strength and thermal conductivity of these nanocomposites, and also to the potential for combustion of percolated nanotubes which opens escape routes to reduce the steam pressure developed in nanocomposites at elevated temperatures. Extended immersion in

hot water had relatively small effects on the dynamic elastic modulus of DSP mortar nanocomposites. Flexural strength, however, experienced a drop after extended hot water immersion, which was not statistically significant with hybrid reinforcement systems comprising PAA-physisorbed carbon nanotubes and carbon microfibers.

- In the case of the high-performance (DSP) concrete also, the accelerated aging effects considered did not damage the flexural attributes and dynamic elastic modulus of plain DSP concrete and that with PVA-physisorbed multiwalled carbon nanotube. These accelerated aging conditions included 300 freeze-thaw or wet-dry cycles, and 56 days immersion in hot water. However, matrices containing polypropylene microfibers and hybrid (polypropylene microfiber and PAA-physisorbed carbon nanotube) reinforcement experienced drops in the mean values of almost all flexural attributes when exposed to accelerated aging effects. These drops, however, were not generally statistically significant. In general, polypropylene microfibers did not perform well under accelerated aging conditions even in a dense DSP concrete matrix. On the other hand, PAA-physisorbed multiwalled carbon nanotubes benefited the durability characteristics of high-performance cementitious matrices.
- Experimental results on the **moisture sorption rates** of different high-performance cementitious matrices reinforced with various volume fractions of graphite nanomaterials and/or microfibers indicated that:
 - o The proper gradation of high-performance cementitious materials yields a dense structure with high barrier qualities.

- Unlike conventional (micro-scale) fibers, graphite nanomaterials significantly enhance the diffusion resistance of cement-based materials. This could be attributed to the close spacing and large surface area of graphite nanomaterials, which significantly increase the tortuosity of diffusion paths within the cement-based matrix. The presence of graphite nanomaterials in the cementitious matrix also partially blocks the pore system at nano-scale, which further benefits the barrier qualities of cementitious materials.
- Addition of either of the two PAA-physisorbed graphite nanomaterials as well as their hybrid combinations with both microfibers resulted in drops in the moisture sorption rate as well as the total water absorbed. The maximum drops (among different reinforcement systems used alone) for all matrices were recorded with 0.24 vol.% PAA-physisorbed graphite nanoplatelet.
- Due to the inherent advantages of being present in the matrix as an inclusion and being relatively inert under weathering effects, graphite nanomaterials, especially graphite nanomaterials, provide a cost-effective solution for enhancing the barrier qualities and thus durability characteristics of cementitious materials. When appropriately combined with microfibers, cementitious nanocomposites offer a desired balance of mechanical, barrier and durability characteristics.
- The experience gained with **industrial-scale production and field construction** of highperformance concrete nanocomposites indicated that:
 - Scaled-up production of concrete nanocomposites requires streamlining of the dispersion process of larger quantities of graphite nanomaterials in water, and their introduction into the plant batching and mixing process.

- O Concrete nanocomposites produced under scaled-up conditions provided statistically similar, but slightly smaller, engineering properties when compared with concrete nanocomposites produced at laboratory scale.
- As was the case in laboratory studies, under scaled-up production and field construction conditions also, optimized hybrid (nano- and micro-scale) reinforcement systems performed better than either of the nano- and micro-scale reinforcement used alone. This confirms the synergistic effects of nano- and micro-scale reinforcement towards enhancement of the high-performance concrete materials properties.
- Scaled-up studies confirmed that the dense matrix in high-strength concrete produced high barrier qualities. Both graphite nanomaterials, when used in combination with polypropylene microfibers, further improved the barrier qualities of high-performance concrete by forcing tortuous diffusion paths and partial blocking of capillary pores. The maximum improvements in barrier qualities were realized with the hybrid reinforcement comprising graphite nanoplatelets and polypropylene microfibers. When used alone, however, polypropylene microfibers did not produce statistically significant gains in the barrier qualities of high-strength concrete.
- A **theoretical framework** was developed for evaluating the contributions of graphite nanomaterials (emphasizing carbon nanotubes) to diverse aspects of concrete engineering properties. The theoretical models were verified and refined using experimental results. These models enabled explanation of the means by which nanomaterials benefit diverse aspects of concrete performance, ranging from toughness and strength to barrier and

durability characteristics, which far surpass the range of properties improved by conventional (micro-scale) fibers. Theoretical explanations were also presented for the synergistic role of carbon nanotubes and conventional (micro-scale) fibers towards achieving balanced gains in diverse engineering properties of concrete

- Percolation of carbon nanotubes can occur at relatively low nanotube volume fractions. This brings about a sharp rise in conductivity (and also fire resistance) of concrete with introduction of relatively low nanotube volume fractions. The electrical conductivity of concrete nanocomposites was found to be sensitive to the damaging effects experienced b concrete. Concrete nanocomposites thus offer inherent health monitoring qualities.
- The trend towards industrial-scale production of multiwalled carbon nanotubes and other graphite nanomaterials is causing a sharp drop in their projected intermediate- and long-term **costs**. This trend together with the significant benefits rendered by nanomaterials to diverse aspects of concrete performance at relatively low dosages make nanomaterials, and especially hybrid (nano- and micro-scale) reinforcement systems, economically viable additives for development of the next-generation high-performance concrete materials.

19.3 Recommendations for Future Research

While this study has advanced the state-of-the-art with respect to the use of suitably modified graphite nanomaterials and/ or microfibers in different high-performance cementitious matrices, further research is required to fully realize the reinforcement potential of graphite nanomaterials in a broad range of cement-based matrices. Some key recommendations for further research in this area are presented in the following.

- The modification conditions of nanomaterials, and procedures used for their dispersion in concrete need to be optimized for enhanced effectiveness at viable cost, and should be streamlined to suit scaled-up production.
- The efficiency of modified nanomaterials in broader categories of concrete materials,
 with different mix proportions and admixtures, need to be evaluated.
- Distinctions between multiwalled carbon nanotubes, carbon nanofibers and graphite
 nanoplatelets should be further clarified, and niche applications for each of these
 nanomaterials should be identified.
- Optimum hybrid (nano- and micro-scale) reinforcement systems should be identified with broader categories of micro-scale fibers, and for different concrete mix proportions.
- More comprehensive laboratory and field test data should be produced on diverse engineering properties of concrete nanocomposites.
- Further micro-structural investigations should be undertaken in order to better understand the impact of modified nanomaterials on the structure of cement hydrates, their role in failure mechanisms and sorption resistance of concrete, and their complementary actions with micro-scale fibers.
- Theoretical models should be refined and expanded for reliable predictions of the nanoscale and hybrid reinforcement systems on diverse aspects of concrete engineering properties.
- Focused laboratory and field investigations should be undertaken to demonstrate the advantages of nanomaterials in niche applications identified for each nanomaterial type.

 The research findings need to be reflected in standard specifications and guides to facilitate transition of modified graphite nanomaterials to selected concrete construction markets.

19.4 Impact of the Research Effort

The pioneering work conducted in this research has produced convincing evidence for the technical value and competitive cost of modified graphite nanomaterials as reinforcement in high-performance concrete materials. The hybrid reinforcement system developed in the project, comprising modified graphite nanomaterials and micro-scale fibers, produces significant and uniquely balanced gains in diverse engineering properties of high-performance concrete. Initial steps were also taken towards scaled-up production and field use of concrete nanocomposites.

The research outcomes point at the value of graphite nanomaterials as a new class of concrete additive, which are distinguished by their impact on a broad range of concrete material properties. Graphite nanomaterials can make important contributions towards development of the next-generation high-performance concrete materials and infrastructure systems offering balanced improvements in diverse mechanical qualities and structural efficiency, barrier and durability characteristics, safety attributes under extreme conditions and life-cycle economy.

REFERENCES

REFERENCES

- Navielle, A.M., N. (1995). Properties of concrete. London, Longman Group Limited.
- Ahlborn, T. M., D. K. Harris, et al. (2011). "Characterization of strength and durability of ultrahigh-performance concrete under variable curing conditions." Transportation Research Record(2251): 68-75.
- Badanoiu, A., M. Georgescu, et al. (2003). "The study of 'DSP' binding systems by thermogravimetry and differential thermal analysis." Journal of Thermal Analysis and Calorimetry 74(1): 65-75.
- Balasubramanian, K. and M. Burghard (2005). "Chemically functionalized carbon nanotubes." Small 1(2): 180-192.
- Banerjee, S., M. G. C. Kahn, et al. (2003). "Rational chemical strategies for carbon nanotube functionalization." Chemistry A European Journal 9(9): 1898-1908.
- Banthia, N. and M. Sappakittipakorn (2007). "Toughness enhancement in steel fiber reinforced concrete through fiber hybridization." Cement and Concrete Research 37(9): 1366-1372.
- Bayard, O. and O. Ple (2003). "Fracture mechanics of reactive powder concrete: Material modelling and experimental investigations." Engineering Fracture Mechanics 70(7-8): 839-851.
- Beaudoin, J. J., R. F. Feldman, et al. (1994). "Pore structure of hardened Portland cement pastes and is influence on properties." Advanced Cement Based Materials 1(5): 224-236.
- Bensebaa, F., F. Zavaliche, et al. (2004). "Microwave synthesis and characterization of Co-ferrite nanoparticles." Journal of Colloid and Interface Science 277(1): 104-110.
- Bentz, D. P. (2000). "Influence of silica fume on diffusivity in cement-based materials. II. Multiscale modeling of concrete diffusivity." Cement and Concrete Research 30(7): 1121-1129.
- Bentz, D. P., O. M. Jensen, et al. (2000). "Influence of silica fume on diffusivity in cement-based materials. I. Experimental and computer modeling studies on cement pastes." Cement and Concrete Research 30(6): 953-962.
- Breuer, O. and U. Sundararaj (2004). "Big returns from small fibers: A review of polymer/carbon nanotube composites." Polymer Composites 25(6): 630-645.
- Camilleri, J., F. E. Montesin, et al. (2006). "Characterization of Portland cement for use as a dental restorative material." Dental Materials 22(6): 569-575.

- Chan, L. Y. and B. Andrawes (2010). "Finite element analysis of carbon nanotube/cement composite with degraded bond strength." Computational Materials Science 47(4): 994-1004.
- Chan, Y.-W. and S.-H. Chu (2004). "Effect of silica fume on steel fiber bond characteristics in reactive powder concrete." Cement and Concrete Research 34(7): 1167-1172.
- Cheyrezy, M., V. Maret, et al. (1995). "Microstructural analysis of RPC (reactive powder concrete)." Cement and Concrete Research 25(7): 1491-1500.
- Childs, P., A. C. L. Wong, et al. (2007). "Measurement of the coefficient of thermal expansion of ultra-high strength cementitious composites using fiber optic sensors." Cement and Concrete Research 37(5): 789-795.
- Chindaprasirt, P., C. Jaturapitakkul, et al. (2005). "Effect of fly ash fineness on compressive strength and pore size of blended cement paste." Cement and Concrete Composites 27(4): 425-428.
- Collepardi, M., V. Corinaldesi, et al. (2002). "Applicazioni e sviluppo dei materiali DSP; DSP materials applications and development progress." Industria Italiana del Cemento 72(JU): 540-545.
- Collins, F., J. Lambert, et al. (2012). "The influences of admixtures on the dispersion, workability, and strength of carbon nanotube-OPC paste mixtures." Cement and Concrete Composites 34(2): 201-207.
- Cwirzen, A., K. Habermehl-Cwirzen, et al. (2009). "SEM/AFM studies of cementitious binder modified by MWCNT and nano-sized Fe needles." Materials Characterization 60(7): 735-740.
- Cwirzen, A., K. Habermehl-Cwirzen, et al. (2008). "Surface decoration of carbon nanotubes and mechanical properties of cement/carbon nanotube composites." Advances in Cement Research 20(2): 65-73.
- Cwirzen, A. and V. Penttala (2005). "Aggregate-cement paste transition zone properties affecting the salt-frost damage of high-performance concretes." Cement and Concrete Research 35(4): 671-679.
- Feylessoufi, A., F. Villieras, et al. (1996). "Water environmental and nanostructural network in a reactive powder concrete." Cement & Concrete Composites 18(1): 23-24.
- Fu, X. and D. D. L. Chung (1998). "Submicron-diameter-carbon-filament cement-matrix composites." Carbon 36(4): 459-462.
- Gao, L., L. Jiang, et al. (2006). "Carbon nanotube-ceramic composites." Journal of Electroceramics 17(1): 51-55.

- Guerrini, G. L. (2000). "Applications of high-performance fiber-reinforced cement-based composites." Applied Composite Materials 7(2-3): 195-207.
- Hall, C. (1989). "Water sorptivity of mortars and concretes: a review." Magazine of Concrete Research 41(147): 51-61.
- Han, B., X. Yu, et al. (2009). "A self-sensing carbon nanotube/cement composite for traffic monitoring." Nanotechnology 20: 1-5.
- Han, B., X. Yu, et al. (2011). "Effects of CNT concentration level and water/cement ratio on the piezoresistivity of CNT/cement composites." Journal of Composite Materials 46(1): 19-25.
- Hawley, M. C. (2002). Microwave processing of polymers and composites Fundamentals and applications. Composites Manufacturing and Tooling 2001, Febrary 21, 2001 Febrary 23, 2001, Orlando, FL, United states, Society of Manufacturing Engineers.
- Hu, A., Y. Fang, et al. (1999). "Humidity dependence of apparent dielectric constant for DSP cement materials at high frequencies." Journal of the American Ceramic Society 82(7): 1741-1747.
- Hu, G., C. Zhao, et al. (2006). "Low percolation thresholds of electrical conductivity and rheology in poly(ethylene terephthalate) through the networks of multi-walled carbon nanotubes." Polymer 47(1): 480-488.
- Kalaitzidou, K., H. Fukushima, et al. (2007). "Mechanical properties and morphological characterization of exfoliated graphite-polypropylene nanocomposites." Composites Part A: Applied Science and Manufacturing 38(7): 1675-1682.
- Kalaitzidou, K., H. Fukushima, et al. (2007). "Multifunctional polypropylene composites produced by incorporation of exfoliated graphite nanoplatelets." Carbon 45(7): 1446-1452.
- Katz, A. and A. Bentur (1994). "Mechanical properties and pore structure of carbon fiber reinforced cementitious composites." Cement and Concrete Research 24(2): 214-220.
- Katz, A. and A. Bentur (1995). "Effect of matrix composition on the aging of CFRC." Cement and Concrete Composites 17(2): 87-97.
- Katz, A. and A. Bentur (1996). "Mechanisms and processes leading to changes in time in the properties of CFRC." Advanced Cement Based Materials 3(1): 1-13.
- Katz, A., V. C. Li, et al. (1995). "Bond properties of carbon fibers in cementitious matrix." Journal of Materials in Civil Engineering 7(2): 125-128.
- Konsta-Gdoutos, M. S., Z. S. Metaxa, et al. (2010). "Highly dispersed carbon nanotube reinforced cement based materials." Cement and Concrete Research 40(7): 1052-1059.

- Konsta-Gdoutos, M. S., Z. S. Metaxa, et al. (2010). "Multi-scale mechanical and fracture characteristics and early-age strain capacity of high performance carbon nanotube/cement nanocomposites." Cement and Concrete Composites 32(2): 110-115.
- Kowald, T. (2004). Influence of Surface-Modified Carbon Nanotubes on Ultra-High Performance Concrete. Proceedings of International Symposium on Ultra High Performance Concrete. Kassel, Germany: 195–202.
- Kubota, K., M. Sano, et al. (2005). "Microwave irradiation for chemical modification of carbon nanotubes for better dispersion." Japanese Journal of Applied Physics, Part 1: Regular Papers and Short Notes and Review Papers 44(1 A): 465-468.
- Lawler, J. S., D. Zampini, et al. (2005). "Microfiber and macrofiber hybrid fiber-reinforced concrete." Journal of Materials in Civil Engineering 17(5): 595-604.
- Lee, M.-G., Y.-C. Wang, et al. (2007). "A preliminary study of reactive powder concrete as a new repair material." Construction and Building Materials 21(1): 182-189.
- Li, G. Y., P. M. Wang, et al. (2007). "Pressure-sensitive properties and microstructure of carbon nanotube reinforced cement composites." Cement and Concrete Composites 29(5): 377-382.
- Li, G. Y., P. M. Wang, et al. (2005). "Mechanical behavior and microstructure of cement composites incorporating surface-treated multi-walled carbon nanotubes." Carbon 43(6): 1239–1245.
- Li, J., M. L. Sham, et al. (2007). "Morphology and properties of UV/ozone treated graphite nanoplatelet/epoxy nanocomposites." Composites Science and Technology 67(2): 296-305.
- Li, V. C. (2002). "Large volume, high-performance applications of fibers in civil engineering." Journal of Applied Polymer Science 83(3): 660-686.
- Makar, J. M. and J. J. Beaudoin (2004). Carbon nanotubes and their applications in the construction industry. Nanotechnology in construction, Proceedings of the 1st international symposium on nanotechnology in construction, Royal Society of Chemistry. P. J. M. Bartos, J. J. Hughes, P. Trtik and W. Zhu: 331–341.
- Makar, J. M. and G. W. Chan (2009). "Growth of cement hydration products on single-walled carbon nanotubes." Journal of the American Ceramic Society 92(6): 1303-1310.
- Makar, J. M., J. Margeson, et al. (2005). Carbon nanotube/cement composites early results and potential applications. Proceedings of the 3rd international conference on construction materials: performance, innovations and structural implications, Vancouver, BC, Canada.

- Manzur, T. and N. Yazdani (2010). "Strength enhancement of cement mortar with carbon nanotubes: Early results and potential." Transportation Research Record(2142): 102-108.
- Matte, V. and M. Moranville (1999). "Durability of reactive powder composites: Influence of silica fume on the leaching properties of very low water/binder pastes." Cement & Concrete Composites 21(1): 1-9.
- Mehta, A. (1993). Concrete, Prentice Hall.
- Metaxa, Z. S., M. S. Konsta-Gdoutos, et al. (2009). Carbon nanotubes reinforced concrete. ACI Fall 2009 Convention, November 8, 2009 November 12, 2009, New Orleans, LA, United states, American Concrete Institute.
- Metaxa, Z. S., M. S. Konsta-Gdoutos, et al. (2010). "Carbon Nanofiber-Reinforced cement-based materials." Transportation Research Record(2142): 114-118.
- Metaxa, Z. S., M. S. Konsta-Gdoutos, et al. (2010). Mechanical properties and nanostructure of cement-based materials reinforced with CNFs and Polyvinyl Alcohol (PVA) microfibers. ACI Spring 2010 Convention, March 21, 2010 March 25, 2010, Chicago, IL, United states, American Concrete Institute.
- Moranville-Regourd, M. (2001). New cementitious systems and composite materials. 7th Conference and Exhibition of the European Ceramic Society, Sep 9-13 2001, Brugge, Trans Tech Publications Ltd.
- Moranville-Regourd, M. (2001). New cementitious systems and composite materials, Brugge, Trans Tech Publications Ltd.
- Morin, V., F. Cohen-Tenoudji, et al. (2002). "Evolution of the capillary network in a reactive powder concrete during hydration process." Cement and Concrete Research 32(12): 1907-1914.
- Musso, S., J.-M. Tulliani, et al. (2009). "Influence of carbon nanotubes structure on the mechanical behavior of cement composites." Composites Science and Technology 69(11-12): 1985-1990.
- Nasibulin, A. G., S. D. Shandakov, et al. (2009). "A novel cement-based hybrid material." New Journal of Physics 11.
- O'Connell, M. J., P. Boul, et al. (2001). "Reversible water-solubilization of single-walled carbon nanotubes by polymer wrapping." Chem. Phys. Lett. 342(3,4): 265-271.
- O'Connell, M. J., P. Boul, et al. (2001). "Reversible water-solubilization of single-walled carbon nanotubes by polymer wrapping." Chem. Phys. Lett. 342(3): 265-271.

- Pfeifer, C., B. Moeser, et al. (2009). Durability of ultra-high-performance concrete. 10th ACI International Conference on Recent Advances in Concrete Technology and Sustainability Issues, October 14, 2009 October 16, 2009, Seville, Spain, American Concrete Institute.
- Ping, X., J. J. Beaudoin, et al. (1991). "Effect of aggregate size on transition zone properties at the portland cement paste interface." Cement and Concrete Research 21(6): 999-1005.
- Poon, C. S., L. Lam, et al. (1999). "Effects of fly ash and silica fume on interfacial porosity of concrete." Journal of Materials in Civil Engineering 11(3): 197-205.
- Richard, P. and M. Cheyrezy (1995). "Composition of reactive powder concretes." Cement and Concrete Research 25(7): 1501-1511.
- Roux, N., C. Andrade, et al. (1996). "Experimental study of durability of reactive powder concretes." Journal of Materials in Civil Engineering 8(1): 1-6.
- Saez De Ibarra, Y., J. J. Gaitero, et al. (2006). Atomic force microscopy and nanoindentation of cement pastes with nanotube dispersions, Wiley-VCH Verlag.
- Sahmaran, M. and V. C. Li (2009). "Influence of microcracking on water absorption and sorptivity of ECC." Materials and Structures/Materiaux et Constructions 42(5): 593-603.
- Sandlar, J., M. S. P. Shaffer, et al. (1999). "Development of a dispersion process for carbon nanotubes in an epoxy matrix and the resulting electrical properties." Polymer 40: 5967-5971.
- Shannag, M., W. Hansen, et al. (1999). "Interface Debonding in Fiber Reinforced Cement-Matrix Composites." Journal of Composite Materials 33(2): 158-176.
- Shannag, M. J., R. Brincker, et al. (1996). "Interfacial (fiber-matrix) properties of high-strength mortar (150 MPa) from fiber pullout." ACI Materials Journal 93(5): 480-486.
- Shannag, M. J., R. Brincker, et al. (1997). "Pullout behavior of steel fibers from cement-based composites." Cement and Concrete Research 27(6): 925-936.
- Shannag, M. J. and W. Hansen (2000). "Tensile properties of fiber-reinforced very high strength DSP mortar." Magazine of Concrete Research 52(2): 101-108.
- Shannag, M. J., W. Hansen, et al. (1995). Interfacial debonding and sliding in brittle cement-matrix composites from steel fiber pullout tests, Boston, MA, USA, Materials Research Society, Pittsburgh, PA, USA.
- Singh, B., P. Kumar, et al. (2001). "High performance composites for the new millennium." Journal of Structural Engineering (Madras) 28(1): 17-26.
- Song, H.-W., J.-C. Jang, et al. (2007). "An estimation of the diffusivity of silica fume concrete." Building and Environment 42(3): 1358-1367.

- Sun, G.-k. and J. F. Young (1993). "Quantitative determination of residual silica fume in DSP cement pastes by 29-Si NMR." Cement and Concrete Research 23(2): 480-483.
- Sun, G. K. and J. F. Young (1993). "Hydration reactions in autoclaved DSP cements." Advances in Cement Research 5(20): 163-169.
- Tibbetts, G. G., M. L. Lake, et al. (2007). "A review of the fabrication and properties of vapor-grown carbon nanofiber/polymer composites." Composites Science and Technology 67(7-8): 1709-1718.
- Tjiptobroto, P. and W. Hansen (1991). "Mechanism for tensile strain hardening in high performance cement-based fiber reinforced composites." Cement & Concrete Composites 13(4): 265-273.
- Tjiptobroto, P. and W. Hansen (1993). "Model for predicting the elastic strain of fiber reinforced composites containing high volume fractions of discontinuous fibers." ACI Materials Journal (American Concrete Institute) 90(2): 134-142.
- Tjiptobroto, P. and W. Hansen (1993). "Tensile strain hardening and multiple cracking in high-performance cement-based composites containing discontinuous fibers." ACI Materials Journal (American Concrete Institute) 90(1): 16-25.
- Tsivilis, S., J. Tsantilas, et al. (2003). "The permeability of Portland limestone cement concrete." Cement and Concrete Research 33(9): 1465-1471.
- Vaisman, L., H. D. Wagner, et al. (2006). "The role of surfactants in dispersion of carbon nanotubes." Advances in Colloid and Interface Science 128-130: 37-46.
- Wang, X., J. Ye, et al. (2007). "Reinforcement of calcium phosphate cement by bio-mineralized carbon nanotube." Journal of the American Ceramic Society 90(3): 962-964.
- Washer, G., P. Fuchs, et al. (2004). "Ultrasonic Testing of Reactive Powder Concrete." IEEE Transactions on Ultrasonics, Ferroelectrics, and Frequency Control 51(2): 193-201.
- Wille, K. and K. J. Loh (2010). "Nanoengineering ultra-high-performance concrete with multiwalled carbon nanotubes." Transportation Research Record(2142): 119-126.
- Wong, A. C. L., P. A. Childs, et al. (2007). "Simultaneous measurement of shrinkage and temperature of reactive powder concrete at early-age using fiber Bragg grating sensors." Cement and Concrete Composites 29(6): 490-497.
- Xie, L., F. Xu, et al. (2007). "Single-walled carbon nanotubes functionalized with high bonding density of polymer layers and enhanced mechanical properties of composites." Macromolecules 40(9): 3296-3305.

- Young, J. F. (1996). Recent advances in the development of high performance cement-based materials, Washington, DC, USA, ASCE, New York, NY, USA.
- Zanni, H., M. Cheyrezy, et al. (1996). "Investigation of hydration and pozzolanic reaction in reactive powder concrete (RPC) using Si NMR." Cement and Concrete Research 26(1): 93-100.
- Zivica, V. (1999). "Possibilities of a novel use of silica fume in mineral binding systems." Construction and Building Materials 13(5): 271-277.